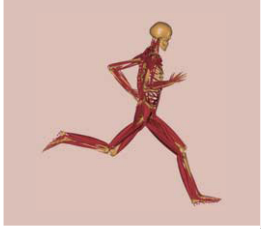

Advances in Transdisciplinary Engineering series

volume 11

DHM2020

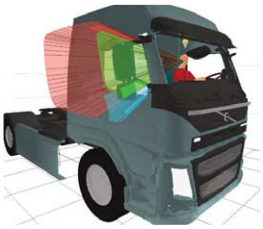

Proceedings of the 6th International Digital Human Modeling Symposium, August 31 – September 2, 2020

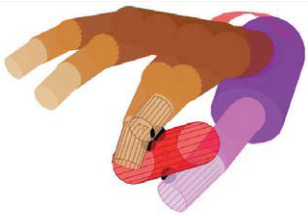
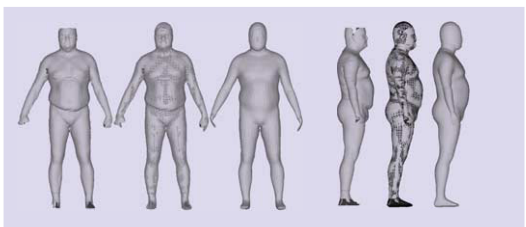

EDITED BY
Lars Hanson
Dan Högberg
Erik Brolin

IOS Press

DHM2020

Digital human modeling (DHM) is an active field of research directed towards the goal of creating detailed digital models of the human body and its functions, as well as assessment methods for evaluating human interaction with products and production systems. These have many applications in ergonomics, design and engineering, in fields as diverse as the automotive industry and medicine.

This book presents the proceedings of the 6th International Digital Human Modeling Symposium (DHM2020), held in Skövde, Sweden from 31 August to 2 September 2020. The conference was also accessible online for those unable to attend in person because of restrictions due to the Covid-19 pandemic. The symposium provides an international forum for researchers, developers and users to report their latest innovations, summarize new developments and experiences within the field, and exchange ideas, results and visions in all areas of DHM research and applications.

The book contains the 43 papers accepted for presentation at the conference, and is divided into 6 sections which broadly reflect the topics covered: anthropometry; behavior and biomechanical modeling; human motion data collection and modeling; human-product interaction modeling; industry and user perspectives; and production planning and ergonomics evaluation.

Providing a state-of-the-art overview of research and developments in digital human modeling, the book will be of interest to all those who are active in the field.

ISBN 978-1-64368-104-7 (print) ISSN 2352-751X (print)
ISBN 978-1-64368-105-4 (online) ISSN 2352-7528 (online)

IOS Press

DHM2020

Advances in Transdisciplinary Engineering

Advances in Transdisciplinary Engineering (ATDE) is a peer-reviewed book series covering the developments in the key application areas in product quality, production efficiency and overall customer satisfaction.

ATDE will focus on theoretical, experimental and case history-based research, and its application in engineering practice. The series will include proceedings and edited volumes of interest to researchers in academia, as well as professional engineers working in industry.

Editor-in-Chief
Josip Stjepandić, PROSTEP AG, Darmstadt, Germany

Co-Editor-in-Chief
Richard Curran, TU Delft, The Netherlands

Advisory Board
Cees Bil, RMIT University, Australia
Milton Borsato, Federal University of Technology – Parana, Brazil
Shuo-Yan Chou, Taiwan Tech, Taiwan, China
Fredrik Elgh, Jönköping University
Parisa Ghodous, University of Lyon, France
Kazuo Hiekata, University of Tokyo, Japan
John Mo, RMIT University, Australia
Essam Shehab, Cranfield University, UK
Mike Sobolewski, TTU, Texas, USA
Amy Trappey, NTUT, Taiwan, China
Wim J.C. Verhagen, TU Delft, The Netherlands
Wensheng Xu, Beijing Jiaotong University, China

Volume 11

Recently published in this series

Vol. 10. K. Hiekata, B. Moser, M. Inoue, J. Stjepandić and N. Wognum (Eds.), Transdisciplinary Engineering for Complex Socio-technical Systems – Proceedings of the 26th ISTE International Conference on Transdisciplinary Engineering, July 30 – August 1, 2019

Vol. 9. Y. Jin and M. Price (Eds.), Advances in Manufacturing Technology XXXIII – Proceedings of the 17th International Conference on Manufacturing Research, incorporating the 34th National Conference on Manufacturing Research, 10–12 September 2019, Queen's University, Belfast, UK

Vol. 8. P. Thorvald and K. Case (Eds.), Advances in Manufacturing Technology XXXII – Proceedings of the 16th International Conference on Manufacturing Research, incorporating the 33rd National Conference on Manufacturing Research, September 11–13, 2018, University of Skövde, Sweden

ISSN 2352-751X (print)
ISSN 2352-7528 (online)

DHM2020

Proceedings of the 6th International Digital Human Modeling Symposium, August 31 – September 2, 2020

Edited by

Lars Hanson

University of Skövde, Sweden

Dan Högberg

University of Skövde, Sweden

and

Erik Brolin

University of Skövde, Sweden

IOS Press

Amsterdam • Berlin • Washington, DC

© 2020 The authors and IOS Press.

This book is published online with Open Access and distributed under the terms of the Creative Commons Attribution Non-Commercial License 4.0 (CC BY-NC 4.0).

ISBN 978-1-64368-104-7 (print)
ISBN 978-1-64368-105-4 (online)
Library of Congress Control Number: 2020943253
doi: 10.3233/ATDE11

Publisher
IOS Press BV
Nieuwe Hemweg 6B
1013 BG Amsterdam
Netherlands
fax: +31 20 687 0019
e-mail: order@iospress.nl

For book sales in the USA and Canada:
IOS Press, Inc.
6751 Tepper Drive
Clifton, VA 20124
USA
Tel.: +1 703 830 6300
Fax: +1 703 830 2300
sales@iospress.com

LEGAL NOTICE
The publisher is not responsible for the use which might be made of the following information.

PRINTED IN THE NETHERLANDS

Preface

This book of proceedings contains papers accepted for the 6th International Digital Human Modeling Symposium (DHM2020), hosted by the University of Skövde in Sweden, and held at the ASSAR Industrial Innovation Arena in Skövde, as well as online, August 31 – September 2, 2020.

The International Digital Human Modeling Symposium provides an international forum for researchers, developers and users to report their latest innovations, summarize new developments and experiences within the field, and exchange ideas, results and visions in all areas of digital human modeling research and applications. It is a major event for researchers, academics and industrialists engaged in topics such as:

- Anthropometry and 3D human body modeling
- Human functional data
- Musculoskeletal human models
- Motion capture and reconstruction
- Posture and motion simulation
- Modeling for subjective responses
- Applications and software demonstration
- Virtual reality and DHM
- Mental/cognitive models and integrated models
- Older, disabled and other populations
- Verification and validation of DHMs
- Model standards and protocols
- Body part modeling
- Virtual humans' appearance
- Biomechanical modeling
- Human vibration modeling
- DHM in safety applications
- DHM in game applications

The International Digital Human Modeling Symposium is a result of collaborations within the worldwide DHM community, and in association with the International Ergonomics Association (IEA) Technical Committee on Digital Human Modeling and Simulation[1]. One of the objectives of the Digital Human Modeling and Simulation Technical Committee is to organize an annual DHM Symposium. Every third year the DHM Symposium is integrated with the IEA Triennial Congress. The current form of the International Digital Human Modeling Symposium builds on a series of SAE International supported digital human modeling conferences.

[1] https://iea.cc/member/digital-human-modeling-and-simulation/

The proceedings of DHM2020 consists of 43 papers subdivided into six parts, reflecting the topics addressed at the symposium.

Part 1 is entitled Anthropometry. It contains papers on the collection and processing of anthropometric data, and on the development of methods for how to use anthropometric data in DHM settings, e.g. in the design of truck interiors and protective equipment. Also included in this part are methods for handling 3D scan data, skewed data, and how to generate full body shapes with a limited number of measures.

Part 2 is entitled Behaviour and Biomechanical Modeling. It contains papers on cognitive modeling of roadside human interactions, and on physical musculoskeletal modelling of jaw motions. Modelling of hand-eye strategies and vision behaviour are covered, representing areas in the intersection of cognitive and physical modelling. Also presented are modelling technologies, including optimal control and neural networks.

Part 3 is entitled Human Motion Data Collection and Modeling. It contains papers on reach and grasp modelling, as well as posture stability and hand trajectories. This part also includes papers on how to gather motion data with 3D textiles and smart clothing, and how to store motion data in databases.

Part 4 is entitled Human-Product Interaction Modeling. It contains papers on how vehicle drivers interact with automotive interiors. Seat interaction for vehicle drivers and pilots is presented, as well as papers on models for human-seat foam interaction. Also included in this part is modelling of exoskeleton as a human support.

Part 5 is entitled Industry and User Perspectives. It contains papers on both industry, health, and medical sector perspectives. Examples are given on applications of DHM software and associated technologies. Future needs and identified gaps are discussed. Several papers focus on usability of DHM software, both on desktop and in VR. Also included in this part is gamification of DHM.

Part 6 is entitled Production Planning and Ergonomics Evaluation. It contains papers on DHM as an ergonomics evaluation tool. Gender perspectives on DHM are presented, as well as a case from the maritime sector. The development of a multi-objective approach for DHM simulation and evaluation is presented. DHM simulations are compared with motion capture data. Also included in this part are DHM tools with VR functionality, combined with motion capture and AI technologies.

We would like to thank:

- all authors of papers,
- the members of the Scientific Committee who assisted with the blind peer-review of the papers submitted and presented at the symposium,
- the key-note speakers Cecilia Berlin, Johan Iraeus, and Kalle Sandzén for sharing their experiences,
- our sponsors ESI, Volvo Group, IPS, and University of Skövde for supporting the event,
- IOS Press and editor-in-chief Josip Stjepandić for accepting to publish the DHM2020 proceedings in the book series Advances in Transdisciplinary Engineering (ATDE),
- everyone who has contributed to the proceedings of DHM2020, and to the realization of the symposium.

In order to allow flexibility and maintain health consciousness due to the Covid-19 pandemic, we decided to organize DHM2020 so that it would be possible to attend the symposium either on-site in Skövde, or online. We would like to thank all participants

for their understanding and their efforts in jointly making DHM2020 a successful symposium, regardless if you are presenting and discussing DHM topics from home or located at ASSAR in Skövde. We are glad that you attended and contributed to DHM2020.

Organizing committee DHM2020
Lars Hanson – General Chair
Dan Högberg – Program Chair
Erik Brolin – Local Chair
Pernilla Klingspor – Event Coordinator
Amila Domi – Finance Officer
University of Skövde, Sweden

This page intentionally left blank

Scientific Committee of DHM2020

Andre Rueckert – ESI Software Germany GmbH, Germany
Bruce Bradtmiller – Anthrotech, USA
Caroline Borot – ESI Group, France
Dan Lämkull – Volvo Cars, Sweden
Erik Billing – University of Skövde, Sweden
Giuseppe Andreoni – POLIMI, Italy
Gregor Harih – University of Maribor, Slovenia
Gunther Paul – James Cook University, Australia
Hans-Joachim Wirsching – Human Solutions GmbH, Germany
James Yang – Texas Tech University, USA
Joachim Linn – Fraunhofer ITWM, Germany
John Rasmussen – Aalborg University, Denmark
Jonas Fredriksson – ESI Northern Europé, Sweden
Josip Stjepandic – PROSTEP AG, Germany
Julie Charland – 3DS – Dassault Systemes, Canada
Lars Fritzsche – imk automotive, Germany
Matt Reed – University of Michigan Transportation Research Institute, USA
Matthew Parkinson – Penn State – The Pennsylvania State University, USA
Maurice Lamb – University of Skövde, Sweden
Mitsunori Tada – AIST – National Institute of Advanced Industrial Science and Technology, Japan
Neil Mansfield – Nottingham Trent University, UK
Pierre-Olivier Lemieux – 3DS – Dassault Systemes, Canada
Riender Happee – TU Delft, Netherlands
Robert Bohlin – Fraunhofer-Chalmers Centre, Sweden
Rush Green – Boeing, USA
Russel Marshall – Loughborough University, UK
Sascha Wischniewski – BAuA – Institute for Occupational Safety and Health, Germany
Serge Van Sint Jan – University of Brussels, Belgium
Sofia Scataglini – University of Antwerp, Belgium
Sudhakar Rajulu – NASA Johnson Space Center, USA
Steve Summerskill – Loughborough University, UK
Thomas Alexander – BAuA – Institute for Occupational Safety and Health, Germany
Xuguang Wang – IFSTTAR – Institut Français des Sciences et Technologies des Transports, de l'Aménagement et des Réseaux, France

International Digital Human Modeling Symposium Series

Hosts of International Digital Human Modeling Symposiums until today:

2011 1st International Digital Human Modeling Symposium (DHM2011)
Université de Lyon, and IFSTTAR
Lyon, France, June 14–16, 2011

2012 2nd International Digital Human Modeling Symposium (DHM2012)
The University of Michigan Transportation Research Institute (UMTRI), and Pennsylvania State University
Ann Arbor, USA, June 11–13, 2013

2014 3rd International Digital Human Modeling Symposium (DHM2014)
Digital Human Research Center at the National Institute of Advanced Industrial Science and Technology (AIST)
Tokyo, Japan, May 20–22, 2014

2016 4th International Digital Human Modeling Symposium (DHM2016)
École de Technologie Supérieure (ÉTS)
Montréal, Québec, Canada, June 15–17, 2016

2017 5th International Digital Human Modeling Symposium (DHM2017)
Fraunhofer-Institute for Communication, Information Processing and Ergonomics (FKIE), and
Federal Institute for Occupational Safety and Health (BAuA)
Bonn, Germany, June 26–28, 2017

2020 6th International Digital Human Modeling Symposium (DHM2020)
University of Skövde
Skövde, Sweden, and online, Aug 31–Sep 2, 2020

Sponsors of DHM2020

ESI Group

Volvo Group

Industrial Path Solutions (IPS)

University of Skövde

This page intentionally left blank

Contents

Preface v
Lars Hanson, Dan Högberg, Erik Brolin, Pernilla Klingspor and Amila Domi

Committees, Organizers and Sponsors ix

Part 1. Anthropometry

Digital Modeling of Law Enforcement Officers: Progress and Challenges 3
Bruce Bradtmiller, Hongwei Hsiao, Mathew Hause and Belva Rockwell

Anthropometric Measure Extraction and Offset Calculation for 3D Body Scan Data, Obtained from an Epidemiological Health Study 11
Dominik Bonin, Sascha Wischniewski, Markus Peters and Dörte Radke

Skewed Boundary Confidence Ellipses for Anthropometric Data 18
Erik Brolin, Dan Högberg and Lars Hanson

Introducing Multivariate Anthropometry in Digital Human Modelling 28
Paulo Eduardo Fragoso

Creating a Personalized Full 3D Body Shape from a Limited Number of Predictors 40
Xuguang Wang, Georges Beurier, Yoann Lafon and Junfeng Peng

Part 2. Behaviour and Biomechanical Modeling

Learning Individual Driver's Mental Models Using POMDPs and BToM 51
Amena Darwish and H. Joe Steinhauer

Automatic Selection of Viewpoint for Digital Human Modelling 61
Erik Billing, Elpida Bampouni and Maurice Lamb

Variational Interpolating Neural Networks for Locomotion Synthesis 71
Janis Sprenger, Han Du, Noshaba Cheema, Klaus Fischer and Philipp Slusallek

Defining Kinematic Chains for Musculoskeletal Optimal Control Simulations via Automatic Differentiation 82
Johann Penner and Sigrid Leyendecker

Grasp Synthesis for Digital Hands with Limited Range of Motion in Their Thumb Using a Grasp Database 91
Reiko Takahashi, Natsuki Miyata and Yusuke Maeda

The Use of Digital Human Modelling for the Definition and Contextualisation of a Direct Vision Standard for Trucks 99
Russell Marshall, Steve Summerskill, Abby Paterson and Anthony Eland

Musculoskeletal Modeling with Jaw Motion Data from a TMD Patient 108
Ryuji Shigemitsu, Keiichi Sasaki and John Rasmussen

Digital Human Motion Planning of Operation Sequences Using Optimal Control of Hybrid Systems 115
Staffan Björkenstam, Peter Mårdberg, Michael Roller and Johan S. Carlson

The Definition of a Common Eye Point for the Virtual Assessment of Truck Direct Vision Performance 121
Steve Summerskill, Russell Marshall, Abby Paterson and Anthony Eland

Multimodality on the Road: Towards Evidence-Based Cognitive Modelling of Everyday Roadside Human Interactions 131
Vasiliki Kondyli and Mehul Bhatt

Part 3. Human Motion Data Collection and Modeling

Precision of Human Movement in the Virtual Reach Envelope – Measurement of Static and Dynamic Precision Depending on Different Movement Speeds 145
André Kaiser and Angelika C. Bullinger

Experimental Evaluation of Postural Stability Using Stepping Strategies During Industrial Tasks 156
Fabrice Latour, Ali Zeighami, Nicola Hagemeister, Julie Charland and Rachid Aissaoui

How to Combine 3D Textile Modeling with Latest FE Human Body Models 166
Hartmut Klein, Marcin Jenerowicz, Niclas Trube and Matthias Boljen

Modelling Take-Over Hand Trajectories Using Linear Mixed Effects Models 178
Martin Fleischer, Arno Hetzenecker and Klaus Bengler

A Pipeline for Creating In-Vehicle Posture Database for Developing Driver Posture Monitoring Systems 187
Mingming Zhao, Georges Beurier, Hongyan Wang and Xuguang Wang

Smart Clothing for Monitoring Gait 197
Sofia Scataglini, Guillaume Abran, Eddy Roosens, Damien Van Tiggelen, Robby Haelterman and Stijn Verwulgen

Optimal Control of Grasping Problem Using Postural Synergies 206
Uday Phutane, Michael Roller, Anja Boebel and Sigrid Leyendecker

Part 4. Human-Product Interaction Modeling

Modelling Interaction Forces at a Curved Physical Human-Exoskeleton Interface 217
Divyaksh Subhash Chander and Maria Pia Cavatorta

Calibration Approach for Muscle Activated Human Models in Pre-Crash Maneuvers with a Driver-in-the-Loop Simulator 227
Fabian Kempter, Florian Bechler and Jörg Fehr

Modelling of Multilayered Foams for Universal Seat Design 237
Gunther Paul, Young Jun Lee and Peter Slattery

On the Development of an Upholstery Database for Simulating the Human-Seat Interaction in Automotive Interiors 249
Hans-Joachim Wirsching and Florian Wagner

Assessment of Aircraft Pilot Seat Performances with Digital Human Models and Virtual Prototypes 259
Jerome Regnault, Caroline Borot and Cecile Cabane

A Digital Human Model for the Simulation of Dynamic Driving Maneuvers 269
Michael Roller, Vanessa Dörlich, Joachim Linn, Staffan Björkenstam and Peter Mårdberg

Part 5. Industry and User Perspectives

Human-Centric Assembly Cell & Line Validation 279
André Rueckert, Marc Niemann and Eric Kam

Employing UX Processes for More Focused Development in Research Projects 288
Ari Kolbeinsson, Jessica Lindblom and Peter Thorvald

The Need for Faster and More Consistent Digital Human Modeling Software Tools 299
Dan Lämkull and Maciej Zdrodowski

Narrowing the Gap of Cognitive and Physical Ergonomics in DHM Through Embodied Tool Use 311
Jessica Lindblom, Ari Kolbeinsson and Peter Thorvald

Gamification of DHM Software 323
Juan Luis Jiménez Sánchez and Adam Palmquist

Digital Human Modeling Technology in Virtual Reality – Studying Aspects of Users' Experiences 330
Julia Rosén, Jessica Lindblom, Maurice Lamb and Erik Billing

Integration of Simulation and Manufacturing Engineering Software – Allowing Work Place Optimization Based on Time and Ergonomic Parameters 342
Oskar Ljung, Aitor Iriondo Pascual, Dan Högberg, Niclas Delfs, Tobias Forsberg, Pierre Johansson, Johanna Dahlvik, Juan Luis Jiménez Sánchez and Lars Hanson

Digital Human Models of Lower Limb Amputees for Socket Modelling and Simulations: An Overview of Current Technologies, Limitations and Future Possibilities 348
Vasja Plesec and Gregor Harih

Part 6. Production Planning and Ergonomics Evaluation

Implementation of Ergonomics Evaluation Methods in a Multi-Objective Optimization Framework 361
Aitor Iriondo Pascual, Dan Högberg, Anna Syberfeldt, Erik Brolin, Francisco García Rivera, Estela Pérez Luque and Lars Hanson

Data-Based Parametric Biomechanical Models for Cyclic Motions 372
John Rasmussen, Morten Enemark Lund and Rasmus Plenge Waagepetersen

Evaluation of Physical Workload Using Simulation Versus Motion Capturing Data for Biomechanical Models 380
Markus Peters and Sascha Wischniewski

The Use and Usage of Virtual Reality Technologies in Planning and Implementing New Workstations 388
René Reinhard, Peter Mårdberg, Francisco García Rivera, Tobias Forsberg, Anton Berce, Mingji Fang and Dan Högberg

Digital Human Modeling as a Risk Assessment Tool for Maritime Workers 398
Sander Zelck, Stijn Verwulgen, Lenie Denteneer and Sofia Scataglini

Closing the Gender Gap in DHM 408
Sofia Scataglini and Estela Perez Luque

Aiding Observational Ergonomic Evaluation Methods Using MOCAP Systems Supported by AI-Based Posture Recognition 419
Víctor Igelmo, Anna Syberfeldt, Dan Högberg, Francisco García Rivera and Estela Pérez Luque

Subject Index 431

Author Index 433

Part 1

Anthropometry

This page intentionally left blank

L. Hanson et al. (Eds.)
© 2020 The authors and IOS Press.
This article is published online with Open Access by IOS Press and distributed under the terms of the Creative Commons Attribution Non-Commercial License 4.0 (CC BY-NC 4.0).
doi:10.3233/ATDE200003

Digital Modeling of Law Enforcement Officers: Progress and Challenges

Bruce BRADTMILLER [a,1], Hongwei HSIAO [b], Mathew HAUSE [b] and Belva ROCKWELL [a]
[a] *Anthrotech, Yellow Springs OH, USA*
[b] *National Institute for Occupational Safety and Health, Division of Safety Research, Morgantown, WV, USA*

Abstract. Over several decades, police officer body dimensions have increased as have the body dimensions of many Americans. But the external dimensions of a law enforcement officer completely outfitted in all of his or her gear has increased dramatically, with the near-constant use of body armor and the addition of body cameras, radios and a host of other work-related items. At the same time, the available space in his or her police cruiser has decreased, with the addition of dash cameras, radios, and computers and the modernization of the bucket seat design. The result is a disaccommodation problem that is increasing with each addition of new equipment for either the officer or the vehicle.

Digital human modeling is an ideal tool to help solve this accommodation problem, by creating realistic models of officers wearing their gear. To create a database for use in that modeling, we recruited approximately 1000 officers from 12 locations around the US and obtained whole body, head, hand, and foot scans from each. In addition, we measured them for a series of traditional anthropometric dimensions both semi-nude and fully equipped in their uniform, body armor and gear. The differences obtained between the equipped and semi-nude officers will allow the verification of future models. Further, we collected data on the vehicles they use, any difficulties with their current vehicles, and the ancillary equipment worn on the body. This paper presents partial results of that study.

The significant challenge going forward will be to create models that take into account the wide diversity in how officers wear their equipment on the body. For example, many officers carry a weapon on the duty belt; some carry it in a thigh holster. Some officers carry a radio on the shirt; others carry it on the duty belt, sometimes in front, and sometimes on the side. We conclude with a suggestion that modelers use data from this survey to accommodate the variability added by the equipment.

Keywords. Anthropometry, Law Enforcement Officer, Vehicle Accommodation

1. Introduction

Anthropometric disaccommodation can affect the ability of any working individual to function safely while carrying out his or her task. For law enforcement officers (LEOs), necessarily encumbered by a considerable amount of bulky equipment, the problem can become critical. And, while anthropometric data are not themselves a solution to

[1] Corresponding Author, Email: bruce@anthrotech.net.

problems of design and accommodation, the lack of appropriate data is a major stumbling block to improving the design of equipment and LEO workspaces.

In 1975, the US National Bureau of Standards funded a study of the nation's male law enforcement officers [1]. Some 23 dimensions were measured on a large sample (approximately 3000) and they were collected in 17 regions throughout the country. For many years, those were the only data available on which to design police vehicles and protective equipment. It is not known whether, or how often, those data were actually used in design. More recently, designers and engineers have become much more accustomed using anthropometric data in design. But by the time designers began to routinely use anthropometric data, the available data for the nation's police force was woefully out of date. The US police force in 1975 bears little resemblance to today's diverse force that contains female as well as male officers.

In 2014, recognizing the workplace mis-match between officers' physical characteristics and their mobile workplaces, the National Institute for Occupational Safety and Health (NIOSH) funded a pilot study to determine the magnitude of the differences between the force of the 1970s and the then-current force 45 years later. That study [2] identified a number of physical changes, but also started to document the tremendous variability in the equipment that officers routinely wore while on duty. The results were striking enough that NIOSH funded a larger nationwide study. Preliminary work began in 2017 and data collection occurred in 2018 and 2019. The complete documentation of the recent study is still underway, and the results have not been reviewed. This paper, addressed to the digital human modeling community, focuses on the aspects of the study that may have the greatest immediate impact for those modeling officers in their vehicles.

2. Methods

A nationwide sampling plan was developed to capture the demographic variability in today's force. Using US Census data from the most recent census, goals were established for racial/ethnic groups, and an appropriate age distribution for each of four regions in the US. The overall goal was 1000 officers. Female officers account for only 17.6% of the US force, so a proportional sampling by sex would not have provided statistical power for decision-making. The female sample was therefore increased to 300 of the 1000 targeted. Male and female data will be reported separately in the final report so the over-representation of females in the sample will not adversely influence the final summary statistics. The sample was collected at 12 police facilities spread over the 4 geographic regions.

A dimension list was created to allow comparison with the earlier Martin et al. study [1], but was also based on experience at NIOSH and Anthrotech in using anthropometric dimensions for vehicle design. In a departure from the Martin study, officers were also measured in their full uniform, including any gear and ancillary equipment that they typically wear while on patrol duty in their car. As police departments in the United States are locally controlled, they vary considerably in what specific equipment constitutes "gear" that officers may wear. We specifically collected information on what items were worn on the duty belt (see below), but additional items of gear that could affect the overall amount of space needed include body armor, body camera, leg holster, leg pads and helmets.

Many of the dimensions are seated dimensions. These were measured in a standard anthropometric sitting posture to allow comparison with earlier datasets, and to minimize the effect of posture on the anthropometric dimensions. At the same time, we acknowledge that anthropometric sitting is not a posture used while driving a vehicle. There is a considerable body of research on automotive seating generally (e.g. [3], [4]) and on driver comfort in police vehicles more specifically [5], [6], [7]. Those issues are not addressed in this paper.

Table 1 shows the dimension list for the lightly clothed (semi-nude measurements as well as the measurements taken over full gear. Dimensions marked with an asterisk are those taken both with gear and without gear.

Table 1. Dimension List.

	Semi-nude		Over Gear
*	Bideltoid Breadth, Sitting		Abdominal Extension Depth, Gear, Sitting
	Buttock Height		Acromion-Troch Surface Length, Gear, Sitting
	Buttock-Knee Length	*	Bideltoid Breadth, Gear, Sitting
	Buttock-Popliteal Length		Bi-trochanter Surface Length, Gear, Sitting
*	Chest Breadth		Boot Breadth
	Chest Circumference		Boot Length
*	Chest Depth		Buttock-Shoetip Length, Gear, Sitting
	Crotch Height	*	Chest Depth, Gear
	Elbow Rest Height	*	Chest Width, Gear
	Eye Height, Sitting	*	Hip Breadth, Gear, Sitting
	Foot Breadth, Horizontal		Shoulder-Grip Length, Gear, Sitting
	Foot Length	*	Stature, footwear
	Front Waist Length, Sitting		Thigh Clearance, Gear, Sitting
	Grip Strength, Sitting (kg)	*	Waist Breadth, Gear, Sitting
	Hand Breadth	*	Weight, Gear, kg
	Hand Length		
	Head Arc Length		
	Head Breadth		
	Head Circumference		
	Head Length		
*	Hip Breadth, Sitting		
	Hip Circumference		
	Knee Height, Sitting		
	Nuchale Height, Sitting		
	Popliteal Height		
	Sitting Height		
*	Stature		
	Thigh Circumference		
	Thumbtip Reach		
*	Waist Breadth, Sitting		
	Waist Breadth Height, Sitting		
	Waist Circumference		
	Waist Height		
*	Weight, kg		

In addition to the traditional measurements, 3D scans were taken of the officers while dressed in Spandex scanwear. Scans were taken of the whole body, the head, the foot, and the hand. There is an incomplete consensus in the scanning community about the most useful position for whole body scans (e.g. [8]). This is in part because different scanning technologies impose differing requirements in order to capture data from the axillary and crotch regions. In this case, we used the body position protocol described in the ANSUR and CAESAR surveys [9], [10]. The data from the scans will not be included

in the survey documentation, but the scans themselves will form a valuable resource for future researchers as well as those designing officers' protective equipment and vehicles.

The study was reviewed and approved by the NIOSH Institutional Review Board, as well as the Office of Management and Budget. A collaborative team of Anthrotech and NIOSH researchers visited each of the sites to collect the data.

3. Results

The team met and exceeded the goal for male officers, and while the female goal was not met, it does exceed the actual representation of female officers in police forces across the country. Table 2 shows the distribution of race/ethnic group and age group by gender.

Table 2. Race/Ethnic Group, Age Group by Gender.

Gender	Age Group	Race/Ethnicity			Total
		White	African-American	Hispanic/Other	
Male	18 - 34	182	30	54	266
	35 - 44	186	30	36	252
	≥ 45	175	34	29	238
	Total	543	94	119	756
Female	18 – 34	51	12	22	85
	35 – 44	62	9	12	83
	≥ 45	29	10	11	50
	Total	142	31	45	218
Total	18 – 34	233	42	76	351
	35 – 44	248	39	48	335
	≥ 45	204	44	40	288
	Total	685	125	164	974

The remaining tables show data that are weighted to account for small mis-matches between the final sample demographics and the 2019 estimates from the US Bureau of Labor Statistics for police race and ethnicity [11].

The full results of the survey will be released when the report is complete, as noted above. However, a preliminary look at the comparably measured dimensions between the current study and the Martin study of 1975 [1] show significant differences in a number of dimensions. Specifically, all the dimensions associated with weight gain, such as breadths, depths, and circumferences, show increases (Table 3). The dimensions that did not show an increase were Thumbtip Reach, Stature, and hand. These differences generally match those seen when comparing the Army's ANSUR survey with ANSUR 2, which took place a quarter-century later [12], [10]. Welch's t is used for significance testing rather than the common Student's t since the variances could not be assumed to be similar between the two studies.

Table 3. Means Test Comparing NIOSH 2020 and Martin 1975 [1]: Males (weight in kg, all other values in mm).

	NIOSH 2020			Martin 1975			Welch's test		
	N	Mean	Std. Deviation	N	Mean	Std. Deviation	Mean Diff.	t	
Bideltoid Breadth, Sit	754	514.1	32.56	2985	494.7	29.42	19.34	14.85	*
Buttock-Knee Length	754	630.9	34.29	2988	615.0	27.11	15.85	11.80	*
Chest Breadth	754	372.5	35.54	2984	346.4	26.35	26.03	18.85	*
Chest Circumference	754	1111.8	100.96	2990	1021.6	78.99	90.20	22.84	*
Front Waist Length, Sit	754	409.4	30.56	2983	413.3	26.91	-3.85	-3.17	*
Hand Breadth	754	90.0	4.65	2987	89.9	4.24	0.08	0.43	
Hand Length	754	193.5	9.93	2989	193.5	9.12	0.04	0.10	
Head Breadth	754	154.9	5.59	2993	154.7	5.67	0.22	0.98	
Head Circumference	754	579.4	15.69	2985	575.0	15.77	4.45	6.95	*
Head Length	754	201.1	6.92	2992	198.0	6.97	3.11	11.02	*
Knee Height, Sit	754	566.3	29.51	2984	559.2	25.26	7.15	6.11	*
Sitting Height	754	929.5	35.36	2993	921.8	34.45	7.68	5.36	*
Stature	754	1776.0	71.37	2989	1781.2	57.84	-5.11	-1.82	
Thumbtip Reach	754	829.7	48.35	2987	829.7	42	-0.01	-0.01	
Waist Circumference,O	754	1026.3	129.11	2988	906.1	94.57	120.18	23.99	*
Weight, kg	754	95.35	17.295	2991	83.31	11.950	12.04	18.06	*

*0.00313 Bonferroni's correction for multiple comparisons, at .05

The remainder of the results have to do with the amount of variability added by the various pieces of equipment officers carry for their own safety as well as for carrying out official duties. An example is seen in Figure 1. To identify the additional space occupied by the equipment, we calculated the differences (delta) between the measurements with gear and the nude measurements. For example, Bideltoid Breadth Delta = Bideltoid Breadth Gear – Bideltoid Breadth. Tables 4 and 5 show, for males and females respectively, both the mean value of the added equipment, as well as selected percentiles. The differences are largest in Hip Breadth, Sitting and Waist Breadth, Sitting. In both cases, the articles worn on the belt have a significant impact on the overall value. Notice also that the range of the deltas – from the 5th to the 95th percentiles of each dimension – is quite large.

Figure 1. Items worn on the torso and duty belt.

Table 4. Differences between Dimensions Measured with and without Gear: Males (weight in kg, all other values in mm).

		Bideltoid Breadth, Sitting Delta	Chest Breadth Delta	Chest Depth Delta	Hip Breadth, Sitting Delta	Stature Delta	Waist Breadth, Sitting Delta	Weight Delta
N		756	756	756	756	756	756	756
Mean		28.9	12.4	44.6	105.2	28.2	90.6	10.9
Std. Deviation		15.69	17.21	20.59	28.11	7.57	52.01	2.55
Percentiles	5	7	-16	16	53	16	12	6
	25	18	1	31	90	23	49	10
	50	28	13	42	108	28	88	11
	75	38	23	56	122	33	134	12
	95	58	40	84	146	41	172	15

Table 5. Differences between Dimensions Measured with and without Gear: Females (weight in kg, all other values in mm).

		Bideltoid Breadth, Sitting Delta	Chest Breadth Delta	Chest Depth Delta	Hip Breadth, Sitting Delta	Stature Delta	Waist Breadth, Sitting Delta	Weight Delta
N		218	218	218	218	217	217	218
Mean		31.7	24.5	40.6	70.2	29.5	120.4	9.2
Std. Deviation		14.79	17.27	21.46	32.08	7.92	51.30	2.09
Percentiles	5	7	-2	12	14	16	28	5
	25	24	13	27	53	25	86	8
	50	29	26	39	72	30	132	9
	75	38	36	55	90	35	159	11
	95	61	51	77	112	43	189	12

An interesting phenomenon occurs for Chest Breadth, where at the small end of the distribution the values are negative. In a handful of cases, the body armor compressed the chest enough that the value with gear was actually smaller than the nude value. The body armor was functioning as a corset for those individuals. We hypothesized that the addition of gear would also increase the variance of the measurements. Table 6 shows that the hypothesis was borne out in some cases, in particular for Bideltoid Breadth, Hip Breadth and Waist Breadth, but in the case of Chest Breadth, the addition of the gear seemed to reduce variability, probably as a result of the corset effect. For the remaining dimensions, the addition of gear did not appear to have much effect on the resulting variance.

Table 6. Standard Deviation Compared between Semi-Nude and Gear Dimensions: Males and Females Combined (weight in kg; all other values in mm).

		Semi-Nude	Gear
	N	Std. Deviation	Std. Deviation
Bideltoid Breadth, Sitting	974	40.83	43.95
Chest Breadth	974	40.52	34.71
Chest Depth	974	31.83	32.11
Hip Breadth, Sitting	974	35.26	37.53
Stature	973	87.00	87.18
Waist Breadth, Sitting	974	42.76	49.73
Weight, kg	974	18.67	19.44

4. Discussion and Conclusion

Previous efforts to model the police officer body envelope have been hampered by the lack of current anthropometric data on active police officers, and by a complete lack of data on the total amount of space occupied by encumbered officers. Since officers carry a wide variety of equipment on their body, these items can have significant impacts on the overall amount of occupied claim. The greatest increases in dimension were found at the waist and the hip. Both of these areas are affected by the items carried on the officer's duty belt. As a part of the questionnaire that accompanied the anthropometric survey, officers were asked to check off from a list of a dozen items that might be worn on the duty belt. Table 7 shows the list of items, ranked in order of frequency (males). The frequencies do not sum to 100% because officers carry many more than one item on their belt. A secondary question was whether items on the duty belt caused discomfort during a shift. Fully 74% of male officers and 85% of female officers reported that they did experience discomfort from belt-worn items. We did not collect data with respect to the specific location of each item on the belt. However, with the number of items carried, it is likely that some duty belt items would interfere with easy placement and fastening of the seat belt. Further, it is also likely that some combination of duty belt items would affect driving posture for at least some officers.

Table 7. Items Carried on the Duty Belt.

	Male		Female	
Handgun	677	92%	190	90%
Handcuffs	674	92%	195	92%
Ammunition pouch	645	88%	183	87%
Radio	639	87%	191	91%
Pepper Spray	588	80%	186	88%
Flashlight	581	79%	173	82%
Baton	447	61%	137	65%
Taser	419	57%	126	60%
Key Holder	375	51%	105	50%
Disposable Gloves	308	42%	93	44%
Knife	238	32%	66	31%
First Aid Kit	104	14%	19	9%

Also, of note is that males and females carry the items on their duty belt in roughly the same proportion. The items carried on the belt are generally not sized items – a taser, for example, is a certain size, no matter who carries it. For officers with smaller waists, and certainly for female officers with smaller waists, the *proportion* of the waist encumbered with equipment must therefore be comparatively larger than when the same equipment is carried on someone with a larger waist. To the extent that items carried on the belt are a cause of discomfort or restrict movement, the effect may be greater on persons with smaller waists and hips. From the perspective of vehicle design, however, the worst case is clearly the individual with wider hips, but who also carries multiple items on the sides of the duty belt.

Creators of digital human models for police vehicle design and protective equipment design may wish to use the updated anthropometric data from this survey when making models for the future. In particular, modelers may wish to take into account the considerable variability added by equipment worn at the waist and hip when configuring worst-case design envelopes. It is not enough to simply model the occupied space of, for example, the 95th percentile of hip breadth with gear. A smaller-hipped person with more

gear, and a larger-hipped person with less gear might have the same overall width. But the models representing each should be different, as the various modeled actions (ingress, egress, behavior during a collision, for example) would be very different from each other. The work here is a very first step in allowing modelers to faithfully represent the equipped bodies of law enforcement personnel.

Disclaimer

The findings and conclusions in this report are those of the authors and do not necessarily represent the official position of the National Institute for Occupational Safety and Health (NIOSH), Centers for Disease Control and Prevention (CDC). Mention of any company or product does not constitute endorsement by NIOSH or CDC.

References

[1] Martin JI, Sabeh R, Driver LL, Lowe TD, Hintze RW, Peters PAC. Anthropometry of Law Enforcement Officers. Naval Electronics Laboratory Center, San Diego, CA 92152, Technical Document 442, 1975.
[2] Hsiao H, Whisler R, Bradtmiller B. Needs and Procedures for a National Anthropometry Study of Law Enforcement Officers. In Press.
[3] Reed MP, Manary MA, Schneider LW. Methods for Measuring and Representing Automobile Occupant Posture. SAE TECHNICAL PAPER SERIES 1999-01-0959. SAE International, 400 Commonwealth Drive, Warrennale, PA, 1999.
[4] Reed MP, Manary MA, Flannagan CAC, Schneider LW. A Statistical Method for Predicting Automobile Driving Posture. Human Factors, 2002, 44, 557-568.
[5] Donnelly CJ, Callaghan JP, Durkin JL. The Effect of an Active Lumbar System on the Seating Comfort of Officers in Police Fleet Vehicles. International Journal of Occupational Safety and Ergonomics, 2009, 15, 295-307, DOI: 10.1080/10803548.2009.11076809
[6] Gruevski KM, McKinnon CD, Dickerson CR, Callaghan JP. The Impact of Mobile Data Terminal Use on Posture and Low-Back Discomfort When Combined With Simulated Prolonged Driving in Police Cruisers. International Journal of Occupational Safety and Ergonomics, 2013, 19, 415-422, DOI: 10.1080/10803548.2013.11076998
[7] Gruevski KM, Holmes MWR, Gooyers CE, Dickerson CR, Callaghan JP. Lumbar postures, seat interface pressures and discomfort responses to a novel thoracic support for police officers during prolonged simulated driving exposures. Applied Ergonomics, 2016, 52, 160-168.
[8] Schwarz-Müller F, Marshall R, Summerskill S. Development of a positioning aid to reduce postural variability and errors in 3D whole body scan measurements. Applied Ergonomics, 2018, 68, 90-100.
[9] Blackwell S, Robinette KM, Boehmer M, Fleming S, Kelly S, Brill T, Hoeferlin D, Burnsides D, Daanen H. Civilian American And European Surface Anthropometry Resource (CAESAR), Final Report, Volume II: Descriptions United States Air Force Research Laboratory, Wright-Patterson Air Force Base, OH. AFRL-HE-WP-TR-2002-0173, 2002.
[10] Gordon CC, Blackwell CL, Bradtmiller B, Parham JL, Barrientos P, Paquette SP, Corner BD, Carson JM, Venezia JC, Rockwell BM, Mucher M, Kristensen S. 2010-2012 Anthropometric Survey of the U.S. Army Personnel: Methods and Summary Statistics. Natick/TR-15/007, U.S. Army Natick Soldier Research, Development and Engineering Center, Natick, MA, 2014.
[11] Bureau of Labor Statistics. Household Data, Annual Averages, 11. Employed persons by detailed occupation, sex, race, and Hispanic or Latino ethnicity. Estimate for 2019. Downloaded May 13, 2020. https://www.bls.gov/cps/cpsaat11.pdf
[12] Gordon CC, Bradtmiller B, Churchill T, Clauser CE, McConville JT, Tebbetts I, Walker RA. 1988 Anthropometric Survey of U.S. Army Personnel: Methods and Summary Statistics. Technical Report Natick/TR-89-044. U.S. Army Natick Research, Development and Engineering Center, Natick, MA, 1989.

DHM2020
L. Hanson et al. (Eds.)

© 2020 The authors and IOS Press.
This article is published online with Open Access by IOS Press and distributed under the terms of the Creative Commons Attribution Non-Commercial License 4.0 (CC BY-NC 4.0).
doi:10.3233/ATDE200004

Anthropometric Measure Extraction and Offset Calculation for 3D Body Scan Data, Obtained from an Epidemiological Health Study

Dominik BONIN[a,1], Sascha WISCHNIEWSKI[a], Markus PETERS[a] and Dörte RADKE[b]
[a] *Federal Institute for Occupational Safety and Health (BAuA), 44149 Dortmund, Germany*
[b] *Institute for Community Medicine - SHIP/KEF, University Medicine Greifswald, 17489 Greifswald, Germany*

Abstract. Digital Human Modeling Systems (DHM´s) benefit from detailed up to date anthropometric data. Whereas the clothing industry focuses on anthropometric measures according to ISO-18825-2, ergonomic- and safety- related measures are defined in ISO 7250-1. For the current research project, body scan data was collected as part of an epidemiological study (Study of Health in Pomerania, SHIP). ISO 20685-1 recommends a validation study for the comparison of manual vs. 3D body scan data from at least 40 persons, if the data should be considered in anthropometric databases. The current study evaluated data of 44 participants. The scans and the manual measurements for each participant were taken successively at the same day. The definition of anatomical landmarks differed for some parameters between the ISO 7250-1 standard and the standard operating procedures (SOP´s) of the SHIP study. As it was not possible to change the methods of the SHIP study, the authors performed a relative offset calculation. With few exceptions, the validation measures exceeded the maximum error allowances from ISO 20685-1:2018. The paper discusses possible root causes of the evaluated differences.

Keywords. Manual Anthropometry, 3D Body Scanning, Data Comparison

1. Introduction

Digital Human Modeling Systems offer the possibility to consider individual, or population based anthropometric data for a human centered product and work system design. To be reliable for a specific population, and to account for multivariate coherences, the anthropometric database needs to be exceptionally detailed. For the German population, percentile based anthropometric data exists, for example within the standards ISO/TR 7250-2 [1] and DIN 33402-2:2005-12 [2]. Other anthropometric databases, with higher level of detail, or with access to raw measures for the German population, are not easy to access as they were collected in a proprietary, commercial setting and are not publicly free available. The manual collection of anthropometric data is time consuming and expensive, therefore the use of 3D body scan devices increased,

[1] Corresponding Author, Email: bonin.dominik@baua.bund.de.

as the scanning procedure is capable of saving time and offering numerous opportunities for further applications. Especially in the clothing industry 3D body scan data is commonly used, even own standards for the vocabulary and terminology used for attributes of the virtual human body exist, e.g. ISO 18825-2:2016 [3]. For ergonomic and safety related applications, the relevant standard is ISO 7250-1:2017 [4]. As there are several differences between classic anthropometry and scan derived anthropometry, ISO 20685-1:2018 [5] provides a standard for internationally comparable anthropometric databases and an evaluation protocol for body dimensions extracted from 3D body scans.

In 2013, the authors got the possibility to establish a cooperation for the collection of 3D body scans within an epidemiological study. The already existing infrastructure offered the possibility, to extract anthropometric measures according to ISO 7250-1:2017, with only little changes in the study protocol. The method, standard operating procedures and the certification process for the examiners and the readers who performed the post processing of the data, have already been published [6]. The main focus of the present paper is to show the results from a validation study according to ISO 20685-1, for the comparison of ISO 7250-1:2017 measures derived from 3D body scan data with manual measures taken with anthropometer, beam caliper and measuring tape.

2. Method

The study was performed as part of a joint project between the Federal Institute for Occupational Safety and Health, Dortmund, Germany (BAuA) and the Institute for Community Medicine - SHIP/KEF, University Medicine Greifswald, Germany. Within the epidemiological Study of Health in Pomerania [7], 4.107 3D body scans were collected within the study waves SHIP-3 (2014 - 2016) and SHIP-Trend-1 (2016 - 2019). The scanning device used was a Vitronic Vitus Smart XXL bodyscanner (Human Solutions, Kaiserslautern, Germany), which fulfills the requirements for anthropometric whole body scanning according to ISO 20685-2:2015 [8, 9]. The measures according to ISO 7250-1 were extracted in a post processing, where human readers manually identified 44 anatomical landmarks on the 3D images of two scan positions, sitting and standing, respectively.

2.1. Validation Study

One prerequisite for the evaluation of anthropometric data derived from body scans is a validation study, which compares the extracted digital measures with manual measure extraction. ISO 20685-1:2018 recommends a minimum of 40 participants, to ensure a 95 % confidence. The present validation study was performed with 44 participants (n = 25 female and n = 19 male). The participants were regular participants of the SHIP-Trend-1 study and volunteered to participate in the extra manual measuring procedure. The participants were provided with an extra expense allowance of 10 € per hour. To avoid examiner or reader effects, all measurements, digital as well as manual, were carried out by one single examiner. The examiner was trained and certified for both methods. The manual measurements were performed at the same day, immediately after the body scan. The measures were calculated using the statistical software tool R [10]. Mean bias and standard deviation were calculated for each measure, combined for female

and male. The corresponding 95% confidence interval was calculated using the method according to ISO 20685-1:2018 (see Eq. (1), N = number of participants).

$$95\ \%\ \text{confidence interval} = mean\ \pm\ sd \cdot \frac{1.96}{\sqrt{N}} \quad (1)$$

2.2. Methodological differences and offset calculation

Two predefined landmark definitions of the SHIP body scan standard operating procedure (SHIP-SOP) showed systematic differences to the ISO 7250-1:2017 landmark definitions. These were the landmarks of the acromion and the olecranon (differences see Figure 1).

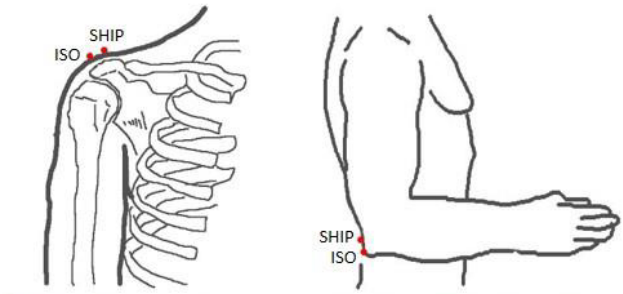

Figure 1. Example (not true to scale) as rough visualization for the landmark location offsets (drawing modified from [4]).

The different landmark locations had an impact to the following measures:

- biacromial breadth,
- shoulder height sitting,
- shoulder height standing,
- shoulder elbow length,
- forearm fingertip length.

As it was not possible to change the study design of the running SHIP evaluation, and to keep the comparability to previous examinations, the authors decided to measure these parameters twice: The first time according to the landmark definition of ISO 7250-1:2017, the second time according to the landmark definition of the SHIP-SOP. As a result, the calculation of a systematic offset was possible. To account for different body sizes (e.g. between fifth percentile female and ninety-fifth percentile male) the offsets were calculated as the relative difference between the two landmarks, taking the mean bias as reference, combined for female and male (see Table 2). Within the validation study, only the SHIP-SOP landmark locations were taken as reference for the comparison.

The parameter crotch height was excluded from the examination, as the landmark definition differed between the SHIP-SOP and the ISO 7250-1:2017 definition in a non-systematic, non-quantifiable manner. As the original landmark location is masked in the body scan images, the SHIP-SOP indexes the lowest visible point between the legs

within the sagittal plane, which in turn is highly influenced by gender as well as type and fitting of the underwear.

Further, the parameter body-depth was excluded due to quality-relevant irregularities on the 3D body scan image and obviously observable differences in body posture (standing upright leaning against a wall vs. standing upright in the body scan without supportive wall).

3. Results

Table 1 shows the mean bias, standard deviation, standard error and 95% confidence interval of the comparison scan measure – manual measure, combined for female and male. MB = Mean Bias, SD = Standard Deviation, SE = Standard Error, - 95% = lower limit of confidence interval, + 95 % = upper limit of confidence interval.

Table 1. Results from the validation study manual vs. body scan, unit: [cm].

Parameter	N	MB	SD	SE	-95%	+95%
bsiso_sta_stature	43	0.28	0.78	0.23	0.05	0.51
bsiso_sta_eye_height	44	-1.11	1.06	0.31	-1.42	-0.80
bsiso_sta_shoulder_height	44	0.12	0.91	0.27	-0.15	0.39
bsiso_sta_tibial_height	44	-0.8	1.5	0.44	-1.24	-0.36
bsiso_sta_grip_axis_height	44	-1.47	1.8	0.53	-2.00	-0.94
bsiso_sta_elbow_height	44	0.1	1.27	0.38	-0.28	0.48
bsiso_sta_iliac_spine_height	44	-1.61	2.36	0.70	-2.31	-0.91
bsiso_sta_hip_breadth	44	0.73	0.67	0.20	0.53	0.93
bsiso_sta_chest_breadth	44	1.11	1.07	0.32	0.79	1.43
bsiso_sit_thigh_clearance	44	-1.81	1.13	0.33	-2.14	-1.48
bsiso_sit_knee_height	44	-0.06	1.04	0.31	-0.37	0.25
bsiso_sit_height	43	-0.29	1.14	0.34	-0.63	0.05
bsiso_sit_cervicale_height	44	-0.69	1.1	0.33	-1.02	-0.36
bsiso_sit_eye_height	44	-1.11	1.31	0.39	-1.50	-0.72
bsiso_sit_shoulder_height	44	-0.41	1.39	0.41	-0.82	0.00
bsiso_sit_elbow_height	44	-0.53	1.79	0.53	-1.06	0.00
bsiso_sit_popliteal_height	44	-0.02	3.34	0.99	-1.01	0.97
bsiso_sit_buttock_poplit_len	44	-0.5	1.85	0.55	-1.05	0.05
bsiso_sit_buttock_knee_len	44	-0.17	1.96	0.58	-0.75	0.41
bsiso_sit_butt_abdomen_depth	44	1.65	1.49	0.44	1.21	2.09
bsiso_sit_abdominal_depth	44	1.1	1.18	0.35	0.75	1.45
bsiso_elbow_grip_len	44	-0.95	1.07	0.32	-1.27	-0.63
bsiso_elbow_wrist_len	44	0.12	0.76	0.22	-0.10	0.34
bsiso_forearm_fingertip_len	44	0.45	0.58	0.17	0.28	0.62
bsiso_shoulder_elbow_len	44	0.01	1.05	0.31	-0.30	0.32
bsiso_biacromial_breadth	44	0.05	1.74	0.51	-0.46	0.56
bsiso_bideltoid_breadth	44	1.21	0.95	0.28	0.93	1.49
bsiso_elbow_to_elbow_breadth	44	3.87	3.87	1.14	2.73	5.01
bsiso_sit_hip_breadth	43	-0.06	1.3	0.39	-0.45	0.33
bsiso_neck_circumference	42	0.49	0.84	0.25	0.24	0.74

Table 2 shows the calculated relative offsets for those parameters, which were affected by SHIP-study specific systematic differences to the ISO 7250-1:2017 landmark locations of the acromion and the olecranon (see Section 2.2).

Table 2. Calculated relative offsets for SHIP-study specific differences to ISO 7250-1:2017 measures. _F = Female, _M = Male, unit: [%].

Parameter	mean_F	sd_F	mean_M	sd_M
bsiso_biacromial_breadth	17.0647	3.5153	16.8904	3.4158
bsiso_forearm_fingertip_len	-3.9810	1.3520	-2.1383	0.9281
bsiso_shoulder_elbow_len	-5.2477	1.9240	-5.1487	1.6193
bsiso_sit_shoulder_height	-2.0419	0.9774	-2.4088	1.2966
bsiso_sta_shoulder_height	-0.9055	0.3194	-1.0168	0.4462

4. Discussion & Conclusion

The present paper showed the methods and results of a body scan evaluation, which was performed as part of an epidemiological study. Some recent research projects already addressed the comparison of manual anthropometry vs. algorithm-based assessment of anthropometric data, e.g. [11-15]. The peculiarity of the present study was the post-processing with manual identification of ISO 7250-1:2017 landmarks on the scan image by a human reader.

Interpretation of the validation study results

ISO 20685-1:2018 allows a maximum mean error between the scan derived data and manual data of 5 mm for segment lengths and body depths, 4 mm for body heights, breadths and small girth, and 9 mm for large girth measurements. The maximum allowable error needs to be smaller than the calculated limits of the 95 % confidence interval. Only four parameters (shoulder height standing, knee height sitting, elbow-wrist length and shoulder-elbow length) fulfilled these requirements. Taking the upper and lower confidence limit as references, six parameter were below 0.5 cm error, eight parameter between 0.5 cm and 1 cm error, eleven parameter between 1 cm and 1.5 cm, four parameter between 1.5 cm and 2.3 cm and one parameter (elbow-to-elbow-breadth) exceeded these values with a confidence interval ranging from 2.73 cm to 5.01 cm (see all values in Table 1). These findings are in line with other comparative studies [12, 16], which also documented higher deviation values, than the above listed maximum error allowances.

As the inter- and intrarater reliability were on a high level within the certification procedure for the manual reading of the present study [6] and the body scanner passed the technical requirements according to ISO 20685-2:2015 [8, 9], it is likely that the root cause for the evaluated differences derive from other influencing factors. One issue might have been differences in landmarking, as landmarking errors are known to have a major influence on the comparability [17]. The scanner used was not capable of detecting manually added landmarks on the participants skin, and a preparation with reflective physical markers on the participant's skin was not possible, due to the limited time frame within the ongoing study procedure. This mainly effects those parameters, where a clear

landmark identification on the scan image is difficult (e.g. thigh-clearance, iliac-spine-height or buttock-abdomen-depth).

Nine out of ten parameter with a negative comparison mean error and a -95 % lower limit of the confidence interval bigger than -1 cm were height measures. This leads to the assumption that the body posture, and especially the placement of the feet might have differed between the trials. This is in line with the results and assumptions of [12], but contrary to other comparison studies that evaluated higher values derived from the 3D body scanner, presumably because of compressed hair underneath the used bathing cap [13, 15, 16].

The parameters with a positive comparison error and a 95 % upper limit of the confidence interval bigger than 1 cm were breadth and depth measures. The parameters elbow-to-elbow breadth, bideltoidal-breadth and chest-breadth seem to suffer from a special sensitiveness to breathing, body composition and arm placement. For the manual measurement of the buttock-abdomen-depth, a buttock plate was placed at the most posterior point of the buttock to ensure a good reference point for the anthropometer. Therefore, a tissue compression at the contact areas from the buttock plate to the participants surface might be a possible reason for the evaluated difference.

Overall, when taking the given methodically difficulties into account, the evaluated differences were in an expected and credible range.

Conclusion

The idea of capturing body scans as part of an epidemiological study is a promising approach to gather a big amount of anthropometric datasets in a comparably short time. Despite a comprehensive quality assurance, the maximum error allowances from ISO 20685-1:2018 for validation studies were hard to achieve, due to several methodically differences. Nevertheless, the values were within a reasonable range and appear to be acceptable for numerous use cases.

However, for the subsequent use of the derived data, it is advisable to take the inter- and intrarater errors of the reader certification as well as the observed errors of the validation study into account. When adding a security supplement, and reporting the source of the data, the authors suggest that it should be possible to use such data, also as a supplement for existing anthropometric databases – which, of course, needs to be discussed with the relevant technical committees.

Acknowledgement

We thank all SHIP participants, examiners, and readers. The Study of Health in Pomerania is part of the Community Medicine Research Network of the University Medicine Greifswald, which was supported by the German Federal State Mecklenburg-West Pomerania. The extension to the body scan examination and reading was funded by the Federal Institute for Occupational Safety and Health (BAuA), Germany.

Special thanks go to Sabrina Geng from the Institute for Community Medicine - SHIP/KEF, University Medicine Greifswald, Germany, for the implementation of the validation study.

References

[1] International Organization for Standardization, ISO/TR 7250-2:2010 + Amd 1:2013: Basic human body measurements for technological design - Part 2: Statistical summaries of body measurements from national populations.

[2] DIN 33402-2:2005-12. Ergonomics - Human body dimensions - Part 2: Values. Beuth Verlag GmbH, Berlin.

[3] International Organization for Standardization, ISO 18825-2:2016: Clothing – Digital fittings – Part 2: Vocabulary and terminology used for attributes of the virtual human body.

[4] International Organization for Standardization, ISO 7250-1:2017 Basic human body measurements for technological design - Part 1: Body measurement definitions and landmarks.

[5] International Organization for Standardization, ISO 20685-1:2018: 3-D scanning methodologies for internationally compatible anthropometric databases – Part 1: Evaluation protocol for body dimensions extracted from 3-D body scans.

[6] Bonin D, Radke D, Wischniewski S. Gathering 3D Body Surface Scans and Anthropometric Data as Part of an Epidemiological Health Study – Method and Results. In: Bagnara S, Tartaglia R, Albolino S, Alexander T, Fujita Y, editors. Proceedings of the 20th Congress of the International Ergonomics Association (IEA 2018). IEA 2018. Advances in Intelligent Systems and Computing, vol 822. Springer, Cham.

[7] John U, Greiner B, Hensel E, Lüdemann J, Piek M, Sauer S, et al. Study of Health in Pomerania (SHIP): a health examination survey in an east German region: objectives and design. Sozial-und Präventivmedizin, 2001, 46, 186-194.

[8] International Organization for Standardization, ISO 20685-2:2015: Ergonomics – 3-D scanning methodologies for internationally compatible anthropometric databases – Part 2: Evaluation protocol of surface shape and repeatability of relative landmark positions.

[9] Kouchi M, Mochimaru M, Bradtmiller B, Daanen H, Li P, Nacher B, et al. A protocol for evaluating the accuracy of 3D body scanners. Work, 2012, 41(Supplement 1), 4010-4017.

[10] R Core Team. R: A language and environment for statistical computing. Vienna, Austria, R Foundation for Statistical Computing, 2019.

[11] Glock F, Vogel M, Naumann S, Kuehnapfel A, Scholz M, Hiemisch A, et al. Validity and intraobserver reliability of three-dimensional scanning compared with conventional anthropometry for children and adolescents from a population-based cohort study. Pediatric Research, 2017, 81(5), 736-744.

[12] Koepke N, Zwahlen M, Wells JC, Bender N, Henneberg M, Rühli FJ, et al. Comparison of 3D laser-based photonic scans and manual anthropometric measurements of body size and shape in a validation study of 123 young Swiss men. PeerJ, 2017, 5, e2980.

[13] Kuehnapfel A, Ahnert P, Loeffler M, Broda A, Scholz S. Reliability of 3D laser-based anthropometry and comparison with classical anthropometry. Sci Rep, 2016, 6, 26672.

[14] Li P, Paquette S, editors. Predicting Anthropometric Measurements from 3D Body Scans: Methods and Evaluation. Advances in Additive Manufacturing Modeling Systems and 3D Prototyping, 2020, Cham, Springer International Publishing.

[15] Jaeschke L, Steinbrecher A, Pischon T. Measurement of Waist and Hip Circumference with a Body Surface Scanner: Feasibility, Validity, Reliability, and Correlations with Markers of the Metabolic Syndrome. PLOS ONE, 2015, 10(3), e0119430.

[16] Han H, Nam Y, Choi K. Comparative analysis of 3D body scan measurements and manual measurements of size Korea adult females. International Journal of Industrial Ergonomics, 2010, 40(5), 530-540.

[17] Kouchi M, Mochimaru M. Errors in landmarking and the evaluation of the accuracy of traditional and 3D anthropometry. Applied Ergonomics, 2011, 42(3), 518-527.

DHM2020
L. Hanson et al. (Eds.)
© 2020 The authors and IOS Press.
This article is published online with Open Access by IOS Press and distributed under the terms of the Creative Commons Attribution Non-Commercial License 4.0 (CC BY-NC 4.0).
doi:10.3233/ATDE200005

Skewed Boundary Confidence Ellipses for Anthropometric Data

Erik BROLIN[a,1], Dan HÖGBERG[a] and Lars HANSON[a,b]
[a] *University of Skövde, School of Engineering Science, 541 28 Skövde, Sweden*
[b] *Scania CV, Södertälje, Sweden*

Abstract. Some anthropometric measurements, such as body weight often show a positively skewed distribution. Different types of transformations can be applied when handling skewed data in order to make the data more normally distributed. This paper presents and visualises how square root, log normal and, multiplicative inverse transformations can affect the data when creating boundary confidence ellipses. The paper also shows the difference of created manikin families, i.e. groups of manikin cases, when using transformed distributions or not, for three populations with different skewness. The results from the study show that transforming skewed distributions when generating confidence ellipses and boundary cases is appropriate to more accurately consider this type of diversity and correctly describe the shape of the actual skewed distribution. Transforming the data to create accurate boundary confidence regions is thought to be advantageous, as this would create digital manikins with enhanced accuracy that would produce more realistic and accurate simulations and evaluations when using DHM tools for the design of products and workplaces.

Keywords. Anthropometry, Skewness, Boundary Cases, Confidence Ellipses

1. Introduction

Digital human modelling (DHM) tools enable simulations and analyses of ergonomics in virtual environments. Functionality for consideration of anthropometric diversity and methods for ergonomics evaluations are central features when using DHM tools for product and production development to ensure that the design fits the intended proportion of the targeted population from a physical perspective. Working with anthropometric data, using mathematical and statistical treatment, it is possible to create boundary confidence regions in the form of ellipses or ellipsoids [1]. This is done under the assumption that the measurement distribution can be approximated with a normal distribution. However, body weight, width and circumference measurements as well as muscular strength often show a positively skewed distribution [2-3]. Comparing older data of a relatively fit population, e.g. ANSUR with military data from 1989 [4], to a more recent civilian population from 3D body scan studies, e.g. CAESAR data from 2002 [5], and to an even more recent data with a bigger sample, e.g. NHANES from 2007 [6], shows clear differences in skewness between both fitness level of different populations and the year when the data was measured [7]. Different types of transformations can be applied when handling skewed data in order to make the data

[1] Corresponding Author, Email: erik.brolin@his.se.

more normally distributed [8-9]. The transformed data could potentially be more representative when creating boundary confidence ellipsoids and selecting subsequent manikin cases, i.e. virtual human models with a number of key anthropometric dimensions defined. This paper visualises how square root, log normal and, multiplicative inverse transformations can affect the data when creating boundary confidence ellipses, i.e. make the shape of the created confidence ellipses more similar to and accurately describing the original data. The paper also shows the difference of created manikin families, i.e. groups of manikin cases, when using transformed distributions or not, for populations with different skewness.

2. Method

The applied methodology for consideration of skewness when defining boundary case manikins includes two parts:

- the first part handles transformation of skewed data to make it more normally distributed as well as transforming the generated boundary case data back to real values for visualisation and input for subsequent DHM simulation
- the second part handles the generation of boundary confidence region and definition of cases on that region

2.1. Transformation of skewed data

Skewness is a measure that describes the asymmetry of the distribution where a positive skew indicates that there is a number of persons that have values relatively far from the median value, thus forming a tail on the right side of the distribution. Skewness is here defined as

$$\frac{n\sum_{i=1}^{n}(x_i-\mu)^3}{((n-1)(n-2))\sigma^3}, \quad (1)$$

where n is the sample size, μ the sample mean and σ the standard deviation. Different methods can be used to consider positively skewed anthropometric data, e.g. using body mass index (BMI) instead of body weight or using the positively skewed log normal distribution instead of the symmetrical normal distribution [7]. Another general method for transforming data, box-cox transformation [8], can also be used. In this study, three different methods for transforming body weight data, *w*, have been evaluated:

- square-root $w^{½}$ (2)
- log normal $\ln(w)$ (3)
- reciprocal or multiplicative inverse w^{-1} (4)

The three transformation methods have in this study been applied only on original body weight data and not using BMI due to space limitations. After the transformed data have been used in statistical methods, e.g. for the generation of boundary confidence region and cases, the data can be transformed back into real values. The three methods are transformed back as:

- square-root $(w^{½})^2$ (5)

- log normal $e^{\ln(w)}$ (6)
- reciprocal or multiplicative inverse $(w^{-1})^{-1}$ (7)

2.2. Generation of boundary region and definition of cases

The transformed data is used, together with stature data, to form boundary regions in the shape of two-dimensional confidence ellipses, and then boundary cases manikins are defined on edges of these ellipses [1]. The mathematical process for calculating boundary case data based on the correlation matrix is described in Table 1.

Table 1. Mathematical process for calculating boundary case data based on the correlation matrix.

Description:		**Mathematical definition:**
1.	Correlation matrix	$\begin{bmatrix} 1 & \rho \\ \rho & 1 \end{bmatrix}$
2.	Eigenvalue matrix	$\lambda = \begin{bmatrix} 1+\rho & 0 \\ 0 & 1-\rho \end{bmatrix}$
3.	Eigenvector matrix	$\boldsymbol{v} = \begin{bmatrix} \frac{1}{\sqrt{2}} & -\frac{1}{\sqrt{2}} \\ \frac{1}{\sqrt{2}} & \frac{1}{\sqrt{2}} \end{bmatrix}$
4.	Two dimensional scale factor k (P=95%)	$k = \sqrt{x_2^2(1-0.95)} = 2.45$
5.	Matrix of scaled axes	$A = \begin{bmatrix} 2.45 \times \sqrt{1+\rho} & 0 \\ 0 & 2.45 \times \sqrt{1-\rho} \end{bmatrix}$
6.	Experimental design plan	$E = \begin{bmatrix} -1 & 0 \\ 1 & 0 \\ 0 & -1 \\ 0 & 1 \\ -\frac{1}{\sqrt{2}} & -\frac{1}{\sqrt{2}} \\ \frac{1}{\sqrt{2}} & -\frac{1}{\sqrt{2}} \\ -\frac{1}{\sqrt{2}} & \frac{1}{\sqrt{2}} \\ \frac{1}{\sqrt{2}} & \frac{1}{\sqrt{2}} \end{bmatrix}$
7.	Boundary cases in standardised space	$C_Z = \boldsymbol{v}(EA)^T$
8.	Boundary cases in real or transformed space	$C = [C_{Z-x} \times \sigma_x + \mu_x, C_{Z-y} \times \sigma_y + \mu_y]$

To give each distribution the same significance in the calculations the data is, in addition to the previous transformation due to skewness, transformed into standard normal distributions in which the mean values are 0 and standard deviation are 1 [10]. The two-dimensional confidence ellipses are defined by the length and direction of the axes, which are given by the eigenvalues and eigenvectors of the correlation matrix. In a two-dimensional standard normal distribution the eigenvalues and eigenvectors are relatively easy to calculate (Table 1). To get the final length of the ellipses axes the square root of the eigenvalues are multiplied with the scale factor k. The scale factor k is calculated from the chi-squared distribution, in this case with two degrees of freedom since we have two dimensions and with a sought accommodation level of 95 %, i.e. the confidence

ellipses are supposed to cover 95 % of the data points. The boundary cases are calculated by using an experimental design matrix that defines four axis cases on the edges of the two axes of the ellipses and four box cases at the corners of a rectangle that spans the biggest area inside the ellipses [11]. The boundary cases are then calculated by multiplying the eigenvector matrix with the transpose of the experimental design plan multiplied with the matrix of scaled axes. The values for the boundary cases are in the end transformed back from standard normal distribution to the real space or transformed space due to skewness.

3. Results

The suggested method was applied on three different populations: 1. ANSUR with military data from 1989 [4], 2. CAESAR with civilian data from 2002 [5], and 3. NHANES with more recent data and a bigger sample from 2011-2014 [12]. The study was, due to space limitations, limited to female data but the three population show a range of skewness and correlation for stature and body weight (Table 2).

Table 2. Skewness and correlation of stature and body weight for three different populations [4,5,12].

Data source	Skewness		Correlation between stature and body weight
	Stature	Body weight	
ANSUR [4]	0.139	0.536	0.529
CAESAR [5]	0.129	1.748	0.296
NHANES [12]	0.020	1.230	0.329

The different transformation methods affect both the skewness and the correlation to stature (Table 3). This can also be visualised using quantile-quantile plots (Q-Q plot) (Figure 1-3). The resulting boundary ellipses with eight boundary cases for each transformation as well as the original weight data are visualised in Figure 4-6 and the corresponding measurement and percentile values are presented in Table 4-6.

Table 3. Skewness and correlation to stature for the three transformation methods.

Data source	Skewness			Correlation to stature		
	Square-root, $w^{½}$	*Log normal,* ln(w)	*Reciprocal,* w^{-1}	Square-root, $w^{½}$	*Log normal,* ln(w)	*Reciprocal,* w^{-1}
ANSUR [4]	0.325	0.119	0.287	0.531	0.533	-0.533
CAESAR [5]	1.285	0.882	-0.203	0.314	0.331	-0.359
NHANES [12]	0.759	0.352	0.388	0.339	0.347	-0.354

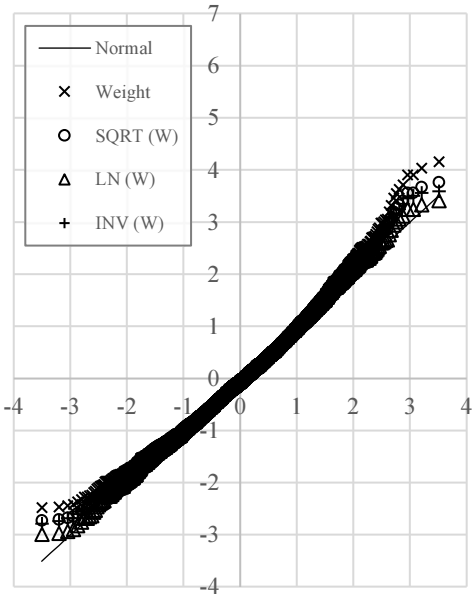

Figure 1. Q-Q plot of the positively skewed distribution of body weight as well as the three transformation methods, data from ANSUR [4].

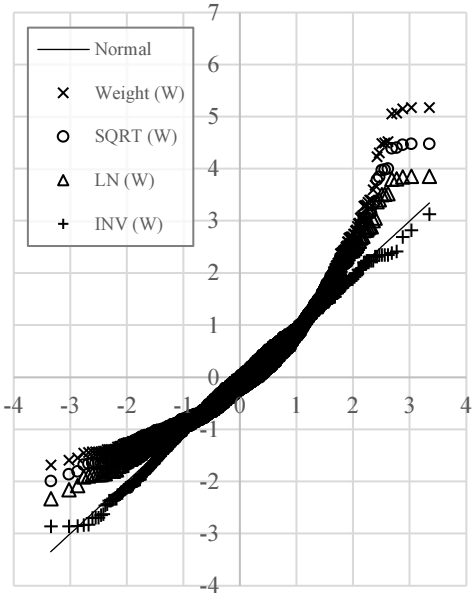

Figure 2. Q-Q plot of the positively skewed distribution of body weight as well as the three transformation methods, data from CAESAR [5].

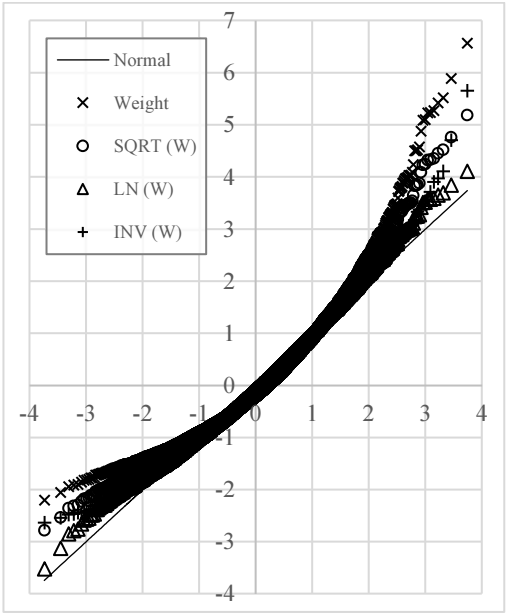

Figure 3. Q-Q plot of the positively skewed distribution of body weight as well as the three transformation methods, data from NHANES [12].

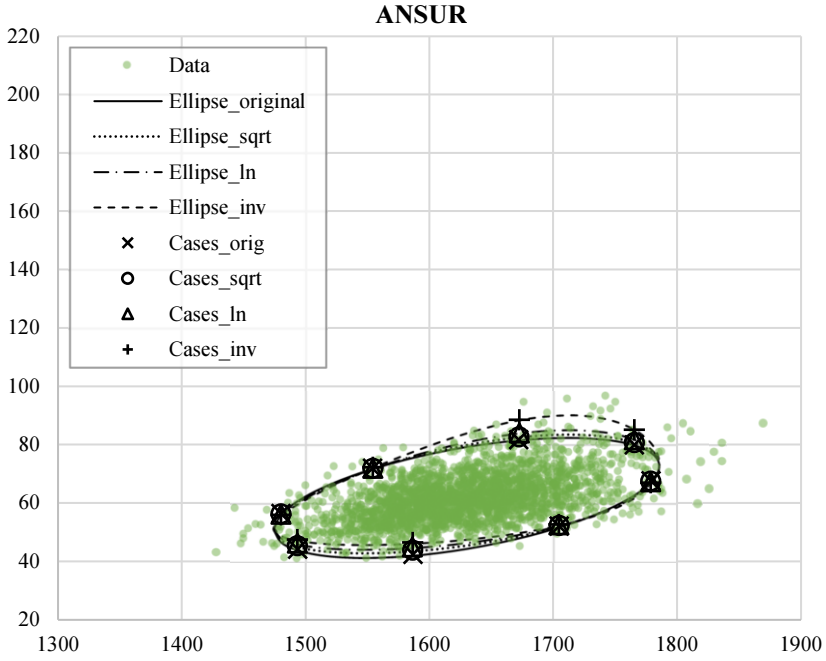

Figure 4. Confidence ellipses and boundary cases for the original body weight data and for the three transformation methods caption, data from ANSUR [4]. Stature (mm) on x-axis and weight (kg) on y-axis.

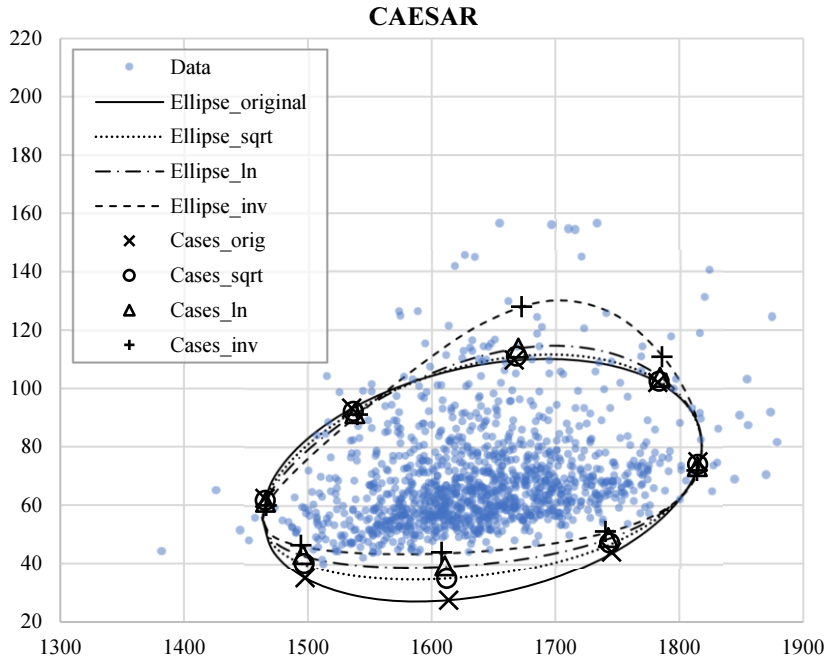

Figure 5. Confidence ellipses and boundary cases for the original body weight data and for the three transformation methods caption, data from CAESAR [5]. Stature (mm) on x-axis and weight (kg) on y-axis.

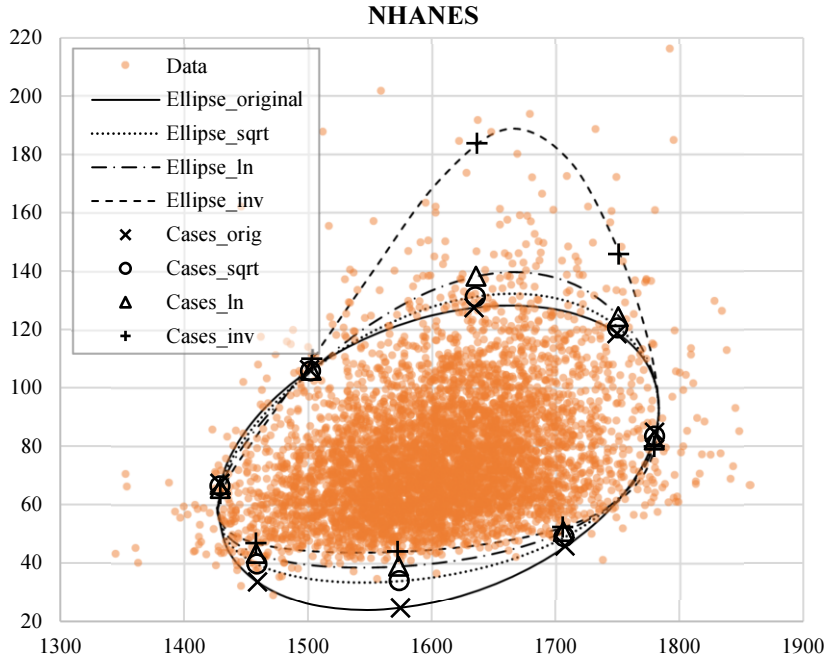

Figure 6. Confidence ellipses and boundary cases for the original body weight data and for the three transformation methods caption, data from NHANES [12]. Stature (mm) on x-axis and weight (kg) on y-axis.

Table 4. Boundary cases for each transformation as well as the original weight data and the corresponding measurement and percentile values, data from ANSUR [4].

ANSUR	Stature [mm,%-ile]	Body weight (w) [kg,%-ile]	Square-root $w^{1/2}$ [kg,%-ile]	Log normal ln(w) [kg,%-ile]	Reciprocal w^{-1} [kg,%-ile]
Case 1	1493 (1.6)	44 (0.6)	45 (0.9)	46 (1.4)	47 (2.6)
Case 2	1766 (98.1)	80 (97.1)	81 (97.5)	82 (97.9)	85 (99.1)
Case 3	1705 (87.6)	52 (10.5)	52 (11.1)	53 (11.9)	53 (12.2)
Case 4	1554 (11.1)	72 (88.0)	72 (88.0)	72 (88.0)	72 (88.7)
Case 5	1586 (25.7)	42 (0.2)	44 (0.5)	45 (0.8)	46 (1.5)
Case 6	1779 (98.9)	68 (77.3)	67 (76.5)	67 (75.9)	67 (74.9)
Case 7	1480 (0.7)	56 (26.0)	56 (25.5)	56 (25.1)	56 (24.2)
Case 8	1672 (75.0)	82 (97.9)	83 (98.3)	84 (98.9)	89 (99.5)

Table 5. Boundary cases for each transformation as well as the original weight data and the corresponding measurement and percentile values, data from CAESAR [5].

CAESAR	Stature [mm,%-ile]	Body weight (w) [kg,%-ile]	Square-root $w^{1/2}$ [kg,%-ile]	Log normal ln(w) [kg,%-ile]	Reciprocal w^{-1} [kg,%-ile]
Case 1	1497 (1.3)	35 (0.0)	40 (0.1)	43 (0.3)	46 (1.9)
Case 2	1784 (97.2)	102 (95.0)	103 (95.0)	104 (95.3)	111 (96.9)
Case 3	1744 (91.7)	44 (0.4)	47 (2.3)	49 (4.1)	51 (6.9)
Case 4	1537 (6.5)	93 (92.0)	92 (91.2)	91 (90.5)	91 (90.5)
Case 5	1612 (36.6)	27 (0.0)	35 (0.0)	39 (0.0)	44 (0.3)
Case 6	1815 (98.5)	75 (74.5)	74 (73.6)	73 (71.8)	72 (69.0)
Case 7	1466 (0.5)	62 (42.1)	62 (39.8)	61 (38.0)	60 (34.2)
Case 8	1668 (67.7)	110 (96.5)	111 (96.9)	114 (97.2)	128 (99.0)

Table 6. Boundary cases for each transformation as well as the original weight data and the corresponding measurement and percentile values, data from NHANES [12].

NHANES	Stature [mm,%-ile]	Body weight (w) [kg,%-ile]	Square-root $w^{1/2}$ [kg,%-ile]	Log normal ln(w) [kg,%-ile]	Reciprocal w^{-1} [kg,%-ile]
Case 1	1459 (2.3)	34 (0.0)	40 (0.3)	43 (1.0)	47 (2.8)
Case 2	1750 (97.6)	119 (95.7)	121 (96.3)	124 (96.9)	146 (99.1)
Case 3	1707 (92.4)	46 (2.2)	49 (4.9)	51 (7.1)	52 (9.2)
Case 4	1502 (8.3)	106 (91.0)	106 (90.7)	106 (90.9)	110 (92.9)
Case 5	1574 (33.6)	25 (0.0)	34 (0.1)	39 (0.2)	44 (1.4)
Case 6	1780 (99.1)	85 (71.8)	83 (70.1)	82 (68.6)	80 (65.1)
Case 7	1429 (0.6)	67 (39.7)	66 (37.7)	66 (35.7)	64 (31.9)
Case 8	1635 (66.3)	128 (97.4)	131 (97.9)	138 (98.7)	184 (99.8)

4. Discussion

The results from the study show that transforming skewed distributions when generating confidence ellipses and boundary cases is possible, suitable and often even necessary to more accurately consider this type of diversity. The shape of the created confidence ellipses are more similar to and accurately describes the original skewed data for the CAESAR and NHANES female population. For the ANSUR female population, which have a less skewed weight distribution, transforming the data does not affect the shape of the ellipses to any great extent. But the tested transformation methods does not either create any subsequent issues or inaccuracies when generating confidence ellipses.

When looking at the measurement and percentile values of the generated cases it is evident that not transforming the data of a skewed weight distribution will generate cases that are relatively far outside or far inside the actual distribution. Case 5 for both CAESAR and NHANES when not transforming the data have an extremely low weight of 25 and 27, respectively. Not transforming the data will also lead to an underestimation of the higher percentile values. Case 8 for all three populations have the highest weight values but at the same time relatively low values when not transforming the data. When transforming the data, the values increases from square-root to log normal and from log normal to multiplicative inverse. For the NHANES data the multiplicative inverse transformation method leads to a boundary case with a weight of 184 kg which can seem extremely high, however that case can still be found within the actual distribution. Future research will also include BMI and other non-normal distributed anthropometric variables as well testing additional transformation methods. To have accurate boundary confidence regions is thought to be advantageous, whether the manikin cases are selected as boundary cases located towards the edges or as distributed cases spread throughout a region, randomly or by some systematic approach. This would give digital human models with anthropometry that better resembles the variance and diversity that exist within human populations. This would in turn produce more realistic and accurate simulations and evaluations and thus give better assistance to engineers and designers using DHM tools when developing products and workplaces.

Acknowledgement

This work has been made possible with support from the Knowledge Foundation and the associated INFINIT research environment at the University of Skövde (projects: Synergy Virtual Ergonomics and ADOPTIVE), and with support from Vinnova in the VIVA project, and SAFER - Vehicle and Traffic Safety Centre at Chalmers, Sweden, and by the participating organizations. This support is gratefully acknowledged.

References

[1] Brolin E, Högberg D, Hanson L. Description of boundary case methodology for anthropometric diversity consideration, International Journal of Human Factors Modelling and Simulation, 2012, 3(2), 204–223. [online] https://doi.org/10.1504/IJHFMS.2012.051097.

[2] Vasu M, Mital A. Evaluation of the validity of anthropometric design assumptions, Industrial Ergonomics, 2000, 26, 19–37.

[3] Pheasant S, Haslegrave CM. Bodyspace: Anthropometry, Ergonomics and the Design of Work. CRC Press, Boca Raton, 2006.

[4] Gordon CC, Churchill T, Clauser CE, Bradtmiller B, Mcconville JT, Tebbetts I, Walker RA. 1988 Anthropometric Survey of US Army Personnel: Methods and Summary Statistics. U.S. Army Natick Research, Development and Engineering Center, Natick, MA, 1989.
[5] Robinette KM, Blackwell S, Daanen H, Boehmer M, Fleming S, Brill T, Hoeferlin D, Burnsides D. Civilian American and European Surface Anthropometry Resource (CAESAR). Final report: Air Force Research laboratory, Wright-Patterson AFB, OH, and Society of Automotive Engineers International, Warrendale, PA, 2002.
[6] U.S. Centers for Disease Control and Prevention. National Health and Nutrition. Examination Survey (NHANES). National Center for Health Statistics, 2008. http://www.cdc.gov/nchs/nhanes.htm.
[7] Parkinson MB, Reed MP. Creating virtual user populations by analysis of anthropometric data. Int. J. Industrial Ergonomics, 2010, 40(1), 106-111.
[8] Box GE, Cox DR. An analysis of transformations. Journal of the Royal Statistical Society: Series B (Methodological), 1964, 26(2), 211-243.
[9] Cole TJ. The LMS method for constructing normalized growth standards. Eur J Clin Nutr, 1990, 44(1), 45-60.
[10] Glenberg A, Andrzejewski M. Learning from Data: An Introduction to Statistical Reasoning, 3rd ed. Routledge Academic, New York, 2007.
[11] Bertilsson E, Högberg D, Hanson L. Using experimental design to define boundary manikins. Work: A Journal of Prevention, Assessment and Rehabilitation, 2012, 41, 4598–4605 [online] https://doi.org/10.3233/WOR-2012-0075-4598.
[12] Fryar CD, Gu Q, Ogden CL, Flegal KM. Anthropometric reference data for children and adults: United States, 2011–2014, National Center for Health Statistics. Vital Health Stat, 2016, 3(39).

DHM2020
L. Hanson et al. (Eds.)
© 2020 The authors and IOS Press.
This article is published online with Open Access by IOS Press and distributed under the terms of the Creative Commons Attribution Non-Commercial License 4.0 (CC BY-NC 4.0).
doi:10.3233/ATDE200006

Introducing Multivariate Anthropometry in Digital Human Modelling

Paulo Eduardo FRAGOSO [1]
Scania CV AB

Abstract. The paper talks about the known concept of Multivariate anthropometry, a term explained in several other studies. The method consists of creating a family of manikins with a combination of more than one anthropometric variable to broaden, or to accommodate more users in a physical ergonomic analysis scenario. The paper explains how this method was adopted at a truck OEM and how it affects the design aspect of ergonomics. The paper also describes how the usage of such a method would be difficult to achieve before the advent of DHMs, CAD environments. Communicating this working method that is within reach of several industries is a history that is worth being aware of and sharing.

Another section of the paper describes how different DHMs deal with this Multivariate method, and what possibilities are open for the users when they create their families in different software.

The statistical concept of percentile is addressed in the paper, and presents it not as being a surpassed method, but rather as being one important variable of the Multivariate approach.

Keywords. Anthropometry, Multivariate, Digital Human Models, Statistics, Ergonomics, Manikins Family

1. Introduction

The Digital Human Model (DHM) software is more accessible today than in years past and is expected to continue to draw appeal to a growing, and diverse, number of users. For this reason, it is an opportune time to explore some of the benefits observed when applying Multivariate Anthropometry (MA) and the Multivariate Anthropometry Family (MAF) to the DHM software. The MA method is not a novel concept. It has previously been introduced and discussed past papers [1,2,3,4,5,6,7].

The purpose of this paper will be to provide an introduction of MA when applied to the DHM software. This will include an outline of some of the historical dates and facts, the statistical method behind the theory, how to interpret the results, how the outcomes can apply in their specific applications, and finally, this paper will discuss some advantages and disadvantages of the MA method within the application of the DHM.

Unique to this paper will be a comparison of the application of MA to two well-known DHMs: (i) IPS IMMA – ***I**ntelligently **M**oving **MA**nikin* (developed in Sweden) and (ii) RAMSIS – ***R**ealistic **A**nthropological **M**athematical **S**ystem for **I**nterior **S**imulations* (developed in Germany).

[1] Corresponding Author, Email: paulo.fragoso@scania.com.

2. Multivariate Anthropometry

2.1. Etymology

The word *Multivariate* is an *adjective that is defined as having or involving a number of independent mathematical or statistical variables, which first appeared in 1920* [8]. 'Multi' signifies many; or more than one. 'Variate' is a verb that refers to a variable that has one of many possible realizations.

Anthropometry is the study human body measurements, especially on a comparative basis, and the first use of this word appears in 1806 [9].

As the name suggests, MA involves a number of independent mathematical and statistical values that variate, and these values are related to body measurements for a comparative basis.

This method is heavily based in the statistical concept of percentiles. Since the number of independent (and dependent) variables are too large to handle manually in this type of work, combined with the fact that the results have a tendency to produce an unnecessarily large number of outputs (considered 'too bulky'), it deterred people from using this method. It was only in the decade of the 1980's, when DHM was created, that we began to see adoption of the MA method.

2.2. Percentiles

The usage of a Multivariate family of manikins does not invalidate the percentile approach, rather it builds on top of that concept. Percentiles according to Speyer [10]:

The α-percentile of an anthropometric measurement (e.g. stature, Figure 1) is the value called **a** of this variable with the following properties:

- The corresponding anthropometric measurement of α% of all subjects in the relevant population is less than or equal to **a**, consequently:
- The corresponding anthropometric measurement of (100 - α) % of all people in the population is greater than **a**.

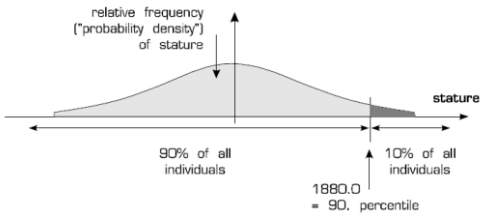

Figure 1. Normal distribution curve and the 90th percentile of stature [10].

The usual way of applying percentiles is done with regards to one variable, the standing height (stature) is by far the most common used variable, and in the automotive industry the most used percentiles are the 5th, 50th and 95th percentiles (Figure 2).

3. From Percentiles into Multivariate

3.1. Adding variables

Expanding on top of the concept of percentiles, it is now possible to imagine applying the same work frame for different anthropometric variables, in the example shown in Figure 3, two other variables were chosen: Sitting height and Waist circumferences.

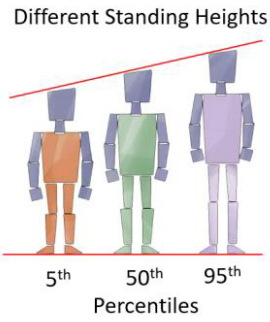

Figure 2. Most common percentiles used at OEMs.

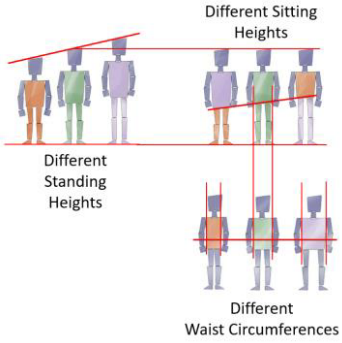

Figure 3. Two other anthropometric variables.

It is these three variables that were chosen by Human Solutions and programmed into the RAMSIS DHM software. According to Speyer [10]:

Based on statistical analysis of anthropometric survey data several anthropological research groups have found the independence and the characterizing property of stature, sitting height, and waist circumference to hold true not only for European populations but also for (e.g.) North America and Korea. It seems to be a universal human property. This is why we call these three body measurements "key dimensions" or "characterizing dimensions".

The existence of independent characterizing body dimensions has the following very important consequences for designing a test sample representing an entire population: it is sufficient to design the sample as to cover the full variation range of each characterizing dimension independently and to use predicted values (most probable values) for all of the other body dimensions. Due to the characterizing property by exploiting the variation ranges of the key dimensions the values of the other body dimensions also widely cover the corresponding variation intervals. Therefore the RAMSIS typology can be easily used for test sample design.

Different from Human Solutions RAMSIS, IPS IMMA users are not constrained to those three variables, according to Brolin [11]:

The comparison can be extended to even more dimensions, using more key anthropometric variables, by calculating the number of measured individuals that are found inside, thus being considered accommodated, a generated multidimensional hyper ellipsoid as well inside a multidimensional hyper cuboid based on the 5th and 95th percentile value for the selected key variables.

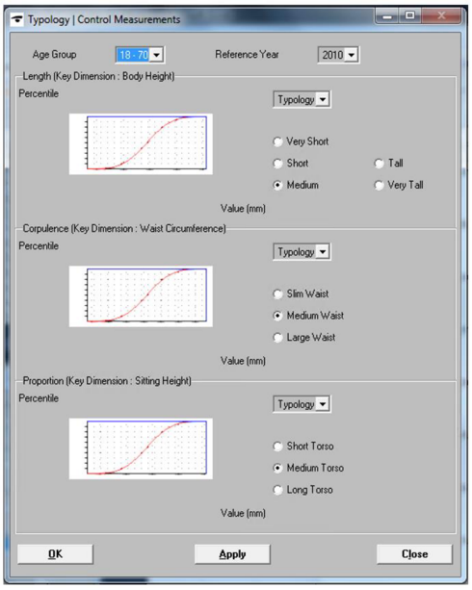

Figure 4. RAMSIS input window for manikin creation.

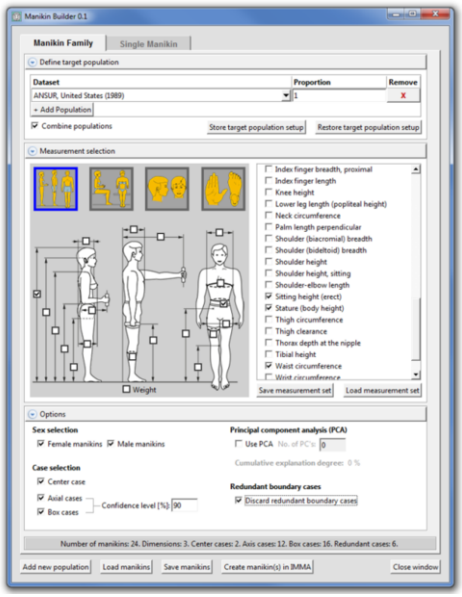

Figure 5. IMMA input window for manikin creation.

In Figure 4 it is possible to see RAMSIS window for manikin creation with the three basic variable options, titled Length, Corpulence and Proportion. In Figure 5 we can see IPS IMMA, with all variables available marked with a clickable box.

3.2. Manikin Family

Regardless of the number of variables used, the next step consists in combining those variables in a way that the entire extent of the population is well represented. That is done using a family of manikins, and each manikin represents a combination of a certain percentile in the variables chosen. As for example the RAMSIS family of manikins is shown in Figure 6.

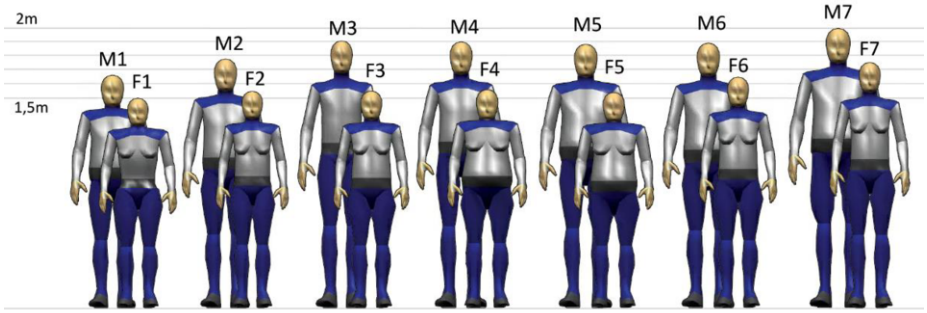

Figure 6. A Multivariate family of manikins created with RAMSIS.

Each manikin can be re-named in a manner that better corresponds to its confining variables (Table 1).

Table 1. Manikin family named (standing height, waist circumference, sitting height).

Female	Male
F1 – Minimum height	M1 – Very short, medium waist, medium torso
F2 – Very short, slim waist, short torso	M2 – Medium, medium waist, medium torso
F3 – Very short, medium waist, medium torso	M3 – Very tall, slim waist, short torso
F4 – Very short, large waist, medium torso	M4 – Very tall, medium waist, short torso
F5 – Very short, large waist, large torso	M5 – Very tall, large waist, medium torso
F6 – Medium, medium waist, medium torso	M6 – Very tall, large waist, large torso
F7 – Very tall, medium waist, medium torso	M7 – Maximum height

Figure 7 is another example of a family of manikins created in IPS IMMA using the following confounding variables: (i) sitting height, (ii) grip reach, and (iii) seat depth. For application purposes, combining these three variables creates a family that would be of interest to, for example, a wheelchair manufacturer.

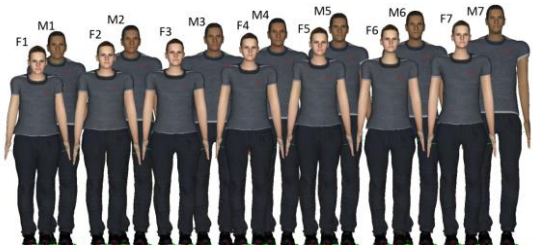

Figure 7. A Multivariate family of manikins created with IPS IMMA.

Similar to what we did in the prior case, each manikin in this software can also be re-named in a manner that better corresponds to its confining variables (Table 2).

Table 2. Manikin family named (sitting height, grip reach, seat depth).

Female	Male
F1- Short torso, short seat depth, short reach	M1- Short torso, short seat depth, short reach
F2- Short torso, medium seat depth, medium reach	M2- Short torso, medium seat depth, medium reach
F3- Medium torso, short seat depth, short reach	M3- Medium torso, short seat depth, short reach
F4- Medium torso, medium seat depth, medium reach	M4- Medium torso, medium seat depth, medium reach
F5- Medium torso, long seat depth, long reach	M5- Medium torso, long seat depth, long reach
F6- Long torso, medium seat depth, medium reach	M6- Long torso, medium seat depth, medium reach
F7- Long torso, long seat depth, long reach	M7- Long torso, long seat depth, long reach

Interestingly, each DHM has its own algorithm to create their families, but they all basically use the same concept of ellipsoids, which will be presented next.

4. How Multivariate compare to Percentiles

In order to understand the advantages of using the multivariate approach in manikin creation, we need to create a situation where results of both a 'percentile family' and a 'multivariate family' can be compared.

Imagine if you were to transform the three variables each of the manikins of the RAMSIS family into points on a coordinate axis system (Figure 8).

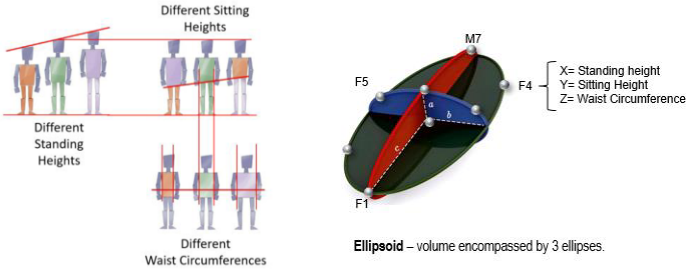

Figure 8. Variables on the manikins transformed in points, and subsequent ellipsoid.

The example above is using only the German population, and most likely the coordinate space would end up containing the ellipsoid shown in Figure 9.

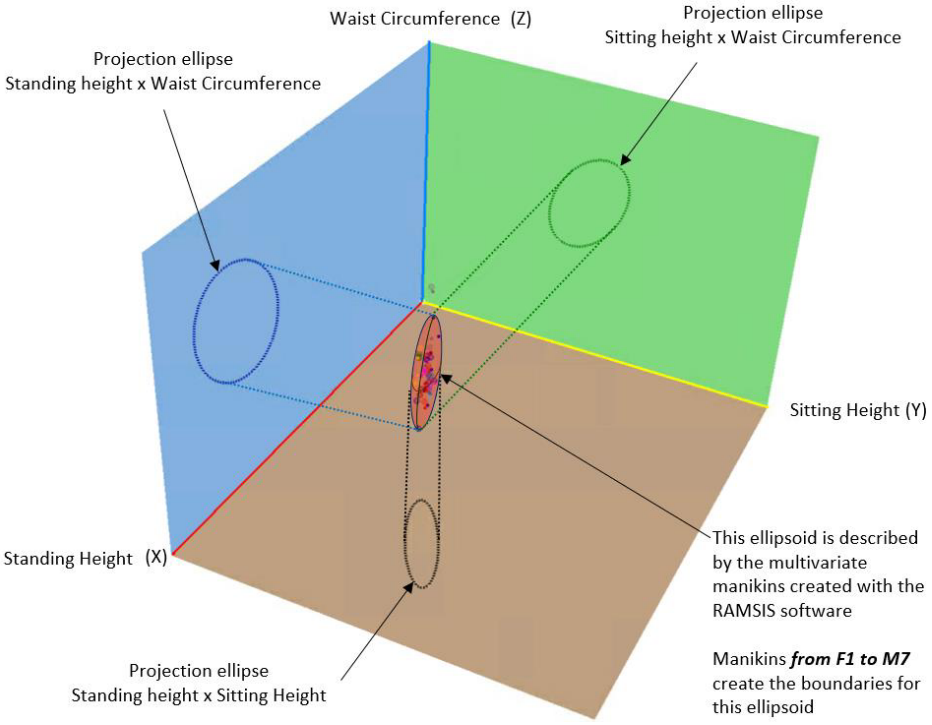

Figure 9. Ellipsoid and projections.

Now it is possible to project an ellipse for each of the sides of the coordinated space, one for each of the two combined axes: XY, XZ and YZ. These ellipses allow us to observe the correlation of the two corresponding axes, and how each manikin is distributed within the ellipse (Figure 10 and Figure 11).

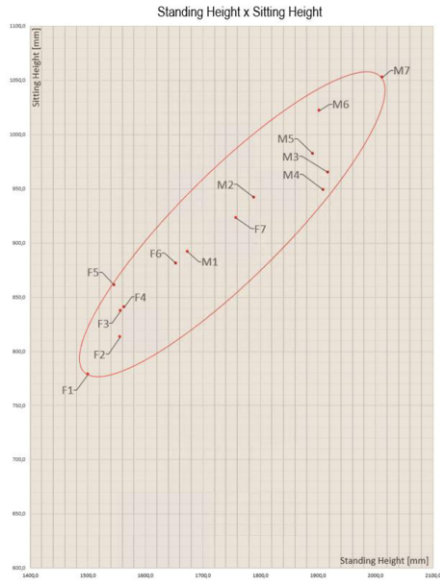

Figure 10. Projected ellipse on the XY plane.

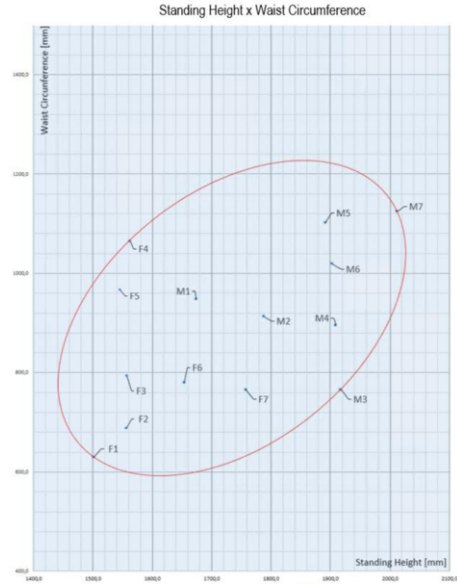

Figure 11. Projected ellipse on the XZ plane.

This is only possible to understand because we can visually represent three dimensions in space. If we were to try to plot manikins with more than three variables, it would not be possible to visualize them, thus, making it more complicated to understand. Nonetheless, note that on the IPS IMMA software, it is feasible to include more than three variables when creating a manikin family, as Brolin demonstrated [11].

Imagine now if we were to plot, in the same coordinated space, a group of manikins that were created using only one variable on the control axis. The example variable used here will be the standing height, from the Swedish [12], Indian [13], and Brazilian [14] anthropometric data set (Figure 12).

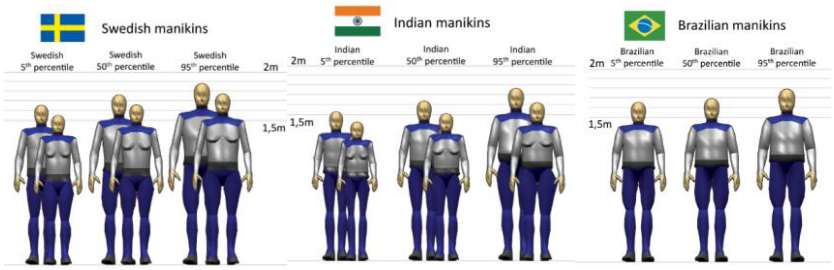

Figure 12. Swedish, Indian and Brazilian percentiles in standing height manikins.

As we can see in Figure 13, they would not appear as more than flat diagonal curves, having only one dimension instead of the inclined ellipse that has two dimensions and thus covering an area. This graphical representation shows that a vastly

bigger group of users are taken into consideration while using the multivariate anthropometry method in comparison to the one variable percentile method.

Another way to interpret this is: By using a multivariate anthropometric family of manikins, which in our example is based in only in one country (Germany), other countries were also being considered indirectly via one variable anthropometry. Making the multivariate family of manikins really an international representation of humans, and enabler of inclusive design.

One last point to observe is the Brazilian data graphical representation. Notice how it is shorter than the other 2 curves? That's because it is only accounting for male users, that curve is there to show how important it is to add female measurements to an anthropometric pool of data.

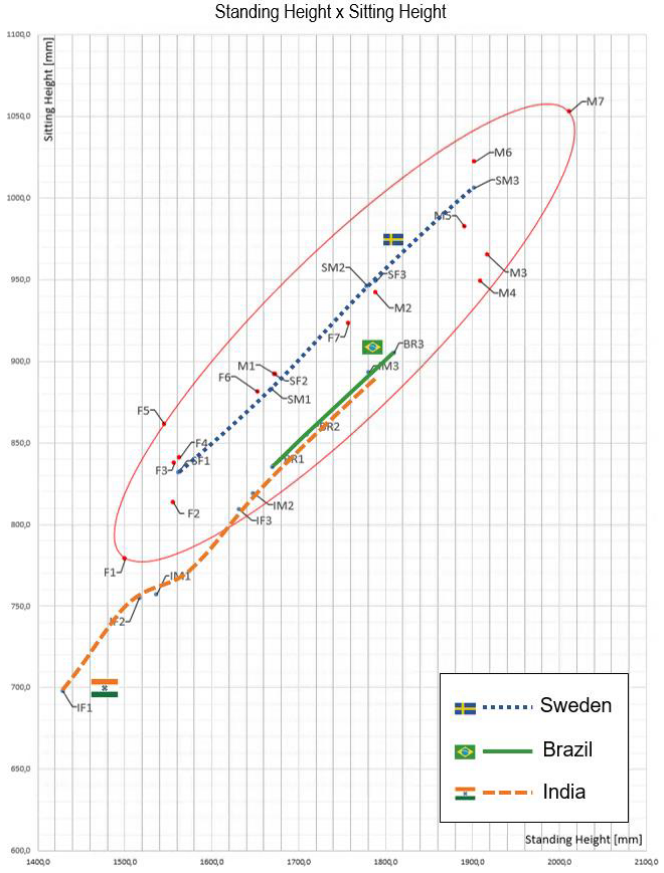

Figure 13. Multivariate generated ellipse and percentile generated curves.

5. Disadvantages of the Multivariate method

One of the disadvantages of the multivariate method is that it is more complicated to explain to your client as to what person you are designing for. In contrast, the primary advantage of using the one variable percentile method is that people can more easily

grasp the concept of a person being taller or shorter; however, this is not as easy when multiple variables are combined.

Another disadvantage is the dependency on having a DHM software to do any useful analysis once the manikin family is created, thus, creating a threshold for on boarding users to this method.

5.1. Discussion

One of the main goals for writing this paper was to help break down the concept of a multivariate system into something that can be more easily understood and communicated. The focus of the paper was to write and provide figures in a way that can achieve this goal, thus making it possible for existing and future users to consider this method with regards to ergonomic-driven work.

6. How it affects the design aspect of ergonomics

Since this method is so dependent on the DHM, the design aspects of ergonomics become really affected by computer-aided design (CAD) computing and the development workflow of different original equipment manufacturers (OEMs). The ergonomist or designer has to find a way to effectively work, give and take input to other engineering or manufacturing areas by using the same CAD system for which the design process is being developed. This makes it necessary for heavy file conversions of complete virtual environments (e.g. VW Ramona) or forcing DHM developers to port their tools to other CAD systems like, for example, the newly ported RAMSIS NextGen into CATIA V5 and RAMSIS in Siemens NX, or IPS IMMA conversion tools to CATIA models.

7. The Multivariate method would be hard to achieve before the advent of DHMs

The application of such method only became possible after the invention of the DHM software. Anthropometry has a long history, longer than the point in time where we will start to describe. We will pick it up from the moment it started to shift from analogue to digital.

In the 1980´s it was becoming the norm for the automotive industry to use CAD to develop new products, and according to Bubb [15]:

In 1980s it became obvious that the traditional procedure of the design and development by drawing machines came to an end and was substituted by the new CAD technologies. Thus, it was necessary to develop a representation of the human shape for the CAD-environment.

And to address this need:

...The German automotive research group (Forschung Automobil Technik, FAT) decided to develop an own 'soft dummy'. Within the FAT an expert group consisting of one person of each German automotive company (Audi, BMW, Ford, Mercedes-Benz, Opel, and Porsche) and each one of the seat manufacturers Keiper-Recaro and Johnson Controls were found. This group developed a matrix of requisitions that define the desired abilities of this soft dummy.

This is done by the application of the stereo metric principle in the body posture-measuring tool PCMAN, which was developed during the RAMSIS project. The idea is to superimpose a

wire frame soft-dummy in photos of a specific working situation which are taken by two or more cameras. In the computer an anthropometrically adjusted soft-dummy-model of the subject is projected virtually on two or more planes by the rules of central perspective and by using the same parameters as in real photography. By adjusting the joint angles in all considered pictures, the 3D position and the posture of the body in space can be described mathematically. The subject's anthropometry and the posture can then be transferred to the RAMSIS environment or be used for other examination such as statistical analysis.

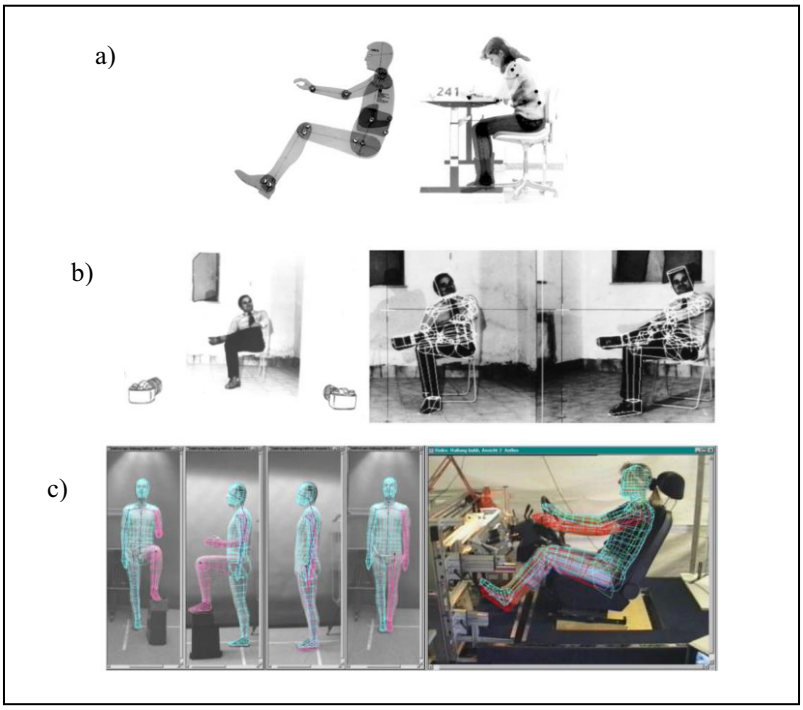

Figure 14. a) 2D template, template over work position, b) Stereo metric principle, soft dummy, c) PCMAN over driving position.

The Swedish industry followed the same steps, later in time (2010) and with a different background, since it first started with manufacturing and assembly line design. From Brolin [11] (Figure 15):

In 2010 research was commenced to develop the DHM tool IMMA (Intelligently Moving Manikins) [16]. IMMA uses advanced path planning techniques to generate collision free and biomechanically acceptable motions for digital human models in complex assembly situations, e.g. vehicle assembly.

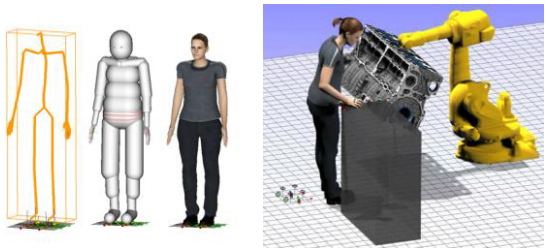

Figure 15. IPS IMMA manikin: bones, colliders, mesh and interaction with a robot in an assembly line.

7.1. DHM manikin creation tools

As it was mentioned before, each DHM has its own method of family creation, but they are only capable of doing this because they have also developed special software tools that only deal with anthropometry.

That is the case for RAMSIS that grounds their anthropometry work on the software called *Body Builder*, a plug-in that can be opened at any time inside any version (Figure 16). The same is true for IPS IMMA, where the anthropometric work is grounded on the *Manikin Builder* add-on (Figure 16).

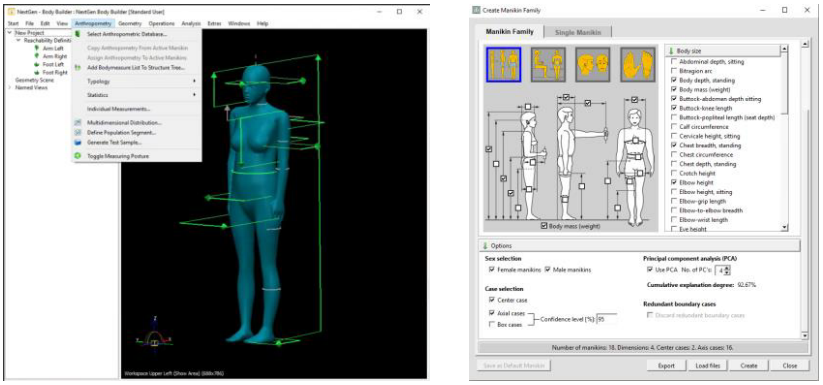

Figure 16. RAMSIS Body Builder (left) and IPS IMMA Manikin Builder (right).

Without those specific tools, it would have been impossible to create such an extended family of manikins, and with such variety. Imagine having to produce a family of manikins in acrylic plastic, and to cover all the anthropometry as well as different views possible. That was the case back in the 60´s and 70´s as attested by Seidl & Bubb [17]:

The SAE template is a 2D template especially developed for use in automotive industry. The data, design and application are on record in the standard SAE J826a (Society of Automotive Engineers). This template has become extremely important in the automotive industry, because it is used not only for ergonomics design but also for the authorization of the vehicles themselves. The template consists only of the torso of the 50th percentile American and a 2D leg simulation of the 95th percentile American.

The DIN 334408 Body contour template for seats was modeled on the SAE template. It is derived from the developments of the Kieler Puppe (shown in Figure 14- a) and encompasses altogether 6 templates in 3 perspectives: front, side and top view. A total of 5 body types are

supported. For the male form, the 5th, 50th and the 95th percentiles are used, whereas for the female form, the 1st to the 5th and the 95th are available.

8. Within reach of several industries

Starting from the car industry, this way of working has developed through the years and now it is starting to show up in other industries. As it was presented in the latest RAMSIS conferences 2017, 2018 and 2019, where a larger number of industries outside of automotive are beginning to show interest in DHMs, such as Recaro seats with the newly developed *Recaro Exo* a gaming seat, KTM motorcycle manufacturing that have presented studies of products using the Multivariate approach of families.

9. Final statement

It is the intent of this paper to help future users of DHM understands the basic principles of the multivariate concept. We sincerely hope that you have understood and found this reading interesting to the point it inspires you into using this method in your work.

References

[1] Zehner GF, Meindl RS, Hudson JA. A multivariate anthropometric method for crew station design: Abridged. Wright-Patterson Air Force Base, Ohio. ALTR-1992-0164. 32, 1993.
[2] Speyer HJ. On the definition and generation of optimal test samples for design problems. Human Solutions GmbH, Kaiserslautern, Germany, 1995.
[3] Johnson RA, Wichern DW. Applied multivariate statistical analysis, Pearson Education, Inc. 2007.
[4] Guan J, Hsiao H, Bradtmiller B, Kau T-Y, Reed MR, Jahns SK, Loczi J, Hardee HL, Piamonte DPT. U.S. truck driver anthropometric study and multivariate models for cab designs. Hum Factors, 2012, 54(5), 849–871.
[5] DINED anthropometry in design – Ellipse. https://dined.io.tudelft.nl/en/ellipse/introduction
[6] Garneau CJ, Parkinson MB. Preliminary validation of a tool for visualizing anthropometric data. Proceedings of the First International Symposium on Digital Human Modeling (DHM2011), 2011.
[7] Multivariate tools at open design lab. https://www.openlab.psu.edu/tools/
[8] Dictionary Merrian-Webster at www.merrian-webster.com search word: Multivariate
[9] Dictionary Merrian-Webster at www.merrian-webster.com search word: Anthropometry
[10] Speyer, HJ. RAMSIS definition of Anthropometric types. Human Solutions GmbH, Kaiserslautern, Germany, 2006.
[11] Brolin, E. Anthropometric diversity and consideration of human capabilities. Doctoral dissertation. Chalmers University of Technology, Sweden, 2016.
[12] Hanson L, Sperling L, Gard G, Ipsen S, Olivares Vergara C. Swedish anthropometry for product and workplace design. Applied Ergonomics, 2009, 40(4), 797–806.
[13] Chakrabarti D. Indian Anthropometric dimensions for ergonomic design practice. National Institute of Design, India, 1997.
[14] Fragoso PE, Nogueira Alves RC, Ormindo TDV. Estudo do perfil antropométrico da população de motoristas de caminhão no Brasil. Brasil, 2013.
[15] Bubb H, Engstler F, Fritzsche F, Mergl C, Sabbah O, Schaefer P, Zacher I. The development of RAMSIS in past and future as an example for the cooperation between industry and university. Int J of Human Factors Modelling and Simulation, 2006, 1(1), 140–157.
[16] Högberg D, Hanson L, Bohlin R, Carlson JS. Creating and shaping the DHM tool IMMA for ergonomic product and production design. Int J Digit Hum, 2016, 1(2), 132–152.
[17] Seidl A, Bubb H. Standards in Anthropometry. In: Handbook of Standards and Guidelines in Ergonomics and Human Factors, 2005, First edition.

DHM2020
L. Hanson et al. (Eds.)
© 2020 The authors and IOS Press.
This article is published online with Open Access by IOS Press and distributed under the terms of the Creative Commons Attribution Non-Commercial License 4.0 (CC BY-NC 4.0).
doi:10.3233/ATDE200007

Creating a Personalized Full 3D Body Shape from a Limited Number of Predictors

Xuguang WANG[a,1], Georges BEURIER[a], Yoann LAFON[a] and Junfeng PENG[b]
[a] *Univ Lyon, Univ Gustave Eiffel, LBMC UMR_T9406, F69622, Lyon, France*
[b] *Decathlon SportsLab, 59650 Villeneuve d'Ascq, France*

Abstract. The use of statistical body shape models (SBSM) offers the possibility to generate a realistic full body shape with a limited number of measures/predictors such as traditional anthropometric dimensions, surface landmarks etc. The purpose of the present work is to explore the possibility to create a personalized surface model with a small set of easily measurable parameters, and to compare the quality of SBSM-based prediction in function of predictors. A sample of 164 full body scans in a standing posture from European and Chinese males were selected based on stature and BMI. After cleaning the raw scans, a non-rigid mesh deformation method was used to fit a customized template onto scans. Then, a principal component analysis (PCA) was performed to build SBSM with different set of predictors, including anthropometric dimensions, landmarks' coordinates, postural parameters. The partial least square regression was used to take into account correlated nature between predictors. As statistical models cannot match the target values of predictors, an optimization was further proposed for better matching targets while not deviating too much from the initial prediction by statistical regression. A leave-one-out (LOO) procedure was used to evaluate the quality of SBSM with different set of predictors.

Keywords. 3D Statistical Shape Model, Human Body Shape, PCA, Anthropometry

1. Introduction

An accurate and personalized full 3D body shape in a position of interest is needed for many applications such as textile industry for specifying product size. In postural and motion analysis, researchers often need to define a subject specific digital human model to understand the interaction between a person and environment [1]. Though a full body surface can be easily scanned using a body scanner, raw scans are generally noisy, incomplete, and require a more or less time consuming post processing to obtain a workable surface model [2]. In recent years, thanks to the development of statistical body shape models (SBSM) [3], researchers used these models to remove noise, complete holes making it possible to create high quality surface models from a low cost depth camera [4] or even from a single image [5]. The use of SBSM also offers the possibility to generate a realistic full body shape with a limited number of measures/predictors such as traditional anthropometric dimensions, surface landmarks etc. Though parametric human body modelling approaches (see for example [6]) have been developed for many

[1] Corresponding Author, Email: xuguang.wang@univ-eiffel.fr.

years, a systematic evaluation of prediction accuracy in function of predictors is missing. The purpose of the present work is to explore the possibility to create a personalized surface model with a small number of easily measurable parameters, and to compare the quality of SBSM-based prediction in function of predictors.

2. Materials and method

2.1. Scan data and processing

A sample of 164 full body scans of European and Chinese males in a standing posture from an existing database of Decathlon SportsLab were selected based on stature and BMI (Table 1). After cleaning the raw scans, a non-rigid mesh deformation method was used to fit a customized template onto scans using mHBM [7]. An experienced researcher identified 27 landmarks manually on the body surface by virtual palpation (Figure 1). They were used for template fitting. An example is shown in Figure 2. Due to artefacts (e.g. hair) and insufficient scan quality, head mesh was re-adjusted according to the head height manually measured at the same time as 3D body scanning, which is defined as the vertical distance from the bottom of the chin to the top of the head.

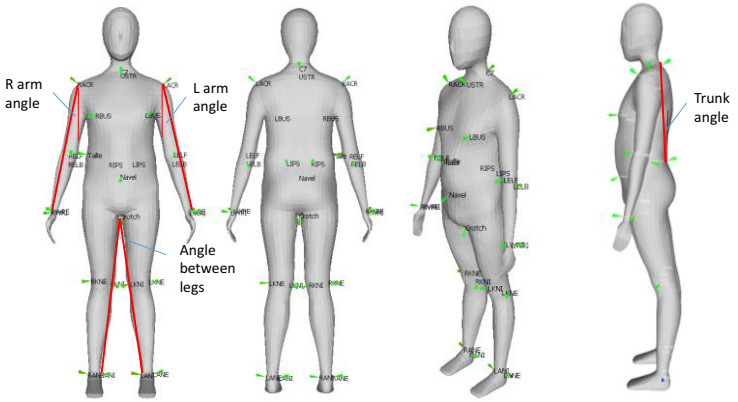

Figure 1. Customized template and landmarks. Four postural angles are also illustrated.

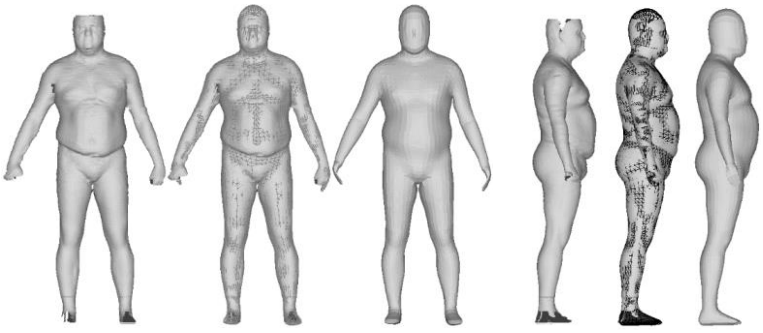

Figure 2. An example showing a raw scan and mesh after template fitting.

Table 1. Summary of the statistics of stature, weight and BMI of selected European and Chinese males.

	Europe			China		
	Stature (mm)	**Weight (kg)**	**BMI (kg/m²)**	**Stature (mm)**	**Weight (kg)**	**BMI (kg/m²)**
N	83	83	83	81	81	81
Average	1744.2	80.3614	26.3973	1723.5	78.9	26.6
Standard deviation	58.46	12.4583	3.79265	74.2661	15.9	4.98
Coeff. of variation	3.35%	15.50%	14.37%	4.31%	20.13%	18.73%
Minimum	1617.3	57.0	18.3	1537.1	53.2	18.3
Maximum	1895.3	134.0	43.8	1871.7	119.0	41.0
Range	278	77.0	25.5127	334.62	65.8	22.7

2.2. Anthropometric and postural parameters

For each scan, a homologous model was created by template fitting, from which 18 anthropometric dimensions were extracted:

- 4 heights: stature, crotch height, C7 height, knee height
- 3 lengths: upper arm length, forearm length, total arm length
- 11 circumferences: at hip, waist, chest, knee, ankle, elbow; thigh circumferences at crotch and middle of thigh, circumferences of lower leg, upper arm and forearm at their middle

To reduce data variability due to postural variation, four postural parameters were extracted with help of pre-defined landmarks (Figure 1):

- Trunk angle: angle between the vertical and the mid IPS (middle between left and right posterior superior iliac spines) to C7 line
- Right and left arm angle: angle between the vertical and the acromion to wrist line
- Angle between legs: angle formed by left internal ankle point, crotch and right ankle point.

2.3. PCA models

All registered scans were at first aligned using the palpated surface landmarks. The 3D coordinates of vertices from *n* subjects were put in a matrix Ψ_{n*r}, with *r* being 3*number of vertices (variables). The *s* (=3*27) coordinates of the 27 landmarks were appended to Ψ_{n*r} resulting in a matrix $\Psi_{n*(r+s)}$. A smaller set of ordered variables, called principal component (PC) scores, was obtained with a principal component analysis (PCA), so that the first PCs retained most of the variation in data. PC scores were calculated for each subject. An intuitive interpretation of the PCs can be performed by varying the scores along each component from (mean -2SD) to (mean +2SD).

From the PCA of $\mathbf{\Psi}$, assume that *m* main PCs $\mathbf{u}_j$ (j=1, *m*) are retained. The vertex coordinates of a body shape $\mathbf{v}_{(r+s)}$ can be approximated:

$$\mathbf{v} \approx \bar{\boldsymbol{\mu}} + \sum_{j=1}^{m} y_j \boldsymbol{u}_j \qquad (1)$$

where $\bar{\boldsymbol{\mu}}$ is the average from the sample data sets Ψ and y_j is the unknown score associated with j^{th} PC. The m unknown scores $\mathbf{y}$ $(y_1, y_2, \ldots y_m)$ can be estimated by statistical regression, optimization or a combination of both. In the present work, m was chosen for accounting for 99.5% of data variance.

2.4. PLS Statistical regression

To estimate of a new body shape from p predictors $x_1, x_2, \ldots x_p$ such as stature, crotch height, waist circumference, etc, the problem now is to estimate m unknown scores $y_1, y_2, \ldots y_m$. As predictors such as anthropometric dimensions are generally correlated, the partial least (PLS) regression is a good technique. As for multiple linear regression, PLS regression takes the same form with the model parameters $\beta_{j,k}$ which relates p predictors $x_k, k = 1, p$ with for m PC scores $y_j, j = 1, m$. The predictors are not limited to anthropometric dimensions. They can be postural variables as well as landmarks.

2.5. Optimisation

Once statistical shape models (SSMs) obtained by PLS regression, they can be used to predict a full body shape using a small number of predictors. An optimization procedure is proposed to find the PC scores $\mathbf{y}$ to better match target predictors while not too much deviating the prediction by SSM. The objective function is defined as

$$f(y_1, y_2, \ldots y_m) = \rho_1 \left(\frac{1}{p_1} \sum_{i=1}^{p_1} \left(x_{ai}^{target} - x_{ai}^{current} \right)^2 \right) + \rho_2 \left(\frac{(H/4)^2}{p_2} \sum_{i=1}^{p_2} \left(x_{pi}^{target} - x_{pi}^{current} \right)^2 \right) + (1 - \rho_1 - \rho_2) \left(\frac{1}{v} \sum_{j=1}^{v} \| \boldsymbol{v}_j^{current} - \boldsymbol{v}_j^{ssm} \|^2 \right) \quad (2)$$

While x_{ai}^{target}, x_{pi}^{target}, $x_{ai}^{current}$, $x_{pi}^{current}$ are i^{th} target and current anthropometric and postural predictor values, $\boldsymbol{v}_j^{current}$, $\boldsymbol{v}_j^{ssm}$ are j^{th} vertex of the current mesh and one predicted by SSM. p_1 and p_2 are number of anthropometric and postural predictors. H is stature. Multiplying the differences between target and current postural angles by H/4 to is to convert postural difference in distance for facilitating the definition of weighting coefficients ρ_1 and ρ_2. In the present work, they were fixed as $\rho_1 = 0.5$, $\rho_2 = 0.3$.

When landmarks are used as predictors, we prefer using the optimization algorithm proposed by Rajamani et al. [8] for reason of efficiency in calculation. PC scores are found by minimizing the distance between target and current landmarks while not too much deviating the mean body shape $\bar{\boldsymbol{\mu}}$.

2.6. Leave-one-out cross validation

Four methods of prediction based on predictors were tested:

1. Stature, Crotch height, Waist circumference, 5 postural angles
2. 1 + Hip circumference + Chest circumference
3. 2 + Arm length + Thigh circumference + Upper arm circumference
4. 27 landmarks

To reduce the body shape variability due to postural change, all five postural parameters were used as predictors for the first three methods.

For each set of predictors, a leave-one-out (LOO) cross validation was performed. For each scan, its data was used to define the predictors, while the rest of scans were used to build SSM. Predicted shapes were aligned with the original one using 27 landmarks. The predictions by optimization were compared with the original body shape model after template fitting. The following parameters are calculated:

- Root mean square errors in the predictors used as targets (RMS_pr)
- Root mean square errors in 18 anthropometric dimensions (RMS_an)
- Root mean square distances between predicted and original vertices for the whole body (RMS_wb)
- Root mean square distances between predicted 27 landmarks and original ones (RMS_lm), which is equal to RMS_pr for Method 4.

3. Results

656 simulations (164 subjects x 4 sets of predictors) were performed for LOO validation. Means and standard deviations for RMS_pr, RMS_an, RMS_wb and RMS_lm are summarized in Table 2. Concerning the error between target and predicted parameters, RMS_pr was all lower than 4 mm on average. For anthropometric dimensions, significant differences in RMS_an between four methods of prediction were observed. Method 3 had the lowest error, while Method 4 obtained the lowest error for whole body vertices and landmarks. Comparing three first methods, lower error in anthropometric parameters was observed when increasing the number of anthropometric predictors. Using 27 landmarks as predictors, the errors in whole body vertices could be highly reduced (lower than 10 mm on average). However, the error in anthropometric dimensions was not reduced as much as for vertices.

Table 2. Means and standard deviations (in mm) of the root mean square errors in the predictors (RMS_pr) and all 18 extracted anthropometric dimensions (RMS_an), root mean square distances between predicted and original vertices (RMS_wb) for the whole body and between predicted 27 landmarks and original ones (RMS_lm) for four sets of predictors.

Method	RMS_pr		RMS_an		RMS_wb		RMS_lm	
1	1.87	±1.15	22.67	±7.45	21.20	±5.46	22.47	±6.29
2	2.73	±1.38	17.67	±5.25	21.29	±5.33	22.64	±6.05
3	2.41	±1.63	14.76	±4.86	21.94	±5.58	23.26	±6.29
4	3.92	±0.54	19.13	±6.28	9.75	±2.11	3.92	±0.54

4. Discussion

In the present work, we have developed PCA based statistical body shape models (SBSM) from 164 European and Chinese males and implemented two optimization algorithms to find PC scores to better match target predictors while preserving the body shape predicted by SBSM. Four methods by predictors were compared by LOO cross validation.

Results are in agreement with *a priori* expectations. More anthropometric predictors resulted in lower errors in extracted anthropometric dimensions. Compared to Method 1 with three anthropometric dimensions as targets (stature, crotch height and waist circumference), five additional anthropometric targets (arm length, circumferences at the hip and chest, thigh and upper arm circumference) reduced the error in 18 extracted anthropometric dimensions by 35% (from 23 to 15 mm on average). However, no significant differences in RMS_wb and RMS_lm were found between three first methods. This is probably because body shape error is much more dependent on posture than error in anthropometric dimensions, and five postural angles used in this work could not fully describe the body shape variation due to postural change between different subjects. Figure 3 shows the predictions by 4 methods for two subjects, one with lower prediction errors in both anthropometric dimensions and body shape, and one with larger errors. Higher errors for the second subject are mainly due to postural difference, especially for the arms.

Method 4 used 27 body landmarks as targets. Less than 10 mm on average in root mean square distances between predicted and original mesh vertices was obtained, much lower than the predictions by the first three methods. However, the error in anthropometric dimensions was higher than the error by Method 3. The 27 landmarks were mainly selected to define internal joint centers. Apart from three landmarks (navel, right and left nipples), all others correspond to bony landmarks. From Figure 3, one can see that Method 4 could predict a body shape with good posture. However, as no landmarks could provide the information about the circumferences of four members, the error in anthropometric dimensions was not much reduced. To further improve the prediction; additional landmarks should be added providing the information about the circumferences of different body segments. We should note that landmarks were virtually palpated on raw scans. Palpation may not be repeatable and there may be large inter-operator even intra palpation variability.

The distances between predicted and original vertices for the whole body (RMS_wb) provide a valuable metric for assessing different prediction methods. The node-to-node distance overestimates the distance between surfaces. A node-to-surface distance could be more relevant and could be considered in the future.

As prediction error depends on the choice of predictors, depending on application, a minimum number of predictors should be determined. One can for example refer to ISO 20685-1 [9] to define the maximum allowable error between predicted and scan extracted values.

In summary, combining a statistical body shape model (SBSM) and an optimization procedure can predict a subject-specific whole body shape with a small number of predictors. Prediction accuracy depends on number of predictors. With only three anthropometric dimensions (stature, crotch height and waist circumference), we observed the root mean square errors in both anthropometric dimensions and whole body shape less than 23 mm. Prediction error could be further reduced by using more postural parameters. We are planning to create a full articulated skeleton with help of bony landmarks and calculate corresponding joint angles. Surface markers attached on the body are usually used for motion and postural analysis. Our results show that it is possible to generate an accurate whole body surface from these landmarks. To improve prediction accuracy, non-bony landmarks should be added to provide information about segment size.

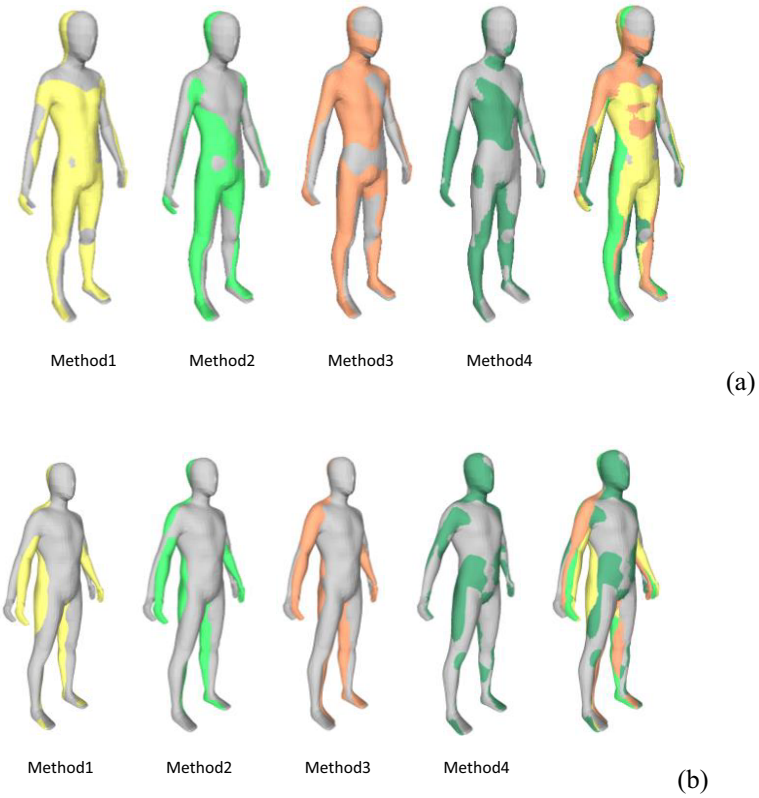

Figure 3. Illustration of the body shapes predicted by four different methods for two subjects. From left to right, predictions by Method 1 to 4 are superimposed with the original model after template fitting. (a) A subject with smaller errors in both anthropometric dimensions and whole body shape with RMS_an=9.1 mm, RMS_wb=18.8 mm for Method 3. (b) A subject with larger prediction errors with RMS_an=20 mm, RMS_wb=33 mm for Method 3.

References

[1] Wang X, Chevalot N, Monnier G, Ausejo S, Suescun Á, Celigüeta J. Validation of a model-based motion reconstruction method developed in the Realman project. SAE 2005 International conference and exposition of Digital Human Modeling for Design and Engineering, Iowa city, IA, Etats-Unis, 14–16 June 2005, SAE Paper 2005–01–2743, 2005.

[2] Shu C, Wuhrer S, Xi P. 3D anthropometric data processing. Int. J. of Human Factors Modeling and Simulation, 2012, 3(2), 133-146.

[3] Allen B, Curless B, Popovic Z. The space of all body shapes: reconstruction and parameterization from range scans. ACM Transactions on Graphics (ACM SIGGRAPH 2003), 22, 3, 587-594

[4] Park BK, Lumeng JC, Lumeng CN, Ebert SM, Reed MP. Child body shape measurement using depth cameras and a statistical body shape model. Ergonomics, 2015, 58(2), 301-309, DOI: 10.1080/00140139.2014.965754.

[5] Bogo F, Kanazawa A, Lassner C, Gehler P, Romero J, Black MJ. Keep it SMPL: Automatic Estimation of 3D Human Pose and Shape from a Single Image. arXiv:1607.08128 [cs], 27 July 2016. http://arxiv.org/abs/1607.08128.

[6] Baek SY, Lee K. Parametric Human Body Shape Modeling Framework for Human-Centered Product Design. Computer-Aided Design, Digital Human Modeling in Product Design, 2012, 44(1), 56-67. https://doi.org/10.1016/j.cad.2010.12.006.

[7] Yamazaki S, Kouchi M, Mochimaru M. Markerless landmark localization on human body scans by non-rigid model fitting. Proceedings of the 2nd International Symposium on Digital Human Modelling (DHM2013), Ann Arbor, Michigan, USA, June 11-14, 2013.
[8] Rajamani K, Styner M, Talib H, Zheng G, Nolte L, Ballester M. Statistical deformable bone models for robust 3D surface extrapolation from sparse data. Medical Image Analysis, 2007, 11(2), 99-109.
[9] NF EN ISO 20685-1:2018. 3-D scanning methodologies for internationally compatible anthropometric databases - Part 1 : evaluation protocol for body dimensions extracted from 3-D body scans. CEN-CENELEC Management Centre: Rue de la Science 23, B-1040 Brussels, 2018.

This page intentionally left blank

Part 2

Behaviour and Biomechanical Modeling

This page intentionally left blank

DHM2020
L. Hanson et al. (Eds.)

© 2020 The authors and IOS Press.
This article is published online with Open Access by IOS Press and distributed under the terms of the Creative Commons Attribution Non-Commercial License 4.0 (CC BY-NC 4.0).
doi:10.3233/ATDE200009

Learning Individual Driver's Mental Models Using POMDPs and BToM

Amena DARWISH [1] and H. Joe STEINHAUER [2]
University of Skövde, School of Informatics, 541 28 Skövde, Sweden

Abstract. Advanced driver assistant systems are supposed to assist the driver and ensure their safety while at the same time providing a fulfilling driving experience that suits their individual driving styles. What a driver will do in any given traffic situation depends on the driver's mental model which describes how the driver perceives the observable aspects of the environment, interprets these aspects, and on the driver's goals and beliefs of applicable actions for the current situation. Understanding the driver's mental model has hence received great attention from researchers, where defining the driver's beliefs and goals is one of the greatest challenges. In this paper we present an approach to establish individual drivers' temporal-spatial mental models by considering driving to be a continuous Partially Observable Markov Decision Process (POMDP) wherein the driver's mental model can be represented as a graph structure following the Bayesian Theory of Mind (BToM). The individual's mental model can then be automatically obtained through deep reinforcement learning. Using the driving simulator CARLA and deep Q-learning, we demonstrate our approach through the scenario of keeping the optimal time gap between the own vehicle and the vehicle in front.

Keywords. Driver Mental Model, Partially Observable Markov Decision Processes (POMDPs), Bayesian Theory of Mind (BToM), Reinforcement Learning

1. Introduction

Advanced driver assistance systems [1] (ADAS) are supposed to aid a car's driver to drive safely and comfortably in various driving situations. For example, the adaptive cruise control [1] (ACC) will dynamically adjust the vehicle's speed in order to keep a safe distance to the vehicle in front. However, human drivers have individual driving styles [2-4], which are based on their previous experience, cultural inheritance and personality traits and will also differ depending on the driving environment. Personalization of ADAS systems is thus of interest for car manufactures in order to enhance the individual's driving experience and satisfaction [5, 6]. With car sharing becoming more popular, the car's driver will change more frequently and a quick adaptation based on relatively little data is needed to personalize the driving experience and to ensure traffic safety.

In cases where the ADAS' actions are not to the individual driver's satisfaction [7], the driver might get annoyed and agitated which might negatively affect their driving capabilities and put them and other traffic participants at risk. Another risk is that the driver becomes preoccupied by trying to counteract the ADAS which takes away their

[1] Corresponding Author, Email: amena.darwish@his.se.
[2] Corresponding Author, Email: joe.steinhauer@his.se.

attention from the traffic situation, or that the driver might simply switch the system off and consequently also loses all its safety features [8, 9].

Hence, efforts should be made to build driver assistance systems that are capable of adapting to the individual driver's preferences within different road and traffic situations. This means that the ADAS should be able to learn the driving style and preferences of the individual driver and adapt to them as long as traffic safety is ensured. The challenges for this endeavor are manifold. Machine learning usually takes time and needs a lot of data, which is not an option when the situation requires that learning takes place online during actual driving in real traffic and driver satisfaction requires that the recognizable learning phase is kept to an absolute minimum.

In recent years, deep reinforcement learning has shown to achieve high performance in many different tasks, ranging from game playing [10, 11] to autonomous driving [12, 13]. The advantage of deep reinforcement learning is that the learner is able to learn from experience and can continue to learn while already in use. For the personalizable ADAS this would mean that on top of the normal ADAS functions, a learning module can be deployed that will, based on the driver's reaction to the ADAS' actions, learn how to better accommodate the driver.

In this paper we will illustrate this approach by focusing on one function within the ADAS, namely the adaptive cruise control (ACC) and the important scenario of keeping an optimal time gap between the own car (ego vehicle) and the car in front (lead vehicle). This distance is usually calculated with regard to the travel speed and given in seconds. A gap of two-three seconds is the usually recommended distance. This time gap is estimated to account for the reaction time of the ego driver to any changes in behavior of the lead vehicle. However, the actual distance that a driver prefers to keep will be influenced by their personality and different aspects of the environment. For example, preferences might depend on if the driving takes place in rural or urban areas, peak or off-peak traffic, dry or wet roads, night or day time conditions with street lights or in darkness, the driver's stress level, the reason for traveling (e.g. cruising for leisure or hurry to the hospital) etc.

In order to apply a time gap that safely accounts for the driver's reaction time, we need to take into account that today's cars free the driver of certain driving tasks, e.g. through dynamic cruise control and lane keeping. When less attention is needed to focus on the driving task a driver's attention might wander to other areas, such as selecting music, attending children, using the telephone, etc. This would call for an increased time gap [14]. However, the engaged and active driver who is fully focused on the traffic situation and, for example, planning to overtake the lead vehicle as soon as possible, might prefer and be safe with a shorter time gap.

The challenge that we will address within this work, is how the ACC can automatically learn the driver's preferences regarding the time gap to the lead vehicle. For this we consider driving to be a Partially Observable Markov Decision Process [15] (POMDP) wherein the individual's driving style depends on their individual mental model for driving. We regard this mental model to be a graph structure that can be represented by the Bayesian Theory of Mind (BToM) e.g. [16, 17]. This makes it possible that the individual's graph structure can then be automatically obtained through deep reinforcement learning. This approach has previously only been used on aggregated drivers' data using a Gaussian learning algorithm where it has led to promising results in mimicking realistic driver behavior in certain situations [18].

In this paper, we provide a novel approach of using deep Q-learning on individual driver's data to personalize the driving experience which we will demonstrate for the

time gap scenario through implementation of an assistant for the ACC (the ACC assistant (ACCA)). The ACCA will based on the driver's reactions learn to suggest the adjustment of the time gap in accordance with driver preferences.

2. Method

We regard driving to be a Partially Observable Markov Decision Process (POMDP) as illustrated in Figure 1. It means that the environment, which at time t is in state s_t, will only be partially observed, these observations o_t, are described by the probability function $P(o_t|s_t)$ based on the observations o_t at time t, the driver makes a decision for an action a_t which will be carried out and leads to changes in the environment in the next time step (t+1) leaving the environment in state s_{t+1}. What impact the action a_t has on the environment is determined by another probability function $P(s_{t+1}|s_t, a_t)$.

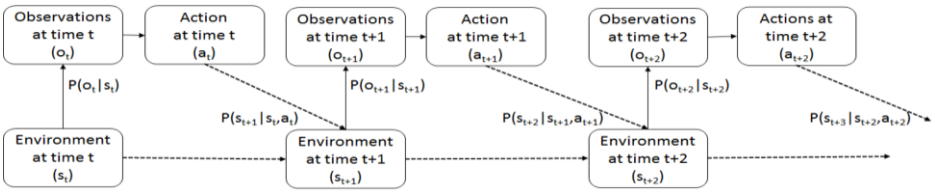

Figure 1. Driving illustrated as a Partially Observable Markov Decision Process (POMDP). The environment at time t is partially observable. Based on these observations o_t the driver will decide on an action a_t. The action will with probability $P(s_{t+1}|s_t, a_t)$ influence the next state of the environment s_{t+1}.

We argue that the driver's mental model that represents the grounds on which the driver is taking his or her decision for an action can be represented through a graph structure using the Bayesian Theory of Mind (BToM), which is commonly used to infer the mental reasoning and mental states of an observed agent by using probabilistic inverse planning [16, 18]. This graph structure captures the driver's knowledge about driving, their beliefs about what actions are applicable in what situation and their goals which will influence which of the applicable actions they will decide on in the given situation. Different individuals will have different graph structures which depend on their experiences, character traits, cultural background, etc. In our case, the observed agent is the vehicle's driver and the observer is the ADAS that needs to understand the driver's mental model in order to be of better assistance to them. In practice this means that the ADAS should be able to map any given state of the environment to the most likely action the driver will take. The "mind of the driver" as the ADAS sees it according to the Theory of Mind [17], denotes the belief that is recursively inferred using a probability distribution over the environment states.

$$b_{t+1} \propto P(o_{t+1}|\, s_{t+1})\, P(s_{t+1}|s_t\,, a_t)\;\; b_t \tag{1}$$

The belief b_{t+1} (at time point t+1) is calculated based on the probability of the observations o_{t+1} given the state of the environment s_{t+1} and on the belief b_t that with probability $P(s_{t+1}|s_t\,, a_t)$ that this state s_{t+1} will have occurred given that action a_t has been executed in the previous state s_t .

Based on the Bellman equation [19] the formula for the quality Q of a state-action pair can be calculated as by [20]:

$$Q\left(s_t, a_t\right) = \alpha\left(r\left(s_t, a_t\right) + \gamma \max_a Q\left(s_{t+1}, a\right)\right) \quad (2)$$

Where the quality, Q of applying action a_t in state s_t is calculated recursively by the sum of the immediate reward $r\left(s_t, a_t\right)$ and the maximum reward that can be obtained in the future over action space $\max_a Q\left(s_{t+1}, a\right)$. α Defines the learning rate and γ represents the discounting factor for the importance of rewards achievable in the future.

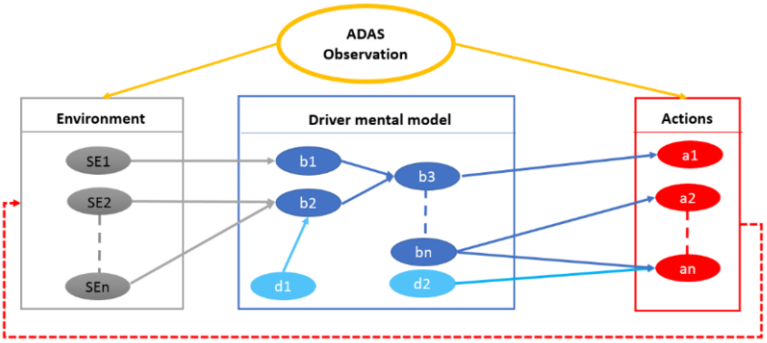

Figure 2. The driver's mental model expressed through the Bayesian Theory of Mind (BToM) (in blue), the input to the mental model will be the environment that can be represented through all observable elements (SEs) in the environment (in grey). The output from the mental model is the driver's action which is one of many possible actions to choose from (in red). The action will influence the environment (represented through the dashed line). The combination of these three results in a structure similar to a deep artificial neural network (ANN). The ADAS is represented as the observer who can observe the observable elements in the envoronment as well as the driver's reaction, but to whom the driver's mental model is a black box.

To update the beliefs we will apply deep Q-learning [21, 22] and regard the graph structure of the mental model to be the hidden layers of a deep ANN as shown (in blue) in Figure 2. The input to this network is the state of the environment, provided by an RGB camera image and the output is the action that the driver is most likely to take in this state. The individual's mental model will hence be expressed by the weights assigned to the connections between the nodes in the network, which will be learned through deep reinforcement learning.

Using an ANN in that way to approximate the POMDPs output is a common approach [23]. Here we use TensorFlow to implement equation (2) and use two different deep Q-learning networks, one to obtain $Q(s_t, a_t)$ and $Q(s_{t+1}, a)$ over the action space, respectively. For the implementation we use the Xception model [24] provided in Keras using RGB camera images with 720x1280 pixels as input. For the simulation we use CARLA (CAR Learn to Act) which is an open source simulator for autonomous driving [25]. Specifically, we use Scenario Runner [26] v.0.9.8, which also is an open source repository containing traffic scenario definitions and an execution engine for CARLA. In CARLA we can simulate the driving environment, choose from different weather and lightning conditions, and include other traffic participants. CARLA provides different sensors for the car, among them the RGB camera images (720x1280 pixels), that will provide the input to the deep Q-learning algorithm.

Initially, our task is to personalize the ACC to the individual driver's preferences, which will be learned from the driver's reactions to the ACC's driving. CARLA, however, does not provide ACC functions that we could build upon. Hence, in order to build an ACC we use the deep reinforcement learning approach for deep Q-learning inspired by [27] and [28, 29]. Once the ACC is in place it will be set to drive the car and a program mimicking an individual driver will intervene through either breaking or accelerating whenever the time gap is not to the driver's liking.

The ACCA that learns the individual driving style, gets as input the environment through the RGB camera image as well as the actions that the ACC performs on this input together with the driver's feedback. The feedback is coupled to the driver's actions, which will be to accelerate if the time gap that is kept by the ACC is too wide, or to break if the time gap is considered to be too small. The ACCA will, based on this, learn the driver's individual preferences. As output it will provide suggestions to the ACC on how to adjust the time gap.

The ACC itself has learned to always follow the lead vehicle in a safe distance, through keeping it in the green zone (see the illustration in Figure 3b) but when the personalized suggestions from the ACCA are added, the ACC will act according to these suggestions instead. This can result in reducing the time gap to an extent where the lead vehicle will be allowed in the yellow zone just adjacent to the red zone. Note, however, that it is not possible for the ACCA to suggest a time gap that would allow the lead vehicle into the red zone.

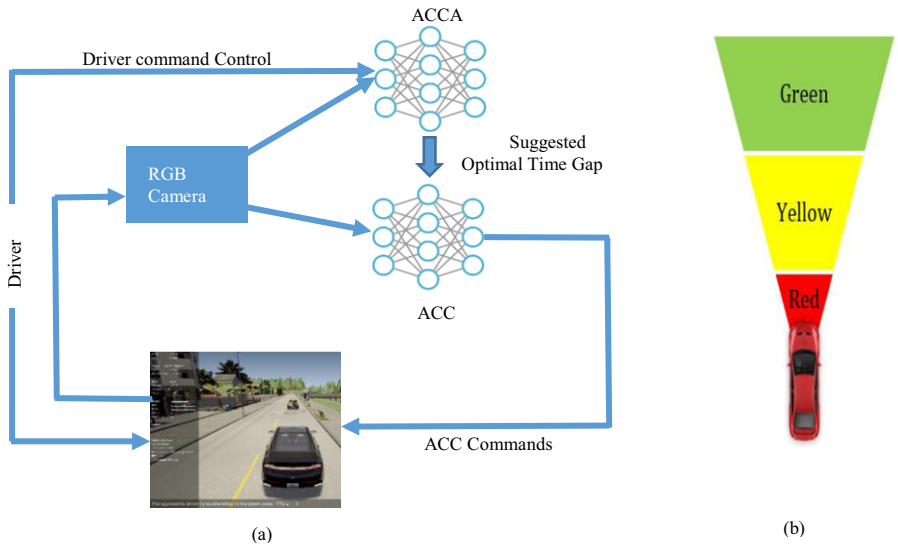

Figure 3. (a) After the system is trained, the RGB image is fed to the ACC and the ACCA alike, the ACCA knows the current time gap (which is part of the environment) and suggests an adjustment to the ACC. The ACC will adjust the time gap accordingly. Note, the ACCA cannot suggest time gaps that are outside safety parameters. (b) An illustration of the different time-gap zones considered in our approach. When the lead vehicle is within the green zone the time gap is considered to be long enough for safe following in all circumstance, when the lead vehicle is in the yellow zone the driver should be actively engaged in driving. The lead vehicle is not allowed in the red zone at all. If the time gap to the lead vehicle becomes larger than the green zone it will be considered to be free driving.

3. Results

The training takes place on the Town01 map in CARLA. The initial distance between ego vehicle and lead vehicle is set to 15 m, the lead vehicle travels with 8 m/s and the initial time gap is set to 5 seconds. We train for 100 episodes; each episode is comprised of 15 steps, unless calculations within steps take unusually long and the episode is ended through a time out after 30 seconds. During training, the ACC learns how to maximize the cumulative sum of rewards (return) over episodes. It receives -200 for a collision with the lead vehicle, +10 when the lead vehicle is kept in the green zone, and -10 if the lead vehicle has entered the red zone. A similar approach has been used by [27] and is formally expressed in equation (3).

$$r = 200\, r_{collision} + 10\, r_{greenzone} + r_{yellowzone} + 10\, r_{redzone} + 0.2\, v_{log}^2 + 0.1 \qquad (3)$$

Where $r_{collision}$ = -1, $r_{colorzone}$ = +1 (within the yellow and green zone) and $r_{colorzone}$ = -1 within the red zone, v_{log} represents the longitudinal speed of the ego vehicle (measured in m/s) and 0.2* v_{log}^2 is needed to prevent the ego vehicle from driving unnecessarily slow, the last summand (0.1) is used to prevent the car from stopping.

How quickly and accurately the algorithm will learn depends, among others, also on the quality of input from the environment. We expect the learning to take longer when sight is poor and hence have chosen to use two different environmental conditions that are available in CARLA. One represents daytime conditions with clear weather, the other sunset illumination on wet roads. The graphs, presented in Figure 4, show that the algorithm learns how to keep an appropriate time gap. They also show, as expected, that the weather condition does influence the learning based on the RGB camera input and that in clear weather conditions a better outcome is received.

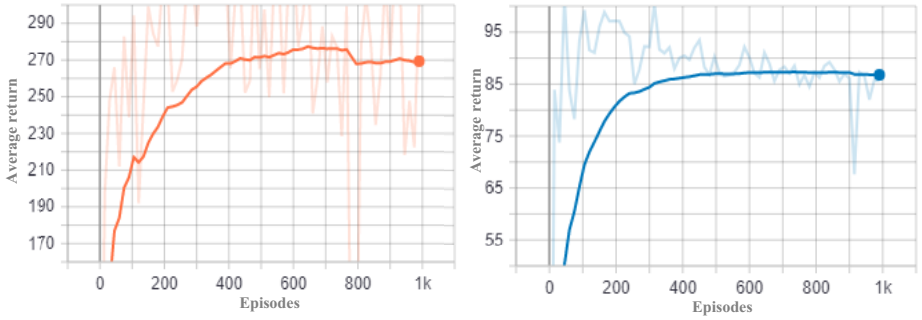

(a) (b)

Figure 4. (a) Average return for the ACC in clear weather. (b) Average return for the ACC in wet sunset weather.

For the ACCA, the deep Q-learning algorithm can choose between three different actions that it will suggest to the ACC: increase the time gap by 0.2 s, decrease the gap by 0.2 s (as long as the new time gap will still be within safety parameters) or keep the time gap as it is. During learning the reward for the ACCA is defined as presented in equation (4).

$$r = 200\, r_{collision} - \sum_{zone=1}^{2} r_{colorzone}\, r_{driver} \left| r_{diff} \right| + 0.2\, v_{log} + 0.1 \qquad (4)$$

With $r_{collision}$ = -1, $r_{colorzone}$ = 1 if the ego vehicle is in the respective color zone, otherwise $r_{colorzone}$ = 0, r_{driver} = 1 when the driver controls the ego vehicle otherwise r_{driver} = 0, r_{diff} represents the difference between the recommended time gap and the predicted optimal time gap, unless there is no difference then r_{diff} =10. v_{log} is the longitudinal speed of the ego vehicle measured in m/s, and also here 0.2* v_{log} is needed to prevent the ego vehicle from being unnecessarily slow as well as the last summand (0.1) is needed to prevent the car from stopping. This assures that the ACCA tries to maximize the return for each episode by keeping the time gap to the driver's satisfaction and does not crash into the lead vehicle.

We test our approach for two different driving styles, one describing a conservative driver who wants to follow the lead vehicle at a distance that in all circumstances would be considered to be safe and would place the lead vehicle into the green zone (illustrated in Figure 3 (b)); the other describing a more aggressive driver who wants to be as close to the lead vehicle as possible which would bring it within the red zone.

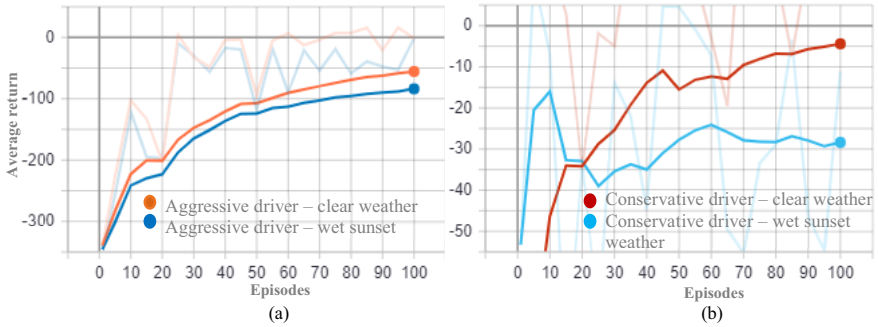

Figure 5. (a) Average return for the aggressive diver. (b) Average return for the conservative driver.

The results presented in Figure 5 show also here that the weather conditions have a significant influence when it comes to the conservative driver. They also show that it is in general harder for the ACCA to please the aggressive driver, due to the fact that the aggressive driver would want to follow the lead vehicle too closely which is not possible with the given safety parameters. However, the weather seems not to influence the learning as much for the aggressive driver. This gives rise to the speculation the ACCA learns just to keep the gap as short as possible and is not analyzing the RGB images of the environment as well as it does for the conservative driver.

To validate our results, we use the success rate that is commonly used in games and robotic domains [30] and describes how many times the agent is able to reach the goal. Here the goal is to suggest a time gap that is accepted by the driver where acceptance means that the driver will not adjust the gap through accelerating or breaking manually during the considered time interval. Table 1 shows the success rate for both our driver types for the clear weather condition.

Table 1. Success and fail rate for the aggressive and the conservative driver and the average time gap in all cases respectively as well as the difference in time gap (in seconds) between average success and average fail for the clear weather condition.

Driver style	Success rate	Average time gap when successful	Fail rate	Average time gap when failed	Difference in time gap
Aggressive	61.91%	1.25	38.09%	2.57	**1.32**
Conservative	63.46%	4.31	36.54%	6.07	**1.76**

4. Discussion

In this study we looked at driving from the perspective of the ADAS, which is supposed to predict the driver's actions from observations of the environment and the driver. The main contribution in our work is hence the approach to use POMDPs wherein the driver's mental model can be represented as a graph structure that follows the BToM and can, together with the input from the environment and the output (action) that the driver choses, be regarded as a deep ANN. For this deep ANN the weights that account for the individual driver's mental model can be learned by deep reinforcement learning (in this case deep Q-learning). Note, that the novelty of our approach lies in the combination of these techniques and their application to personalize the driving experience for the individual driver.

From an applicational point of view the personalization of the driving experience, where the ADAS learns the preferences of the individual driver while at the same time ensuring traffic safety is an important task for the automobile industry. Achieving personalization requires data-driven approaches and requires that the system is able to adapt quickly to the driver's needs and habits and keeps adapting while the driver's behavior and preferences evolve as well over time and with experience [5, 6]. Hence, the system should be able to adapt in real time which means on the bases of very little data. This exceeds previous work done for example for aircraft autopilots e.g. [31] or to model human driving on a general, not individual, level [32]. Our work describes personalization for the relatively simple driving scenario of following a lead vehicle. In reality the system should be able to adapt to many different scenarios in parallel (e.g. overtaking, turning, approaching traffic light, approaching zebra crossing).

So far, validation of the system has been done by looking at the success rate. Further research is needed to see if this can be further improved when using a different reward function. Once the system is tested within a real car and against a human driver further validation will be done by the drivers through questionnaires about the driving experience and satisfactions.

Future work will include to broaden the driving scenario where individual preferences are also dependent on the type of road, the amount of surrounding traffic, and the in-car situation. There is increasing work on autonomously driving cars, several of which are implemented in CARLA with very good results (see for example [27]). Approaches similar to them could replace the ACC in our example and represent a complex driver assistant system that then will, following the approach presented here, become personalizable through deep Q-learning.

Acknowledgement

This work has been supported by VINNOVA, the Swedish Government Agency for Innovation Systems, proj. "Intention Recognition for Real-time Automotive 3D situation awareness (IRRA)", in the funding program FFI: Strategic Vehicle Research and Innovation (DNR 2018-05012)

References

[1] American Automobile Association. Advanced driver assistance technology names: AAA's recommendation for common naming of advanced safety systems. AAA News Room, January, 2019.
[2] Witt M, Wang L, Fahrenkrog F, Kompaß K, Prokop G. Cognitive Driver Behavior Modeling: Influence of Personality and Driver Characteristics on Driver Behavior. In: Stanton N, editor. Advances in Human Aspects of Transportation. AHFE 2018, 751-763. Springer, Cham.
[3] Bellet T, Bornard JC, Richard B, Laverdure. Use of a cognitive simulation model of the driver to support the Virtual Human Centred Design (V-HCD) of ADAS and automated vehicles, 2018. In: Graz Symposium Virtual Vehicle: Artifical Intelligence Meets Model-Centric Design.
[4] Chen H, Zhao F, Huang K, Tian Y. Driver behavior analysis for advanced driver assistance system. In: 2018 IEEE 7th Data Driven Control and Learning Systems Conference (DDCLS), 2018, May, 492-497. IEEE.
[5] Hasenjäger M, Heckmann M, Wersing H. A Survey of Personalization for Advanced Driver Assistance Systems. IEEE Transactions on Intelligent Vehicles, 2019, 5(2), 335-344.
[6] Yi D, Su J, Hu L, Liu C, Quddus MA, Dianati M, Chen WH. Implicit personalization in driving assistance: State-of-the-art and open issues. IEEE Transactions on Intelligent Vehicles, 2019.
[7] Strand N, Nilsson J, Karlsson IC, Nilsson L. Interaction with and use of driver assistance systems: a study of end-user experiences. In: Proceedings of the 18th ITS World Congress. Washington, DC: ITS America, 2011.
[8] Aziz T, Horiguchi Y, Sawaragi T. Towards understanding the development of driver's mental model of a Lane Departure Warning system while driving. Journal of Advanced Mechanical Design, Systems, and Manufacturing, 2014, 8(3), JAMDSM0032-.
[9] Heikoop DD, de Winter JC, van Arem B, Stanton NA. Psychological constructs in driving automation: a consensus model and critical comment on construct proliferation. Theoretical Issues in Ergonomics Science, 2016, 17(3), 284-303.
[10] Mnih V, Kavukcuoglu K, Silver D, Graves A, Antonoglou I, Wierstra D, Riedmiller M. Playing atari with deep reinforcement learning. arXiv preprint arXiv:1312.5602, 2013, Dec 19.
[11] Mnih V, Kavukcuoglu K, Silver D, Rusu AA, Veness J, Bellemare MG, Graves A, Riedmiller M, Fidjeland AK, Ostrovski G, Petersen S. Human-level control through deep reinforcement learning. Nature, 2015, 518, 529-533.
[12] Kiran BR, Sobh I, Talpaert V, Mannion P, Sallab AA, Yogamani S, Pérez P. Deep reinforcement learning for autonomous driving: A survey. arXiv preprint arXiv:2002.00444, 2020, Feb 2.
[13] Sallab AE, Abdou M, Perot E, Yogamani S. Deep reinforcement learning framework for autonomous driving. Electronic Imaging, 2017, (19), 70-76.
[14] Salvucci DD. Predicting the effects of in-car interface use on driver performance: An integrated model approach. International Journal of Human-Computer Studies, 2001, 55(1), 85-107.
[15] Bai H, Cai S, Ye N, Hsu D, Lee WS. Intention-aware online POMDP planning for autonomous driving in a crowd. In: 2015 IEEE international conference on robotics and automation (icra), 2015, May, 454-460. IEEE.
[16] Sukthankar G, Geib C, Bui HH, Pynadath D, Goldman RP, editors. Plan, activity, and intent recognition: Theory and practice. Newnes, 2014, Mar 3.
[17] Doherty M. Theory of mind: How children understand others' thoughts and feelings. Psychology press, 2008, Aug 26.
[18] Eilers M, Möbus C, Tango F, Pietquin O. The learning of longitudinal human driving behavior and driver assistance strategies. Transportation research part F: traffic psychology and behavior, 2013, 21, 295-314.
[19] Sutton RS, Barto AG. Reinforcement learning: An introduction. MIT press, 2018, Oct 19.
[20] Stekolshchi, R. How does the Bellman equation work in Deep RL? 2020, Towards Data Science.
[21] Hausknecht M, Stone P. Deep recurrent q-learning for partially observable mdps. In: 2015 AAAI Fall Symposium Series, 2015, Sep 23.
[22] Egorov M. Deep reinforcement learning with pomdps, 2015.

[23] Hauskrecht M. Value-function approximations for partially observable Markov decision processes. Journal of artificial intelligence research, 2000, 13, 33-94.
[24] Chollet F. Xception: Deep learning with depthwise separable convolutions. In: Proceedings of the IEEE conference on computer vision and pattern recognition, 2017, 1251-1258.
[25] Dosovitskiy A, Ros G, Codevilla F, Lopez A, Koltun V. CARLA: An open urban driving simulator. arXiv preprint arXiv:1711.03938, 2017, Nov 10.
[26] GitHub. 2020. Carla-Simulator/Scenario_Runner. [online] Available at: <https://github.com/carla-simulator/scenario_runner> [Accessed 13 May 2020].
[27] Chen J, Li SE, Tomizuka M. Interpretable end-to-end urban autonomous driving with latent deep reinforcement learning. arXiv preprint arXiv:2001.08726, 2020, Jan 23.
[28] Bojarski M, Del Testa D, Dworakowski D, Firner B, Flepp B, Goyal P, Jackel LD, Monfort M, Muller U, Zhang J, Zhang X. End to end learning for self-driving cars. arXiv preprint arXiv:1604.07316, 2016, Apr 25.
[29] Dharmawan W, Nambo H. End-to-End Xception Model Implementation on Carla Self Driving Car in Moderate Dense Environment. In: Proceedings of the 2019 2nd Artificial Intelligence and Cloud Computing Conference, 2019, Dec 21, 139-143.
[30] Zhang F, Leitner J, Milford M, Upcroft B, Corke P. Towards vision-based deep reinforcement learning for robotic motion control. arXiv preprint arXiv:1511.03791, 2015, Nov 12.
[31] Wickens CD, McCarley JS, Alexander AL, Thomas LC, Ambinder M, Zheng S. Attention-situation awareness (A-SA) model of pilot error. Human performance modeling in aviation, 2008, 213-39.
[32] Bellet T, Bailly-Asuni B, Mayenobe P, Banet A. A theoretical and methodological framework for studying and modelling drivers' mental representations. Safety Science, 2009, 47(9), 1205-1221.

DHM2020
L. Hanson et al. (Eds.)

© 2020 The authors and IOS Press.
This article is published online with Open Access by IOS Press and distributed under the terms of the Creative Commons Attribution Non-Commercial License 4.0 (CC BY-NC 4.0).
doi:10.3233/ATDE200010

Automatic Selection of Viewpoint for Digital Human Modelling

Erik BILLING [a,1], Elpida BAMPOUNI [a], and Maurice LAMB [a]
[a] *Interaction Lab, University of Skövde, Sweden*

Abstract. During concept design of new vehicles, work places, and other complex artifacts, it is critical to assess positioning of instruments and regulators from the perspective of the end user. One common way to do these kinds of assessments during early product development is by the use of Digital Human Modelling (DHM). DHM tools are able to produce detailed simulations, including vision. Many of these tools comprise evaluations of direct vision and some tools are also able to assess other perceptual features. However, to our knowledge, all DHM tools available today require manual selection of manikin viewpoint. This can be both cumbersome and difficult, and requires that the DHM user possesses detailed knowledge about visual behavior of the workers in the task being modelled. In the present study, we take the first steps towards an automatic selection of viewpoint through a computational model of eye-hand coordination. We here report descriptive statistics on visual behavior in a pick-and-place task executed in virtual reality. During reaching actions, results reveal a very high degree of eye-gaze towards the target object. Participants look at the target object at least once during basically every trial, even during a repetitive action. The object remains focused during large proportions of the reaching action, even when participants are forced to move in order to reach the object. These results are in line with previous research on eye-hand coordination and suggest that DHM tools should, by default, set the viewpoint to match the manikin's grasping location.

Keywords. Cognitive modelling, Digital Human Modelling, Eye-hand coordination

1. Introduction

With the shift towards Industry 4.0 and an increased use of simulation and visualization software in all design phases, Digital Human Modelling (DHM) has become an important asset allowing engineers to evaluate ergonomics of new products and workplaces early in the design phase, long before the first physical prototype is built. While most DHM tools were primarily developed to evaluate aspects of physical ergonomics, there has recently been increased interest in modelling various aspects of human cognition [1]. Many DHM tools today allow modelling of view cones or volumetric projections. These tools are commonly used to evaluate driver environments by identifying blind spots around the vehicle [e.g. 2].

[1]Corresponding Author: Erik Billing, University of Skövde, Högskolevägen, 541 28 Skövde, Sweden; E-mail: erik.billing@his.se.

While these tools can effectively determine what is visible, a realistic estimate of what a DHM manikin sees also requires simulation of where they are looking [3]. Currently, a manikin's viewpoint is either manually specified by the designer or the simple result of other task related movements, e.g. the viewpoint moves forward and down as the manikin leans forward to reach for an object. However, from research on visual attention, it is well known that human beings display specific eye-gaze behaviors during daily activities [4], including reaching actions [5]. As a result, accurate manual specification of viewpoints for individual tasks is a challenging and potentially impossible process, but one that can be supported by both designer training and automated software features grounded in vision research.

In the present work, we take the first steps towards automating selection of viewpoint, with the goal of improving the quality of DHM simulation while also reducing the time and effort needed to create these simulations. Since object manipulation in the form of reaching and grasping are very common elements of tasks simulated using DHM software, the present study investigates eye-gaze behavior in a pick-and-place (PAP) task. This is done by recording eye-gaze of 10 participants executing a PAP task in a virtual reality (VR) environment. Collected data is analyzed and validated against existing literature. Based on these findings we present 4 principles for automatic selection of realistic viewpoints in DHM software.

The rest of this paper is organized as follows. Previous research on visual attention, eye-hand coordination, and modelling is presented in Section 2. The procedure for the experimental study is presented in Section 3, followed by analysis and presentation of results in Section 4. Finally, the paper concludes with a discussion in Section 5.

2. Background

Our selection of where to look is tightly linked to motions of the rest of our body and highly consistent between individuals [6, 7]. Visual attention is typically discussed in terms of *overt attention*, referring to the act of selecting fixation points, and *covert attention*, which refers to a psychological shift of focus without moving the eyes. In a DHM context, we are primarily interested in the former, often not only in eye-motion, but also in head motion and relevant shifts in posture [7, 8]. Thus, realistic simulation of overt attention is not only relevant from a cognitive perspective, but may also improve ergonomic simulations.

Overt visual attention is mostly studied as a response to stimuli in the form of an image. In this context, bottom-up control of eye-gaze refers to the effect that the image has on eye motion, while top-down control refers to cognitive influences and task context [e.g. 9]. In these studies, participants are typically seated in a relatively static position, though recent advances in eye-tracking allow for more naturalistic participant activity.

Extensive experimental research on eye-hand coordination over the last 40 years has established a high correlation between eye-gaze and hand position [e.g. 5, 7, 10, 11]. This correlation is proactive in the sense that the eyes specify the target for the upcoming action. When reaching for an object, we will typically first fixate on that object, and then the hand follows executing the reach. The eye-gaze will remain fixated on the target until the reaching action is completed. As soon as the action is finished, the gaze will shift to the next goal in a highly coordinated fashion [10]. A similar pattern emerges during

transportation of objects. People first look at the object being grasped, then shift their gaze towards the goal of the action. During object transport, the gaze typically remains fixated on the goal location until the release of the object occurs [5]. This proactive relationship between eye-gaze and body motion is likely to stem from simultaneous neural activity connecting both eye and body, while the temporal relationship is primarily resulting from differences in inertial properties between eye and body [10].

While this basic proactive eye-gaze pattern appears very stable between individuals, it is affected by several factors. Johansson et al. [5] demonstrate that participants consistently fixate on obstacles during object manipulation, shifting gaze towards the goal only after the hand has passed the obstacle. In cases involving sub-tasks or usage of both hands, earlier gaze transitions may occur in order to visually guide other pending tasks [12, 13].

The dominant approach to modelling visual attention is Koch and Ullman's [14] saliency map method. Models of visual attention is also a big research field in computer vision, see Borji et al. [15] for a review of 65 different models. The vast majority of these are bottom-up models, but there are also mixed models that incorporate both bottom-up and top-down aspects.

Although there is a growing body of literature describing visual attention in more ecological task related terms (see Hayhoe & Ballard [16] for a review), this approach to modelling eye-gaze is less developed. Moreover, careful consideration of eye-gaze in relation to the rest of the body is rare also in this area. One recent initiative was taken by Abboott et al. [11] who proposed a linear autocorrelation model of eye-body coordination. While this model is highly relevant for the present work, it requires training data from real participants executing the task and is thus difficult to apply in a DHM setting.

3. Method

The present study investigates a PAP task in VR where participants pick up objects lying on a table and place them in a bin (see Figure 1). Each participant performed 150 trials, in which a single object appeared on the left side of the table at a random distance between 0.2 and 1.4. meters from the participant's starting location. The aim of this layout was to ensure that in some trials the participant was able to pick up the object from the initial starting position, i.e. direct reach (DR), while other trials required the participant to walk before reaching for the object, i.e. relocate and reach (RAR).

During the experiment, participants were wearing a HTC Vive Pro Eye VR headset and two motion trackers (HTC Vive Trackers) placed on the right shoulder and left ankle. Participants also held an HTC Vive controller in their right hand. The virtual environment and task interactions were developed and run using Unity3D 2019.4 LTS. The virtual environment was comprised of a sparse office room (see Figure 1) that contained a table, a bin, and the object to be moved. A physical table of 95x160cm standing at 87cm height was placed in the middle of the lab space and configured to precisely match the position of its virtual counterpart, allowing participants to touch and lean on the (virtual) table. The bin and objects were solely virtual with the bin located 120cm from the table. Participants were allowed to move around freely within the open physical space. The exact position of headset, hand controller, and motion sensors were tracked using

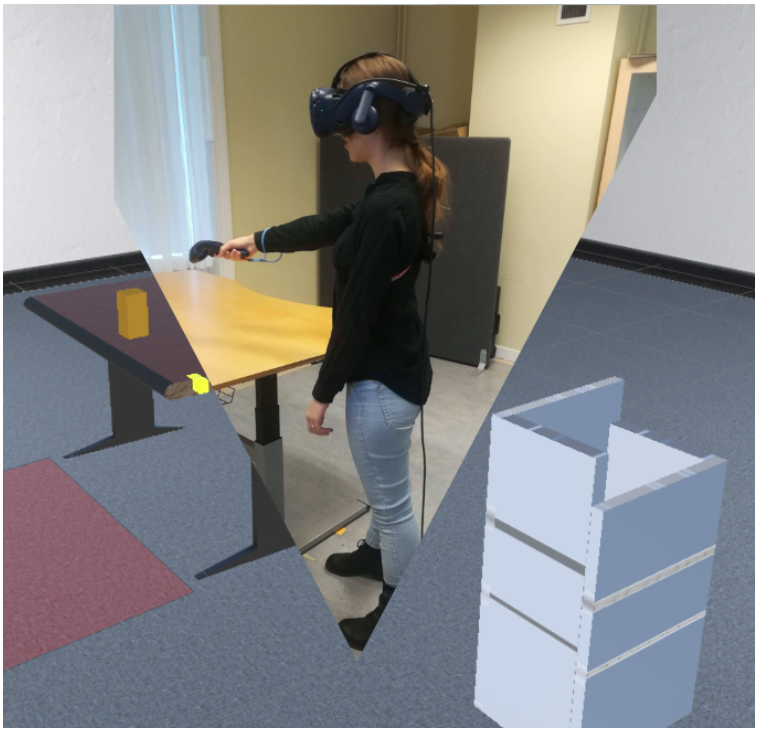

Figure 1. Example image of the experimental setting in VR and the physical room (overlay). Second author demonstrating. When participants moved into the red region on the floor, their action was classified as RAR, otherwise the action was classified as DR, (for analysis only, not visible to participants).

the SteamVR 2.0 tracking system. In order to avoid accidents, the limits of the physical space were indicated in the virtual environment using the VR system's built-in boundary system. The task object was a dark yellow box of size $10x10x20$cm and the participant could see their hand position represented by a virtual version of the hand controller.

3.1. Procedure

A detailed script had been constructed and was followed for each participant in order to ensure similar treatment. First, written and verbal consent was obtained from each participant after a brief description of the task expectations. After the consent process a more detailed explanation of what their task entailed was provided. This included verbal and visual instructions regarding the use of VR equipment in order to complete the task. Participants were reminded that they could take breaks or withdraw consent and cease their participation at any time without having to explain themselves and without losing any compensation.

An identification number was assigned to ensure data de-identification prior to eye tracking calibration and the beginning of the task. Upon entering the virtual lab room, participants were given the instruction *"You will be picking up boxes and placing them into the bin. Some of the boxes might be too far to reach and so you may move around the table to grasp them"*. After all the trials were finished, participants would sit next to the experimenter and verbally answer a questionnaire regarding the task, demographics, and

previous VR experience. Physical measurements of height, arm and leg length were also recorded. Participants then received a cinema ticket as compensation and were provided the opportunity to ask study-related questions during the debriefing. The complete procedure took about 35 minutes out of which approximately 16 minutes were spent within the virtual environment.

3.2. Participants and Data collection

Data was collected from 12 healthy right handed individuals of age (19 - 29) with full vision or corrected to full vision. Two participants were excluded as a result of not following task instructions and problems with the data collection. The final sample comprised 10 participants with a mean age of 22 years. Four identified as female, 5 as male, and 1 as non binary. All of them were students and all but one had minimal exposure to VR in daily life.

The position and orientation of headset, hand controller, motion trackers and the object were recorded with a temporal resolution of 90 Hz. In addition, eye-gaze vectors, viewpoint in the virtual environment, and fixated object were recorded with a temporal resolution of 120 Hz. Eye gaze data was pulled from the the headset through HTC's SRanipal plugin[2]. An eye gaze vector and origin were used along with the headset's position and orientation to calculate the participant's current focus point in the virtual environment. These values were calculated in real-time in the Unity environment, allowing focus points to be calculated with respect to the first virtual object that the headset relative eye gaze vector intersected in the scene. SRanipal provides processed eye values relative to the headset with a delay from eye record to provided data due to processing of approximately 16.6 ms. As a result, given Unity's 90hz framerate for the HTC Vive, eye tracking values have an expected latency of up to 33.2 ms.

The project was submitted for ethical review to the Ethical Review authority of Sweden (#2020-00677, Umeå) and was found to not require ethical review under Swedish legislation (2003:615).

4. Results

For the purpose of analysis, the data from each trial is divided into two phases. The first phase begins with the appearance of the object on the table and ends with the participant grasping the object. We refer to this phase as *appear-to-grasp (ATG)*. The second phase starts with the grasp and ends with the object landing in the bin. This object transport phase will not be analysed in this paper.

On any given trial participants executed one of two action strategies during the ATG phase; DR or RAR. Trials where the participant moved such that the left foot was located at the side of the table during the ATG phase were defined as RAR, otherwise the trial was labeled as a DR (c.f., Figure 1). Out of 1500 trials in total, 620 trials (41%) were labeled as RAR.

[2]HTC's SRanipal plugin for Unity, `https://developer.vive.com/resources/knowledgebase/vive-sranipal-sdk/`

Table 1. *The most frequently observed gaze sequences during the ATG phase.*

Action	Fixation seq.	Frequency	Percentage
DR	table → object	444	71%
	table → object → table → object	76	12%
	table → object → table	57	9%
	object	42	6%
RAR	table → object → floor → object	58	9%
	table → object → table → object	46	7%
	table → object	44	7%
	table → floor → object	44	7%

4.1. Fixation points

In order to analyze where people were looking when reaching for objects, a low-pass filter of 15 frames (8 Hz) was applied to the eye-gaze data. Gaze fixations were identified and grouped into 6 categories of eye-focus points: *hand, object, bin, table, floor,* and *surrounding*. Surrounding included gazes towards e.g. walls and ceiling. Gazes within a radius of 15 cm from the center point of the object were labeled as ”object”.

The most frequently observed fixation sequences during ATG are presented in Table 1. In most cases, participants started a trial by looking at the table and thereafter shifting their gaze to the object once it had appeared. During DR trials, the object typically remains fixated upon until grasp, sometimes combined with a gaze shift to the surrounding area on the table. The object was fixated at least once during reach in 99% of all DR trials, and remained fixated during 65% of the reaching phase. These numbers are even higher if we include the immediate surrounding of the object. 82% of all gazes during DR landed within 30 cm from the object.

In a small proportion of all DR trials (6%), the ATG phase begins with the participant looking at the object’s appearance location. Relevantly, the object initial position varies randomly along the dimension extending from the participant, but not along the orthogonal dimensions. Thus, in these cases, it is likely that the participant is looking at the table in the task relevant region before the ATG phase, and just happens to be looking in a region that is occluded by the object when it appears.

RAR trials comprise much more variability in fixation sequences but typically involve combinations of the object, table, and the floor. Notably, the four most common fixation sequences only account for 30% of all trials. Similar to DR, the object was fixated at least once in 99% of all RAR trials, and remained fixated during 47% of the reaching phase (60% within 30 cm from the object).

As can be seen in Figure 2, the differences between DR and RAR are also visible in the eye-gaze distribution over the room. While there are fixations around the room in both conditions, gazes during DR are more tightly grouped along the left side of the table (where the object appears). As indicated by the sequential analysis presented in Table 1, the RAR trials frequently (but not always) comprise gaze shifts towards the floor. Here we can see that these gazes are primarily located within the region where the participant is about to go, but also include scanning gazes around the room.

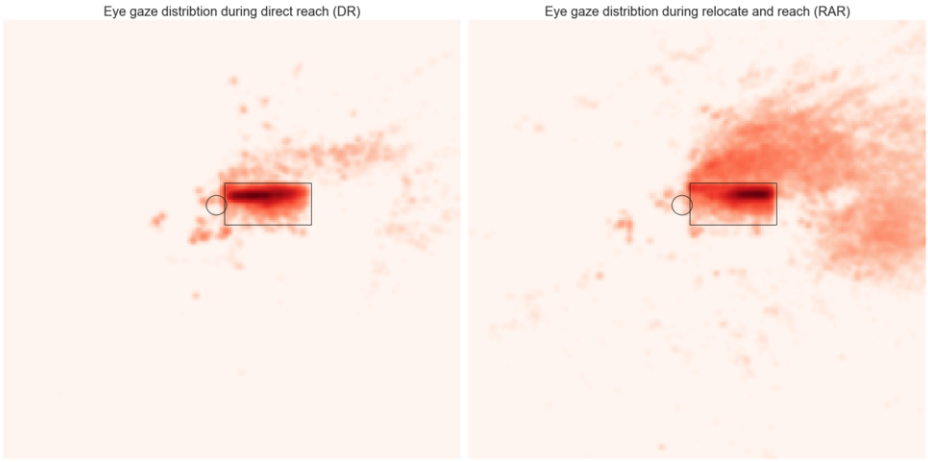

Figure 2. Distribution of eye-gaze during the ATG phase, over the room seen from above. Circle and rectangle represents the initial location of the participant and the location of the table, respectively. Intensity of red represents frequency of eye-gaze, scaled logarithmicly to make sparse gaze patterns more visible.

4.2. Temporal dynamics

The analysis presented in the previous section provides insight on *where* participants are looking when reaching for objects. This section will target the *when*. One dominant pattern observed during both DR and RAR trials was an initial shift of gaze from the table to the object. In order to analyse when this shift occurs, the time of the first gaze on the object was calculated relative to action onset. Action onset was here defined as 5% of peak velocity of the right hand, along the X-dimension (forward in relation to the participant's starting position). Results are presented in Figure 3.

We are also interested in the temporal coordination between the eye and the hand motion. In the present task, this is primarily visible in the sideways motion of the participant, when reaching for the object. If previous literature stipulating a strong coordination between eye-gaze and hand motion is correct, we expect to see the hand motion following the eye-focus point, with a certain delay. Results are presented in Figure 4. Here we also include the motion of the left foot, which has been less studied in relation to eye-gaze. Interestingly, results reveal a high correlation between both eye-hand and hand-ankle, with an approximate delay of about 1.0 s and 0.3 s, respectively.

5. Discussion

In the present work, we have taken the first steps towards a model for automatic selection of viewpoint. While the present study does not result in a fully developed computational model, we suggest the following principles for automatic viewpoint selection in DHM software. These principles are based on the experimental results from the present study combined with previous literature. Although these formulations do not account for the full variability in human visual behavior, we hope that they will constitute *implementable* formulations of automatic viewpoint selection in DHM tools.

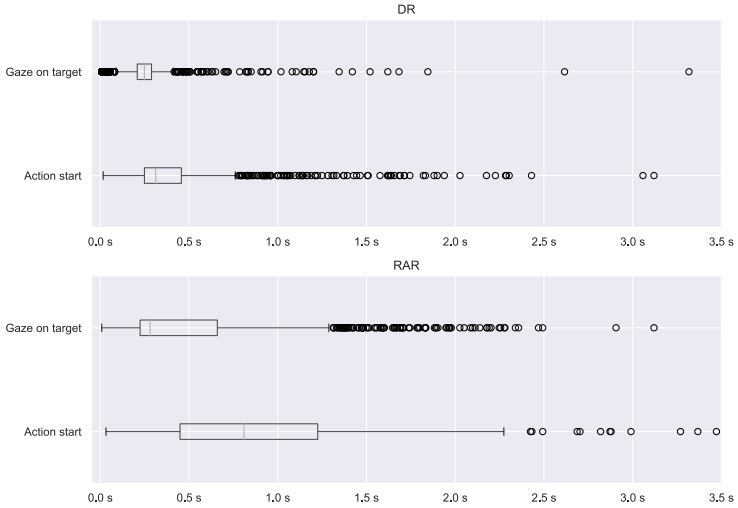

Figure 3. Timing of eye-gaze on target object and action onset relative to the appearance of the object on the table.

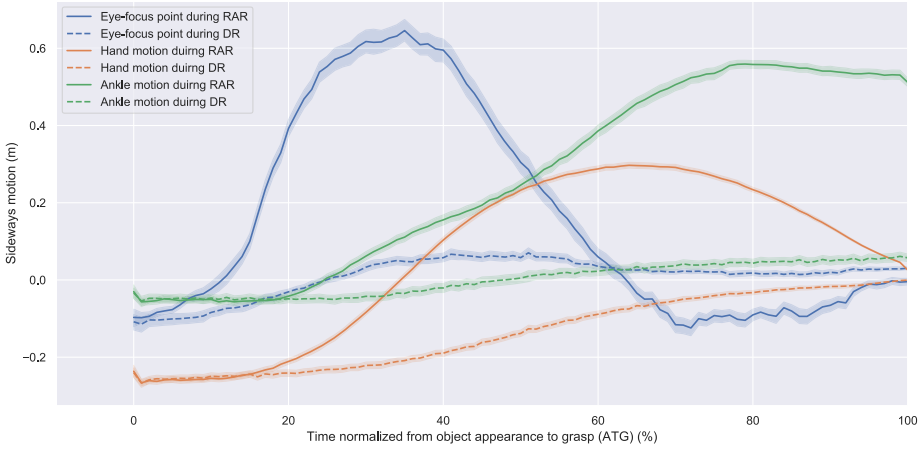

Figure 4. Sideways motion of the eye-focus point, hand, and ankle during the ATG phase, relative to the position of the target object. The plot shows mean values from all 10 participants. Envelopes represents the 95% confidence interval of the mean.

1. *Eyes on target.* This principle is highly dominating during direct reaching behaviors when the participant is standing still, and aligns well with previous research [e.g. 5, 7]. Somewhat surprisingly, this appears to be also valid when participants relocate, as more than half of all gazes were directed on to the object or in its near surrounding in RAR trials.
2. *Eyes on floor.* Similar to previous research [5], we here observe a shorter fixation on intermediate targets, in this case the floor where participants are about to relocate. This intermediate eye-gaze appears to interrupt the otherwise dominating

principle of looking at the main target for the action.

3. *Coordinated onset.* As visible in Figure 3, the first eye-gaze on target object appears to be highly coordinated with the onset of the action. Here, there is a greater variability in previous literature and there are certainly many situations where individuals look at targets long before initiating an action. However, our results align well with the seminal study of Biguer et al. [10], describing eye-gaze, head motion, and hand motion during reaching as initiated by a single "neural command". Although there may be exceptions, we believe this principle constitutes a simple and yet realistic approach to the timing between eye-gaze and reaching actions for DHM tools.
4. *Eyes in the lead.* Although onset of eye movements appear to be synchronous with the action, the eye-gaze is leading motion of the rest of the body. This has been repeatedly expressed in literature, and is also obvious in our data (Figure 4). We believe this constitutes good basis for modelling the relationship between hand motion and eye-gaze, while recognizing the fact that DHM tool developers may want to describe eye-gaze as a product of hand movements; the opposite is likely a more accurate description of the cognitive mechanisms.

Acknowledgements

This work was financially supported by the synergy Virtual Ergonomics funded by the Swedish Knowledge Foundation, dnr 20180167. `https://www.his.se/sve`

References

[1] Scataglini S, Paul G, editors. DHM and Posturography. 1st ed. London: Elsevier, Academic Press; 2019.

[2] Summerskill S, Marshall R, Cook S, Lenard J, Richardson J. The use of volumetric projections in Digital Human Modelling software for the identification of Large Goods Vehicle blind spots. Applied Ergonomics. 2016;53:267–280.

[3] Fletcher L, Zelinsky A. Driver inattention detection based on eye gaze - Road event correlation. International Journal of Robotics Research. 2009;28(6):774–801.

[4] Raudies F, Mingolla E, Neumann H. Active Gaze control improves optic flow-based segmentation and steering. PLoS ONE. 2012;7(6).

[5] Johansson RS, Westling G, Bäckström A, Flanagan JR. Eye–Hand Coordination in Object Manipulation. Journal of Neuroscience. 2001 9;21(17):6917–6932.

[6] Land MF, Furneaux S. The knowledge base of the oculomotor system. Philosophical Transactions of the Royal Society of London Series B: Biological Sciences. 1997 8;352(1358):1231–1239.

[7] Land MF, Mennie N, Rusted J. The Roles of Vision and Eye Movements in the Control of Activities of Daily Living. Perception. 1999 11;28(11):1311–1328.

[8] Herst AN, Epelboim J, Steinman RM. Temporal coordination of the human head and eye during a natural sequential tapping task. In: Vision Research. vol. 41. Pergamon; 2001. p. 3307–3319.

[9] Schutz AC, Braun DI, Gegenfurtner KR. Eye movements and perception: A selective review. Journal of Vision. 2011 9;11(5):9–9.

[10] Biguer B, Jeannerod M, Prablanc C. The coordination of eye, head, and arm movements during reaching at a single visual target. Experimental Brain Research. 1982;46(2):301–304.

[11] Abbott WW, Harston JA, Faisal AA. Linear Embodied Saliency : a Model of Full-Body Kinematics-based Visual Attention. PrePrint by bioRxiv. 2020;.

[12] Land MF. Vision, eye movements, and natural behavior. Visual Neuroscience. 2009;26(1):51–62.

[13] Srinivasan D, Martin BJ. Eye-hand coordination of symmetric bimanual reaching tasks: Temporal aspects. Experimental Brain Research. 2010;203(2):391–405.

[14] Koch C, Ullman S. Shifts in selective visual attention: Towards the underlying neural circuitry. Human Neurobiology. 1985;4(4):219–227.

[15] Borji A, Itti L. State-of-the-art in visual attention modeling. IEEE Transactions on Pattern Analysis and Machine Intelligence. 2013;35(1):185–207.

[16] Hayhoe M, Ballard D. Modeling task control of eye movements. Cell Press; 2014.

DHM2020
L. Hanson et al. (Eds.)

© 2020 The authors and IOS Press.
This article is published online with Open Access by IOS Press and distributed under the terms of the Creative Commons Attribution Non-Commercial License 4.0 (CC BY-NC 4.0).
doi:10.3233/ATDE200011

Variational Interpolating Neural Networks for Locomotion Synthesis

Janis SPRENGER [a,b,1], Han DU [a,b], Noshaba CHEEMA [a,b,c], Klaus FISCHER [a] and Philipp SLUSALLEK [a,b]

[a] *German Research Center for Artificial Intelligence (DFKI)*
[b] *Saarland University, Saarbrücken, Germany*
[c] *Max-Planck Institute for Informatics, Saarbrücken, Germany*

Abstract. Natural human locomotion contains variations, which are important for creating realistic animations. Most of all when simulating a group of avatars, the resulting motions will appear robotic and not natural anymore if all avatars are simulated with the same walk cycle. While there is a lot of research work focusing on high-quality, interactive motion synthesis the same work does not include rich variations in the generated motion. We propose a novel approach to high-quality, interactive and variational motion synthesis. We successfully integrated concepts of variational autoencoders in a fully-connected network. Our approach can learn the dataset intrinsic variation inside the hidden layers. Different hyperparameters are evaluated, including the number of variational layers and the frequency of random sampling during motion generation. We demonstrate that our approach can generate smooth animations including highly visible temporal and spatial variations and can be utilized for reactive online locomotion synthesis.

Keywords. Neural Networks, Procedural Animation, Variational Motion Synthesis

1. Introduction

Human locomotion is composed out of two characteristics: consistency and variation. It is quite often considered as a cyclic problem (e.g., [1, 2, 3]), as consecutive steps are quite similar while walking with the same velocity and direction. On the other hand, it is very hard for humans to accurately replicate the same motion twice. Hence every step during locomotion is slightly different. In order to generate natural locomotion animations, it is not only important to accurately and fluently replicate the mean motion but to generate the intrinsic variation as well. In a third-person gaming context, this might not be a major issue, as the user is controlling the avatar and thus is incorporating a certain amount of variation due to his input. However, as soon as the avatar is perceived for a long time with the same input (e.g. walking straight ahead) or is displayed from an outside angle, the lack of variation becomes apparent. This problem increases with the number of avatars using the same type of locomotion variation. In this case, even a very natural locomotion clip will appear robotic and unnatural. In the gaming context, for example, different walk-cycles are generated and randomly assigned to different avatars in order

[1] Corresponding Author. janis.sprenger@dfki.de

to diminish this effect. Considering advanced motion synthesis techniques, this approach is rarely possible.

The recent publications for reactive motion synthesis (e.g. [2, 3, 4]) generate motions of very high quality, but these approaches usually lack variability due to their deterministic nature. Given the same initialization and user input, all motions will appear the same. In novel application fields, like a digital reality [5] simulating pedestrian agents for testing autonomous driving systems, the variation is not only preferred but highly required. If an autonomous vehicle is trained or validated in a virtual scene using avatars with only a single animation clip, the systems will overfit or only be proven to work with this single animation. Hence, it is necessary to accurately replicate the variation apparent in reality.

Although there are already approaches using variational autoencoders, they lack either the ability to control the motion synthesis [6] or the fidelity of the generated motion is not comparable with the results of state-of-the-art models [7]. Currently, the most promising work for locomotion synthesis are **Feedforward Interpolating Neural Networks (FINN)**. These networks consist of a core motion network and an interpolation method [2, 3, 8]. The core motion network is a fully connected neural network and performs the regression step from the current to the next frame (feedforward step). The interpolation method is used to generate the optimal network weights of the motion network for the current regression step.

In this work, we are presenting a novel approach adapting the core motion network of a FINN to learn and reproduce the variation intrinsic to the training data while retaining the motion quality and responsiveness. Similar to a variational autoencoder the parameters of a hidden layer are considered to correspond to the mean and variance of a normal distribution. During model training as well as during motion synthesis, a random variable is sampled from a normal distribution and scaled by the parameter. Hence the model can learn the distribution inherent to the motion capture training dataset inside the hidden layer. The approach is based on a phase-functioned neural network [2]. We evaluated the impact of different numbers and positions of variational layers inside the network against adding random noise and a vanilla phase-functioned neural network. Our approach greatly increases the inter- and intra-individual variation of locomotion, while retaining the quality and naturalness of the original motion. This work has the following contributions:

- a novel approach of Variational Interpolating Neural Networks (VINN) is presented,
- evaluation of the impact of multiple hidden distributions in a single variational network,
- novel insights for the usage of variational generative networks with a high frame rate,
- novel approach to the evaluation of the variation of generated motions.

2. Background

2.1. Data-Driven Motion Synthesis

Motion capturing produces natural and high-quality motions that can be used to train data-driven synthesis models. Kovar et al. [9] used motion clips from a dataset and build

a *motion graph* encoding the different possibilities to reassemble the original clips. A constrained graph walk can generate target-specific animations based on the control input. There are multiple extensions for motion graphs, e.g. [10, 11]. Lee et al. [4] encode individual frames as motion states and model all possible transitions using a motion field rather than a graph. A Markov decision process (MDP) is built to model the possible decisions in terms of actions for each motion state. Motion synthesis can be considered as a concatenation of individual discrete poses over time. Using simple fully-connected regression models to reproduce this time-series data suffers from pose averaging. Similar intermediate poses in different sequences, e.g. when both legs are crossing each other in a walk cycle, are averaged and prevent a natural transition of frames. Due to missing information on the recent past, the network can become unable to distinguish the foot going forward and does not accurately continue the walk cycle. There are different approaches, trying to solve this problem using recurrent neural networks (RNNs) [12, 13, 14]. However, training RNNs reportedly is very complex, time-consuming, and uncontrolled generation of motion using RNNs suffers from dying out of motion and accumulation of error [12, 13, 2].

Recently, [2] proposed a novel network architecture that interpolates the network weights depending on the phase of the walk cycle. This methodology was further extended by [3] to generate complex quadruplet motion of dogs. A prove of concept of the same idea for reach motions was recently published by [15]. All of these approaches have in common, that the network weights of the regression network are interpolated and use a similar, fully-connected network structure for motion synthesis. While these forward interpolating neural networks (FINN) are providing a natural motion synthesis that can be controlled responsively, they are deterministic by nature and unable to create variations in the generated motion. Although the animation of a single avatar appears convincing, the animation of multiple avatars appears highly unnatural and robotic. Therefore, including natural variations as a statistical model is attractive for crowd animation and realistic simulation.

2.2. Statistical Motion Modeling

Another trend of approaches for motion synthesis task is to learn the distribution from motion capture data. The new motions can be generated by sampling and optimizing the learned distribution based on constraints. Many conventional models have been used to model the motion distribution, for instance, the variants of Hidden Markov Models (HMMs) [16, 17, 18], Gaussian Mixture Models (GMMs) in low-dimensional space [10, 19, 11, 20] and Gaussian Processes (GP) and its many variants for temporal variations [21, 22, 23]. Min and Chai [11] combine a motion graph [9] with statistical motion modeling. The motion data is modeled as a directed graph with each node being a cluster of semantically and structurally similar motion clips. Each edge in the graph represents the possible transition between clips. Motion clips in each motion primitive are projected into low-dimensional space and a GMM is used to learn the distribution. The transitions between motion primitives are modeled by Gaussian Processes. Recently, variational autoencoders (VAE) have been proposed as non-parametric, unsupervised approaches for manifold learning. Since it is a non-parametric model, no prior knowledge about data distribution is assumed. It uses the computational power of neural networks to learn a transform from a normal distribution to any kind of complex distribution. Holden et al.

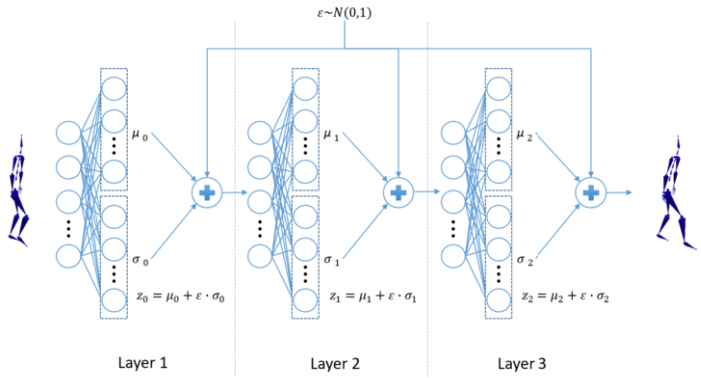

Figure 1. Network Structure using three Variational Layers (var1n2n3). A single sample is drawn from a normal distribution and used to scale the trained distribution in the hidden layers.

[24] first apply convolutional autoencoders to learn a continuous manifold space for a large, heterogeneous motion database. Other solutions are combining VAE with long short-term memory nodes (LSTM) [7] to model and predict motion sequences. These models, however, cannot model the high-level control of a user intuitively.

3. Variational Interpolating Neural Networks (VINN)

By considering animation as a concatenation of individual poses, we can consider the whole process as a time-series problem where each individual step can be predicted by a regression model. In order to allow a user to control the motion generation, a separate imperative controller is required, storing the global state of the avatar. Considering fully connected or feedforward interpolating neural networks, a single latent representation performs the regression steps deterministically. We propose a novel approach for learning not a single representation, but the distribution present in the training data. The approach is built upon a phase-functioned neural network ([2]), one of the state-of-the-art models for locomotion synthesis.

3.1. Neural Network Structure

For a single variational layer, the output of a fully connected layer is split into the mean (μ) and the standard deviation (σ) of a normal distribution. The output of the layer is computed by drawing a normal distributed variable $\varepsilon \sim N(0,1)$ and scaling it by the values computed in the fully connected layer:

$$v(\mu,\sigma,\varepsilon) = \mu + \varepsilon \cdot \sigma \tag{1}$$

Using a suitable split function to separate the mean and standard deviation (e.g. $split(x) = (x[0:0.5\cdot|x|], x[0.5\cdot|x|:|x|])$), a single variational layer for an input vector x, weights W and bias b can be defined as

$$\mathrm{VAR}(x,W,b) = v(split(Wx+b)) \tag{2}$$

Using the exponential rectified linear function [25] as an activation function, the variational layer can be written as:

$$\mathrm{VAR}^{(e)}(W,b,x) = v(split(ELU(Wx+b))) \tag{3}$$

Given an input parameter $x \in \mathbb{R}^n$, output parameters $y \in \mathbb{R}^m$ and a phase parameter $p \in \mathbb{R}$, we construct a three layer network as visualized in figure 1.
Mathematically, the network can be described as

$$\Phi(x;A) = \mathrm{VAR}_3(W_2,b_2,\mathrm{VAR}_2^{(e)}(W_1,b_1,\mathrm{VAR}_1^{(e)}(W_0,b_0,x))) \tag{4}$$

A network model A can be completely defined by $A = \{W_0 \in \mathbb{R}^{2h\times n}, W_1 \in \mathbb{R}^{2h\times h}, W_2 \in \mathbb{R}^{m\times h}, b_0 \in \mathbb{R}^{2h}, b_1 \in \mathbb{R}^{2h}, b_2 \in \mathbb{R}^m\}$. Here, $h = 512$ is the size of hidden state, $n = 301$ is the dimension of the input vector and $m = 245$ the dimension of the output vector. Similar to [2] we are employing a phase-functioned structure on this network. Hence, the network weights are computed by a phase function before each regression step, depending on the phase and the input parameters θ. In this case, a cyclic cubic Catmull-Rom spline is chosen as the phase function, using for control points $\theta = \{\alpha_0\ \alpha_1\ \alpha_2\ \alpha_3\}$. A definition of this function is shown in the appendix eq. (9).

3.2. Number of Variational Layers and Dimensionality of Random Sample

Variational autoencoders learn a single distribution in the latent space after encoding. Here, a fully connected network is utilized and hence, there are multiple possibilities to incorporate the variation. In practice, each conventional layer of a phase-functioned neural network (PFNN) [2] can be replaced with a variational layer. We configured network models for all different positions (e.g. *var1n3* starts with a variational layer, has a regular layer in between, and ends with a variational layer. For each pass, a single random sample is used to draw from the latent distributions to enable a correspondence between distributions. The dimensionality of the random sample is equal to the dimensionality of the hidden layer.

3.3. Input and Output Format

The network performs a single regression step from the past to the future frame. The input and output vectors are defined as a combination of control input and joint configurations. The input vector contains trajectory positions $p_i \in \mathbb{R}^{2f}$, trajectory directions $d_i \in \mathbb{R}^{2f}$ and gait controls $g_i \in \mathbb{R}^{f\times s}$ of $f = 12$ surrounding frames and the $s = 6$ target gaits (standing, walking, jogging, etc.). The past joint configuration is provided as joint positions $l_{i-1} \in \mathbb{R}^{3j}$ and joint velocities $v_{i-1} \in \mathbb{R}^{3j}$ for all $j = 31$ joints.

The output vector contains global translation $r_i^x \in \mathbb{R}^2$, the change of forward direction $r_i^a \in \mathbb{R}^2$ projected on the ground plane, the phase delta (elapsed phase) $\Delta_i \in \mathbb{R}$. In addition, it contains the predicted future trajectory positions $p_{i+1} \in \mathbb{R}^f$ and directions $d_i \in \mathbb{R}^f$. Last but not least the predicted next posture as joint positions $l_i \in \mathbb{R}^{3j}$ and velocities $v_i \in \mathbb{R}^{3j}$ for all $j = 31$ joints.

$$\begin{aligned} x_i &= \{p_i\ \ d_i\ \ g_i\ \ l_{i-1}\ \ v_{i-1}\} \in \mathbb{R}^{306} \\ y_i &= \{r_i^x\ \ r_i^a\ \ \Delta_i\ \ p_{i+1}\ \ d_{i+1}\ \ l_i\ \ v_i\} \in \mathbb{R}^{215} \end{aligned} \tag{5}$$

3.4. Random Sampling during Motion Synthesis

A simple motion controller similar to [2, 26] was implemented. During motion synthesis, the network is executed at 60 frames per second. Random sampling at such a high frequency is problematic for two reasons: first, drawing a random sample at each frame can produce jittering. Second, the more samples are drawn, the more will the average of these samples converge towards the mean of the distribution thus reducing the variability. Similar to Du et al. [20], a single step can be considered as motion primitive. Thus drawing a new random sample at each step rather than at each frame and keeping this sample constant throughout the step should generate variational steps rather than variational frames.

4. Evaluation

4.1. Dataset

All frames from the motion capture library published by Holden et al. [2] containing only the locomotion on a flat surface were utilized. After pre-processing, the raw motion capture data in the required format, 179,586 frame-pairs were extracted. The decision to focus on the reduced dataset was taken, to reduce the variability introduced by external factors, for example, the terrain.

4.2. Network Training

The network architecture was implemented using the TensorFlow framework [27]. Each network was trained on the same dataset for 50 epochs using the stochastic gradient descent algorithm Adam [28], already included in the framework.Dropout [29] was applied with a retention probability of 0.7. All models were trained in mini-batches of size 32. Cosine decay with warm restarts was utilized to adjust the learning rate over time. The initial learning rate was set to 0.0001. The restarts were performed at 10 and 30 epochs.

4.3. Measuring Variation

An experimental setup was utilized to compare the variation in locomotion generation. Using a vanilla PFNN, 10 seconds of straight forward walking were simulated to initialize a walk cycle. Based on this initialization all models generated 100 separate walk cycles of 4 seconds or about 5 steps. We measure three variables for each of the walk cycles. The **inter-individual variation**, comparing variation between the walk cycles for each time-step. For the baseline-method (PFNN) this variation should be zero. The **intra-individual variation**, describing variation throughout a single walk cycle. And the **error**, measuring violations of smoothness, foot drifting and large inconsistencies between steps (stumbling).

The **inter-individual variation** (V_{inter}) was computed by the sum

$$V_{\text{inter}} = V_{\text{inter pose}} + V_{\text{inter step}} \tag{6}$$

The *inter-pose variation* ($V_{\text{inter pose}}$) was measured as the median deviation of local joint positions of the mean joint configuration for each time step. The *inter step velocity* ($V_{\text{inter step}}$) was measured as the average standard deviation of step velocity of temporally aligned steps generated by the different models. The sum of both variables was used to measure the inter-individual variation.

The **intra-individual variation** (V_{intra}) was computed as the sum

$$V_{\text{intra}} = V_{\text{intra pose}} + V_{\text{intra step}} \tag{7}$$

The *intra-pose variation* ($V_{\text{intra pose}}$) was measured by first, grouping all generated local joint positions to their respective phase of the walk cycle (in 0.01 increments) and second computing the average deviation of joint positions for each phase increment in the same way, as the inter-pose variation. The *intra step velocity* ($V_{\text{intra step}}$) was measured as the average deviation of step velocity of all steps generated from the specific motion model.

The **error** was measured as the sum

$$\text{error} = e_{\text{smooth}} + e_{\text{drift}} + e_{\text{distance}} + e_{\text{duration}} \tag{8}$$

Smoothness (e_{smooth}) was computed as the average of the 95-percentile of velocities generated by each model. *Foot drifting* (e_{drift}) was computed for each generated walk cycle and averaged. *Step distance consistency* (e_{distance}) and *step duration consistency* (e_{duration}) are computed by taking the differences of distance and duration of consecutive steps. The resulting standard deviation of the differences should be reasonably small. The variables are computed by taking the standard deviation of all respective differences. Consistency and smoothness should be reasonably small but not zero, as there would be no dynamic movement in this case.

4.4. Numerical Results

We compare the VINN models against a vanilla PFNN implementation as well as random models, where instead of sampling from a distribution random noise is added to the layers of a PFNN, as this could generate variation as well. In addition, we compare sampling at each frame and sampling at each step. In figure 2 we present the results as scatter plots of variation measure versus the error. The baseline model produces zero inter-individual variation and only minor intra-individual variation. All random models generate motion with high error scores and do not necessarily generate more variation. Sampling at each step rather than each frame can double the variation scores without a large increase of error in the VINN models. The best performing model for inter- and intra-variation as well as with an error comparably with the baseline model contains only variational layers (var1n2n3).

4.5. Qualitative Results

The different models were used to generate locomotion in different scenarios. The rendered videos of these scenarios can be found in the supplementary material.

(a) Scatterplot of the inter-individual variation vs error for variational models

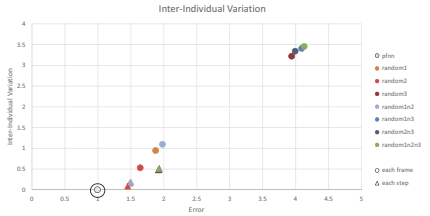

(b) Scatterplot of the inter-individual variation vs error for random models

(c) Scatterplot of the intra-individual variation versus error for variational models

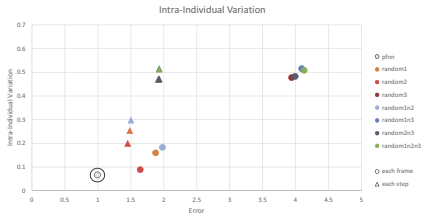

(d) Scatterplot of the intra-individual variation versus error for random models

Figure 2. Scatterplots of the variation versus error for inter- and intra-variation factors of all models. The baseline and the best performing model are encircled. All random models generated inconsistent and noisy motion.

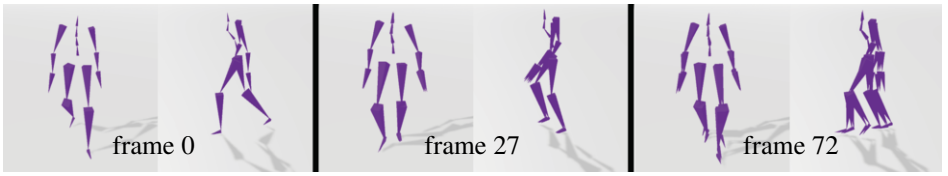

Figure 3. Development of motion variation within the first 72 frames (1.2 s). The display shows 5 overlayed skeleton walkers fixed at their hip position from front and side view. The motion is generated using single-step sampling with the vinn1n2n3 model.

Figure fig. 3 displays the result for the target model (vinn1n2n3). The qualitative analysis supports the numerical evaluation. Adding random noise creates a high amount of jitter when sampling at each frame. When sampling at each step, fewer variations in motion but a lot of floating can be observed, where the global translation did not match the body movements. In the case of VINN, the visible variation increases for all models, when sampling at each step. The body movement is corresponding to the global translation very accurately. Although there is a small numeric discontinuity at the specific frame of the change of random sample, the discontinuity is barely visible in the animations.

5. Discussion

The evaluation results suggest, that the proposed generative network can capture and replicate variation in motion best if a distribution is trained in each layer. In comparison to a vanilla PFNN, it generates a significant amount of variations. In comparison to

adding random noise at each layer, it generates consistent motions with respect to foot placement, step length, and smoothness.

We selected sufficiently straight walking examples from the training dataset and performed the same evaluation on these training samples. As the data was captured in a restricted space and not on a treadmill, there are only a few samples of straight-line walking. To find a sufficient amount of sequences for the evaluation, small deviations from a straight line were accepted. The results show an error of 0.93 and an intra-individual variation of 3.2. Although the variation is twice as large as generated by our model, it shows a comparable error. For future data capturing of locomotion, we suggest to include treadmill walking to have better means of evaluation, as the larger variation may be due to different trajectories.

Due to the high frame-rate (60fps) the variation is regressing to the mean if a random sample is drawn at each frame. Sampling at each step, however, creates natural motions with high variability. The discontinuity between two steps is comparably small and can be further reduced by smoothing the random sample. However, future work should investigate the usage of more temporally stable sampling methods.

The proposed approach demonstrates, that concepts of VAE can be integrated into a fully-connected interpolating network structure while retaining the controllability and visual quality of the original approach. This opens the potential for further experiments with similar network structures ([3, 8]). In addition, it builds a basis for future work in the direction of conditional variation and stylistic motion synthesis.

References

[1] Troje NF. Decomposing biological motion: A framework for analysis and synthesis of human gait patterns. Journal of Vision. 2002;2(5):2.

[2] Holden D, Komura T, Saito J. Phase-functioned Neural Networks for Character Control. ACM Trans Graph. 2017 Jul;36(4):42:1–42:13.

[3] Zhang H, Starke S, Komura T, Saito J. Mode-adaptive Neural Networks for Quadruped Motion Control. ACM Trans Graph. 2018 Jul;37(4):145:1–145:11.

[4] Lee Y, Wampler K, Bernstein G, Popović J, Popović Z. Motion Fields for Interactive Character Locomotion. ACM Trans Graph. 2010 Dec;29(6):138:1–138:8.

[5] Dahmen T, Trampert P, Boughorbel F, Sprenger J, Klusch M, Fischer K, et al. Digital reality: a model-based approach to supervised learning from synthetic data. AI Perspectives. 2019;1(1):1–12.

[6] Motegi Y, Hijioka Y, Murakami M. Human Motion Generative Model Using Variational Autoencoder. International Journal of Modeling and Optimization. 2018;8(1).

[7] Habibie I, Holden D, Schwarz J, Yearsley J, Komura T. A Recurrent Variational Autoencoder for Human Motion Synthesis. 2017.

[8] Starke S, Zhang H, Komura T, Saito J. Neural state machine for character-scene interactions. ACM Transactions on Graphics. 2019 Nov;38(6):1–14. Available from: https://dl.acm.org/doi/10.1145/3355089.3356505.

[9] Kovar L, Gleicher M, Pighin F. Motion Graphs. ACM Trans Graph. 2002 Jul;21(3):473–482.

[10] Lee J, Chai J, Reitsma PSA, Hodgins JK, Pollard NS. Interactive Control of Avatars Animated with Human Motion Data. ACM Trans Graph. 2002 Jul;21(3):491–500.
[11] Min J, Chai J. Motion Graphs++: A Compact Generative Model for Semantic Motion Analysis and Synthesis. ACM Trans Graph. 2012 Nov;31(6):153:1–153:12.
[12] Fragkiadaki K, Levine S, Felsen P, Malik J. Recurrent Network Models for Human Dynamics. In: Proceedings of the 2015 IEEE International Conference on Computer Vision (ICCV). ICCV '15. Washington, DC, USA: IEEE Computer Society; 2015. p. 4346–4354.
[13] Li Z, Zhou Y, Xiao S, He C, Li H. Auto-Conditioned LSTM Network for Extended Complex Human Motion Synthesis. CoRR. 2017;abs/1707.05363.
[14] Lee K, Lee S, Lee J. Interactive Character Animation by Learning Multi-objective Control. ACM Trans Graph. 2018 Dec;37(6):180:1–180:10.
[15] Gaisbauer F, Fröhlich P, Lehwald J, Agethen P, Rukzio E. Presenting a Deep Motion Blending Approach for Simulating Natural Reach Motions. In: Proceedings of the 39th Annual European Association for Computer Graphics Conference: Posters. EG '18. Goslar Germany, Germany: Eurographics Association; 2018. p. 5–6.
[16] Brand M, Hertzmann A. Style Machines. In: Proceedings of the 27th Annual Conference on Computer Graphics and Interactive Techniques. SIGGRAPH '00. New York, NY, USA: ACM Press/Addison-Wesley Publishing Co.; 2000. p. 183–192.
[17] Bowden R. Learning statistical models of human motion. In: IEEE Workshop on Human Modeling, Analysis and Synthesis, CVPR. vol. 2000; 2000. .
[18] Lehrmann AM, Gehler PV, Nowozin S. Efficient nonlinear markov models for human motion. In: Proceedings of the IEEE Conference on Computer Vision and Pattern Recognition; 2014. p. 1314–1321.
[19] Min J, Chen YL, Chai J. Interactive generation of human animation with deformable motion models. ACM Transactions on Graphics (TOG). 2009;29(1):9.
[20] Du H, Hosseini S, Manns M, Herrmann E, Fischer K. Scaled Functional Principal Component Analysis for Human Motion Synthesis. In: Proceedings of the 9th International Conference on Motion in Games. MIG '16. New York, NY, USA: ACM; 2016. p. 139–144.
[21] Lawrence ND, Moore AJ. Hierarchical Gaussian process latent variable models. In: Proceedings of the 24th international conference on Machine learning. ACM; 2007. p. 481–488.
[22] Wang JM, Fleet DJ, Hertzmann A. Gaussian Process Dynamical Models for Human Motion. IEEE Transactions on Pattern Analysis and Machine Intelligence. 2008 Feb;30(2):283–298.
[23] Zhou L, Shang L, Shum HP, Leung H. Human motion variation synthesis with multivariate Gaussian processes. Computer Animation and Virtual Worlds. 2014;25(3-4):301–309.
[24] Holden D, Saito J, Komura T, Joyce T. Learning motion manifolds with convolutional autoencoders. In: SIGGRAPH Asia 2015 Technical Briefs. ACM; 2015. p. 18.
[25] Clevert D, Unterthiner T, Hochreiter S. Fast and Accurate Deep Network Learning by Exponential Linear Units (ELUs). CoRR. 2015;abs/1511.07289.
[26] Clavet S. Motion matching and the road to next-gen animation. In: Proc. of GDC; 2016. .

[27] Abadi M, Barham P, Chen J, Chen Z, Davis A, Dean J, et al. TensorFlow: A System for Large-scale Machine Learning. In: Proceedings of the 12th USENIX Conference on Operating Systems Design and Implementation. OSDI '16. Berkeley, CA, USA:
USENIX Association; 2016. p. 265–283.

[28] Kingma DP, Ba J. Adam: A Method for Stochastic Optimization. CoRR. 2014;abs/1412.6980.

[29] Srivastava N, Hinton G, Krizhevsky A, Sutskever I, Salakhutdinov R. Dropout: A Simple Way to Prevent Neural Networks from Overfitting. Journal of Machine Learning Research. 2014;15:1929–1958.

A. Appendix

A.1. Definition of a Cubic Catmull-Rom Spline

$$\begin{aligned}\Theta(p;\theta) &= \alpha_{k_1} + w(\frac{1}{2}\alpha_{k_2} - \frac{1}{2}\alpha_{k_0}) + w^2(\alpha_{k_0} - \frac{5}{2}\alpha_{k_1} + 2\alpha_{k_2} - \frac{1}{2}\alpha_{k_3}) \\ &\quad + w^3(\frac{3}{2}\alpha_{k_1} - \frac{3}{2}\alpha_{k_2} + \frac{1}{2}\alpha_{k_3} - \frac{1}{2}\alpha_{k_0}) \\ w &= \frac{4p}{2\pi} \mod 1 \\ k_n &= (\left\lfloor \frac{4p}{2\pi} \right\rfloor + n - 1) \mod 4\end{aligned} \tag{9}$$

DHM2020
L. Hanson et al. (Eds.)
© 2020 The authors and IOS Press.
This article is published online with Open Access by IOS Press and distributed under the terms of the Creative Commons Attribution Non-Commercial License 4.0 (CC BY-NC 4.0).
doi:10.3233/ATDE200012

Defining Kinematic Chains for Musculoskeletal Optimal Control Simulations via Automatic Differentiation

Johann PENNER [a,1], Sigrid LEYENDECKER [a]
[a] *Chair of Applied Dynamics, Friedrich-Alexander-Universität Erlangen-Nürnberg, Germany*

Abstract. Many digital human model applications are based on optimal control simulations of the musculoskeletal system. These simulations usually involve the derivatives of the underlying kinematic and dynamic model, which are in general not easy to derive analytically. In the direct transcription method DMOCC, we use the discrete Euler-Lagrange equations together with a discrete null space matrix and a nodal reparametrization, which are embedded into a constrained optimization problem. The abstract and formalizable structure of this method offers many possibilities for automation. Therefore, we use the CasADi nonlinear optimization and algorithmic differentiation tool to automatically derive the discrete Euler-Lagrange equation and a valid discrete null space matrix. This allows us an efficient and easy implementation of the DMOCC method for large multibody systems.

Keywords. musculoskeletal optimal control simulations, discrete mechanics, automatic differentiation

1. Introduction

The representation of musculoskeletal systems with multibody dynamics and cable-like muscles has become an essential tool to analyse human movement [1]. The actuation of these models via Hill muscles requires the calculation of the muscle paths, their lengths and changes in length during the movement, which is determined by the muscle wrapping problem [2,3]. In order to model and solve complex human motion tasks, an appealing approach is to formulate optimal control problems and to approximate their solution numerically. The development of automatic differentiation in resent years reveals efficient ways to create and solve these optimal control problems, which we make use of in this paper. We thereby focus on an automatic generation of the discrete Euler-Lagrange equations and the discrete null space matrix, see [4–6].

When simulating the dynamics of musculoskeletal systems, we formulate the dynamics of multibody system representing bones and joints and the dynamic muscle paths [2, 3, 7, 8], which wrap smoothly over adjacent obstacles, in terms of discrete Lagrange mechanics [4–6]. Setting up new musculoskeletal models in the present formula-

[1]Corresponding Author: Johann Penner, Chair of Applied Dynamics, Friedrich-Alexander-Universität Erlangen-Nürnberg, Immerwahrstrasse 1, 91058 Erlangen, Germany; E-mail: johann.penner@fau.de.

tion is an abstract, formalizable process that offers a wide range of options for automation. In particular for open kinematic chains, we use a discrete null space matrix and a nodal reparametrization of the unknowns (redundant director based coordinates) via incremental generalized coordinates in order to reduce the dimension of the system size in two steps [5, 6].

Note that the discrete null space matrix is not unique and can be found in different ways [5, 6]. In fact, a particularly elegant way is to represent the discrete null space matrix as the Jacobian of the nodal reparametrization, which describes the kinematics of the multibody system. This Jacobian can be calculated using automatic differentiation. Consequently, since higher order derivative information is needed anyway for the optimisation tasks, this offers opportunities for simplifying and automating the model creation.

Efficient methods for the implementation of the discrete Euler–Lagrange equations for generic mechanical systems with tree structured, rigid multibody system are shown in [9–11]. The benefits of a derivation of the underlying system dynamic with automatic differentiation has for example been shown in [12]. The idea of this work is to generate the discrete Euler-Lagrange equations, the discrete null space matrix and all higher order derivatives for the direct transcription method discrete mechanics and optimal control for constrained systems (DMOCC) [13] with the help of automatic differentiation. This significantly shortens and simplifies model creation compared to manual implementations. The interaction of the skeleton with the muscles and the contact formulation is currently formulated in detail in another paper.

CasADi [14] is an open-source tool for nonlinear optimization and algorithmic differentiation that provides an easy framework for the implementation of the DMOCC method. Here, the director formulation allows us a very modular and automated design of discrete Euler-Lagrange equations, once the discrete Lagrangian of the system and a nodal reparametrisation are setup. The derivatives of these functions, i.e. the variational integrator, can easily be nested into the nonlinear optimization program with CasADi.

2. Method

The main objective of the simulations in this work is the control of a musculoskeletal system, which must be steered from a given initial state to a predefined final state. Therefore, we apply the DMOCC formulation [13] to a biomechanical system, where bones and joints are represented as multibody system [5, 6] and the muscle path is modelled as the shortest connection between two points on obstacle surfaces [2,3]. As a result of that, the infinite dimensional optimal control problem is transcribed into a finite dimensional nonlinear programming problem that can be solved by any suitable standard algorithm.

2.1. Musculoskeletal Optimal Control Problem

To solve the optimization problem, we require higher order derivatives of the underlying dynamical system. The implementation these derivatives by hand is generally not an easy task. In addition, derivations are required for the discrete Euler-Lagrange equations and the discrete null space matrix. Consequently, the automation of all derivatives brings a great advantage for the creation and solution of optimal control problems.

2.1.1. Constrained Optimization Problem

The DMOCC [13] method can be summarized as

$$\min_{\boldsymbol{x}_d} J_d(\boldsymbol{x}_d)$$

$$\text{subject to} \quad \begin{array}{l} \cdot \text{ discrete Euler-Lagrange equations} \\ \cdot \text{ boundary and path conditions} \end{array}$$

where $\boldsymbol{x}_d = \{\boldsymbol{x}_n\}_{n=0}^{N}$ is the discrete optimisation vector with $N \in \mathbb{N}$, J_d is the discrete objective function, that is to be minimized subject to the discrete Euler-Lagrange equations of the system and further boundary and path conditions.

2.1.2. Discrete Euler-Lagrange Equations of the Musculoskeletal System

In our model, the discrete path $\boldsymbol{q}_d = \{\boldsymbol{q}_n\}_{n=0}^{N}$ is an approximation of the continuous path on a discrete time grid with constant time step $\Delta_t \in \mathbb{R}$ and $N+1$ time nodes. The discrete muscle path vector $\boldsymbol{\gamma}_d = \{\{\boldsymbol{\gamma}_{k,n}\}_{k=0}^{K}\}_{n=0}^{N}$ is defined on a discrete arc length grid with fixed arc length fraction $\Delta_s \in \mathbb{R}$ with $K \in \mathbb{N}$ and $K+1$ nodes. Note that, we have to solve for all $K-1$ unknown muscle path configurations $\boldsymbol{\gamma}_{k,n}$ at every time node.

We further choose the midpoint quadrature and finite differences to specify the discrete Lagrangian [4] for the mechanical system L_d and the geodesic L_γ. In addition, we use the discrete null space matrix $\boldsymbol{P}_d(\boldsymbol{q}_n)$ and the nodal reparametrisation $\boldsymbol{q}_{n+1} = \boldsymbol{F}_d(\boldsymbol{u}_{n+1}, \boldsymbol{q}_n)$ in terms of discrete local coordinate $\boldsymbol{u}_n$, see [5, 6]. The surface constraint function $\phi_d(\boldsymbol{q}_n, \boldsymbol{\gamma}_k)$ and the integrals of the scalar product of the constraints and the Lagrange multipliers $\mu_{k,n}$ are approximated in a similar way. This leads to the following discrete Euler-Lagrange equations

$$\boldsymbol{P}_d(\boldsymbol{q}_n)^T \cdot \left[\frac{\partial L_d(\boldsymbol{q}_{n-1}, \boldsymbol{q}_n)}{\partial \boldsymbol{q}_n} + \frac{\partial L_d(\boldsymbol{q}_n, \boldsymbol{q}_{n+1})}{\partial \boldsymbol{q}_n} - \frac{\partial \phi_d(\boldsymbol{\gamma}_k, \boldsymbol{q}_n)}{\partial \boldsymbol{q}_n}^T \cdot \mu_{k,n} \right] = 0 \tag{2}$$

$$\frac{\partial L_\gamma(\boldsymbol{\gamma}_{k-1}, \boldsymbol{\gamma}_k)}{\partial \boldsymbol{\gamma}_k} + \frac{\partial L_\gamma(\boldsymbol{\gamma}_k, \boldsymbol{\gamma}_{k+1})}{\partial \boldsymbol{\gamma}_k} - \frac{\partial \phi_d(\boldsymbol{\gamma}_k, \boldsymbol{q}_n)}{\partial \boldsymbol{\gamma}_k}^T \cdot \mu_{k,n} = 0 \tag{3}$$

$$\phi_d(\boldsymbol{\gamma}_k, \boldsymbol{q}_n) = 0$$

for $0 < n < N$ and $0 < k < K$, see [7, 8].

2.2. Automatic Derivation of the System Equations

The first step in creating a multibody simulation model, is the definition of the number, shape and connection of the rigid bodies. Knowing the dimensions, weight and location of every rigid body, one can easily define the Lagrangian of the system. The coupling of rigid bodies is achieved via configuration constraints that form a kinematic chain. The augmentation of the Lagrangian and discretization of Hamilton's principle then leads to time stepping equations that inherit certain characteristic properties of the continuous solution, the discrete Euler-Lagrange equations. To reduce the dimension of the resulting equations, it is possible to apply a discrete null space matrix and a nodal reparametrization [4–6].

This is an abstract and formalizable process that offers a wide range of options for automation. The main tasks here are the derivation of the Euler-Lagrange equations and the derivation of a null space matrix. Within this work, we use MATLAB for the implementation of the examples. Thereby, our formulation supports the null space method with a user defined reparametrization for oben kinematics chains and is internally based on CasADi [14].

2.2.1. Derivation of the Euler-Lagrange Equations

Lets consider a multibody system consisting of a kinematic chain with b rigid bodies. This yields a $12b$-dimensional configuration variable

$$\boldsymbol{q}(t) = \begin{bmatrix} \boldsymbol{q}^1 \\ \vdots \\ \boldsymbol{q}^b \end{bmatrix} \in \mathbb{R}^{12b}. \tag{4}$$

with $\boldsymbol{q}^\beta$, $\beta = 1,\dots,b$ representing the redundant coordinates of a rigid bodies. The Lagrangian of the system

$$\mathscr{L}(\boldsymbol{q},\dot{\boldsymbol{q}}) = \mathscr{T}(\boldsymbol{q},\dot{\boldsymbol{q}}) - \mathscr{V}(\boldsymbol{q}) \tag{5}$$

is composed by the kinetic energy $\mathscr{T}(\boldsymbol{q},\dot{\boldsymbol{q}})$ and potential energy $\mathscr{V}(\boldsymbol{q})$, where $\dot{\boldsymbol{q}}(t) \in \mathbb{R}^{12b}$ is the velocity of the system. Approximating the integral over the Lagrangian in the interval $[t_n, t_{n+1}]$ via midpoint quadrature and finite differences, yield the discrete Lagrangian

$$L_d(\boldsymbol{q}_n,\boldsymbol{q}_{n+1}) = \Delta_t \mathscr{L}\left(\left(\frac{\boldsymbol{q}_{n+1}+\boldsymbol{q}_n}{2}\right),\left(\frac{\boldsymbol{q}_{n+1}-\boldsymbol{q}_n}{\Delta_t}\right)\right) \tag{6}$$

where $\boldsymbol{q}_n$ is approximating $\boldsymbol{q}(t_n)$. Whit the mass matrix $\boldsymbol{M}$ and the gravity vector $\boldsymbol{g}$ of right dimension, the first derivatives of the discrete Lagrangian contribute to the discrete Euler-Lagrange equations and hence the variational integrator. A pseudo code in a syntax similar to MATLAB can be read as

```
function [L_d] = d_Lagrangian(q_n,q_np1)
    q = (q_np1+q_n)/2;
    q_dot = (q_n-q_np1)/dt;
    L_d = dt*(q_dot'*M*q_dot/2 - q'*M*g);
end

import casadi.*
q_np1 = MX.sym('qnp1',number_of_bodies*12,1);
q_n = MX.sym('qn',number_of_bodies*12,1);
q_nm1 = MX.sym('qnm1',number_of_bodies*12,1);

d_EulerLagrange = casadi.Function('DEL',{q_nm1,q_n,q_np1}, ...
    {gradient(d_Lagrangian(q_n,q_np1),q_n) + ...
    gradient(d_Lagrangian(q_nm1,q_n),q_n)});
```

The discrete Euler-Lagrange equations `d_EulerLagrange(q_nm1,q_n,q_np1)` are a function of three consecutive configurations, which can easily be nested to the constrained optimization problem. Thereby, CasADi provides the functionality to take further higher-order derivatives of the discrete Euler-Lagrange equations and to generate C code from them.

2.2.2. *Derivation of the Null Space Matrix for Open Kinematic Chains*

Lets now assume that the b rigid bodies are connected via $b-1$ joints and one anchor, such that the incremental update function reads

$$\boldsymbol{q}_{n+1} = \boldsymbol{F}_d(\boldsymbol{u}_{n+1}, \boldsymbol{q}_n) = \begin{bmatrix} \boldsymbol{F}_d^1(\boldsymbol{u}_{n+1}, \boldsymbol{q}_n) \\ \vdots \\ \boldsymbol{F}_d^b(\boldsymbol{u}_{n+1}, \boldsymbol{q}_n) \end{bmatrix} \in \mathbb{R}^{12b} \tag{7}$$

with F_d^α, $\alpha = 1, \ldots, b$. The entries of the incremental coordinate $\boldsymbol{u}_n$ represent the degrees of freedom of all kinematic pairs in the chain. The total degrees of freedom DoF define the dimension of the discrete local coordinate, i.e. $\boldsymbol{u}_n \in \mathbb{R}^{DoF}$. The first rigid body of every kinetic chain is assumed to be either anchored or free in space. In this setup, the Jacobian of the nodal reparametrization

$$\boldsymbol{P}_d(\boldsymbol{q}_n) = \left. \frac{\partial \boldsymbol{F}_d(\boldsymbol{u}_{n+1}, \boldsymbol{q}_n)}{\partial \boldsymbol{u}_{n+1}} \right|_{\boldsymbol{u}_{n+1}=\boldsymbol{0}} \tag{8}$$

evaluated at $\boldsymbol{q}_n$ is a suitable null space matrix. A pseudo code can be read as

```
function [F_d] = n_Reparam(u_np1,q_n)
    F_d = [F_1(u_np1,q_n);...
           ...
           F_b(u_np1,q_n)];
end

import casadi.*
u_np1 = MX.sym('unp1',DoF,1);
q_n = MX.sym('qn',number_of_bodies*12,1);

d_NullSpace = casadi.Function('P',{u_np1,q_n}, ...
    {jacobian(n_Reparam(u_np1,q_n),u_np1)});
```

Thereby, the properties of the reparametrization are to be defined by the user. This gives our implementation a maximum of flexibility, while standard connections can be provided by a library. The function `d_NullSpace(u_np1,q_n)` is calculated in a preprocessing step and is hand over to the optimization problem.

3. Results

We show two examples of musculoskeletal optimal control simulations. While the first example serves as validation with simplified complexity, a model of the kinematic model

of the upper body is presented in the second example. As mentioned before, we use the direct transcription method DMOCC to transcribe the optimal control problem into a nonlinear program that adopts the properties of structure preserving integrators. The constrained optimisation problem is solved via IPOPT [15]. Alternately, `fmincon` or to search for global optima `multistart` [16] from MATLAB can be used.

3.1. Two Muscle Arm Model

In this example (Figure 1), the multibody system consists of two rigid bodies and a revolute joint, which represent the upper and lower arm connected by the elbow joint. The upper arm is fixed in space, the configuration of the lower arm is given as $\boldsymbol{q} = [\boldsymbol{x}_s, \boldsymbol{d}_1, \boldsymbol{d}_2, \boldsymbol{d}_3]^T \in \mathbb{R}^{12}$, $\boldsymbol{n} \in \mathbb{R}^3$ is the joint axis and $\boldsymbol{\rho} \in \mathbb{R}^3$ is the joint location. The centre of mass is given by the vector $\boldsymbol{x}_s(t) \in \mathbb{R}^3$ and the orientation is indicated by an orthonormal body frame $\boldsymbol{d}_I(t) \in \mathbb{R}^3$ with $I = 1,2,3$ spanning a rotation matrix. In this example, the dynamics are discretized with $N = 50$ time nodes and the muscle path is discretized with $K = 20$ nodes per muscles. Furthermore, the nodal reparametrization in terms of the rotational degree of freedom $\boldsymbol{\theta}_n = u_n \boldsymbol{n}$ is given as

$$\boldsymbol{F}_d(u_{n+1}, \boldsymbol{q}_n) = \begin{bmatrix} \boldsymbol{x}_s - \mathrm{cay}(\widehat{\boldsymbol{\theta}_{n+1}}) \cdot \boldsymbol{\rho}_n \\ \mathrm{cay}(\widehat{\boldsymbol{\theta}_{n+1}}) \cdot \boldsymbol{d}_{I_n} \end{bmatrix} \tag{9}$$

where we use the Cayley map $\mathrm{cay} : so(3) \to SO(3)$. Herein $\widehat{(\bullet)} \in so(3)$ denotes a skew-symmetric matrix. We use the Cayley map because the differentiation of the Rodrigues formula for the evaluation of the exponential map does not work easily with automatic differentiation. The model comprise two muscles (biceps, triceps) and the actuation is

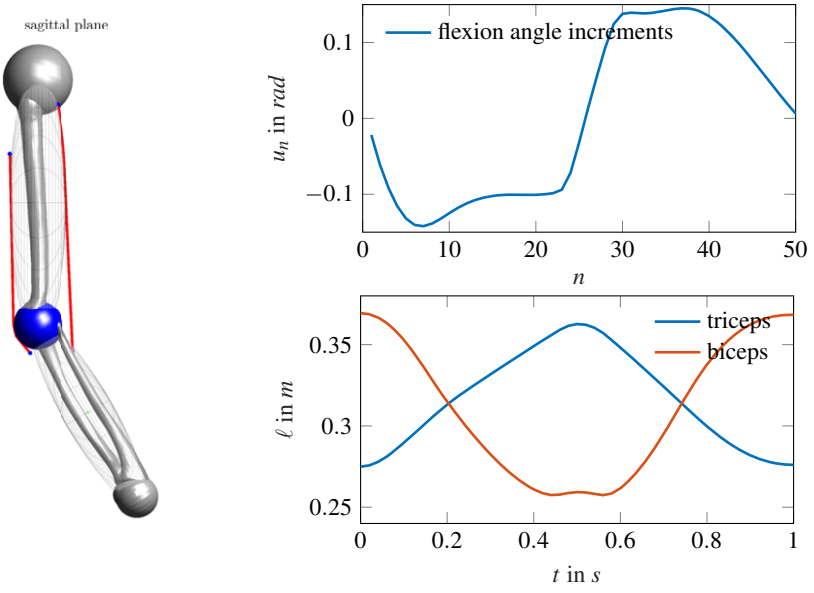

Figure 1. Configuration, joint angle change and muscle length evolution of the two muscle arm model[2] for a rest-to-rest manoeuvre are shown. The muscle path is plotted in red and the revolute joint is marked in blue.

realized by Hill-type muscle forces, similar to [2]. We solve a rest-to-rest manoeuvre from a given initial state to a predefined final state. The gradient, Jacobian and Hessian information for the optimization problem in IPOPT is carried out by CasADi. The incremental joint angle change and the muscle length evolution are shown in Figure 1 on the right side. The results show that the integrator and the optimal control simulation with the automatic differentiation work as expected. Due to the structure preserving properties of the integrator, the simulation works robustly even with coarse discretizations.

3.2. Upper Body Kinematic Model

The second multibody system comprises a kinematic chain with $b = 9$ rigid bodies, 8 joints and 12 degrees of freedom. Figure 2 shows the numbering of the rigid body and the joint list. The torso ($\beta = 1$) is fixed in space and is connected to the right humerus ($\beta = 2$) and left humerus ($\beta = 6$) via spherical joints, with $\boldsymbol{\theta}_n^{\{2,6\}} \in \mathbb{R}^3$. The ulna of the right arm ($\beta = 3$) and left arm ($\beta = 7$) is connected to the respective humerus via revolute joints, where $u_n^{\{3,7\}} \in \mathbb{R}$. Between the right ($\beta = 4$) and left ($\beta = 8$) radius and ulna, a revolute joint with $u_n^{\{4,8\}} \in \mathbb{R}$ is defined respectively. The right hand ($\beta = 5$) and the left hand ($\beta = 9$) are connected via revolute joints with $u_n^{\{5,9\}} \in \mathbb{R}$ to the respective radius. The rotation of a revolute joint $\boldsymbol{\theta}_n = u_n \boldsymbol{n}$ follows with the definition of the joint axis $\boldsymbol{n}$ and the joint location of the α-th joint with respect to the β-th body is given as $\boldsymbol{\rho}_\alpha^\beta$. With respect to Eq. (7) the mapping for the fixed torso reads

$$\begin{bmatrix} \boldsymbol{x}^1_{s_{n+1}} \\ \boldsymbol{d}^1_{I_{n+1}} \end{bmatrix} = \begin{bmatrix} \boldsymbol{x}^1_{s_n} \\ \boldsymbol{d}^1_{I_n} \end{bmatrix} \tag{10}$$

for $I = 1,2,3$. The mapping for the right arm with bodies $\beta = \{2,3,4,5\}$ reads

$$\begin{bmatrix} \boldsymbol{x}^\beta_{s_{n+1}} \\ \boldsymbol{d}^\beta_{I_{n+1}} \end{bmatrix} = \begin{bmatrix} \boldsymbol{x}^{\beta-1}_{s_{n+1}} + \operatorname{cay}(\widehat{\boldsymbol{\theta}^{\beta-1}_{n+1}}) \cdot \left(\boldsymbol{\rho}^{\beta-1}_\beta - \operatorname{cay}(\widehat{\boldsymbol{\theta}^\beta_{n+1}}) \cdot \boldsymbol{\rho}^\beta_\beta \right) \\ \operatorname{cay}(\widehat{\boldsymbol{\theta}^\beta_{n+1}}) \cdot \boldsymbol{d}^\beta_{I_n} \end{bmatrix} \tag{11}$$

where $I = 1,2,3$. The mapping for the left arm with bodies $\beta = \{6,7,8,9\}$ follows in the same way. The definition of the kinematic tree – with all rigid bodies and joints – and with that the reparametrization completes the model setup. No additional assembly of a null space matrix is necessary. With that, the extension of the DMOCC method to kinematic trees with a relatively large number of bodies is now much easier than through manual implementation. The next step is to automate the derivation of muscle path equations in a similar way.

4. Discussion

This work focuses on the definition and implementation of the discrete Euler-Lagrange equations for open kinematic chains with automatic differentiation, which are used to de-

[2]For the 3d bone model see https://www.thingiverse.com/thing:1543880.

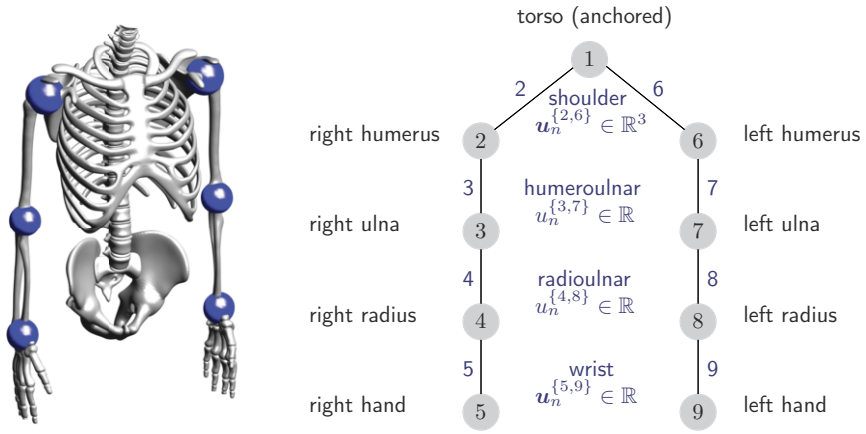

Figure 2. The configuration and the kinematic tree for the upper body model[2] is shown. The model comprises 9 rigid bodies with 12 degrees of freedom.

fine optimal control problems with DMOCC. All necessary derivatives were carried out with the help of the nonlinear optimization and algorithmic differentiation tool CasADi. This not only simplifies the solution to the optimization problem, but also the model creation benefits from that. In particular, we use a user defined reparametrization to calculate the discrete null space matrix for which no separate implementation is required. This simplifies and accelerates the creation and solution of the optimization problems transcribed by DMOCC.

By using CasADi to calculate the discrete null space matrix, it is possible to automate and simplify one of the most challenging tasks in our model assembly. Usually, the null space matrix $\boldsymbol{P}_d(\boldsymbol{q}_n) \in \mathbb{R}^{12b \times DoF}$ has to be assembled by traversing piecewise through the kinematic chain or has to be implemented by hand. Furthermore, the discrete Euler-Lagrange equations in Eqs. (2) and (3) are based on a nodal reparametrization $\boldsymbol{F}_d \in \mathbb{R}^{12b}$, which defines a suitable null space matrix by calculating its Jacobian. Thus, an additional implementation of the $12b \times DoF$ dimensional null space matrix is no longer necessary. Since the reparametrization remains definable by the user, our formulation also remains very flexible.

However, the presented method is limited to open kinematic chains and difficulties may arrive for practical application with inherent closed chains in the human skeleton, e.g. the shoulder girdle, forearm, grasping. However, for closed kinematic chains, one can formulate the open loop system a null space matrix and formulate an additional closure constraint. This procedure will still be much more efficient than formulating the complete system without a null space reduction. Our next steps include musculoskeletal optimal control simulations with a relative large number of rigid bodies (for example the upper body), muscles and general smooth wrapping surfaces that perform certain movement tasks. Therefore, we will automate the derivation of muscle path equations and contact formulation in a similar way.

Acknowledgements

The authors acknowledge the financial support by the German Federal Ministry of Educaiton and Research of Germany in the framework of DYMARA (project number 05M16WEB).

References

[1] Delp SL, Anderson FC, Arnold AS, Loan P, Habib A, John CT, Guendelman E and Thelen DG. OpenSim: Open-Source Software to Create and Analyze Dynamic Simulations of Movement. IEEE Transactions on Biomedical Engineering, November 2007, 54(11):1940–1950.

[2] Maas R, Leyendecker S. Biomechanical optimal control of human arm motion. Proceedings of the Institution of Mechanical Engineers, Part K: Journal of Multi-body Dynamics, December 2013, 227(4):375–389.

[3] Scholz A, Sherman M, Stavness I, Delp S, Kecskeméthy A. A fast multi-obstacle muscle wrapping method using natural geodesic variations. Multibody System Dynamics, 2016, 36(2):195–219.

[4] Marsden JE, West W. Discrete mechanics and variational integrators. Acta Numerica, 2001, 10:357–514.

[5] Betsch P, Leyendecker S. The discrete null space method for the energy consistent integration of constrained mechanical systems. Part II: Multibody dynamics. International journal for numerical methods in engineering, 2006, 67(4):499–552.

[6] Leyendecker S, Marsden JE, Ortiz M. Variational integrators for constrained dynamical systems. ZAMM-Journal of Applied Mathematics and Mechanics/Zeitschrift für Angewandte Mathematik und Mechanik: Applied Mathematics and Mechanics, 2008,88(9):677–708.

[7] Penner J, Leyendecker S. Multi-Obstacle Muscle Wrapping Based on a Discrete Variational Principle. In: Faragó I, Izsák F, Simon P, editos. Progress in Industrial Mathematics at ECMI 2018, volume 30, Cham, 2018: Springer International Publishing, p. 223–229.

[8] Penner J, Leyendecker S. A Hill Muscle Actuated Arm Model with Dynamic Muscle Paths. In: Kecskeméthy A, Geu Flores F, editos. Multibody Dynamics 2019, volume 53, Cham, 2019: Springer International Publishing, p. 52–59.

[9] Johnson ER, Murphey TD. Discrete and continuous mechanics for tree representations of mechanical systems. In 2008 IEEE International Conference on Robotics and Automation, Pasadena, CA, USA, May 2008, p. 1106–1111.

[10] Johnson ER, Murphey TD. Scalable Variational Integrators for Constrained Mechanical Systems in Generalized Coordinates. IEEE Transactions on Robotics, December 2009, 25(6):1249–1261.

[11] Björkenstam S, Leyendecker S, Linn J, Carlson JS, Lennartson B. Inverse Dynamics for Discrete Geometric Mechanics of Multibody Systems With Application to Direct Optimal Control. Journal of Computational and Nonlinear Dynamics, October 2018, 13(10):101001.

[12] Giftthaler M, Neunert M, Stäuble M, Frigerio M, Semini C, Buchli J. Automatic differentiation of rigid body dynamics for optimal control and estimation. Advanced Robotics, November 2017, 31(22):1225–1237.

[13] Leyendecker S, Ober-Blöbaum S, Marsden JE, Ortiz M. Discrete mechanics and optimal control for constrained systems. Optimal Control Applications and Methods, 2010, 31(6):505–528.

[14] Andersson J, Gillis J, Horn G, Rawlings JB, Diehl M. CasADi: a software framework for nonlinear optimization and optimal control. Mathematical Programming Computation, March 2019, 11(1):1–36.

[15] Wächter A, Biegler LT. On the implementation of an interior-point filter line-search algorithm for large-scale nonlinear programming. Mathematical Programming, March 2006, 106(1):25–57.

[16] Ugray Z, Lasdon L, Plummer J, Glover F, Kelly J, Martí R. Scatter Search and Local NLP Solvers: A Multistart Framework for Global Optimization. INFORMS Journal on Computing, August 2007, 19(3):328–340.

DHM2020
L. Hanson et al. (Eds.)

© 2020 The authors and IOS Press.
This article is published online with Open Access by IOS Press and distributed under the terms of the Creative Commons Attribution Non-Commercial License 4.0 (CC BY-NC 4.0).
doi:10.3233/ATDE200013

Grasp Synthesis for Digital Hands with Limited Range of Motion in Their Thumb Using a Grasp Database

Reiko TAKAHASHI [a,1], Natsuki MIYATA [b] and Yusuke MAEDA [a]
[a] *Yokohama National University, Graduate School of Engineering Science, Yokohama, Japan*
[b] *National Institute of Advanced Industrial Science and Technology, Artificial Intelligence Research Center, Tokyo, Japan*

Abstract. For virtual evaluation of universal design products, it is necessary to synthesize natural grasps for various hands including those with disability. As one of the disabilities, we focused on the limitation of the thumb's range of motion (ROM). For example, carpal tunnel syndrome (CTS) is a typical disease that limits thumb's ROM. Though there is no doubt that the range of motion affects the whole grasp, detailed grasp strategy has not been studied so far due to the difficulties in collecting data from such patients. Therefore, in this paper, we propose to synthesize grasping postures by the thumb's ROM-limited digital hands based on the observation of an actual subject whose hand is artificially-disabled. The synthesized postures of the healthy hand and the thumb's ROM-limited hand were obviously different. We applied a contact-region-based method for grasp synthesis for ROM-limited hand and succeeded in synthesizing the grasping postures that reflect the features of the thumb's ROM-limited hands' grasps.

Keywords. grasp synthesis, universal design, digital hands, virtual evaluation

1. Introduction

For the virtual evaluation using a digital hand, it is necessary to synthesize natural grasps for arbitrary product model. In [1], studies about data-driven grasp synthesis were surveyed. Examples of data-driven grasp synthesis approaches are [2]–[6]. Data-driven approaches use the database of real human grasps and the necessary data are identified based on known grasp classification (e.g., [7]–[11]). Therefore, it is possible to synthesize natural grasps that are more similar to human real grasps than analytical approaches. Previous studies on grasp synthesis have been focusing mainly on healthy hands. However, non-healthy hands should also be considered as designing universal design products. Grasps by non-healthy hands differ from those of healthy hands. Thus, in the virtual evaluation of universal design products, it is important to synthesize natural grasps by various hands including non-healthy ones.

[1]Corresponding Author. [takahashi-reiko-cf@ynu.jp]

Grasps by hands with limited range of motion (ROM) are typical examples of grasps different from those of healthy hands. In particular, because the thumb is used for 98–99% of the grasps [12], the change of grasping posture becomes noticeable when the ROM of the thumb is limited. Therefore, in our research, hands with limited thumb's ROM are focused on. Patients with carpal tunnel syndrome (CTS) are a typical example of those whose thumbs' ROM is limited. CTS is the most common peripheral nerve entrapment syndrome worldwide [13]. Particularly in patients with severe CTS, it is known that the palmar abduction of the carpometacarpal (CM) joint is restricted (e.g., [14]). Since the opposition of the thumb is hindered, significant change in grasping posture of the hands is expected when their palmar abduction of the CM joint is limited.

We have investigated the grasp features when the ROM of palmar abduction of the thumb's CM joint was artificially limited [15] and attempted synthesizing the grasps when the thumb's palmar abduction is limited based on the features [16]. However, the grasps of the thumb's ROM-limited hand cannot be synthesized well. For thumb's ROM-limited hands, two grasp styles were observed, but it was not possible to control the two observed grasp styles in grasp synthesis using the method proposed in [16]. Therefore, in this paper, we present a newer method that can synthesize the grasps both of the healthy hand and the thumb's ROM-limited hand. Realization of grasp synthesis for ROM-limited hands would contribute to evaluation of usability of universal design products virtually.

2. Method of grasp synthesis

2.1. Algorithm of grasp synthesis

In this paper, the method of grasp synthesis for healthy hands proposed in [5] and [6] is applied to grasp synthesis for ROM-limited hands. This section explains an overview of the algorithm of grasp synthesis. It is cited from [16].

The greatest feature of this method is the use of grasp database based on the "contact regions." The outline of the method of grasp synthesis proposed in [5] and [6] is shown in Fig. 1. The contact regions are the hand surface areas that touch the object when grasping. Hirono et al. divided the hand surface into 34 regions, and classified grasps that appear in the taxonomy proposed in [7] and [8] based on the contact regions. Furthermore, additional grasping postures with different number of used fingers and with different inter-fingertip distance were selected, and finally, a grasp database including 801 natural grasps was created. The postures with different number of used fingers were added to the grasp database in order to cover expected possible grasps. In addition, the postures with different inter-fingertip distance were added to synthesize the grasp for a newly given object by interpolating a few postures in the grasp database.

The advantage of the grasp database based on the contact regions is that the posture in the grasp database whose contact regions are same as the input regions can be used to synthesize the initial posture even if the grasped object is different. Therefore, it is expected to have wide applicability to object variations of size and shape.

The input information of grasp synthesis is the contact regions and the points of grasping targets on the object surface. In the method, postures having the same contact regions as the input data are searched from the database firstly. Then, an initial posture is

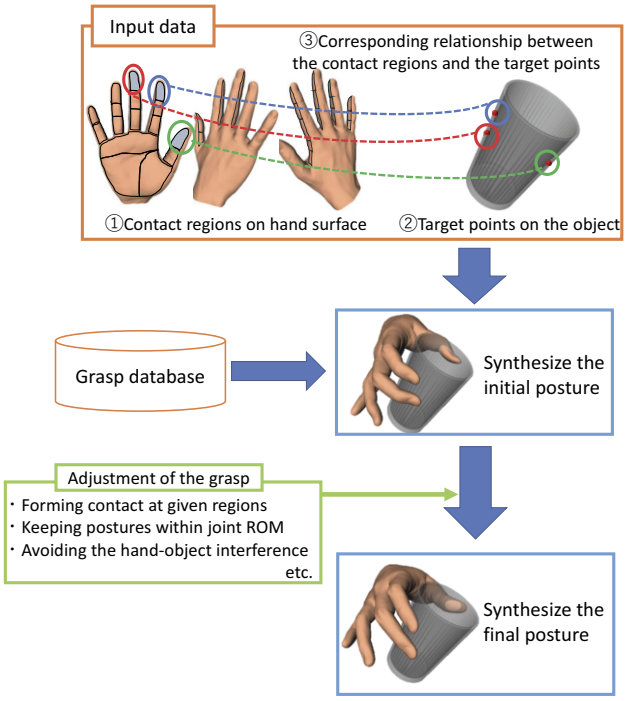

Figure 1. Outline of the method of grasp synthesis proposed in [5] and [6]

synthesized by interpolating the reference grasps whose contact regions are same as the input data based on the distance between the target points on the object surface. In this step, the hand model is also aligned with the object by matching the contact points on the hand with the corresponding contact target points on the object.

As the initial posture is not guaranteed to be a natural and proper grasp, the initial posture is adjusted through optimization, that considers following points: forming a contact in appropriate orientation, self-interference and hand-object interference avoidance, and keeping postures within joint ROM.

2.2. Grasp synthesis method for thumb's ROM-limited hand

In [15], we observed the grasp features of the thumb's ROM-limited hand based on the contact regions. Two grasp styles were observed to be typically different from the healthy hand. One was the style that uses the same contact regions as the healthy hand and the other was the style that uses the thumb's lateral region. The style that uses the thumb's lateral region means the grasp style that uses the thumb's radial region in the power grasp, to wrap an object with fingers, and uses the palm and the thumb's ulnar region in the precision grasp, to support an object with fingertips.

In [16], we tried to synthesize the grasping postures using the Hirono et al.'s algorithm explained in Sec. 2 with the limited ROM data. However, it was not possible to control the two observed grasp styles in grasp synthesis. In other word, two typical styles

of thumb's ROM-limited hands cannot be synthesized absolutely using the Hirono et al. 's method because this is developed for healthy hands.

Therefore, in this paper, we add the postures that use the thumb's lateral region to the grasp database proposed by Hirono et al., and further modify the calculation algorithm when synthesizing the posture to synthesize the grasp that reflects the features of the thumb's ROM-limited hand. The algorithm was implemented on DhaibaWorks, a platform software developed by the National Institute of Advanced Industrial Science and Technology. The details of changing points from the method for healthy hands are described below.

2.2.1. Database extension

In our previous study [15], the grasp style that uses the thumb's lateral region was not observed in healthy hands. Therefore, the conventional grasp database for the healthy hand [6] did not include postures in the style. In [16], it was shown that it was possible to synthesize the grasp using the thumb's lateral region from the conventional database by changing the grasping target points, but it was also predisposed to synthesize an unnatural postures.

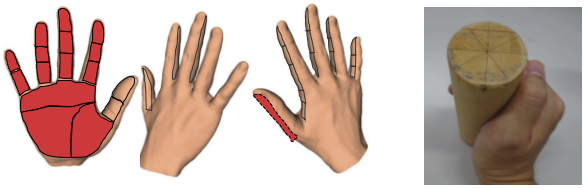

(a) Using the thumb's palmar side

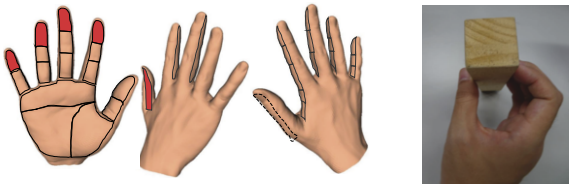

(b) Using the thumb's ulnar side

Figure 2. Grasping styles of the thumb's ROM-limited hands

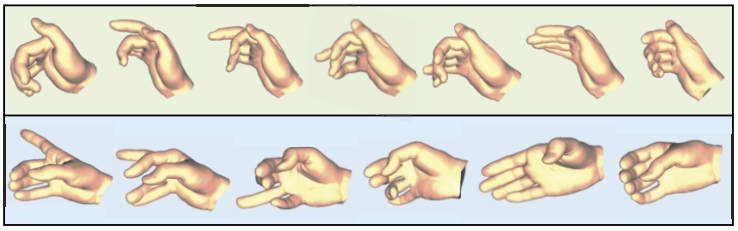

Figure 3. Added postures for the grasp database

Therefore, we aim to synthesize the grasps that reflects the features of the thumb's ROM-limited hand by adding grasping postures using the thumb's lateral region to the grasp database. For other postures, the database for healthy hands is used, and the limitation of their ROM is dealt with in the optimization calculation part. It is unrealistic to recreate all the database according to various hand function states considering the number of postures included in the database. Therefore, we try to synthesize the grasp that reflects the features peculiar to the hand function by adding only the necessary grasping postures to the database for healthy hands.

The grasp styles actually added to the database are shown in Fig. 2. We do not consider grasping styles with fewer fingers, which tend to be unstable in the thumb's ROM-limited hand. Therefore, the number of fingers is not changed, and the postures in which only the distance between the fingertips is changed are added to the database. Since an initial posture is synthesized by interpolation of postures in the database, it is necessary to include the postures with different distance between the fingertips for each finger in the database. The added postures are shown in Fig. 3. These postures were measured when grasping the actually objects. When measuring the postures in which one finger was extended, an object with a wide diameter at the contact position of that finger was used. The 13 postures that were newly measured as the unique grasping postures of the thumb's ROM-limited hand are added to the 801 postures obtained by converting the database by Hirono et al. according to the development environment of this study. Thus the new grasp database has 814 postures in total.

2.2.2. Changing the calculation algorithm

In this study, the following four points are used as the evaluation indices in the optimization process. (1) The degree of coincidence between the coordinates and the directions of the normal vectors of the contact regions and the grasp target points, (2) The margin for the ROM boundary that considers joint coordination, (3) The amount of interference between the hand model and the object model, (4) Degree of contact with the object between the contact regions where the grasp target points are not given. We implemented optimization calculation by Powell's method. The position of the wrist joint and the angles of all joints are used as variables.

In particular, the margin for the ROM boundary was determined by the maximum and minimum joint angles in the previous method [6]. However, due to joint coordination, the ROM should be expressed in a higher dimensional space. Therefore, the information of the joints' angles in the high-dimensional space are projected onto two-dimensional planes to model the ROM. In this modeling, the ROM data actually measured by a healthy hand or a ROM-limited hand is used. Although the thumb joint can move complicatedly, it is possible to properly reflect the ROM limitation of the thumb on the synthesized posture by considering the joint coordination for each two joint angles in this way.

3. Results and Discussions

Grasp synthesis was attempted using the proposal method. Grasping postures were synthesized under the following three conditions: (1) a healthy hand, (2) a thumb's ROM-limited hand using the same style as a healthy hand, (3) a thumb's ROM-limited hand

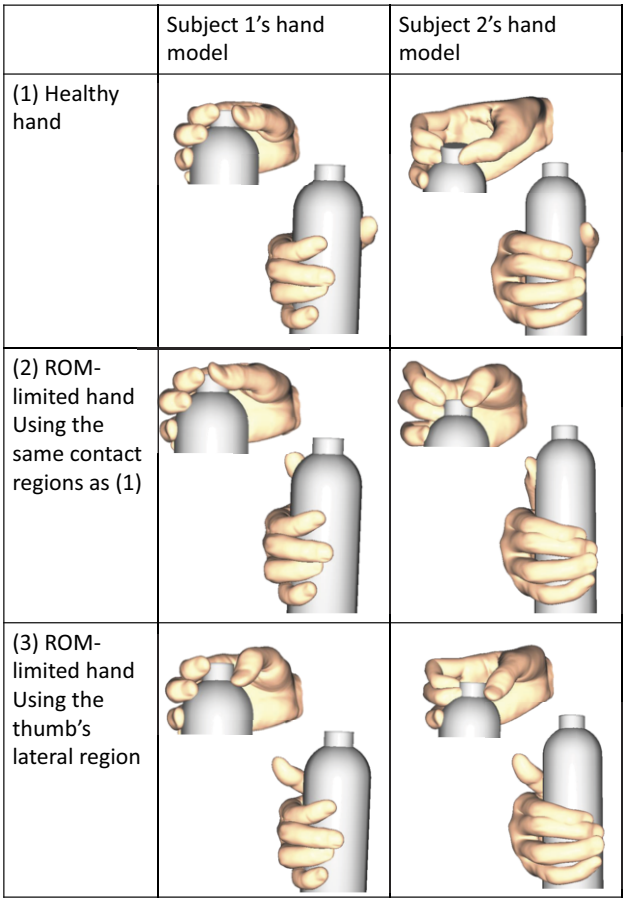

Figure 4. Examples of the results of the grasp synthesis

using the thumb's lateral region. The same contact regions were given in (1) and (2), and the region on the thumb to be used was changed in (3). The measured ROM of a healthy hand was used in (1), and the measured ROM of a thumb's ROM-limited hand was used in (2) and (3). The grasp target points were changed by trials and errors under all conditions. We used hand models that imitate two different subjects. and confirmed that the grasps can be synthesized even if the hands' shapes and their ROMs are different.

Examples of synthesized grasping postures are shown in Fig. 4. The object to be grasped was a bottle, and two postures were synthesized for the bottle. One was the posture of power grasp with the whole hand, assuming to drink the bottle, and the other was the posture of precision grasp with fingertips assuming to open the cap. According to the previous study [6], the validity of the synthesized posture were confirmed visually. It was visually confirmed that the specified contact regions were in proper contact with the object in Fig. 4. In addition, it was also confirmed numerically that the joints' angles were inside the ROM. Therefore, it was concluded that valid grasps were synthesized under all conditions.

The self-interference seemed to remain slightly in Fig. 4. However, it was thought that this self-interference was an effect of skin deformation. The hand model could not reproduce skin deformation because it was defined as rigid body, so the range of possible skin deformation was excluded from the amount of self-interference in the optimization process. It was considered that the self-interference remaining in Fig. 4 had no problem because it was due to this skin deformation.

However, the angle of the index finger's metacarpophalangeal (MP) joint was unnatural in the power grasp of subject 1. The joint angle was inside the ROM and it could be realized as a hand posture, but it was seemed unnatural as a grasping posture. The index finger was expected to be oriented along the middle finger. This is a remaining problem, and it is necessary to consider how to eliminate these unnaturalness.

4. Conclusion

In this study, we synthesized grasps for the thumb's ROM-limited hand, which can be used to evaluate universal design products virtually. The grasp synthesis method for a healthy hand [6] was extended by augmented grasp database and consideration of joint coordination for this purpose. It was confirmed that both grasps for healthy hands and grasps that reflected the features of thumb's ROM-limited hands were synthesized using the proposed method.

In the future, we will increase the number of grasping objects, evaluate the validity of the synthesized postures, and improve the optimization process to synthesize more natural grasps. Also, the current program's calculation time is very long. Therefore, it is necessary to reduce the calculation time. In addition, adjustment of the grasp target points, which is made by trial and error in our current method, should be automated.

Acknowledgement

This work was partly supported by JSPS KAKENHI Grant Number JP17H05918 and JP20J20651.

References

[1] Bohg J, Morales A, Asfour T, Kragic D. Data-driven grasp synthesis-a survey. IEEE Transactions on Robotics, 2014, 30(2), 289–309.

[2] Kyota F, Watabe T, Saito S Nakajima M. Detection and evaluation of grasping positions for autonomous agents. In: Proceedings of 2005 International Conferende on Cyberworlds, 2005 Nov, Singapore, 453–460.

[3] Ciocarlie MT, Allen PK. Hand posture subspaces for dexterous robotic grasping. The International Journal of Robotics Research, 2009, 28(7), 851–867.

[4] Goldfeder C, Allen PK. Data-driven grasping. Autonomous Robots, 2011, 31(1), 1–20.

[5] Miyata N, Hirono T, Maeda Y. Grasp database that covers variation of contact region usage. In: Proceedings of 2013 IEEE International Conference on Systems, Man, and Cybernetics, 2013 Oct, Manchester, UK, 2635–2640.

[6] Hirono T, Miyata N, Maeda Y. Grasp synthesis for variously-sized hands using a grasp database that covers variation of contact region. In: Proceedings of the 3rd International Digital Human Modeling Symposium, 2014 May, Tokyo, Japan, 11.

[7] Feix T, Pawlik R, Schmiedmayer H-B, Romero J, Kragic D. A comprehensive grasp taxonomy. In: Robotics, Science and Systems Conference: Workshop on Understand the Human Hand for Advanced Robotic Manipulation, 2009, USA.

[8] Feix T, Romero J, Schmiedmayer H-B, Dollar AM, Kragic D. The GRASP taxonomy of human grasp types. IEEE Transactions on Human-Machine Systems, 2016, 46(1), 66–77.

[9] Napier JR. The prehensile movements of the human hand. The Journal of Bone and Joint Surgery, 1956, 38(4), 902–913.

[10] Kamakura N, Ohmura M, Ishii H, Mitsuboshi F, Miura Y. Positional patterns for prehension in normal hands. Journal of Rehabilitation Medicine (in Japanese), 1978, 15(2), 65–82.

[11] Lee K-S, Jung M-C. Common patterns of voluntary grasp types according to object shape, size, and direction. International Journal of Industrial Ergonomics, 2014, 44, 761–768.

[12] Gonzalez F, Gosselin F, Bachta W. Analysis of hand contact areas and interaction capabilities during manipulation and exploration. IEEE Transactions on Haptics, 2014, 7(4), 415–429.

[13] Padua L, Coraci D, Erra C, Pazzaglia C, Paolasso I, Loreti C, Caliandro P, Hadson-Webb L-D. Carpal tunnel syndrome: clinical features, diagnosis, and management. The Lancet Neurology, 2016, 15(12), 1273–1284.

[14] Marquardt TL, Nataraj R, EvansPJ, Seitz Jr WH, Li Z-M. Carpal tunnel syndrome impairs thumb opposition and circumduction motion. Clinical Orthopaedics and Related Research, 2014, 472(8), 2526–2533.

[15] Takahashi R, Miyata N, Maeda Y, Fujita K. Grasps under Artificially-limited Thumb's Joint Range of Motion –Posture Analysis with ROM Boundary and Muscle Loads–. In: Proceedings of 2018 International Symposium on Micro-NanoMechatronics and Human Science, 2018 Dec, Nagoya, Japan, 253–255.

[16] Takahashi R, Miyata N, Maeda Y, Fujita K. Grasp Synthesis for Digital Hands with Limited Range of Motion in Their Thumb Joints. In: Proceedings of 2019 IEEE International Conference on Systems, Man, and Cybemetics, 2019 Oct, Bari, Italy, 191–196

DHM2020
L. Hanson et al. (Eds.)

© 2020 The authors and IOS Press.
This article is published online with Open Access by IOS Press and distributed under the terms of the Creative Commons Attribution Non-Commercial License 4.0 (CC BY-NC 4.0).
doi:10.3233/ATDE200014

The Use of Digital Human Modelling for the Definition and Contextualisation of a Direct Vision Standard for Trucks

Russell MARSHALL[1], Steve SUMMERSKILL, Abby PATERSON and Anthony ELAND
Loughborough University, School of Design and Creative Arts, Loughborough, LE11 3TU, UK

Abstract. This paper presents research performed on behalf of Transport for London in the UK addressing the over representation of trucks involved in accidents with vulnerable road users where issues with driver vision are often cited as the main casual factors. A Direct Vision Standard for London and potentially for Europe has been developed that utilizes a volumetric assessment of field of view performance. This paper presents research into how to contextualize the somewhat abstract volumetric performance scores into real world metrics using digital human models. The research modelled 27 trucks currently available from major manufacturers and analyzed their volumetric performance. It also explored a supplementary process using digital human models define the minimum threshold of field of view performance. The current proposal utilizes thirteen human models, representing 5th %ile Italian females, positioned to front, left and right of the cab. The minimum standard was developed to ensure that no blind spot exists between the regulations for mirror coverage and the new Direct Vision Standard. The research is ongoing in line with the finalization of the standard at a European level.

Keywords. DHM, Human Modelling, Direct Vision, Trucks, Vulnerable Road Users, Standardization

1. Introduction

In 2014 Transport for London (TfL) commissioned research to better understand the variability in driver vision in Trucks (Heavy Goods Vehicles – HGVs) on UK roads. The impetus for this research was a growing concern that blind spots exist around the cab of trucks that prevent the driver from being able to see other road users, and in particular so-called Vulnerable Road Users (VRUs) namely cyclists and pedestrians. This concern was supported by road accident data analysis performed on the UK STATS 19 database that showed that whilst road accident casualties in the UK were falling (49% reduction between 2000 and 2012) the trend was the opposite for cyclists, with a National increase of 21% and a 59% increase in Greater London [1], [2]. Furthermore, whilst only accounting for 4% of road miles, category N3 Trucks (>12 tonnes) were overrepresented in accidents with VRUs.

[1] Corresponding Author, Email: R.Marshall@lboro.ac.uk.

One of the main findings from the research was that standard truck configurations have blind spots in direct vision that can hide VRUs from the driver's view. The research therefore highlighted the need for a new vehicle standard for direct vision in HGVs [3].

In 2015 TfL responded by commissioning further research into the development of a novel Direct Vision Standard (DVS) to define methods for measuring drivers' Field of View (FoV) and to establish both a minimum standard for direct vision and a means to rate existing and future vehicles for their direct vision performance [4].

This paper discusses a key aspect in the development of the DVS namely where the minimum standard should be set. This posed two main challenges: the first was what should be measured to quantify direct vision? the second was what measure is appropriate for a minimum requirement?

2. Methods

2.1. Overview

Based on previous research the DVS was developed to exploit a volumetric FoV technique [5], [6] implemented initially in the SAMMIE DHM system [7]. The volumetric technique provides a number of advantages for the development of a DVS in particular it provides opportunities to obtain objective measures of driver vision.

As shown in Figure 1, the volumetric projection forms an extended cone from a driver's eye point through a window or reflected via a mirror. In terms of direct vision performance, the first challenge was to identify how the projections should be measured

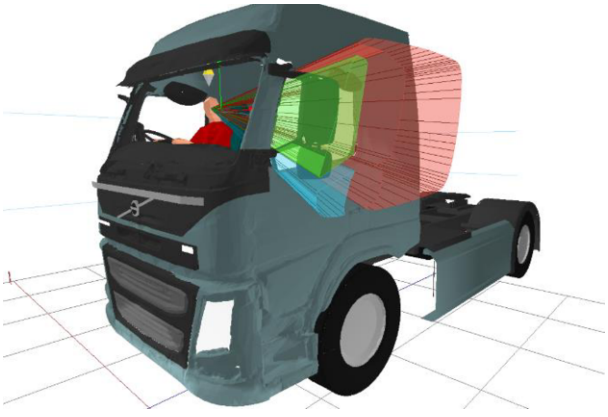

Figure 1. Volumetric projection of FoV in SAMMIE.

The starting point for these investigations explored accident data for insights into the area of greatest risk as a basis for the evaluation. Insights from accident data analysis identified that cyclists were more likely to be involved in collisions to the passenger side of the vehicle typically in a turning manoeuvre. Conversely pedestrians were more likely to be involved in collisions to the front when the truck pulls away from stationary [8]. However, the data do not provide a means to further define this area of greatest risk. To resolve the issue the research explored compatibility with other standards.

At the time there were no existing direct vision standards for trucks. There are however, standards that mandate FoV requirements for indirect vision such as UNECE

Regulation 46 [9]. It was therefore decided to ensure that the DVS should be compatible with the existing FoV requirements for indirect vision such that there would be no blind spots around the vehicle when combining direct and indirect vision. The FoV limits specified around the truck cab mandated to be visible via indirect vision formed the basis of the area of greatest risk for the DVS. Unlike the specification of indirect vision the DVS did not rely on only a 2-dimensional area, but instead extended the area on the ground vertically to form an 'Assessment Volume' around the cab. The proportion of that volume that could then be seen via direct vision would then form the basic metric for the objective rating of direct vision performance.

2.2. Setup

2.2.1. Vehicle Sample

It was critical to the research that the majority of the Euro 6 truck fleet were accounted for in the vehicle sample. All major manufacturers were contacted and vehicles from DAF, Mercedes, Scania, Volvo, MAN, Renault, and Dennis were evaluated in CAD. The final sample consisted of 27 unique vehicles.

2.2.2. The Driver's Eye Point

The projection technique is reliant upon an eye point definition as this is the source of the projections. The process ultimately used a combination of existing standards such as SAE J1050 [10], SAE J1516 [11] together with a hip to neck point offset that took into account anthropometric variability across the European population. Three eye points were ultimately defined to represent forward, left and right vision.

2.2.3. Projection of Direct Field of View

The analysis utilized Rhinoceros 3D (Rhino) for the volumetric projections to take advantage of additional geometry editing tools such as 'MeshOutline' and various Boolean operations. The use of Rhino also allowed demonstrated that the process could be applied using available and relatively inexpensive CAD tools.

2.2.4. Assessment Volume

As previously discussed the Assessment Volume was formed from the limits of the indirect vision coverage as specified in Regulation 46 [9], as shown in Figure 2. The volume also extended 1m rearwards of the driver's eyepoint. Additionally, the Dutch male population were used together with the premise that a driver being able to see the head and shoulders of a person would allow recognition. Thus, the volume height was set to correspond to the shoulder height of the 99th %ile Dutch male, resulting in vertical dimension of 1.602 m.

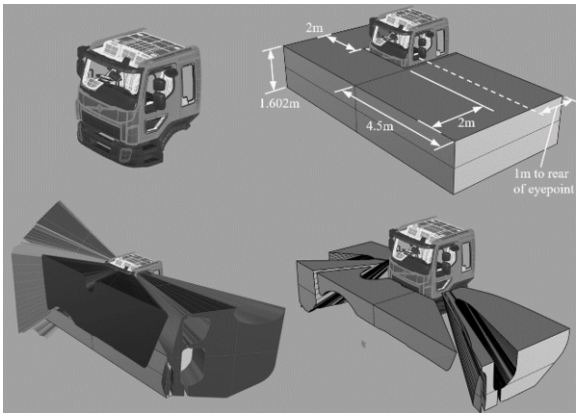

Figure 2. Assessment volume and its intersection with the projected FoV.

2.3. Calculation of Volumetric FoV

The FoV afforded the driver of the area of greatest risk is calculated by intersecting the projected FoV with the Assessment Volume (Figure 2). The remaining volume therefore represents what the driver would be able to see in proximity to the truck cab. The volume can then be calculated in mm^3 to provide an objective measure of FoV performance.

3. Results

The results consisted of a set of volumetric scores for each vehicle. Figure 3 shows a summary of these data for each vehicle in its maximum and minimum cab mounting height.

The variability in performance ranges from around 2.5 m^3 through to nearly 20 m^3. There is a clear differentiation in performance across the best to worst performing vehicles. However, what these data do not convey is what should be considered an appropriate baseline of performance, especially when the total volume of the Assessment Volume is more in the region of 50 m^3 and therefore even the best performing vehicle only provides direct vision of less than half of the area of greatest risk.

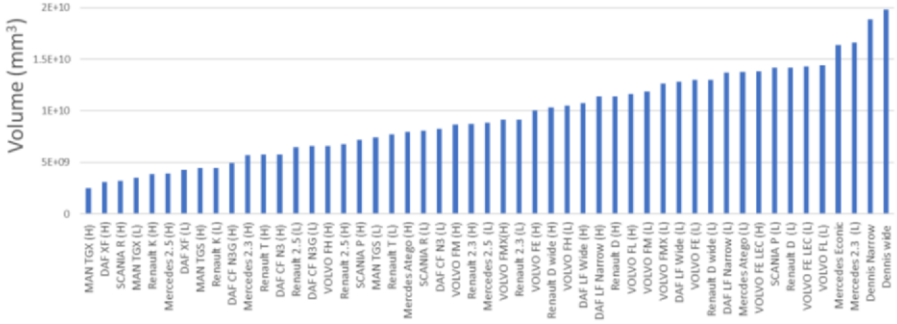

Figure 3. Volumetric scores for all trucks.

4. Methods 2

4.1. Overview

The volumetric scores provide a high resolution, objective, measure of the FoV and a means to compare vehicle performance. However, the data are abstract (what does 20 m^3 mean?), they lack context (how many m^3 are enough?) and ultimately fail to answer the question of where should a minimum threshold be placed? An alternative approach was required to contextualize the volumetric data.

Previous research in this area had taken an approach of using human models of VRUs in proximity to the cab [2], [3]. This allowed some objective measures to be determined, such as how far can a cyclist be from the side of the cab before they are no longer visible to the driver, but these approaches consistently raised issues with what needs to be seen of a VRU to be visible and recognizable to the driver? However, it was deemed essential to have some element of real road users in the assessment for context. Being able to define that a particular VRU is visible in a particular location provides the basis for determining a minimum performance standard. This is much easier to visualize, to comprehend and for stakeholders to agree is appropriate, than a more abstract volumetric score. It is also important that the contextualization is seen as an augmentation to the volumetric score. The volumetric score, whilst abstract is ideal for manufacturers to work with to optimize their performance and accounts for the full FoV. Thus, the aim was to develop a method that provided synergy with the volumetric approach but not replace it.

4.2. VRU Human Models

It was acknowledged that other standards such as FMVSS 111 [12] use cylindrical visual markers for assessments of vision and electronic sensing around vehicles. However, from the outset these were discounted. One of the primary aims of this additional test was to add context, and empathy, to the assessment. Thus, the use of human models was seen as essential. As stated previously, accident data suggested that two main accident scenarios involved cyclists and pedestrians. This led to the evaluation of a range of options exploring three variables. The first was the type of human model, including humans in a cycling posture and a bicycle model, and humans in a standing posture as pedestrians. The second was the number of human models, taking into account the characteristics of the FoV and the complexity of the assessment. The final variable was the locations of these models around the cab. Having explored a range of options and balancing complexity with performance, an assessment was defined and agreed.

It was decided that pedestrians would be used as the VRU models throughout. This was due to their simpler geometry and thus a more straightforward assessment of what should be seen. For example, if a cyclist were to be used, would seeing part of the bicycle be acceptable? If the cycle is ignored then a human model in a cycling posture is arguably just pedestrian in a standing posture with a different stature. In order to ensure a high degree of coverage a 5^{th} %ile Italian female, by stature, was employed. This ensured that over 99% of the European population would be visible. The use of child anthropometry was explored. However, accident data suggested that children were very rarely involved in accidents with trucks though it was noted that this may be different outside the UK. In addition, 5^{th} %ile Italian female stature is around 1500 mm, this is broadly equivalent to a 50^{th} %ile 11 / 12 year old child in most European countries and it was argued that most

children below that age would not likely be in the road environment unaccompanied by an adult.

It was decided to place VRU models to all three sides and to orientate these as though the pedestrians were crossing the road in front of the cab or waiting to cross the road. The number of VRUs was explored though correlation with the volumetric scores (see 5. Results). Figure 4 shows the final configuration of the VRU models around the truck cab. Three VRU models are positioned to the front, and five to either side. A greater number of VRUs to either side were defined to provide greater resolution to account for obscuration around the mirrors. In terms of determining an objective measure to explore correlation it was decided that the distance, from the front / sides of the cab to the VRU model, would be calculated as shown in Figure 4. The distance the VRU would be placed at was then final variable to explore.

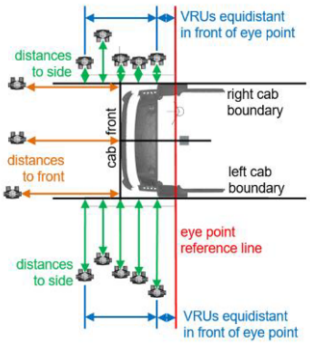

Figure 4. VRU human models positioned around the vehicle to contextualize the volumetric analysis.

This was the most complex aspect of the approach and one that most of the research had sought to avoid to this point. The fundamental challenge is what is considered 'enough' of another road user for the driver to recognize them as something they need to attend to. A broad range of options were explored before finally setting a visual requirement of being able to see the head and shoulders of the VRU models. The inclusion of the head and shoulders was informed primarily by research into the effects of eye contact between the driver and other road users that suggests that eye contact can have a substantial influence on behavior [13]. The benefits of eye-contact were interpreted into a need to be able to see a complete head, and not just the eyes, as the familiarity aspect of the interaction is reinforced by what is being seen as recognizable as a human. This was extended to include the shoulders to account for the downward angle of vision and situations where only a partial head might be visible if only head were specified but when shoulders are taken into account the appropriate recognition and interaction can take place.

4.3. VRU Assessment

Each of the vehicles in the sample were assessed again, this time for their VRU performance. For each vehicle the VRUs were loaded into the truck model and arranged as specified in Figure 4. Each VRU was then moved linearly away from the cab to the point at which their head and shoulders were just visible as shown in Figure 5. Once all of the VRUs were located, the average of the linear distances to each side were calculated and summed. This provided an overall distance measure in mm.

Figure 5. Intersection of the volumetric projections of FoV and the VRU models.

As expected the process was not without its challenges. In this assessment it was stated that head and shoulders of the VRU model needed to be seen. However, even this raises degrees of interpretation. For example, in Figure 5 (right) the right most human model is positioned such that the mid point of the shoulder level (sternum) is aligned with the lower limit of the window line. This results in the right shoulder (as viewed) being partially obscured, and the left shoulder being fully visible, together with part of the upper arm. The analysis is partially under assessing performance with more of the VRU visible to the left, and over assessing performance with less than the specified requirement visible to the right. Thus, even at the individual VRU level a degree of averaging is being performed. This could be avoided by insisting that both shoulders must be visible but this increases the distances and was agreed to over penalize vehicle performance when it is clear that the human would be both visible and recognizable in the position shown. More complex examples of this also proved a challenge. The leftmost humans in the right hand image of Figure 5 have been pushed back to avoid obscuration due to the mirrors. In some cases those humans could be brought much closer to the side of the vehicle and were partially visible through the gap between the mirror and the A-pillar. In some cases it could be argued that a human in this position between the mirror and A-pillar could be seen and be recognized as their full head may be visible. However, it was decided that this deviated too greatly from the head and shoulders specification and so was not allowed. Due to these complexities the analysis was performed manually and each decision validated by the team. More automated methods were considered but the subjectivity in some instances precluded an automated method at this point.

5. Results

The results of the VRU assessment were presented via a correlation graph with the previously reported volumetric scores. Figure 6 shows the strength of the correlation (0.97 Pearson) between the two sets of data. The strength of the correlation validates that the VRU analysis can serve as a good indicator of volumetric performance. Fundamentally it provides a more understandable context, using real world measures, of FoV performance for direct vision. For example the best performing vehicle, the Dennis Eagle (wide) has an average VRU distance from the side of the cab of 0.45 m. This means that a small Italian female's head and shoulders can be seen on average only 0.45 m from the cab to the font and sides. Conversely for the MAN TGX in its highest configuration the average is 3.84 m. The visualization of this top down on the vehicles is shown in Figure 7, arguably this is a much stronger message that the 20 m^3 and 2.5 m^3 from the volumes alone.

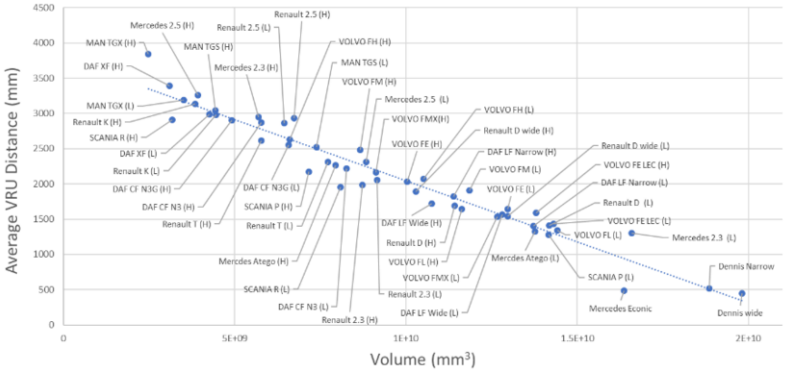

Figure 6. Volumetric scores correlated with average VRU distance for all trucks.

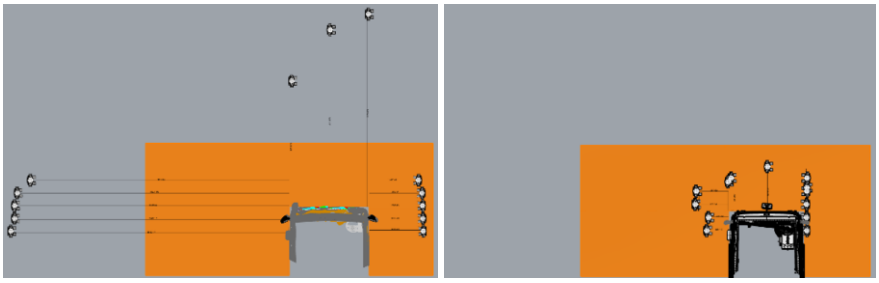

Figure 7. Comparison of extremes of VRU distance performance.

6. Discussion

The final aspect to this part of the research was to set a minimum performance level. For the London DVS this was mostly emergent from the process already followed. To the front, it was decided that the minimum performance must be such that the 5th%ile Italian female's head and shoulders must be visible, on average, 2 m from the front of the cab. This would mean that there would be no blind spot between the coverage of the Class VI mirror that provides indirect vision directly in front of the vehicle and direct vision through the windscreen to the front. The same rationale was used to define a limit of 4.5 m to the passenger side. The driver's side was ultimately set at 0.6 m. Regulation 46 [9] does not mandate mirror coverage immediately to the driver's side of the cab. The 2 m limit to this side for the assessment volume was considered too far with no indirect vision to assist and so the 0.6 m limit was determined through experimentation with an aim of achieving the greatest correlation with the volumetric scores. This minimum performance level then formed the 1 star boundary limit in the London DVS and approximates to a volumetric score of 10 m^3. The London DVS then defines further star ratings up to 5, evenly splitting the volumetric performance shown in Figure 6 across the star ratings. London will begin restricting access to vehicles rated lower than 1 star from 2020 and below 3 stars from 2024, unless they also fit a range of other safety equipment as part of a safe system.

At the time of writing this research is ongoing with the volumetric approach agreed at a European level and written into the General Safety Regulation. However, where the

minimum performance requirement will be set is, as yet, undecided. The DVS has significant implications for general road safety and for VRUs in particular across Europe. However, it also poses significant challenges for trucks and their manufacturers.

7. Conclusion

This paper reports on the development of a two stage methodology for the assessment of FoV as part of the development of a new Direct Vision Standard for trucks. The use of a volumetric assessment in close proximity to the cab provides a high resolution objective measure of performance. However, it also provides little context. A VRU approach, using human models, provides a lower resolution assessment but with much greater context and a much more understandable measure of direct vision performance. The correlation of the two differing approaches provides the ideal compromise addressing all of the requirements and allowing a meaningful measure of the problem to be made and for viable performance limits to be mandated for future truck designs.

References

[1] Talbot R, Reed S, Barnes J, Thomas P, Christie N. Pedal Cyclist Fatalities in London: Analysis of Police Collision Files (2007-2011). Research Report. Transport Safety Research Centre, Loughborough University, Centre for Transport Studies, University College London. 2014. URL: https://dspace.lboro.ac.uk/2134/16487.

[2] Cook SE, Summerskill S, Marshall R, Richardson JH, Lawton C, Grant R, Bayer SH, Lenard J, Clemo K. The development of improvements to drivers' direct and indirect vision from vehicles. Phase 2. Loughborough University. Report for Department for Transport. 2011. URL: https://dspace.lboro.ac.uk/2134/8873.

[3] Summerskill S, Marshall R, Paterson A, Reed S. Understanding direct and indirect driver vision in heavy goods vehicles: Final report prepared on behalf of Transport for London. Loughborough: Loughborough University. 2015. URL: https://dspace.lboro.ac.uk/2134/8874.

[4] Summerskill S. Marshall R. Paterson A. Eland A, Lenard J. The Definition, Production and Validation of the Direct Vision Standard (DVS) for HGVs: Final report prepared on behalf of Transport for London. Loughborough: Loughborough University. 2019. URL: https://dspace.lboro.ac.uk/2134/36622.

[5] Marshall R, Summerskill S, Cook S. Development of a volumetric projection technique for the digital evaluation of field of view. Ergonomics, 2013, 56 (9), 1437-1450. URL: http://dx.doi.org/10.1080/00140139.2013.815805.

[6] Summerskill S, Marshall R, Cook SE, Lenard JA, Richardson JH. The use of volumetric projections in Digital Human Modelling software for the identification of large goods vehicle blind spots. Applied Ergonomics, 2016, 53, pt.A, 267-280. http://dx.doi.org/10.1016/j.apergo.2015.10.013.

[7] Case K, Marshall R, Summerskill S. Digital human modelling over four decades. International Journal of the Digital Human, 2016, 1(2), 112. https://doi.org/10.1504/IJDH.2016.077408.

[8] Marshall R, Summerskill S, Lenard J. The analysis of UK road traffic accident data and its use in the development of a direct vision standard for trucks in London. 2019, Washington D.C, 427-439. DOI: 10.1007/978-3-030-20503-4_39.

[9] UNECE Regulation 46. Uniform Provisions for Devices for Indirect Vision and of Motor Vehicles with Regard to the Installation of these Devices. UN ECE Vehicle Regulations. 2009.

[10] SAE J1050. Describing and Measuring the Driver's Field of View. Society of Automotive Engineers, Surface Vehicle Recommended Practice, 2009.

[11] SAE J1516. Accommodation Tool Reference Point for Class B Vehicles. Society of Automotive Engineers, Surface Vehicle Recommended Practice, 2011.

[12] FMVSS 111. Laboratory Test Procedure for FMVSS 111 Rear Visibility. U.S Department of Transportation, National Highway Traffic Safety Administration, TP-111V-01, 2018.

[13] Milner R, Western-Williams H. Direct vision vs indirect vision: A study exploring the potential improvements to road safety through expanding the HGV cab field of vision. London: Ove Arup & Partners Ltd. 2016.

DHM2020
L. Hanson et al. (Eds.)
© 2020 The authors and IOS Press.
This article is published online with Open Access by IOS Press and distributed under the terms of the Creative Commons Attribution Non-Commercial License 4.0 (CC BY-NC 4.0).
doi:10.3233/ATDE200015

Musculoskeletal Modeling with Jaw Motion Data from a TMD Patient

Ryuji SHIGEMITSU[a,1], Keiichi SASAKI[a] and John RASMUSSEN[b]
[a] *Division of Advanced Prosthetic Dentistry, Tohoku University Graduate School of Dentistry, Sendai 980-8575, Japan*
[b] *Department of Materials and Production, Aalborg University, Fibigerstraede 16, Aalborg East DK-9220, Denmark*

Abstract. Temporomandibular disorder (TMD) is a prevalent dental disease in common with dental caries and periodontitis. The major symptoms of TMD are masticatory muscle pain, temporomandibular joint (TMJ) pain and impairment of jaw movement due to the pain and pathologic derangement of TMJs. However, there are few studies using TMD patient-specific motion data to drive the musculoskeletal model that can elucidate kinematic and biomechanical characteristics of the patient. The purpose of this study is to develop the workflow of musculoskeletal modeling of the mandible with jaw motion data obtained from a TMD patient. This involves the establishment of patient-specific boundary conditions representing the characteristics of the TMJ. The jaw motion of a TMD patient was recorded and used as an input for driving the model.

Keywords. Musculoskeletal Modeling, Jaw Motion, Temporomandibular Disorder, Inversed Dynamics

1. Introduction

Along with dental caries and periodontitis, temporomandibular disorder (TMD) is one of the prevalent dental diseases. The major symptoms of TMD are pain/dysfunction of the masticatory muscles and temporomandibular joints (TMJs), and impairment of jaw movement including restricted range-of-motion of the jaw, clicking and crepitation of TMJs [1]. In clinical situations, it is typically observed that both limited jaw movement and pain could be improved after adequate TMD management by specialists. Tracking record of jaw motion can be used for effective functional assessment for TMD patients, because it is important to record and interpret the changes of jaw movement during a treatment sequence. Additionally, the jaw motion capture data can be input data for reverse engineering of the patients' condition and outcomes of treatment. Although the etiology of TMD is considered as multi factorial, kinematic factors in the etiology and phenomenology of TMD are poorly understood, thus their relative importance is still controversial [2].

On the other hand, inverse dynamics simulation is an effective computational method to determine the internal forces which are difficult to measure *in vivo*. Inverse dynamics-based software has been used for simulating muscle activations, muscle forces

[1] Corresponding Author, Email: ryuji.shigemitsu.d7@tohoku.ac.jp.

and TMJ reaction forces in various types of tasks [3-4], but there are few studies using TMD patient-specific motion data to drive the musculoskeletal model.

The purpose of our project was, therefore, to develop a patient-specific musculoskeletal model of a patient who has dysfunction in her masticatory system. As the first step, we implemented identification of the patient-specific boundary condition representing the bony surface characteristics of TMJ from motion capture data.

2. Method

2.1. Recording of jaw motion in patient

A 25-year old female patient was selected as the subject of this study. Informed consent relating to the purpose of study and management of personal information was obtained. As having imitated jaw movement and pain on the masticatory muscles at the first examination, the occlusal splint therapy (OST) and cognitive behavioral therapy were prescribed by a TMD specialist to improve the symptoms [5] (Figure 1). An orthodontic motion capture system (ARCUS Digma, Kavo dental excellence, Germany) was used to record and analyze the jaw motion during jaw opening (Figure 2). The bite fork was fixed to her lower dental arch for recording jaw motion at three virtual markers indicating the incisor point and left and right condyles. After recording, the data of marker's tracking were exported in text format files. The recording was conducted at three times during her treatment sequence: before treatment, *i.e.* starting OST, three months and six months after treatment, for assessing the treatment outcome and clinical course. In this study, we used the jaw motion data at before treatment, when the patient showed limitation of range-of-motion caused by TMJ pain. The measured motion data were digitally filtered with a low-pass filter (LPF) and a third order Butterworth filter. Particular noise problems existed at the maximal opening point, and the filter parameters had to be calibrated iteratively to retain the characteristics of the motion (Figure 7). The filtered jaw motion data were used as input driver data for musculoskeletal simulations in the AnyBody Modeling System (AMS) ver. 7.2 (AnyBody Technology, Aalborg, Denmark).

Figure 1. The inter-oral view of the patient.

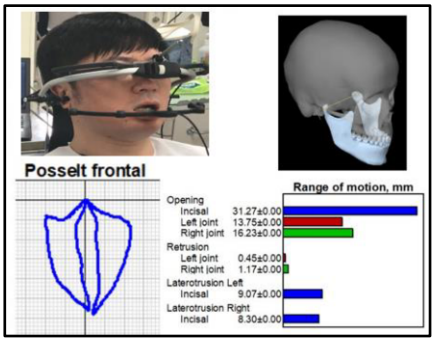

Figure 2. Measurement of jaw motion using orthodontic motion capture system.

2.2. Description of the model with patient-specific constraint

The model of the skull and mandible in AMS were based on CT-scans of a 30-year old male (Figure 3) [4]. The entire skull and mandible were segmented in AMS and used for defining the muscle insertions and visualization. To represent the actual patient anatomy, the right and left TMJ fossa, *i.e.* the contact surfaces to the TMJ condyles, were modeled with parametric biphasic constraining planes (Figure 4). The two planes meet at a patient-specific origin and form patient-specific angles, α and β, with the skull reference frame. These parameters in turn constrain the movement of the condyle in the patient. This movement is detected by the motion capture system from where it can be reverse-engineered into patient-specific fossa parameters for the model. Each condyle has the possibility to rotate in all three dimensions and to translate along the specified constraining planes which means both condyles move with five degrees-of freedom. The model was equipped with 24 jaw muscles; 16 masticatory muscles and 8 suprahyoid muscles, actuating the movement of mandible. Each muscle was modelled as a Hill-type muscle consisting of contractile, parallel elastic and serial elastic elements, with the stiffness contribution of the tendon included in the serial elastic element. The details of model parameters were implemented from the study done by M. de Zee et al. [3]. The kinetic analysis was conducted after defining the constraint.

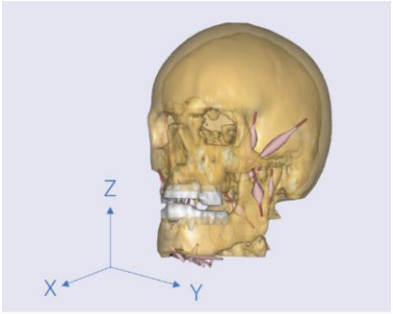

Figure 3. The musculoskeletal model of the human mandible.

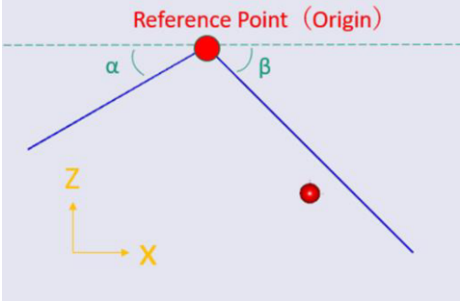

Figure 4. The schema of biphasic behavior.

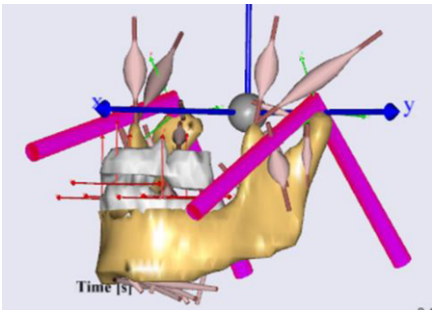

Figure 5. Patient-specific constraining plane.

3. Results and Discussion

3.1. Results

Figure 6 shows the trajectory of the three markers in sagittal, horizontal, and frontal planes (Figure 7). In the sagittal plane, the motions of both condyles show biphasic behavior during the opening-closing movement. Regarding the incisor point in frontal plane, the maximum unassisted jaw opening was 22 mm from which the subject has limitation of mandibular movement caused by the pain.

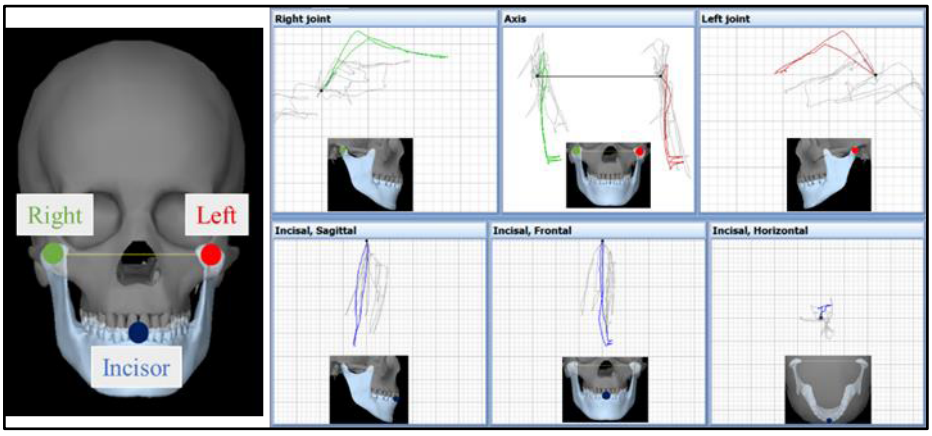

Figure 6. The trajectory of 3 marker positions in each plane.

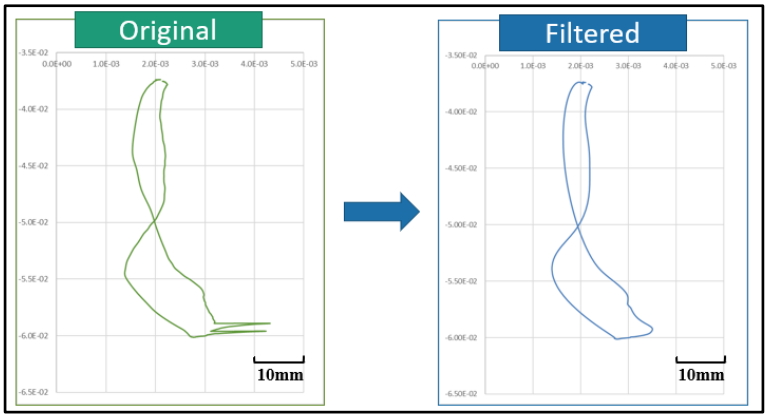

Figure 7. Filtered data of incisor point in frontal plane.

Figure 8 shows the trajectory of both condyles in the subject and patient-specific model. Although the slight difference of each condyle position could be observed between the model and subject during opening, the ranges of motion and angle between 2 constraining planes in the model were consistent with the input data from which it can be concluded the characteristics of the motion were properly represented in the model.

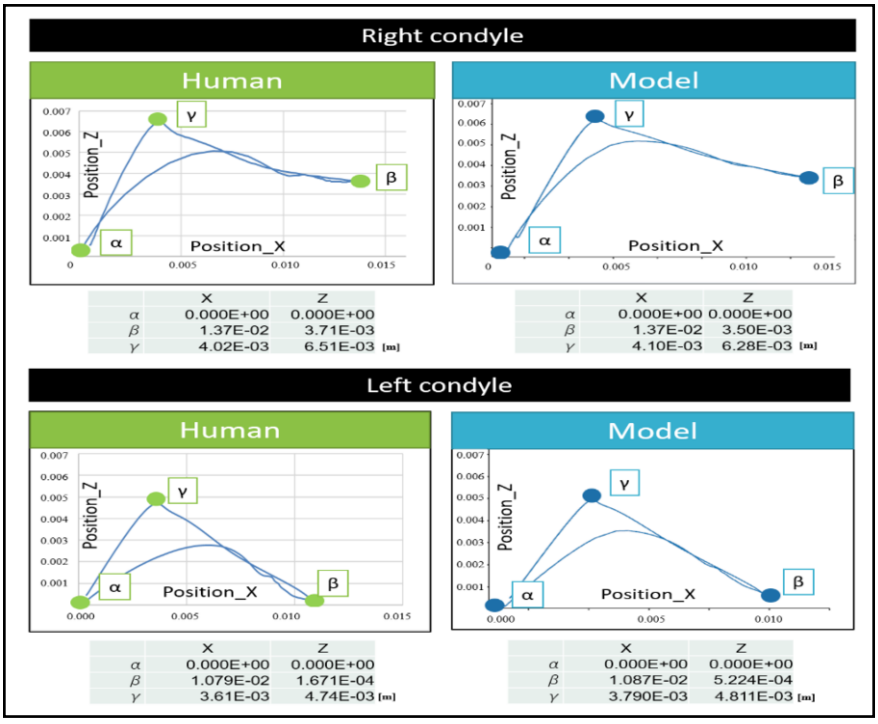

Figure 8. The trajectory of condyle in the subject and patient-specific model.

Figure 9 shows the results of kinetic analysis of condyle motions in the simple demo model prepared in AMS and patient specific model constructed in the present study. The characteristics of the condyle's curved motions are successfully represented in the patient-specific model.

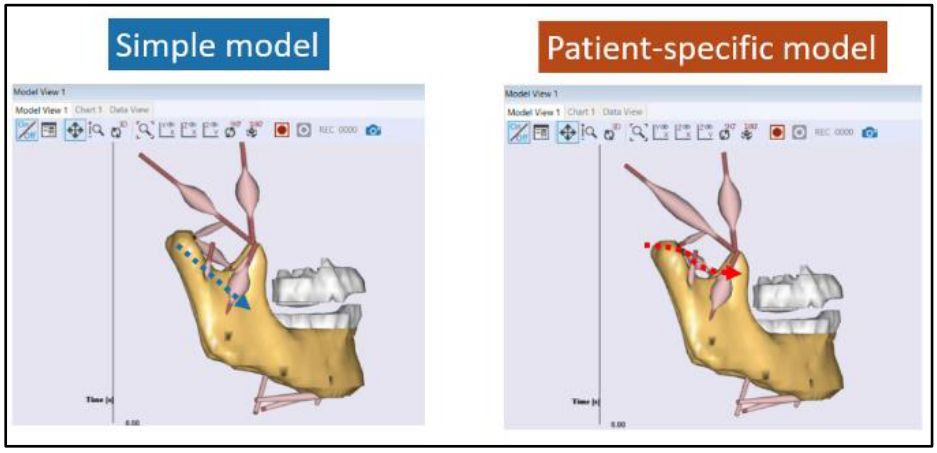

Figure 9. The motion of condyle in simple model and patient-specific model.

3.2. Discussion

The TMD is a comprehensive diagnostic label of syndrome including various signs and symptom with different pathology, hence the exact etiology is still controversial [2, 6-7]. The methodology developed in this paper is the first step of a process, in which biomechanics can contribute to the knowledge of the problem. The orthodontic motion capture employed in this study is a relatively simple and accessible procedure, and the developed model shows possibility to extract patient-specific features from motion capture data and to implement them into a biphasic and patient-specific model with the TMJ fossa constraints. This will facilitate the use of musculoskeletal modelling for an investigation of larger cohorts of patients and might enable clinical use of digital human modelling in orthodontic and prosthodontic treatment.

Although the noise of recorded data can be minimized by experimental procedures using an accurate measuring device, it can never be completely removed. It turned out that the measured jaw motion data needed to be filtered with the settings obtained in an iterative process before using the data for kinetic analysis. An automated procedure for processing of the motion capture data will probably be necessary for use of the modelling technique on a larger, clinical scale.

In the present musculoskeletal model, the motion of each condyle was properly consistent with the motion-captured jaw motion data. The temporomandibular joints are hinging and sliding joints, so that their correct, patient-specific representation is important for the credibility of the kinetic model. In this study, small displacements between the measured motions and model's motions were observed, which is considered to be the consequence of using soft drivers in the musculoskeletal model to compromise between redundant positional information from the motion capture markers. Since the skull and mandible used in this study were based on a demo model representing a different patient, incompatibility between measured jaw motions from the patient in question and bony geometries from the template model might influence the result. Future work must include patient-specific scaling of the template model [8].

The model neglects the influence of ligaments, which are also constraining the motion during jaw opening. Future work will attempt to also identify ligament properties based on the relevant part of the motion capture data using parameter identification [9], thus extending the patient-specific adaptation of the model from motion capture data.

Although only jaw motion data at before treatment were included in this study, the jaw motion was improved with the progress of the treatment. Future comparative studies based on patients' jaw motions as treatment progresses could be clarify the interaction between the clinical symptoms and musculoskeletal systems such as muscle activations, muscle forces and TMJ reaction forces. This will be helpful to elucidate the TMD etiology and phenomenology from a biomechanical point-of-view. Additionally, the musculoskeletal simulation could provide boundary conditions for a patient-specific finite element analysis [10]. These types of digital human simulation could pave the way for simulation-based diagnostics and assessment systems [11] and would link well with future CAD/CAM systems in dentistry.

Acknowledgement

This work was supported by JSPS KAKENHI Grant Numbers JP20K10047.

References

[1] Schiffman E, Ohrbach R, Truelove E, Look J, Anderson G, Goulet JP, et al. Diagnostic Criteria for Temporomandibular Disorders (DC/TMD) for Clinical and Research Applications: recommendations of the International RDC/TMD Consortium Network* and Orofacial Pain Special Interest Groupdagger. J Oral Facial Pain Headache, 2014, 28(1), 6-27.
[2] Scully C. Oral and Maxillofacial Medicine-E-Book: The Basis of Diagnosis and Treatment: Elsevier Health Sciences, 2012.
[3] de Zee M, Dalstra M, Cattaneo PM, Rasmussen J, Svensson P, Melsen B. Validation of a musculoskeletal model of the mandible and its application to mandibular distraction osteogenesis. J Biomech, 2007, 40(6), 1192-1201.
[4] Basafa E, Murphy RJ, Gordon CR, Armand M. Modeling the biomechanics of swine mastication – An inverse dynamics approach. Journal of Biomechanics, 2014, 47(11), 2626-2632.
[5] Wassell RW, Naru A, Steele J, Nohl F. Applied occlusion. Quintessentials of Dental Practice. 2008.
[6] Huang G, LeResche L, Critchlow C, Martin M, Drangsholt M. Risk factors for diagnostic subgroups of painful temporomandibular disorders (TMD). Journal of dental research, 2002, 81(4), 284-288.
[7] Watanabe M, Sasaki K, Inai T, Tsuboi A, Jung-in H. A role of occlusion in the etiology of TMD. Dentistry in Japan, 2000, 36, 62-65.
[8] Lund ME, Andersen MS, de Zee M, Rasmussen J. Scaling of musculoskeletal models from static and dynamic trials. International Biomechanics, 2015, 2(1), 1-11.
[9] Andersen MS, Damsgaard M, MacWilliams B, Rasmussen J. A computationally efficient optimisation-based method for parameter identification of kinematically determinate and over-determinate biomechanical systems. Comput Methods Biomech Biomed Engin, 2010, 13(2), 171-183.
[10] Shigemitsu R, Yoda N, Ogawa T, Kawata T, Gunji Y, Yamakawa Y, et al. Biological-data-based finite-element stress analysis of mandibular bone with implant-supported overdenture. Computers in biology and medicine, 2014, 54c, 44-52.
[11] Sasaki K. Examination and diagnosis for masticatory and swallowing function. Nihon Hotetsu Shika Gakkai Zasshi, 2002, 46(4), 463-474.

DHM2020
L. Hanson et al. (Eds.)

© 2020 The authors and IOS Press.
This article is published online with Open Access by IOS Press and distributed under the terms of the Creative Commons Attribution Non-Commercial License 4.0 (CC BY-NC 4.0).
doi:10.3233/ATDE200016

Digital Human Motion Planning of Operation Sequences Using Optimal Control of Hybrid Systems

Staffan BJÖRKENSTAM[a,1], Peter MÅRDBERG[a], Michael ROLLER[b] and Johan S. CARLSON[a]
[a] *Fraunhofer-Chalmers Centre, Göteborg, Sweden*
[b] *Fraunhofer Institute for Industrial Mathematics, Kaiserslautern, Germany*

Abstract. In IPS-IMMA the operation sequence planning tool offers an easy and powerful way to construct, analyze, and simulate sequences of human operations. So far, the simulations created using this tool have been quasi-static solutions to the operation sequence. In this paper we present new functionality for motion planning of digital human operation sequences which also takes the dynamics of the human into consideration. The new functionality is based discrete mechanics and optimal control and will be seamlessly integrated into to the IPS-IMMA software through the operation sequence planning tool. First, the user constructs an operation sequence using the operation sequence planning tool in IPS-IMMA. The operation sequence is then converted into a discrete optimal control problem which is solved using a nonlinear programming solver. Finally, the solution can be played back and analyzed in the graphical interface of IPS-IMMA. In order to obtain physically correct solutions to complex sequences consisting of several consecutive and dependent operations, we view the digital human as a hybrid system, i.e. a system containing both continuous and discrete dynamic behavior. In particular, the optimal control problem is divided into multiple continuous phases, connected by discrete events. The variational integrators used in discrete mechanics are particularly well suited for modelling the dynamics of constrained mechanical systems, which is almost always the case when considering complex human models interacting with the environment. To demonstrate the workflow, we model and solve an industrial case where the dynamics of the system plays an important part in the solution.

Keywords. Optimal Control, Discrete Mechanics, Human Motion Planning

1. Introduction

To describe operations and facilitate motion generation, it is common to equip the manikin with coordinate frames attached to end-effectors like hands and feet. The inverse kinematic problem is to find joint values such that the position and orientation of hands and feet matches certain target frames. For the quasi-static inverse kinematics this leads to an underdetermined system of equations since the number of joints exceeds the end-effectors' constraints. Due to this redundancy there exist a set of solutions, allowing us to consider ergonomics aspects, collision avoidance, and maximizing comfort when choosing one solution [1].

[1] Corresponding Author, Email: staffan.bjorkenstam@fcc.chalmers.se.

Traditionally, human simulation tools use these static poses to emulate motion, which severely limits the possible set of motions which can be produced. Our goal is to extend the model in IMMA to be able to generate dynamically feasible motions for the manikin based on a performance index, which could typically include quantities such as comfort, muscle strain, and cycle time. Furthermore, we want to be able to realistically simulate highly dynamic motions, where modelling of inertial effects become crucial. To do this, we model the manikin as a dynamical system, and use optimal control methods to compute the motions. Optimal control is the problem of determining a control function for a dynamical system in order to minimize a given performance index. In order to solve the optimal control problem on a computer, we discretize the continuous problem into a nonlinear programming problem using discrete mechanics. The idea of using optimal control to generate human motion is not new, see for example [2],[3],[4],[5].

In this paper we work with the DHM tool IMMA [6] and show how to generate motions for complex operation sequences using hybrid optimal control techniques. The paper builds on the work presented in [7],[8],[9], and is a part of the VIVA (Virtual Vehicle Assembler) project.

2. Method

Here we briefly describe the kinematical model of the manikin in the DHM tool IMMA. We also describe how we introduce dynamics and optimal control in the model. In this paper we control the manikin by directly applying torques in the joint.

2.1. Kinematics

The manikin model is a tree of rigid bodies connected by joints. Each body has a fixed reference frame, and we describe its position relative to its parent body by a rigid transformation T(q), where q is the coordinate of the joint. To position the manikin in space, with respect to some global coordinate system, it has an exterior joint positioning the manikin relative to a fixed inertial frame – as opposed to the interior links representing the manikin itself, see (1).

The exterior joint is modeled as a rigid transformation that completely specifies the position of the lower lumbar in the world. In turn, the lower lumbar represents an interior root, i.e. it is the ancestor of all interior joints. Note that the choice of the lower lumbar is not critical. In principal, any link can be the interior root, and the point is that the same root can be used through a complete simulation. No re-rooting or change of tree hierarchy is needed.

For a given configuration of each joint, collected in the joint vector q, we can calculate all the relative transformations by traversing the tree, beginning at the root and propagating the transformations to get the global position of each body. We say that the manikin is placed in a pose, and the mapping from a joint vector into a pose is called forward kinematics. Furthermore, a continuous mapping q(t), where $t \in R$, is called a motion, or a trajectory of the system.

2.2. Dynamics and optimal control

The dynamic motion planning problem is stated as the following optimal control problem:

Minimize

$$\chi\left(\boldsymbol{q}(t_f), \dot{\boldsymbol{q}}(t_f)\right) + \int_{t_0}^{t_f} \mathcal{L}\big(\boldsymbol{q}(t), \dot{\boldsymbol{q}}(t), \boldsymbol{u}(t)\big)dt \tag{1}$$

subject to

$$\frac{\partial L}{\partial \boldsymbol{q}}\big(\boldsymbol{q}(t), \dot{\boldsymbol{q}}(t)\big) - \frac{d}{dt}\frac{\partial L}{\partial \dot{\boldsymbol{q}}}\big(\boldsymbol{q}(t), \dot{\boldsymbol{q}}(t)\big) + \boldsymbol{F}\big(\boldsymbol{q}(t), \dot{\boldsymbol{q}}(t), \boldsymbol{u}(t)\big) + \boldsymbol{\Phi}^{\boldsymbol{T}}\big(\boldsymbol{q}(t)\big)\boldsymbol{\lambda}(t) = \boldsymbol{0}, \tag{2}$$

$$\boldsymbol{\phi}\big(\boldsymbol{q}(t)\big) = \boldsymbol{0}, \tag{3}$$

$$\boldsymbol{g}\big(\boldsymbol{q}(t), \dot{\boldsymbol{q}}(t), \boldsymbol{u}(t)\big) \geq \boldsymbol{0}, \tag{4}$$

$$\boldsymbol{\psi_0}\big(\boldsymbol{q}(t_0), \dot{\boldsymbol{q}}(t_0)\big) = \boldsymbol{0}, \tag{5}$$

$$\boldsymbol{\psi_f}\left(\boldsymbol{q}(t_f), \dot{\boldsymbol{q}}(t_f)\right) = \boldsymbol{0}, \tag{6}$$

for $t \in [t_0, t_f]$.

Thus, we want to minimize the performance index (1), consisting of the terminal cost, χ, and the integral of the control Lagrangian, $\mathcal{L}$, along the trajectory, while satisfying the dynamics (2)-(3), path constraints (4), and boundary conditions (5)-(6).

The optimal control problem is then discretized. This results in a nonlinear constrained optimization problem, which can be solved using standard nonlinear programming solvers. Furthermore, this general problem formulation makes it straight forward to include very general constraints and objectives. The differential equation in the optimal control problem is discretized using discrete mechanics. In discrete mechanics, the variational principle is directly discretized into a set of nonlinear equations known as the discrete Euler-Lagrange equations. The discrete equations of motions derived in this way have been shown to be superior compared to standard discretizations since they preserve characteristics of the continuous system such as conservation of momentum and a good energy behavior [10]. This results in very stable integrators, which in practice allows us to use large time steps when solving our problems.

In order to efficiently use the discrete equations for these potentially high dimensional systems in a direct optimal control method, it is important to exploit both the structure of the optimal control problem as well as the structure of the dynamics [7].

3. Results

3.1. Hybrid optimal control and operation sequence planning

In this section we use the operation sequence planning tool in IMMA to create an optimal control problem for a given operation sequence. We will use the task of climbing a loader to illustrate the process (Figure 1). Foot attachment points are created at the ground and the steps of the loader. We also put attachment point for the left hand on the rail of the loader. Currently, the placement of the attachment points must be chosen by the user, but functionality to let, for example the attachment point for the hand, grab anywhere on a line segment representing the rail, is in the works.

We are now ready to create our operation sequence. We attach the manikin to the foot attachment points on the ground, and choose this as the start configuration (Figure 1). Operations are then added to the sequence according to Table 1.

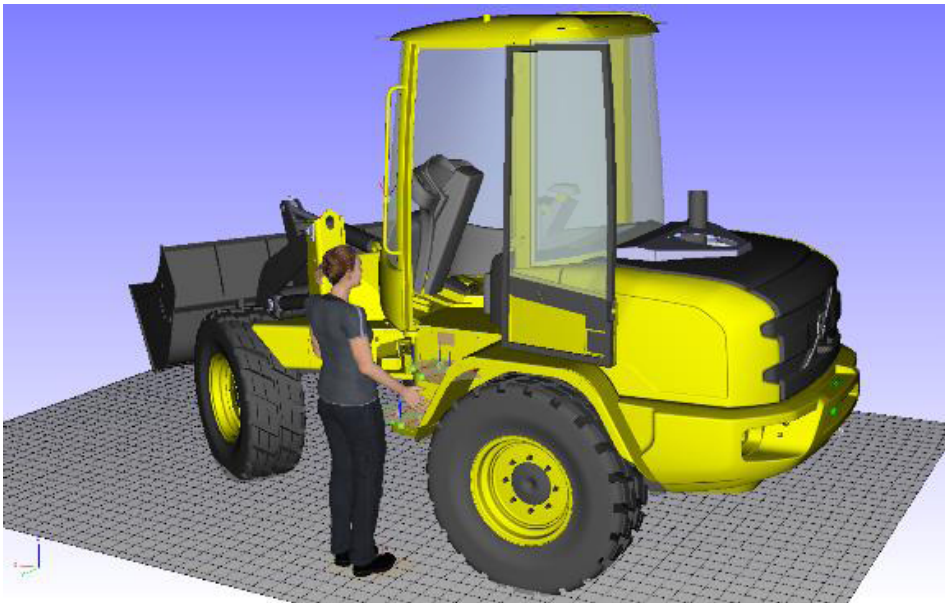

Figure 1. IPS scene.

Table 1. Operations with the resulting duration for each operation. The duration of each operation is determined by the solution to the optimal control problem, except for the final pause with is fixed to 1 s.

Operation	Duration [s]
Start	-
Attach left hand to rail	0.515
Detach left foot from ground	-
Attach left foot to first step of the stairs	0.383
Detach right foot from ground	-
Attach right foot to top of the stairs	0.566
Detach left hand from rail	-
Detach left foot from first step of the stairs	-
Attach left foot to top of the stairs	0.301
Pause	1.00

The detach operations are instantaneous, i.e. have no durations, whereas the duration of the attach operations are initialized to 0.5 s but free to be changed during the optimization, i.e. the durations are variables in the optimization problem. The duration for the pause at the end, however, is fixed to 1 s, otherwise the optimization would simply drive the duration to zero since that would introduce zero cost for the operation. Additionally, the manikin is constrained to end the operation sequence in rest.

Note that the optimal control problem includes discrete points in time where the dynamics of the problem changes discontinuously, namely the opening and closing of the contacts, this type of optimal control problem is called a hybrid problem. We approach this by splitting the optimal control problem into several phases and connecting the phases with appropriate boundary constraints. It is, however, important to note that the operation sequence is solved as one optimal control problem, although containing several phases, i.e. the obtained solution is an optimal solution to the complete operation sequence.

Figure 2. The operation sequence dialog in IPS

Now that our operation sequence is defined **(Figure 2)**, we click the plan-button in the operation sequence dialog **(Figure 2)**. The operation sequence is then converted to a hybrid optimal control problem, which in turn is discretized and solved using a nonlinear programming solver.

The complete operation sequence takes the manikin 2.76 seconds to perform, and can be replayed and analyzed further in IPS **(Figure 3)**.

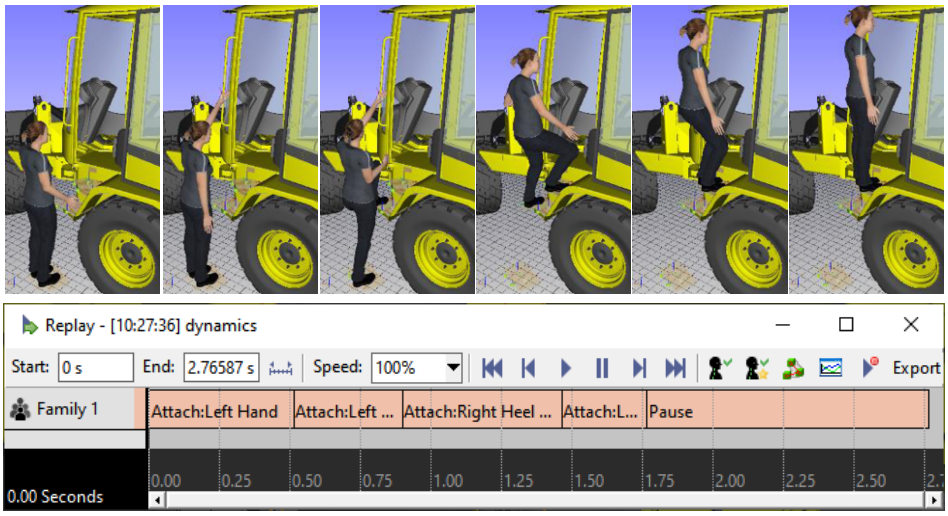

Figure 3. The solution in IPS.

4. Discussion

We conclude that hybrid optimal control is an excellent technique to create dynamic motions from operation sequences created in the operation sequence tool in IPS. Comparing the resulting solution in Section 3.1 to the regular quasi-static solution to the same operation sequence, we see that the dynamics indeed plays an important role in generating a human-like motion. The fact that paths generated by the DHM tool are now dynamic and have a time stamp for each manikin position allows for extended comparisons between simulation results and measures made in the physical world, something we view as one of the great benefits added to the IMMA software.

By modifying the cost functional of the optimal control problem, different motions and behavior can obtained. For example, if more weight is put on completing the operation fast the manikin will use more of its available strength, which results in more aggressive, “athletic”, motions.

In this paper we control the manikin by directly applying torques in the joint. However, more advanced control mechanisms, such as muscles and muscle synergies, are possible, see for example [11],[12].

Acknowledgement

This work was supported by VINNOVA (the Swedish Governmental Agency for Innovation Systems) within the VIVA project.

References

[1] Bohlin R, Delfs N, Hanson L, Högberg D, Carlson J. Unified solution of manikin physics and positioning. Exterior root by introduction of extra parameters. In: Proceedings of the 1st International Symposium on Digital Human Modeling (DHM2011), Lyon. 2011, 27–39.
[2] Lo J, Huang G, Metaxas D. Human motion planning based on recursive dynamics and optimal control techniques. Multibody Syst Dyn. 2002, 8(4), 433–458.
[3] Xiang Y, Chung H-J, Kim JH, Bhatt R, Rahmatalla S, Yang J, et al. Predictive dynamics: an optimization-based novel approach for human motion simulation. Struct Multidiscip Optim. 2009, 41(3), 465–749.
[4] Koch MW, Leyendecker S. Structure Preserving Optimal Control of a Three-Dimensional Upright Gait. In: Font-Llagunes JM, editor. Multibody Dynamics: Computational Methods and Applications [Internet]. Cham: Springer International Publishing, 2016. 115–146.
[5] Maas R, Leyendecker S. Biomechanical optimal control of human arm motion. Proc Inst Mech Eng, Part K, J Multi-Body Dyn, 2013, 227(4), 375–389.
[6] Hanson L, Högberg D, Bohlin R, Carlson J. IMMA–intelligently moving manikins–project status 2011. In: Proceedings of the 1st International Symposium on Digital Human Modeling (DHM2011), Lyon. 2011, 1–5.
[7] Björkenstam S, Leyendecker S, Linn J, Carlson JS, Lennartson B. Inverse Dynamics for Discrete Geometric Mechanics of Multibody Systems With Application to Direct Optimal Control. J Comput Nonlinear Dyn, 2018, 13(10).
[8] Roller M, Björkenstam S, Linn J, Leyendecker S. Optimal control of a biomechanical multibody model for the dynamic simulation of working tasks. In: ECCOMAS, 2017.
[9] Björkenstam S, Carlson JS, Nyström J, Roller M, Linn J, Hanson L, et al. A framework for motion planning of digital humans using discrete mechanics and optimal control. In: 5th International Digital Human Modeling Symposium (DHM2017), Bonn, 2017.
[10] Marsden JE, West M. Discrete mechanics and variational integrators. Acta Numer, 2001, 10, 357–514.
[11] Obentheuer M, Roller M, Björkenstam S, Berns K, Linn J. Comparison of different actuation modes of a biomechanical human arm model in an optimal control framework. In: Proceedings of the 5th Joint International Conference on Multibody System Dynamics IMSD, Lisbon, 2018.
[12] Obentheuer M, Roller M, Björkenstam S, Berns K, Linn J. Human like motion generation for ergonomic assessment-a muscle driven digital human model using muscle synergies. ECCOMAS Multibody Dyn, Prague, 2017.

DHM2020
L. Hanson et al. (Eds.)

© 2020 The authors and IOS Press.
This article is published online with Open Access by IOS Press and distributed under the terms of the Creative Commons Attribution Non-Commercial License 4.0 (CC BY-NC 4.0).
doi:10.3233/ATDE200017

The Definition of a Common Eye Point for the Virtual Assessment of Truck Direct Vision Performance

Steve SUMMERSKILL[1], Russell MARSHALL, Abby PATERSON and Anthony ELAND
Loughborough University, School of Design and Creative Arts, UK

Abstract. Accidents between vulnerable road users and trucks have been linked to the inability of drivers to directly see the areas in close proximity to the front and sides of the vehicle cab. The lack of direct vision is mitigated through the use of mirrors. The coverage requirements of mirrors are standardized in Europe. Direct Vision for trucks is not currently standardized in any way. Research by the authors identified key requirements for a Direct Vision Standard (DVS). Transport for London funded this work. This standard is now being applied in London, and a European version is in development. A key element of the definition of this standard was the application of DHM software to define a standardized eye point. This is used to create simulations of the volume of space to the exterior of the cab that a driver can see. Eye point definitions exist in standards for trucks, but the standards are defined in a manner which allows variability in the eye point location. This variability allowed some truck designs to gain an advantage over their competitors, leading to the requirement for a new definition for a common eye point. The paper describes the process that has been followed to define this eye point.

Keywords. Direct Vision, Safety, Accidents, Trucks, Blind Spot, Standards

1. Introduction

In the UK there has been a considerable reduction in the number of accident fatalities on the roads with a halving of the number of fatalities since 2004 [1]. In contrast to this, the number of cyclists that are being killed or seriously injured has increased [2]. There are multiple factors involved in each of these situations including improved vehicle design, and an increase in cycling as a method of commuting [2]. In particular a review of the UK accident database (STATS 19) has highlighted that the number of accidents between Heavy Goods Vehicles (HGVs) and Vulnerable Road Users (VRUs) such as cyclists and pedestrians is disproportionate to the number of miles driven by HGVs. In addition, when an accident occurs between a VRU and a HGV the outcome is much more likely to be a VRU that is Killed or Seriously Injured (KSI, 47% for pedestrians and 35% for cyclists) compared to the rates for the whole STATS 19 database (13% KSI) [3].

These issues have led to multiple research projects which have explored the reasons for an increased prevalence of accidents between HGVs and VRUs in the UK and elsewhere. For example, [4] explored the three-dimensional modelling of the volume of

[1] Corresponding Author, Email: s.j.summerskill2@lboro.ac.uk.

space that can be directly seen by a truck driver using direct vision through windows and indirect vision through mirrors. This project highlighted that blind spots existed between direct and indirect vision which subsequently led to revision of UNECE regulation 46, [4] which increased the coverage of a key mirror to reduce the identified blind spot. Other work [5] has highlighted potential design interventions to improve direct vision. A more comprehensive project that explored the design of 19 HGV designs [6] highlighted the key design variables which affect blind spot size. [4] and [6] build a case for understanding the disproportionate nature of accidents between HGVs and VRUs being at least partly accounted for by the requirement of a HGV driver to use the combination of direct vision and indirect vision through six mirrors. These visual interactions allow situational awareness to be maintained regarding the location of VRUs in close proximity to a vehicle during maneuvers. There is however a time cost for reviewing each mirror which potentially leads to the situation in mirror one changing by the time that mirror six is observed, e.g. a cyclist or pedestrian has moved into location that can lead to a collision. This rationale, combined with other research [7] which highlights that the use of indirect vision increases driver reaction time by close to 1 second, led to the recommendation for a Direct Vision Standard [8] for HGVs including a minimum safety requirement. Direct Vision should be prioritized over indirect vision to improve safety. The work to define the DVS has been completed [3] and the DVS came into force in London 2019. This bans vehicles from entering London which fail to meet the DVS minimum safety requirement.

The authors were commissioned to design and validate the London DVS by Transport for London. The brief that was provided to the authors was built upon previous work. The basic premise for the DVS was a that a volume of space should be established around a vehicle cab, and the proportion of that volume that is seen by direct vision provides a score. This process is performed in a Digital Human Modelling environment or other CAD system. Figure 1 (A) shows the assessment volume around a vehicle cab. Figure 1 (B) shows the projection of the volume of space visible to the driver, and Figure 1 (C) shows the intersection of the assessment volume and visible volume. The result in Figure 1 (C) is represented as a visible volume in m^3. A key element of this process is the representation of the Driver's eye point for the projections shown in Figure 1 (B).

The project was supported by a stakeholder group that included representatives from eight HGV manufacturer design teams along with other government and safety group representatives. All decisions relating to the design of the DVS were reviewed and commented upon by the stakeholder group. The following paper describes the options that were considered for the definition of the DVS eye point, the analysis of those options and the method by which the final eye point was defined.

2. Method & Results

2.1. Review of existing options for an eye point definition in vehicle standards

The combination of a literature review and consultation with the TfL stakeholder group highlighted two main options for the definition of an eye point. The first option that was considered allowed the generation of an optimized H-point envelope (the H-point (or hip-point) is the theoretical, relative location of an occupant's hip: specifically the pivot point between the torso and upper leg portions of the body, the H-Point envelope shows

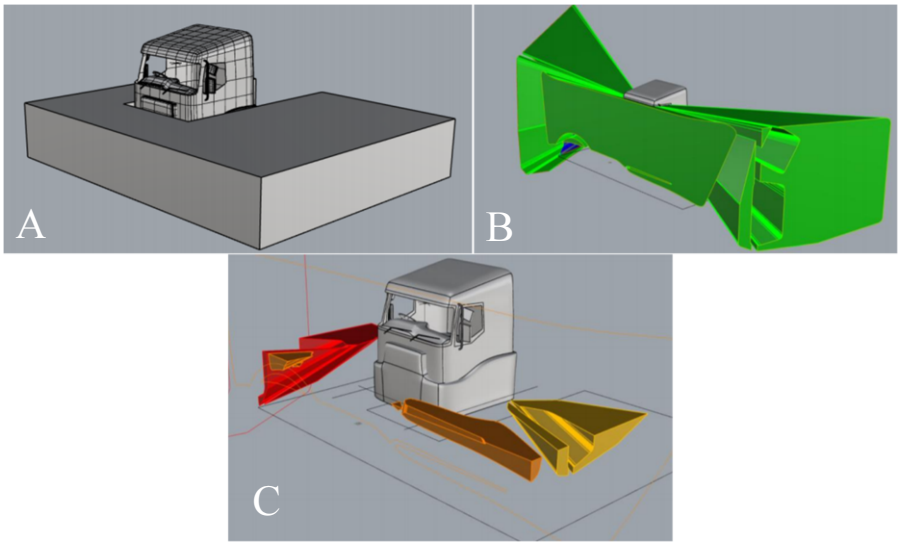

Figure 1. The premise of the London DVS.

the design intent with regard to the range of H-points that are accommodated by the design), steering wheel adjustment and the resultant eye point locations. This method produced by Matt Reed [9] was defined in response to issues with SAE J941 [10]. SAE J941 defined H-point envelopes for HGVs, but needed to be updated as it did not account for modern height adjustable seat designs. The Reed method applies a set of equations to the definition of vehicle package adjustability through the use of user defined variables for adjustability and predicts a H-point envelope and Eyellipse definition to account for the desired accommodation. This method is based upon a data collection exercise utilizing a range of real-world trucks and selected seat and steering wheel locations for a sample of 17 males and 7 females. This method had been applied in previous work assessing the direct and indirect vision performance of HGVs [6]. The stakeholder group highlighted concerns about the use of the Reed method highlighting the sample of HGVs used, which were generally of a different form factor compared to EU HGVs, the size of sample used to define the underlying data, and the complexity of applying the method which could lead to errors. The stakeholder group had a strong preference for methods which were already written into standards, and therefore recommended the much more simple method defined UNECE Regulation 46 [11]. This method simply uses a manufacturer defined Seating Refence Point (SgRP) and vertical offset from that point of 635 mm. In order to explore this method it was requested that all manufacturers supplied SgRP data and CAD data of the vehicles. Volvo, Renault, Mercedes, DAF, Dennis and Iveco provided full CAD data, Accelerator Heel Point (AHP) and SgRP data for all models sold in Europe. Scania and MAN declined to provide vehicle CAD data and so scanned data was collected for those vehicles. This was followed by an analysis of the data provided. These data identified an issue with applying the methods in UNECE Regulation 46 [11]. Three manufacturers had applied the definition of the SgRP location in a different manner to the other manufacturers. See figure 2 for a diagram which shows the relative position of the SgRPs for each manufacturer within the H-point envelope.

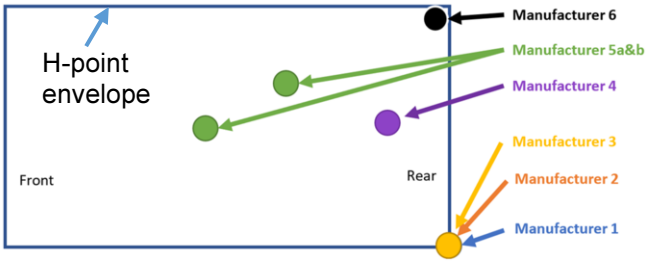

Figure 2. The relative position of the SgRP in the H-point envelope for each manufacturer.

The variability of the application of the SgRP shown in Figure 2 created a situation where manufacturers 4, 5 and 6 would gain advantage in the assessment. This is because when the 635 mm offset defined in [11] is applied those three manufacturers which have an eye point which is higher and further forward in the cab compared to manufacturers 1, 2 & 3. This would create an unfair advantage as this would allow improved vision of areas to the front and side of the vehicle cab. These results were reported to the stakeholder group and it was therefore deemed inappropriate to use the method defined in [11].

2.2. Definition of requirements for a new common eye point

The further meetings were held with the stakeholder group to define the requirements for the 'new common eye point'. The stakeholder group preferred an option which could be applied in the same manner by all manufacturers, was simple to apply, and could not allow manipulation to improve the results. Two options were presented to the stakeholder group with the following positive and negative aspects defined by the stakeholder group.

Option 1. To define a H-point based upon the same relative location in the H-point envelope for each vehicle, which will be used to define an eye point

Positives: This would produce the most fair result for existing vehicles as it accounts for the current location of windows and other elements that effect direct vision with reference to the specific H-point envelope for each cab design

Negatives: As highlighted by a number of stakeholders including manufacturers, the H-point envelope could be moved in future designs, or redefined for existing redesigns to improve a DVS score without adding any real Direct Vision benefit.

Option 2. To define a single H-point with reference to the AHP which will be used to define an eye point for all vehicles

Positives: A consistent approach which will avoid manufacturers adapting H-point envelopes as discussed above

Negatives: A single point will potentially disadvantage some manufacturers as the relative position of the single point will be different in each vehicle's H-point envelope

Option 2 was selected by the stakeholder group as this method was based around the AHP which is defined in SAE standards [13, 14]. The rationale was that option 2 could not be manipulated to provide an improved DVS score without actual direct vision benefit. Any change in the AHP would directly affect the whole occupant accommodation package if a single eye point was defined. The approach taken by the research team was to define a common H-point which all manufacturers can achieve, and then to define an offset from that H-point to allow a common eye point to be defined.

2.3. Definition of a common H- point

In order to define a common H-point each of the H-point envelopes were plotted with reference to the AHP. Figure 3 shows the outcome of this process where the common area for all H-point envelopes for 26 vehicle designs in the sample is highlighted.

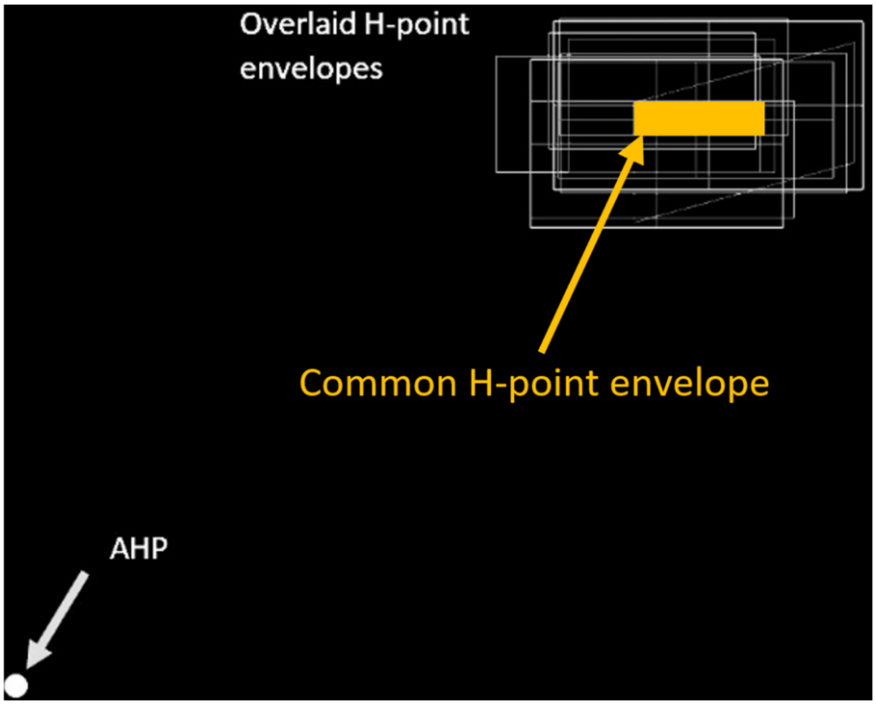

Figure 3. The definition of a common area that all 26 H-point Envelopes can meet.

The process for defining a H-point within the common H-point envelope was then explored using calculations derived from;

- SAE J1516: Accommodation Tool Reference Point for Class B Vehicles [14]
- SAE J1517: Driver Selected Seat Position for Class B Vehicles - Seat Track Length [15]

All approaches define an offset from the AHP to a H-point which matches the intent described by the stakeholder group, notably the Accommodation Tool Reference Point (ATRP) can vary in position based upon a supplied H30 value (vertical offset between the AHP and the H-point).
SAE J1516 and J1517 use the following equations for a 90:10 Male:Female ratio:

$x = 855.31 – 0.509z$ 50^{th} %ile (SAE J1516)
$x = 922.49 – 0.494z$ 95^{th} %ile (SAE J1517)

The equations were used to plot the H-point location lines for a series of points between the maximum and minimum H30 values.

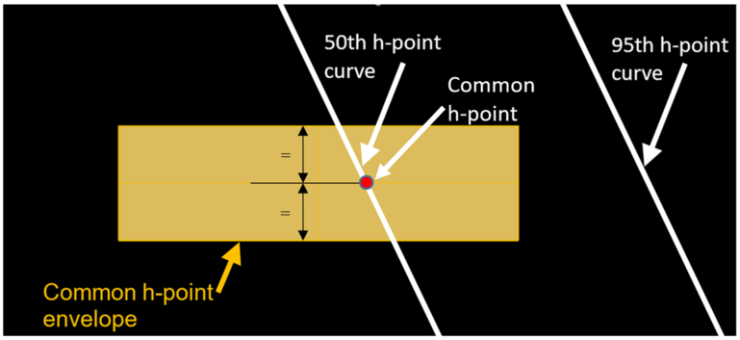

Figure 4. Plotting the 50th %ile and 95th %ile H-point curves on the common H-point Envelope and defining the new common H-point.

As can be seen from Figure 4 the 95th H-point curve does not coincide with the common H-point envelope and so the 50th H-point curve was used. The intersection of the 50th %ile H-point curve and the common H-point envelope was then used to define a single reference point that became the new common H-point. As the H-point curve was based on 50th %ile anthropometry the mid-point between the maximum and minimum common H30 (z) [14] value was used as shown in Figure 4. In this manner, the common H-Point was defined and this was agreed by the vehicle manufacturer's representatives in a further stakeholder meeting. The next step in the process was to explore the offset from the defined common H-point to the eye point that would be used for all vehicles.

2.4. Definition of a common eye point through an offset from the common H-point

The approach taken in UNECE Regulation 46 [11] defines a vertical offset from the SgRP of 635 mm. This was option was initially explored. 635 mm is equivalent to an offset from the H-point to the eye point of a 6th %ile UK female as shown in Figure 5. Figure 5 shows the SAMMIE DHM system [15] with a 6th %ile UK female based upon anthropometric data provided by the UK Department of Trade and Industry [12].

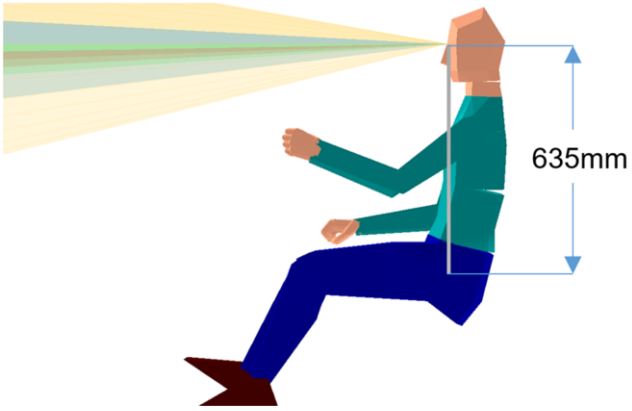

Figure 5. A representation of the DHM size equivalent to a vertical offset from the H-point to the eye point of 635 mm.

The fact that the UNECE Regulation 46 eye point offset represented a 6th %ile European female was reported to the stakeholder group, and it was noted that using this in conjunction with a 50th %ile H-point would not be logical. Therefore, the research team was requested to define a new offset that was representative of the whole European population at the 50th %ile level. To this end, as shown in Figure 6, the average European eye height above H-point (Z-axis), and rearwards offset between the hip and eye location (X-axis) was defined. This was done using a back rest angle of 18° (as agreed by the stakeholder group as the mid-point in the variability in the 'design' back rest angle used for the driving position by each manufacturer, i.e. 16-20°) and the average value was found for 50th %ile digital human models.

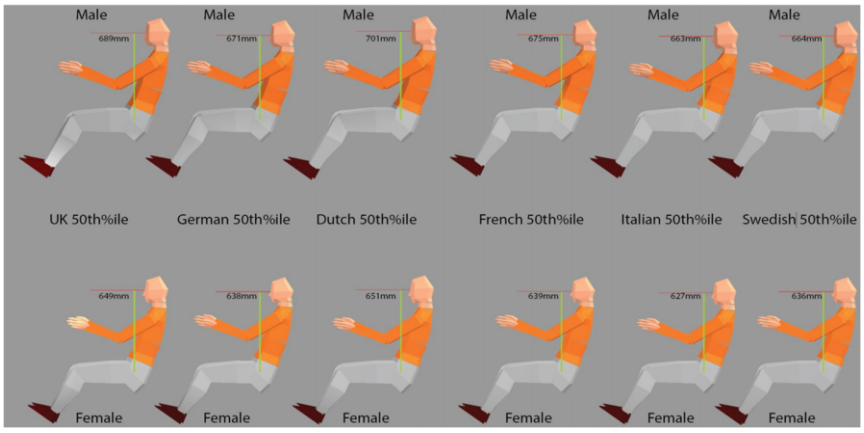

Figure 6. Defining the vertical (Z axis) and Horizontal (X axis) offsets from the H-point to the eye point for six different European nationalities with an 18° backrest angle.

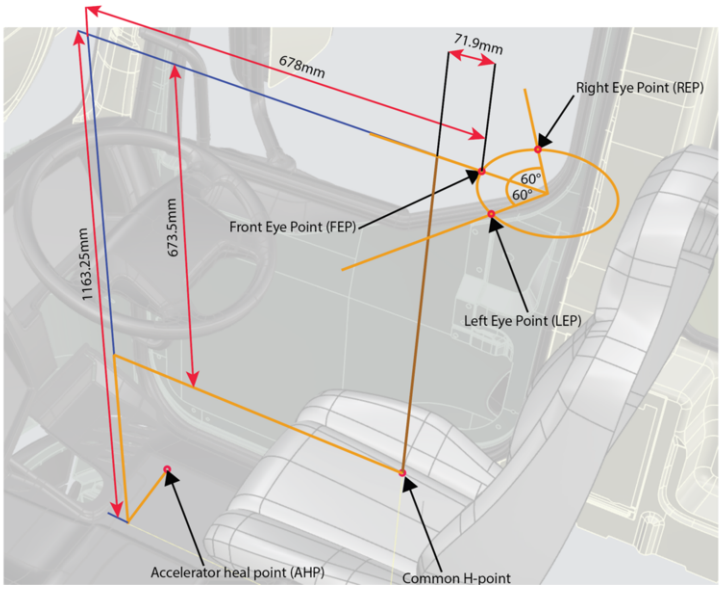

Figure 7. Illustrating the offset from the AHP to FEP, and the subsequent use of SAE 1050 to define the LEP and REP.

The sample included 50th %ile male and female offsets identified for UK, Germany, Holland, France, Italy and Sweden, and then this was averaged with a 90:10 male female split to reflect the proportion of male and female drivers that was acceptable to the stakeholder group. This reflects the values used in other standards. The result is an eye point that is 673.5 mm above the H-point and 71.9 mm rearwards of the H-point in X. When these values are offset from the common H-point, the proposed common eye point is 1163.25 mm above the AHP and 678 mm rearwards of the AHP. This defined the forward eye point. SAE J1050 [16] was then used to define a neck point 98 mm rearwards of the forward eye point, and two further eye points were then defined by a 60° rotation about the neck to the left and right of the forward point as shown in Figure 7. This defines three eye points (Front Eyepoint (FEP), Left Eye Point, (LEP) and Right Eye Point, (REP)). Figure 8 shows the newly defined eye point plotted along with the eye points that are produced by an 635 mm offset from the SgRP points shown in Figure 2 as the UNECE regulation 46 method.

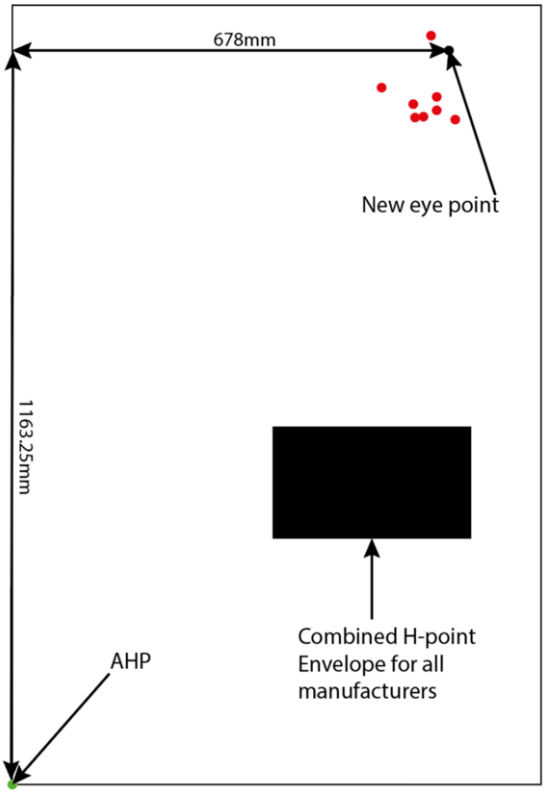

Figure 8. The position of the eye point defined by the new method, compared to the range of eye points created by the UNECE Regulation 46 method.

Figure 9 shows an example of the three eye points that have been defined being used to analyze the performance of a typical UK HGV (right hand drive). In the Figure 9 the volume of space visible to the driver is projected through the driver's door window, the passenger door window and a lower door window which is used to improve direct vision to the passenger side.

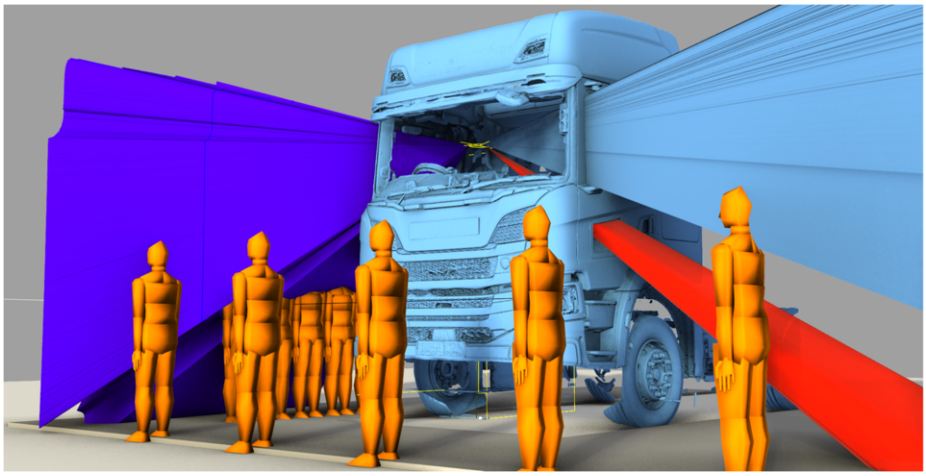

Figure 9. An example of the LEP and REP being used as the origin of projection through the passenger door and driver door windows.

3. Discussion

The previous sections have described the process by which a new eye point definition has been created for use in a process that allows the direct vision of HGV designs to be quantified. The process was driven by the research team in collaboration with a stakeholder group which included design team members from eight European HGV manufacturers and so has been rigorously reviewed by industry. As with many standardization definitions there are compromises that have been made. The definition of single eye point for all HGV designs inherently means that some vehicle designs will perform better or worse than if the manufacturers own eye point definitions had been used, but the driver for this process has been the creation of a measurement process which cannot be unfairly manipulated by a manufacturer changing variables which do not give a genuine improvement to direct vision. Figure 9 shows that the new eye point is generally higher than the points defined using the UNECE Regulation 46 approach of offsetting 635 mm from the SgRP. This is to be expected given that a 635 mm offset represents a 6th %ile female European as opposed to the 50th %ile data used in the new eye point definition. The new method is simple to apply by vehicle design teams as it simply requires an offset from the AHP, allowing a consistent and repeatable approach.

4. Conclusions

The requirement for a new eye point definition for HGVs for use in the assessment of direct vision was highlighted. A process was followed to define a new approach based upon an analysis of the limitations of existing standards. The result is a method that can be applied to all HGV designs in Europe, and this has been successfully implemented in the UK capital, London. This method is now under consideration by the European Union as a method to standardize a minimum requirement for direct vision from trucks in Europe.

References

[1] Department for Transport. Reported road casualties in Great Britain: 2018 annual report. 2019. (https://assets.publishing.service.gov.uk/government/uploads/system/uploads/attachment_data/file/834585/reported-road-casualties-annual-report-2018.pdf. (accessed 12/05/2020)

[2] Talbot R, Reed S, Barnes J, Thomas P, Christie N. Pedal cyclist fatalities in London: analysis of police collision files (2007-2011). 2014. https://dspace.lboro.ac.uk/2134/16487.

[3] Summerskill S, Marshall R, Paterson A, Eland A, Lenard J. The definition, production and validation of the direct vision standard (DVS) for HGVS. Final Report for TfL review. Version 1.1. London: Transport for London. 2019.

[4] Cook S, Summerskill S, Marshall R, Lawton C, Grant R, Lenard J, Clemo K. The development of improvements to drivers' direct and indirect vision from vehicles. Phase 2. Loughborough University. Report for Department for Transport. 2011. https://dspace.lboro.ac.uk/2134/8873.

[5] Summerskill S, Marshall R, Lenard J. The design of category N3 vehicles for improved driver direct vision. Loughborough Design School. 2014. https://dspace.lboro.ac.uk/2134/15922.

[6] Summerskill S, Marshall R, Paterson A, Reed S. Understanding direct and indirect driver vision in heavy goods vehicles: Final report prepared on behalf of Transport for London. Loughborough: Loughborough University, 1-432. 2015.

[7] Mole CD, Wilkie RMG. Looking forward to safer HGVs: The impact of mirrors on driver reaction times. Accident Analysis and Prevention, 2017, 107, 173–185. doi:10.1016/j.aap.2017.07.027.

[8] Mayor. Mayoral press release. New Measures To Rid London of Dangerous Lorries. 2016. Available at: https://www.london.gov.uk/press-releases/mayoral/new-measures-to-rid-london-of-dangerous-lorries. Accessed 19/12/19.

[9] Reed MP. Development of a New Eyellipse and Seating Accommodation Model for Trucks and Buses. University of Michigan Transportation Research Institute, Ann Arbor, MI, Tech. Report No. UMTRI-2005-30. 2005.

[10] SAE J941, Motor Vehicle Drivers' Eye Locations. Warrendale, PA: Society of Automotive Engineers, Inc., 2010

[11] UN ECE regulation 46. Uniform Provisions for Devices for Indirect Vision and of Motor Vehicles with Regard to the Installation of these Devices. UN ECE Vehicle Regulations. 2019.

[12] Peebles L, Norris B. Adultdata. The handbook of adult anthropometric and strength measurements - Data for design safety. (London: Department of Trade and Industry), DTI publication 2917/3k/6/98/NP URN 98/736. 1998.

[13] SAE J1516, Accommodation Tool Reference Point. Warrendale, PA: Society of Automotive Engineers, Inc., 2011

[14] SAE J1517, Driver Selected Seat Position. Warrendale, PA: Society of Automotive Engineers, Inc., 2011.

[15] Case K, Marshall R, Summerskill S. Digital human modelling over four decades. International Journal of the Digital Human, 2016, 1(2), 112–131.

[16] SAE J1050, Describing and Measuring the Driver's Field of View, Warrendale, PA: Society of Automotive Engineers, Inc., 2019.

DHM2020
L. Hanson et al. (Eds.)

© 2020 The authors and IOS Press.
This article is published online with Open Access by IOS Press and distributed under the terms of the Creative Commons Attribution Non-Commercial License 4.0 (CC BY-NC 4.0).
doi:10.3233/ATDE200018

Multimodality on the Road: Towards Evidence-Based Cognitive Modelling of Everyday Roadside Human Interactions

Vasiliki KONDYLI, and Mehul BHATT
Örebro University, Sweden
CoDesign Lab – Cognitive Vision
www.codesign-lab.org/cognitive-vision

Abstract We propose an evidence based methodology for the systematic analysis and cognitive characterisation of multimodal interactions in naturalistic roadside situations such as driving, crossing a street etc. Founded on basic human modalities of embodied interaction, the proposed methodology utilises three key characteristics crucial to roadside situations, namely: explicit and implicit mode of interaction, formal and informal means of signalling, and levels of context-specific (visual) attention. Driven by the fine-grained interpretation and modelling of human behaviour in naturalistic settings, we present an application of the proposed model with examples from a work-in-progress dataset consisting of baseline multimodal interaction scenarios and variations built therefrom with a particular emphasis on joint attention and diversity of modalities employed. Our research aims to open up an interdisciplinary frontier for the human-centred design and evaluation of artificial cognitive technologies (e.g., autonomous vehicles, robotics) where embodied (multimodal) human interaction and normative compliance are of central significance.

Keywords. multimodal interaction, interpersonal communication, naturalistic perception, joint attention, virtual reality, autonomous driving

1. Introduction

Interpersonal communication and interactions are vital for safe and effective coordination of actions in everyday roadside engagements: walking around, driving, riding a bike etc. Failure in interpersonal communication leads to a lack of mutual understanding of a situation and it is responsible for a great number of roadside accidents [1, 2]. With further strides in the autonomous vehicles industry and the present impetus on high-level visual intelligence technologies [3, 4], it will therefore be necessary to account for the role of interpersonal communication on the street and articulate human-centred performance benchmarks, e.g., from the viewpoint of training, testing and validation as part of statutory compliance measures.

Evidence-Based Design Issues pertaining to human-centred design and human-machine interaction have been barely addressed in the autonomous driving sector. Presently, autonomous vehicles do not have the capacity to communicate intentions, or to anticipate or predict interactions based on deep semantic analysis of observations of behavioural patterns. Considering how ambiguous interpersonal communication is within the context of driving, the interpretation is not trivial for contemporary systems, especially if we take into consideration socio-cultural normative behaviour, environmental and situational context. For this reason, people-centred datasets for training and testing the capabilities of systems will be necessary [6, 7]. These datasets should be based on behavioural analysis from real-world situations, and they should incorporate diverse real-world cases of interactions as they accrue amongst roadside stakeholders.

Interpersonal Communication by Multimodal Interaction Understanding how interpersonal communication develops is about understanding how emotions and intentions are expressed, and how gestures, facial expressions and body posture support, complement, and occasionally override verbal communication. Interpersonal communication involves single or multicomponent signals, together with informative cues and feedback [8].[1] Often communication takes place with the use of different modalities and often these phenomena occur in synchrony. Multimodality refers to a person's way of communicating by using more than one modalities at the same time, or from a perceptual approach, it refers to more than one modality being received based on the receiver's perception of the signal [9, 10].

Multimodality in Embodied Human Interaction The reason why and the point when people utilise multimodal signals for interaction is a question that has been explored from different perspectives [8, 10, 11]. It is primarily related to the circumstances (e.g. environment, events, participants), as well as to efficacy issues of signal structure and permanence to environmental noise, all of which are (most) likely to differ across modalities [8, 12]. For instance, signals expressed in different modalities have different transmission distances and different permanence to environmental noise; hence, by combining modalities the signal has a better chance to get transmitted. Moreover, examining correlations between cognitive load and multimodal communication shows that people respond to dynamic changes in their cognitive load by shifting to multimodal communication when load increases due to task difficulty or communication complexity [13].

Core Contribution Driven by fine-grained modelling of human behaviour and considerations in human-centred cognitive interaction technology design, we develop a systematic method for the evidence-based modelling of embodied multimodal interactions in an everyday roadside context with a particular focus on cognitive aspects pertaining to visual attention during activities such as driving and crossing a street. We propose a model categorising and characterising the instances of communication based on:

- embodied (inter)action modalities, e.g. involving gestures, head movement, gaze
- explicit, or implicit mode of interaction
- means of signalling, e.g., formal or informal, body-based, device-based
- levels of (visual) social attention achieved (e.g. common, mutual, joint) amongst interacting stakeholders such as Drivers, Pedestrians, Cyclists.

[1] A multicomponent signal is different than a multimodal signal and it refers to a number of sensory unimodal elements in a signal. It is considered complex signalling within the same modality.

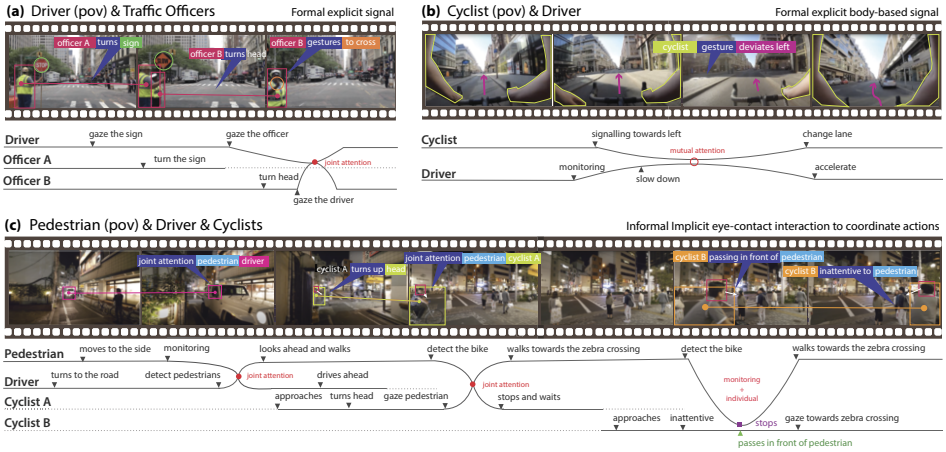

Figure 1. Multimodal interactions in streetscape, characterised based on Table 1; **(a)** From the point of view of the driver, a formal explicit device-based signal from the traffic officers using a sign and gestures (New York); **(b)** From the point of view of the cyclist, a formal explicit gesture indicates change of lane and ask for priority to the driver who follows (Berlin); **(c)** From the point of view of the pedestrian, several interaction episodes back to back involving a driver and two cyclists and focusing on the establishment of joint attention (Tokyo).

Even though real-world instances are the most valuable source for investigating the nature of interpersonal communication, controlling for external factors in naturalistic virtual reality (VR) scenes and projecting the roles of roadside stakeholders to a virtual agent and a participant are a significant addition for the investigation of synchronisation and dynamics between modalities during the course of interaction. To this effect, we also present instances from a work-in-progress dataset of roadside multimodal interactions combining real and VR episodes with the purpose of studying the variations of modalities involved in a sample of scenarios of interactions and the process of achieving joint attention.

2. A Cognitive Characterisation of (Roadside) Multimodal Interactions

Interactions between roadside users are mostly based on non-verbal communication and they are significant in resolving traffic ambiguities considering communication is precarious because of the lack of a homogeneously accepted social set of signals, and their dependance on the circumstantial aspects as situations, country, etc. [14, 15, 16] (Fig. 1). Non-verbal signals serve greatly social functions, creating bonds and shared knowledge, as well as reflecting attitudes, mood, and emotions [17]. In this context non-verbal communication can be characterised as *Spontaneous* (e.g. yawning, scratching their head, stretching their muscles), *Symbolic* (sign language, body movements or facial expressions), and *Pseudo-spontaneous* (performing an action that looks spontaneous) [18]. Focusing on the modalities used, the users, and the cognitive nature of the interaction we further characterise the interactions in the streetscape as follows (Table 1):

Interaction Modalities Roadside users handle a set of modalities to convey their intentions or to give feedback during an interaction. Each modality conveys a great deal of information regarding one's intentions that can be categorised according to its semantic

EMBODIED INTERACTIONS	INTERPRETATION
A1. MODE	
Explicit Interaction	Joint Attention - Facial Expressions - Gestures - Speech - Nodding
Implicit Interaction	Body Posture - Head Rotation - Behaviour Changes (pace, direction change) - Gaze Allocation (referential, aversion) - Stigmergy
A2. METHOD	
Formal Device-based	Hazard lights - Turn signal - Honking
Informal - Device-based	Head-light flashing for warning - Head-light blinking for acknowledgement - Honking as social etiquette - Honking for expressing displeasure - Honking for gratitude
Formal Body-based	Cyclist gesture to turn - Hand signals by traffic officer
Informal Body-based	Nodding for encouragement - Gesture to order yield - Gesture as gratitude for yielding - Eye contact to encourage yielding
A3. LEVEL (OF SOCIAL ATTENTION)	
Individual	Individual A attends objects/event X and individual B
Monitoring	Individual A attends to B's attention to objects/event X
Common	Individual A attends to B's attention to X and him/herself
Mutual	Individual A attends to B who attends to X and him/herself characterised by non-communicative eye contact
Joint (Shared)	Individual A attends to B who attends to X and him/herself characterised by communicative eye contact and/or other bi-directional communication
MODALITIES	EXAMPLES
HEAD MOVEMENTS (HM)	Turn towards the street - Tilt to a direction - Nod for disapproval - Slide for notice - Protrusion for warning
FACIAL EXPRESSIONS (FE)	Smiles - Frowns - Wrinkle - Eye Rolling - Cut Eye - Eyebrows Raising - Lips Movement - Mouth Movement
GESTURES (GE)	Emblematic (thumbs up, hitchhiking, stop) - Iconic (direction of movement) - Deictic (pointing) - Beat (irritation, gratitude)
BODY POSTURES (BP)	Crossing arms - Idle - Stand with the back to the street - Lean towards the car/ a kid's stroller - Stand besides a car/bike
GAZE (GZ)	Eye contact - Seek attention - Follow other's gaze - Follow a moving object - Aversion - Point towards a direction(Referential) - Look the traffic light
AUDITORY CUES (AU)	Honking - Car engine - Traffic light sound - Brakes - Siren - Voice
SPEECH (SP)	Ask - Warn - Shout - Scold - Give directions

Table 1. A Cognitive Characterisation of Roadside Interactions and the Modalities Involved.

functions. The classification is based on measurable properties of the modality such as direction, intensity, angle, fluidity, which can provide details for fine-grained modelling of interactions. For instance, manual gestures are classified with respect to their semantic function by McNeill [19] into *emblematic* (bare conventionalised meaning e.g. "thumbs up"), *iconic* (convey the shape of an object, direction of movement), *metaphoric* (resemble abstract concepts e.g. shape hands into a heart), *deictic* (point out locations in space), *beat* (keep the rhythm of speech with no semantic content). Head gestures vary in their exact of kinematic realisations (angles, extent), as well as overlap with other movements. However, the main categorisation includes *tilt, nod, turn, slide and protrusion*, and the relevant measurable properties include the pitch rotation in the up-down direction, roll in X axis, yaw and translation in X and Y axes [20].

A1. Mode of Interaction Signals of interpersonal communication can be expressed explicitly, e.g. via a handwave (Fig. 1a), or a gesture (Fig. 1b); however an implicit mode of signal deliverance is more common in streetscape scenarios, such as eye-contact (Fig. 1c). In implicit interactions, intending any practical action primarily aimed to reach a practical goal, can also lead to achieving a communicative purpose, without any predetermined (conventional or innate) specialised meaning. For instance, changing the speed of a vehicle indicates driver's intention to give or take priority. There are several steps in the scale between pure action and direct communication, with the general principle that the message is based on observation and it exploits simple side effects of acts and the agent's natural disposition to observe and interpret the behaviour of others [21].

A2. Method of Interaction The role and the tools that different roadside users have at their disposal also indicate the types of modalities they use and the nature of interaction they get involved in. Pedestrians and cyclists use their body as a communication

tool (e.g. hand gesture - Fig. 1b; eye gaze and subtle movement towards the side of the road - Fig. 1c). Drivers also use body-based configurations and additionally the available technological device such as hazard lights, or horn. With or without equipment roadside users produce a range of formal and informal signals that they integrate into their interactions [22]. Formal signals refer to established traffic rules such as gesturing before changing lane for a cyclist (Fig. 1b), or traffic officer's sign (Fig. 1a), while informal signals vary widely, as they are highly context and culture dependant (e.g. gesture for gratitude, gesture to give priority).

A3. Levels of Social Attention Gaze has a crucial role in non-verbal communication in the streetscape. Naturalistic studies show that pedestrians often establish eye contact with drivers to make sure they are seen, and drivers also often gaze at the face of other road users to assess their intentions [23]. Gaze in combination with gestures or speech, aims to establish a common ground between the road users and achieve a high level of social attention. The levels of social attention correspond to different degrees of situation awareness, and are defined in a scale from *individual* to *joint (or shared)*[2], where *individual* refer to one person attentional engagement with the environment from a first-person perspective only, while in every additional state of the scale (*monitoring, common, mutual, and joint*) the person's engagement is modified to second or third person perspective in order to acquire common knowledge with others [24]. The ultimate state of interaction is *joint* attention, the state where both participants have awareness of the situation and are also both aware that they are engaged. The different levels can be established with a combination of multiple interaction modalities.

Joint Attention In developmental psychology, the ability to share attention and to coordinate behaviour is defined under the joint attention framework, or visual co-orientation [25]. Joint attention traditionally refers to a triadic relationship between two interacting parties and a shared object or event [26, 27], and it is mostly related to the ability to follow a person's gaze to an objects or event [26, 27]. However, in recent work joint attention is also interpreted as *mental focus* [28] or *shared intentionality* [29]. Even though joint attention has been investigated in more sensory modalities other than vision (such as touch [30]), in the context of interpersonal communication in streetscape the focus is on joint *visual* attention between the roadside users. We address joint attention as the ability of a person to engage with another for the purpose of a common objective, or task, which may not involve explicit gaze following action or specific object involved.

Factors Influencing Roadside Interactions Multimodal interactions highly vary and they can convey very different meanings depending on the users involved (F1-Table 2), their intentions, and activities in the streetscape (Table 2, F2), as well as the environmental and situational context (Table 2, F3). For example, *social* factors refer to differences in behaviour recorded as a result of the group size of users, or the compliance levels to traffic rules; while *demographics* refers to correlations between age or gender groups with attentive behaviour from themselves and a cautious treatment from others [1]. Although we emphasise the importance of these factors to the overall outcome of the interactions, we do not provide further analysis in this paper, however, we address parts of topic on our previous work focusing on visuospatial complexity of naturalistic driving stimuli [7].

[2]The terms *joint attention* and *shared attention* have a very similar meaning however there is not one widely acceptable term for the phenomenon. For this paper we will refer to it as *joint attention*.

ROADISE INTERACTIONS | STAKEHOLDERS – ACTIONS – CONTEXT	
F1. Roadside Users	
Pedestrian - Motorcyclist - Cyclist - Driver Kid's stroller - Wheelchair - Truck Driver - Bus Driver Emergency Vehicle Driver - Trailer Driver - Animal Rider - Traffic Control Person - Pedal-cyclist	
F2. Intentions – Activities	
Slow down/Accelerate - Cross - Overtake - Stop/Start - Enter/Exit Point - Turn - Ask - Perform work - Play - Retrieving an object - Warn - Regulate traffic	
F3. Context — Environmental – Situational	
VISUOSPATIAL COMPLEXITY	Spatial Configuration - Street Width - Visibility - Auditory Cues - Clutter - Luminance - Traffic Density - Order - Regularity - Motion - Speed - Direction
DEMOGRAPHICS	Age - Gender - Culture
INDIVIDUAL DIFFERENCES	Psychical Capability - Cognitive Capability - Experience - Emotions - Attitude and beliefs - Personality traits
SOCIAL	Group Size - Social Norm - Law Compliance to Traffic Rules - Behavioural Imitation/Observation - Movement Flow - Informal Best Practices

Table 2. Factors influencing the behaviour of roadside users and the multimodal interactions developed during roadside actions.

3. Human-Centred Interaction Modelling: From Real-World to Naturalistic Virtual Scenes

To develop evidence-based modelling on frequently encountered multimodal interactions in the streetscape we firstly analyse incidents from real-world dynamic scenes recorded from the perspective of a driver, cyclist, or pedestrian (select scenes in Table 3). The analysis is based on the cognitive categorisation in Table 1, with the aim to examine:

1. What kind of interpersonal communication does take place between roadside users and which modalities are used?
2. What kind of interrelations can be found among the modalities during the course of interaction and how do they vary in similar scenarios?
3. Can properties of the modalities be measured systematically to serve in fine-grained modelling for the purpose of design multimodal interaction in VR?

As a second step, a number of incidents from the chosen scenes are subsequently (re)constructed in a virtual environment with variations on the modalities used for communication and the level of social (visuoauditory) attention established between the participating roadside users. We present two example scenarios with their corresponding variations (Scenarios A and B; Fig. 2-3):

Scenario A. Zebra-Crossing Situation (Fig. 2)
Pedestrian (P) with a kid's stroller is crossing a two-lane road on a zebra crossing while two drivers (D1 and D2) are approaching. P turns the head towards D1 as he approaches a zebra crossing, and establishes eye contact with D1. P then looks straight. D2 approaches the zebra crossing in the second lane without detecting P. Momentarily P turns the head, detects D2, stops and expresses disapproval towards D2 by extending his leg and using frowns and lip movements.

► *Scenario A Analysis based on Table 1.* Pedestrian P performs informal body-based explicit interaction with drivers D1 (via eye contact) and D2 (via body posture and facial expressions). P establishes joint attention with D1, as both parts engage in eye contact and both slow down or stop indicating intentional communication and situation awareness. On the contrary, for the interaction between P and D2 we only annotate monitoring attention for P towards D2. Concerning the interrelations between the modalities used, P uses body posture together with facial expressions instead of gestures (because of his

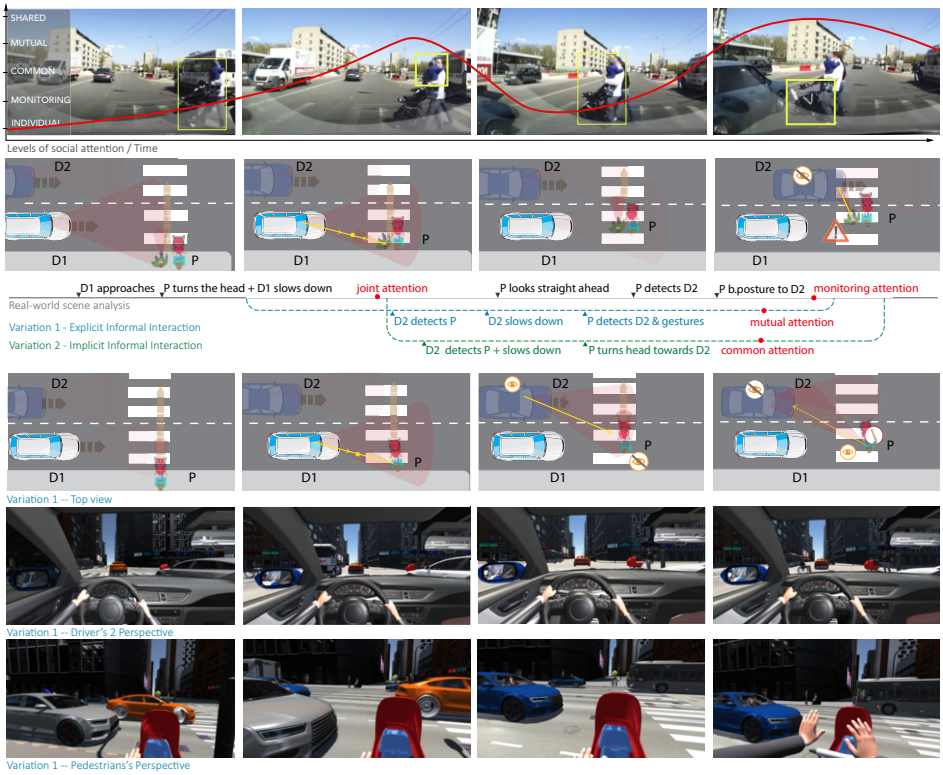

Figure 2. Zebra-Crossing Situation (**Scenario A**) / Real-world scene analysis involving an interaction incident between pedestrian(s) with a kid's stroller and drivers on two-lane zebra crossing. Two variations of this scenario developed in VR, differ from the original scene in terms of the embodied interaction factors (A1-A3) and the combination of modalities involved (Table 1).

occupied hands) to communicate agitation. Social attention levels change three times (represented with the red line on Fig. 2) as a result of P's distraction after interacting with D1, and the head movements that follow. In this scenario measurements of the angle of head rotation in both interaction instances, the synchronisation between the gaze allocation and the reaction time among users are significant for modelling. In variations 1 and 2 we manipulate the series and the number of events, as well as the timing between them, in order to examine via behavioural studies in VR (Section 4) the establishment of lower levels of social attention (e.g. mutual and common).

Scenario B. Cyclist changes lane / turns in front of a car (Fig. 3)
(Motor)Cyclist (C) changes lane / turns in front of a car and the driver (D). C slightly deviates from his lane, D who is following C slows down and starts monitoring C, C listens to the car approaching, performs overhead check and establishes common attention with D, then C looks ahead and changes lane.

► *Scenario B Analysis based on Table 1.* (Motor)Cyclist C performs an informal body-based implicit interaction with D by the action of changing direction of movement, and

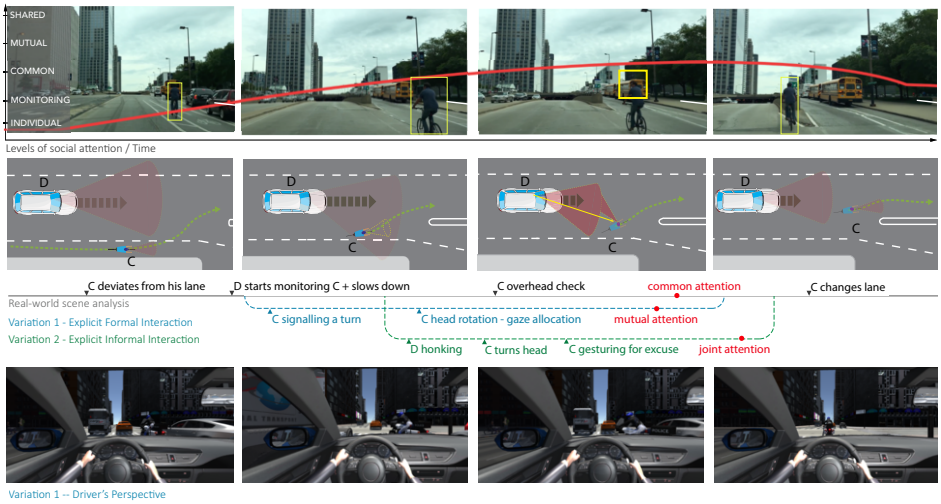

Figure 3. Cyclist changes lane / turns in front of a car (Scenario B.) / Real-world scene analysis involving a driver and a cyclist, and two variations that differ on the formalisation and the configuration of the signal and the modalities involved (based on Table 1). In variation 1 an explicit formal interaction is developed using formal gestures and gaze by the (motor)cyclist.

then via an overhead check. D's monitoring attention and C's overhead check overlap in time and lead to a safe change of lane for C in front of the car. During the overhead check, C uses his peripheral vision to detect D and to confirm the auditory cue of car's engine, but C and D do not perform eye contact. Consequently, D and C are aware of each others presence and they achieve common knowledge about the events via recursive assumptions, inferences, and perspective-taking since there are no specific external behaviours (beyond monitoring attention). To examine the temporal coordination of actions we record head rotation angle, reaction times, the speed and acceleration changes of the car, and the duration of monitoring attention and overhead check. Two variations of explicit communication signals are developed to test how they may lead to higher levels of social attention.

4. Towards a Naturalistic Dataset of Human Interactions in Everyday Driving

Work is in progress to develop a multimodal interaction dataset (following the methodology discussed in Section 3) consisting of the original real-world scenes together with scenes representing variations (in VR). Specifically, we collect and analyse a set of 20 dynamic scenes, covering 15 scenarios (A-O, Table 3) recorded from the egocentric perspective of a driver, cyclist, or pedestrian. The scenes are chosen such that there exists diversity with respect to typically occurring events and hazardous situations published by the Accident Research report of the German Insurance Association ("Unfallforschung der Versicherer") [31].

Behavioural Analysis The overall analysis of the real-world scenarios suggests that the behaviour of roadside users varies significantly even for similar scenarios with the

SCENARIOS	ROADSIDE MULTIMODAL INTERACTIONS	MODALITIES
A	P with a kid's stroller is crossing a two-lanes road while D1-D2 are approaching.	HM, BP, GZ, FE
B	C changes lane / turns in front of a car.	HM, GZ, AU
C.	Inattentive group of P crossing the street, D approaches seeking attention and signalling	GE, GZ, BP
D.	P looks at the traffic light that turns red, signalling and taking to other P on the other side of the street and crossing inattentively, D approaches the crossing	SP, FE, GE, BP, GA
E.	P emerges between parked cars and enters a parked car. D approaches	HM, GZ, AU
F.	P on wheelchair approaches a zebra crossing, D and C approach from different sides and give priority to P	HM, FE, GE, GA
G.	D turns to the street and P who are walking on the street move to the side	AU, HM, BP
H.	P (or group of pedestrians) cross half way a double-way street, they do not check the second lane, D approaches	AU, BP
I.	Low traffic road, P on the side of the street negotiate crossing with D, while M and C are passing between stopped cars	GZ, AU, HM
J.	P exits a shop/parking slot and walks on the street, D approaches	HM, BP, GA
K.	P is close to a zebra crossing, talking on the phone or texting with no clear intention to cross, D approaches	BP, FE, SP
L.	C standing close to a bike, and get on the bike, with no clear intention to start driving	BP, HM
M.	P steps on the road because of an obstacle on the pavement, C avoids pedestrian and changes lane, while D approaches	HM, GE, BP, GA
N.	M overtakes a car, looking for occluded pedestrians, and gives priority to P who is crossing	GZ, HM
O.	Policemen regulates traffic, instruct D for the direction too follow	BP, AU, GE

Table 3. Select scenarios of multimodal interactions based on the real-world dynamic scenes. The modalities involved are represented by the acronyms as per Table 1: **SP** (Speech); **HM** (Head Movements); **FE** (Facial Expressions); **GE** (Gestures); **BP** (Body Postures); **GZ** (Gaze); **AU** (Auditory Cues). The stakeholders involved are: D (Driver), C (Cyclist), M (Motorcyclist), P (Pedestrian).

same user roles (Pedestrian-Driver, Cyclist-Driver), and the same goals (crossing, turning). This observation highlights the effect of external factors such as visuospatial complexity, traffic dynamics, culture. Moreover, in line with previous studies we observe some modalities to differentiate more between cases than others [13, 20]. For instance, the number of gestures seems to be the same on average across the users in similar interactions, while the number of head and body movement differ greatly. However, even though the use of multimodal cues differ a lot in manner and frequency, there are some underline commonalities rooted in human basic perception and cognition concerning visual attention, spatial cognition and decision-making on the use of communication signals. For instance, drivers are more likely to use a turn signal if they have to turn left instead of right, or if they gaze at the vehicle in front of them that approaches an intersection [32]. Additionally, analysis of interrelations between modalities suggests that different interaction modalities are closely related to different cognitive processes, e.g. gestures with thinking and motor control of speech, body movements and facial expression with emotions [33].

Additionally, we observe more implicit than explicit interactions, and many of the explicit ones in more hazardous situations. This is in line with studies suggested that there is a trade off between the complexity of the communication mode and the reaction time required to respond [34]. Explicit interaction requires more cognitive processing to be perceived and it occasionally leads to slower reactions and collisions. However, this does not mean that explicit communication is counter-productive, but it shows the need for the communication strategies to start well in advance. Moreover, a major weight of interpersonal communications in this dataset was held by gaze. Pedestrians employ direct gaze to indicate intention to cross, to make the drivers to yield and more. Eye contact many times supported by facial expressions, is used by pedestrians to gain attention, while lack

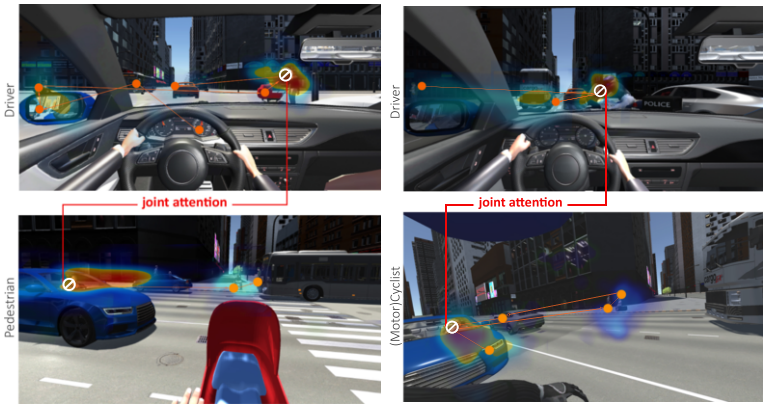

Figure 4. Sample eye-tracking data (presented as scanpath and heatmap) corresponding to the moment of joint attention (fixations during joint attention represented by ⊘): **(a)** Joint attention established between a Pedestrian with a stroller and a Driver (Situation corresponding to Scenario A in Fig. 2); **(b)** Joint attention established between a (Motor)Cyclist and a Driver (Situation corresponding to Scenario B in Fig. 3).

of gaze coordination, as a result of gaze deviation to distractors or aversion, indicates low level of social attention and it is related to hazardous scenes.

Empirical Evaluation in VR[3] Considering that the real-world scenes analysis shows a lot of variance between the behavioural patterns mostly because of external factors, the naturalistic VR scenes provide the controlled conditions for a behavioural study on fine-grained behavioural traits during interactions. By developing the scenarios in VR, we project the roles of pedestrians, drivers or (motor)cyclists to a pair of a user and a virtual agent. We manipulate variables related to the establishment of embodied interactions (mode of deliverance, formalisation and configuration of the signals), and the modalities used and we examine how they affect the establishment of different levels of social attention (Scenarios A-B). By manipulating aspects of the original events in VR we also explore how the complexity of the event may trigger the use of different modalities for interpersonal communication. In the ongoing behavioural study we collect physiological measurements (e.g. eye-tracking – Fig. 4), as well as observation on behavioural patterns and expressions (e.g. head rotation, steering wheel rotation, acceleration, intensity of gestures). This work adds empirical knowledge to the process of fine-grained modelling of interactions, concerning typical everyday scenarios in streetscape that may seem trivial and monotonic however they are complex problems for today's autonomous systems. It also contributes to evaluation of the human-centred interaction modelling and experimentation in respect to behavioural patterns and differences between people in the course of interaction.

[3] **Technical Setup (VR and Immersive Eye-Tracking)**. We implement full-body animated VR characters and several urban scenes built within the Unity Game Engine (v2019.2.2). The virtual scenarios are inherently multiperspective, e.g., from the POV of driver(s), pedestrian(s), cyclists(s). For the behavioural study, we use the HTC Vive Pro Eye system with embedded eye-tracking, accelerometer, gyroscope, and dual front-facing cameras with display resolution of 2880x1600 and 90Hz refresh rate. For the control of motion by the participants, we use a Logitech steering wheel with two pedals for the driver / cyclist, and a hand-held controller for the pedestrian.

5. Outlook

Within autonomous driving, the need for ethical regulation has most recently garnered interest [6, 7, 35]; therefore, qualitatively specified human-centred behavioural and normative benchmarks and evaluation for machine intelligence are imminent. Embedding evidence-based modelling in the process of designing agent-user multimodal interactions provides an ecologically rooted naturalistic basis for the development of human-centred technologies such as autonomous vehicles and social robotics.

As an example application of the proposed methodology, we have reported work-in-progress concerning the development of a dataset (including real-world and VR scenes) emphasising a cognitive characterisation of roadside multimodal interactions. In synergy with recent work on evaluating the visuospatial complexity of dynamic scenes [7], such a dataset provides an empirical foundation for the human-centred design of cognitive (computational) vision components within cognitive interaction technologies in general, and autonomous vehicles in particular [3, 4, 6]. That said, even from the singular viewpoint of behavioural research alone, we believe that ecologically valid naturalistic datasets such as the ones resulting from this research (and [7]) can provide a shared foundation for conducting naturalistic studies in perception and interaction, e.g., in the context of established paradigms such as event perception [5], ensemble perception [36], visual search and foraging [37], change blindness [38]. We posit that such a confluence of computational and behavioural studies combining cognitive psychology, AI, digital media, HCI, and design science [39] is needed to better appreciate the complexity and spectrum of varied human-centred challenges in the design of cognitive (assistive) technologies and other artefacts in everyday life and work.

References

[1] Stanciu S, Eby D, Molnar L, Louiss R, Zanier N, Kostyniuk L. Pedestrians/ Bicyclists and Autonomous Vehicles: How will they communicate? Transportation Research Record. 2018;2672(22):58–66.
[2] Risser R. Behavior in traffic conflict situations. Accident Analysis and Prevention. 1985;17(2):179–197.
[3] Suchan J, Bhatt M. Driven by Commonsense: On the Role of Human-Centred Visual Explainability for Autonomous Vehicles. In: 24th European Conference on Artificial Intelligence (ECAI). Santiago de Compostela, Spain.; 2020. .
[4] Bhatt M, Suchan J. Cognitive Vision and Perception: Deep Semantics Integrating AI and Vision for (Declarative) Reasoning about Space, Action, and Motion. In: 24th European Conf. on AI. Spain; 2020. .
[5] B. Tversky and J. M. Zacks. Event perception. In D. Reisberg, editor, *The Oxford Handbook of Cognitive Psychology*, Oxford Library of Psychology. ISBN 9780195376746.
[6] Suchan J, Bhatt M, Varadarajan S. Out of Sight But Not Out of Mind: An Answer Set Programming Based Online Abduction Framework for Visual Sensemaking in Autonomous Driving. In: Proc. of the 28th Intl. Joint Conf. on Artificial Intelligence, IJCAI 2019, China, August 10-16, 2019; 2019. p. 1879–1885.
[7] Kondyli V, Bhatt M, Suchan J. Multimodal Interaction in Autonomous Driving. Towards Human Visual Perception Driven Standardisation and Benchmarking. In: STAIRS @ ECAI 2020: 9th European Starting AI Researchers Symposium (STAIRS)., at ECAI 2020, 24th European Conf. on AI; 2020.
[8] Higham JP, Hebets EA. An introduction to multimodal communication. Behavioral Ecology and Sociobiology. 2013;67(9).
[9] Smith CL, Evans CS. A new heuristic for capturing the complexity of multimodal signals. Behavioral Ecology and Sociobiology. 2013;67(9).
[10] Partan SR, Marler P. Issues in the classification of multisensory communication signals. The American Naturalist. 2005;166(2):231–45.
[11] Healey P, Colman M, Thirlwell M. Analysing Multimodal communication. Repair-Based Measures of Human Communicative Coordination. van Kuppevelt et al JCJ, editor. Springer; 2005.

[12] Heymann EW. The neglected sense-olfaction in primate behavior, ecology, and evolution. Am J Primatol. 2006;68(6):519–524.
[13] Oviatt S, Coulston R, Lunstord R. When Do We Interact Multimodally? Cognitive Load and Multimodal Communication Patterns. Pennsylvania, USA: ICMI; 2004. .
[14] Rasouli A, Kotseruba I, Tsotsos KJ. Are They Going to Cross? A Benchmark Dataset and Baseline for Pedestrian Crosswalk Behavior. In: IEEE Inter Confon Computer Vision Workshops; 2017. p. 206–213.
[15] Sucha M, Dostal D, Risser R. Pedestrian-driver communication and decision strategies at marked crossings. Accident Analysis and Prevention. 2017;102:41–50.
[16] Wilde G. Immediate and delayed social interaction in road user behaviour. Applied Psychology. 1980;29(4):439 – 460.
[17] Feldman RS, Rim B. Fundamentals of Nonverbal Behavior. Cambridge University Press; 1991.
[18] Buck R, VanLear CA. Verbal and nonverbal communication: Distinguishing symbolic, spontaneous, and pseudo-spontaneous nonverbal behavior. Journal of Communication. 2002;52(3):522–541.
[19] McNeill D. Hand and Mind: What Gestures Reveal about Thought. Leonardo. 1992;27(4).
[20] Wagner P, Malisz Z, Kopp S. Gesture & speech in interaction: An overview [Editorial]. Speech Communication. 2014;57:209–232.
[21] Beckers R, Holland OE, Denebourg JL. From Local Actions to Global Tasks: Stigmergy and Collective Robotics. Fourth International Workshop on the Synthesis and Simulation of Living Systems (Artificial Life IV). Cambridge: MIT Press; 1994. p. 181–189.
[22] Renge K, Weller G, Schlag B, Peraaho M, Keskinen E. Comprehension & Evaluation of Road Users' Signaling - An International Comparison between Finland, Germany, & Japan. International Conference on Traffic and Transport Psychology- ICTTP; 2000. p. 91–100.
[23] Walker I, Brosnan M. Drivers gaze fixations during judgements about a bicyclists intentions. Transportation research part F: Traffic psychology and behaviour. 2007;10(2):90–98.
[24] Siposova B, Carpenter M. A new look at joint attention and common knowledge. Cognition. 2019;189:260–274.
[25] Butterworth G, Cochran E. Towards a mechanism of joint visual attention in human infancy. International Journal of Behavioral Development. 1980;3(3):253–272.
[26] Dube WV, MacDonald RP, Mansfield RC, Holcomb WL, Ahearn WH. Toward a behavioral analysis of joint attention. The Behavior Analyst. 2004;27(2):197.
[27] Moore C, Angelopoulos M, Bennett P. The role of movement in the development of joint visual attention. Infant Behavior and Development. 1997;20(1):83–92.
[28] Holth P. An operant analysis of joint attention skills. Journal of Early and Intensive Behavior Intervention. 2005;2(3):160.
[29] Tomasello M, Carpenter M. Shared intentionality. Developmental science. 2007;10(1):121–125.
[30] Botero M. Tactless scientists: Ignoring touch in the study of joint attention. Philosophical Psychology. 2016;29(8):1200–1214.
[31] GDV. Compact Accident Research by the German Insurance Association (Unfallforschung der Versicherer); 2017.
[32] Sullivan JM, Bao S, Goudy R, Konet H. Characteristics of turn signal use at intersections in baseline nauralistic driving. Accident Analysis and Prevention. 2015;74:1–7.
[33] De Stefani E, De Marco D. Language, Gesture and Emotional Communication: An Embodied View of Social Interaction. Frontiers in Psychology. 2019;10.
[34] Walker I. Signals are Informative but slow down responsess when drivers meet bicyclists at road junctions. Accident Analysis and Prevention. 2005;37(6):1074–1085.
[35] BMVI. Report by the ethics commission on automated and connected driving. BMVI. 2018.
[36] Whitney D, Yamanashi-Leib A. Ensemble perception. Annual review of Psychology. 2017.
[37] Kristjánsson T, Thornton IM, Chetverikov A, Kristjánsson A. Dynamics of visual attention revealed in foraging tasks. Cognition. 2020;194.
[38] Simons DJ, Levin DT. Change blindness. Trends in Cognitive Sciences. 1997;1(7):261 – 267.
[39] Bhatt M. Minds. Movement. Moving image. Cognitive Processing;19(Suppl. 1):S5–S5. Available from: www.codesign-lab.org/www/ICSC2018.pdf.

Part 3

Human Motion Data Collection and Modeling

This page intentionally left blank

DHM2020
L. Hanson et al. (Eds.)

© 2020 The authors and IOS Press.
This article is published online with Open Access by IOS Press and distributed under the terms of the Creative Commons Attribution Non-Commercial License 4.0 (CC BY-NC 4.0).
doi:10.3233/ATDE200020

Precision of Human Movement in the Virtual Reach Envelope - Measurement of Static and Dynamic Precision Depending on Different Movement Speeds

André KAISER[1] and Angelika C. BULLINGER
Chemnitz University of Technology, Chair for Ergonomics and Innovation, 09125 Chemnitz, Germany

Abstract. The precision of human movements within the reach envelope has been poorly described, but could play an important role, particularly in the simulation of human movements or in virtual interactions. We therefore describe an experiment in which virtual target points need to be reached. The targets are visualized in the three-dimensional reach envelope using the HTC-Vive Pro and participant movements are recorded using an optical motion-capturing system. The targets consist of 60 spheres which appear at different ranges, height angles and side angles. We measured 43 test subjects in three test conditions (fast as possible, precise as possible, fast and precise). Two forms of human movement precision were measured: static holding precision and dynamic reaching precision. As a result, the static and dynamic precision is described in terms of the speed, the distance between the hand and the virtual target, as well as the position within the reach envelope. Fast movements seem to be more precise at the end of the movement phase (26 mm deviation). Precise movements result in better dynamic precision at the end of the adjustment (7 mm deviation) and holding precision (5 mm deviation). Future works involve the evaluation of movement strategies.

Keywords. Precision of Human Movement, VR Interaction Using Collider, Simulation of Human Movements, Static Precision, Dynamic Precision

1. Introduction

When designing ergonomic virtual interactions, the design of the reach envelope is of importance [1]. Beside anthropometry, other influencing factors can be found in literature, guidelines, standards and methods for work planning, e.g. the field of vision [2], muscle forces [3] [4] [5] or the precision of manual actions [6] [7]. The precision in particular has so far been poorly described but could have an important role in the simulation of human movements or in the interaction with virtual objects using colliders.

Within the field of ergonomics, some works have measured the precision, but due to the use of touch displays only measured them in two dimensions (2D) [7] [8]. Sports science subdivides the precision into target accuracy and sequence accuracy [9]. This includes the deviation of spatial and/or temporal target points in positions (targets) or movements (sequences). Considering the sequence accuracy of movements towards

[1] Corresponding Author, Email: andre.kaiser@mb.tu-chemnitz.de.

target points, the literature [10] [11] [12] indicates, that joint angles along the involved chains are depending on hand positions, but due to the physical environment, the accuracy of the hand positioning is not directly observed in these works. Other works [13] [14] [15] describe the target accuracy of 1D, 2D or 3D movements using Fitt´s Law [6]. This literature also indicates, that gestures using more joints lead to a lower throughput and a higher error rate (representing the accuracy) in the given interaction task. This corresponds to Hick´s Law [16] [17], which concludes that more joints result in higher inaccuracy. Some of these works did not change the eye-object distance [7] [10] [13] [14] [15], did not change the position of the objects in the reach envelope [13] [14] [15], or did not measure the precision in 3D [7] [8] [10] [11] [12] [13] [14] [15]. A movement within the reach envelope contains all of those elements. Consequently, it is not possible to predict the precision of the hand movement in the reach envelope, especially if the haptic feedback of a real object is missing. This is important for the interaction with virtual objects using natural movements. Focusing on the hand/controller position, such interactions consist of two essential parts. First the ability of the hand/controller to reach the virtual object to select it. Second the ability to hold this position, if for example the selection task is based on a short timer.

Therefore, the aim of the paper is to describe the 3D target accuracy of human hand/controller in the virtual reach envelope. Hence, the authors designed an experiment where the difference between virtual positions and physical hand positions was measured, which corresponds to the definition of precision as the difference between an aimed and an actual value [9].

2. Method

2.1. Test setup and procedure

To investigate 3D target accuracy of human hand/controller in the virtual reach envelope, we conducted two studies. Study 1 compared two instructions, precise ('please be as **precise** as possible') and fast movements ('please be as **fast** as possible') as a within-subjects design. Study 2 mixed the instructions ('please be as **precise and fast** as possible') and can be compared to the data of study 1 as between subject design. Mixed instructions should be a better replication of a real situation. For the experiment, a hardware and software system was created that synchronised data and combined the coordinate systems of a VR-headset and a motion capturing system (Figure 1).

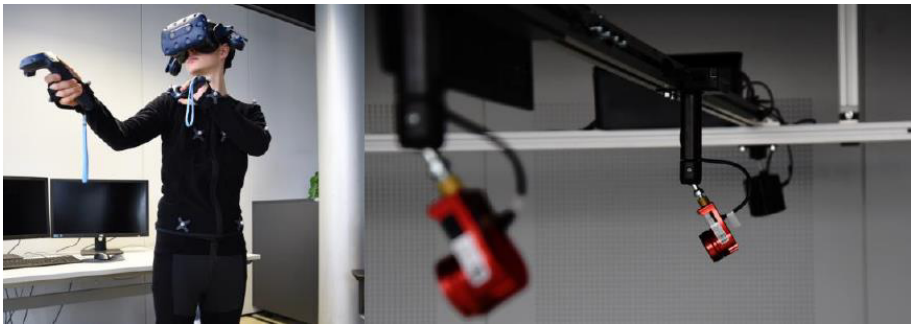

Figure 1. left: subject with motion capturing suit and HTC-Vive Pro, right: Flex 13 camera and lighthouse station installed on top of the capturing area [18].

The hardware consists of an optical motion capturing system (OptiTrack, Flex13) as well as an HTC Vive Pro headset, HTC Vive controller and two lighthouse stations. The HTC Vive Pro uses optical tracking as well to correct the drift of the IMU based tracking in the headset and controllers. Interference between the two systems was tested and could not be found. The software system consists of the Motive Body software from OptiTrack, which streams the marker and skeleton data. The software Unity was used to synchronize the motion capturing data with the position of the HTC controller and the Headset. Additionally, the application generates the virtual environment in which the subject should reach virtual spheres. For measuring precision, we tracked the distance between the virtual target sphere and the actual position of an equal sphere on top of the controller. The sphere on top of the controller was presented to the participant. In the following, this distance is described as **delta**.

At the beginning of the study, the length of the arm was measured as the distance between the shoulder pivot point of the OptiTrack skeleton and the center of the sphere on top of the controller in a position with a stretched arm to the side. After that each subject conducted a tutorial with five target spheres.

In the experiment the virtual environment consists of 60 invisible target spheres, each with a 15 mm radius. The target spheres are positioned in accordance to the subject's arm-length, the orientation towards a fixation cross on the eye level and the right shoulder pivot point, which was recalculated at the start for each of the target spheres. They appear at 0.4, 0.6 and 0.8 times the arm length. In addition, all points appear in four elevation angles, each with 30 ° rotation, and in five side angles, each with 30 ° rotation (Figure 2). For the starting position the controller needs to be in a specific area, defined by a loose hanging arm. The subject's gaze is focused on the fixation cross at eye level. Pressing a controller key within the starting position switches one target sphere to a visible state in a random order. The fixation cross turned then to an arrow pointing at the visible target sphere. If the surface of the sphere on top of the controller enters the target sphere (delta = 30 mm), a timer counts for two seconds and then the target disappears.

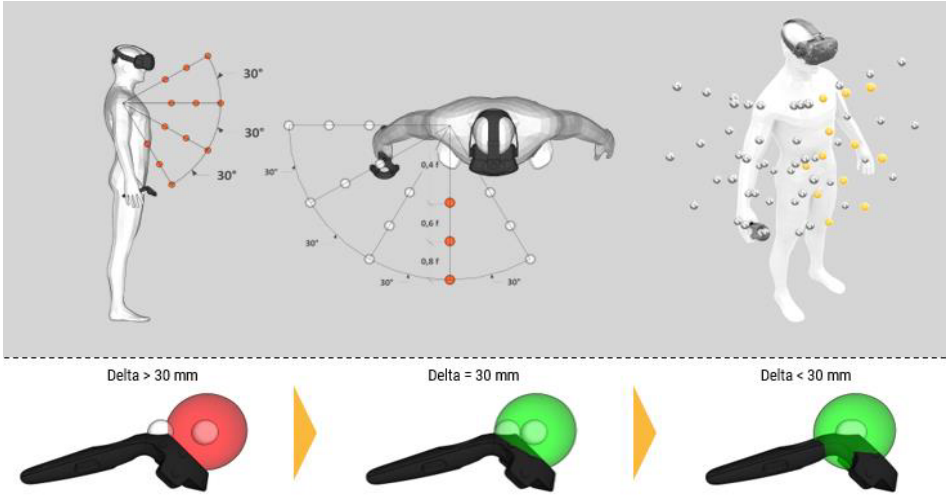

Figure 2. target positions depending on three arm length, four elevation angles and five side angles [18] and the visualization of the sphere on top of the controller entering the target sphere (including delta).

To visualize the start of the timer, a transparent sphere surrounding the target switches its color from red to green (Figure 2). The joint angles of the wrist, elbow, and shoulder, as well as delta are recorded.

2.2. Test subjects

We measured 43 subjects, consisting of students and scientist. 20 subjects for study 1 and 23 for study 2. The collected demographic is presented in Table 1. In addition, we asked for their sport activities, pre-existing conditions like injuries within the upper arm or restrictions in the vision. The authors also controlled simulator sickness using the virtual reality sickness questionnaire [19] [20]. No signs of unease were found.

Table 1. Test subjects. Data showing mean (SD).

criteria	**Study 1**	**Study 2**
Number [n]	20 (15 male; 5 female)	23 (15 male; 8 female)
Age [n]	25.1 (3.5)	27.0 (4.3)
Height [cm]	178.3 (7.9)	178.0 (9.7)
Weight [kg]	72.4 (13.7)	71.1 (14.5)
Arm length [cm]	65.9 (4.4)	65.3 (5.0)
Dominant side	14 right; 6 left	18 right; 5 left

2.3. Calculating dynamic and static precision

After the experiment, the authors excluded all collisions between controller and the physical environment from the dataset, which occur in certain cases due to a subject's anthropometry and neutral posture. Especially positions near the head, breast and abdomen, caused such collisions. Attempts in which the subject performed unusual movements were also excluded. Such movements were found when a subject started to move the controller before the target sphere is even detected. This could lead to a decreasing, then increasing and later again decreasing delta. Making sure to detected movement phases right, the authors only used straightforward movements. This results in data schematically shown in Figure 3.

Algorithms were used to detect different phases of the recorded data. These phases include searching and processing, moving, fine adjustment and holding. To calculate the start and end of the movement, the author used the elbow/knee of the curve. While the problem of knee detection in curves seems clear, to our knowledge, neither an accepted, nor a general approach for detecting one exists [21]. Here, the "kneedle algorithm" for the detection was used. Hence, a line from the first to the last point was drawn. The maximum and minimum perpendicular distance indicates the knee points [21].

To detect the fine adjustment phase, a point was calculated at which the movement is stopped for the first time within the two second timer. To reduce the influence of noise in the data and rise the probability of a consciously stop, we used 10 frames to calculate the slope of delta representing the movement speed. If the speed changed sign when adding the next value, we chose the middle value as the end of the fine adjustment phase.

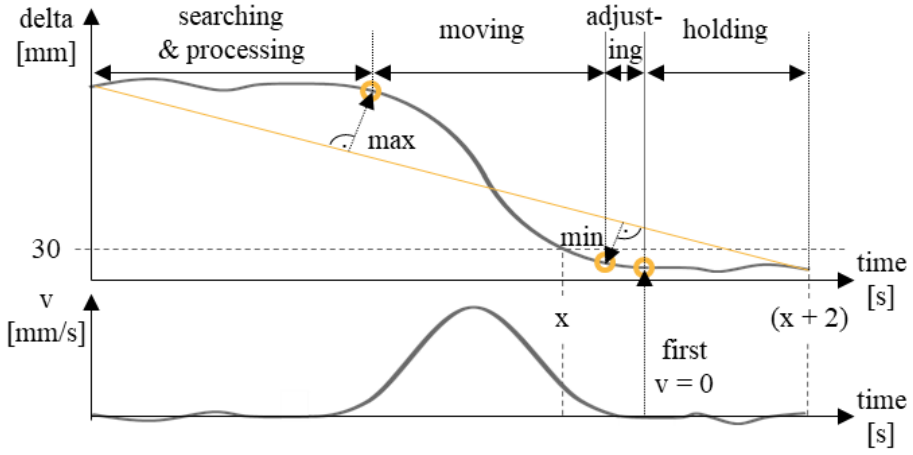

Figure 3. Detecting the phases using the kneedle algorithm and a first stop in schematic data.

Knowing these points allows the calculation of the target accuracy in the different phases. Especially for reaching motions towards virtual objects, the delta of the movement and adjustment phases seem to be relevant. Whereas the movement towards bigger objects could feel normal without the adjustment phase, the reach towards smaller objects could feel more natural if a short adjustment needs to be done. Because the delta is constantly decreasing in the movement and adjustment phase, the authors defined their accuracy as **dynamic precision**. This precision is measured for both phases separately *using delta at the end of both phases*.

If a selection is characterized as staying with the hand/controller in position for a short period of time, the delta within the holding phase is relevant for designing the space to select objects. Because the position is hold nearly static, the authors defined the accuracy during this phase as **static precision**. To *calculate the static precision, center (as arithmetic mean [mean]) and spread (as standard deviation [SD]) of the delta for the whole holding phase* was used. Whereas the center represents the distance to the virtual object during the holding phase, the spread represents the calmness of the hand. The definitions are graphically shown in Figure 4.

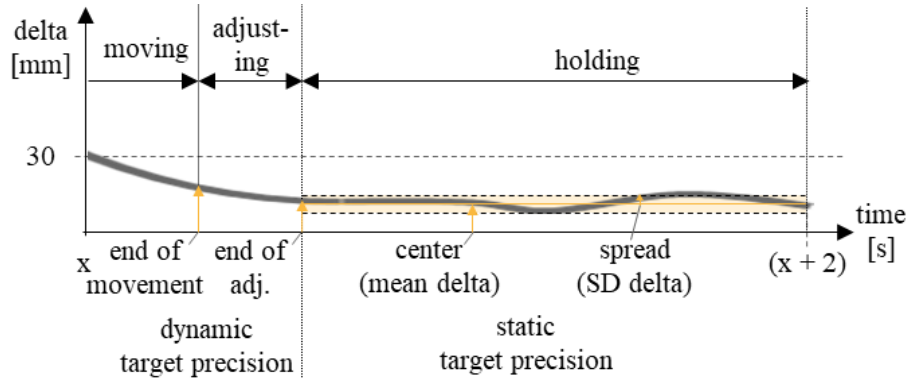

Figure 4. Definition of dynamic and static precision.

Additional the movement time, the adjusting time, and the movement speed, which equals the mean speed of the controller sphere during the movement phase was calculated. To compare the positions in the reach envelope, the data was normalized by using the length of the arm. The data included the values of both studies, not differentiating between movement speeds.

To calculate significance, we used a two-sample t-test for independent samples to compare study 1 and study 2 or a paired t-test to compare the results within study 1. Even though the distribution of the data shifts slightly sideward, a t-test was used due to its robustness to changed distributions. All described calculations where done using R studio.

3. Results

3.1. Dynamic reaching precision

The results show differences between **precise**, **fast** and the combined **fast and precise** movements. The values are shown in Table 2 and Figure 5.

Table 2. Dynamic precision. If not described the data are given in mean (SD).

criteria	**precise (n=1053)**	**fast (n=1012)**	**precise & fast (n=1030)**
movement time [s]	0.70 (0.22)	0.53 (0.19)	0.71 (0.22)
movement speed [m/s]	1.01 (0.34)	1.41 (0.57)	1.03 (0.43)
End of movement dynamic precision [mm]			
Mean (SD)	33.47 (21.33)	25.90 (15.32)	31.93 (18.84)
Median [Min, Max]	29.51 [2.55, 58.30]	23.30 [1.19, 49.08]	28.27 [1.21, 61.64]
adjusting time [s]	0.48 (0.46)	0.34 (0.38)	0.43 (0.34)
End of adjusting dynamic precision [mm]			
Mean (SD)	7.22 (6.96)	11.48 (9.35)	9.45 (7.69)
Median [Min, Max]	5.04 [0.25, 14.69]	8.71 [0.26, 26.33]	7.10 [0.41, 23.76]

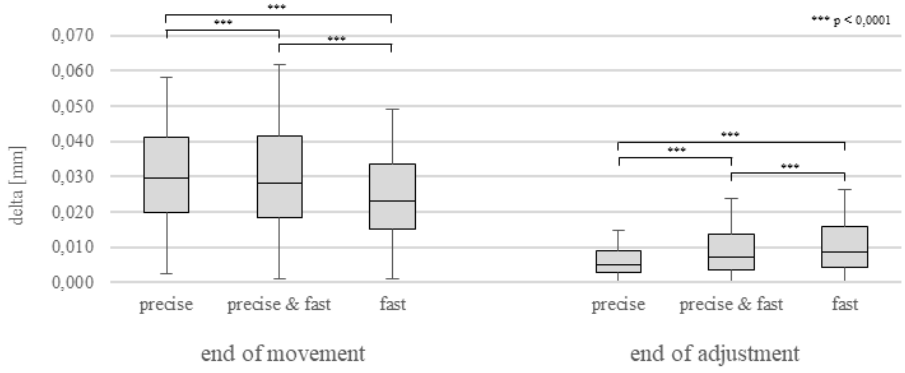

Figure 5. Boxplots for the dynamic precision.

As expected, the movement speed increases and the movement time decreases, when comparing the fast to the precise movements. Comparing the dynamic precision of the movement phase, fast movements enter the adjustment phase with a significantly ($p < 0.0001$) lower distance to the goal position. When comparing precise with fast and precise movements, the movement phase shows no significant differences. This changes, when looking at the adjustment phase. Doing precise adjustment takes more time and results in significantly ($p < 0.0001$) higher accuracy.

3.2. Static holding precision

Because the movement and adjusting phase takes more time in precise movements, the holding time decreases, when comparing **precise, precise and fast, and fast** movements. Table 3 and Figure 6 are showing, that the center value of the static precision is even closer to the target position than our detected ending of the adjusting phase (Table 2). Precise movement show significantly ($p < 0.0001$) lower distances to the target positions as well as significantly ($p < 0.0001$) less spread compared to the fast or the precise and fast movements.

Table 3. Static precision. If not described the data are given in mean (*SD*).

criteria	**precise (n=1053)**	**fast (n=1012)**	**precise & fast (n=1030)**
holding time [s]	1.47 (0.32)	1.61 (0.29)	1.51 (0.31)
center value static precision [mm]			
Mean (SD)	5.54 (5.20)	7.17 (5.96)	8.15 (5.76)
Median [Min, Max]	4.31 [1.08, 8.52]	5.68 [0.96, 11.35]	6.36 [0.96, 15.21]
spread value static precision [mm]			
Mean (SD)	2.33 (1.74)	3.51 (2.44)	2.59 (2.04)
Median [Min, Max]	1.80 [0.19, 13.89]	2.82 [0.18, 13.80]	1.96 [0.05, 14.69]

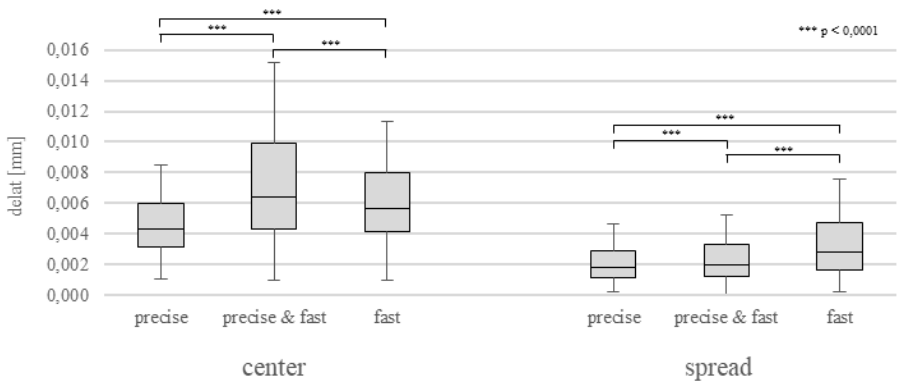

Figure 6. Boxplots for the static precision.

3.3. Precision within the reach envelope

Within the reach envelope the authors could find different areas, which result in higher or lower precision. The data can be found online (https://ebol.shinyapps.io/Kugeln3D/), where the x-axis runs to the front, the y-axis runs upwards and the z-axis runs to the right side. The black dot symbolises the shoulder pivot point. Figure 7 shows exemplary data prepared with a human model for better visualisation. The colors of spheres represent the dynamic precision at the end of the adjusting phase. The positions near a hanging arm, as well as positions with the hand crossing the sagittal plane of the human seem to be less accurate.

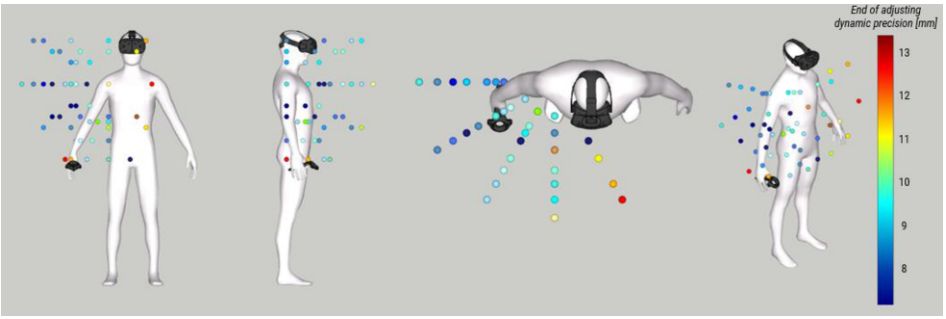

Figure 7. Precision within the reach envelope.

4. Discussion

Compared to results of Schmidtke [7] where the movement speed of 1 m/s until physical contact on a surface, for subjects between 20 and 30 years, leads to precision around 5 mm, the dynamic precision at the end of the adjusting phase shows higher values around 7 mm. The center value of the static precision shows that the adjustment didn´t reach its maximum during the first stop of the movement. This value of 5.5 mm is closer to the compared value. But taking the extra time for adjustment and holding phase into account, the movement speed would decrease. Looking up a movement speed of 0.5 m/s in the data of Schmidtke would lead to a precision of 1.0 mm.

Comparing the precision within the reach envelope to data of Rüffert, Mühlstedt and Bullinger [8] shows differences as well. The data of the 2D study describe two areas with increased precision within a 2D reach envelope. One area in front of the body (< 6 mm) and one around the elbow position (< 7 mm). For the other areas, precision values between 7 mm and 12 mm were measured. This data was obtained using a touchscreen at elbow height with the fast movement instruction. In our data, areas in front of the body or when crossing the sagittal plain lead to lower precision (Figure 4), regardless of the height. The second area of lower precision, which occurs around the hanging arm position, is not comparable due to the experimental setting. Overall, mean values of Rüffert et al. show a higher precision in comparison to our values for fast movements at the end of the adjustment phase. Inclusion of the holding phase and use of the static precision center minimizes these differences.

The differences to both compared studies [7] [8] could be explained by the use of the hardware setup. Due to the short experimental time (around 5 min), drift of up to 3

mm per 20 min (HTC Vive Pro) [23] has a minor impact. Latency and precision of the system seem to be more important. The HTC Vive Pro has a precision of 0.2 mm and a trueness of 2.63 mm, depending on environment, setup and scenario [23]. But because the authors didn´t use the direction of the delta and did take a high number of trails into account, the mean value should be meaningful. The app-to-display latency of 31.3 ms [24] could influence the subjects' tendency to adjust their position constantly. This would be an additional explanation why the center of the static precision is more accurate than the dynamic precision at the end of the adjusting phase. A more reasonable explanation could be that adjusting doesn´t simply end after the first detected stop or possibly doesn´t end at all. The differences within the reach envelope could also be influenced due to the hardware setup. It is possible that one of the two lighthouse stations had trouble tracking the controller near the body. This could have had an influence on values with the controller near the body, e. g. near the hanging arm and in front of the subject.

In general, the differences to both studies [7] [8] could also be caused by additional distance in the third dimension, as well as missing information in VR (e. g. shadows). Both increase difficulty in perception. Other than perception, the missing physical contact and the additional third dimension, also increase the difficulty in muscle coordination. Focusing on our data, the relationship of movement speed to time, dynamic precision, and static precision, was predictable. It was found that the speed of the movement phase doesn't influence precision. However, the adjusting time is influenced by the effort the subjects put into being precise. The essential difference between being precise and being precise and fast, is that the adjustment time and the precision changes. Focusing on just being fast increases the movement speed significantly.

Knowledge of these values allows for the design of more natural interactions in virtual environments, without the help of other technologies like eye-tracking. Hence, the collider of objects that need to be grasped, should be given an extra 5 mm to 30 mm radius, depending on the task given to users. Of course, small objects will lead to more precise movement, so the collider should only get a small extra radius, whereas bigger objects may need a larger additional radius value. This data could be used, for example, to design workplaces where you might want to add a chamfer to increase the radius of specific goal positions for plugins or clips. Since it is clear that such a chamfer would reduce the assembly time [25], measured 3D values would now be available to design the dimensions within a 3D reach envelope.

It is also possible to use the data for static interactions such as a virtual selecting task, where you would need to stay in one position for a short amount of time. Within the selection time, designers need to take a spread of movement into account. This spread of 2 mm to 4 mm is compensated by an additional adjustment of the hand/controller during the holding phase, which leads to even higher accuracy than the position at the end of the adjusting phase.

Knowing the relationship between movement, adjusting and holding could be used in the simulation of human movements as well. To extend on this knowledge, further analysis of the OptiTrack motion capturing data should be done. They can be used to compare movement strategies for reaching and holding different positions. This includes the sequence of the joint movements, as well as the influence of the joints towards the final precision. Further studies should analyze changing target sizes and forms, holding times, demographics, as well as evaluating the usability of virtual grasping then applying the precision values.

Acknowledgement

This contribution would have been impossible without the support of the "Future of Work" program from the Federal Ministry of Education and Research and the European Social Fund. (Project: VirMont, 02L17C050).

References

[1] Schlick C, Bruder R, Luczak H. Arbeitswissenschaft. Springer-Verlag, 2018.
[2] DIN Deutsches Institut für Normung e. V. DIN 15996. Bild- und Tonbearbeitung im Film-, Video- und Rundfunkbetrieben - Grundsätze und Festlegungen für den Arbeitsplatz. Beuth Verlag, Berlin, 2008.
[3] DIN Deutsches Institut für Normung e. V. DIN 33411-4. Körperkräfte des Menschen. Maximale statische Aktionskräfte (Isodynen). Beuth Verlag, Berlin, 1987.
[4] Wakula J, Berg K, Schaub KH, Bruder R, Glitsch U, Ellegast R. Der montagespezifische Kraftatlas. In: DGUV, editor. BGIA-Report 03/2009, 2009, ISBN: 978-3-88383-788-8.
[5] Kaiser A. Modellierung maximaler menschlicher Muskelmomente auf Basis digitaler Menschmodelle. Universitätsverlag Chemnitz, Chemnitz, 2018 ISBN 978-3-96100-048-7
[6] Fitts PM. The information capacity of the human motor system in controlling the amplitude of movement. Journal of Experimental Psychology, 1954, 47, 381–391.
[7] Schmidtke H. Untersuchung motorischer Koordinationsleistungen des Menschen. In: Bundesamt für Wehrtechnik und Beschaffung, editors. Ergonomische Studien Nr. 26, Koblenz, 1988.
[8] Rüffert D, Mühlstedt J, Bullinger AC. Ergonomie im Griff?. Bewegungsstudie zu Präzision im Greifraum. In: Gesellschaft für Arbeitswissenschaft e.V., editors. Tagungsband GfA-Frühjahrskongress. Verantwortung für die Arbeit der Zukunft, February 2015, Karlsruhe.
[9] Meinel K, Schnabel G. Bewegungslehre Sportmotorik. Abriss einer Theorie der sportlichen Motorik unter pädagogischem Aspekt. Meyer & Meyer Verlag, Aachen, 2007.
[10] Desmurget M, Prablanc C, Rossetti Y, Arzi M, Paulignan Y, Urquizar C, Mignot JC. Postural and synergic control for three-dimensional movements of reaching and grasping. Journal of Neurophysiology, 1995, 74(2), 905-910.
[11] Desmurget M, Prablanc C, Arzi M, Rossetti Y, Paulignan Y, Urquizar C. Integrated control of hand transport and orientation during prehension movements. Experimental brain research, 1996, 110(2), 265-278.
[12] Paulignan Y, Frak VG, Toni I, Jeannerod M. Influence of object position and size on human prehension movements. Experimental brain research, 1997, 114(2), 226-234.
[13] Mackenzie IS, Buxton W. Extending Fitts' law to two-dimensional tasks. In: Proceedings of the SIGCHI conference on Human factors in computing systems, 1992, 219-226.
[14] Mackenzie, IS. Fitts' law as a research and design tool in human-computer interaction. Human-computer interaction, 1992, 7(1), 91-139.
[15] Burno RA, Wu B, Doherty R, Colett H, Elnaggar R. Applying fitts' law to gesture based computer interactions. Procedia Manufacturing, 2015, 3, 4342-4349.
[16] Hick WE. On the rate of gain of information. Quarterly Journal of experimental psychology, 1952, 4(1), 11-26.
[17] Logan GD, Ulrich JE, Lindsey DRB. Different (key) strokes for different folks: How standard and nonstandard typists balance Fitts' law and Hick's law. Journal of Experimental Psychology: Human Perception and Performance, 2016, 42(12), 2084-2102.
[18] Kaiser A, Bernhagen M, Trezl J, Bartzke T, Lorenz T, Dittrich F, Bullinger AC. Erfassung der Bewegungstrajektorien und der Präzision im dreidimensionalen Greifraum. In: Gesellschaft für Arbeitswissenschaft e.V., editors. Tagungsband GfA-Frühjahrskongress. Arbeit interdisziplinär analysieren - bewerten - gestalten, February 2019, Dresden.
[19] Kim HK, Park J, Choi Y, Choe M. Virtual reality sickness questionnaire (VRSQ): Motion sickness measurement index in a virtual reality environment. Applied Ergonomics, 2018, 69, 66–73.
[20] Neukum A, Grattenthaler H. Kinetose in der Fahrsimulation (Project: Simulation von Einsatzfahrten im Auftrag des Präsidiums der Bayerischen Bereitschaftspolizei, Abschlussbericht – Teil II). University of Würzburg, Germany, 2006.
[21] Satopaa V, Albrecht J, Irwin D, Raghavan B. Finding a" kneedle" in a haystack: Detecting knee points in system behavior. In: 2011 31st international conference on distributed computing systems workshops. IEEE, 2011, 166-171.

[22] Luckett E. A Quantitative Evaluation of the HTC Vive for Virtual Reality Research. 2018. Doktorarbeit. The University of Mississippi.
[23] Groves LA, Carnahan P, Allen DR, Adam R, Peters TM, Chen EC. Accuracy assessment for the co-registration between optical and VIVE head-mounted display tracking. International journal of computer assisted radiology and surgery, 2019, 14(7), 1207-1215.
[24] Chénéchal ML, Goldman JC. HTC Vive Pro time performance benchmark for scientific research. In: Bruder G, Yoshimoto S, Cobb S, editors. In: Proceedings of ICAT-EGVE 2018 - International Conference on Artificial Reality and Telexistence and Eurographics Symposium on Virtual Environments, 2018.
[25] Zadeh HS. Einflüsse von Greif-und Kontaktbedingungen auf die Montage von Clipsverbindungen aus der Automobilindustrie. Ergonomia, 2011.

DHM2020
L. Hanson et al. (Eds.)
© 2020 The authors and IOS Press.
This article is published online with Open Access by IOS Press and distributed under the terms of the Creative Commons Attribution Non-Commercial License 4.0 (CC BY-NC 4.0).
doi:10.3233/ATDE200021

Experimental Evaluation of Postural Stability Using Stepping Strategies During Industrial Tasks

Fabrice LATOUR [a], Ali ZEIGHAMI [a], Nicola HAGEMEISTER [a], Julie CHARLAND [b] and Rachid AISSAOUI [a,1]
[a] *Laboratoire de Recherche en Imagerie et Orthopédie (LIO), École de Technologie Supérieure (ÉTS), Centre de Recherche du CHUM, Montréal, Québec, Canada*
[b] *Dassault Systèmes Canada, Montréal, Québec, Canada*

Abstract. Foot positioning has a significant impact on human body stability control when completing a manufacturing task. In classical Digital Human Models (DHM), the use of stepping strategies to generate stable postures relies on simplistic models, which generally locate the DHM center of mass (COM) at half distance between feet contact or limit the zero moment point (ZMP) projection within the base of support (BOS). Developing more comprehensive stepping models requires rigorous experimental studies to extract human movement coordination strategies during manufacturing tasks, which can be used to validate DHM models. The objective of this study is to develop an experimental test bench representing industrial conditions and to carry out experiments to provide these DHM models with parameters of postural stability. The assessed postural stability parameters in this study were the support length which is a variation of the step length, and the ZMP position with respect to the BOS. Results obtained from a pilot subject showed that the contralateral and ipsilateral legs move respectively to expand the BOS in the direction of ZMP displacement to maximize stability.

Keywords. Posture, Stability, Stepping, Zero Moment Point

1. Introduction

A common aspect digital human models (DHM) strive to improve is their autonomy to position the human manikin in a biomechanically plausible posture under specific task conditions. Currently, few models allow for semi-autonomous placement of the manikin in the simulated environment requiring manual interactions by the user to refine the final simulated postures [1,2]. For models simulating standing tasks, stability criteria are important to ensure the generation of biomechanically plausible postures. In industrial conditions, the use of stepping to maintain a stable posture is frequent as workers will often need to reach or apply forces when accomplishing tasks [3].

Classical DHMs that utilize stepping behaviors to generate stable postures rely on simplistic models, which generally locate the DHMs center of mass (COM) at half distance between the feet contact position [4]. Predictive stepping models use experimentally collected data and calculations to predict data-based feet placement.

[1] Corresponding Author, Email: rachid.aissaoui@etsmtl.ca.

These models rely on regression equations with the task characteristics as the inputs to position the manikin's feet [3,5,6]. They can predict transition stepping, but pose some challenges when simulating more complex asymmetrical handling or tool manipulation tasks with task parameters different from the experimentally collected data.

Optimization-based stepping models compute the feet position and posture through minimizing an objective function (e.g., joint torques) [7,8]. The main stability criterion for these models is accomplished by limiting the calculated zero moment point (ZMP) projection to stay inside the base of support (BOS), which is the convex hull of the feet contact points with the support plane. This basic formulation respects minimal stability requirements that maintain feet placement as long as stability is not compromised. The ZMP represents a virtual point where the total tilting moments generated from gravitational and external forces applied to the manikin are zero [9]. Although this method generates stepping according to external requirements, it has not yet been validated with suitable experimental data to verify if the feet placement is accurate.

This study is motivated by the Smart Posture Engine (SPE) technology to enhance the stability control of the DHM. The SPE is a posture prediction model used to generate biomechanically plausible final postures of a DHM given the simulated environment and the task information [10,11]. The SPE uses an inverse kinematics solver with selective filtering and prioritized constraints similar to Baerlocher [12] while avoiding the collision with the environment. The more recent stepping model proposed was developed as part of an improvement to the SPE [13]. The main stability difference in this model is that the ZMP and the feet placement are controlled more precisely with respect to the functional stability region, a smaller region than the BOS situated between feet contact. This allows the manikin to be simulated adopting the most stable posture possible depending on the required target reach, height, and loads. However, no experimental data has yet been produced to validate this concept.

In the literature, the majority of studies that have proposed foot positioning models studied general two-handed push-pull tasks [3,7,14], which is not representative of the observations found in the industrial field [15]. The study by Baril-Gingras and Lortie [15], conducted in industrial settings, allowed the identification of different postural strategies. Of the 944 material handling tasks observed, one-handed tasks and two-handed asymmetrical tasks represented respectively 55.4% and 35.6% of the handlings, which accounted for more than 90% of all evaluated handlings. This indicates that one-handed and out of sagittal plane tasks should be preferred when studying industrial tasks. In this same study, horizontal pushing and pulling (48.2%) was seen almost twice as often as vertical lifting and lowering (26.6%), where tasks accomplished with horizontal and transverse components were the most frequent. When reviewing the literature, accurate stepping behavior models derived from specific industrial task experiments providing human movement coordination are very scarce. No feet prediction model assessed tasks involving hand tools. Also, no study evaluated the effects of a transverse obstacle imposing spatial constraints and requiring subjects to execute tasks out of the sagittal plane without prescribing specific feet placement, which has been underlined by Wilkinson, Pinder, and Grieve [16] to require further investigation. Imposing specific feet position for out of sagittal plane tasks shows a strong indication that foot placement and posture constraints may have an important effect on force exertion capability [16,17,18]. Granata and Bennett [19] studied the effects of split and side-by-side stances on stability during pushing tasks, where stability was found to be significantly influenced by feet placement. In order for DHMs to become fully autonomous, the stepping prediction models need to be enhanced.

Although bracing and other postural strategies exist in the industrial field, this study focuses on maintaining stability through the stepping strategy, while executing tasks in different hand conditions, by limiting the use of other postural strategies. In this study, the subject is free to position their feet as wanted in order to adopt a preferred posture. Moreover, the use of a transverse obstacle requires the subject to execute the conditions without centering themself with respect to the line of the applied hand force. The use of a tool while completing the same tasks allows the evaluation of its influence on feet placement when compared to typical push and pull conditions. Because no previous study evaluated a transverse obstacle, the scaling of the target position was based on other scaled parameters found in the literature [18,19,20,21].

The primary objective of this study was to develop an experimental test bench that would allow the evaluation of the required parameters to assess the ZMP and human postural stability, such as the support length with respect to the BOS. It is hypothesized that during either centered tasks or tasks with a transverse obstacle, the contralateral and ipsilateral legs move respectively to expand the BOS in the direction of ZMP displacement in order to maximize the stability.

2. Method

2.1. The Conception of an Experimental Test Bench

A test bench was custom designed with two sliding rails mounted on articulated pantograph arms allowing the adjustment of a hand target position in all three axes and the addition of a transverse obstacle to impose spacial constraints for out of sagittal plane tasks (Figure 1). Lockable adjustments ensure no movement occurs during trials.

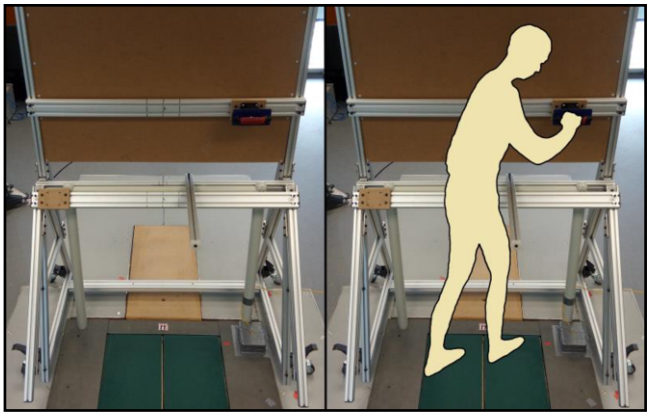

Figure 1. Experimental test bench positioned with a transverse obstacle.

For evaluating pushing and pulling, a 5 3/16" (131.7 mm) handle interface with a projection of 2" (50.8 mm) was built (Figure 2). It consists of a high-friction rubber handle with an anti-slip shape that enhances hand-handle grip. The second interface is for evaluating the use of a tool (Figure 2). Three reflective markers were fixed on each capture interface which is attached to a load cell and three other markers were affixed on the screwdriver, to locate their position in the environment.

2.2. Experimental Setup

Experiments were conducted in the Laboratoire de recherche en imagerie et orthopédie (LIO) of the Centre de recherche du Centre hospitalier de l'Université de Montréal (CRCHUM). Three synchronized acquisition systems were used to collect human kinematic data at a sampling frequency of 200 Hz and kinetic data at 1000 Hz (Figure 2): (1) AMTI MC3A 6-DOF load cell attached to the capture interface, (2) Twelve VICON MX T20-S motion capture cameras, and (3) ground force platforms. As shown in Figure 2, the experimental test bench is centered with the force platforms and is affixed in this position using anchor screws.

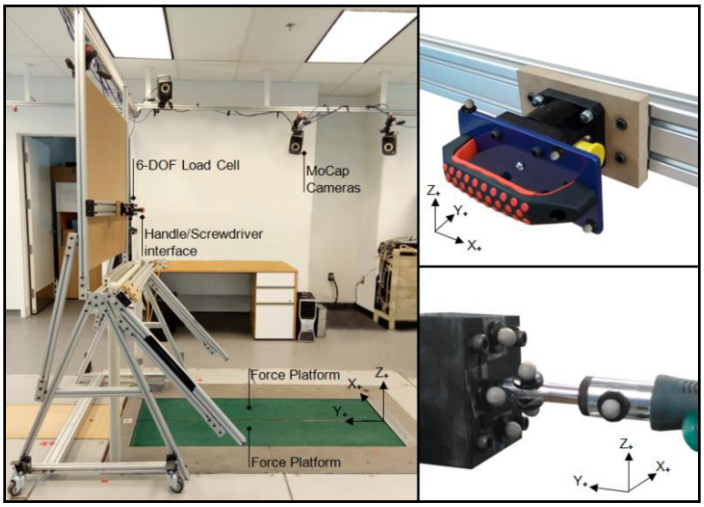

Figure 2. Experimental setup: Left, test bench affixed to the laboratory floor with acquisition systems. Right, two different capture interfaces developed. Pushing and pulling handle interface and screwdriver interface.

2.3. Pilot Subject

The subject assessed in this study was a right-hand dominant female with the following age, stature, weight, arm span, and hip-width: 24 years, 165 cm, 67 kg, 167 cm, and 31.12 cm, respectively. A total of 50 passive reflective markers were affixed on subject body landmarks as shown in Figure 3 [22].

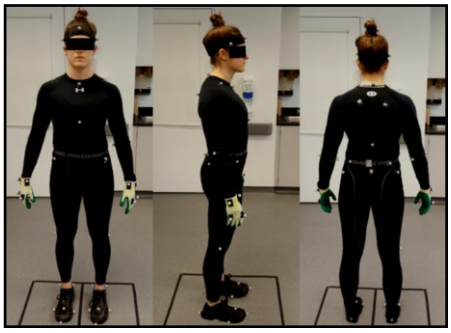

Figure 3. Passive reflective marker placement on the subject.

2.4. Experimental Procedure

Experiments were conducted with the right hand only, at an overhead position, and with two handle locations as presented in Table 1. For each handle locations, the subject performed four (4) task conditions. At least one practice trial of the presented target configuration was required to ensure that the preferred posture was adopted and that the subject was comfortable achieving the required force levels. For the transverse offset trials, the target was placed at 25% of the subject's arm span in X+ direction. The obstacle was fixed at the waist level and hip-width minus 5 cm transverse to the center of the force platforms. These positions were chosen to account for subject variability in arm span as well as anthropometric measurements that could influence reach and physical limitations in the experimental setup.

Table 1. Experimental protocol conditions and the number of trials analyzed.

Task Height	Handle location	Condition	Number of trials analyzed
Overhead	Centered	Reach	5
		Push	5
		Pull	5
		Tool	5
	Transverse offset	Reach	5
		Push	5
		Pull	5
		Tool	5

Experimental trials assessed in this study were conducted with a target height of 10 cm over stature (overhead), which was also studied by Hoffman et al. [21], as it is a position where the stepping strategy is isolated since the use of other postural stability strategies is limited. At this height, subjects won't favor the use of the squatting strategy as it will not benefit the vertical reach of the target. An overhead target has been seen to create more balance perturbation when leaning in a side-by-side stance and limit the use of body mass to increase applied hand force [16,18]. Although overhead work isn't a preferred working posture, it remains present in some industrial fields [23,24] and its study is important as it still represents a high impact risk from an ergonomic point of view [25,26].

The subject started facing the target with feet side-by-side outside of the posterior end of the force platforms. A verbal indication instructed the subject that the trial had started. The subject was required to take a few steps towards the target and adopt a preferred posture while, with their dominant hand, executing and maintaining for 5 seconds the required condition. After the specified time, another verbal indication was given, instructing the subject to stop and return to the start position. Audio feedback was produced once the minimum force of 40 N was obtained, announcing to the subject that the posture had to be maintained for at least 5 seconds. A different sound was produced if the maximum force exceeded 100 N, indicating to the subject to unload. For the tool condition using a screwdriver, the minimum required torque was 3 Nm and the maximum torque was 6.5 Nm [27]. Audio feedback was also produced once the minimal torque was achieved and if the maximal torque was exceeded.

2.5. Data Modeling

The body COM was calculated using the center of mass segmental distances presented by Dempster [22]. The individual adjusted segmental weight ratios presented by Clauser, McConville, and Young [28] were used. They were adjusted because the sum of Dempster's [22] ratios equaled 97.7% of total body mass. The body COM was estimated using a 14 segment model (Head, Trunk, Upper Arms, Forearms, Hands, Thighs, Tibias, and Feet) arising from individual marker position and subject mass.

The support length is the line passing through the projected points ML and MR, which are virtual points obtained from the intersection of the longitudinal axes (straight lines connecting the Phalanx Distal II and the heel) of the feet with the balance line [4]. The balance line is a line passing through the mean center of gravity (COG) during quiet standing and its direction is found by connecting the left and right mid malleolus. The COG is the vertical projection of the COM on the ground. Figure 4 illustrates this definition for our subject.

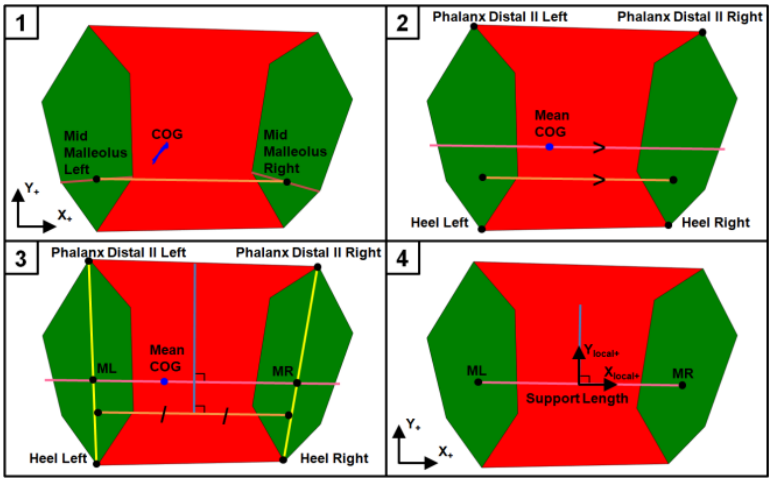

Figure 4. ML and MR points, support length, and local coordinate system definition during quiet standing.

Ground contact regions of the feet were estimated by comparing the vertical position of the feet markers against their vertical positions in the reference quiet standing trial. If a marker was 3 mm above the reference position, the part of the left or right foot was considered raised. The 3 mm threshold was set to account for possible variations (e.g., foot soft tissue deformation) [29].

3. Results

Marker position and kinetic data were low-pass filtered at specific cut-off frequencies (5-10 Hz, 4th order zero-lag Butterworth). Screwdriver weight was neglected because it was considered light enough and because pure torsion is applied directly in the center of the hand. It is considered that the tool COM nearly coincides with the hand COM which are both approximately in line with the applied moment as a diagonal volar grip is used with the screwdriver. The ZMP coordinates, defined by ZMP_X, ZMP_Y, and

ZMP_Z, were computed using Eq. (1) where X_{COG} and Y_{COG} are the COG coordinates, and f_bx, f_by, f_bz, M_bx, and M_by are the hand reaction forces and moments measured by the load cell [8]. The support surface is the ground, therefore ZMP_Z is set to 0. X, Y, and Z are the center coordinates of the capture interfaces and mg is the subject's weight.

$$\mathbf{ZMP_X} = \frac{(\mathbf{M_by} + \mathbf{f_bx} \times \mathbf{Z} - \mathbf{f_bz} \times \mathbf{X} + \mathbf{mg} \times \mathbf{X_{COG}})}{(\mathbf{mg} - \mathbf{f_bz})}$$

$$\mathbf{ZMP_Y} = \frac{(-\mathbf{M_bx} + \mathbf{f_by} \times \mathbf{Z} - \mathbf{f_bz} \times \mathbf{Y} + \mathbf{mg} \times \mathbf{Y_{COG}})}{(\mathbf{mg} - \mathbf{f_bz})}$$

$$\mathbf{ZMP_Z} = \mathbf{0} \tag{1}$$

After processing the raw data, parameters were obtained as illustrated in Figure 5. The BOS includes the left and right foot regions in contact with the ground as it is defined by the external polygonal line of the contact points between the feet with the ground. The D_2 ratio is a normalized ratio between 0.00 and 1.00 from the root foot (trailing leg), specified by the square projection of the mean 5-second static posture ZMP position (ZMP_X and ZMP_Y) on the support length. Consequently, if the D_2 ratio is superior to 1.00 the ZMP projection is situated outside of the support length.

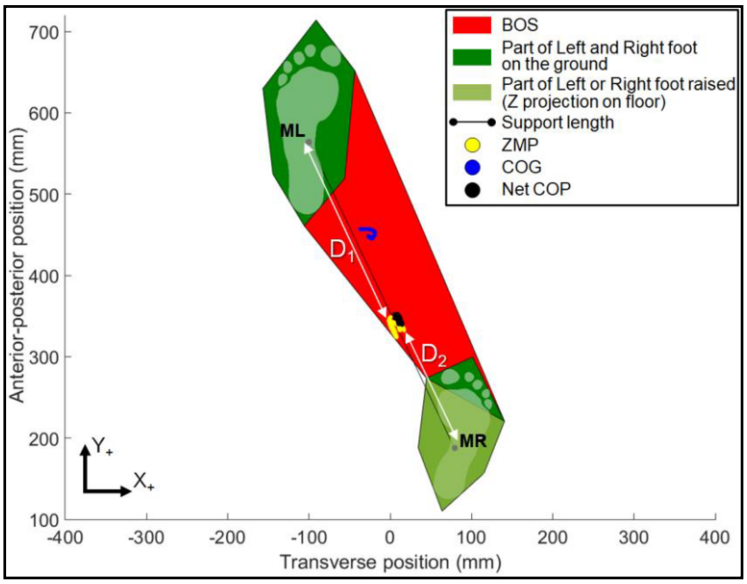

Figure 5. Processed trial parameters (XY plane projection) for a pushing centered trial.

Of the forty trials that were analyzed, one transverse offset-reach and one transverse offset-pull trials were removed from the analysis because bracing against the obstacle was seen in their video recording. Individual trial statistics of the calculated normalized D_2 ratio, the support length magnitude, and the occurrence of the dominant right foot being the lead foot are presented in Figure 6. The mean feet placement, the

mean projected ZMP, and the mean projected COG on the support length for each condition and handle location are also illustrated. As hypothesized, the ipsilateral and contralateral legs moved accordingly to ensure the ZMP displacement remained collinear to the support length in the most stable direction. Across conditions requiring load exertions, the D_2 ratio varied in the direction of the hand reaction load. The ZMP and COG nearly coincide for the reach condition as no external force is present.

		Condition			
		Reach	Push	Pull	Tool
Handle location	Centered	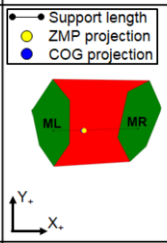	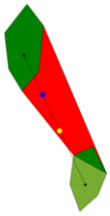	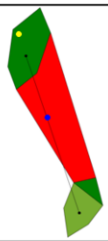	
	D_2 ratio	0.65 (0.04)	0.42 (0.04)	1.11 (0.06)	0.88 (0.05)
	Support length magnitude (mm)	256.79 (10.15)	425.47 (34.98)	470.62 (32.68)	356.30 (30.35)
	Occurrence of right foot being lead foot	1/5	0/5	0/5	0/5
	Transverse offset	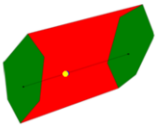	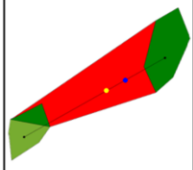	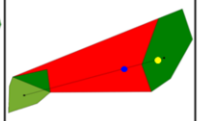	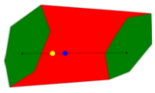
	D_2 ratio	0.40 (0.05)	0.59 (0.06)	0.95 (0.04)	0.28 (0.06)
	Support length magnitude (mm)	317.38 (45.87)	418.32 (21.64)	403.59 (8.88)	325.30 (13.89)
	Occurrence of right foot being lead foot	4/4	5/5	4/4	5/5

Figure 6. ZMP projection in yellow and COG projection blue on the support length between ML and MR. Mean normalized (and standard deviations) D_2 ratio, support length magnitude, and lead foot occurrence across trials. Reference quiet standing trial support length of 250.73 mm.

Experimental trials also indicate that the projected COG is not predominantly located at half distance (0.50) between feet. The mean COG for each trial was found in a range varying from 0.40 to 0.86 normalized to the support length from the root foot.

4. Discussion

This study presents an experimental test bench capable of measuring hand forces and moments simultaneously with feet position when completing tasks in industrial conditions. It is noted that the sample size is limited, hence the conclusions remain partial. Ideally, subjects of different ages and anthropometry should be included to have an accurate representation of what is seen in the industrial field. Also, the number

of tasks evaluated in this pilot study is limited, where variations of target position would allow the full integration of target parameters in a stepping prediction model.

Our exploratory experiments showed that task requirements vary the position of feet placement whether an obstacle is present or not. Over all trials, the subject moved the contralateral leg backward when the transverse obstacle was present, as feet were not constraint. During the centered trials, because the subject was able to center in line with the applied force direction, stability was maintained by expanding the BOS in the same direction as the applied force. These observations agree with Hoffman et al. [21], who stated that when possible subjects will prefer to position their body in line with the applied force direction to maximize applied forces by limiting lateral forces. During the transverse offset location trials, because the obstacle prevented the subject from positioning in line with the applied force, a more transverse feet placement strategy was used, possibly to develop sufficient torque at the foot base to compensate for the moment created by the hand force and the out of plane distance. This observation is consistent with Wilkinson et al. [16], where out of sagittal plane forces required the production of higher feet torque to ensure stability when standing with feet centered to the target. The mean support length appeared smaller for the transverse offset trials, which indicates hand-target reach might have been favored over stability.

These preliminary results indicate that feet placement varies according to task requirements, which will help validate the developed feet placement model for the SPE. In future works, it is intended to carry out an experimental protocol consisting of ten tasks varying in target height, reach, and obstacle. This protocol should be applied to a larger population size in order to develop a nonlinear regression model able to predict accurately the support length with respect to the ZMP position as well as its orientation about the target and the hand load requirements.

Acknowledgment

This study was part of the Smart Posture Engine project in collaboration with Dassault Systèmes Canada and the CRCHUM LIO. The project is supported by Natural Science Engineering Research Council (NSERC) Canada, and PROMPT Québec.

References

[1] Chaffin DB. Digital human modeling for workspace design. Rev Human Factors and Ergon, 2008, 4(1), 41-74.

[2] Berlin C, Adams C. Production ergonomics: designing work systems to support optimal human performance [Internet]. London (GB): Ubiquity Press, 2017. Chapter 9, Digital Human Modeling; [cited 2020 Mar 19]. 161-174. Available from: www.jstor.org/stable/j.ctv3t5qtf.13

[3] Wagner DW, Reed MP, Chaffin DB. The development of a model to predict the effects of worker and task factors on foot placements in manual material handling tasks. Ergonomics, 2010, 53(11), 1368-1384.

[4] Badler NI, Phillips CB, Webber BL. Simulating humans: computer graphics, animation, and control. New York, NY: Oxford University Press, 1993. Chapter 4, Behavioral Control, 101-136.

[5] Faraway JJ. Data-Based Motion Prediction. Warrendale, PA: SAE International, 2003, 13 p. Report No.: 2003-01-2229.

[6] Reed MP, Wagner DW. An integrated model of gait and transition stepping for simulation of industrial workcell tasks. Warrendale, PA: SAE International, 2007, 13 p. Report No.: 2007-01-2478.

[7] Marler T, Knake L, Johnson R. Optimization-based posture prediction for analysis of box lifting tasks. In: Duffy V.G., editor. Digital human modeling. Proceedings of the Third International Conference (ICDHM2011); July 2011; Orlando (US). Berlin (DE): Springer, 2011, 151-160.
[8] Howard B, Yang J, Ozsoy B. Optimal posture and supporting hand force prediction for common automotive assembly one-handed tasks. J Mechanisms Robotics, 2014, 6(2), 1-10.
[9] Vukobratović M, Borovac B. Zero-moment point-thirty five years of its life. Int J Humanoid Robot, 2004, 1(1), 157-173.
[10] Lemieux PO, Barré A, Hagemeister N, Aissaoui R. Degrees of freedom coupling adapted to the upper limb of a digital human model. IJHFMS, 2017, 5(4), 314-337.
[11] Lemieux PO, Barré A, Aissaoui R, Hagemeister N, inventor; Dassault Systemes Americas Corp., assignee. Method and system of constraint-based optimization of digital human upper limb models. United States patent 10,621,384 B2, 2020, Apr 14.
[12] Baerlocher P. Inverse kinematics techniques of the interactive posture control of articulated figures [dissertation]. Lausanne (CH): EPFL, 2001. 156 p.
[13] Zeighami A, Lemieux PO, Charland J, Hagemeister N, Aissaoui R. Stepping behavior for stability control of a digital human model. Presented at: International/American Society of Biomechanics. ISB/ASB 2019, 2019, Jul 31-Aug 4; Calgary (CA).
[14] Hoffman SG, Reed MP, Chaffin DB. A study of the difference between nominal and actual hand forces in two-handed sagittal plane whole-body exertions. Ergonomics, 2010, 54(1), 47-59.
[15] Baril-Gingras G, Lortie M. The handling of objects other than boxes: Univariate analysis of handling techniques in a large transport company. Ergonomics, 1995, 38(5), 905-925.
[16] Wilkinson AT, Pinder AD, Grieve DW. Relationships between one-handed force exertions in all directions and their associated postures. Clin Biomech, 1995, 10(1), 21-28.
[17] Warwick D, Novak G, Schultz A, Berkson M. Maximum voluntary strengths of male adults in some lifting, pushing and pulling activities. Ergonomics, 1980, 23(1), 49-54.
[18] Haslegrave CM, Tracy MF, Corlett EN. Force exertion in awkward working postures-strength capability while twisting or working overhead. Ergonomics, 1997, 40(12), 1335-1362.
[19] Granata KP, Bennett BC. Low-back biomechanics and static stability during isometric pushing. Hum Factors, 2005, 47(3), 536-549.
[20] Jones ML, Reed MP, Chaffin DB. The effect of bracing availability on one-hand isometric force exertion capability. Ergonomics, 2013, 56(4), 667-681.
[21] Hoffman SG, Reed MP, Chaffin DB. Postural behaviors during one-hand force exertions. SAE Int J Passeng Cars-Mech Syst, 2008, 1(1), 1136-1142.
[22] Dempster WT. Space requirements of the seated operator. Wright-Patterson Air Force Base, Ohio: Wright Air Development Center, 1955. 254 p. Report No.: TR-55-159.
[23] Forde MS, Buchholz B. Task content and physical ergonomic risk factors in construction ironwork. Int J Ind Ergon, 2004, 34(4), 319-333.
[24] Marchand D, Giguère D. Les risques de troubles musculo-squelettiques aux membres supérieurs dans le secteur des services à l'automobile. Montreal (CA): L'Institut de recherche Robert-Sauvé en santé et en sécurité du travail (IRSST), 2010. 103 p. Report No.: R-645.
[25] van Rijn RM, Huisstede BM, Koes BW, Burdorf A. Associations between work-related factors and specific disorders of the shoulder-a systematic review of the literature. Scand J Work Environ Health, 2010, 36(3), 189-201.
[26] van der Molen HF, Foresti C, Daams JG, Frings-Dresen MH, Kuijer PP. Work-related risk factors for specific shoulder disorders: a systematic review and meta-analysis. Occup Environ Med, 2017, 74(10), 745-755.
[27] Kong YK, Lowe BD, Lee SJ, Krieg EF. Evaluation of handle design characteristics in a maximum screwdriving torque task. Ergonomics, 2007, 50(9), 1404-1418.
[28] Clauser CE, McConville JT, Young JW. Weight, volume, and center of mass of segments of the human body. Wright-Pattersen Air Force Base, Ohio: Aerospace Medical Research Laboratory, 1969. 101 p. Report No.: TR-69-70.
[29] Mochimaru M, Kouchi M, Dohi M. Analysis of 3-D human foot forms using the free form deformation method and its application in grading shoe lasts. Ergonomics, 2000, 43(9), 1301-1313.

DHM2020
L. Hanson et al. (Eds.)
© 2020 The authors and IOS Press.
This article is published online with Open Access by IOS Press and distributed under the terms of the Creative Commons Attribution Non-Commercial License 4.0 (CC BY-NC 4.0).
doi:10.3233/ATDE200022

How to Combine 3D Textile Modeling with Latest FE Human Body Models

Hartmut KLEIN, Marcin JENEROWICZ, Niclas TRUBE, and Matthias BOLJEN [1]
Fraunhofer Institute for High-Speed Dynamics, Ernst-Mach-Institut, EMI, Germany

Abstract. Current finite element (FE) approaches to model clothing on the human body in terms of personal protective equipment (PPE) are mainly bound to the discretization of the outer element layer of the human body model (HBM) and the given posture. Costs for PPE prototyping could be lowered drastically if an efficient and posture-independent clothing modeling method would be available, so that the effectiveness of PPE in terms of injury risk mitigation could be assessed in a donned configuration. In the present study, an FE modeling method was developed to map 2D planar clothing structures on arbitrary 3D human body contours. The method was successfully applied to the GHBMC M50-PS with a modular design based ballistic vest including all components, joints and fasteners. The 3D shaped clothing models in combination with arbitrary HBM allow to analyze the structural interaction of protective clothing with the human body in unforeseen dangerous situations. The presented method facilitates the building of full featured FE models of PPE in donned configurations.

Keywords. Clothing modeling, finite element method, human body models, personal protective equipment

1. Introduction

The idea of clothing simulation generally involves two main focuses that are interrelated, i.e. clothing models for engineering applications and clothing models for visualization purposes and computer graphics industry [1]. Since fabric models for engineering applications need to follow physical guidelines, these models are often computationally quite demanding compared to the much simpler, visualization-driven models of animation industry. However, engineering models usually focus on aspects regarding comfort, reliability, performance and ensuring safety for specific operations and because of that, they need to consider the non-trivial fabric characteristics on the material level [2]. Fabrics specially designed for personal protection in automotive, civil and military applications are outstanding materials often combining low weight and high flexibility at high tensile stiffness and tenacity [3]. The benefit of these materials comes with the burden to handle the constitutive non-linearities with regard to finite deformations, anisotropy, hysteretic properties, and failure mechanisms at comparatively affordable computational costs. While there are continuum and non-continuum based constitutive models, only

[1]Corresponding Author: M. Boljen, Fraunhofer EMI, Ernst-Zermelo-Straße 4, 79104 Freiburg, Germany; E-mail: matthias.boljen@emi.fraunhofer.de.

the continuum models seem to be able to accurately handle all possible modes of deformation, including buckling and wrinkling, and are therefore preferable towards non-continuum models [4].

With FE models of anthropomorphic test devices (dummies) and virtual HBM coming into play, the interest in donning clothes to the body contours of these models has increased. If product designers and textile manufactures could assess the effectiveness of their products directly on the human body by virtual simulation, financial and temporal costs for prototyping could be drastically decreased [1]. Nevertheless, a universal modeling technique capable of fitting a particular piece of clothes to a given body shape and posture is – to the knowledge of the authors – currently not available.

Therefore, the aim of the present study is to propose a universal method for donning 2D representations of clothes to complex and arbitrary 3D body shapes as a pre-staged modeling step for FE simulations. FE models of clothes in 2D shape are considered to require much less modeling effort than for 3D models, while an arbritary element mesh size can be defined. The method shall be able to consider arbitrary HBM types with respect to body size, stature, gender and arbitrary postures to enable its use in applications other than the automotive domain, e.g. body armor, work safety, sports and healthcare applications. This study also presents a reasonable alternative to the current commonly used methodology of skin mesh based extrapolation of body contours for 3D textile modeling [5,6,7], which is not able to capture more complex textile setups on the level of individual layers and is restricted to the mesh discretization of the body skin. The modeling workflow and the implementation of the developed algorithm will be demonstrated for a complex ballistic vest consisting of soft and hard ballistic components and several joints and fasteners. The present study is limited to the modeling method and the creation of the FE input deck. Simulation and post-processing of results are subject of future work.

Literature Review

Though there is an endless list of constitutive models for describing the structural behavior of fabric materials [8,9,10], there are only a few studies dealing with FE clothing models in a donned shape directly on a dummy model or HBM (Figure 1). Ishimaru et al. developed an FE model to dress knitted fabrics to an HBM, sew the pieces together, and calculate the resulting clothing pressure and therefore introducing a method to design virtually tight-fitting clothing [11]. Long et al. analyzed draping effects of single layer clothes on the human body due to gravity [12]. Aggromito et al. investigated how distributing equipment on the body of military helicopter pilots affects the injury potential during a crash [5]. For this study the primary survival gear carrier sitting on top of the flight suit and the body armor of the upper torso had to be modeled. The discretization of the carrier was based on the given mesh of the torso. Brolin and Wass used a virtual HBM to investigate dangerous accidents in equestrian sports [6]. The protective capacity of a safety vest with respect to falls, kicks and horse trample had been assessed. Again, the mesh of the vest model had been based on the external torso geometry. Li et al. applied the modeling approach of Brolin and Wass to a study where protective vests shall reduce the injury risk of aged people when falling down accidentally [7]. The model was based on CT scanning data of a 65-year-old female. Again the bulk mesh had been constructed by offsetting the nodes of the skin. Grassi et al. introduced the concept of a belted safety jacket for powered-two wheelers, and by design of experiment, they verified the effec-

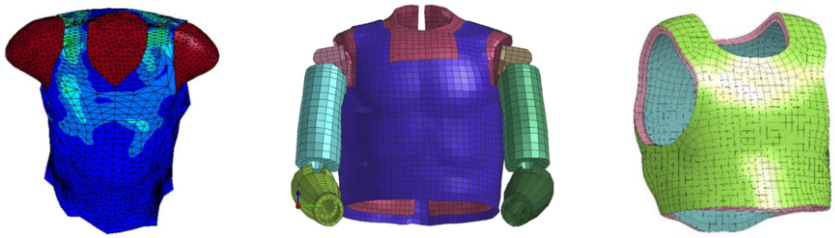

(a) Single layer shirt [12] **(b)** Survival gear carrier [5] **(c)** Equestrian vest [6]

Figure 1. Examples on textile simulation with HBM and dummy models from literature: (a) Shirt draping study; (b) primary survival gear carrier; (c) equestrian protective vest.

tiveness of such a jacket in collisions with other vehicles and the potential to reduce the injury risk of the rider [13].

2. Methods

Preparing an HBM simulation for an injury risk analysis usually requires to include the HBM from-the-shelf into the main input deck, add a proper position and orientation and include all mandatory constraints, e.g. contact definitions. For occupant scenarios, a pre-loading phase will allow the occupant model to settle into the seat under gravity, and seat belts to tighten [5,14]. When it comes to other domains of application and arbitrary body postures, the user relies on the pre-processor's capability of altering the position of upper and lower extremities of the HBM. Considering the influence of PPE, one needs to include additional modeling steps to the conventional workflow.

Basic principle. The authors assume that it is feasible to build an FE model of the protective equipment in its 2D tailored or undonned shape and propose the workflow illustrated in Figure 2. The body hull of the HBM in the posture of interest has to be extracted from the FE model and a simplified target geometry has to be defined. The latter shall be so small in scale that it fits into the interior space of the modeled protective equipment. No information about the FE nodes and the element connectivity of the original HBM mesh shall be lost during this transformation. If successful, contact definitions can be installed between the miniaturized HBM skin and the interior surface of the protective equipment. A kinematic boundary constraint shall shift back each node to its original position on the body hull. Hence, the protective equipment will be transformed to the individual body contour of the HBM of which the skin has been extracted from. This method has the benefit that the clothes will be perfectly shaped according to the contour of the applied HBM. A drawback is that compression effects that might be exerted by tight clothes on the human body currently cannot be taken into account.

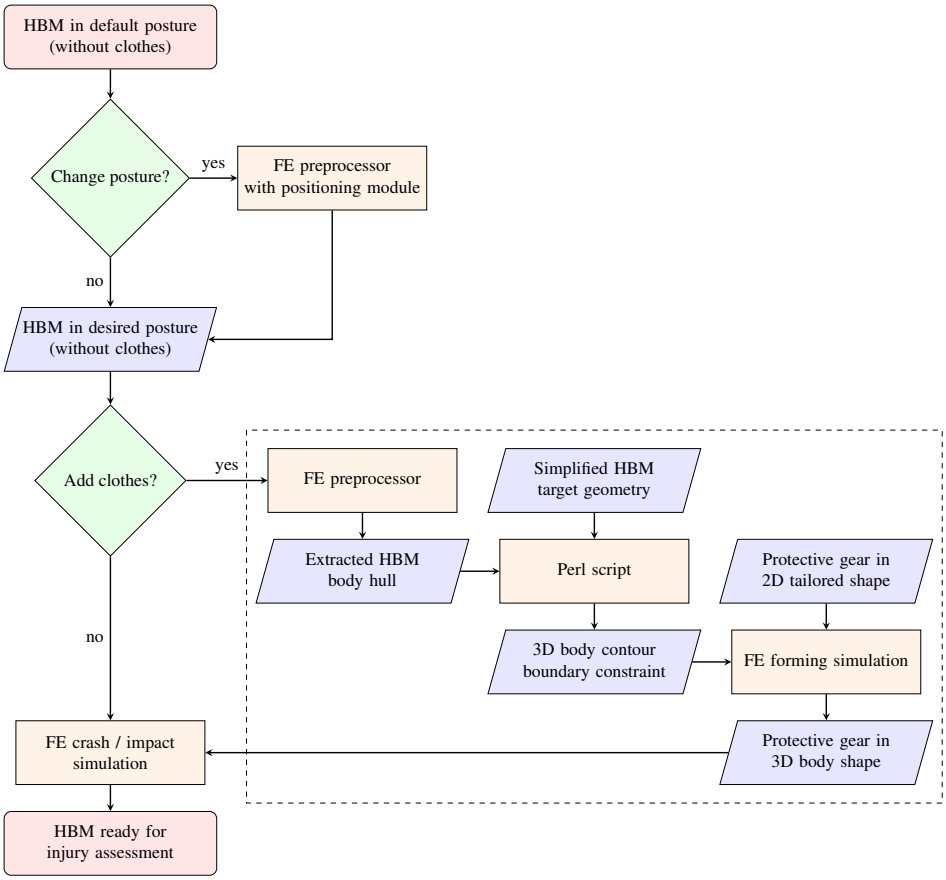

Figure 2. Workflows for preparing human body models for FE simulation and injury risk assessment with and without clothes. The integration of clothes in a donned shape with regard to HBM requires additional modeling steps (denoted by the dashed box).

2.1. Algorithm

For the scope of this work, the authors implemented a Perl script[2]. to automatically map the FE mesh of a body hull geometry on a simplified target geometry. The script has been designed for input decks of the FE code LS-DYNA and makes use of the specific command `*BOUNDARY_PRESCRIBED_FINAL_GEOMETRY` [15] that implements a linear transformation of nodes from one configuration to another.

Phase 1 – Connectivity

When the surface mesh of the body hull is extracted, it has to be associated to a simplified and scalable target geometry that is defined by the user. The authors used a linearized mesh of 21 target nodes and 20 target elements for the current study. The connectivity of these elements is shown in Figure 3a. The coordinates of the nodes (Figure 3b) have

[2] https://gitlab.cc-asp.fraunhofer.de/human-body-dynamics/perl-dynaskin

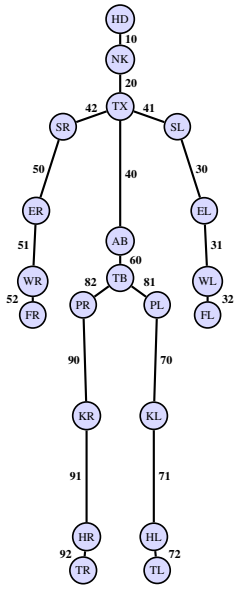

(a) Target mesh geometry.

Node	Joint / End
HD	Head
NK	Neck
TX	Thorax
SL	Shoulder (L)
SR	Shoulder (R)
EL	Elbow (L)
ER	Elbow (R)
WL	Wrist (L)
WR	Wrist (R)
FL	Fingers (L)
FR	Fingers (R)
AB	Abdomen
TB	Tailbone
PL	Pelvis (L)
PR	Pelvis (R)
KL	Knee (L)
KR	Knee (R)
HL	Heel (L)
HR	Heel (R)
TL	Toes (L)
TR	Toes (R)

(b) Target nodes.

Elm	Body part
10	Head
20	Neck
30	Arm (L)
31	Lower Arm (L)
32	Hand (L)
40	Thorax
41	Shoulder (L)
42	Shoulder (R)
50	Arm (R)
51	Lower Arm (R)
52	Hand (R)
60	Abdomen
70	Leg (L)
71	Lower Leg (L)
72	Foot (L)
81	Pelvis (L)
82	Pelvis (R)
90	Leg (R)
91	Lower Leg (R)
92	Foot (R)

(c) Target elements.

Figure 3. Discretization serving as simplified HBM target geometry. The chosen level of the discretization is arbitrary, i.e. a finer level of discretization could have been used if needed as long as the target geometry is placed in the interior of the HBM body hull.

to be aligned with the centers of the corresponding body parts in the posture of interest. The script will then loop over each element of the source mesh and look for the closest element of the target mesh (Figure 3c). This search is implemented by a linear nearest neighbor search [16] based on the closest distance between both elements. The algorithm is extended by a conical search domain aligned in the direction of the element normal. This constraint will filter out target elements which otherwise would have been wrongly associated as shown in Figure 4a. Body regions that require this constraint have been identified near the fingers and toes and along the whole upper extremities if positioned very close or in contact to the torso.

Phase 2 – Fragmentation

The nearest neighbor search will yield results where adjacent elements of the source mesh are connected to different target elements. The nodes connecting those source elements will be projected to either the one or the other target element, which in return will produce highly distorted elements unsuitable for FE simulation. In order to avoid such distortions, the algorithm applies a nodal splitting technique that obviously results in a fragmentation of the source mesh.

Phase 3 – Morphing

The final step is to shift the nodes of the source elements to the projected locations on the target elements. The target elements are assumed to be of cylindrical shape with a non-

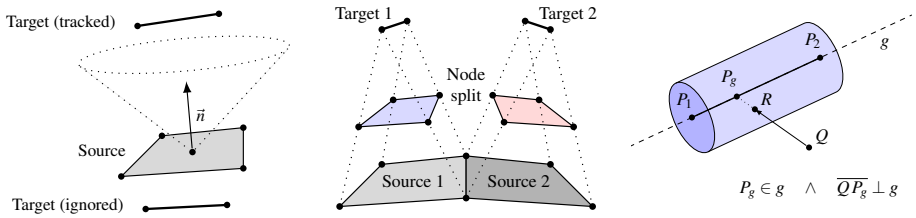

(a) Connectivity **(b)** Fragmentation **(c)** Nodal projection

Figure 4. Algorithm to implement the 3D body contour boundary constraint: (a) Nearest neighbor search to find element connectivity; (b) source mesh fragmentation where required; (c) nodal projection on target element surface.

zero radius and hemispherical ends (Figure 4b). Nodes can either be projected directly on the element's surface or scaled by a constant ratio with respect to the original distance between source and target node. Each source node will be mapped via an orthogonal projection on the closest point on the center line of the target element (Figure 4c). In order to disable the evaluation of constitutive equations, all source elements are associated with material card `*MAT_NULL`.

2.2. Examples

The algorithm has been tested successfully for five different human body models of three different HBM suppliers, i.e. the GHBMC pedestrian models for adult 5th percentile females and adult 50th and 95th percentile males [17], the THUMS occupant model for adult 50th percentile males [18], and the ViVA OpenHBM for adult 50th percentile females [19].

In Figure 5 and Figure 6, the results of the mapping algorithm have been illustrated for the body contours of the GHBMC model variants F05-PS and M50-PS. The latter (1.75 m height, 77 m weight, 593 components, 840,000 elements) has been used for the final part of this study, i.e. the donning of a ballistic vest to an arbitrary body posture.

Figure 7 and Figure 8 illustrate the extrusions of the body contours of the occupant model of the THUMS M50 and the ViVA OpenHBM model. The implemented method thus works successfully independently of the model type and the body posture.

3. Results

3.1. Model Setup

A body armor protective vest manufactured by MVS (Figure 9a) was used as reference for the model development [20]. The vest consists of a modular structure with long range rifle protection in the front, back and abdominal area and all-round protection in the flank area. The main two components of the protective vest are the front and the back structures which are connected with Velcro fasteners on the shoulders and in addition, on the sides of the torso to adapt the vest to the body. The protective vest is supplemented by a removable collar and groin protection. These parts are not considered in the model. The

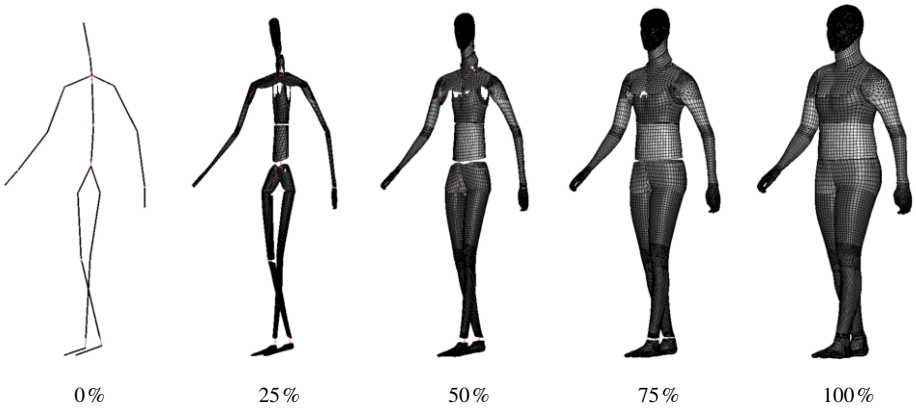

Figure 5. GHBMC adult female 5th percentile as pedestrian in walking posture (F05-PS).

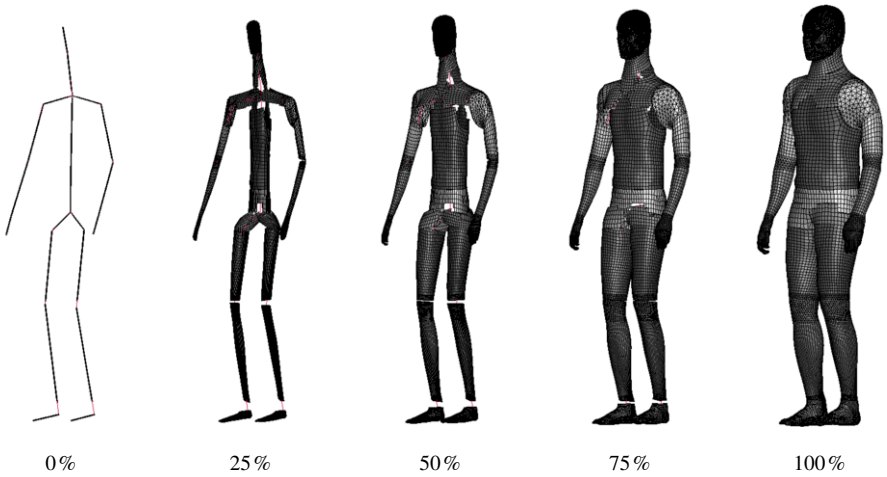

Figure 6. GHBMC adult male 50th percentile as pedestrian in standing posture (M50-PS).

Figure 7. THUMS adult male 50th percentile as occupant (AM50-Occ).

Figure 8. ViVA OpenHBM for adult female 50th percentile as occupant.

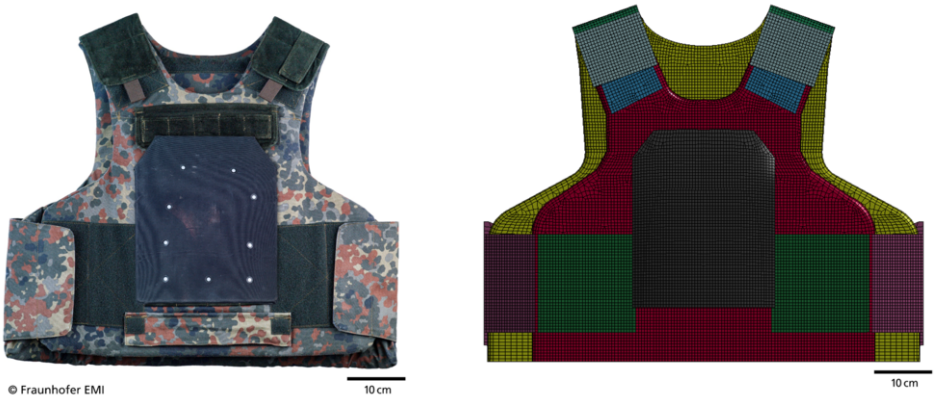

(a) Vest used as reference

(b) Developed vest model

Figure 9. Front view of the body armor protective vest. Hard armor plate removed and placed on the carrier component. (a) Reference vest; (b) FE model.

front and back components have the same structure and differ only in their dimensions. They consist of an outer shell (the carrier), the trauma reduction layer (foam shock absorbent), the soft ballistic armor (three aramid fiber packages, total 40 layers), and a hard armor (boron carbide or silicon carbide with an additional ultra-high molecular weight polyethylene composite plate).

All components of the vest were modeled and meshed using the pre-processor Femap [21]. The textile components were created as planar 2D surfaces with a defined thickness. The front and rear carrier contain a soft ballistic component and a shock absorber component and an additional pocket for the placement of the hard armor. This modular structure allows the exchange of the individual components in order to carry out parameter variation studies of the materials and geometry. The implemented material models for the expansion process are simplified and after the expansion subsequently adapted. The material stiffness and contact definitions were iteratively adjusted to avoid fabric folds and strong element distortions.

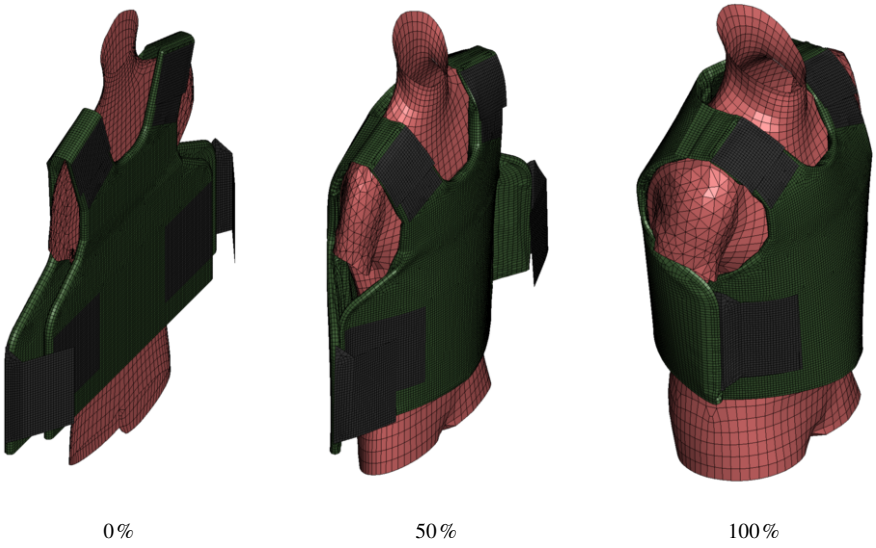

Figure 10. Expansion of the FE vest model from 2D planar to 3D state with the body contour of the GHBMC M50-PS.

3.2. Model Expansion

In the initial state of the FE forming simulation (Figure 9b), the main components are placed over each other with a small gap in between. The flattened skin shell of the GHBMC M50-PS is positioned in the gap (Figure 10). The hard armor plates are placed over the location of the designated pockets in the carrier components. As these are made of high-strength material and are not being bent during the simulation, the plates diffuse into the pockets during the expansion. The Velcro fasteners in the shoulder area lie on top of each other and are closed up via contact conditions. The Velcro fasteners in the flank area are half-open and progressively fastened during the FE forming simulation via load curves and contact conditions. Predefined load vectors ensure that the lateral Velcro fasteners close during the fitting simulation. All formable structures are aligned to the body surface (Figure 11a). Subsequently, a new initial state is defined in LS-DYNA, which is free of initial stresses, since the material models are adjusted. The full GHBMC M50-PS model is placed in the expanded protective vest (Figure 11b) and is ready for further analysis.

4. Discussion

In this study, a nodal mapping method has been applied to the body contour of a full HBM in order to transform the FE clothing model of a ballistic vest from a 2D planar shape to a 3D donned configuration. The process is implemented using a forming simulation to determine the final nodal positions of the PPE model. The stamping tool, which is usually rigid in forming simulations is replaced by a dynamic geometric boundary constraint that forces the flexible textile from the inside to the final 3D body shape.

(a) Expanded vest including inner structure

(b) GHBMC M50-PS in expanded vest

Figure 11. FE protective vest model in donned configuration: (a) Detailed view of the expanded ballistic vest including inner structure; (b) full body HBM combined with protective vest.

Using the proposed method, the authors showed that complex FE models of 3D body shaped clothes based on the much simpler 2D representation can be obtained in an efficient way (Figure 9 and Figure 10). Textile models in 2D shape are considered to require much less modeling effort than 3D models while an arbitrary element mesh size can be defined. Further, it could be shown that the method can be applied to any HBM type and many body postures (Figure 5, Figure 6 Figure 7). This allows not only to apply this method to any other protective clothing besides ballistic vests, such as PPE for motorcyclists, vulnerable road users on micromobility-vehicles, American football players or alpine skiers, it also presents a reasonable alternative to the current commonly used methodology of skin mesh based extrapolation of body contours for 3D textile modeling [5,6,7].

4.1. Limitations

While the method has been tested successfully for HBM of several distributors and various body postures, the method is still limited to postures that are close to a neutral position with adjacent upper and lower extremities. This restriction still poses difficulties to the modeling of textile preforms. In future studies, the method shall be improved in such a way that textile preforms can be modeled in perfectly flat 2D shape, allowing a miniaturized HBM contour in a neutral posture being inserted and expanded to an arbitrary body posture that is required for the load case simulation of interest. The validation of the implemented FE models and their usability will be realised in future works.

4.2. Outlook

In forthcoming studies, the ballistic vest FE model will be adapted to the GHMBC variants F05-PS and M95-PS to provide comparability analysis. Furthermore, the imple-

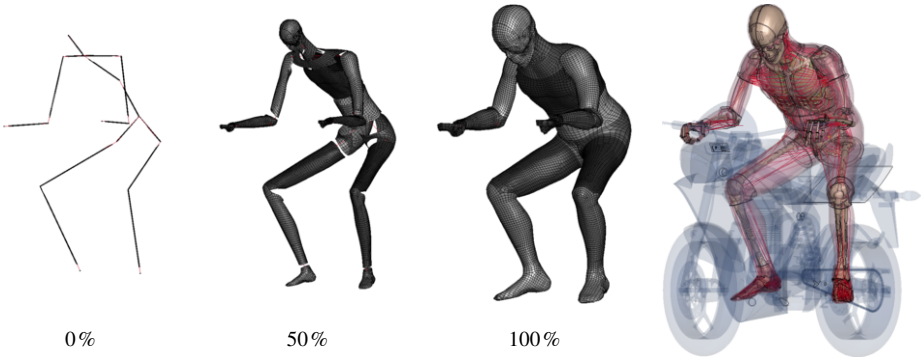

Figure 12. THUMS AM50 as a motorcycle rider to assess the efficiency of PPE (under development).

mentation of advanced material models and an investigation of various armor piercing projectiles will be carried out.

A positioning and forming simulation of a THUMS AM50 to a motorcyclist model is currently under investigation (Figure 12). In addition, a motorcycle jacket FE model is under development that will demonstrate the effectiveness and the protective capabilities of PPE in traffic accident scenarios.

References

[1] Long J, Burns K, Yang JJ. Cloth Modeling and Simulation: A Literature Survey. In: Duffy VG, editor. Digital Human Modeling. Berlin, Heidelberg: Springer Berlin Heidelberg; 2011. p. 312–320.

[2] Kawabata S, Masako N, Kawai H. The Finite-deformation Theory of Plain-weave Fabrics – Parts 1, 2 and 3. Journal of the Textile Institute. 1973;64:21–85.

[3] Boljen M, Hiermaier S. Continuum constitutive modeling of woven fabrics. European Physical Journal Special Topics. 2012;206:149–161.

[4] Choi KJ, Ko HS. Research problems in clothing simulation. Computer-Aided Design. 2005;37(6):585–592. CAD Methods in Garment Design.

[5] Aggromito D, Thomson R, Wang J, Chhor A, Chen B, Yan W. Effect of body-borne equipment on injury of military pilots and aircrew during a simulated helicopter crash. International Journal of Industrial Ergonomics. 2015;50:130–142.

[6] Brolin K, Wass J. Explicit Finite Element Methods for Equestrian Applications. Procedia Engineering. 2016;147:275–280.

[7] Li J, Chen D, Tang X, Li H. On the protective capacity of a safety vest for the thoracic injury caused by falling down. Biomedical Engineering Online. 2019;18(1):40.

[8] Boisse P, Borr M, Buet K, Cherouat A. Finite Element Simulations of Textile Composite forming Including the Biaxial Fabric Behaviour. Composites Part B: Engineering. 1997;28(4):453–464.

[9] Kato S, Yoshino T, Minami H. Formulation of Constitutive Equations for Fabric Membranes Based On the Concept of Fabric Lattice Model. Engineering Structures. 1999;21(8):691–708.

[10] King MJ, Jearanaisilawong P, Socrate S. A Continuum Constitutive Model for the Mechanical Behaviour of Woven Fabrics. International Journal of Solids and Structures. 2005;42(13):3867–3896.

[11] Ishimaru S, Isogai Y, Matsui M, Furuichi K, Nonomura C, Yokoyama A. Prediction method for clothing pressure distribution by the numerical approach: attention to deformation by the extension of knitted fabric. Textile Research Journal. 2011;81(18):1851–1870.

[12] Long J. Simulation-Based Assessment for Construction Helmets and Clothing [mathesis]. Texas Tech University; 2012.

[13] Grassi A, Barbani D, Baldanzini N, Barbieri R, Pierini M. Belted Safety Jacket: a new concept in Powered Two-Wheeler passive safety. Procedia Structural Integrity. 2018;8:573–593.
[14] Schap JM, Koya B, Gayzik FS. Objective evaluation of whole body kinematics in a simulated, restrained frontal impact. Annals of Biomedical Engineering. 2019;47(2):512–523.
[15] DYNAmore. LS-DYNA Manual R11 Vol. 1, 2, 3; 2020. Livermore Software Technology Corporation (LSTC).
[16] Weber R, Schek HJ, Blott S. A Quantitative Analysis and Performance Study for Similarity-Search Methods in High-Dimensional Spaces. In: Gupta A, Shmueli O, Widom J, editors. Proceedings of 24rd International Conference on Very Large Data Bases. New York: Morgan Kaufmann; 1998. p. 194–205.
[17] Global Human Body Models Consortium. GHBMC; 2020. Elemance, LLC.
[18] Toyota Motor Corporation and Toyota Central R&D Labs. Total Human Model for Safety - THUMS; 2020. ANSYS / LST.
[19] Brolin K, Svensson M, Putra IPA, Iraeus J. Open HBM ViVA: Virtual Vehicle-Safety Assessment: Open Source Human Body Models addressing gender diversity; 2016. Chalmers.
[20] Mehler Vario System GmbH. Ballistische Schutzprodukte; 2020.
[21] Siemens PLM Software. FEMAP V11.1.0; 2020. Siemens Digital Industries Software.

DHM2020
L. Hanson et al. (Eds.)
© 2020 The authors and IOS Press.
This article is published online with Open Access by IOS Press and distributed under the terms of the Creative Commons Attribution Non-Commercial License 4.0 (CC BY-NC 4.0).
doi:10.3233/ATDE200023

Modelling Take-Over Hand Trajectories Using Linear Mixed Effects Models

Martin FLEISCHER[1], Arno HETZENECKER and Klaus BENGLER
Technical University of Munich, Chair of Ergonomics, Germany

Abstract. Automated driving is currently one of the most important research areas in the automotive industry. If automation reaches its system limits, the driver is obliged to take over the driving of the vehicle again. In that scenario, the driver first has to put his hands on the steering wheel again if he was occupied with a non-driving task. This work shows a method to precisely model these hand movements from a specific task back to the steering wheel. These movements are analyzed depending on the individual parameters of each person, such as age, gender, body height. For this purpose, a test stand was developed and assembled, on which a study with 52 participants was carried out. It can be observed that the hand trajectories are lying in a plane in the three-dimensional space, with orthogonal deviation from the plane smaller than 10 mm. This finding allows to model the trajectory as a combination of a polynomial and the orientation of the individual plane. The results show that the trajectory of the hand movement only averaged about 2 mm from their main movement plane. The trajectories from this study were fitted using polynomials. Trajectories were parametrized and fitted to a linear mixed effects model using the "lmer" [1] and "afex" [2] R-packages.

Keywords. Linear Mixed Effects Models, Take-Over, Automated Driving, Hand Trajectories, Digital Human Modeling, Grasping Movement

1. Introduction

With increasing automation of cars, new non-driving-related tasks will be feasible scenarios for future interior design and thus for digital human models (DHMs) [3]. One of the critical scenarios in automation level 3 according to SAE J3016 [4] is the take-over, when the passenger needs to reassume control over the vehicle. Research about take-over-performance indicates, that personal as well as environmental circumstances influence the outcome of such situations [5]. It is yet unknown in detail, how a person will move from the non-driving-related task to the steering wheel. Some insight is given by [6].

Motion simulation is often carried out through kinematic models. While those models can give detailed information about forces and momentums in- and outside the human body, they may require motion capturing data for inverse kinematics, highly trained specialists, long setup or calculation time. Not all of those might be available in every company using DHMs for their product design processes. Thus, for the described study, an empirical-based approach is used. Similar approaches were found for general hand trajectories and ingress into and egress out of cars [7-9]. The idea is to model the hand trajectory through environmental and demographic predictors, as well as general

[1] Corresponding Author, Email: martin.fleischer@tum.de.

data that is easy assessable by the DHM-user. The hand of the DHM is then dragged along this path, while the body follows through a closed inverse kinematic chain. As a result, the user of the modeling tool gets a geometric shape visualizing the space needed for unhindered movement.

The elemental premise of the three models found in literature [7-9] and the model described in this paper is that the leading body part geometrically moves on a two-dimensional plane. To apply the trajectory to the real-world scenario, the orientation of the plane where the movement takes place in three-dimensional space is needed for the model. In practice this leads to two major models – the trajectory model and the plane model. The presented study differs in the use of quartic functions modeled with mixed linear effects models from the other mentioned studies. The assumption derived from the literature is that individualistic factors of the moving person as well as the environment play a major role for the form of the trajectory.

2. Methodology

A test stand was set up to examine the hand movement from a varying resting position to a target hold resembling the steering wheel. Four grasping elements [9] (Figure 1) were designed to achieve a similarity in the start and end position of movement:

1. 1-finger-contact-handle
2. 3-finger-contact-handle
3. Spherical handle (diameter 50 mm)
4. Cylindrical handle (diameter 30 mm)

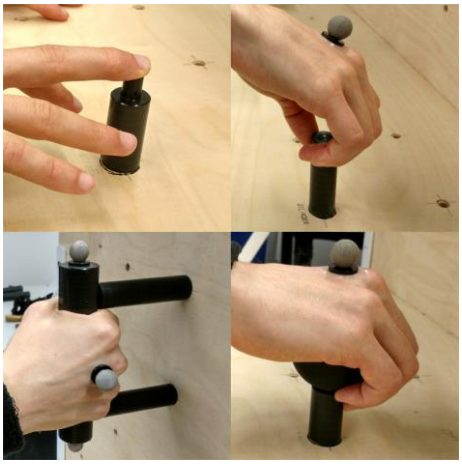

Figure 1. From top left to bottom right: 1-finger-contact-handle, 3-finger-contact-handle, cylindrical handle and spherical handle.

The target handle was a vertically oriented cylindrical handle representing the steering wheel grabbed at the 3 o'clock position. In total eight different scenarios were tested: The four handles were mounted beneath the target handle as well as translated to the right side. Figure 2 shows the setup with four of the scenarios. The test stand was reconfigured between the trails. The participants were instructed to place the right hand on the handle on the horizontal plane and then grasp for the handle on the vertical plane. The stand was designed in a way that every person invited could do the task sitting

without moving their shoulder. The setup represents a highly abstracted environment that is comparable to a take-over scenario. That way reliable data with consistent start and end points is guaranteed.

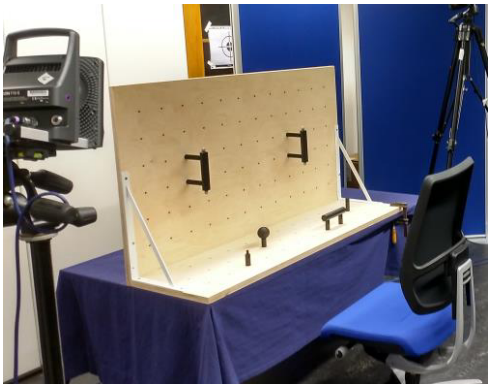

Figure 2. Example scenario setup of the test stand with four of the eight possible scenarios from left to right: 1-finger-contact-handle straight beneath the target, spherical handle to the right side of the target, cylindrical handle straight beneath the target and 3-finger-contact-handle to the right side of the target.

A total of 52 participants were invited to the experiment. They were instructed to grasp from the start handle close to them and then move to the target handle with their right hand. Before the movements were recorded via motion capturing (VICON Nexus using 4 MX T10S and four MX10 cameras), the subjects were instructed to do a few test runs to reduce learning effects. Afterwards, each of the eight scenarios was completed three time by every participant. A total of 1152 grasping movements were recorded that way.

Anthropometric and demographic data for every participant was collected and is presented in Table 1:

1. Gender
2. Age
3. Dominant hand
4. Body height

Table 1. Participant data.

	All	Male	Female
N	48	30	18
Average Age (SD) in years	23.97 (3.28)	24.02 (3.30)	23.75 (3.15)
Percentage of dominant left hand	12.5%	10%	16.67%
Average body height (SD) in mm	1743 (77)	1747 (74)	1736 (72)

Recorded trajectories were transformed from three dimensional discrete points into quartic functions through the following steps:

First, the plane closest to all points was determined for each individual trajectory. Then, every point was projected onto the plane and the distance from point to plane was calculated for later quality assessment. No distance above 10 mm was found, and the average distance was 2 mm. A quartic polynomial (see (1)) was fitted on the projected points. This polynomial degree showed the best performance between under and over

fitting the recorded data. C_0 was then set to 0 making every trajectory start at the same point.

$$f(x) = C_4 x^4 + C_3 x^3 + C_2 x^2 + C_1 x + C_0 \quad (1)$$

A mixed linear effects model for each of the four remaining C_x was fitted with the "lme4" [1] in R with the syntax seen in (2). Environmental and demographic factors were modelled as fixed effects, while the individual participant was modeled as a random intercept effect. Every fitted polynomial with $R^2 > .95$ was discarded reducing the amount to 624 of the initial 1152 trajectories. A model with participant as a random slope would not converge. Far more than three data points from every participant and scenario would have been necessary.

$$C_x \sim Gender + Age + Dominant\ Hand + Body\ Height + Handle\ Position + Handle\ Type + (1|Participant) \quad (2)$$

The four fitted C_x -models were analyzed further using "afex" [2] to find the relevant predictors. The afex-package performs type 3 test, KR-method ANOVA between the reduced model compared to the full model regarding the fixed effects. For further reference, see [10].

3. Results

For all four models the plots of the scaled residuals (Figure 3) show a linear, homoscedastic behavior. The Q-Q plots (Figure 4) show a tendency for heavy tailed distributions with growing index number of C_x.

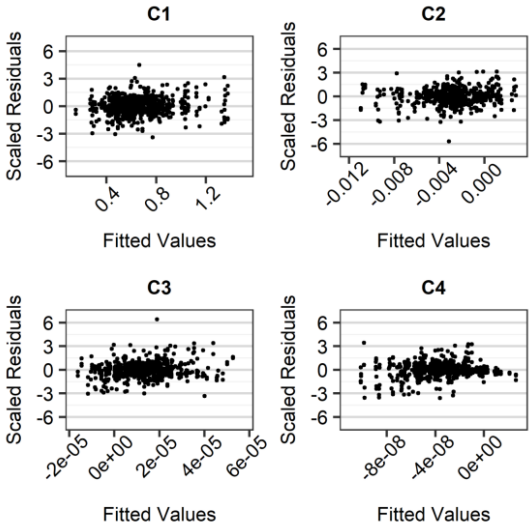

Figure 3. Scaled residuals of the models of the constants C_x

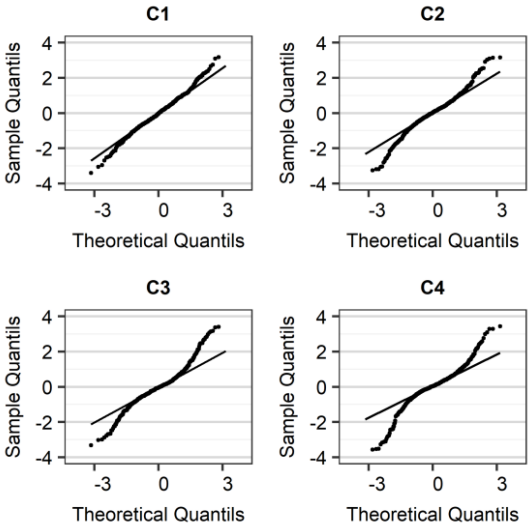

Figure 4. Q-Q plots of the models of the constants C_x

For detailed results please contact the corresponding author as only the core of the data can be displayed here, which is the model comparison of the afex-package, the marginal and the conditional R^2 of the model.

3.1. Factor C_1

As seen in Table 2 only the factor handle type becomes significant, while every other fixed effect shows no significant influence. It is to be noted, that body height is closest to becoming significant. In Table 3 the big difference between the marginal and conditional R^2 can be seen.

Table 2. ANOVA table for factor C_1

Effect	df	F	p-value
Gender	1, 42.07	0.18	.672
Age	1, 41.65	0.11	.745
Dominant Hand	1, 38.82	0.26	.613
Body Height	1, 41.48	1.96	.169
Handle Position	1, 583.47	1.05	.307
Handle Type	3, 583,75	6.58	<.001

Table 3. Marginal and conditional R^2-values for C_1

R^2_m	R^2_c
.044	0.333

3.2. Factor C_2

Table 4 shows similar results for C_2 compared to C_1: The handle type is significant and body height with the second lowest p-value. As for the R^2-values a big discrepancy is observed (Table 5).

Table 4. ANOVA table for factor C_2

Effect	df	F	p-value
Gender	1, 41.71	0.12	0.729
Age	1, 41.12	0.03	0.854
Dominant Hand	1, 37.49	0.26	0.613
Body Height	1, 40.77	2.82	0.101
Handle Position	1, 587.73	0.17	0.679
Handle Type	3, 587.94	3.32	0.02

Table 5. Marginal and conditional R^2-values for C_2

R^2_m	R^2_c
.035	0.232

3.3. Factor C_3

For C_3 none of the factors becomes significant, but it is observable that handle type and position are the most relevant. Body height remains on the verge to significance (Table 6). For the factor the difference between R^2_m and R^2_c is the smallest (Table 7).

Table 6. ANOVA table for factor C_3

Effect	df	F	p-value
Gender	1, 41.53	0.2	0.657
Age	1, 40.85	0.01	0.933
Dominant Hand	1, 36.92	0.09	0.765
Body Height	1, 40.40	2.69	0.109
Handle Position	1, 589.70	3.50	0.062
Handle Type	3, 589.83	2.49	0.059

Table 7. Marginal and conditional R^2-values for C_3

R^2_m	R^2_c
.033	0.198

3.4. Factor C_4

For C_4 the handle type and position have the most influence according to the p-values, while body height has the lowest p-value of the non-significant fixed effects (Table 8). The R^2-values show the same trend as for the other factors, as seen in Table 9.

Table 8. ANOVA table for factor C_4

Effect	df	F	p-value
Gender	1, 41.37	0.43	0.515
Age	1, 40.59	0.11	0.742
Dominant Hand	1, 36.45	0.00	0.945
Body Height	1, 40.06	2.59	0.115
Handle Position	1, 591.41	7.20	0.007
Handle Type	3, 591.46	9.19	<.001

Table 9. Marginal and conditional R^2-values for C_4

R^2_m	R^2_c
.063	0.200

4. Conclusion and Discussion

Three major findings can be extracted from the data:

1. Environmental factors (handle type and handle position) play the major role for the grasping trajectory.
2. Body height plays a role in the modelling of hand trajectories. Gender, age, and dominant hand only show negligible influence on the trajectory.
3. Other individual human factors not evaluated in this study seem to heavily influence the hand movement.

For 1.:

Looking at the p-values from the model comparison (Table 2,4,6,8) the handle type becomes significant for C_1, C_2, and C_4 while the handle position becomes relevant for C_3 and C_4. Those variables describe the whole scenario, thus making the hand-arm orientation and configuration a dominant factor in the assessment of human grasping movement. This might lead to the conclusion that the participant him/herself is not relevant. This assumption is wrong as explained in 3.

For 2.:

Opposing to the other three individual factors, body height has an effect in this context despite the non-significant results in this experiment. Several things need to be considered for this statement. Every factor will become significant if the data collective is big enough and mixed linear effects models profit from big collectives. It is not the single most goal to find significances, when using mixed linear effects models. They just pose an indicator to what is more important, and this model has quite many factors for the sample size regarding statistical power [11]. A bigger sample size will reduce the Type II error without increasing the Type I error badly. This is important for the body height as the near significant value might be a consequence of the underlying experiment. The young age, the rather homogeneous body height and low sample size may interfere with the results in an unknown way. The fitting of the polynomials to the data was carried out in an automated way and not manually supervised. This results in high reject numbers in the data through the $R^2 > .95$ filter.

For 3.:

As stated above the environment is important for the model. Still, the human itself plays a major role in the process, but not the aspects gender, age or dominant hand. This can be extracted from the R^2-values. For social science standards, the R^2_m can be interpreted as small, but R^2_c reaches into moderate effect sizes [12]. The addition of the random slope for the individual to the model raises the quality greatly. Thus, the individual is important – just not the aspects gender, age, or dominant hand.

As by the points discussed above, the assumption that personal factors play the same role as the environmental ones can be declined conditionally, as in the data gathered here shows no such trend.

5. Future work

Mixed linear effects models are an appealing method for DHM, because of their ability to handle asymmetric data. This opens the possibility to have missing data and still generate good results. The process used in this experiment will be improved to gain a higher yield in future experiments.

Highly relevant factors were found in the environmental factors. External circumstances like the movement speed or obstacles need to be researched. It is also important to tackle different individual factors in future experiments to raise the R^2_m.

Acknowledgement

This study was conducted in the context of the project INSAA funded by the Bundesministerium für Bildung und Forschung of Federal Republic of Germany. The project aims to develop the DHM RAMSIS to handle non-driving related tasks and take-over scenarios.

References

[1] Bates D, Maechler M, Bolker B, Walker Steven, Christensen RHB, Singmann H, et al. lme4, 2020.
[2] Singman H, Bolker B, Westfall J, Aust F, Ben-Shachar M, Højsgaard S, et al. afex, 2020.
[3] Yang Y, Fleischer M, Bengler K. Chicken or Egg Problem? New Challenges and Proposals of Digital Human Modeling and Interior Development of Automated Vehicles. In: Di Nicolantonio M, Rossi E, Alexander T, editors. Advances in Additive Manufacturing, Modeling Systems and 3D Prototyping: Proceedings of the AHFE 2019 International Conference on Additive Manufacturing, Modeling Systems and 3D Prototyping, July 24-28, 2019, Washington D.C., USA. 1st ed. Cham: Springer International Publishing; Imprint: Springer, 2020, 453–463. doi:10.1007/978-3-030-20216-3_42.
[4] On-Road Automated Driving (ORAD) committee. Taxonomy and Definitions for Terms Related to Driving Automation Systems for On-Road Motor Vehicles, J3016_201806. Warrendale, PA, US: SAE International. doi:10.4271/J3016_201806.
[5] Gold C. Modeling of Take-Over Performance in Highly Automated Vehicle Guidance [Dissertation]. München: Technische Universität München, 2016.
[6] Kerschbaum P, Omozik K, Wagner P, Levin S, Hermsdörfer J, Bengler K. How does a symmetrical steering wheel transformation influence the take-over process ? In: de Waard D, Toffetti A, Wiczorek R, Sonderegger A, Röttger S, Bouchner P, … Brookhuis K, editors. Proceedings of the Human Factors and Ergonomics Society Europe Chapter 2016 Annual Conference, 2017.

[7] Faraway JJ, Choe SB. Modelling orientation trajectories. Statistical Modelling, 2009, 9, 51–68. doi:10.1177/1471082X0800900104.
[8] Cherednichenko A. Funktionales Modell der Einstiegsbewegung in einen PKW [Dissertation]. München: Technische Universität München, 2007.
[9] Arlt F. Untersuchung zielgerichteter Bewegungen zur Simulation mit einem CAD-Menschmodell: Herbert Utz Verlag, 1999.
[10] Singmann H, Kellen D. An Introduction to Mixed Models for Experimental Psychology. In: Spieler D, Schumacher E, editors. New Methods in Cognitive Psychology: Routledge, 2019, 4–31. doi:10.4324/9780429318405-2.
[11] Field A, Miles J, Field Z. Discovering statistics using R. Reprint. Los Angeles, Calif.: Sage, 2013.
[12] Ferguson CJ. An effect size primer: A guide for clinicians and researchers. Professional Psychology: Research and Practice, 2009, 40, 532–538. doi:10.1037/a0015808.

DHM2020
L. Hanson et al. (Eds.)

© 2020 The authors and IOS Press.
This article is published online with Open Access by IOS Press and distributed under the terms of the Creative Commons Attribution Non-Commercial License 4.0 (CC BY-NC 4.0).
doi:10.3233/ATDE200024

A Pipeline for Creating In-Vehicle Posture Database for Developing Driver Posture Monitoring Systems

Mingming ZHAO[a,b], Georges BEURIER[a], Hongyan WANG[b] and Xuguang WANG[a,1]
[a] *Univ Lyon, Univ Gustave Eiffel, LBMC UMR_T9406, F69622, Lyon, France*
[b] *Tongji University, School of Automotive Studies, 200092, Shanghai, China*

Abstract. Driver posture monitoring is beneficial for identifying driver physical state as well as for optimizing passive safety systems to mitigate injury outcomes during collisions. In recent years, depth cameras are increasingly used to monitor driver's posture. However, good driver posture data is missing for developing accurate posture recognition methods. In this study, we introduce a method to build an in-vehicle driver posture database for training posture recognition algorithms based on a depth camera. Driver motion data was collected from 23 participants performing both driving and non-driving activities by an optical motion capture system Vicon. Motions were reconstructed by creating personalized digital human skeletons and applying inverse kinematics approach. By taking advantage of the techniques developed in computer graphics, a recorded driver motion can be efficiently retargeted to a variety of virtual humans to build a large database including synthetic depth images, ground truth labels of body segments and skeletal joint centers. Examples from motion reconstruction, data augmentation and preliminary posture prediction results are given.

Keywords. Driver Posture, Motion Reconstruction and Animation, Motion Database, Driver Monitoring

1. Introduction

According to the global status report on road safety released by World Health Organization in 2018, road traffic accidents claimed over 1.35 million fatalities and more than 50 million serious injuries worldwide each year. In spite of the advances in vehicle safety technologies, most of these accidents are still caused by human driver errors [1] and therefore could be avoidable. Driver monitoring has been an important research topic for many years. Especially with the background of driving automation of level 3 (SAE standard), researchers are struggling to find efficient ways to assess driver state and develop driving assistance systems that can deal with the human-machine transition in a smooth and safe manner [2][3]. Driver posture is an important source of information to evaluate driver's state, such as distraction [4] and inappropriate operation [5]. Furthermore, dynamic tracking of driver posture is necessary for developing future intelligent restraint systems that can be automatically adapted to driver's position to prevent or reduce injury during collision [6].

[1] Corresponding Author, Email: xuguang.wang@univ-eiffel.fr.

Recently, thanks to the progress in 3D modeling and depth perception in computer vision community, several non-invasive measuring methods for human posture recognition have been proposed [7]. As opposed to conventional cameras, depth cameras are not subject to varying illumination conditions, color, and texture in the scene and most importantly demonstrate a good compromise between real-time performance and 3D measurement [8]. Thanks to these characteristics, depth cameras have been introduced to monitor driver's upper body posture [2][4][9]. In these studies, Microsoft Kinect camera was adopted along with the integrated real-time posture recognition algorithm predicting 3D joint positions from a single depth image [10]. This algorithm was featured by the classification of body parts using Random Forest classifier [11] followed by the estimation of 3D joint positions using Meanshift [12]. Millions of human pose depth images with ground truth labels were artificially generated to train the algorithm. However, the algorithm was mainly intended for gaming. Training samples were collected from entertainment activities, such as dancing, fighting, etc. When directly used to monitor drivers, posture recognition suffers due to body occlusions and suboptimal camera placement in the vehicle cabin [13]. Therefore, there is a need to develop more performant in-vehicle postural monitoring algorithm based on depth images.

A reliable posture recognition algorithm requires a large amount of data samples for training and evaluation to avoid overfitting. To facilitate the research of driver posture recognition using depth cameras, more and more in-vehicle driver posture databases including depth images are now publicly available [14][15][16]. The database in [16] even provided drivers' ground truth motion capture data for reference. One crucial information still missing in these databases is the body segmentation label. To annotate on depth images of a real driver is challenging. To this end, Yamada et al. [17] dressed two drivers with a color-coded T-shirt to generate labeled depth images in order to customize the existing posture recognition algorithm [10]. However, the ground truth joint centers were not collected in the experiment. Apart from that, this method for generating body part labels is time consuming and the T-shirt only covered the trunk and arms.

The aim of this work was to establish a pipeline for creating in-vehicle driver posture database necessary for developing driver posture monitoring systems based on a depth camera. Our goals for building this pipeline are two-fold. On one hand, the data samples generated by this pipeline contain a good coverage of realistic posture variations, more specifically the appearance variations in depth images. On the other hand, the ground truth labels including body part segmentation and joint centers should be accurately obtained in an efficient way.

2. Materials and method

Figure 1 presents an overview of the pipeline, which mainly consists of three parts: data collection, motion reconstruction and data augmentation. We first perform experiments to collect a large set of driver posture data using both a motion capture (mocap) system VICON and a Microsoft Kinect. Then, driver motion is reconstructed from the raw mocap data using RPx [18], a customized human model based motion analysis and simulation tool. A personalized skeleton template is defined and inverse kinematics is applied to calculate the orientation and position of each body segment during movement.

Although depth images are also collected from the experiment and ground truth joint centers are estimated, it is not a good idea to directly use these samples to train the posture recognition algorithm due to the complexity in manual body part labeling, because this is tedious and cumbersome at best and potentially could lead to label inaccuracy. In addition, participants in an experiment are usually dressed with tight gym suits. Thereby depth images obtained in lab conditions are clearly different from those in real conditions.

Inspired by the work in [10], we resort to data augmentation by means of computer graphics techniques to obtain a large number of synthetic depth images covering a wide variety of driver postures and more importantly to simplify the collection of the ground truth labels. The basic idea is to animate rigged virtual human characters with realistic external envelopes including skin, clothes, hair and predefined body part labels using reconstructed motions captured in lab condition. This allows us to synthesize artificial depth images by rendering and meanwhile provides ground truth labels including body part segmentation and joint centers. The virtual human characters are created in MakeHuman (MH) [19], an open source tool designed to prototype realistic 3D human models. The motion retargeting, image rendering and data recording process are performed in MAYA [20], a 3D computer animation, modeling, simulation, and rendering software.

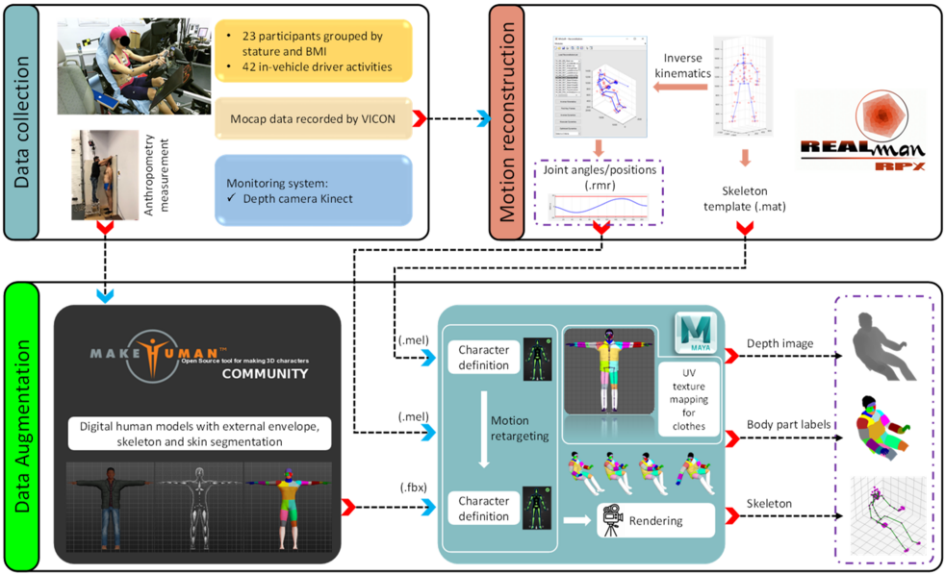

Figure 1. Overview of proposed pipeline.

2.1. Driver motion data collection

Twenty-three drivers (12 males and 11 females) with driving experience, ranged in age from 22 to 65 years, in height from 153 cm to 195 cm, in Body Mass Index (BMI) from 18.2 kg/m^2 to 43.4 kg/m^2, took part in this study. All participants provided written informed consent prior to participation in this study. The experimental protocol was approved by the ethical committee of Gustave Eiffel University (formerly known as French Institute of Science and Technology for Transport, Development and Networks).

We captured motions corresponding to 42 representative in-vehicle driver activities with reference to the work in [21]. They included primary driving operations, such as switching gear, turning steering wheel, etc., common secondary behaviors, such as interacting with phone, reading the dashboard, etc., and non-driving activities that might be present in autonomous vehicles, such as holding a book with both hands, relaxing both feet on the floor, etc. During experiment, participants were instructed to perform these tasks one by one on an experimental mockup (Figure 2a).

A motion capture system Vicon Giganet® MXT (Vicon Motion Systems, Oxford, United Kingdom) with 14 infrared cameras was used to track reflective markers placed on participants (Figure 2b) at a frequency of 50 Hz. A Microsoft Kinect camera was placed right front of the driver to observe upper body posture through depth perception with a frequency of 25 Hz. The synchronization between two systems was realized by an electronic trigger.

Figure 2. Experimental mockup (b) and marker arrangement (a).

2.2. Motion reconstruction

From measured marker trajectories, body motion was reconstructed using RPx. First, a subject specific articulated skeleton was created for each participant from a reference standing posture (Figure 3a). The joint positions related to hips, spine, shoulders and neck were estimated by statistical models [22][23]. Regarding limbs and head, joint positions were simply determined as the center of the marker pair attached close to the target joint or body part. Once the personalized skeleton template was created, joint angles were calculated by minimizing the distance between model based marker positions and measured ones (Figure 3b). Note that the real hand gestures of the participants were not collected in detail. The default hand gesture from RPx was adopted for all participants. Refer to [24][25][26] for more details. Motion reconstruction process was implemented in Matlab.

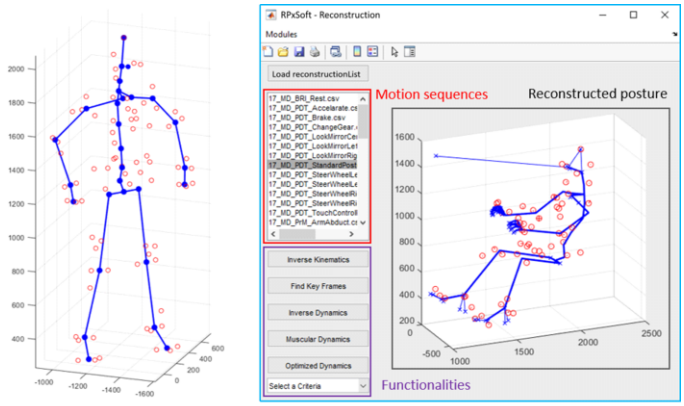

Figure 3. Personalized skeleton template (a) and RPx motion reconstruction module (b).

2.3. MH human character

The basic human character in MakeHuman was composed of a rigged skeleton and a skin mesh that forms the body surface shape. The skeleton (Figure 4 left) was linked to the mesh (Figure 4 middle) using the linear blend skinning technique available in the Blender software [27] so that changes of joint positions led to an adaptation of skin mesh. To impersonate the real participants, the attributes for each virtual model (e.g., age, gender, weight, height, body proportion etc.) were adjusted according to subject's anthropometry measurements. We also randomly configured clothes and hairstyle materials for each base character to yield more realistic driver appearances in depth images. We defined 30 color-coded body parts that densely cover the body, as suggested by [10]. These parts were specified in a texture map that can be applied to the body skin of different models (Figure 4 right). The resulting models were exported in standard FBX files that can be seamlessly manipulated in MAYA.

Figure 4. Digital human models for each participant. Skeleton (left), body shape with clothes and hair (middle) and body shape with segmentation labels on the skin (right).

2.4. Synthetic data generation

The reconstructed motion data including the RPx skeleton template and joint angles were recompiled using mel (the scripting language of MAYA) so that they were compatible with the animation engine in MAYA. With help of Autodesk® HumanIK® (HIK)

animation middleware (a full-body inverse kinematics (IK) solver and retargeter), the motion of RPx skeleton could be easily retargeted to MH skeleton.

Since the clothes would shadow the colors attached to the body skin during rendering, we mapped the same texture onto various clothes in MAYA UV editor as to the body skin in MH, so that the body segmentation labels were consistent across different characters dressed with different clothes (Figure 5).

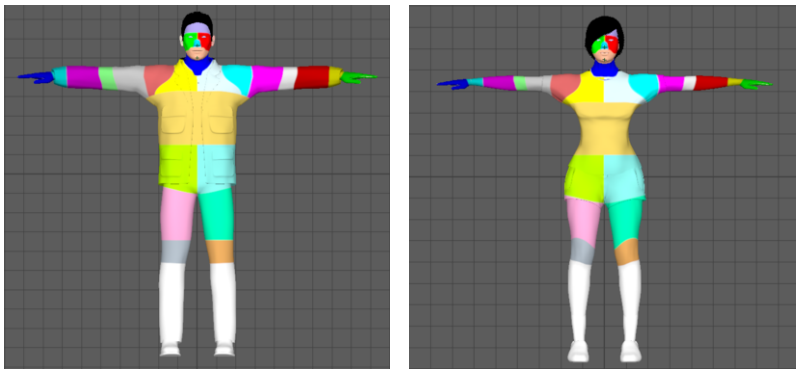

Figure 5. Body segmentation labels from skin and clothes.

During animation, the scene was rendered into color and depth images by using Arnold Renderer for MAYA (an advanced Monte Carlo ray tracing renderer) and the joint centers were recorded. In addition, we marked some key points on the head with the expectation that these points could be useful for monitoring head orientation. The motion retargeting, image rendering and data recording in MAYA were automatized by a hybrid programming of Python and mel.

3. Results

The motion database consists of approximately 2.4 Million frames in the driver motion sequences. Figure 6 gives one example after motion reconstruction. The reconstructed postures were from a motion when the driver moved the left foot and right hand to switch gear. The joint angles of left hip (GHUL) and the positions of left foot (GFBL) during motion are plotted.

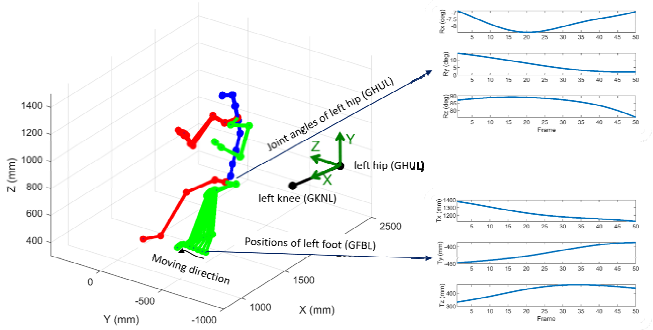

Figure 6. Motion reconstruction.

Figure 7 shows an example where we retargeted the real driver motion when reaching the phone with right hand onto a MH character. The generated depth images, body segmentation color labels and skeletal joint centers are given.

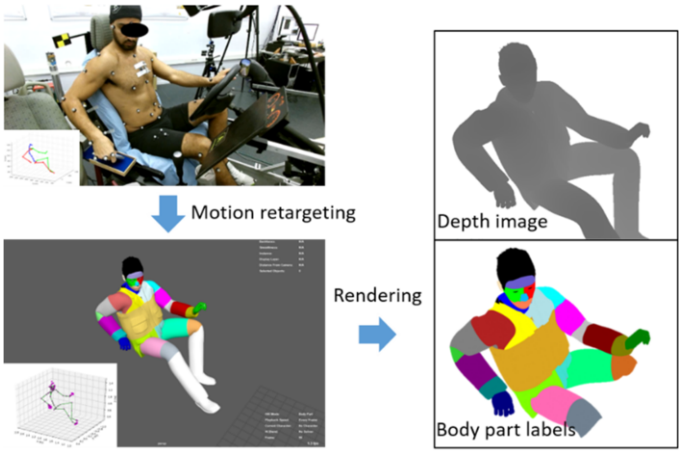

Figure 7. Data augmentation.

Given the synthetic dataset generated by the proposed pipeline, we adapted the algorithm from [10] and extracted some key joint centers and key points for prediction. As mentioned before, this algorithm transformes the body segmentation as a per-pixel classification task. After identifying the relevant body parts, the joint centers beneath the mesh surface and key points on the head could be directly inferred. Assume that the background is subtracted, our algorithm could discern different body parts and predict driver's posture from a depth image and an example is shown in Figure 8. Note that the lower body parts are merged into a single part annotated by white color and fall out of our interest, because they are practically invisible by a single camera in a real car.

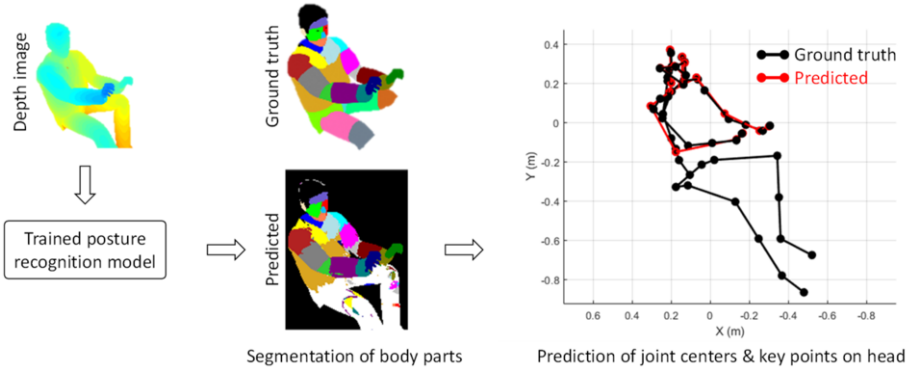

Figure 8. An example of posture recognition.

4. Discussion and conclusion

The aim of this paper is to introduce a pipeline to generate diver posture depth images and high quality ground truth labels required by the development of in-vehicle posture recognition algorithms. The pipeline is built by taking advantage of existing techniques

including RPx, MakeHuman and MAYA. Results show that real driver motions can be reliably reconstructed even when some markers were missing and synthetic dataset including realistic depth images and accurate ground truth labels can be generated in an efficient manner. Compared to the publicly existing driver posture databases [14][15][16], the dataset generated by this pipeline contains more information including complete ground truth labels for depth images. In contrast to the T-shirt method used in [17], the data augmentation process proposed in the present work allows us to obtain the body part labels more efficiently.

It should be noted that the motion retargeting in MAYA is not limited inbetween the MakeHuman character and mocap character of the same participant, although this was performed in this work. Theoretically and technically, motion retargeting can be performed across different participants. By generating more characters in MakeHuman, the dataset can be potentially enlarged to an infinitive scale based on the limited mocap data.

Another advantage of data augmentation is that the virtual environment provides us the opportunity to find the optimum depth camera position in the vehicle cabin, as proposed by Plantard et al. [28].

The main limitation of the proposed pipeline lies in the nature of marker-based optical motion capture system. In order to reduce relative movement of markers with respect to body segment, participants were required to dress with tight gym suits and markers were directly attached to the skin. In addition, the seatbelt was not used. In the motion retargeting and animation process, the clothes deformed in accordance with the skeletal posture of the character but not vice versa. Therefore, possible effects of clothing were not considered in the present study.

In addition, realistic driving operations were not imposed on the experimental mockup. Although we designed 42 different trials for participants to simulate the real driver motions in various scenarios, this list was by no means exhaustive. In fact, to cover all the driver motions in realistic driving conditions is not possible and also not our primary goal. According to [10], a wide range of posture combinations of different body parts would be sufficient for generalizing the prediction model to unseen postures.

More research will be performed to further improve the data augmentation process including the segmentation layout of body parts, the integration of driver hand gesture details, etc. In addition, the driver posture recognition algorithm trained on the synthetic dataset will be tested on the real depth images collected from the experiment.

Acknowledgement

This study was funded by China Scholarship Council (CSC 201806260131) and partly supported by the French National Project ANR AutoConduct (ANR-16-CE22-0007). The authors would like to express sincere gratitude to Ilias Theodorakos and Richard Roussillon for their contribution during the design and implementation of the experiment as well as to the volunteers who participated in the experiments for their efforts and time.

References

[1] Singh S. Critical reasons for crashes investigated in the national motor vehicle crash causation survey. Traffic Safety Facts Crash-Stats. Report No. DOT HS 812 115. National Highway Traffic Safety Administration, Washington, DC, 2015 Feb.

[2] Shia VA, Gao Y, Vasudevan R, Campbell KD, Lin T, Borrelli F, Bajcsy R. Semiautonomous vehicular control using driver modeling. IEEE Transactions on Intelligent Transportation Systems, 2014, 15(6), 2696-2709.

[3] Okabe K, Watanuki K, Kaede K, Muramatsu K. Study on Estimation of Driver's State During Automatic Driving Using Seat Pressure. In: International Conference on Intelligent Human Systems Integration, 2018, 35-41. Springer, Cham.

[4] Xing Y, Lv C, Zhang Z, Wang H, Na X, Cao D, Velenis E, Wang FY. Identification and analysis of driver postures for in-vehicle driving activities and secondary tasks recognition. IEEE Transactions on Computational Social Systems, 2017, 5(1), 95-108.

[5] McCall JC, Trivedi MM. Driver behavior and situation aware brake assistance for intelligent vehicles, In: Proceedings of the IEEE, 2007, 95(2), 374-387.

[6] Filatov A, Scanlon JM, Bruno A, Danthurthi SS, Fisher J. Effects of Innovation in Automated Vehicles on Occupant Compartment Designs, Evaluation, and Safety: A Review of Public Marketing, Literature, and Standards. SAE Technical Paper, 2019, Apr 2.

[7] Berretti S, Daoudi M, Turaga P, Basu A. Representation, analysis, and recognition of 3D humans: A survey. ACM Transactions on Multimedia Computing, Communications, and Applications (TOMM), 2018, 14(1s), 1-36.

[8] Wang H, Zhao M, Beurier G, Wang X. Automobile Driver Posture Monitoring Systems: A Review. China Journal of Highway and Transport, 2019, 32(2), 1-18.

[9] Chuang YW, Kuo CH, Sun SW, Chang PC. Driver behavior recognition using recurrent neural network in multiple depth cameras environment. Electronic Imaging, 2019, (15), 56-1.

[10] Shotton J, Sharp T, Kipman A, Fitzgibbon A, Finocchio M, Blake A, Cook M, Moore R. Real-time human pose recognition in parts from single depth images. Communications of the ACM, 2013, 56(1), 116-124.

[11] Breiman L. Random forests. Machine learning, 2001, 45(1), 5-32.

[12] Comaniciu D, Meer P. Mean shift: A robust approach toward feature space analysis. IEEE Transactions on Pattern Analysis & Machine Intelligence, 2002, (5), 603-619.

[13] Zhao M, Beurier G, Wang H, Wang X. In vehicle diver postural monitoring using a depth camera kinect. SAE Technical Paper, 2018, Apr 3.

[14] Martin M, Roitberg A, Haurilet M, Horne M, Reiß S, Voit M, Stiefelhagen R. Drive&Act: A Multi-modal Dataset for Fine-grained Driver Behavior Recognition in Autonomous Vehicles. InProceedings of the IEEE International Conference on Computer Vision, 2019, 2801-2810.

[15] Jegham I, Khalifa AB, Alouani I, Mahjoub MA. MDAD: A Multimodal and Multiview in-Vehicle Driver Action Dataset. InInternational Conference on Computer Analysis of Images and Patterns, 2019, 518-529. Springer, Cham.

[16] Feld H, Mirbach B, Katrolia J, Selim M, Wasenmüller O, Stricker D. DFKI Cabin Simulator: A Test Platform for Visual In-Cabin Monitoring Functions. arXiv preprint arXiv:2002.03749, 2020, Jan 28.

[17] Yamada T, Irie H, Sakai S. High-accuracy joint position estimation and posture detection system for driving. In: Adjunct Proceedings of the 13th International Conference on Mobile and Ubiquitous Systems: Computing Networking and Services, 2016, 219-224.

[18] Monnier G, Renard F, Chameroy A, Wang X, Trasbot J. A motion simulation approach integrated into a design engineering process. SAE Transactions, 2006, 1118-1123.

[19] http://www.makehumancommunity.org/

[20] https://www.autodesk.com/education/free-software/maya

[21] Dingus TA, Klauer SG, Neale VL, Petersen A, Lee SE, Sudweeks J, Perez MA, Hankey J, Ramsey D, Gupta S, Bucher C. The 100-car naturalistic driving study, Phase II-results of the 100-car field experiment. United States. Department of Transportation. National Highway Traffic Safety Administration, 2006.

[22] Reed MP, Manary MA, Schneider LW. Methods for measuring and representing automobile occupant posture. SAE Technical Paper, 1999, Mar 1.

[23] Peng J, Panda J, Jan SV, Wang X. Methods for determining hip and lumbosacral joint centers in a seated position from external anatomical landmarks. Journal of biomechanics, 2015, 48(2), 396-400.

[24] Monnier G, Wang X, Verriest JP, Goujon S. Simulation of complex and specific task-orientated movements-application to the automotive seat belt reaching. SAE transactions, 2003, 715-721.

[25] Wang X, Chevalot N, Monnier G, Ausejo S, Suescun Á, Celigüeta J. Validation of a model-based motion reconstruction method developed in the Realman project. SAE transactions, 2005, Jan 1, 873-879.

[26] Ausejo S, Suescun A, Celigüeta J, Wang X. Robust human motion reconstruction in the presence of missing markers and the absence of markers for some body segments. SAE Technical Paper, 2006, Jul 4.

[27] https://www.blender.org/
[28] Plantard P, Auvinet E, Pierres ASL, Multon F. Pose Estimation with a Kinect for Ergonomic Studies: Evaluation of the Accuracy Using a Virtual Mannequin. Sensors, 2015, 15(1), 1785-1803.

DHM2020
L. Hanson et al. (Eds.)

© 2020 The authors and IOS Press.
This article is published online with Open Access by IOS Press and distributed under the terms of the Creative Commons Attribution Non-Commercial License 4.0 (CC BY-NC 4.0).
doi:10.3233/ATDE200025

Smart Clothing for Monitoring Gait

Sofia SCATAGLINI[a,b,d,1], Guillaume ABRAN[c], Eddy ROOSENS[a,c], Damien VAN TIGGELEN[a], Robby HAELTERMAN[b] and Stijn VERWULGEN[d]
[a] *Military Hospital Queen Astrid, 1120 Brussels, Belgium*
[b] *Royal Military Academy, 1000 Brussels, Belgium*
[c] *Haute Ecole Libre de Bruxelles Ilya Prigogine 1070 Brussels, Belgium*
[d] *Department of Product Development, Faculty of Design Sciences, University of Antwerp, Antwerp, Belgium*

Abstract. This paper presents a method to calculate spatiotemporal parameters using a chest-worn accelerometer. Accuracy was compared with an optical system that consists of a walkway of transmitting and receiving bars (Microgait, Optogait, Bolzano, Italy). To this purpose, seventeen healthy male wore a smart shirt based worn accelerometer performing five meters of walkway delimited by five meters of optical bars OptoGait™ for three times. Spatiotemporal parameters such as gait cycle and gait phases were analysed and compared using the two systems. Smart shirt based on chest-worn accelerometer revealed to be a non-intrusive way of calculating gait cycle, phases and sub-phases. In addition, the inverted pendulum model based on chest body-worn accelerometer revealed to be a good model for calculating step length variation and consequently the speed. Our results, are in line with previous literature presenting an average of 60.24 % of stance phase, 39.75% of swing phase, a foot flat subphase of 17.60%, a terminal stance subphase of 21.42%, a pre-swing subphase of 10.65%, a step length of 0.74 m for an average speed of 1.37 m/s using the smart shirt.

Keywords. Smart Clothing, Gait Analysis, Monitoring, Spatio-Temporal Parameters, Human Kinematics, Biomechanical Modelling, DHM

1. Introduction

Monitoring and modeling physical functions in rehabilitation is becoming important to achieve/establish new and improved rehabilitation [1]. Instrumented gait analysis is commonly used to quantify and evaluate pathologies manifested by gait disorders [2-5]. Related to the lower body part, gait analysis is used to assess patients with affected physical activity [2-4].

This laboratory-based technique requires the use of a gold standard device, such as an optoelectronic system. Gold standard measurement devices are often costly, not intuitive, time-consuming and not suitable for outdoor use and evaluating subjects in an ecological context [6]. Nowadays smart clothing based on a body-worn accelerometer can respond to the problem [7]. This results in an intelligent garment that contains embedded sensors for monitoring bio-signals but also accelerometers or Inertial Measurement Unit (IMU) sensors for monitoring the subject's kinematics over an extensive period in a non-intrusive way and in an ecological approach [7-9].

[1] Corresponding Author, Email: sofia.scataglini@mil.be; sofia.scataglini@uantwerpen.be.

Previous studies demonstrated the use of wearable technology for measuring gait parameters [10-12] but few studies demonstrated the possibility to monitor gait using a smart cloth [13]. The majority of wearable devices are attached to shoes or to the body by straps, that revealed to be uncomfortable, limiting the wearer's movements and consequently his/her performance. Wearable technology integrated into a smart cloth can respond to user needs during daily activities, where monitor locomotion is essential [14].

Natural walking consists of consecutive gait cycles [2,3]. Each cycle is characterizing by two phases: the stance (60% of the gait cycle) where the foot remains in contact with the ground and the swing (40% of the gait cycle) where the foot is in the air (Figure 1).

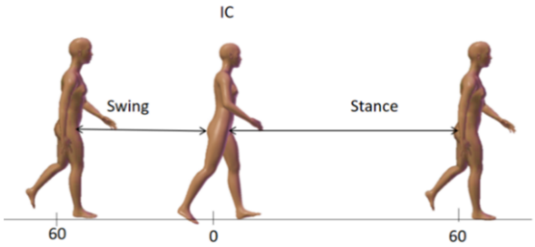

Figure 1. Gait cycle and phases. In order to show the concept, a dedicate DHM was created using MakeHuman and rigged in Blender with a BVH file of walking captured data acquired in one subject of this study [8].

Additionally, each phase is divided by sub-phases initial contact (IC), loading response (foot flat), mid-stance, terminal stance and pre-swing (toe-off) for the stance phase and initial, mid and terminal swing for swing [2,3,15] (Figure 2).

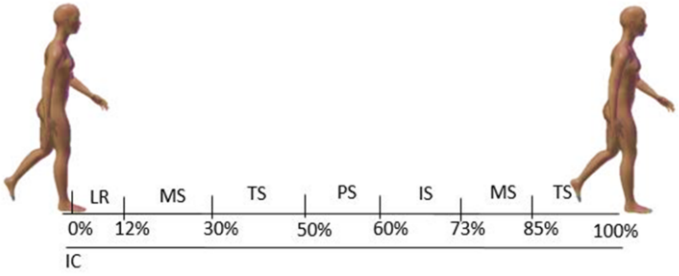

Figure 2. Gait cycle and the related sub-phases (IC=initial contact, MS=mid-stance, TS=terminal stance, PW=pre-swing, IS=initial swing, MS=mid-swing, TS=terminal swing).

Together with all the phases, there are other spatio-temporal parameters [2,3,15,16]: step length, cadence (step/min) and speed.

The step length (m) is the distance between the initial contact of one foot and the initial contact of the other foot [16]. The cadence (step/min) corresponds to the number of steps in a defined time; often expressed as a number of steps per minute [15]. The speed, also referred as the "sixth vital sign", can predict health status [17].

Starting from the previous assumptions, the objective of our research is to present a study that investigates the use of smart clothing for measuring spatio-temporal gait parameters in healthy individuals.

2. Methods

2.1 Participants

Seventeen healthy male volunteers participated in this study. Their anthropometric characteristics are summarized in Table 1. Subjects were instructed about the experiment and signed the informed consent. This study was also approved by the ethical committee (CE2019/32).

Table 1. Anthropometric characteristic of study population.

Anthropometric parameters	Mean (SD)	Minimum	Maximum
Age (years)	25.647 (6.123)	21	47
Stature (m)	1.807 (0.065)	1.71	1.92
Body mass (kg)	74.882 (7.398)	60	89
BMI (kg/m²)	22.873 (1.263)	20.047	24.915
Leg length (m)	0.94 (0.053)	0.84	1.05
Chest height (m)	1.31(5.992)	1.22	1.43

2.2 Protocol

Subjects were instructed to perform five meters of walkway delimited by five meters of optical bars OptoGait™ (Bolzano, Italy), wearing a smart t-shirt (Politecnico di Milano, SensibiLab, Lecco, Italy, Figure 3) for three times (Figure 4). To obtain a subject specific normal walking speed, subjects were first asked to perform a few laps without recording, to familiarize themselves with the environment and find their comfort speed [18].

Figure 3. Smart shirt realized by Politecnico di Milano (SensibiLab, Lecco, Italy).

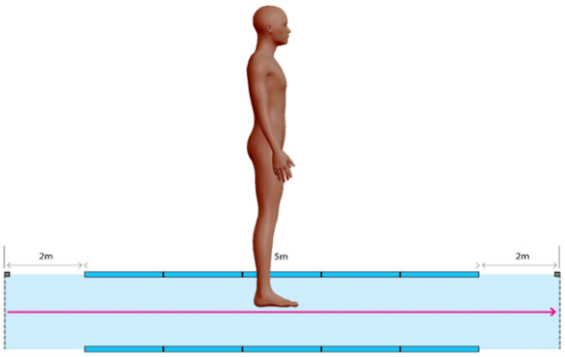

Figure 4. The five-meter walkway using the Optogait (OptoGait™, Microgait, Bolzano, Italy).

The five-meter walkway, OptoGait™ (Microgait, Bolzano, Italy) consists of five transmitting bars (each one contains 96 LEDs) and five receiving bars (each one contains 96 LEDs) communicating on an infrared frequency [19]. The smart shirt created by the (Politecnico di Milano, SensibiLab, Lecco, Italy) integrates two textrodes embedded into the cloth and a three-axial accelerometer, connected by two fasteners (nickel-free material). The t-shirt is connected with a dedicated App for collecting and managing data of tri-axial-acceleration (anterior-posterior, medio-lateral and vertical) and ECG recording in real-time [20-22].

Spatiotemporal parameters such as the time of the gait cycle (s), the duration of the swing and stance phase (s), the percentage of the swing phase, stance phase (%), the percentage of the loading response, flat foot, terminal stance and pre-oscillation (%), the percentage of the phase double contact (%), cadence, speed (m/s) and the gait to stance ratio were measured with the two devices and successively calculated. We have analysed 204 datasets (17 subjects x 3 trials of 4 steps each=204 datasets).

Spatio-temporal parameters using the OptoGait™ (Microgait, Bolzano, Italy) were automatically calculated by their software. In the smart shirt the vertical acceleration was used for calculating the gait cycle and their eight phases according to Auvinet et al. [23] (Figure 5).

Step length was calculated using two methods (SL_1 and SL_2).

The first one is represented by the product between the stature S and an anthropometric coefficient C, Eq.(1), [24-25].

$$SL1 = C*S \quad (1)$$

While the second method considers the pendulum model, according to Fusca et al. [12-25, 26], Eq.(2).

$$SL = 2\sqrt{2L * hCOM - hCOM^2} \quad (2)$$

In this equation, L is the length of the lower limb and hCOM is calculated by using the following formula based on the work of Fusca et al. [12]:

$$hCOM = 2 * Av * \left(\frac{T}{2\pi}\right)^2 \quad (3)$$

where in our case, Av is the maximum value of the vertical acceleration calculated at chest level and T is the period of the step.

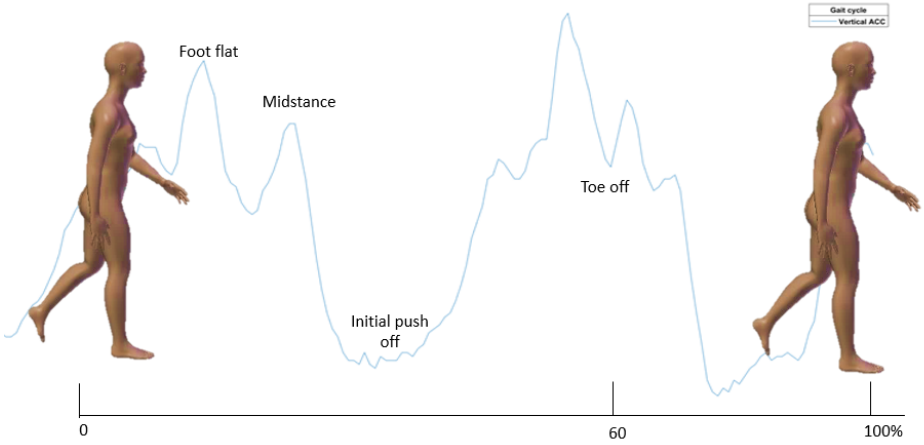

Figure 5. Gait phases identification using the vertical acceleration extrapolated by the smart shirt realized by Politecnico di Milano (SensibiLab, Lecco, Italy).

Introducing the Eq.(3) in the Eq.(2) with a quadratic relationship, SL2 can be determinate as follow:

$$SL2=\sqrt{SL} \quad (4)$$

While, two different speed (S_1, S_2) for the SL_1 and SL_2 respectively were calculated using the following formula:

$$S = \frac{2*K}{GC} \quad (5)$$

In this equation K is the step length and CG is the gait cycle duration.

3. Results and Discussions

Spatio-temporal parameters measured with the smart t-shirt and the OptoGait are shown in Table 2 and 3. In particular, the smart shirt showed to have a stance time of 0.653 ± 0.033 seconds, a swing time of 0.431± 0.027 seconds and an average time cycle of 1.085 ± 0.047 seconds according to the previous literature [12, 23-27]. These values were observed to be different in the case of the Optogait where we had an average stance time of 0.705 (±0.045) seconds for an average oscillation time of 0.393 (± 0.026) seconds and an average time cycle of 1.098 (± 0.055) seconds (Table 2). A Spearman correlation test between these parameters demonstrated a medium correlation with the time of the stance and the swing and the time of gait cycle with p<0,0001. By contrast, the resulting percentage of stance and swing, being 60.24 % and 39.75% for the smart shirt and 64.18% and 35.81% for swing were not correlated using the Spearman correlation test (Table 2). The percentage of foot flat, terminal stance and pre-swing were not correlated between the two devices. In term of step length calculation, the two formulas, Eq.(1) and Eq.(2) were applied for determining the step length using the smart shirt (Table 4).

Table 2. Mean, minimum, maximum and correlation of spatio-temporal parameters (Tps-CG=gait cycle duration, Tps-ST= stance phase duration, Tps-SW= swing phase duration, ST=stance, SW=swing, DS=double support, LR=loading response, FFL=foot flat, TS=terminal stance, PSW=pre-swing) calculated using the smart shirt and the Optogait.

	Smart t-shirt		***Optogait***			
Spatio-temporal parameters	**Mean (SD)**	**Minimum Maximum**	**Mean (SD)**	**Minimum Maximum**	**Spearman's rs**	**p-value**
Tps GC (s)	1.085 (0.047)	0.967 1.209	1.098 (0.055)	0.972 1.286	0.6725	<.0001
Tps ST (s)	0.653 (0.033)	0.546 0.748	0.705 (0.045)	0.614 0.848	0.4176	<.0001
Tps SW (s)	0.431 (0.027)	0.351 0.514	0.393 (0.026)	0.338 0.473	0.5410	<.0001
ST (%)	60.247 (1.770)	55.118 65.648	64.189 (1.998)	59.6 69.9	0.1377	0.0854
SW (%)	39.752 (1.770)	34.351 44.881	35.81 (1.998)	30.1 40.4	0.1375	0.0859
DS (%)	20.991 (2.950)	9.655 28.057	27.321 (3.107)	20.3 36.8	0.2010	0.0116
LR (%)	10.631 (1.618)	7.246 15.441	12.654 (6.335)	0.2 25.4	0.0758	0.3453
FFL (%)	17.606 (2.368)	10.791 24.489	13.846 (1.605)	10.1 25.4	0.1191	0.0904
TS (%)	21.428 (2.527)	14.084 27.941	38.489 (8.487)	21.5 59.3	-0.2285	0.0010
PSW (%)	10.658 (1 .648)	7.092 15.714	13.491 (1.648)	9.8 18	0.0937	0.2430

Table 3. Mean, SD (standard deviation), Minimum, Maximum, Median (SLO=step length calculated with the Optogait, SO=speed calculated with the Optogait, SL1=step length calculated using Eq.(1), SL2=step length calculated with smart shirt using Eq.(4), S1=speed calculated using the SL1in Eq.(5), S2=speed calculated using the SL2 in Eq.(5) (Figure 6).

Variable	**Mean**	**SD**	**Minimum**	**Median**	**Maximum**
SLO	0.786	0.038	0.69	0.780	0.89
SL1	0.750	0.027	0.710	0.747	0.797
SL2	0.743	0.033	0.654	0.742	0.865
SO	1.456	0.047	1.260	1.460	1.55
S1	1.385	0.060	1.249	1.386	1.571
S2	1.371	0.071	1.180	1.360	1.606

Optogait step length detection (SLO) was automatically determined using the Optogait software, (Table 3). A small correlation ($r=0.229$, $p<0.005$) was found between the SLO and SL1. By contrast the speed calculated with Optogait was not correlated with the speed S2 but with the SL2 ($r=-0.201$, $p<0.005$) and SL1 ($r=-0.230$, $p<0.005$). While the step length SL1 was correlated with SL2 ($r=0.456$, $p<0.0001$) (Table 4). As a result, their speed was also correlated ($r=0.544$, $p<0.0001$) as shown in Table 4.

While, the step length calculated with Eq.(1) does not take in consideration the step length variation as the inverted pendulum model Eq.(4). According to the previous studies, 1.4 m/s is considered the natural walking speed and this corresponds to a value of the stance phase between 60-62% and 38-40% of the swing, [12, 23-27]. This result is in accordance with our evaluation using the smart shirt and calculating the speed with Eq.(5) and this is the case when we are calculating the variation of the chest height using Eq.(4).

Table 4. Step length and speed correlation between the smart shirt and the Optogait (SLO=step length calculated with the Optogait, SO=speed calculated with the Optogait, SL1=step length calculated using Eq.(1), SL2=step length calculated with smart shirt using Eq.(4), S1=speed calculated using the SL1in Eq.(5), S2=speed calculated using the SL2in Eq.(5).

Variables	Spearman's rs	95% CI		p-value
SLO, SL1	0.229	0.090	to 0.355	0.0010
SO, SL2	-0.201	-0.329	to -0.065	0.0042
SO, SL1	-0.230	-0.356	to -0.095	0.0009
S2, SLO	-0.289	-0.411	to -0.158	<0.0001
S1, SLO	-0.288	-0.354	to -0.0931	0.0011
SL1, SL2	0.456	0.340	to 0.558	<0.0001
S1, S2	0.544	0.439	to 0.634	<0.0001

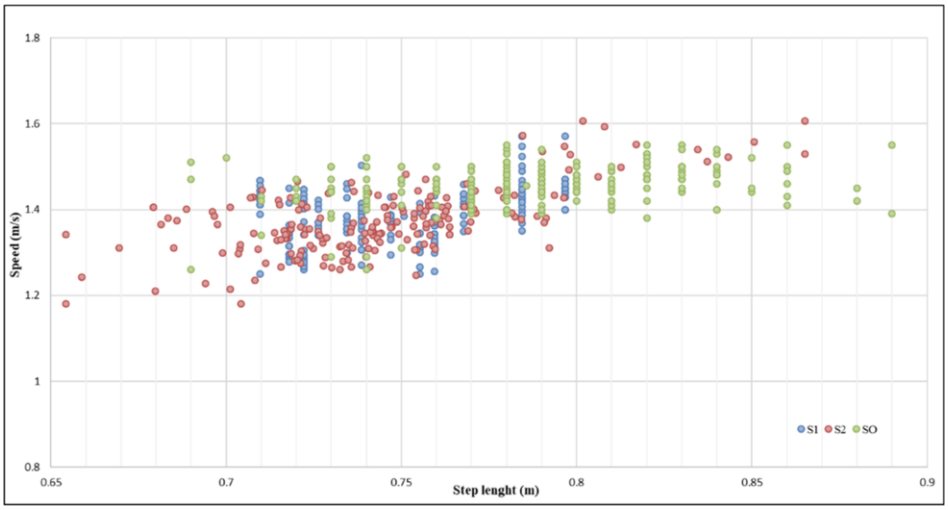

Figure 6. Step length and walking speed (SL1=step length calculated using Eq.(1), SL2=step length calculated with smart shirt using Eq.(4), S1(in blue)=speed calculated using the SL1in Eq.(5), S2(in red)=speed calculated using the SL2in Eq.(5) and SO (in green)=speed calculated using the Optogait).

4. Conclusion

In conclusions, the smart shirt based on a chest-worn accelerometer revealed to be a non-intrusive way of calculating the spatio-temporal parameters in an ecological approach according with the previous literature.

In fact, our results, are in line with previous literature presenting an average of 60.247 % of stance phase, 39.752% of swing phase, a foot flat of 17.60%, a terminal stance of 21.42%, a pre-swing of 10.65%, a step length of 0.74 m for an average speed of 1.371 m/s using the smart shirt.

Several methods were used for calculating either the step length and the speed. Indeed, this study presents a study limitation regarding the comparison of these measurements using a commercial system that not correspond the gold standard scientific method such as camera based (e.g. Vicon system). And, in this study Spearman correlation test demonstrates that the chest inverted pendulum model adopted in this study can be used for calculating step length variation and speed.

As a result, future perspective will be addressed in evaluating this method using the gold standard scientific method to assess gait analysis.

Acknowledgement

This work was supported by the Belgian Royal Higher Institute for Defence (RHID), Military Hospital Queen Astrid, Haute école libre de Bruxelles Ilya Prigogine and the University of Antwerp. We would also like to thank all the participants in this study for their subjects, commitments and motivated collaboration.

References

[1] Agarwal V, Smuck M, Tomkins-Lane C, Shah NH. Inferring Physical Function From Wearable Activity Monitors: Analysis of Free-Living Activity Data From Patients With Knee Osteoarthritis. JMIR mHealth and uHealth. JMIR Publications Inc, 2018, 6(12).

[2] Whittle M. Normal gait. Gait Analysis, Elsevier, 1998.

[3] Roberts A. Gait analysis: normal and pathological function (2nd edition). The Journal of Bone and Joint Surgery British volume. British Editorial Society of Bone & Joint Surgery, 2010, 92-B(8), 1184–1184.

[4] Ciprandi D, Bertozzi F, Zago M, Ferreira CLP, Boari G, Sforza C, Galvani C. Study of the association between gait variability and physical activity. European Review of Aging and Physical Activity. Springer Science and Business Media LLC, 2017, 14(1).

[5] Muro-de-la-Herran A, Garcia-Zapirain B, Mendez-Zorrilla A. Gait Analysis Methods: An Overview of Wearable and Non-Wearable Systems, Highlighting Clinical Applications. Sensors. MDPI AG, 2014, 14(2), 3362–3394.

[6] Vastola R, Medved V, Daniele A, Coppola S, Sibilio M. Use of Optoelectronic Systems for the Analysis of Technique in Trials. Journal of Sports Science. David Publishing Company, 2016, 4(5).

[7] Scataglini S, Danckaers F, Huysmans T, Sijbers J, Andreoni G. Design smart clothing using digital human models. In: Scataglini S, Paul G, editors. DHM and Posturography, 2019, 683–698.

[8] Scataglini S, Paul G. Open-source software to create a kinematic model in digital human modelling. In: Scataglini S, Paul G, editors. DHM and Posturography, 2019, 201–213.

[9] Scataglini S, Moorhead AP, Feletti F. A Systematic Review of Smart Clothing in Sports: possible Applications to Extreme Sports. Muscle Ligaments and Tendons Journal, Edra SpA, 2020, 10(2), 333-342.

[10] Caldas R, Mundt M, Potthast W, Buarque de Lima Neto F, Markert B. A systematic review of gait analysis methods based on inertial sensors and adaptive algorithms. Gait & Posture, Elsevier BV, 2017, 57, 204–210.

[11] Chen S, Lach J, Lo B, Yang G-Z. Toward Pervasive Gait Analysis With Wearable Sensors: A Systematic Review. IEEE Journal of Biomedical and Health Informatics. Institute of Electrical and Electronics Engineers (IEEE), 2016, 20(6), 1521–1537.

[12] Fusca M, Negrini F, Perego P, Magoni L, Molteni F, Andreoni G. Validation of a Wearable IMU System for Gait Analysis: Protocol and Application to a New System. Applied Sciences. MDPI AG, 2018, 8(7), 1167.

[13] Ascioglu G, Senol Y, Erdem D. A Smart Garment for Gait Analysis. Journal of Fashion Technology & Textile Engineering, 2018, S4:004.
[14] Scataglini S, Andreoni G, Gallant J. Smart Clothing Design Issues in Military Applications. Advances in Intelligent Systems and Computing. Springer International Publishing, 2018, 158–168.
[15] Levine D, Whittle MW. Whittles gait analysis. Edinburgh: Churchill Livingstone/Elsevier, 2012.
[16] Porciuncula F, Roto AV, Kumar D, Davis I, Roy S, Walsh CJ, et al. Wearable Movement Sensors for Rehabilitation: A Focused Review of Technological and Clinical Advances. PM&R.Wiley, 2018, 220–232.
[17] Fritz S, Lusardi M. White Paper:"Walking Speed: the Sixth Vital Sign". J Geriatr. Phys. Ther, 2009, 32(2), 46-49.
[18] Paterson KL, Lythgo ND, Hill KD. Gait variability in younger and older adult women is altered by overground walking protocol. Age and Ageing. Oxford University Press (OUP), 2009, 38(6), 745–748.
[19] Healy A, Linyard-Tough K, Chockalingam N. Agreement Between the Spatiotemporal Gait Parameters of Healthy Adults From the OptoGait System and a Traditional Three-Dimensional Motion Capture System. Journal of Biomechanical Engineering. ASME International, 2018, 141(1).
[20] Scataglini S. Ergonomics of gesture: effect of body posture and load on human performance. PhD thesis, Politecnico di Milano, 2017.
[21] Scataglini S, Truyen E, Perego P, Gallant J, Van Tiggelen D, Andreoni G. Smart clothing for human performance evaluation: biomechanics and design concept evolution. In: Proceedings of the 5th International Digital Human Modeling Symposium (DHM2017), 2017, Bonn, Germany, 9-17.
[22] Scataglini S, Andreoni G, Truyen E, Warnimont L, Gallant J, Van Tiggelen D. Design of smart clothing for Belgian soldiers through a preliminary anthropometric approach. In: Proceedings of the 5th International Digital Human Modeling Symposium (DHM2016), 2016, Montréal, Québec, Canada.
[23] Auvinet B, Berrut G, Touzard C, Moutel L, Collet N, Chaleil D, Barrey E. Reference data for normal subjects obtained with an accelerometric device. Gait & Posture. Elsevier BV, 2002, 16(2), 124–134.
[24] Carrington E. PT Exam Review — The essential guide for the foreign-trained physical therapist. Physiotherapy. Elsevier BV, 1996, 82(4), 278.
[25] Fusca M, Perego P, Andreoni G. Method for Wearable Kinematic Gait Analysis Using a Harmonic Oscillator Applied to the Center of Mass. Journal of Sensors. Hindawi Limited, 2018, 1–14.
[26] Zijlstra W, Hof AL. Assessment of spatio-temporal gait parameters from trunk accelerations during human walking. Gait & Posture, 2003, 18(2), 1–10.
[27] Iosa M, Morone G, Paolucci S. Golden Gait: An Optimization Theory Perspective on Human and Humanoid Walking. Frontiers in Neurorobotics. Frontiers Media SA, 2017, 11.

DHM2020
L. Hanson et al. (Eds.)
© 2020 The authors and IOS Press.
This article is published online with Open Access by IOS Press and distributed under the terms of the Creative Commons Attribution Non-Commercial License 4.0 (CC BY-NC 4.0).
doi:10.3233/ATDE200026

Optimal Control of Grasping Problem Using Postural Synergies

Uday PHUTANE [a,1], Michael ROLLER [b], Anja BOEBEL [a] and Sigrid LEYENDECKER [a]

[a] *Chair of Applied Dynamics, Friedrich-Alexander-Universität Erlangen-Nürnberg, Erlangen, Germany*
[b] *Fraunhofer ITWM, Kaiserslautern, Germany*

Abstract. The human hand has a complex musculoskeletal structure which acts as an effective end-effector to perform grasping effectively. Optimal control is a productive method to execute predictive simulations for many biomechanical activities. Optimal control for grasping simulations has been demonstrated for precision grasps for two fingers. However, the procedure to expand it to a full hand is laborious, primarily due to a large computational cost. Furthermore, a full hand performs with a high degree of coordination. These issues can be challenged by the inclusion of kinematic or postural synergies in the multibody framework. In this work, we implement the modelling of kinematic synergies to perform grasping simulations.

Keywords. hand kinematics, postural synergies, grasping, model order reduction

1. Introduction

Grasp path planning is an extensive research area with primary applications in humanoid robotics, industrial ergonomics and also, clinical applications. While the robotics influence aided to formalise grasping concepts of velocity and force transmission, see [1,2], the ergonomics and medical concerns motivated the research to anatomically characterise hand models, see [3,4]. Overall, it also established grasp types from power and precision grasps as defined by Napier [5] to an exhaustive taxonomy, [6]. We have demonstrated two-finger precision grasp examples in [8] with the discrete mechanics and optimal control with constraints (DMOCC, see [7]) approach. Here, a hybrid dynamical system with known switching sequence and unknown switching times was modelled to perform a *reaching* phase and a *grasping* phase in a non-linear optimisation problem. The reaching phase is the prehension phase during which the fingers approach the object surface, and the grasped action is performed during the grasping phase.

While the extension from the two finger model to the complete hand grasping optimal control is modular, the size of the overall optimisation problem increases tremendously. This imposes an enormous computational challenge on the optimiser. Fortunately, the human hand exhibits a highly coordinated motion due to its complicated underlying musculoskeletal network, see [9]. The coordinated motion has been quantified

[1] uday.phutane@fau.de.

into eigen modes, called as synergies by Santello in [10]. The concept of synergies arose from a neuroscience perspective where it was observed that the hand motion can be expressed as a linear combination of a basis of a fairly reduced configuration space. Overall, it was observed that the hand can be kinematically operated through a relatively reduced number of degrees of freedom (DoFs). The objective is this work is to implement the kinematic synergies into our multibody grasping framework. Here, we concentrate only on the reaching or prehension phase, so as to only see the viability of using the synergies to be able to close contact as well as possible.
The contribution continues with the description of the multibody model and the inclusion of synergies in Section 2, followed by the results and conclusions in Sections 3 and 4, respectively.

2. Multibody model

The grasping multibody model relies on the joint description, leading to the total number of degrees of freedom. A small introduction is provided on the method of hand postural synergy extraction, followed by the gap closure mechanism.

2.1. Synergy actuated hand model

We describe a rigid body in the director formulation as in [7]. In short, a body is with twelve DoFs with configuration $\boldsymbol{q} = [\,\boldsymbol{\varphi},\, \boldsymbol{d}_1,\, \boldsymbol{d}_2,\, \boldsymbol{d}_3]$, with center of mass $\boldsymbol{\varphi}$ and an orthonomal director triad $\{\boldsymbol{d}_I\}_{I=1,2,3}$. The hand is composed of twenty such rigid bodies connected in a tree like structure through a combination of revolute, cardan and joints with two rotation axes that are non-intersecting and non-orthogonal (nino). With rigid body internal constraints and joint constraints, the model comprises of twenty-six DoFs. These include six DoFs for the wrist is free to move in space and twenty degrees of freedom for the joint angles. The complete structure is depicted in Figure 1. The motion of the hand in time can approximated by through discrete configuration $\boldsymbol{q}_n \approx \boldsymbol{q}(t_n)$, i.e. the approximate configuration at time node t_n. To update the configuration from time node n to $n+1$, we apply a discrete nodal reparameterisation

$$\boldsymbol{q}_{n+1} = \boldsymbol{F}_d(\boldsymbol{u}_{n+1}, \boldsymbol{q}_n) \tag{1}$$

Here, $\boldsymbol{u}_{n+1}$ represents the increment in the minimal coordinates from time nodes n to $n+1$. The finger digit geometries are modelled as cylinders.

Although there are multiple ways to obtain these eigen grasps, see [11], we focus briefly on the one by Santello, see [10]. Herein, five subjects were made to visualise and mime hand postures for fifty-seven different objects. The joint angles in these poses were captured and a covariance matrix for the captured data was created. Using singular value decomposition, the eigen vectors form the required reduced configuration space or the principal components (PCs), while the corresponding eigen values represented the amount of variance. As per Santello, more than 80% of the posture variance was accounted by the first two PCs. Nevertheless, the study prescribed fifteen PCs, where the fifteenth eigen value or amplitude was approximately zero. The MATLAB Toolbox *Syngrasp*, see [12], provides a function `SGsantelloSynergies()`, which provides the eigen grasps extracted by Santello in the forms of a matrix $\boldsymbol{S} \in \mathbb{R}^{20\times 15}$. Here, the twenty

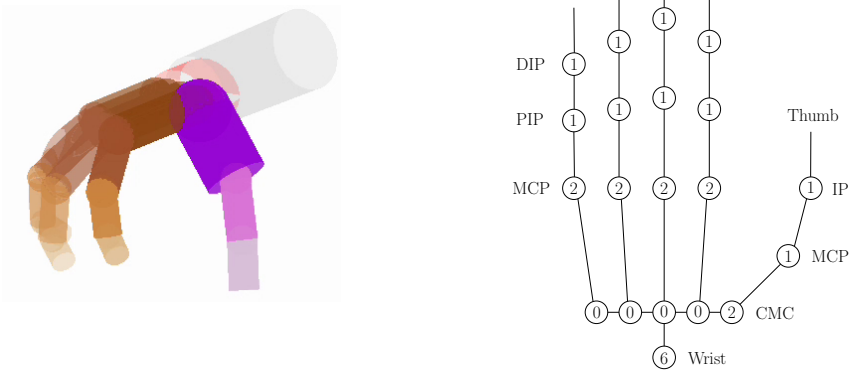

Figure 1. The multibody hand model. Left: the modelling of the digits as cylindrical geometries. Right: the tree structure with the number of DoFs in the circles. The one and two DoF joints are modelled as revolute and cardan (fingers) / nino (thumb), respectively.

rows prescribe the joint angles while 15 columns represent the eigen vectors or synergies. The matrix $\boldsymbol{S}$ is ordered column-wise, as per their eigen values in the decreasing order. Using a discrete change in the synergies, say $\boldsymbol{z}_{n+1} \in \mathbb{R}^{n_z}$, the increment in the joint angles $\boldsymbol{u}_{n+1}$ can be be calculated using

$$\boldsymbol{u}_{n+1} = \boldsymbol{S}\boldsymbol{z}_{n+1} \tag{2}$$

Consequently, Equation 1 can now be written as,

$$\boldsymbol{q}_{n+1} = \boldsymbol{F}_d\left(\boldsymbol{S}\boldsymbol{z}_{n+1}, \boldsymbol{q}_n\right) \tag{3}$$

2.2. Gap closure

A grasp can be assessed through closure properties, namely form and force closures. While form closure would imply as many contact points as degrees of freedom, force closure would suggest lesser contact points, but maintaining the grasp through friction. While such properties can be analysed mathematically, see [2], a coarse way to differentiate between the two is that force closure is ensured through a better contact patch i.e., a tangential contact between the finger and object surfaces. The object to be grasped is described with the configuration $\boldsymbol{q}^O = \left[\boldsymbol{\varphi}^O, \boldsymbol{d}_1^O, \boldsymbol{d}_2^O, \boldsymbol{d}_3^O\right]$. The object surface depends on the configuration $\boldsymbol{q}^O$ and certain dimensions such as radius, length etc. We formulate a contact point $\boldsymbol{\rho}$, which is constrained to lie on the finger digit cylindrical surface. These are, in other words, defined in the digit coordinate system. To close the contact, we define contact closure functions $\boldsymbol{g}$ between the contact point $\boldsymbol{\rho}$ and the object surface, as shown in Figure 2 for a spherical object. For n_c such contact points, we can define an objective

$$J_1 = \sum_{i=1}^{n_c} (\boldsymbol{g}_i^T \boldsymbol{g}_i), \qquad \boldsymbol{g}_i = \boldsymbol{g}_i\left(\boldsymbol{q}, \boldsymbol{q}^O, \boldsymbol{\rho}_i\right) \tag{4}$$

The minimisation of J_1 Equation 4 will result in grasp closure with no requirement on relative positional orientation and may also result in partial penetrations. To improve

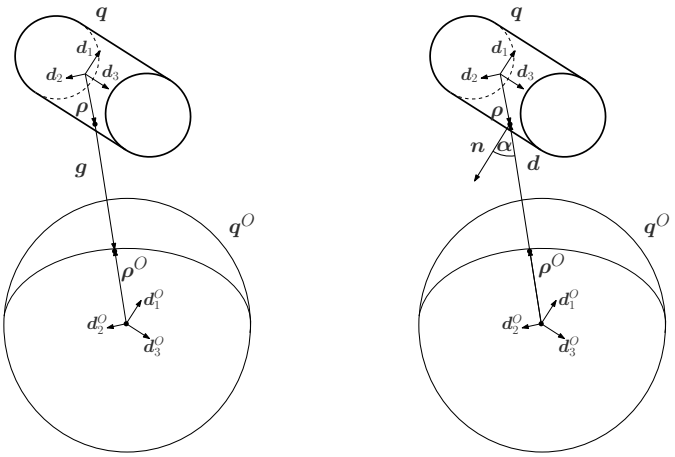

Figure 2. Left: the contact closure condition expressed in Equation 4. Right: the tangential contact condition expressed in Equation 5.

the contact, we calculate the cosine of the angle α between the shortest distance $\boldsymbol{d}$, between the contact point and the object centre, and the normal $\boldsymbol{n}$ to the finger surface at the contact point. Similar to the contact closure condition, we can write the tangential contact objective as,

$$J_2 = \sum_{i=1}^{n_c} \left(1 + \frac{\boldsymbol{d}_i^T \boldsymbol{n}_i}{|\boldsymbol{d}_i| \cdot |\boldsymbol{n}_i|} \right) \tag{5}$$

To achieve gap closure which may lead to proper force closure, it is essential to minimise both objectives J_1 and J_2. Note that, it will require a complete mathematical analysis to ascertain the force closure property of the generated grasps through minimisation and is beyond the scope of this contribution.

3. Results

We perform a two-fold analysis to determine the synergy effectiveness for grasping. Firstly, the grasping simulation is done for the complete hand model. In this model, we impose coordination between the finger interphalangeal joints and the metacarpophalangeal joints among the fingers through constraints, as described in [15]. Secondly, we perform grasping with the synergy based model, wherein the simulation is performed with a varying number of synergies. Assuming, we prescribe N time nodes for the optimisation, for n_z synergy optimisation variables, the number of variables reduces by $(26 - n_z) \cdot N$. The main goal here is to determine the minimum number of synergies that needs to be applied to obtain a good grasp in the sense of minimising J_1 or $J_1 + J_2$ objectives. The grasping simulation is performed for two grasps, namely the prismatic 2-finger grasp, i.e. grasping a cylinder, and the tripod grasp, i.e. grasping a sphere. Both grasps are performed with three contact points, one each on the distal phalanges of the thumb, index and middle fingers.

We implement our grasping simulation framework in the MATLAB environment, by optimising the objective $J = J_1$ or $J = J_1 + J_2$ subject to the kinematic path constraints,

specifically Equation 1 for the complete hand model and Equation 3 for the synergy based model. The optimisation is performed with the interior-point optimiser, IPOPT, see [13], with CasADi as a automatic differentiation tool, see [14].

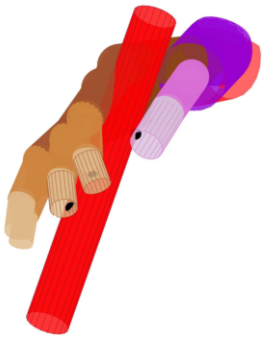

Figure 3. Synergy actuated model ($n_z = 15$) with prismatic 2-finger grasp, see [6], by minimising $J_1 + J_2$ objective. The contact points are shown with ($\bullet$) symbol.

For the prismatic 2-finger example, the resulting grasp posture is shown in Figure 3, with a model actuated through $n_z = 15$ synergies by minimising $J_1 + J_2$ objective. Though the contact is defined for the first three fingers only, we see a coordinated posture for the ring and little fingers as well. We can compare this posture with other models, as shown in Figure 4. In Figure 4 left, we present a grasp posture for a non-synergy actuated model by minimising $J_1 + J_2$ objective. Here, only the index and middle fingers are flexing to close the contact. The ring and little fingers show little flexion at the metacarpophalangeal and interphalangeal joints. In Figure 4 middle, the grasp posture is obtained by only minimising the J_1 objective for a synergy actuated model with $n_z = 15$, due to which we see clear penetration of the three distal phalanges. This posture illustrates the need of the tangential contact objective J_2. We also present the grasp posture obtained with a synergy actuated model with $n_z = 5$ synergies by minimising both $J_1 + J_2$ objectives in Figure 4 right.When comparing the different resulting grasp postures, we can clearly observe the variation in the placement of the contact points. In particular, the inclusion of the tangential contact objective leads to an increased contact area.

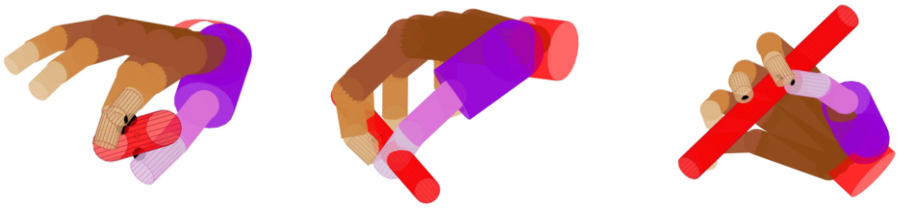

Figure 4. From left to right, we see the grasp posture for prismatic 2-finger grasp with (left) non-synergy actuated model while minimising $J_1 + J_2$ objectives, (middle) synergy actuated model with $n_z = 15$ synergies and only J_1 objective to be minimised and (right) synergy actuated model with $n_z = 5$ synergies while minimising $J_1 + J_2$ objectives. The contact points are shown with ($\bullet$) symbol.

The objective values for the synergy analysis is shown in Table 1. It can be observed that the objective value stays at the same order $\left(10^{-12}\right)$ when performing the grasp from 15 synergies to 5 synergies. The values, thereafter till 3 synergies, are still acceptable though higher than 10^{-12}. The optimiser could not obtain solutions with lesser number of synergies. It can be comfortably asserted that this grasping simulation can be performed with 5 synergies while minimising $J_1 + J_2$ objectives. However, when minimising only the J1 objective, we can see that it is possible to obtain gap closure from the last column in Table 1 even with a single synergy.

Table 1. Objective values for synergy actuated model with prismatic 2-finger grasp, see [6].

number of synergies	$J_1 + J_2$	J_1	J_2	only J_1
15	-6,06E-14	2,10E-12	-2,16E-12	1,46E-13
14	-2,87E-12	1,04E-12	-3,92E-12	7,01E-14
13	1,31E-11	2,41E-12	-1,55E-11	7,83E-14
12	-1,56E-12	2,23E-12	-3,79E-12	2,17E-13
11	2,00E-12	2,00E-12	-2,11E-15	1,70E-13
10	5,82E-10	2,92E-12	5,79E-10	2,21E-13
9	-1,67E-13	2,79E-12	-2,96E-12	3,01E-13
8	9,89E-12	9,96E-12	-7,04E-14	1,24E-13
7	-4,21E-12	2,91E-12	-7,12E-12	1,29E-13
6	4,63E-12	5,80E-12	-1,17E-12	1,02E-13
5	3,32E-12	6,09E-12	-2,77E-12	4,85E-13
4	8,64E-09	8,65E-09	-1,57E-11	2,40E-12
3	1,06E-05	1,06E-05	2,72E-10	1,29E-13
2				8,93E-14
1				1,18E-13

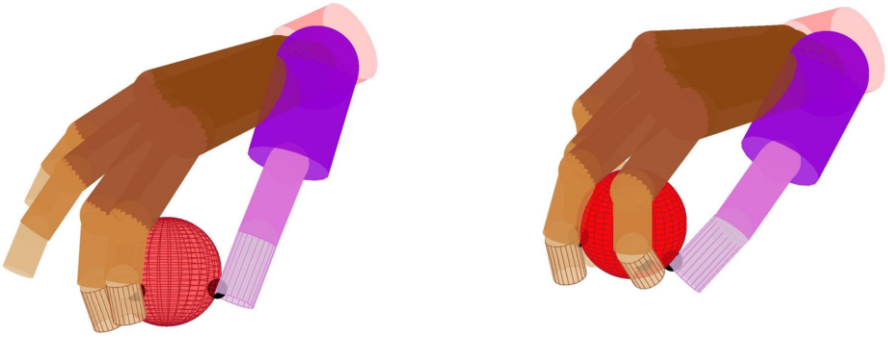

Figure 5. Synergy actuated model with tripod grasp, see [6], with $n_z = 15$ (left) and $n_z = 5$ synergies. The contact points are shown with (•) symbol.

For the tripod grasp we see a similar grasp performance when the model is actuated with $n_z = 15$ and $n_z = 5$ synergies in Figure 5, left and right respectively, while minimising $J_1 + J_2$ objective. With $n_z = 15$, the index and ring fingers are closer to each other as compared to the posture obtained with $n_z = 5$ synergies, which also lead to different contact points. The objective values retains a similar order $\left(10^{-11}\right)$ with even 3 syner-

gies, as seen in Table 2, exhibiting a substantial reduction in the number of actuated DoFs. Thereafter, it is still possible to obtain solutions with slightly higher objective values while using even a single synergy. As with the previous grasp, it is possible to obtain grasp postures while minimising only J_1 objective for all possible synergy combinations.

Table 2. Objective values for synergy actuated model with tripod grasp, see [6].

number of synergies	$J_1 + J_2$	J_1	J_2	only J_1
15	-2,80E-09	4,03E-13	-2,80E-09	4,13E-13
14	3,49E-13	3,53E-13	-3,77E-15	2,06E-12
13	-3,14E-12	4,79E-14	3,19E-12	1,32E-14
12	-7,05E-11	7,13E-14	-7,06E-11	3,75E-13
11	-1,49E-09	2,58E-13	-1,49E-09	4,76E-12
10	1,81E-12	1,84E-12	-3,20E-14	7,70E-17
9	-3,70E-11	2,98E-14	-3,70E-11	3,38E-13
8	3,35E-10	5,74E-14	3,35E-10	1,38E-12
7	-2,09E-11	1,14E-13	-2,10E-11	9,56E-12
6	2,46E-12	2,45E-12	1,11E-15	3,75E-11
5	-7,85E-11	2,02E-13	-7,87E-11	4,56E-13
4	-3,79E-11	8,45E-13	-3,87E-11	7,12E-13
3	-1,49E-11	1,54E-12	-1,64E-11	2,78E-22
2	1,01E-08	1,01E-08	1,18E-12	2,51E-10
1	2,15E-07	2,15E-07	4,68E-11	6,99E-13

4. Conclusion

We have demonstrated a kinematic grasping methodology with coordinated hand motion achieved through synergies. The grasping performance of the synergy based model has been compared with an independent joint model. The synergy analysis shows the possibility of a significant reduction in the number of independent joint angle DoFs. It also enables the formulation of synergistic actuation torques, as per [16]. This will result in a considerable reduction in problem size when the method is ported to optimal control simulations for grasping where the number of optimisation variables, i.e. DoFs and controls, are multiplied by the number of discrete time nodes. The method, however, is not free from certain drawbacks. In particular, the kinematic hand model is dependent on the description of the synergy matrix and hence is not readily subject to change. For example, the synergy matrix used in this work from *Syngrasp*, does not allow flexion motion for the ring and little finger CMC joints. Also, the thumb CMC joint is modelled as a universal joint in the synergy matrix. Thus, the thumb cannot perform the passive internal rotation motion as observed in human beings. Thus, to add more realism to the grasps, a kinematically appropriate synergy matrix must be used. As an outlook, we plan to include non-interpenetration constraints in our model for the optimal control. The grasps obtained therein will be analysed for force closure properties and their performance will be compared as per grasp quality metrics, as given in [17].

Acknowledgements

This work was supported by the Fraunhofer Internal Programs under Grant No. MAVO 828424.

References

[1] Bicchi A. On the problem of decomposing grasp and manipulation forces in multiple whole-limb manipulation. Robotics and Autonomous Systems. 1994 Jul 1;13(2):127-47.
[2] Prattichizzo, D., Trinkle, J. Grasping. Springer Handbook of Robotics 2008; 671–700.
[3] Buchholz B, Armstrong TJ. A kinematic model of the human hand to evaluate its prehensile capabilities. Journal of Biomechanics. 1992 Feb 1;25(2):149-62..
[4] Sancho-Bru JL, Mora MC, León BE, Pérez-González A, Iserte JL, Morales A. Grasp modelling with a biomechanical model of the hand. Computer methods in biomechanics and biomedical engineering. 2014 Mar 12;17(4):297-310.
[5] Napier JR. The prehensile movements of the human hand. The Journal of bone and joint surgery. British volume. 1956 Nov;38(4):902-13.
[6] Feix T, Romero J, Schmiedmayer HB, Dollar AM, Kragic D. The grasp taxonomy of human grasp types. IEEE Transactions on Human-Machine Systems. 2015 Sep 4;46(1):66-77.
[7] Leyendecker S, Ober-Blöbaum S, Marsden JE, Ortiz M. Discrete mechanics and optimal control for constrained systems. Optimal Control Applications and Methods. 2010 Nov;31(6):505-28.
[8] Phutane U, Roller M, Björkenstam S, Leyendecker S. Optimal Control Simulations of Two-Finger Precision Grasps. In Multibody Dynamics 2019, volume 53, pages 60–67, Cham, 2019. Springer International Publishing.
[9] The physiology of the joints. Volume I, Upper Limb. Second edition. By I. A. KAPANDJI, Paris. 11 x 9 in. Pp. 203, with 346 illustrations. 1970. Edinburgh: S. & E. Livingstone Ltd. 50s. Br J Surg, 57: 640-640.
[10] Santello M, Flanders M, Soechting JF. Postural hand synergies for tool use. Journal of Neuroscience. 1998 Dec 1;18(23):10105-15.
[11] Vinjamuri R, Patel V, Powell M, Mao ZH, Crone N. Candidates for synergies: linear discriminants versus principal components. Computational intelligence and neuroscience. 2014;2014.
[12] Malvezzi M, Gioioso G, Salvietti G, Prattichizzo D. Syngrasp: A matlab toolbox for underactuated and compliant hands. IEEE Robotics & Automation Magazine. 2015 Sep 4;22(4):52-68.
[13] Wächter A, Biegler LT. On the implementation of an interior-point filter line-search algorithm for large-scale nonlinear programming. Mathematical programming. 2006 Mar 1;106(1):25-57.
[14] Andersson JA, Gillis J, Horn G, Rawlings JB, Diehl M. CasADi: a software framework for nonlinear optimization and optimal control. Mathematical Programming Computation. 2019 Mar 14;11(1):1-36.
[15] Lee J, Kunii TL. Model-based analysis of hand posture. IEEE Computer Graphics and applications. 1995 Sep;15(5):77-86.
[16] Gabiccini M, Bicchi A, Prattichizzo D, Malvezzi M. On the role of hand synergies in the optimal choice of grasping forces. Autonomous Robots. 2011 Oct 1;31(2-3):235.
[17] Roa MA, Suárez R. Grasp quality measures: review and performance. Autonomous robots. 2015 Jan 1;38(1):65-88.

This page intentionally left blank

Part 4

Human-Product Interaction Modeling

This page intentionally left blank

DHM2020
L. Hanson et al. (Eds.)

© 2020 The authors and IOS Press.
This article is published online with Open Access by IOS Press and distributed under the terms of the Creative Commons Attribution Non-Commercial License 4.0 (CC BY-NC 4.0).
doi:10.3233/ATDE200028

Modelling Interaction Forces at a Curved Physical Human-Exoskeleton Interface

Divyaksh Subhash CHANDER [1] and Maria Pia CAVATORTA
Department of Mechanical and Aerospace Engineering, Politecnico di Torino, Corso Duca degli Abruzzi, 24, 10129 Torino, Italy

Abstract. In virtual modelling of exoskeletons, the human-exoskeleton interface is often simplified by modelling the interface forces at a single point instead of contact forces due to the straps or cuffs. In the past, force-generating elements (FGEs) have been used to predict ground reaction forces. However, unlike the ground, which is a planar surface, the human-exoskeleton interface presents curved surfaces. This work discusses the modifications required for using the FGEs for predicting the curved human-exoskeleton interface forces of a passive lower-limb exoskeleton, the Chairless Chair. A pressure mat was positioned at the human-exoskeleton interface to measure the area of contact and the centre of pressure (CoP) in three different sitting conditions. The strength of the FGEs was analysed in detail and its optimization based on the model outputs is discussed. The strength affects the model assistance and the CoP, and these outputs could be used to identify the optimal value of the strength. The strength of the FGEs affects the biomechanical outputs from the model also. Therefore, it is crucial to select the correct value of the strength. The results of this work would be useful for the detailed modelling of the human-exoskeleton interface.

Keywords. Human-Exoskeleton Interaction, Interface Forces, Curved Surface, Passive Exoskeleton, Musculoskeletal Model

1. Introduction

Virtual assessment of exoskeletons is often used during the design and redesign phase to optimize the exoskeleton. The level of assistance or the design of the exoskeleton could be optimized considering the end-user or the activity [1–3]. As the end-user of an exoskeleton is a human, biomechanical analysis plays a key role in assessing the exoskeleton. Virtual assessment of the exoskeleton through multibody dynamics is often used in the literature for biomechanical analysis. Such an assessment requires a model of the human, a model of the exoskeleton and an interaction model to connect the human and the exoskeleton models. Subsequently, a comparison is made between the with and without exoskeleton cases for the target activity.

Often in multibody dynamics, the interaction between the human and the exoskeleton is modelled through kinematic joints [1, 4, 5]. Rigid kinematic joints are used to fix the different attachment points of the exoskeleton to the corresponding points on the human model. Such joints constrain all the translational and rotational degrees of freedom and provide reaction forces and moments in these constraints. Another approach to model the interface forces between the human and the exoskeleton

[1] Corresponding Author, Email: chander.divyaksh@polito.it.

is to use force-generating elements (FGEs) to create reaction forces in the necessary constraints in the model [6]. However, both the approaches are not a realistic representation of the actual interface between the human and the exoskeleton. The human-exoskeleton interface usually consists of straps or moulded surfaces to fix the exoskeleton to the user and to provide support and assistance. The presence of straps or moulded surface leads to the generation of frictional forces. The straps must be closed tightly for generating enough frictional and normal forces to rigidly attach the exoskeleton to the user. Frictional forces are not accounted for by the kinematic joints or the FGEs (unless the FGEs are configured to). Not modelling friction at the interface could result in an unrealistic interaction force at the human-exoskeleton interface.

The FGEs could be configured to simulate contact forces, including frictional forces. Such an approach has been used extensively to predict ground reaction forces (GRFs) [7, 8]. Recently, this approach has also been used to predict reaction forces at the human-exoskeleton interface. The effect of the interface model on the biomechanical outputs was studied in [9] and it was observed that using the GRF prediction method at the human-exoskeleton interface resulted in a more reasonable trend of the knee moment compared to using a rigid kinematic joint at the interface. However, a limitation of the GRF prediction method, as far as the human-exoskeleton interface is concerned, is that the method is suitable for predicting contact forces at planar surfaces only, such as the ground. In the case of exoskeletons, the straps wrap around the body or the moulded surfaces are shaped according to the shape of the matching body part. Thus, the approach must be modified to predict contact forces at the human-exoskeleton interface.

The aim of this work is to modify the approach of the GRF prediction method to predict the contact forces at a curved human-exoskeleton interface. In this work, the modifications required to the existing method for planar surfaces will be discussed and indications would be provided for selecting the parameters of the modified method suitable for curved surfaces.

2. Method

This work builds on the existing work [9] that used the GRF prediction method to estimate the interface forces at the human-exoskeleton interface of a passive exoskeleton for the lower limbs, the Chairless Chair® (noonee AG, Switzerland). The exchange of forces was considered in a limited area of contact on the seat that was assumed planar in [9]. The curved surface of the seat prevented the use of the entire seated area for the exchange of forces by the GRF prediction method as the method is intended for planar surfaces, such as the ground. The current work aims to modify the approach of the GRF prediction method to estimate interface forces at curved surfaces so that the entire seated area of the Chairless Chair could be used for the exchange of forces at the human-exoskeleton interface.

The Chairless Chair consists of two mechanical legs that are loosely attached behind the user's legs. The exoskeleton allows the user to walk and as the user starts to sit, the exoskeleton legs touch the ground and bend at their central revolute joint. The exoskeleton legs block at a user-selected position and provide static support to the user in the seated posture, like a regular chair. The sitting height of the exoskeleton can be continuously adjusted between a minimum height, defined as the low-seat configuration, and a maximum height, defined as the high-seat configuration.

2.1. Experimental pressure maps

The human-exoskeleton interface was studied in three different sitting conditions: the low-seat, the high-seat, and the comfort-seat configuration, which is defined as the seat height selected by the user as the most comfortable. The different seat heights provided different seat inclinations and contact conditions, resulting in a changed seated posture and the support available from the exoskeleton. Previous studies have reported that the high seat configuration led to an increased tendency of slip [10, 11]. A pressure mat (PX200:20.40.05, XSensor) was placed on the exoskeleton seat for the right leg and recorded the human-exoskeleton interface pressure at 60 Hz. The pressure mat served to determine the area of contact at the interface and to compare the empirical and the virtual centre of pressure (CoP). The data of the pressure mat was mirrored about the sagittal plane for the left leg due to the symmetry of the posture. The pressure mat had a total of 800 cells arranged in an array of 40 x 20, with each cell having an area of 0.51 x 0.51 cm^2. The body weight distribution between the human and the exoskeleton was measured using a scale. A static resting posture was used across the conditions to avoid unnecessary variables in this study. The trials were done by a male subject (163.0 cm and 73.8 kg) who was trained in the use of the exoskeleton. As described in a prior study, the percentage of body weight supported by the exoskeleton was consistent among different users provided that they were trained in the use of the Chairless Chair [11]. The Chairless Chair was adjusted to the anthropometry of the user by setting both the lower and the upper half of the exoskeleton leg to their smallest lengths in these trials. After the subject assumed the seated posture and provided a verbal confirmation of feeling stable, data were recorded for at least three seconds in the static resting posture (Figure 1). For each test condition, three trials were done, and the data were averaged over the three trials.

2.2. Musculoskeletal modelling

A commercially available software, AnyBody Modelling Systems (AMS) (version 7.1.2, AnyBody Technology A/S, Denmark) was used to develop the model for the biomechanical analysis using the musculoskeletal human model available in the AnyBody Managed Model Repository version 2.1.1 [12]. The human model was scaled to the subject height and weight using length-mass-fat scaling law. AMS models human muscles as unidirectional FGEs and uses a multibody dynamics approach to analyse the musculoskeletal system. It uses inverse dynamics analysis to estimate the internal muscle and joint reaction forces given the external forces and motion data. As the body contains an excess of muscles than necessary to solve the dynamic equilibrium, the inverse dynamics analysis equations are framed as an optimisation problem to determine the muscle recruitment. In this work, the polynomial criterion with power 3 was used for the muscle recruitment problem [13].

A computer-aided design (CAD) model of the exoskeleton was created using SolidWorks® 2017 (Dassault Systèmes SOLIDWORKS Corporation) and translated into an AMS compatible script file using the AnyExp4SOLIDWORKS® plugin (version 1.1.0, AnyBody Technology A/S, Denmark). The central revolute joint between the upper and the lower half of the exoskeleton was defined to produce all the reaction forces and moments necessary to support the user in the seated posture.

A static model of the trials was developed with the human and the exoskeleton models positioned according to the experimentally observed postures and positions

(Figure 1). GRFs at the human foot and the exoskeleton base were estimated in the model as described in [9], using the method reported in [8], by creating virtual force plates (VFPs) in the model.

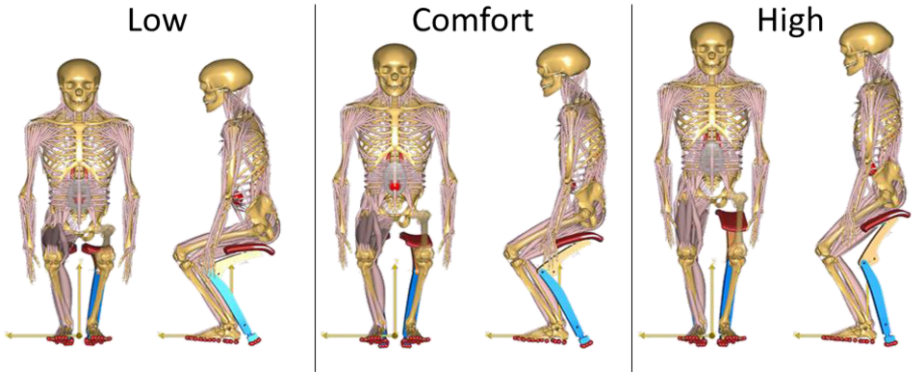

Figure 1. Virtual models of the low, comfort and high seat. Muscles of the left leg are hidden.

2.3. Human-exoskeleton interaction forces

The human-exoskeleton interaction forces were estimated by modifying the approach of GRF prediction method to predict reaction forces at the human-exoskeleton interface, which usually consists of a curved surface. Instead of using a single VFP with multiple contact nodes, multiple VFPs were distributed over the surface of the exoskeleton seat. Each VFP was positioned tangentially at its centre to the seat surface and consisted of a single contact node positioned correspondingly on the human model to ensure contact. The orientation of the VFP determined the normal and shear directions. The approach of using multiple VFPs has been used previously in [14] for predicting GRFs.

The presence of multiple VFPs allowed not just a more realistic representation of the curved surface but also allowed individual control of these VFPs. This was especially needed for the Chairless Chair, where different sitting heights resulted in different areas of contact. Thus, the empirically observed area of contact was used as an input in the model. The model also consisted of an array of 40 (rows) x 20 (columns) VFPs, each corresponding to the individual cell of the pressure mat. The VFP was inactive if the pressure mat reading of the corresponding cell was zero.

At each contact node, five artificial muscles were created and configured to produce the contact forces just as in the GRF prediction method [8]. The contact forces from the individual VFPs were processed to obtain the location of the centre of pressure (CoP) relative to the seat surface. Whereas the percentage of body weight supported by the exoskeleton was calculated as the difference between the subject weight and the weight supported by the legs of the subject.

A key parameter of these artificial contact muscles is the strength of the muscles or the maximum force that these contact muscles can produce. In [14], the maximum force was selected based on a parametric study. Similarly, a parametric study was performed in this work as well. Figure 2 shows the empirical pressure maps for the left leg and the corresponding virtual pressure maps for different values of the strength (S_0) of the artificial contact muscles. The first (top) and the last (bottom) row of the pressure maps correspond to the back and the front edges of the seat. It can be observed that high values of the strength resulted in an uneven utilization of the surface of the

seat. The solver found the exchange of the interaction forces at the rear of the exoskeleton seat to be biomechanically advantageous, such that at S_0 = 150 N, most of the seat surface was left unutilized. Consequently, the pressure in the limited area of contact far exceeded the pressure threshold of 2 N/cm^2 for discomfort [15]. On the other hand, at low values of strength, a greater surface of the exoskeleton seat was used for the interaction forces, nonetheless, with a preference for the rear portion of the exoskeleton seat for the exchange of forces.

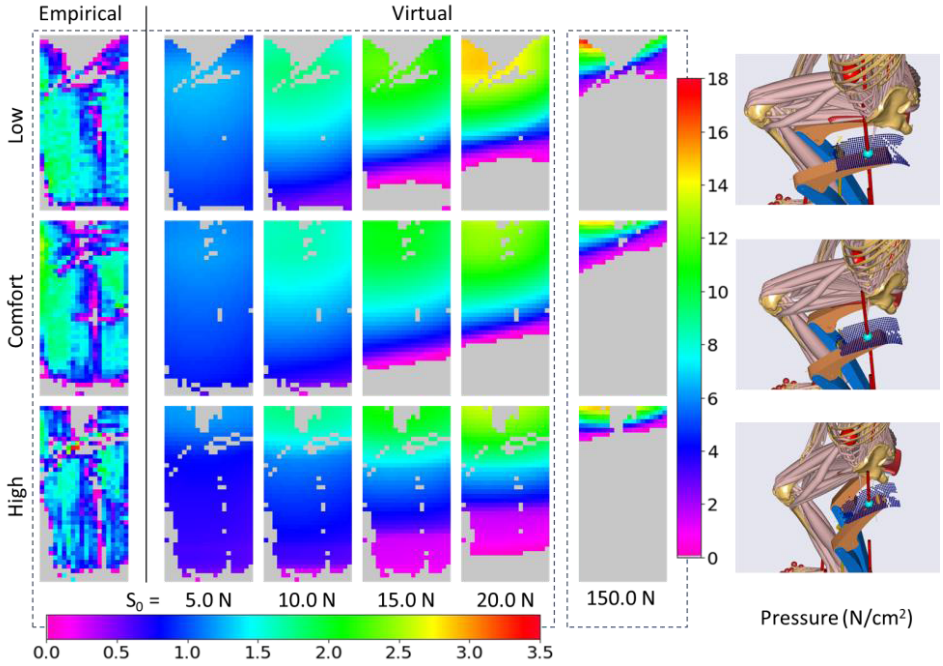

Figure 2. Empirical and virtual pressure maps for the left leg. S_0 is the strength of the contact muscles.

The preference of the solver for utilizing the rear portion of the seat to support the subject was manually offset. The strength of the artificial contact muscles at the rear of the seat was reduced relative to the front of the seat. The row of the VFP determined its position along the length of the seat. The strength of the artificial contact muscles at each VFP was given as:

$$S_{ij} = \begin{cases} 0.0 & \text{if } P_{ij} = 0.0 \\ S_0 \text{ x } [c_1 + (i\text{-}1) \text{ x } (c_2 - c_1)/39] & \text{if } P_{ij} > 0.0 \end{cases} \quad (1)$$

Where,

S_{ij} is the strength of the contact muscles at the i^{th} row and j^{th} column.

P_{ij} is the recorded pressure of the cell at the i^{th} row and j^{th} column.

S_0 is a constant factor for multiplying the strength.

c_1 and c_2 are constants for controlling the linear gradient of strength.

i is the row number.

Thus, strength at the first row (i = 1) was S_0 x c_1, while the strength at the last row (i = 40) was S_0 x c_2.

3. Results and discussion

This work aimed to model the human-exoskeleton interface forces for a curved surface, study the model parameters in detail, and identify strategies to select these parameters. This section discusses the results of the change in the strength of the contact muscles and its effect on the interaction forces and the biomechanical outputs.

3.1. Interaction forces

Figure 3 plots the percentage of body weight supported by the exoskeleton and the centre of pressure (CoP) for different values of the strength of the contact muscles, along with the empirically observed values. The position of the CoP was measured from the front edge of the seat along the length of the seat. The length of the seat is 20.5 cm. Only the front-rear location of the CoP is plotted. The location of the CoP along the seat width was not significantly affected by the strength of the artificial contact muscles and matched well with the empirically observed values. The figure shows various values of strength (defined by S_0 and indicated in the callouts in the figure) as well as the different gradients (defined by c_1 and c_2) of the strength of the contact muscles, including the constant strength without any gradient ($c_1 = c_2 = 1$).

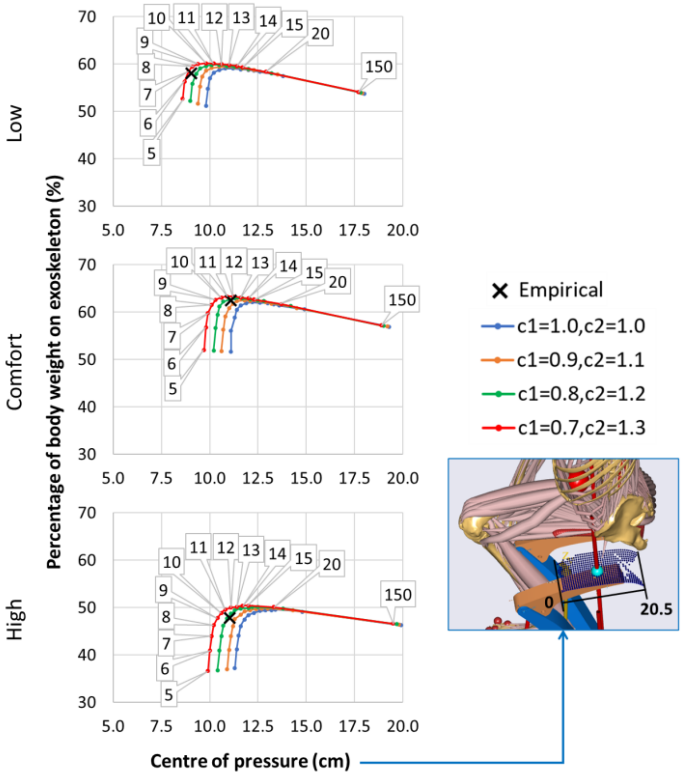

Figure 3. Exoskeleton support and the centre of pressure for different strength and gradient of the contact muscles.

An important observation is the shape of the curves in Figure 3. The curves have a similar shape for all the seat heights as well as for different gradients. It can be

observed that the exoskeleton could not provide adequate support to the user at low values of the strength of the contact muscles. Increasing the strength resulted in a uniform increase of support throughout the seat surface such that the CoP did not change until the vertex of the curve was reached. Once the vertex was reached, increasing the strength further did not increase the support provided by the exoskeleton. Instead, it resulted in a rearward shift of the CoP. The rearward shifting of the CoP could be linked to the observation made in Section 2.3 that the front part of the seat remained unutilized if the strength was large enough to allow it. Thus, the shape of the curves of Figure 3 indicates that an optimum value of strength exists around the vertex of the curve. This optimal zone of the strength should allow the required exchange of interface forces at a reasonable CoP. Figure 3 also shows that the gradient in strength resulted in an offset in the CoP location towards the front part of the seat. Higher the gradient, greater the offset. The gradient increased the strength of the contact muscles in the front of the seat relative to the rear part, resulting in a forward shift of the CoP.

The observations of Figure 3 could be compared with the approach used in [14] for selecting the maximum force of the FGEs. The authors of [14] performed a parametric study and selected the lowest value of the maximum force of the FGEs at which the GRF converged for the rest of their analyses. Similar to the observations of Figure 3, the GRF was inadequate at low values of the maximum force of the FGEs, while increasing the maximum force beyond the threshold for adequate GRF did not increase the GRF further.

3.2. Biomechanical outputs

The human-exoskeleton interface is a crucial component in the analysis of the exoskeletons. The interface forces determine the assistance received by the user and can affect the biomechanical analysis. Figure 4 plots the moments at the knee and the ankle, and the activation of the vastus lateralis and gastrocnemius muscles for different strengths of the contact muscles. The figure shows that the biomechanical outputs depend on the strength of the artificial contact muscles. At values of strength lower than the optimal zone, inadequate support was available from the exoskeleton (Figure 3), and thus a greater knee extension moment was required from the user. On the other hand, high values of the strength led to an underestimation of the knee moment. At values of the strength greater than the optimal zone, the support received by the user reduced slightly, however, the CoP shifted rearwards unrealistically, resulting in a higher overall external extension moment at the knee, and thereby reducing the demand from the user. Similarly, effects on the ankle plantarflexion moment can be observed. The changes in the joint moments were also supported by the changes in the muscular effort. The activation of vastus lateralis, a knee extensor was reduced as the knee moment requirement reduced due to the increased strength of the contact muscles. Whereas the activation of the gastrocnemius increased as the plantarflexion moment at the ankle increased due to the increase in the strength of the artificial contact muscles.

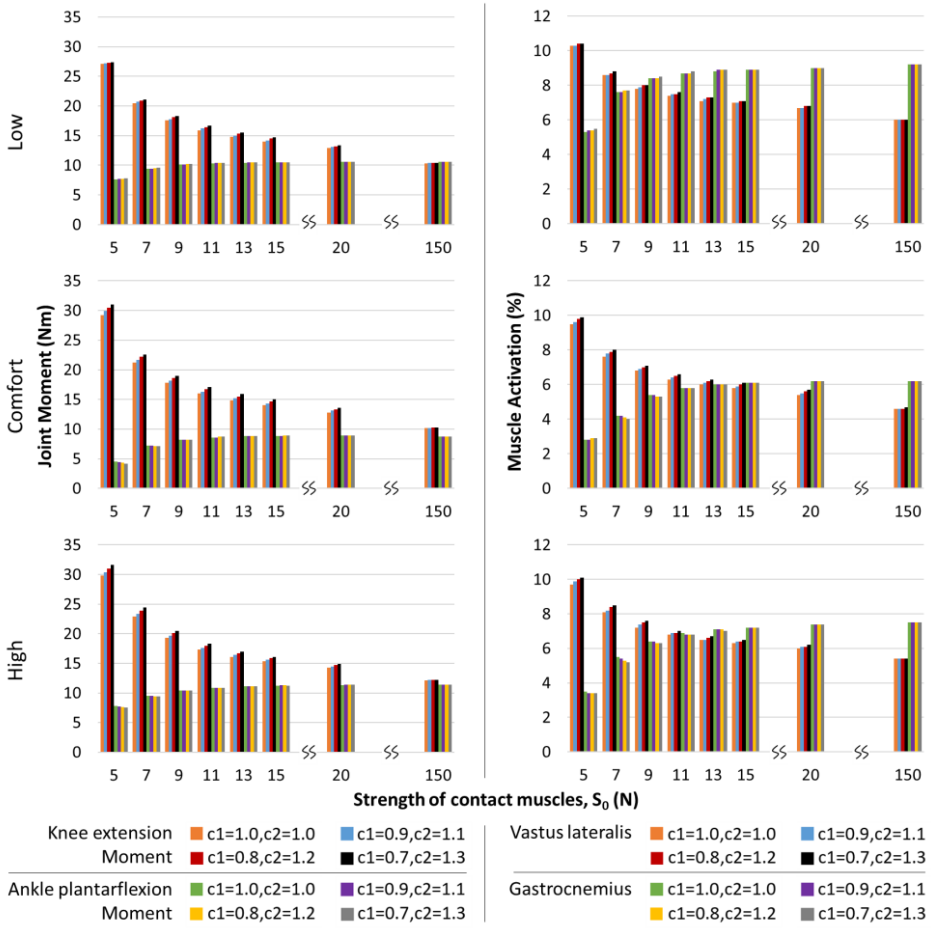

Figure 4. Joint moment and muscle activation for different strength and gradient of the contact muscles.

Figure 4 also shows a marginal effect of the strength gradient on the biomechanical outputs. For the same value of the strength (S_0) of the contact muscles, a slight variation in the biomechanical outputs was seen due to the gradient in the strength. The CoP for the gradient $c_1 = 0.8$, $c_2 = 1.2$ resulted closest to the empirically observed CoP (Figure 3). The difference in the CoP due to the strength gradient was less than 1.0 cm in the zone of optimal strength value compared to the CoP for no strength gradient. 1.0 cm is 2.7% of 37.1 cm, which is the length of the thigh of the mannequin. It is likely that this small offset in the CoP due to the strength gradient causes a small and less significant effect on the biomechanical outputs than that due to the absolute value of the strength of the contact muscles.

The model is unable to account for the deformation of the soft tissue or the seat compression and is unable to provide a realistic distribution of pressure. However, the amount of external force and its point of application are significant details in multibody analysis and can influence the biomechanical outputs as seen in this work. Thus, it is critical to pay attention to the strength of the artificial muscles introduced in this approach of distributed VFPs to simulate the human-exoskeleton interface forces.

3.3. Application to other exoskeletons

This work presented a modified approach of the GRF prediction method to estimate the human-exoskeleton interface forces at a curved surface. This approach was applied to the Chairless Chair at three different seat heights that resulted in different inclinations of the seat, different contact conditions, and different support received by the user. In this section, some considerations are discussed for applying this modelling approach to other exoskeletons.

Empirical data from the pressure mat were used as an input in the model. The contact area was used to determine the VFPs that had to be deactivated. However, this problem of determining the area of contact is also specific to the Chairless Chair as the seat is loosely attached to the user to allow different sitting heights. The area of contact, especially in the upper portion of the seat, changes with the sitting height (Figure 2). In the case of other exoskeletons, often, the human-exoskeleton interface is firmly secured using straps. In such a case it could be reasonable to assume that the entire surface area of the human-exoskeleton interface is in contact. Secondly, this work used the pressure maps to justify the use of the gradient of the strength of the contact muscles and identify the optimal gradient values. However, when no experimental data is available, the results without the strength gradient could be reasonably reliable as shown in this work. Identification of the correct strength would be a more critical factor for the analysis than the finer refinement allowed by the strength gradient.

The pressure maps highlight an important aspect of the model regarding the optimal strength of the contact muscles. Besides the convergence of the interface force, the muscle activation of the contact muscles could also be relevant. The solver cannot differentiate between the physiological and contact muscles in the optimization problem to determine the muscle forces. Low strength of the contact muscles could result in highly activated contact muscles to provide the interface forces. If the activation of the contact muscles is comparable to that of the physiological muscles, the solver might recruit some under-activated physiological muscles to unload the contact muscles. On the other hand, high strength of the contact muscles, far beyond the optimal zone, can result in the solver "exploiting" the contact muscles to reduce the biomechanical load unrealistically as seen in Figure 2 and Figure 4. Thus, it is important to find a strength of the contact muscles that is neither too high nor too low, as is also mentioned in [6]. In this study, a maximum activation of 1.5% was seen for the artificial contact muscles at strength S_0 = 5.0 N, and it reduced as S_0 was increased.

There could also be other unknowns when applying this approach to another exoskeleton, such as the behaviour of the model in dynamic activities. Depending on the phase of the movement, the model might show an unrealistic preference towards either side of the interface. In such a case, it could be desirable to taper down the strength of the artificial contact muscles on both the sides of the interface. Also, additional functions of the gradient could be explored. Further, as the strength is optimized based on the assistance received by the user, if the exoskeleton offers various assistance levels, the optimal strength could be different for each assistance level. Analogously, in this study, a subject with a substantially different body weight would require a different strength value for the Chairless Chair to support about 60% of the body weight as in the low and comfort-seat heights. A similar adjustment for the GRF estimation of obese subjects was also suggested in [14].

In conclusion, this work presented an approach to model the interaction forces at the human-exoskeleton interface. The advantage of this approach over other methods is

its ability to simulate contact forces over curved surfaces, which are typical in human-exoskeleton interfaces. On the other hand, the application of this approach requires greater attention to the model parameter than for other approaches as the model parameter can significantly affect the biomechanical outputs. It is recommended to start with a coarse grid of VFPs on the interface and make a parametric study of the strength of the artificial contact muscles without any gradient and subsequently proceed towards refining and identifying an optimal value of the strength of the contact muscles.

References

[1] Agarwal P, Neptune RR, Deshpande AD. A Simulation Framework for Virtual Prototyping of Robotic Exoskeletons. J Biomech Eng, 2016, 138(6), 061004.
[2] Jensen EF, Raunsbæk J, Lund JN, Rahman T, Rasmussen J, Castro MN. Development and simulation of a passive upper extremity orthosis for amyoplasia. J Rehabil Assist Technol Eng, 2018, 5, 1–10.
[3] Zhou L, Li Y, Bai S. A human-centered design optimization approach for robotic exoskeletons through biomechanical simulation. Rob Auton Syst, 2017, 91, 337–347.
[4] Gordon DFN, Henderson G, Vijayakumar S. Effectively Quantifying the Performance of Lower-Limb Exoskeletons Over a Range of Walking Conditions. Front Robot AI, 2018, 1–16.
[5] Harant M, Sreenivasa M, Millard M, Sarabon N, Mombaur K. Parameter optimization for passive spinal exoskeletons based on experimental data and optimal control. IEEE-RAS Int Conf Humanoid Robot, 2017, 535–540.
[6] Fournier BN, Lemaire ED, Smith AJJ, Doumit M. Modeling and Simulation of a Lower Extremity Powered Exoskeleton. IEEE Trans Neural Syst Rehabil Eng IEEE, 2018, 26(8), 1596–1603.
[7] Fluit R, Andersen MS, Kolk S, Verdonschot N, Koopman HFJM. Prediction of ground reaction forces and moments during various activities of daily living. J Biomech Elsevier, 2014, 47(10), 2321–2329.
[8] Skals S, Jung MK, Damsgaard M, Andersen MS. Prediction of ground reaction forces and moments during sports-related movements. Multibody Syst Dyn Springer Science+Business Media Dordrecht, 2017, 39(3), 175–195.
[9] Chander DS, Cavatorta MP. Modelling friction at the mechanical interface between the human and the exoskeleton. Int J Hum Factors Model Simul, 2019, 7(2), 119–136.
[10] Luger T, Cobb TJ, Seibt R, Rieger MA, Steinhilber B. Subjective Evaluation of a Passive Lower-Limb Industrial Exoskeleton Used During simulated Assembly. IISE Trans Occup Ergon Hum Factors Taylor & Francis, 2019, 7(3–4), 175–184.
[11] Spada S, Ghibaudo L, Carnazzo C, Pardo M Di, Chander DS, Gastaldi L, Cavatorta MP. Physical and Virtual Assessment of a Passive Exoskeleton. In: Proceedings of the 20th Congress of the International Ergonomics Association (IEA 2018), Springer International Publishing, Cham, 2019.
[12] Lund ME, Tørholm S, Jung M. The AnyBody Managed Model Repository (AMMR) (Version 2.1.1), 2018.
[13] Damsgaard M, Rasmussen J, Christensen ST, Surma E, Zee M de. Analysis of musculoskeletal systems in the AnyBody Modeling System. Simul Model Pract Theory, 2006, 14(8), 1100–1111.
[14] Jung Y, Jung M, Lee K, Koo S. Ground reaction force estimation using an insole-type pressure mat and joint kinematics during walking. J Biomech Elsevier, 2014, 47(11), 2693–2699.
[15] Zenk R, Mergl C, Hartung J, Sabbah O, Bubb H. Objectifying the Comfort of Car Seats. SAE Technical Paper 2006[Online], SAE International, 2006.

DHM2020
L. Hanson et al. (Eds.)

© 2020 The authors and IOS Press.
This article is published online with Open Access by IOS Press and distributed under the terms of the Creative Commons Attribution Non-Commercial License 4.0 (CC BY-NC 4.0).
doi:10.3233/ATDE200029

Calibration Approach for Muscle Activated Human Models in Pre-Crash Maneuvers with a Driver-in-the-Loop Simulator

Fabian KEMPTER, Florian BECHLER and Jörg FEHR[1]
University of Stuttgart, Institute of Engineering and Computational Mechanics, Pfaffenwaldring 9, 70569 Stuttgart, Germany

Abstract. Active human body models (AHBM) are essential engineering tools to provide further biomechanical knowledge. For example, to predict injury risks and kinematic behaviour in a wide range of possible scenarios such as low-g and multiaxial loading scenarios where muscle activity has shown to affect head and neck kinematics. The validation of the AHBM, in particular, the tuning and selection of an appropriate control strategy is a significant challenge. There are two main contributions of this paper. First, a Driver-in-the-Loop (DiL) simulator, used for reproducible and safe data acquisitions of human behaviour, is presented. Second, subject-specific control parameter identification to replicate the unique behaviour of each subject by using a modular calibration approach. The DiL setup is modelled in Madymo using the active human model (AHM) as a representation of the human. The Matlab/Simulink interface of Madymo is extended to implement in Matlab two new individual muscle control strategies for the head-neck region of the AHM; (i) PD controllers based on the muscle length – motivated by the equilibrium point control theory and (ii) the in-vivo stretch reflex – based on the strain measuring capabilities of the muscle spindles. Any optimization procedure available in Matlab, i.e. a particle swarm optimizer, can be used to calibrate the control parameters to achieve a good agreement between DiL measurement data and the simulation output. Finally, this modular workflow is used to identify two subject-specific sets of control parameters. These subject-specific parameters play an important role in a robust representation of human occupants.

Keywords. Active Human Body Models, Pre-Crash, Muscle Activation, Subject-Specific Calibration

1. Introduction

Traditional crash test dummy models fail to represent the dynamic behaviour of humans in integral safety concepts. Therefore, digital human models suited for the dynamic analysis of safety and comfort are becoming more critical.

For instance, realistic predicted kinematic behaviour influences the injury risk assessment in pre-crash manoeuvers. Essential in these investigations is the consideration of the active behaviour of the occupants. In [1] an overview of existing active human body models (AHBM) in the field of vehicle safety with the corresponding muscle control approach is provided. For the validation and calibration of these models, volunteer tests need to be performed and evaluated. The active control intervention and

[1] Corresponding Author, Email: joerg.fehr@itm.uni-stuttgart.de.

the chosen passive characteristics need to match real human behaviour for valid kinematic predictions. The improvements in passive properties of AHBM are not part of this work. The focus is on muscle controller parameterization, which defines the control intervention. Due to the variation in human behaviour which is pervasive in volunteer tests [2, 3] and real-world traffic, there is no characteristic controller setup which is representative of all This distribution of individual human reaction types is considered relevant to predict realistic occupants' kinematics in events of moderate acceleration values. These Pre-Crash movements of the occupants affect their injury risks and need to be accounted for in the development of future mobility solutions, where each individual is protected as best as possible.

In standard parameter identification and validation approaches, the experimental results are often averaged. Afterwards, parameter identification for the mean trajectory is performed. Nevertheless, for at least some volunteer tests the observed variance in the experimental results cannot be sufficiently modelled by a mean trajectory in addition with a variance of the identified mean parameter values, as the subject show different motion patterns. Therefore, averaging the experimental results before the identification process is debatable. In the worst-case, such an approach isn't even representative for any of the subjects.

In our approach, we try to find parameters for each individual in a first step and process the identified parameters afterwards. These individual results could be clustered to gain a set of representative controller parameterizations for different groups of human with similar characteristics, for example, level of consciousness or the individual motion strategy. Additionally, the variability of the experimental results inside the clusters can be replicated by using fuzzy valued parameters [4] instead of nominal parameter sets. In case of large data sets also information about the likelihood of parameter ranges can be considered. The behaviour of each individual itself is not the goal of our research but a first necessary step towards a more representative parameterization of AHBMs.

Current implementations of muscle controllers mainly focus on PD controllers based on joint angles in combination with spatial tuning patterns gained from experimental results, e.g. [5], – mapping angular deviations into appropriate muscle activation to decrease the control error, e.g. [1, 6]. These spatial tuning approaches need quite large input data to ensure adequate muscle activation based on angle deviations and the current posture. Alternative approaches on muscle level, like reflex control [7] or equilibrium point control [8, 9] could be beneficial in non-nominal postures because there is no need to adapt and identify spatial tuning patterns for a large variety of individual postures.

Therefore, the main contribution of this work is to present a workflow which allows the identification of individual muscle controller parameter for each individual subject. In Section 2.1, a Driver-in-the Loop setup is presented, which is used to gain the necessary experimental data for muscle parameter identification in a reproducible and safe way. In Section 2.2, the simulation setup in Madymo which emulates the experiments is presented. Afterwards, it is motivated why only a head-neck submodel is used in the identification procedure. A modular structure enabled by the Madymo coupling with Matlab/Simulink is used to parametrize and optimize the muscle level controller, which makes the workflow very flexible. The clear separation into subtasks, i.e. dynamic simulation in Madymo, muscle controller in Simulink and optimization in Matlab, increases the usability. In Section 3 Results, the experimental results of a braking scenario presented in [10] are used to calibrate the two different individual muscle neck controller. The PD control strategy and the reflex control strategy is compared. The suitability of the muscle controller definitions and the performance of the calibration

approach is investigated. The paper finishes in Section 4 with a conclusion and an outlook.

2. Methods

The methods of this contribution are subdivided into three parts. i) Obtaining experimental results using a dynamical Driver-in-the-Loop simulator, ii) modelling the experimental setup in the simulation, including muscle controller and iii) optimizing the muscle controller parameters with a submodel for computational efficiency. This work combines the following software tools to a modularised workflow. The multi-body simulation performed in Madymo is separated from muscle controller modelling and parameter calibration/identification both performed in Matlab/Simulink. Furthermore, Madymo is controlled and evaluated with a Matlab-Madymo interface routine. This allows the simple adaptation of the muscle controller of each of the 136 muscle separately in Matlab/Simulink without the need of changing any input files of Madymo during the calibration/identification process.

2.1. Driver-in-the-Loop Simulator Experiments

The approach of using a DiL-simulator instead of traditional sled tests or real-car experiments possesses the following features: (i) a safe and reproducible environment, (ii) kinematic feedback in all six degrees of freedom, (iii) unconventional trajectories with superposed rotations to emulate translational accelerations, (iv) visual feedback of a virtual driving environment, e.g. by using head-mounted displays, (v) excellent accessibility for measurements and, (vi) fast application and testing of early alert systems. The whole setup is depicted in **Figure 4**. It consists of a 6-DOF motion platform, a force-feedback wheel and a bass-shaker at the back of the driving seat. The software implementation is based on a Matlab-Simulink-model, initially generated in Simcenter Prescan.

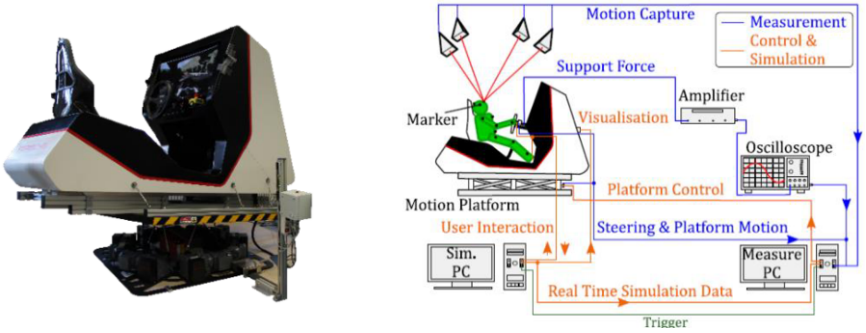

Figure 1. Driver-in-the-Loop simulator (left) with internal and external signal flow for simulation and experimental data acquisition.

Measurements. To analyze the driver's behaviour in the simulator during Pre-Crash situations, the kinematics, as well as muscle activation, can be monitored. The subjects and the simulator platform are tracked by a motion capture system Optitrack Prime with four Prime13W cameras using computer stereo vision with reflective infrared markers. Muscle activation measures are performed for the neck muscles sternocleidomastoid and

trapezius using surface electromyographics [10]. Additional sensors can be applied easily using the interfaces in the Simulink model of the DiL simulation. For example, a force sensor mounted at the steering wheel allows measuring the support of the driver applied on the steering wheel [10]. This force can be considered as an indication of the amount and timing of pre-stressing in an emergency braking situation. Additionally, it affects the T1 motion and lead to head displacements. All measures are synchronized using udp or TCP/IP network communication.

Platform motion. The motion of the platform is calculated based on the state of the virtual vehicle model using motion cueing algorithms to emulate virtual vehicle accelerations [11]. Instead of performing a pure translational trajectory, in this setup, a combined translational and rotational excitation is used to emulate the vehicle accelerations. The longitudinal platform motion is extended by a superposed pitch motion **(Figure 2)**.

2.2. Modelling of the Experiments

A simulation setup of the DiL-simulator is modelled with the multibody simulation software Madymo to enable the calibration of human models with the experimental results gained in the simulator. This simulation setup is based on the default Madymo application model of a car interior with an active occupant model under gravitation of 9.81 m/s^2. The occupant is represented by the active human body model of a 50-percentile male human (1.74 m, 75.7 kg). The trajectories performed by the platform in the experiment are applied in the simulation using an ideal joint between interior parts and the inertial frame at the identical location as the platform rotational centre in the experiment, see Figure 3. First, the model needs to be initialised, with a settling run. From this settling run, a constant stimulation set $Stim_{\text{init}}$ is gained, which ensures a stable posture under gravitational load. This stimulation values $Stim_{\text{init,}}$ from the settling run, will be used in all the simulations of this paper. In a subsequent simulation, the model is run with Madymo default head neck controller with the parameters (headRef = 1, reaction time = 100 ms, no co-contraction and no arm bracing). The simulation run with the full model is only performed to extract the T1 motion of the model, to enable a submodel simulation with a head-neck model, described in the following section. In the field of vehicle safety, a common approach is to investigate submodels instead of the whole human model to decrease computational cost, the number of parameters, the complexity of the simulation model and to separate effects. For studying human neck control, for instance, it can be useful to neglect the influence of changes in neck control on the upper body motion and fix the T1 motion to experimental results [1, 12, 13] or to the values gained in simulations of the whole human model with default parameterizations **(Figure 3)**. The HN-model is only applicable to identify neck controller parameters with a given T1 trajectory. Aspects influencing T1 trajectory need to be investigated separately, e.g. effects of boundary conditions or arm bracing against the steering wheel. In case of distinct arm bracing behaviour in the experimental results, the T1 trajectory of the full model needs to be reconciled before using it as an input of the HN-submodel simulations. As we aim for a separate calibration process for each subject, the reduction of computational cost of the full model (computation time 21 min 37 s) is important and can be reduced by over five times (4 min 8 s) by using a Head-Neck (HN) submodel. All the presented simulations were performed on Linux with Madymo R7.7 and Matlab/Simulink R2019b on a 12 core Intel i7-8700 processor with 3.20 GHz and 64 GB RAM.

2.2.1. Head Neck model with muscle control in Matlab/Simulink

To increase computational efficiency and to allow larger optimization runs, an extracted HN-model is derived based on the default AHBM. Muscle insertion points, which are used to be part of the upper body, are fixed to T1. The trajectory of T1 obtained in the nominal AHBM is used in the HN-model as kinematic excitation $\boldsymbol{r}_{\mathrm{T1}}^{\mathrm{HN}} := \boldsymbol{r}_{\mathrm{T1}}^{\mathrm{full}}$ (**Figure 3**). In this phase of the investigations, the influence of changes in the neck controller parameterization on the upper body motion will be neglected. In this contribution, we want to focus on muscle level controller and their suitability in reflex-based scenarios with superposed rotations. The Madymo-Simulink coupling [14] is used to allow an easier muscle controller modelling for the 136 individual muscles.

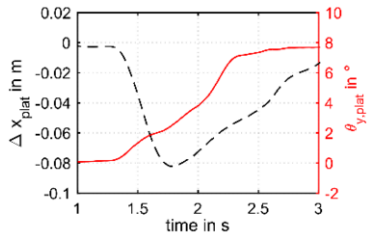

Figure 2. Platform motion longitudinal (black, dashed) and rotational (red) displacement in the braking scenario.

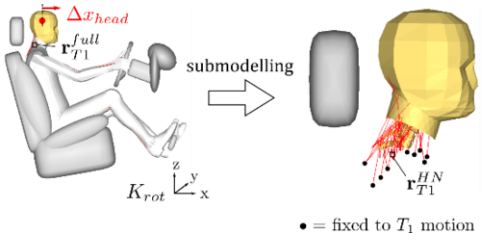

Figure 3. Madymo application model with rotational centre K_{rot} used to apply rotational and translational trajectories (left). Derived simplified HN- model with headrest and applied T1-trajectory r_{T1} (right).

While the muscle controller can be modelled more freely and intuitive in Matlab/Simulink, providing the mapping of muscle length and muscle activation signals, the dynamical simulation is performed inside the Madymo software without the need of any further adaptions during the calibration process. An overview of the Simulink structure is shown in Figure 4 exemplary for the reflex controller implementation. It consists of three main components: 1) the Madymo model with input/output definitions to Simulink, 2) the muscle controller serving the neural excitation $Stim$ at each time step based on the muscle length of the corresponding muscle element, 3) muscle activation dynamics which provides the muscle activation a based on previous activation value and neural excitation $Stim$ of the controller.

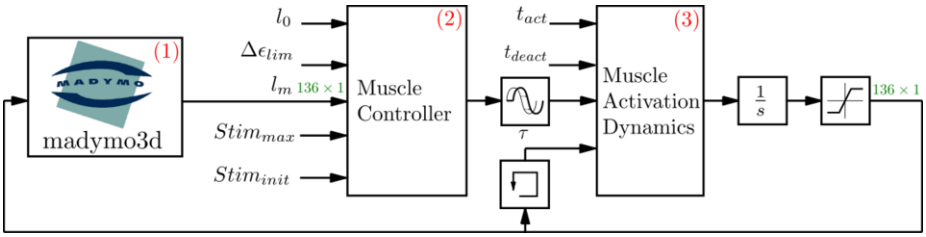

Figure 4. Structure of the Madymo-Simulink coupling: 1) Madymo transfer block with muscle activation signals a ϵ $\mathbb{R}^{136\times1}$ as input and resultant muscle lengths at current time step l ϵ $\mathbb{R}^{136\times1}$ as output, 2) muscle controller and 3) muscle activation dynamics.

2.2.2. Muscle Controller

In the following two muscle controller implementations are considered i) reflex controller and ii) PD controller both working only on the muscle length.

The muscle controller calculates stimulation values $Stim_i = f\left(l_i, \dot{l}_i, Stim_{\mathrm{init},i}, p\right)$ of muscle i is a function of its length conditions, initial constant stimulation value $Stim_{\mathrm{init},i}$ resulting from the Madymo settling run, and controller specific options p. Next, the two investigated controller definitions are described.

Reflex Controller. The reflex controller is modelled by the following relation between muscle length and muscle stimulation

$$Stim_{\mathrm{reflex,i}} = \begin{Bmatrix} Stim_{\max} & for\ \epsilon_i > \Delta\epsilon_{\lim} \\ Stim_{\mathrm{init},i} & else \end{Bmatrix} \text{ with } \epsilon_i = \frac{l_{\mathrm{m},i}(t-\tau)-l_{0,i}}{l_{0,i}},$$

where ϵ_i represents the strain of the muscle, τ the delay and $\Delta\epsilon_{\lim}$ the strain threshold. In case of no or moderate muscle strains $\epsilon_{\mathrm{i}} < \Delta\epsilon_{\lim}$ the muscle controller is inactive and outputs the constant muscle stimulation level $Stim_{\mathrm{init},i}$ provided as input. In the optimization procedure the parameters $Stim_{\max}$, τ and $\Delta\epsilon_{\lim}$ are used as optimization parameters, as they are assumed to have the highest relevance in the used controller hypothesis to match differences in subject behaviour in reaction time τ, trigger for activating muscles $\Delta\epsilon_{\lim}$ and level of counteracting $Stim_{\max}$.

PD controller. The PD muscle controller, is modelled by the following relation between the muscle activation $Stim_{\mathrm{PD},i}$, the target value for the muscle length l_0 at the beginning of the simulation and the current (delayed) muscle length $l_{\mathrm{m},i}$ and its derivative $\dot{l}_{\mathrm{m},i}$

$$Stim_{\mathrm{PD},i} = Stim_{\mathrm{init},i} + k_p\left(\frac{l_{\mathrm{m},i}(t-\tau)-l_{0,i}}{l_{0,i}}\right) + k_d\left(\frac{\dot{l}_{\mathrm{m},i}(t-\tau)}{l_{0,i}}\right).$$

During the optimization process, the parameters k_{p}, k_{d} and τ are adapted.

In a first approach, the controller parameters $\Delta\epsilon_{\lim}, Stim_{\max}, k_{\mathrm{p}}$, k_{d} and τ are assumed to be equal for all muscles. An individual parametrization for muscles or muscle groups can be implemented easily but leads to increased optimization times and risk of overfitting or unphysiological parameterizations.

The activation dynamics, calculating the muscle activation a based on the neural excitation $Stim$ is modelled according to [7]. For the activation phase $t_{\mathrm{act}} = 10\,ms$ and for the deactivation phase to $t_{\mathrm{deact}} = 40\,ms$ is used.

2.3. Optimization

The optimization target is to decrease the deviations between simulation and experiment. In a first approach, the longitudinal head displacements Δx_{head}, expressed in coordinates of the moving platform coordinate system, are used to calculate a cost function J formulated via a mean square error

$$J = \frac{1}{m}\sum_{t_1}^{t_m}\left(\Delta x_{\mathrm{head}}^{\mathrm{sim}} - \Delta x_{\mathrm{head}}^{\mathrm{exp}}\right)^2,$$

evaluated at discrete timesteps $t_m \in$ [1.2:0.01:2.2]. More proper cost functions, e.g. based on CORA evaluation [7] or multiple target signals are conceivable. Local optimization approaches with reconstructed gradients did not show good convergence behaviour. Therefore, global optimization using a particle swarm optimizer [15] in Matlab is applied to find parameter sets to minimize deviations between experimental results and simulation. The swarm size per generation is set to 20. As hybrid function the Matlab optimization routine *fmincon* is used.

3. Results

In the following, the simulation results of the head-neck model with optimized parameters are investigated. Additionally, the convergence of the optimization process is shown. Furthermore, the long-term stabilization properties of the presented muscle-controller are outlined.

3.1. Kinematic Results

The observed kinematics of one subject in a single take is compared to the HN model with the parameter sets found during optimization. In this first investigation, we considered only Δx_{head} . It is possible to consider other parameters in future investigations by adding them to the cost function calculation. The calibrated controller settings are evaluated in the time corridor t ϵ [1.2,2.2] used in the optimization process to calculate the cost function *J*. In this phase of the scenario, a good agreement can be achieved for both PD and reflex controller after optimization. Due to the lack of proportional stimulation capabilities and its on-off characteristics, the reflex controller show less smooth behaviour and higher deviations (*J*=0.0098 vs. *J*=0.0041) (**Figure 5** and Table 1. Calibrated muscle controller parameters after optimization to further investigate this issue, the mean muscle activation values of the n=136 muscles $a_{\text{mean}}(t) = \frac{1}{n}\sum_{i=1}^{n} \text{a}_i(t)$ are calculated at each timestep (**Figure 6**). The limited consistency of the reflex controller behaviour can be explained by the higher level of activation. The used reflex controller implementation with a unique stimulation level in combination with high values of τ shows excessive behaviour.

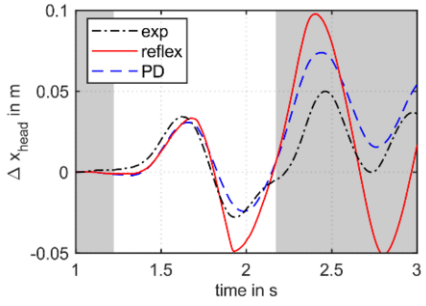

Figure 5. Head longitudinal displacement described in coordinated of the platform of simulations with optimized reflex control (red, solid) and PD control (blue dashed) in comparison to experimental target line (black dash-dotted). Only the time range of 1.2 to 2.2 s (white) is considered during optimization.

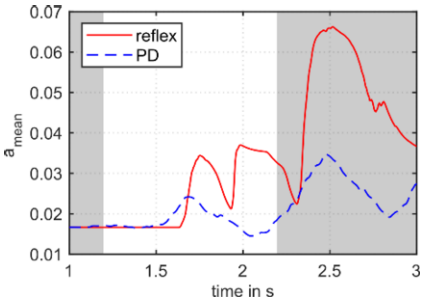

Figure 6. Mean muscle activation signals of calibrated reflex controller (red, solid) and PD controller (blue dashed). Grey shaded areas are not considered during calibration process.

Table 1. Calibrated muscle controller parameters after optimization.

Reflex controller	$\boldsymbol{Stim_{\max}}$	$\boldsymbol{\Delta\epsilon_{\lim}}$	$\boldsymbol{\tau}$ **in s**	$\boldsymbol{J}$
	0.0896	0.0154	0.1084	0.0098
PD controller	$\boldsymbol{k_p}$	$\boldsymbol{k_d}$	$\boldsymbol{\tau}$ **in s**	$\boldsymbol{J}$
	0.448	0.05	0.1032	0.0041

To demonstrate the robustness of the calibration approach, also the parameters of the PD controller for another subject in a single take are identified showing slightly different muscle controller parameters $\text{k}_\text{p} = 0.360$, $\text{k}_\text{d} = 0.103$ and $\tau = 0.158$, while the rating J is similar with a value of 0.0054, indicating good convergence. Due to the modularized

structure of the approach, it can be applied for more complex controllers or more complex calibration tasks by extending the calculation of cost function to multiple signals and/or scenarios as well.

3.2. Convergence behaviour

In the following section, the convergence behaviour of the particle swarm optimizer is analyzed. For both reflex and PD control, the optimizer finds suitable parameter sets and converge to an optimal solution **(Figure 7)**. Starting from a broad swarm contribution in the initial population (dark blue), the parameter sets converge to optimal solutions in the later populations (red) **(Figure 8)**. In the PD controller with pure particle swarm optimization without hybrid function, the parameter k_d converges to its lower limit, while the values of k_p and τ are more spread, indicating a good exploration of the result field spanned by τ and k_p. The combined optimization approach of particle swarm optimizer with hybrid function *fmincon* used in the reflex controller shows better convergence behaviour towards the local optima, while requiring additional simulation evaluations. With the presented approach, a parameter set for one subject take can be identified with a total amount of approximately 150 simulations with computational time of 2 min 28 s each. In total, a parameter set is found approximately after six to eight hours.

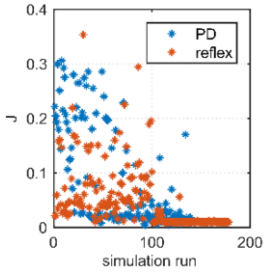

Figure 7. Convergence behaviour of the PD controller (blue) and reflex controller (red).

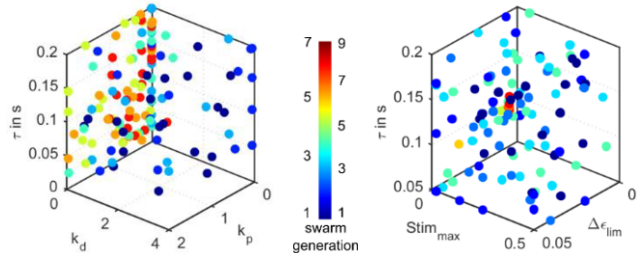

Figure 8. Contribution of data points of swarm generations during optimization. Initial population (blue) towards last swarm population (red) in optimization of PD-controller (left) and reflex-controller (right).

The expansion of the parameter space should be done cautiously. An expansion of the parameter space increases the risk of overfitting, especially if using very few evaluation sets to calculate *J*.

3.3. Long-Term Stabilization

Besides the focused phase of reflex behaviour which can be tackled quite well by the simple muscle approaches used in this study, a short outline is given to the subsequent phase. The performance and suitability for long-term stabilization of the calibrated controllers can be investigated in a time corridor that exceeds the one used in the optimization process, see the grey area in **Figure 5**. For the given data set, the calibrated PD controller shows good agreement to the experimental results. In contrast, the reflex controller seems to be less suited to enable stabilization after the initial phase.

Nevertheless, if investigating the phase after the reflex in the experimental data, there can be identified quite large deviations between the subjects. The simple controller definitions are not suited to model all the additional influences which are relevant, as for instance the control strategy or target of the individual subject. To further analyze

subject-specific differences, additional experimental data with statistical evidence and evaluations of important influences is required.

4. Discussion and Outlook

The calibration and validation of active human models is a challenging topic due to the different requirements of the disciplines. Challenges are: (i) the high reproducibility and identification of representative behaviour in experimental tests and (ii) the modelling and calibration of the biomechanical models in the simulation. This contribution aims to show an approach to combine these separate subtasks in a modular way to empower users from different disciplines to improve subtasks.

In the future, large sets of calibration data with the natural variance in human behaviour will become available due to driver monitoring systems for instance. To account for this variance in the simulation models as well, semi-automatic calibration of individual subjects parameters becomes more prominent. Together with possibilistic methods, such as fuzzy valued parameters [4], the variance in experimental result can be reproduced based on individually identified parameter sets.

We presented a subject-specific identification of muscle-level controller parameters based on head kinematics gained in volunteer tests performed on a dynamic DiL-simulator. The DiL-simulator approach allows replicable investigations of driver behaviour in Pre-Crash scenarios, with and without the interaction of driver assistance systems. The transferability of the driver behaviour gained in the simulator compared to drivers in an emergent situation on the road is not finally evaluated. However, the presence of different reaction types of drivers in the simulator as well as in real cars undergoing an emergent situation is considered likely. We think that methods to address these variations can be developed and tested with data gained in the simulator, even if no direct transferability is ensured. The calibration process of the muscle-level controller using particle swarm optimizer shows good convergence behaviour, usability and good agreement in the reflex phase. However, pure muscle level control without any high-level controller seems to be less suitable for long-term stabilization tasks exceeding the human reflex phase.

Further improvements could be achieved by increasing the level of detail of the controller modelling, like different gain factors for each muscle group or a more complex cost function. For example, a CORA analysis could be performed to calculate the cost function J. Furthermore, a frequency dependency of the muscle controller could be useful to enable the emulation of human behaviour which depends on the level of external excitation or accelerations [16]. Due to the modelling as muscle-level controller, the controllers can be easily deployed in complex FE simulations. For example using the extended Hill-type muscle model presented in [17, 9].

Acknowledgement

The work presented in this paper was carried out at the Institute of Engineering and Computational Mechanics and the Cluster of Excellence Simulation Technology of the University of Stuttgart. Funded by state Baden-Wuerttemberg and the German Research Foundation (DFG) through the financial support of the project within the Juniorprofessor program and the Cluster of Excellence Simulation Technology (EXC 310/1) and Data-

Integrated Simulation Technology (EXC 2075) of the University of Stuttgart. Funded by Deutsche Forschungsgemeinschaft (DFG, German Research Foundation) under Germany's Excellence Strategy – EXC 2075 – 390740016). Additionally, the authors want to thank Francesco Labanti for his support in MADYMO modelling during his master thesis.

References

[1] Östh J, Mendoza-Vazquez M, Sato F, Svensson MY, Linder A, Brolin K. A Female Head-Neck Model for Rear Impact Simulations. Journal of Biomechanics, 2017, 51, 49–56.

[2] Bastien C, Blundell MV, Neal-Sturgess C. A Study into the Kinematic Response for Unbelted Human Occupants during Emergency Braking. International Journal of Crashworthiness, 2017, 22(6), 689–703. Available from: https://doi.org/10.1080/13588265.2017.1301080.

[3] Ghaffari G, Brolin K, Brase D, Pipkorn B, Svanberg B, Jakobsson L, et al. Passenger Kinematics in Lane Change and Lane Change with Braking Manoeuvres Using Two Belt Configurations: Standard and Reversible Pre-Pretensioner. In: Proceedings of the IRCOBI Conference. IRC-18-80. Athens, Greece, 2018, 493–511.

[4] Hanss M. The Transformation Method for the Simulation and Analysis of Systems with Uncertain Parameters. Fuzzy Sets and Systems, 2002, 130, 277–289.

[5] Ólafsdóttir JM, Brolin K, Blouin JS, Siegmund GP. Dynamic Spatial Tuning of Cervical Muscle Reflexes to Multidirectional Seated Perturbations. SPINE, 2015, 40(4), E211–E219. Available from: https://-doi.org/10.1097/brs.0000000000000721.

[6] Larsson E, Fice J, Pipkorn B, Jakobsson L, Brynskog E, Brolin K, et al. Active Human Body Model Predictions Compared to Volunteer Response in Experiments with Braking, Lane Change, and Combined Manoeuvres. In: Proceedings of the IRCOBI Conference. Florence, Italy, 2019, 349–369.

[7] Feller L, Kleinbach C, Fehr J, Schmitt S. Incorporating Muscle Activation Dynamics into the Global Human Body Model. In: Proceedings of the IRCOBI Conference. Malaga, Spain, 2016, 512–523.

[8] Kistemaker DA, Wong JD, Gribble PL. The cost of Moving Optimally: Kinematic Path Selection. Journal of Neurophysiology, 2014, 112(8), 1815–1824.

[9] Martynenko O, Kempter F, Kleinbach C, Schmitt S, Fehr J. Integrated Physiologically Motivated Controller for the Open-Source Extended Hill-type Muscle Model in LS-DYNA. In: Proceedings of the IRCOBI Conference. Athens, Greece, 2018, 239–241.

[10] Kempter F, Fehr J, Stutzig N, Siebert T. On the Validation of Human Body Models with a Driver-in-the-Loop Simulator. In: The 5th Joint Int. Conference on Multibody System Dynamics (IMSD 2018). Lisboa, Portugal, 2018, 15–31.

[11] Kempter F, Fehr J. Layout of a Driver-in-the-Loop Simulator for Validation of Human Body Models. In: Proceedings in Applied Mathematics and Mechanics, 2018.

[12] Happee R, de Bruijn E, Forbes PA, van der Helm FCT. Dynamic Head-Neck Stabilization and Modulation with Perturbation Bandwidth Investigated Using a Multisegment Neuromuscular Model. Journal of Biomechanics, 2017, 58, 203–211. Available from: http://www.sciencedirect.com/science/-article/pii/S0021929017302579.

[13] Putra IPA, Iraeus J, Thomson R, Svensson MY, Linder A, Sato F. Comparison of control strategies for the cervical muscles of an average female head-neck finite element model. Traffic Injury Prevention, 2019, 1–7. PMID: 31617760. Available from: https://doi.org/10.1080/15389588.2019.1670818.

[14] Nemirovsky N, van Rooji L. A New Methodology for Biofidelic Head-Neck-Postural Control. In: Proceedings of the IRCOBI Conference, 2001, 18.

[15] Kennedy J, van Eberhart RC. Particle Swarm Optimization. In: Proceedings of the IEEE International Conference on Neural Networks. Perth, Australia, 2001, 1942–1945.

[16] Happee R, de Bruijn E, Forbes PA, van Drunen P, van Dieën JH, van der Helm FCT. Neck postural stabilization, motion comfort, and impact simulation. In: Scataglini S, Paul G, editors. DHM and Posturography. Academic Press, 2019, 243–260.

[17] Kleinbach C, Martynenko O, Promies J, Haeufle DFB, Fehr J, Schmitt S. Implementation and Validation of the Extended Hill-Type Muscle Model with Robust Routing Capabilities in LS-DYNA for Active Human Body Models. BioMedical Engineering OnLine, 2017, 16(109), 1–28.

DHM2020
L. Hanson et al. (Eds.)

© 2020 The authors and IOS Press.
This article is published online with Open Access by IOS Press and distributed under the terms of the Creative Commons Attribution Non-Commercial License 4.0 (CC BY-NC 4.0).
doi:10.3233/ATDE200030

Modelling of Multilayered Foams for Universal Seat Design

Gunther PAUL [a,1], Young Jun LEE [b] and Peter SLATTERY [b]
[a] *James Cook University, Australian Institute of Tropical health and Medicine, Mackay QLD 4710, Australia*
[b] *Queensland Health Department, Rehabilitation Engineering Centre, Brisbane QLD 4000, Australia*

Abstract. Patients with chronic disability, or in a transient disability state post-surgery may require a mobility device for their safety and convenience. Patients with a low to mid-level severe mobility impairment are mostly comfortable to leave hospital in a factory wheelchair without further modifications, however in particular chronically disabled wheelchair bound patients require wheelchair cushion modifications specifically designed for their condition. Such personalized cushions minimise pain from sitting, avoid pressure ulcers, and correct patient posture to prevent musculoskeletal and spinal damage. To identify physical properties of a complex seat cushion design with multiple layers, for the simulation of optimum seat cushions for mobility impaired users, long-term testing was undertaken with multiples of different layer combination samples. Physical indentation results for reorganised cushions were obtained and further evaluated. We present the first study where a complex, multi-layered foam cushion structure is cycle-tested using a custom-specific human-shape indenter, derived from 3-D body scanning of a 95th percentile stature subject. The test provides physical material properties of the complex foam structure under realistic human shape indentation for the selected anthropometry. The test results feed and validate a realistic material model, and confirm durability and stability over time of the complex foam.

Keywords. Rehabilitation, Wheelchair, Seat Cushion, Pressure Ulcer

1. Introduction

In 2018, 4.4 million or 17.7% of Australians had a disability; 47.8% of the disabled in working age were employed, compared to 80.3% of people without disability. Only 28.3% of the disabled working population worked full-time, showing how people with disability experienced employment restrictions [1]. Overall, 4.4% of disabled used a wheelchair in Australia in 2015-16, and 189,200 Australians were wheelchair bound. In 2011, between 11,300 and 19,000 Australians lived with a spinal cord injury [2]. People with a physical disability or patients after spinal surgery may require a mobility device for their mobility, safety and convenience. According to the level of medical condition, health practitioners can suggest wheelchairs for early patient discharge post-surgery to return to normal lifestyle. This practice increases patient turnover and thus capacity at hospitals. Chronically disabled people are often fully dependent on a wheelchair for good. Wheelchairs come in different sizes and are mostly customizable to cover a larger range

[1] Corresponding Author, Email: gunther.paul@jcu.edu.au.

of patient anthropometry. Patients with mid-level severity conditions are mostly comfortable with an off-the-shelf factory wheelchair without further modifications, but others with more severe conditions require modifications specifically designed for the patients' condition to minimize pain from sitting, correct their posture to prevent spinal damage, and prevent pressure ulcers [3]. In 2015-16, 4,313 pressure injuries were reported by Australian public hospitals as hospital acquired, at a rate of 9.7 per 10,000 hospitalisations, causing significant cost [4]. Pressure ulcers are a medically critical complications as they are likely to cause further infections, abscess, sepsis and cancer after onset. The focus in this study was to assess cushion performance for severely affected patients.

PU foams are elastic materials that allow easy structural deformation however they eventually return to their initial shape [5]. The downside of repeated loading is loss of elasticity over time, which then causes a change in geometry and hardness.

A large proportion of patients visiting the Queensland Health Rehabilitation Engineering Centre (REC) have difficulty controlling body functions or have lost sensation below their waist. While in a healthy body the brain naturally senses build-up of pressure about the buttocks and lower limb area, and relieves pressure by changing posture or through micromotion, a significant proportion of these patients cannot independently correct their posture or sense pain from hazardous seating conditions. One solution to mitigate this problem are pressure relieving cushions which optimize distribution of pressure across weight bearing body parts.

To prevent such injuries and improve patients' quality of life, a pressure relieving cushion was formerly designed based on experience, trial and error [6]. While this design had been successfully used over the past decade, durability remained a problem to solve. Moreover, increasingly complex surgery required more intricate cushion solutions to prevent pressure injuries. The original design consisted of a simple cushion with three layers of foams with the hardness increasing from top to bottom so that the top layer provided high elasticity to deform and an even distribution of pressure over the contact area. With the aim to minimize pressure discomfort, a similar combination of foams with alternating hardness was then layered into cushions of high geometric complexity to provide both softness for comfort and hardness for durability [7], where the expectation from increased durability is to reduce instances of patients having to re-visit REC for a replacement.

As a result of the evolved structural complexity of such new pressure optimized cushions (Figure 1), purely physical development and testing is now uncommon. New designs are developed in analytical dynamic models [8] which represent both the cushion and human subject for testing in CAE [9]. However, to determine mechanical properties of multi-layered foam materials under realistic human like indentation, and in order to validate analytical modelling, physical studies are still required. The physical testing described here is a novel approach and deviates from standardised material testing, which measures indentation force/load deflection (IFD/ILD) with an indenter foot according ASTM D3574 [10], ISO 2439 [11] or DIN 53579-1 [12]. The purpose of this study is to inform future FEM analytical models with relevant material parameters.

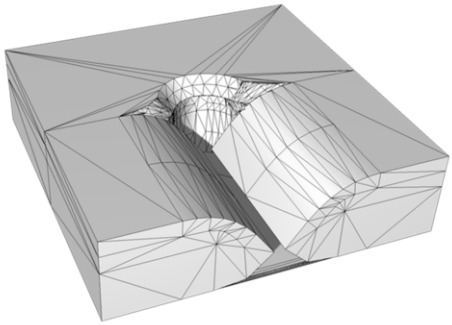

Figure 1. Complex multi-layered pressure optimizing cushion, see [6].

2. Methods

This physical study required multiple repetitive tests being conducted on three differently configured cushion PU foam samples. Initially a controller was programmed for a previously developed indentation rig [13] to perform a cycled loading test on cushion samples. Fatigue loading response of the three foam samples was compared, and the effect of fluid on the mechanical properties of different types of cushion was investigated.

2.1. Foam specification

Three different foams were used, with their hardness indicated by colour from light green to pink. The numbering for each foam type is indicative of the foam density and hardness, where the first number after the letters represents density and the following value indicates hardness. Foams were sourced from Dunlop (Table 1). Green and pink foams (Figure 2) have similar density, while the hardness of the pink foam is about 5 times stiffer than green. Yellow foam has the highest density, while providing a mid-range hardness within the types of foams used. Hardness values are measurements determined by Dunlop using the industry standard ASTM D3574 indentation force deflection (IFD) method with a standard probe. This involves compression of a given thickness and size foam sample block to a deflection of X percent of its initial height, using an indenter of 200 mm diameter [10]. IFD values differ depending on foam sample height, size, and the compression factor. Common sample heights are 50-100 mm [14]; common sample sizes are 380x380 mm and 500x500 mm; and common compression factors are X=25%, X=40% and X=65%. Lower hardness foam has a better capability to recover from deformation caused by a load. All foams used were premium quality, flame retarded and with antimicrobial protection, and came in four different thicknesses, 10 mm, 25 mm, 50 mm, and 75 mm. This made it possible to test cushions of 150 mm total thickness composed of different foam layers. Length and width of each foam layer block was 600 mm x 460 mm.

Table 1. Standard foam density and IFD hardness specification for each type of foam used.

Foam type	Colour	Density [kg/m³]	IFD hardness [N]	Resilience	Grade description
EN36-90	Green (G)	36 -1/+1.5kg	90 -10/+30N	50%	Soft cushioning foam
EN40-230	Yellow (Y)	40 -1/+2kg	230 ± 20N	45%	Firm cushioning foam
MA35-600	Pink (P)	35.0 +2kg	600 ± 50N	30%	Extra firm impact cushioning foam

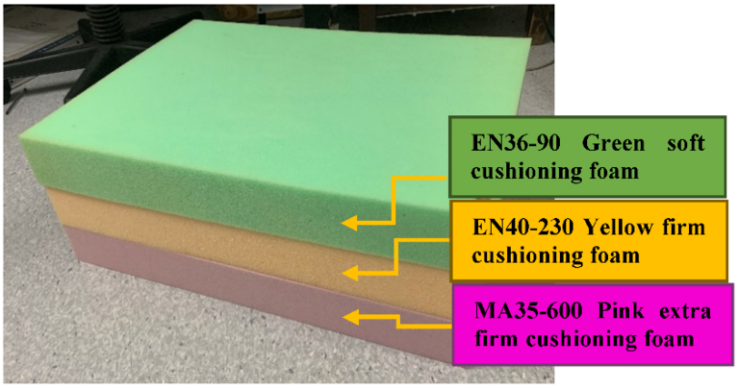

Figure 2. Three different foams piled in order of increasing hardness from top to bottom.

2.2. Indenter rig

The axial indenter rig had been previously developed [13]. It consists of a vertically mounted worm drive actuator, driven by a stepper motor that allows precise control of the rod movement along the vertical axis, allowing a precise specific load to be generated and held still at any given position. The rotation and torque created by the servo motor is fed to the worm drive supported by ball bearings. A strain gauge load cell (Honeywell, 500lbsf/227kgf range; accuracy 0.05%) is mounted between indenter and actuator (Figure 3) for the precise measurement of the three-dimensional indentation force. Weight plates are used to prevent cushion movement. The indenter mechanism was designed to apply high loads with low internal friction, permitting high precision and stabilised movements, and reducing power requirements to allow loads of over 80 kg.

2.3. Indenter probe

The indenter probe form was derived from 3D scans of a 95th percentile stature (2011), median corpulence healthy Australian young man [9] (Figure 4). This same indenter form had been previously used in investigating automotive seat pressure comfort, both in physical and virtual environments as a model in ANSYS [15]. In this study, a

simplified physical model was used with identical geometry, however as rigid form with hard surface (Figure 5).

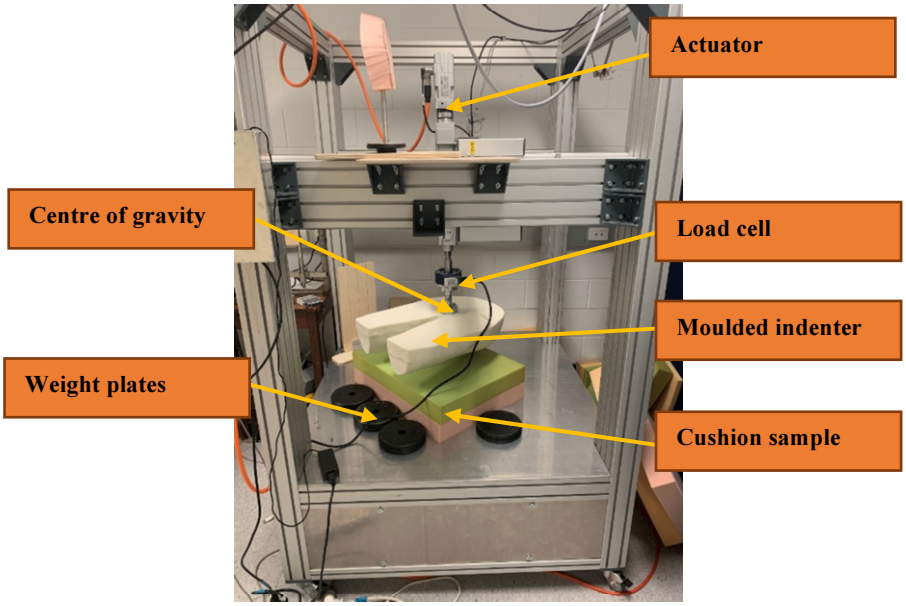

Figure 3. Setup of the axial indenter rig, consisting of actuator, load cell, moulded indenter and cushion sample.

Figure 4. Indenter shell. This picture shows a shell version with a surface layer of soft neoprene, however using the same geometry as the indenter shell in the experiment.

Figure 5. Hard surface indenter shell, from [6].

2.4. Software

The software to control the indenter rig was programmed using C# on Visual Studio. Two test features were implemented, normal and fatigue test. For a normal test, the cycle time is selected in minutes and the total run time in hours. For fatigue testing, instead of selecting a total run time, the number of cycles is chosen, and delays between each cycle if a resting period is required. The software provides a live graph feature to observe real-time results. At the end of each test all recorded data (time, force and indenter position) are saved in an Excel file.

2.5. Procedure

Multiple layered foam cushions have mechanical properties which deviate from the material data sheets. In addition to testing hardness change over normal use, a wet cushion test was implemented to further understand effects of incontinence on cushion durability for each foam type.

A creep compression test (one cycle loading of 60 kg load for one hour; 1.5 m/min), which was also used to calculate stiffness ilo IFD and durability test (0.2 Hz; 15,000 cycles; 80 kg maximum load) were conducted on each foam type. Durability testing was also performed on wet cushions to determine the impact. The creep test was run for the cushions to obtain their intended property, as foam requires conditioning before it reaches its nominal strength. Durability testing for wet cushions was run for 8 hours, and 5 days for normal cushions. Standardised wet set testing has shown good correlation with fatigue and is thus predictive of durability [16]. Hysteresis was not tested. All tests were performed according to the aims of the study:

Experiment 1: Creep test and stiffness calculation of multilayered foams with different ratios of each foam type.
Experiment 2: Durability test on normal cushion.
Experiment 3: Durability test on wet cushion.

Each foam combination was tested so that the cushion front edge was placed at 300 mm distance from the centre of gravity (Figure 6). The ratio of foam types in each sample varied, with a total cushion thickness of 150 mm. The samples tested in this experiment were according to Table 2.

Table 2. Foam combinations used as study samples. Numbers next to the colour indicate the ratio of foam types used in each sample, for example: pink2:yellow1:green3 indicates the use of 50 mm pink, 25 mm yellow and 75 mm green foam.

Number	Foam combination and ratio
1	green
2	green1:pink5
3	green2:pink4
4	green2:pink4
5	green3:pink3
6	green4:pink2
7	green: yellow
8	yellow
9	yellow1:pink5
10	yellow2:pink4
11	yellow3:pink3
12	yellow4:pink2
13	pink
14	pink2:yellow1:green3
15	pink2:yellow2:green2
16	pink2:yellow3:green1
17	pink3:yellow1:green2
18	pink3:yellow2:green1

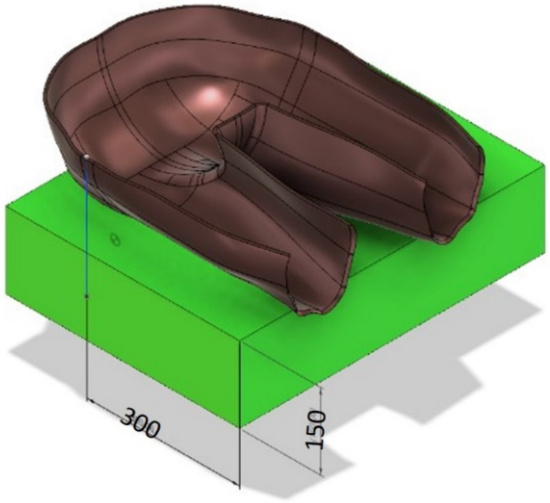

Figure 6. Indenter placement.

The wet test experiment followed the same procedure as outlined for the fatigue test. Each cushion sample was treated with 800 ml of room temperature tap water. An average person urinates between 800 ml to 2 l per day, however foams will not absorb more than 1 l of water without expelling. The foams had hydrophobic surface characteristic due to their antimicrobial protectant treatment, therefore 1/3 cup of water was added during the experiment every 10 cycles for 10 times. This test ran with reduced cycles for 8 hours on a single day.

3. Results

3.1. Creep test

Creep for various foam and layered cushion configurations is shown in Figure 7. Green and pink foam cushions settled and reached equilibrium in hardness within 20 minutes of creep testing, whereas the yellow cushion showed an ongoing and continuous change in hardness. Creep for the green foam was over 100 mm, while yellow foam creep was about 40 mm and pink foam creep was less than 20 mm. It can be seen that while the P2:Y3:G1 or P3:Y1:G2 configurations achieved a creep reduction to about 55 mm, **P3:Y2:G1** yielded a significantly better creep of about 45 mm, similar to the two layer configuration P2:Y4. The two latter ones appear as a reasonable compromise between hardness and creep behaviour.

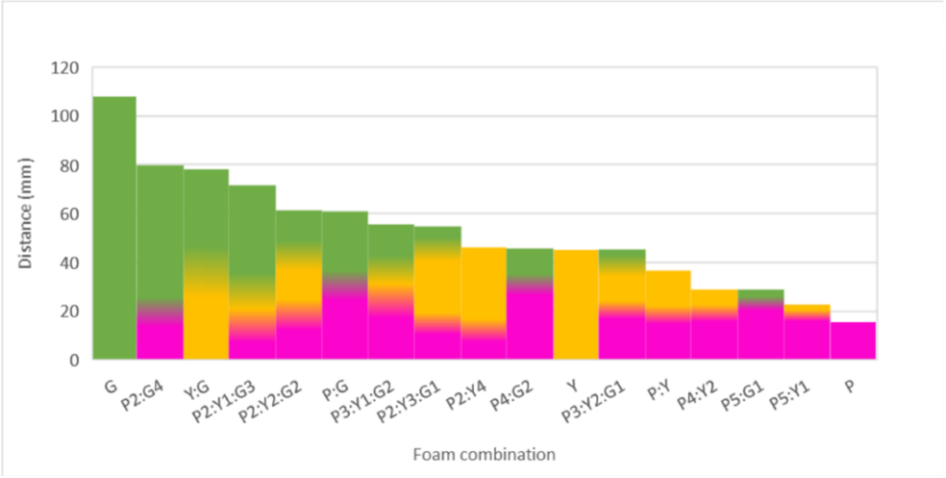

Figure 7. Creep under 60 kg load over 1 hour. 150 mm total height of cushion layered with different hardness, indicated by P (pink), Y (yellow) and G (green). Numbers represent the thickness ratio of each foam used.

3.2. Stiffness

Stiffness as a comparison value to indentation hardness (IFD) of different cushion configurations was calculated from creep test measurements with new foams; results are shown in Figure 8.

The common configuration used for average patients at REC is P2:Y2:G2. This configuration has a good low overall stiffness of about 10 N/mm, similar to P3:Y1:G2 and P2:Y3:G1. It is however inferior to **P3:Y2:G1** which provided a similar stiffness, yet yielded significantly better creep. The two-layer configuration P2:Y4 is slightly harder, however performs better in creep and appears to be a good low-cost alternative to the three-layer configurations.

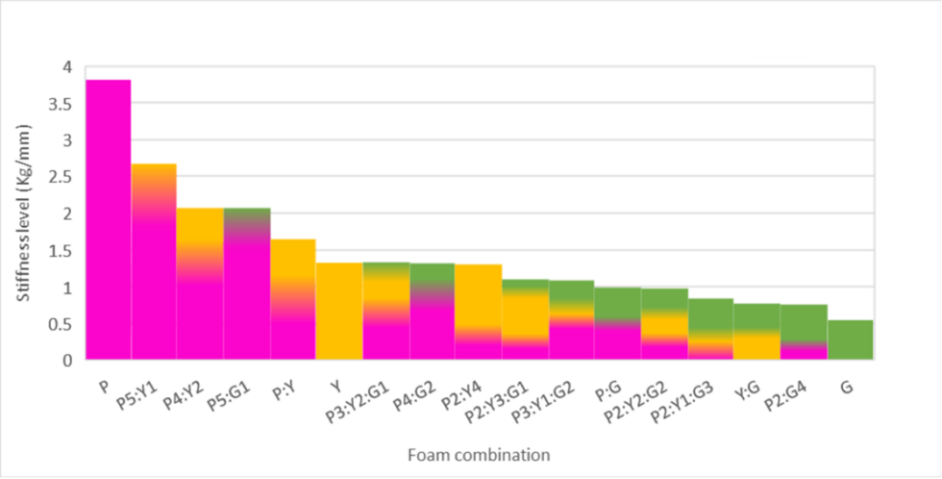

Figure 8. Stiffness as calculated from creep test measurements with a human form indenter probe at 60 kg load. 150 mm total height of cushion layered with different hardness, indicated by P (pink), Y (yellow) and G (green). Numbers represent the thickness ratio of each foam used.

3.3. Durability test

Foam cushion combinations were tested as green on pink (G:P), yellow on pink (Y:P), and pink (P) (all 1:1 ratio). While G:P and P achieved a settled state on the first day after start of the experiment, Y:P settled after 5 days (Figure 9). No fatigue was recorded after 15,000 cycles.

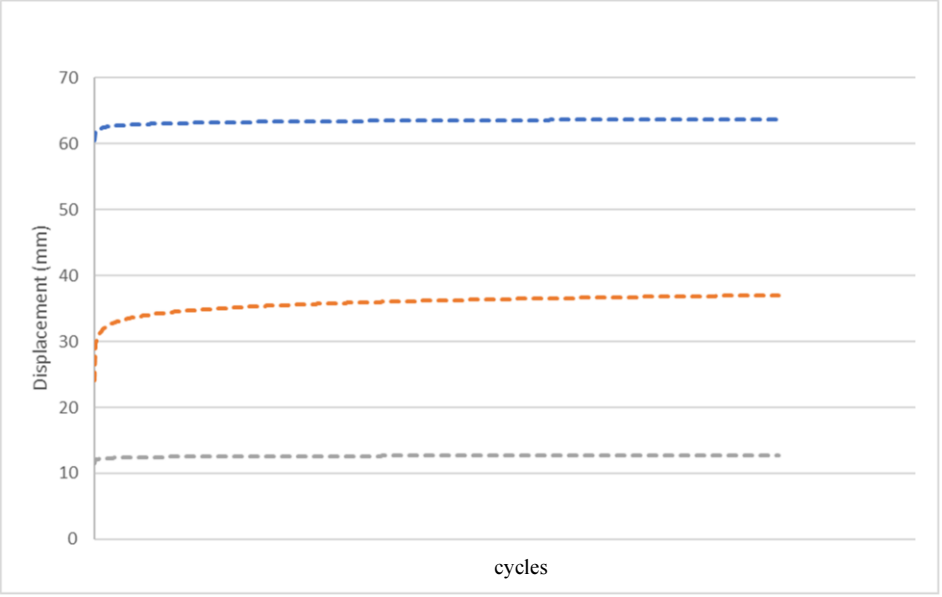

Figure 9. Foam cushion durability test over 5 days and 15,000 cycles on three different samples. Blue line: G:P; Orange line: Y:P; Grey line: P. Measured with human indenter form under 80 kg cycled.

3.4. Wet compression test

The tests showed a continuous increase in compression rate for all three water treated samples P, Y and G, while P and G dry/unconditioned samples had reached a settled state, and dry Y increased at a much smaller rate. Exemplary results are shown for Y (Figure 10). Wet Y reached 40 mm compression after 2:45 hrs, which was not reached after 5 days in a dry condition; at the same time, dry Y reached 33 mm compression.

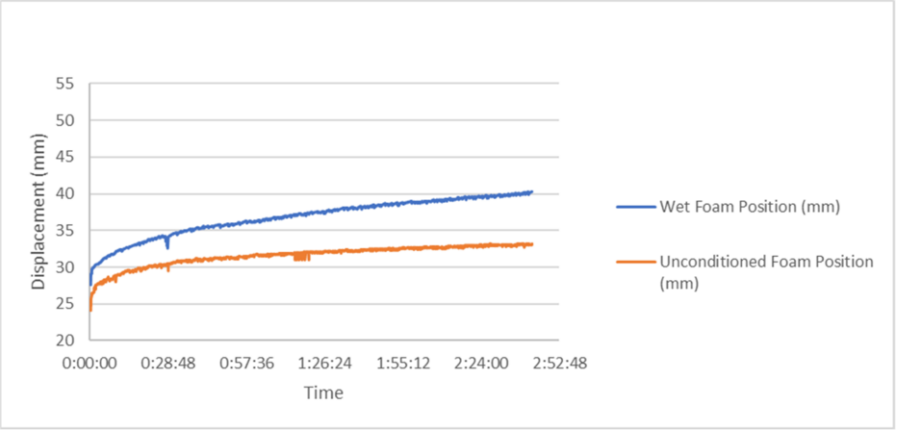

Figure 10. Foam cushion ageing/fatigue test over 1 day on wet (blue line) and dry (orange line) Y samples. Measured with human indenter form under 80 kg cycled.

4. Discussion

While cushion indentation hardness can be optimized to prevent pressure ulcers, pressure comfort may require more firmness which contributes to a feeling of support. Evaluating the perfect balance between firmness and softness was not an aim of this study and could not be determined in the evaluation. The use of pressure mapping is suggested for further analysis to find the cushion configuration that most evenly distributes pressure around areas of medical concern, such as the rectum.

Due to inaccuracies of the mechanical and servo motor control assembly, load accuracy at full load was 5% or ± 2 kg as each step of movement triggered by the motor created 4kg change in load. Due to its non-linear and time-dependent compression behaviour, indentation force changes at a set point over time. Therefore, the control program was set to step up the indenter rod when the load had eased to 2 kg below the intended load. For example, for a target of 80 kg, the motor was set to increase indentation when the load measured by the load cell decreased to 78 kg, to obtain 82 kg, therefore applying a load of between 78 kg to 82 kg. While this issue did not affect smaller indentation, load control became less accurate for higher loads. This could be improved by reducing the amount of worm drive rotation in each step; however, this will require a different drive gear or position control to be implemented on the worm drive.

While quasi-linearized stiffness measurements of single foam type cushions compare with standardised IFD indentation hardness values, more complex multilayer foam cushions show significant deviation from an averaged stiffness prediction in a linear model. For example, P5:Y1 was measured at 25.5 N/mm while P had a stiffness

of 37.3 N/mm and Y had a stiffness of 12.7 N/mm. When predicting averaged stiffness of P (IFD 40% 600 N) and Y (IFD 40% 230 N) in a linear model however, combined averaged stiffness would be 33.2 N/mm, and combined averaged IFD would yield 538 N. The addition of a thin layer of softer foam to a layered cushion thus had a significantly over-proportional effect on overall stiffness. Similarly, in IFD hardness the 25 mm softer foam layer will contribute over-proportionally to a 40% compression of 60 mm. This was confirmed when comparing P4:Y2 to P5:G1. While measured stiffness of both samples was equally 20 N/mm, predicted stiffness (hardness) is 29.1 N/mm (IFD 40% 477 N) for P4:Y2, and 31.9 N/mm (IFD 515N) for P5:G1.

The ratios of stiffness, i.e. P:Y=2.937, P:G=7.612, Y:G=2.592, were found consistently larger (P:Y=+12.6%; P:G=+14.2%; Y:G=+1.4%) than the ratios of IFD hardness (P:Y=2.608; P:G=6.666; Y:G=2.555), indicating an increasing influence of foam IFD hardness on foam stiffness as measured with a human indenter form under quasi-static/quasi-linear conditions. Because harder foams cannot be avoided in cushions for a variety of reasons shown before, a key finding of this study is therefore the deduction that cushions must use a combination of at least one softer and one harder PU foam for comfort reasons. Findings are summarized in Table 3. Results from this study will be used to inform a finite element model, which will be used in combination with indenters modelled from patient specific 3D scans. The results are essential to provide realistic parameters for the wheelchair cushion FE model; these are currently unavailable, as neither dry nor wet stiffness of such wheelchair cushion foams have ever been established, and tabulated standardised data has been shown to be misleading. While durability was confirmed to be no issue in dry foams, it was shown that fatigue behaviour of the wet foams requires further study [17] to formulate time-dependent elasticity in the FE model.

Table 3. Summary of foam stiffness measurements using human form indenter vs IFD hardness specification for each type of foam used.

Foam type	Density [kg/m³]	IFD hardness [N]	Stiffness [N/mm]	Hardness ratio		Stiffness ratio	
EN36-90 (G)	36 -1/+1.5kg	90 -10/+30N	4.9	2.555	6.666	2.592	7.612
EN40-230 (Y)	40 -1/+2kg	230 ± 20N	12.7	2.608		2.937	
MA35-600 (P)	35.0 +2kg	600 ± 50N	37.3				

The results show that medical device cushion foams are likely to lose their expected indentation hardness and durability under wet condition, and appropriate treatments are suggested to prevent contact with moisture. Climate chamber tests will be required to investigate this behaviour further.

Through experimental variation of geometric parameters in such a correctly parametrized wheelchair cushion FE model, we expect to optimize seat pressure of occupants, with a particular focus on medically relevant areas.

References

[1] Australian Bureau of Statistics. Disability, Ageing and Carers, Australia: Summary of Findings, 2018. [Accessed May 2020]. https://www.abs.gov.au/ausstats/abs@.nsf/mf/4430.0
[2] New P et al. Estimating the Incidence and Prevalence of Traumatic Spinal Cord Injury in Australia. Archives of Physical Medicine and rehabilitation, 2015, 96(1), 76-83.
[3] Regan MA, Teasell RW, Wolfe DL, et al. A systematic review of therapeutic interventions for pressure ulcers after spinal cord injury. Arch Phys Med Rehabil, 2009, 90, 213-231.
[4] Nguyen K-H et al. PI costs in Australian public hospitals. Australian Health Review, 2015, 39, 329–336.
[5] McEvoy J, McRoberts T, Yamasaki R. Test of Dynamic Properties in Different Environmental Conditions with Different Occupant Weight, Polyurethanes Expo 2003, October 1-3, 2003, Arlington VA, 205-215.
[6] Paul G, Briceno L, Condon J. Customization of the user-wheelchair seat interface through an iterative experimental-computational process. 10th International Conference on Applied Human Factors and Ergonomics (AHFE), July 24-28, 2019, Washington D.C., USA.
[7] Slattery P, Paul G, Condon J, Veivers J. Evidence into Practice - Designing Better Custom Cushions. Australian Assistive Technology Conference (AATC), Melbourne Convention Centre, 14.-16.11.2018.
[8] Bui HT, Lestriez P, Nguyen TNP, Nguyen LV, Tao QB, Debray K, Nguyen THV, Taiar R. The Evaluation of the Interaction Between Human Buttocks Thighs and Wheelchair Seat Cushion to Prevent Pressure Ulcers Using Finite Element Analysis. In: Ahram T, Karwowski W, Taiar R, editors. Human Systems Engineering and Design (IHSED 2018). Advances in Intelligent Systems and Computing, Vol 876, Springer, Cham, 2019, 904-910.
[9] Paul G, Miller J, Pendlebury J. Soft tissue human thigh and buttock finite element model to simulate vehicle seat cushion indentation. International Journal of Human Factors Modelling and Simulation (IJHFMS), 2014, 4(3/4), 220-232.
[10] ASTM D3574-17. Standard Test Methods for Flexible Cellular Materials—Slab, Bonded, And Molded Urethane Foams. ASTM International, West Conshohocken, PA, 2017, www.astm.org.
[11] ISO 2439:2008. Flexible cellular polymeric materials — Determination of hardness (indentation technique).
[12] DIN 53579-1:2015. Testing of flexible cellular materials - Indentation test on finished parts.
[13] Slattery P, Sivakumar A, Paul G. Virtualization in Physical Ergonomics: Seat Indenter Testing Rig. In: Proceedings of the AHFE 2017 International Conference on Physical Ergonomics, July 2017, Los Angeles, California, USA.
[14] Blair GR, McEvoy J, Weierstall M, Ali A. Hardness Test Methods comparison and Correlation with H-Point Measurements. In: API Conference Proceedings, The Grand America, Salt Lake City, Utah 2006 Sep 25, 526-542.
[15] Paul G, Miller J, Pendlebury J. A finite element model of seat cushion indentation with a soft tissue human occupant model. In: Reed M, Parkinson M, editors. Proceedings of the 2nd International Digital Human Modeling Symposium (DHM2013), University of Michigan & Pennsylvania State University, Michigan Union, University of Michigan, Ann Arbor, 2013.
[16] Pask R, Blair GR, Weierstall M. The Time is Right for Harmonization of Foam Standards. CPI Conference, September 29 – October 1, 2008, San Antonio, TX.
[17] Zenkert D, Shipsha A, Burman M. Fatigue of Closed Cell Foams. Journal of Sandwich Structures & Materials, 2006, 8(6), 517–538. https://doi.org/10.1177/1099636206065886

DHM2020
L. Hanson et al. (Eds.)

© 2020 The authors and IOS Press.
This article is published online with Open Access by IOS Press and distributed under the terms of the Creative Commons Attribution Non-Commercial License 4.0 (CC BY-NC 4.0).
doi:10.3233/ATDE200031

On the Development of an Upholstery Database for Simulating the Human-Seat Interaction in Automotive Interiors

Hans-Joachim WIRSCHING [1] and Florian WAGNER
Human Solutions, Europaallee 10, 67657 Kaiserslautern, Germany

Abstract. A corner stone in digital ergonomics is the positioning of digital human models into occupant configurations. Since seats play a major role for interiors, the human-seat interaction has to be considered for simulating postures. In most applications the classical H-Point model has been used. Since this approach is limited, the prediction has been refined by considering seat parameters like kinematics, upholstery surfaces and stiffness. But the necessity of stiffness parameters often hinders applying this method, since it requires extensive measurements based on a special indenter. To reduce this bottleneck, two improvements have been introduced. First, the measurement has been enhanced to be more generic and easier to perform. The process has been standardized in line with SAE J2896 and supports user-defined indenters. Second, an upholstery database has been implemented as alternative to measure the stiffness. The database is based on a sample of German vehicle seats and a statistical analysis of their measured force-deflection curves. A GUI supports the definition of characteristic curves. This can be done by selecting a referential curve, by setting individual parameters or by predicting a curve from the cushion stiffness. The final curves are suited for predicting the manikin or seat positions in interior designs.

Keywords. Posture Simulation, Human-Seat Interaction, Upholstery Database, Upholstery Stiffness Measurement

1. Introduction

A crucial feature of digital vehicle ergonomics tools is the realistic and automatic task-specific positioning of a digital human model into a given occupant configuration. Since the seat has a major influence on the occupant behavior in vehicle interiors, the human-seat interaction has to be considered properly by a digital human model for the simulation and evaluation of occupant postures [1].

In most applications the classical and pragmatic H-Point model has been used to predict sitting postures. This model addresses the offset between the seating reference point and the occupant's hip center and dates back to the start of using human models in automotive applications [2]. Since the quality and evaluation potential of this approach is limited, the prediction has been refined by an advanced human-seat simulation method [3]. This method can be used to predict a manikin posture in a given seat or the seat position for a given sitting manikin. It takes into account several user-defined seat

[1] Corresponding Author, Email: hans-joachim.wirsching@human-solutions.com.

parameters like kinematics, cushion and back rest surfaces, attachments, H-Point travel field and upholstery stiffness.

However, poor availability of stiffness parameters impedes the application of this method in ergonomic vehicle design, because extensive seat stiffness measurement has to be conducted by moving a special indenter device into the upholstery and measuring the corresponding forces and deflections [4]. Such procedures are commonly used to evaluate the dynamic seat comfort concerning vibrations caused by driving dynamics [5]. This global approach is a simplification of measuring local foam characteristics for the simulation of seat foam structures in complex FEM models [6] and of measuring local seat pressure distributions for the prediction of static seat comfort ratings [7,8].

This bottleneck was defused by a measurement procedure that is more generic and easier to perform. In addition, a seat upholstery database has been implemented as a functional alternative for explicitly measuring the seat stiffness. These two improvements will be described in the following sections.

2. Method

2.1. Seat measurement

The measurement of upholstery stiffness is an extension of a procedure which essentially is based on the determination of the force-dependent deformation of the complete seat surface [4]. A machine moves an indenter into the seat surface at specific locations with varying forces and constant speed, while taking its travel length to measure the upholstery deflection. The measurement appliance and the rigid indenter (shaped like human buttocks) are displayed in Figure 1.

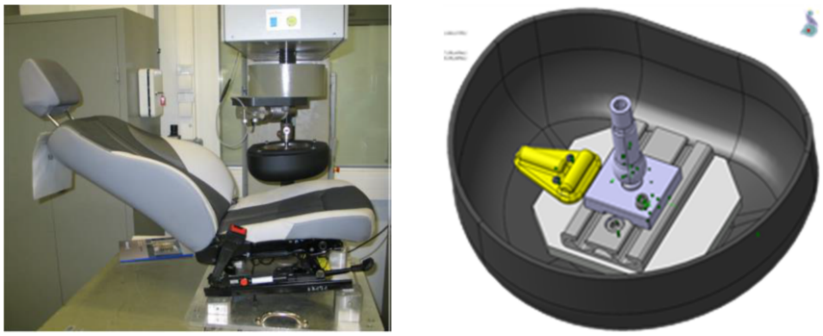

Figure 1. Measurement appliance and indenter.

In order to cover the entire upholstery area, the procedure is applied to various locations on the seat. The cushion and back rest are fixed and aligned such that the indenter subsides orthogonally into the upholstery surface. The forces are measured perpendicular to the indenter. The four measurement locations and directions are illustrated in Figure 2 and Figure 3.

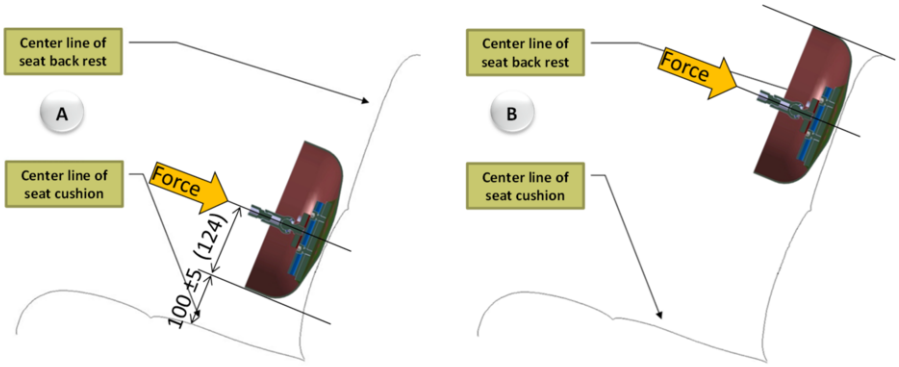

Figure 2. Measurement locations on back rest: bottom and top.

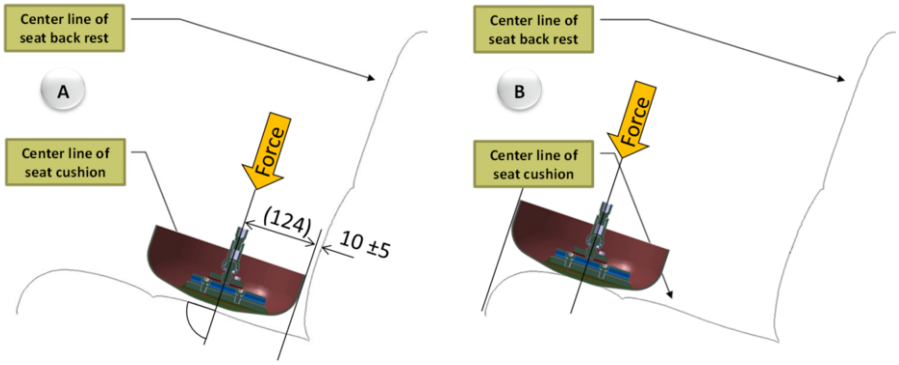

Figure 3. Measurement locations on cushion: rear and front.

The measurement forces are uniformly increased up to 750 N (cushion) and 250 N (back) at a constant speed of 50 mm/min (loading) and decreased to 0 N under the same conditions (unloading) without time delay. This procedure is repeated four times with 5 minutes break between the takes. Finally, the last trial is used for further processing. The measured force-deflection pairs build the characteristic load-deflection curve at the specific location (Figure 4).

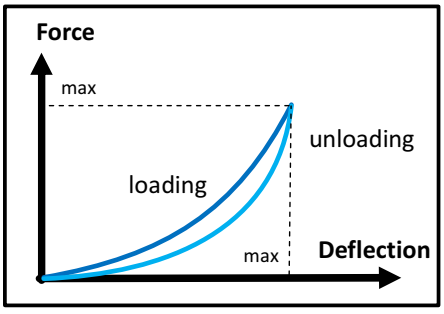

Figure 4. Characteristic force-deflection curve.

This procedure is essentially compatible with the standard SAE J2896 ”Motor Vehicle Seat Comfort Performance Measures” [9]. Selective differences with regard to

recommendations such as maximum applied forces and measurement direction are neglected, because their application in the presented method has already been approved [4]. Basically, the principal procedure and results of the standard correspond to our approach.

The scope of SAE J2896 is a recommendation for test procedures applied to complete seat systems in manufacturing quality. The specified test methods stipulate a range of indenter shapes (buttform, disk or oval). This open indenter specification is addressed in the measurement processing software presented in Section 2.3.

A representative set of 24 automotive and light truck seats from German vehicle manufacturers were measured using the method described above. The resulting force-deflection curves (loading) show quite homogenous trends (Figure 5).

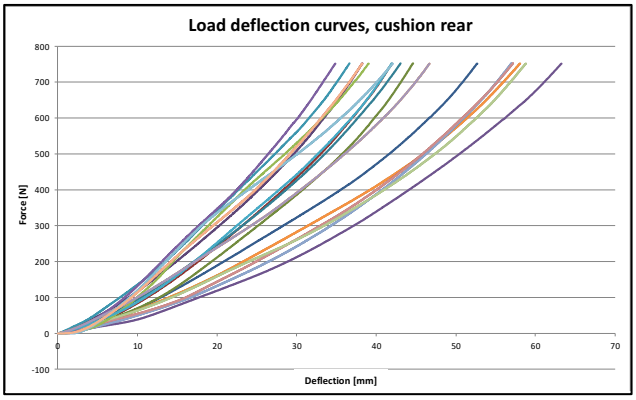

Figure 5. Load-deflection curves of all seats (cushion-rear).

The analysis of repeated measurements showed that all trial curves are similar with exception of the first take (Figure 6, left). The diagram in Figure 6 (right) shows small deviations between the maximal forces and deflections over all locations and seats for trial 2-4 and large deviations between trial 1 and the averages of trial 2-4. This confirms the guideline instructions given in Section 2.1 to use the last measurement in further practice.

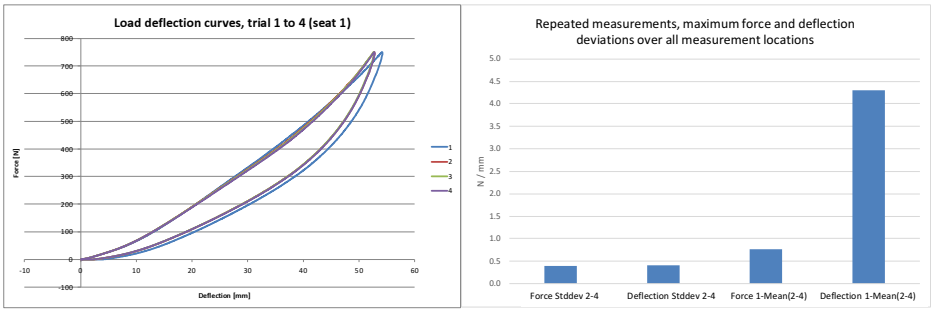

Figure 6. Deviations between maximal forces and deflections over all locations and seats for repeated trials.

2.2. Seat curve analysis and modeling

The goal is the creation of a database from a representative set of seats providing the two main features:

1. Representation of upholstery load-deflection curves by percentiles
2. Selection, adjustment or prediction of user-defined load-deflection curves

Since the trend of these curves (loading part) is quite similar over all seats (Figure 5), the principal idea of the database model is to represent each curve by two characteristic parameters: Absolute deflection d_{max} under maximal force and deflection $d_{50\%}$ (relative to d_{max}) under half of maximal force (Figure 7, left). For these two parameters the percentiles are calculated over all elements of the data pool at each of the four seat locations (Figure 7, right).

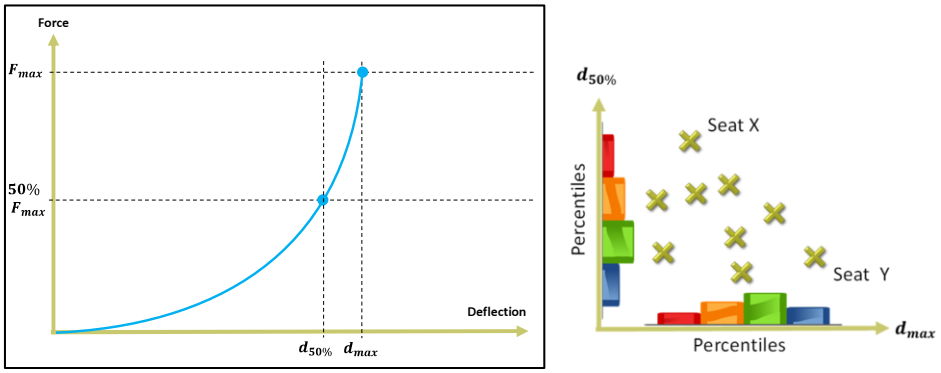

Figure 7. Two characteristic parameters (left) and percentiles in 2-dimensional parameter space (right).

In addition, the correlations between these parameters for different locations are studied as a basis for a regression model predicting a curve at a certain location from the data of the other seat locations (Figure 8). Since the cushion-rear measurement is most important for posture prediction, all further locations should be predictable from there. This enables users to model the upholstery properties of the entire seat by just providing the cushion-rear measurement.

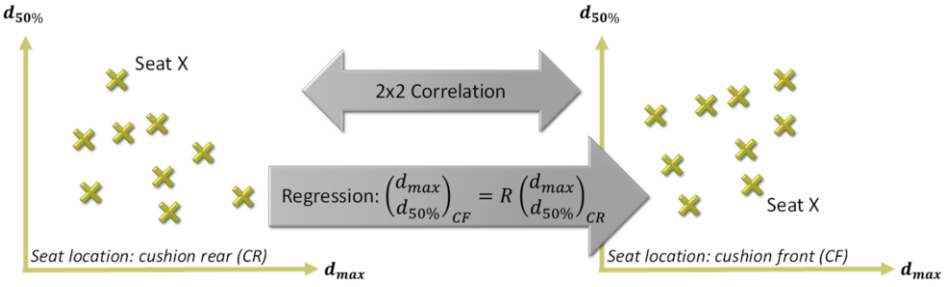

Figure 8. Correlation analysis between parameters of different seat locations.

Finally, the model for deriving a curve from the two characteristic parameters is generated by normalizing measured curves (with respect to maximal force and deflection) and clustering them in three groups at each seat location. The group "mean" contains 60% of curves around the average d_{max} over all seats. The groups "min" and "max" contain the remaining curves below (hard) and above (soft) the average d_{max}. In each group the average curve is pointwise calculated as a representative of the group.

These three curves provide the trends which are locally interpolated to create a user defined curve (Figure 9).

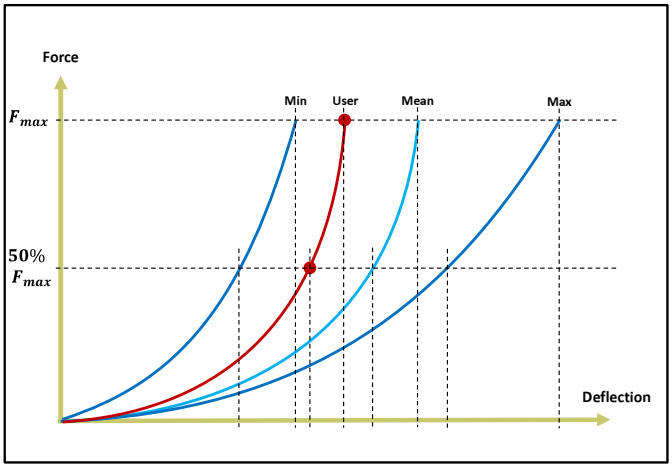

Figure 9. Representative trends for hard (min), mean and soft (max) seat curves interpolated for user curve.

2.3. Measurement processing

The load-deflection curves exemplified above deliver force data that have to be converted to pressure data using the indenter dimensions, thus facilitating the posture simulation to account for various manikin dimensions. In order to handle user-defined indenter shapes in the seat measurement, the processing tool provides a parameterization of the shape with respect to crucial properties.

Modelling the measurement locations on the virtual seat requires the main geometric indenter dimensions, namely the maximal depth and the height at the location of the maximal depth can be defined for each of the rear and the front part (Figure 10, left). The generation of the pressure data requires the effective pressure areas of the indenter during the measurement. Therefore, the pressure area values of horizontal intersections at various heights above the bottom can be defined (Figure 10, right).

To process the seat measurement results, the values of the characteristic load-deflection curves (Figure 4) are stored in a specific protocol. This EXCEL data sheet provides two table fields for the trial pairs of movement and normal force at both measurement locations on each of cushion and back (Figure 11, right).

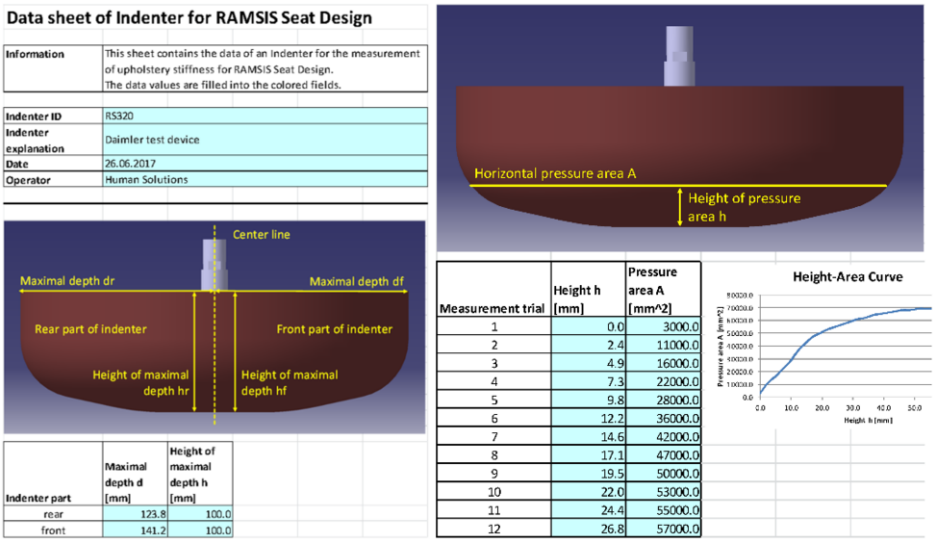

Figure 10. Protocols for indenter dimensions (left) and height specific pressure areas (right).

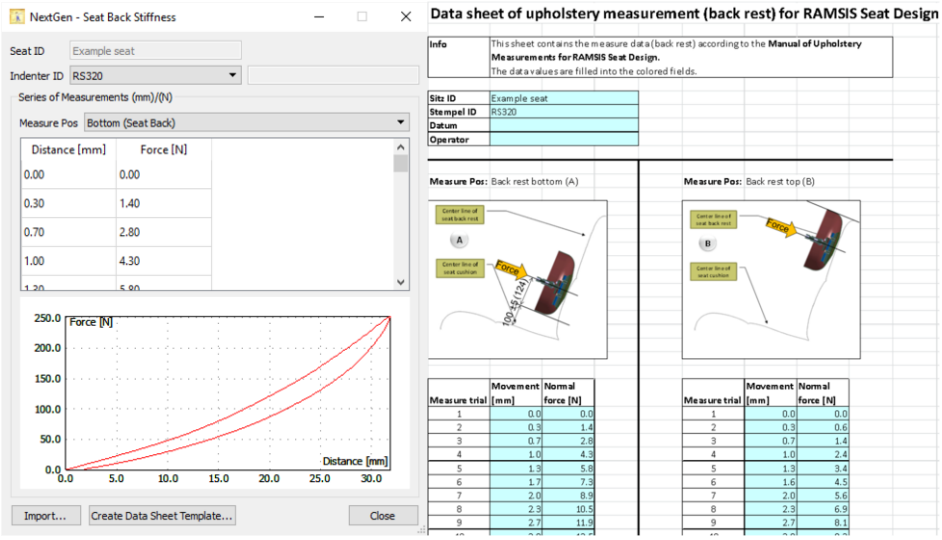

Figure 11. GUI (left) and protocol for load-deflection curve (right).

These sheets can be imported by the processing software which displays the load-deflection curves for each location as well as the indenter positions on the virtual seat and transfers the force data to pressure data using the specified indenter (Figure 11, left). Since the posture simulation addresses the sinking into the seat of a manikin, it refers only to the loading part of the load-deflection curves.

3. Results

The methods introduced in Section 2.2 were applied to the German seat measurements to create an upholstery database predicated on the extracted 2-dimensional parameters from which the percentiles were calculated (Figure 12).

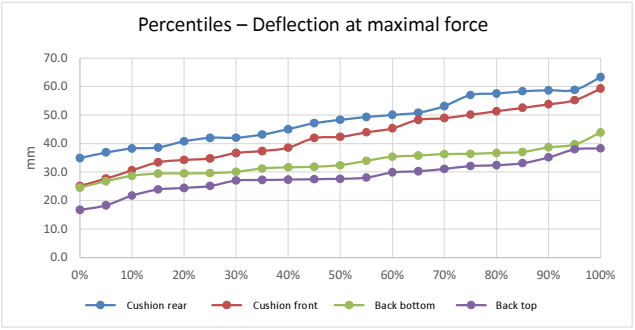

Figure 12. Percentiles for parameter: deflection at maximal force ($\boldsymbol{d_{max}}$).

The clustering process was applied on the normalized raw curve data to get the three representative curve trends for a hard, mean and soft upholstery (Figure 13).

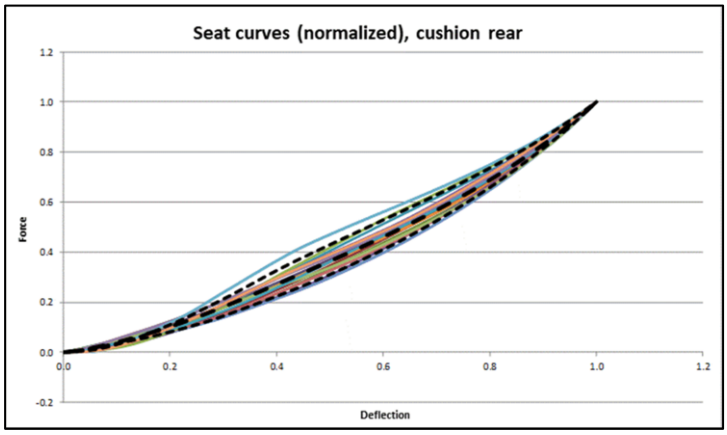

Figure 13. Representative curve trends for hard, mean and soft upholstery.

The correlations of the 2-dimensional parameters between the seat locations cushion-rear and -front, back-top and -bottom were calculated. Additionally, the determination coefficients between the locations were calculated to check the significance of predicting curves from the cushion-rear parameters by regression. According to the results in Figure 14, the prediction of cushion-front and back-bottom from the cushion-rear parameters is satisfying. Back-top parameters should rather be predicted from the back-bottom data if provided. All in all, the prediction order cushion-rear to -front and to back-bottom as well as back-bottom to -top was implemented.

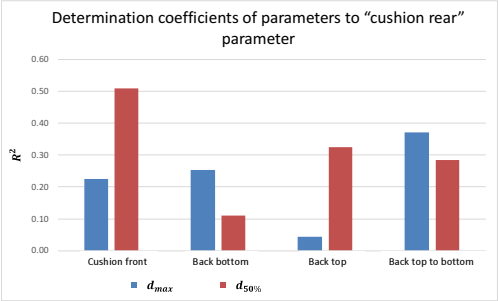

Figure 14. Determination coefficients between parameters and "cushion rear" parameters & prediction order.

All statistical figures were integrated into an upholstery database. The corresponding software interface provides several possibilities to create individual load-deflection curves from the database (Figure 15). In the diagram referential curves such as "very hard", "medium" or "very soft" are plotted (blue) together with the current user defined curve (red). This curve can be defined directly by selecting a referential curve from the database, or by setting the individual characteristic parameters (d_{max}, $d_{50\%}$), or by predicting them from the cushion rear stiffness data. Both parameters can be provided within a reasonable range observed in the measurements. The corresponding pressure and percentile values are automatically displayed.

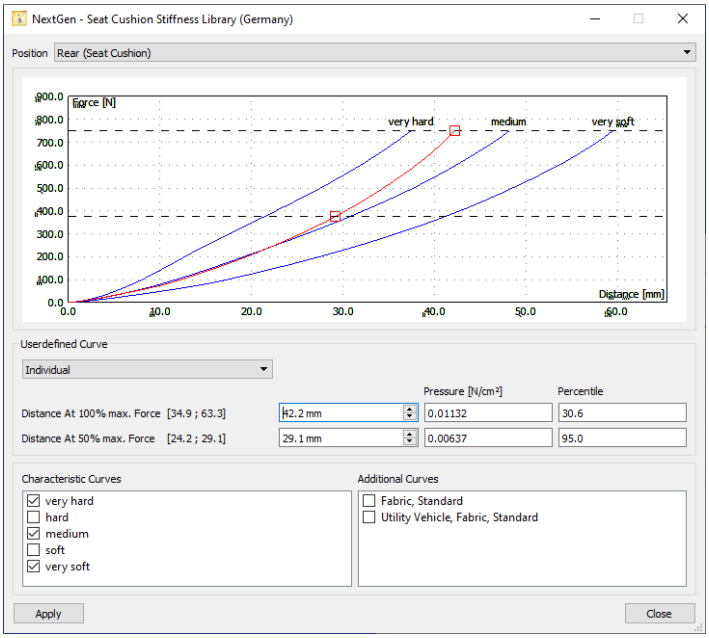

Figure 15. Software interface to upholstery database.

The final curves are ready for direct use in the human seat interaction predicting the manikin or seat positions. For this purpose, the force-deflection curves are transferred into pressure-deflection curves by the processing tools described in Section 2.3. The simulation calculates the position of the manikin or seat such that the manikin body weights are compensated along the manikin-seat collision areas by the reaction pressure from these seat curves [3].

4. Discussion

The presented measurement procedure is less complex and easier to perform than earlier instructions. In addition, it is more generic and in line with the international standard SAE J2896. All this makes individual upholstery measurements more acceptable for users.

The measurement has been extensively performed using a buttock-like indenter. For practical reasons, the same indenter is used for all seat locations. In future, the usage of additional indenter types, especially for the back rest, should be validated.

The usage of horizontal indenter intersections to transfer force to pressure data is a simplification of the indenter pressure distribution in the upholstery. This is a pragmatic compromise, since real pressure areas are difficult to determine during the measurement process and the vertical force component is the most essential one for the prediction of manikin postures.

The current upholstery database is based on a representative set of seats available in German cars and light trucks. The question remains if it can be applied to seats manufactured in additional regions like France, America or Asia. This certainly depends on the international manufacturing differences of vehicle seats and should be elaborated in future. Anyway, the proposed procedure is suited to create further international upholstery databases.

The software interface to the database has been successfully validated by users. It is a proper compromise between a pragmatic reduction of complexity and a range of possibilities to parameterize individual seats.

Acknowledgement

This study was carried out thanks to the financial and technical support of the RAMSIS Industrial Advisory Panel.

References

[1] Bubb H, Bengler K, Grünen RE, Vollrath M. Automobilergonomie. ATZ/MTZ-Fachbuch, Springer Vieweg, 2015.
[2] Balzulat J, Schmidtke H, Bubb H. H-Punktbestimmung für das Menschmodell RAMSIS. Report, Lehrstuhl für Ergonomie, Technical University Munich, Germany, 1995.
[3] Wirsching HJ, Schaller F. On the compatibility of two different simulation approaches for human-seat interaction. In: Proceedings of 3rd International Digital Human Modeling Symposium (DHM2014), May 2014, Tokyo, Japan, Paper #35.
[4] Wirsching HJ, Tomp C, Wiedemann J. A new practical approach for measuring and simulating human-seat interactions. In: Proceedings of 1st International Digital Human Modeling Symposium (DHM2011), 2011, Lyon, France, Paper #2259.
[5] Akamatsu M. Handbook of Automotive Human Factors. CRC Press, 2019.
[6] Siefert A, Pankoke S. CASIMIR/Automotive: A Software for the virtual Assessment of Static and Dynamic Seating Comfort. Paper 2009-01-2311, SAE Digital Human Modeling Conference, 2009.
[7] Ulherr A, Zeller F, Bengler K. Simulating Seat Discomfort: An Experimental Design for Using Digital Human Models. Advances in Intelligent Systems and Computing, Proceedings of the AHFE 2017 International Conference on Human Factors in Simulation and Modeling, Springer International Publishing, 2018.
[8] Jones M, Park J, Ebert-Hamilton S, Kim K, Reed M. P. Effects of Seat and Sitter Dimensions on Pressure Distribution in Automotive Seats. SAE Technical Paper 2017-01-1390, 2017.
[9] SAE J 2896 - Motor Vehicle Seat Comfort Performance Measures. 2012-01-06.

DHM2020
L. Hanson et al. (Eds.)

© 2020 The authors and IOS Press.
This article is published online with Open Access by IOS Press and distributed under the terms of the Creative Commons Attribution Non-Commercial License 4.0 (CC BY-NC 4.0).
doi:10.3233/ATDE200032

Assessment of Aircraft Pilot Seat Performances with Digital Human Models and Virtual Prototypes

Jerome REGNAULT [1], Caroline BOROT and Cecile CABANE
ESI Group, France

Abstract. In the aeronautic industry, some research is currently carried out to improve pilot seating and lying comfort, as well as cockpit ergonomics and accessibility. Pilots spend indeed a lot of time on their seat during a flight. If seats are uncomfortable and pilots are in a wrong posture, risks of injuries and fatigue increase a lot. But taking into account these comfort requirements for the pilot seat and the cockpit design is very challenging. In fact, the very strict aeronautics standards for certification may sometimes jeopardize initial design ambitions regarding comfort. The necessary innovations to address certification and comfort cannot rely on a classical trial-and-error approach on real prototypes with human volunteers. This way of working presents several disadvantages related to test repeatability and human subjectivity. From one real test to another, volunteers' morphology, posture and mood may change and sometimes do not represent the range of possible occupants. In addition, as tests happen late in the development process, at a time where there are limited possibilities to improve the seat and cockpit designs, or propose radically innovative solutions, it becomes very complicated for engineers to reach their initial objectives. To avoid these issues related to real tests, OEMs and suppliers are beginning to change their development process to adopt alternative ways to iterate earlier in the conception phase. In the scope of a project on pilot cabin development, done with Dassault Aviation, Safran and ESI Group, a tool dedicated to aircraft pilot seat virtual prototyping has been developed to integrate earlier in the industrial process comfort aspects and seat integration inside the cockpit. It has been adapted from ESI's Virtual Seat Solution already used in the automotive industry. This paper will describe an application of this virtual prototyping on industrial examples and how designers can virtually create a seat model right from the early design phases and start assessing its performances. Seating simulations of human models have been performed to evaluate static and postural comfort. Those simulations can be then extended to address, in a second step, other performances such as vibratory or thermal comfort, or static comfort for a different seat adjustment such as the reclined posture. Finally, these results have been compared to real measurements to give some insights into the predictivity of ESI Seat and Interior Solutions.

Keywords. Aircraft Pilot Seat, Virtual Prototyping, Digital Human Modeling, Static Comfort, Postural Comfort, Vibratory Comfort, Thermal Comfort, ESI's Virtual Seat Solution for Aero

[1] Corresponding Author, Email: Jerome.Regnault@esi-group.com.

1. Introduction

Pilots spend a considerable amount of time on seats. This leads to disorders such as lower back pain and fatigue. And this is a matter of great concern because uncomfortable workspace for pilots leads to a reduction in alertness while flying the plane. Pilot comfort depends upon several factors such as seat dimensions and adjustments, the seating posture they make possible, the ability to reach easily every part of the control panel, the softness of the trim parts and other design parameters related to the seat and the cockpit [1]. As a consequence, aeronautic OEMs and suppliers want to have the ability to change easily seat and cockpit design to improve this comfort, while respecting safety standards and delivery time. However, seat comfort is usually tested late in the development process, at a time where it is not possible anymore to make a change which may impact the safety performance. To optimize time and costs developments while ensuring the right level for all types of performance, OEMs and suppliers want to iterate earlier on seat to avoid these kinds of issues.

In the scope of the SEFA IKKY [2] project, managed by CORAC French organization, and particularly in the work package focusing on cockpit layout, done with Dassault Aviation, Safran and ESI Group, virtual prototyping has been applied on a specific example to enable this integration of comfort considerations early in the development process. ESI-Group has adapted its automotive solution which is widely adopted by the automotive industry to the specificities aeronautics performance tests [3,4,5,6].

This paper will provide an example of how virtual prototyping can be applied during the early stage of seat conception to address first comfort requirements. Then, it will be used during the phase of detailed design to consider vibration response and thermal comfort as well. A variant of the pilot seat being manufactured, this paper will propose some correlations between real tests and simulation results to validate the software predictive capability at all stages of the seat development cycle.

2. Challenges of Aircraft Pilot Seat Performances Evaluation

Traditional seat development process is usually done after design freeze with a focus on safety. Some simulations are performed, but the seat model they use has been usually calibrated through tests on real prototypes. The outcome of those simulations is therefore limited. Furthermore, after seat design freeze, if issues are discovered on performance types other than safety, engineers and seat designers must take costly counter measures with associated delays or deliver their seat below the expected performance levels.

Using human volunteers to test static or vibratory comfort is also inconvenient to ensure the right performance levels. The first issue is the repeatability. The seat static comfort performance is evaluated through the measurement of pressure distribution for a given occupant posture [7]. Ensuring that the same volunteer will adopt the same posture on different variants of the seat is a challenge. Therefore, it is difficult, with volunteers, to make a reliable comparison on comfort, between two design iterations of the same seat. A second issue related to those tests with volunteers, is the ability to recruit and keep available along the years, people representing the range of possible end-users from small female to large male.

Combining virtual seat prototypes and digital human models is one way to overcome the challenges previously described. Seat designers and engineers can create easily reliable seat models with data available during the early stages. They can anticipate potential comfort issues with human models of different anthropometries. With tools to quickly explore different seat design changes, it is also possible to make some choices very early in the development cycle. By addressing with the same seat model both safety and comfort, it is finally affordable to develop a seat ensuring comfort and prepare virtually its certification before producing any physical prototype.

3. Preliminary Comfort Performance Evaluation in Early Development Phase

In early development phase, designers and engineers may have very few information and available data to build a seat model. Indeed, all decisions have not been taken yet, and this is the purpose of the development process itself, to select the adequate materials and shape, which will lead to the best performances. In addition, people in charge of this initial concept phase are not necessarily used to simulation techniques and need support to make the best use of them.

3.1. Management of Missing Information at the Early Stage

The different seat components are made of selected materials, whose properties will influence significantly the seat performance. Consequently, in order to be predictive, the model needs to include a description of those properties. But as mentioned here before, the goal at this stage is to use simulation in order to choose the right material based on targeted performance levels. Therefore, at this stage only a first material assumption will be required (coming from a previous seat for instance), and simulation will be used to update those materials in order to reach the targeted performance, as for instance the occupant position. This is made possible with one of the tools developed in the frame of the project. Indeed, it includes first a material database with materials of different kinds (foams, textiles, metals, plastics) which are automatically assigned to the different seat parts based on the component they belong to (Figure 1). For example, if a part is recognized as being a cover, a textile material will be automatically assigned to it. Then, the user will give his targeted occupant position and the simulation will handle the optimization of the materials to reach this target. The output is here the choice of the materials to reach a prescribed performance.

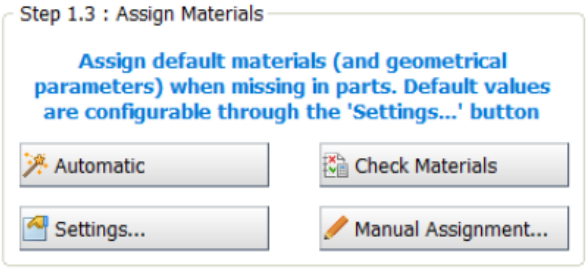

Figure 1. Material Assignment with ESI Interior Solution.

This automated material assignment is one step of a larger automated workflow, developed to guide people non-familiar with the building of seat models.

3.2. Human Models to Test Several Anthropometries

To ensure cockpit design will deliver a good level of static comfort while optimizing the living space, ESI has developed a finite element human models' database with anatomically precise features and deformable tissues. Several kinds of anthropometries from different populations and including elderly and overweighed people are embedded and can be scaled to match with real users (Figure 2). Those models have been developed based on real people and validated regarding their ability to predict pressure distribution and vibratory behavior [8][9][10].

Figure 2. Comfort Human Model Library embedded in ESI Interior Solution.

3.3. Occupant seating simulations for preliminary layout design choices

Regulations impose a precise seating position for pilots, ensuring that they will have the best visibility within the cockpit. This position is determined by the pilot's eyes position once seated. They should be at the Eye Reference Point (ERP) position, which is materialized by aircraft manufacturers with a marker in the cockpit. When seating, the pilot has to adjust the seat settings in order to make sure to have his eyes at the level of this marker. This being done, he will have adopted the optimum position to operate the aircraft.

Designers must design a seat with settings adjustments which enable to have the actual eyes location on the cockpit ERP for several extreme anthropometries. ESI has therefore developed an automatic process to simulate the pilot seating and an automated adjustment of the seat settings to reach the ERP (Figure 3). This process is as simple as the workflow for the seat modelling described here before. Users must only choose the pilot anthropometry, define the cockpit ERP location, and then, the process is done in 3 main steps. The first one consists in seating human model and tightening belt. Then the cylinder located under the seat is adjusted to reach the vertical coordinate of ERP and finally the horizontal seat adjustment is done. The output of this simulation is not only the eyes position of the pilot for a given seat, but the adequate seat settings adjustments to reach the targeted ERP.

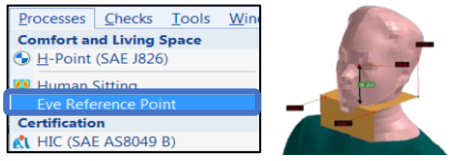

Figure 3. ERP process with ESI Interior Solution.

Fig a)

Fig b)

Figure 4. Simulation with the ERP process of ESI Interior Solution: before a) and after b) horizontal seat adjustments, applied on Safran Seat inside a Dassault Aviation Falcon Environment.

Thanks to these numerical tests, engineers have an idea of solutions they could incorporate in a future seat before any virtual and/or real prototype has been built (Figure 4). At this stage of development, engineers could explore virtually the seat integration inside the cockpit and can easily iterate.

4. Exhaustive Comfort Performance Evaluation during Detailed Design Phase

4.1. Seat Model

During detailed design phase, the main objective is to predict very accurately the performances of the seat. For this purpose, the virtual model of the seat is defined as close as possible to the future real production seat. Regarding comfort, foam properties have a major influence. Tensile and quasi-static compression tests must be carried out on samples of material to obtain stress as a function of strain for static comfort. Those data are directly applicable to the seat model. For vibrations responses, similar tests must be performed, and their results can be converted directly by the software into proper dataset for the simulation. Those properties are purely physical, and no numerical tuning is needed. Engineers have the possibility to fill their own material database into the software and assign a specific behavior to each seat part of the foam cushions (Figure 5).

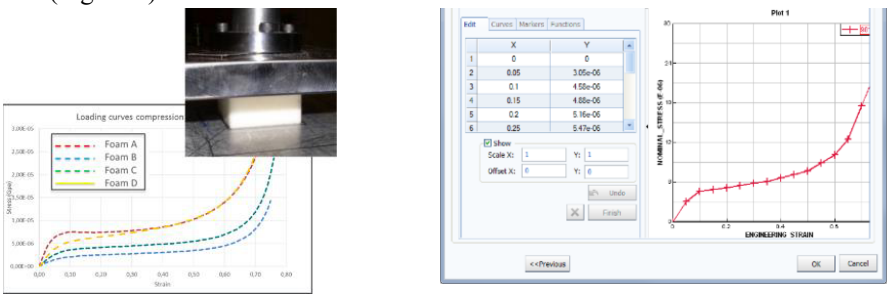

Figure 5. Material Mechanical Properties: As measured in test on the left, as pasted in the model on the right with ESI Interior Solution.

For the frame modelling, different strategies are adopted based on the performance to be simulated. For both certification and vibrations testing, the frame deformation must be considered. On the opposite, for static comfort, loads supported by the frame are not in a range where the frame is likely to deform. A semi-rigid modelling is used to save

some simulation time. As a consequence, the model contains two alternative modellings for the frame which can be activated automatically based on the performance to be tested (Figure 6):

- Deformable Modeling: each frame part is deformable and all connections between all parts and the frame are precisely defined,
- Semi-Rigid Modeling: frame parts are modeled with large rigid bodies linked with kinematic joints.

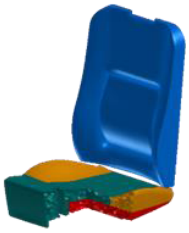

Figure 6. Different foam materials assignment on the Safran seat cushions with ESI Interior Solution.

4.2. Static Performance

Safran has done several real tests with three volunteers to assess postural comfort. Digital human models have been generated by Safran engineers to match with volunteers. Real male volunteers correspond to small, medium and large statures [8][9].

Table 1. Pilot morphology: Real Volunteers & virtual human models from ESI Interior Solution.

	Small		Medium		Large	
Properties	Size (cm)	Weight (kg)	Size (cm)	Weight (kg)	Size (cm)	Weight (kg)
Real Tests	161	51	192	82	194	118
Virtual Model	157	51	180	82	191	118

The first simulation step consists in seating the human model. Contacts between occupant and seat are then defined automatically. Then the automatic ERP process adjusts the seat position on longitudinal and vertical axis. Once the seat has been correctly positioned, pressure maps and pressure distributions from simulation and real tests have been compared.

Numerical pressure maps are very close to real maps (Figure 7). Average pressures and pressure distributions are also near experimental results (0,54 N/cm² for simulation tests and 0,50 N/cm² for real tests. Moreover, overpressure areas have the same locations. These areas are below ischium tuberosities and on lateral zones where the foam is stiffer. However, demarcation line with the forward foam is not present on virtual simulation because it wasn't included in the CAD file. Moreover, real test reports did not contain any precise information on each occupant posture. This could affect results.

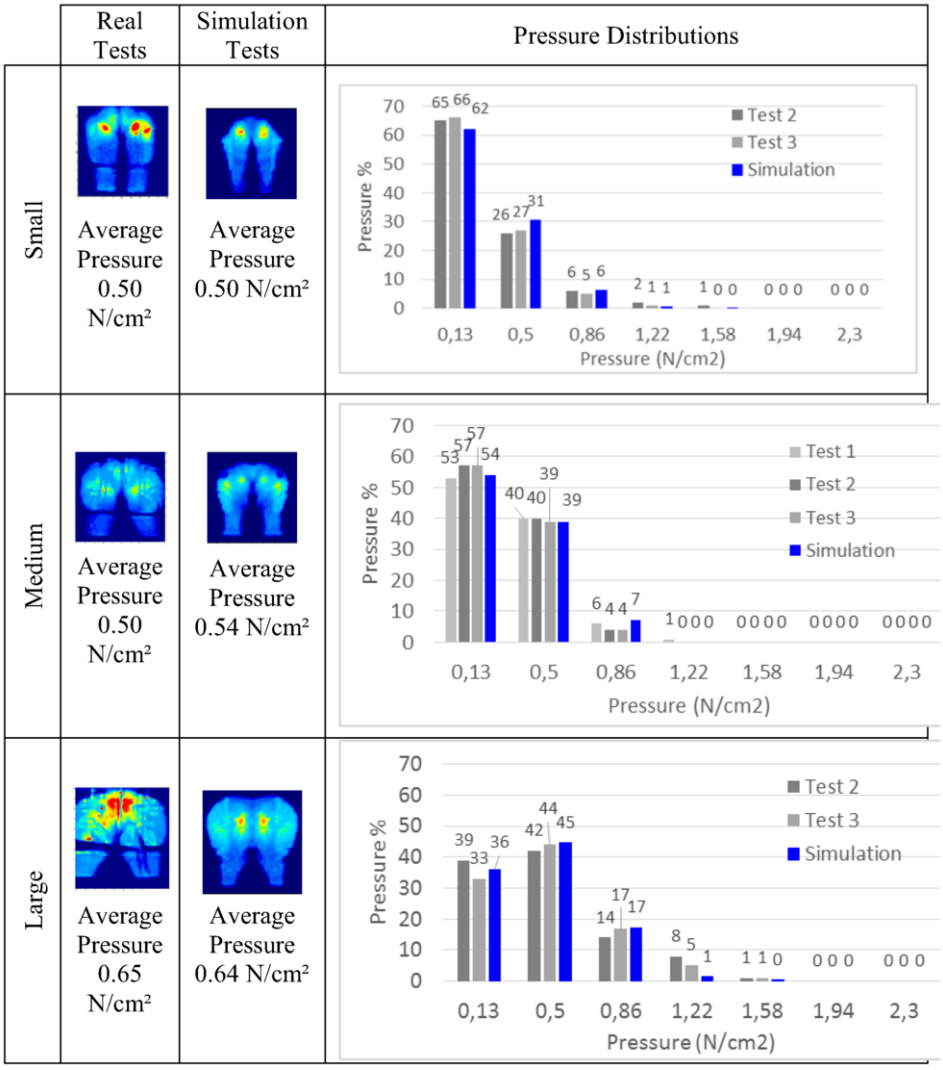

Figure 7. Static seating pressure map comparison between real tests and virtual tests done with ESI Interior solution.

4.3. Dynamic Comfort Performance

To ensure vibratory seat performance, seat coupled with human system transfer function has been measured. In these tests, the same human volunteers as for postural studies have been positioned on the seat. Regarding simulations, the previous seating simulations are extended to replicate seat excitations based on confidential experimental data and monitor how much those vibrations are absorbed or increased by the seat at the level of the occupant. Occupant comfort only depends on low frequencies around peak of resonance [11].

The numerical model presents results which are in the range of the experimental scattering (Figure 8). The movement observed at the peak of resonance is a movement mainly vertical with a slight flexion of the pelvis around the sagittal axis. The natural frequency for the foam material is always around this value.

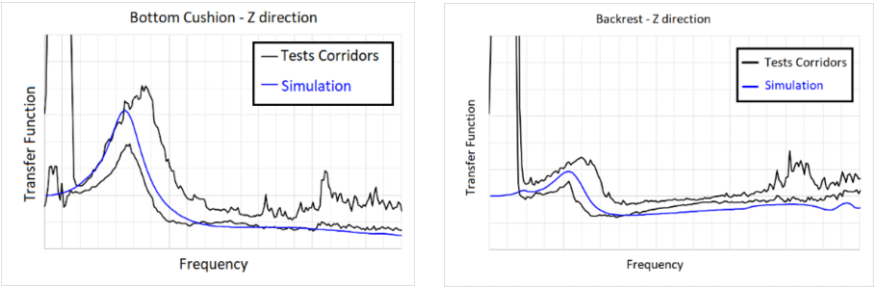

Figure 8. Examples of vibratory response and correlation between simulation done with ESI Interior Solution and experiment.

4.4. Thermal Comfort Performance

To evaluate thermal comfort performance the seat model has been updated, by adding some thermal material properties to the mechanical properties already defined before. Two main parameters are fulfilled: the conductivity and the specific heat capacity. Both can be set as constant or temperature dependent. Conductivity can also be made dependent on the level of compression reached by the material after an occupant is seated. Pilot seats are also covered with sheepskin including wool. The main function of sheepskin cover is to keep pilots cool in the summer and warm in the winter – whatever the temperature in a cockpit is, sheepskin covers remain of almost the same temperature and keep a pilot dry. Sheepskin is also a perfect seat cover for aircraft seats since it is totally flame resistant and self-extinguishing. Sheepskin and wool cover were modelled as a porous material retaining air flows. Its width is 10 mm. Such covers were placed both on the backrest and on the cushion.

At the level of contact interfaces if two interfaces are in contact, the heat is transferred without loss and, the more the two interfaces are distant, the less heat is transferred. The loss of heat by convection with air is modelled through a uniform and constant coefficient applied on all external surfaces of the seat [6]. Regarding human models, mathematical models predicting human thermal behavior are included and rely on the computation of the body thermal balance. The human body can be considered as a combination of two thermoregulation systems: one active and one passive system. The active system model mimics the behavior of the central nervous system which manages the temperature regulation, and the passive system simulates the heat and mass transfers within the body but also with the body environment. In addition to the simulation of the thermoregulation and the calculation of the temperature distribution, the human models can provide comfort scores [6]. The aim of defining such scores is to have an objective criterion to support the design of seat heating and cooling system or global thermal management of the cockpit. The thermal comfort criterion which has been developed is partially based on the work of Zhang [12]. Based on experimental data, Zhang has established a direct relationship between objective values (skin temperature, skin temperature variation…) and the subjective feeling of comfort/discomfort [5] [6].

After calculations, engineers can have access to temperature distribution on seat and occupant, sensation and comfort scores, and can explore several seat variants to diminish the thermal loads on pilots, which have a direct influence on dehydration, fatigue and alertness (Figure 9).

Figure 9. Temperature Distribution on Safran Seat done with ESI Interior Solution.

5. Conclusion

In order to deliver a seat prototype meeting standard and performances requirements, Safran & Dassault Aviation have decided to adopt virtual prototypes. Indeed, usual traditional seat development process doesn't allow to test seat comfort very early in the development process and a large margin to correct defaults.

This study showed the benefits of using Virtual Seat Prototyping and digital human models to anticipate pilot seat integration inside a cockpit. Thanks to dedicated workflows, Safran & Dassault Aviation engineers and designers could start to explore new designs with few data and almost no finite elements background and compare results coming from simulations with real tests, validating software predictivity for static comfort and vibration response evaluation. They were able to iterate on existing seat designs for future seat development projects.

References

[1] Paul G. Occupant comfort. In: Scataglini S, Paul G, editors. DHM and Posturography. 2019, 471-486. Academic Press, London, UK.
[2] SEFA (Systèmes Embarqués et Fonctions Avancées) IKKY (Intégration du cockpit et de ses Systèmes) Project, managed by CORAC (Conseil Pour La Recherche Aéronautique Civile).
[3] Dooge D, Cabane C, Marca C, Dwarampudi R, Cohen D, Pearson S. Utilizing finite element model objective seat comfort results. SAE Technical Paper 2012-01-0074, 2012.
[4] Montmayeur N, Marca C, Dwarampudi R, Kolich M, Nunez S. Virtual Seat Manufacturing and Testing for FMVSS 202a Backset Prediction. SAE Transactions. SAE Technical Paper 2007-01-2460, 2007.
[5] Doroudian M, Kolich M, Almasi G, Medoro M, Dwarampudi R, Salokhe S. Virtual Temperature Controlled Seat Performance Test. SAE Technical Paper Technical Paper 2018-01-1317, 2018.
[6] Adel Z, Marca C, Borot C. Development of a human thermal model to predict seat occupant thermal comfort. In: 1st International Comfort Congress, Salerno, 2017.
[7] Wang X, Savonnet L, Theodorakos I, Beurier G, Duprey S. Biomechanical human models for seating discomfort assessment. In: Scataglini S, Paul G, editors. DHM and Posturography, 2019, 643-656. Academic Press, London, UK.
[8] Montmayeur N, Marca C, Choi HY, Sah S. Experimental and numerical analyses of seating pressure distribution patterns. SAE Technical Paper 2005-01-2703, 2005.
[9] Beaugonin M, Borot C. ESI unique human model for seat (dis) comfort evaluation. In: Scataglini S, Paul G, editors. DHM and Posturography, 2019, 139-153. Academic Press, London, UK.

[10] Borot C, Marca C, Jammet-Reynal O. Predict passenger comfort in aircraft cabin to improve seat design. AEGATS Conference 12, 2016.
[11] Griffin MJ. Handbook of human vibration. Academic Press Inc, 1996.
[12] Fiala D. Dynamic simulation of human heat transfer and thermal comfort. Doctoral Thesis, De Montfort University, UK, 1998.

DHM2020
L. Hanson et al. (Eds.)

© 2020 The authors and IOS Press.
This article is published online with Open Access by IOS Press and distributed under the terms of the Creative Commons Attribution Non-Commercial License 4.0 (CC BY-NC 4.0).
doi:10.3233/ATDE200033

A Digital Human Model for the Simulation of Dynamic Driving Maneuvers

Michael ROLLER [a,1], Vanessa DÖRLICH [a], Joachim LINN [a], Staffan BJÖRKENSTAM [b] and Peter MÅRDBERG [b]
[a] *Fraunhofer ITWM, Germany*
[b] *Fraunhofer Chalmers Center, Sweden*

Abstract. In this work, a digital human model based on multibody system dynamics is used in a car pre-crash scenario. An optimal control approach is used to generate motion and control signals. The arms of the manikin are actuated by Hill muscles, while the rest of the body is controlled by joint torques. A full braking maneuver is investigated as an application case.

Keywords. Digital human model, Hill muscle, Optimal control, Dynamic driving, Pre-crash

1. Introduction

Digital human models (DHM) are widely used in automotive industry to simulate the driver in very early stages of product development, where no physical prototypes of the car exist. In case of crash simulation, detailed finite element (FE) models of the human body are used to simulate the highly dynamic impact and the resulting injuries in the human body [1,2,3]. Models with multibody system (MBS) kinematics are widely used when the reachability and the ergonomic assessment of the driver is investigated [4,5, 6,7]. These types of models are only used in static scenarios, where the car is standing or driving with constant velocity. In dynamic driving scenarios like cornering, sudden braking or pre-crash scenarios, neither FE nor MBS model types are applicable. Besides being difficult to control, FE models are too time consuming, as the simulated time span in dynamic driving is longer than in crash simulations. The kinematic models are not able to take into account dynamic loads and contact forces. Furthermore, the motion generation is difficult, because these models are usually based on forward or inverse kinematics.

2. Methods

In this work, we will present an approach for the enhancement of a multibody based DHM to generate human like motions for dynamic driving maneuvers. The human is

[1]Corresponding Author: Michael Roller, Fraunhofer ITWM, Fraunhofer-Platz 1, 67663 Kaiserslautern, Germany; E-mail: michael.roller@itwm.fraunhofer.de

modelled as a multibody system for that purpose, where the limbs are rigid bodies, which are connected via joints. Hill muscles are used to implement digital versions of the real muscles in the human body and to actuate the multibody system. An optimal control algorithm, which is able to handle opening and closing of contacts, is developed in order to generate the dynamic human motion. It allows for the simulation of the dynamic interaction of the DHM with the car interior such as the seat, pedals or the steering wheel. In this approach, only some basic boundary conditions have to be described. These include the sitting posture of the human at starting time with two hands on the steering wheel and the trajectory of the car. Using a certain objective function, the optimal control approach then generates the desired control (muscle actuation) and the human motion. This approach has already been applied successfully to simulate dynamic motions of workers [8,9,10]. In this work we will show that it is also applicable in pre-crash scenarios, like full braking.

2.1. Biomechanical Multibody Model of the Human

The limbs of the human are modelled as rigid bodies with the mass and inertia tensor as physical properties. Their respective position and orientation in space are given by a translational vector and a rotation matrix. These rigid bodies are connected with rotational joints in a tree structure starting from the hip. In Figure 1, all degrees of freedom of the DHM are displayed. It is essentially the same manikin which was used in [9] to do a full body box lift. The degrees of freedom of each joint q control the position and

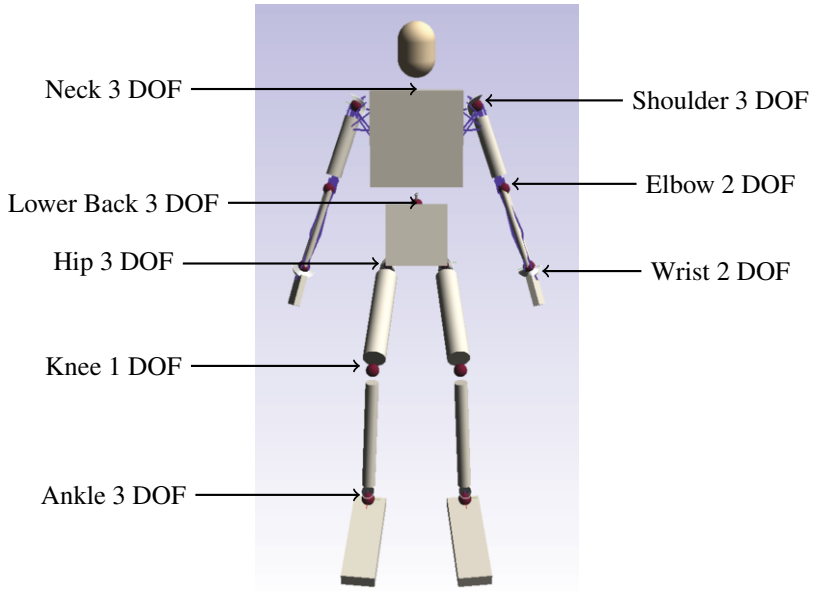

Figure 1. DHM with 40 degrees of freedom including the rigid body joint, which has 6 DOF

orientation of the corresponding child body in terms of the parent body, see [11] for more details. The hip is connected to the fixed world frame by a rigid body joint, which allows the DHM to translate and rotate freely in space. All of these degrees of freedom are col-

lected in the vector $\mathbf{q} = (q_1, ..., q_N)$, which describes the position and orientation of each body and therefore the state of the multibody system.

A digital version of the human muscles is used to actuate the multibody model representing the human skeleton. As in [12,13], muscles of simple Hill-type are utilized. The rheological model of the muscle consists of a contractile element (CC) and an elastic spring (PEC), which are connected in parallel. The force generated by the CC depends

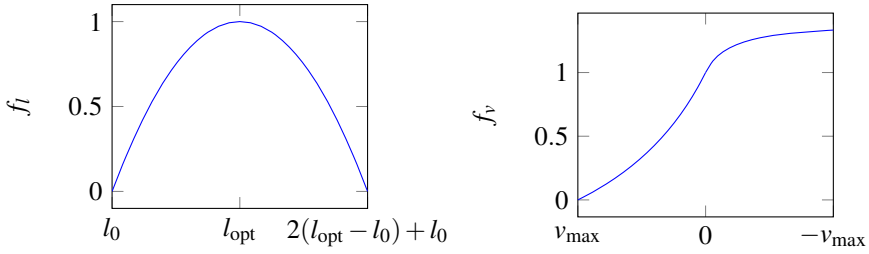

Figure 2. Left: Force-length relation of CC-element. **Right:** Force-velocity relation of CC-element, where $v > 0$ corresponds to an eccentric and $v < 0$ to a concentric motion.

on the current length l, the contraction velocity $\dot{l}$, the actuation level $u \in [0,1]$ and the maximum isometric force $F_{\max}$ of the muscle and is given by

$$F_{CC} = f_l(l) f_v(\dot{l}) u F_{\max} \, . \tag{1}$$

The force-length and the force-velocity dependencies are visualized in Figure 2. Here, l_0 represents the minimum and l_{opt} the optimal muscle length. The negative scalar $v_{\max} < 0$ is the maximal contractive velocity of the muscle.

The PEC element is modelled using a linear elastic spring $F_{PE} = k(l - l_0)$ with stiffness $k \in \mathbb{R}_+$. Since the elements are connected in parallel, the muscle force is a linear superposition of both,

$$F_m = F_{CC} + F_{PE} = f_l(l) f_v(v) u F_{\max} + k(l - l_0) \, . \tag{2}$$

In order to use the rheological Hill elements in a MBS, a piecewise linear string is used to represent the muscle path. This string is defined by $M \geq 2$ points $\mathbf{x}_i$, where each point is positioned on the surface of a rigid body. The length of the muscle is calculated by summarizing the distances between points. With these quantities and an activation u, the scalar muscle force $F_m \in \mathbb{R}$ is calculated using equation (2). Then, a force pointing in the direction of neighbouring points with magnitude F_m is applied in every point $\mathbf{x}_i$, which induces a force and torque on the corresponding body.

In this work, both arms are actuated by Hill muscles. Each arm consists of the same 27 muscles which were used in [10] to control the seven degrees of freedom of the arm. In Figure 3, all digital muscles of the right arm are visualized in detail. The remaining joints of the human are controlled by joint torques, which are the ankles, knees, hips and neck.

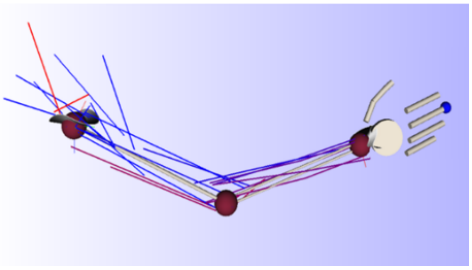

Figure 3. Multibody model of the arm including 27 muscles.

2.2. Discrete Mechanics and Optimal Control with Constraints

Traditionally, human simulation tools use quasi-static poses to emulate motion, which severely limits the possible set of producible motions. For pre-crash simulations, we want to be able to realistically simulate highly dynamic motions, where modelling of inertia effects becomes relevant. To that end, we model the manikin as a dynamical system and use optimal control methods to compute the motions. This approach was already used for the simulation of different working tasks [8,9,10,14].

An optimal control problem is defined abstractly by the following formulas

$$\min_{\mathbf{q},\mathbf{u}} J = \int_{t_0}^{t_f} \phi\left(\mathbf{q},\dot{\mathbf{q}},\mathbf{u},\dot{\mathbf{u}}\right) \mathrm{d}t \tag{3}$$

s.t.

$$\frac{\partial L}{\partial \mathbf{q}}(\mathbf{q},\dot{\mathbf{q}}) - \frac{\mathrm{d}}{\mathrm{d}t}\frac{\partial L}{\partial \dot{\mathbf{q}}}(\mathbf{q},\dot{\mathbf{q}}) + \mathbf{F}(\mathbf{q},\dot{\mathbf{q}},\mathbf{u}) + \mathsf{G}^T(\mathbf{q})\lambda = 0\,, \tag{4}$$

$$\mathbf{g}(\mathbf{q}) = 0\,, \tag{5}$$

$$\mathbf{h}(\mathbf{q}|_{t_0},\mathbf{q}|_{t_f},\dot{\mathbf{q}}|_{t_0},\dot{\mathbf{q}}|_{t_f},t_0,t_f) = 0\,, \tag{6}$$

$$\mathbf{c}^- \leq \mathbf{c}(\mathbf{q},\mathbf{u},\lambda) \leq \mathbf{c}^+\,. \tag{7}$$

As already introduced in Section 2.1, the variable $\mathbf{q}$ represents the temporal trajectory of the MBS between the starting time t_0 and the end time t_f. The control signals for the muscles and the joint torques are combined in the variable $\mathbf{u}$. In (3), the objective function J is introduced, where ϕ is a measure for the state of the system. As a side constraint, the constrained Euler Lagrange equations (4)-(5) have to be fulfilled, where the function L represents the Lagrangian of the system, the function $\mathbf{g}$ summarises the constraints and the variable λ is the corresponding Lagrangian multiplier. A general formulation of the boundary conditions is given by (6) with the function $\mathbf{h}$. Additional equality and inequality constraints can be included in the optimal control problem by (7). Here $\mathbf{c}^-$ is the lower and $\mathbf{c}^+$ is the upper bound of the constraint function $\mathbf{c}$. This is a general description of many different constraints like box constraints on the controls, constancy of a function or path constraints. Altogether, the optimal control problem is an optimization problem and the solutions are temporal trajectories of the MBS $\mathbf{q}$, the control signals $\mathbf{u}$ and the Lagrangian multiplier λ.

In order to solve the optimal control problem, the continuous problem (3)-(7) is discretised into a non-linear programming problem using discrete mechanics, see [15,16] for more details. This approach is called DMOCC (discrete mechanics and optimal control with constraints). The discrete equations of motions derived in this way have been shown to be superior compared to standard discretisations since they preserve characteristics of the continuous system such as conservation of momentum and a good energy behaviour. This results in very stable integrators, which in practice allows us to use large time steps when solving our problems. The resulting non-linear programming problem is solved with the interior point method [17].

3. Simulation Results of a Sudden Braking Maneuver

As application case we investigate the dynamic scenario of full braking of a car with the DHM as the driver. The car is modelled as a plate, where two pedals, a seat and a steering wheel are rigidly mounted. This sledge is mounted using a one dimensional translation joint on the fixed root frame. The car model is visualized in Figure 4.

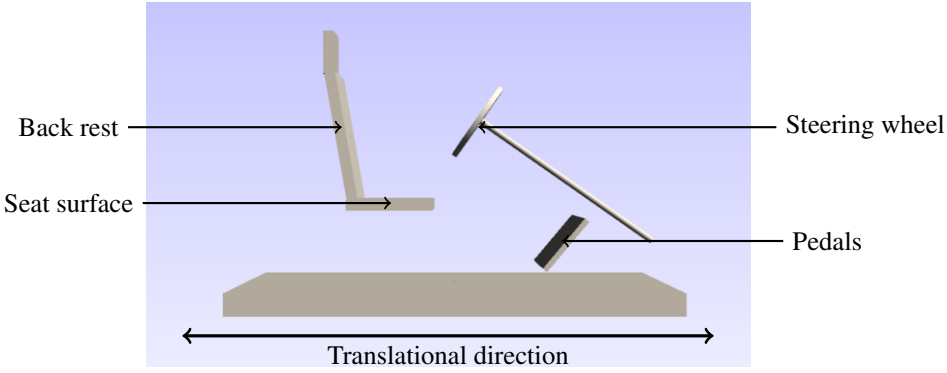

Figure 4. Simplified model of a car used in the simulation.

The manikin specified in Section 2.1 is seated into the simplified car model as follows. Both feet are rigidly mounted on the pedals in an arbitrary position, but fixed over the time span of the simulation, which means that the position on the pedals is a free variable in the optimal control problem. Also the constraint forces are restricted, such that Coulomb's law of static friction holds. The buttocks of the human are connected in the same way to the lower seat surface. Both hands are connected rigidly to the steering wheel in a fixed position and orientation. In case of the hands, the constraint forces are not restricted, such that the constraint force realizes grabbing the wheel with a closed hand. For more details on how this is technically implemented we refer to [10].

The simulation is split in two connected phases. In the first phase the car is accelerated to $5\,m/s$ from starting at standstill. The manikin is constrained to an arbitrary but fixed position during the whole phase. This is done to avoid a dynamic preparation for the sudden deceleration of the manikin by moving the upper body against the direction of driving, which would be unnatural behaviour. The duration of the phase is fixed, because a constant force is used to accelerate the car. It has to be noted, that due to the choice

of special time stepping algorithm, it is sufficient to discretise this phase by only one interval. This reduces the number of variables and therefore decreases the computation time.

At the beginning of the second phase the slide stops immediately to $0 m/s$, which is done by adding an additional dynamic constraint, see [10,18]. Therefore, the kinetic energy of the car is completely absorbed by a phase specific constraint force. At the end of the phase, the manikin is forced to be at rest as well. The DHM has to use the muscle and control torques to eliminate the kinetic energy during the phase as there are no additional constraint forces. The duration of this phase is free, which means that it is an additional variable of the optimization problem. Minimal control is used as objective function for this application case, which means that in objective function (3) $\phi = \mathbf{u} \cdot \mathbf{u}$ is used.

In Figure 5, the movement of the manikin during the second phase is visualized in a series of pictures. The simulation starts at the top left corner at picture **(a)** and time is moving through the rows to the right. At the end of the row the simulation continues at the left side of the next row. It can be observed that the upper body of the manikin is moving towards the steering wheel at the beginning of the simulation, see picture **(b)**. This is caused by a lack of strength of the muscles in the arms and the control torques in the lower back to eliminate the remaining kinetic energy immediately. After some time, this movement stops and the body is moving in direction of the back rest until it is at rest, see picture **(c)**.

4. Discussion

It has to be noted that the motion was generated by the DMOCC method with only the constraints described in section 3. Thus, no time demanding forward kinematic positioning of the manikin has to be performed. Additionally, all specified muscle forces and actuation signals are computed by this method as a by-product, which could be used in a further physiological evaluation. The computation time for such a model on a modern personal computer is in the range of minutes. Therefore, it is possible to do many different variations using this simulation approach, e.g. in the positioning of the seat, the position of the steering wheel or the velocity of the car as well as different posture, anthropometry and weight of the driver.

In this work, we have shown that an optimal control approach including muscles as actuators can be used to create a realistic motion of a manikin in a pre-crash simulation. The simulation times of such a model are in the range of minutes, which is much faster than detailed FE simulations. These FE models usually run for hours without having any active control of the DHM. We observed that in this type of optimal control simulation of a DHM in a dynamic pre-crash scenario, the computational model anticipates the sudden perturbation and prepares dynamically in an unnatural manner for it. In this work, this behaviour was suppressed by fixing the degrees of freedom of the DHM during the first phase. However, this can also be used as a method to determine physically optimal behaviour of a human in dynamic scenarios using a suitable formulation of the optimal control problem.

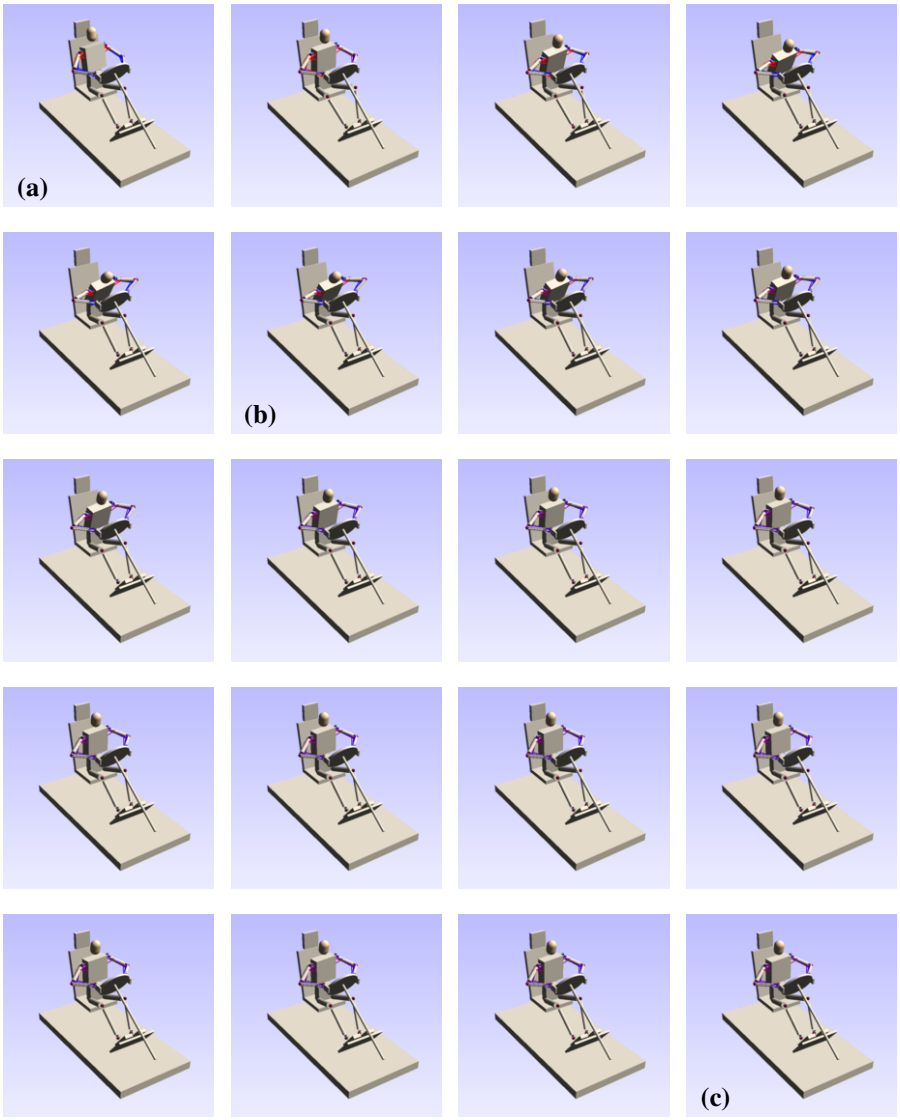

Figure 5. Screenshots at different time stamps of the DHM during the second phase. The time is running from left to right through the rows and from top to bottom.

References

[1] Iwamoto M, Kisanuki Y, Watanabe I, Furusu K, Miki K, Hasegawa J. Development of a finite element model of the total human model for safety (THUMS) and application to injury reconstruction. In: Proceedings of the international IRCOBI Conference; 2002. .

[2] Forman JL, Kent RW, Mroz K, Pipkorn B, Bostrom O, Segui-Gomez M. Predicting rib fracture risk with whole-body finite element models: development and preliminary evaluation of a probabilistic analytical framework. In: Annals of Advances in Automotive Medicine/Annual Scientific Conference. vol. 56. Association for the Advancement of Automotive Medicine; 2012. p. 109.

[3] Östh J, Mendoza-Vazquez M, Linder A, Svensson MY, Brolin K. The VIVA OpenHBM finite element 50th percentile female occupant model: whole body model development and kinematic validation. In: IRCOBI Conference; 2017. p. 13–15.

[4] van der Meulen P, Seidl A. Ramsis–the leading cad tool for ergonomic analysis of vehicles. In: International Conference on Digital Human Modeling. Springer; 2007. p. 1008–1017.

[5] Blanchonette P. Jack human modelling tool: A review. DEFENCE SCIENCE AND TECHNOLOGY ORGANISATION VICTORIA (AUSTRALIA); 2010.

[6] Hanson L, Högberg D, Carlson JS, Delfs N, Brolin E, Mårdberg P, et al. Industrial Path Solutions–Intelligently Moving Manikins. In: DHM and Posturography. Elsevier; 2019. p. 115–124.

[7] Högberg D, Hanson L, Bohlin R, Carlson JS. Creating and shaping the DHM tool IMMA for ergonomic product and production design. International Journal of the Digital Human. 2016;1(2):132–152.

[8] Björkenstam S, Nyström J, Carlson JS, Roller M, Linn J, Hanson L, et al. A framework for motion planning of digital humans using discrete mechanics and optimal control. In: 5th International Digital Human Modeling Symposium, Bonn Germany, June 26-28, 2017. Federal Institute for Occupational Safety and Health; 2017. p. 64–71.

[9] Björkenstam S, Leyendecker S, Linn J, Carlson JS, Lennartson B. Inverse Dynamics for Discrete Geometric Mechanics of Multibody Systems With Application to Direct Optimal Control. Journal of Computational and Nonlinear Dynamics. 2018;13(10):101001.

[10] Roller M, Björkenstam S, Linn J, Leyendecker S. Optimal control of a biomechanical multibody model for the dynamic simulation of working tasks. In: Proceeding of the 8th ECCOMAS Thematic Conference on Multibody Dynamics; 2017. .

[11] Featherstone R. Rigid body dynamics algorithms. Springer; 2014.

[12] Maas R, Leyendecker S. Optimal control of biomechanical motion using physiologically motivated cost functions. In: The 2nd joint international conference on multibody system dynamics; 2012. .

[13] Maas R, Leyendecker S. Biomechanical optimal control of human arm motion. Proceedings of the Institution of Mechanical Engineers, Part K: Journal of Multi-body Dynamics. 2013;227(4):375–389.

[14] Obentheuer M, Roller M, Björkenstam S, Berns K, Linn J. Comparison of Measured EMG Data with Simulated Muscle Actuations of a Biomechanical Human Arm Model in an Optimal Control Framework–Direct Vs. Muscle Synergy Actuation. In: IFToMM World Congress on Mechanism and Machine Science. Springer; 2019. p. 26–33.

[15] Marsden JE, West M. Discrete mechanics and variational integrators. Acta Numerica. 2001;10:357–514.

[16] Leyendecker S, Ober-Blöbaum S, Marsden JE, Ortiz M. Discrete mechanics and optimal control for constrained systems. Optimal Control Applications and Methods. 2010;31(6):505–528.

[17] Wächter A, Biegler LT. On the implementation of an interior-point filter line-search algorithm for large-scale nonlinear programming. Mathematical programming. 2006;106(1):25–57.

[18] Koch M, Leyendecker S. Structure preserving optimal control of a three-dimensional upright gait. In: Multibody Dynamics. Springer; 2016. p. 115–146.

Part 5

Industry and User Perspectives

This page intentionally left blank

DHM2020
L. Hanson et al. (Eds.)

© 2020 The authors and IOS Press.
This article is published online with Open Access by IOS Press and distributed under the terms of the Creative Commons Attribution Non-Commercial License 4.0 (CC BY-NC 4.0).
doi:10.3233/ATDE200035

Human-Centric Assembly Cell & Line Validation

André RUECKERT [1], Marc NIEMANN [2] and Eric KAM [3]
ESI Software Germany GmbH, Liebknechtstrasse 33, 70565 Stuttgart, Germany

Abstract. Further digitalization is in progress for production processes which creates new challenges for both human centric assembly line management and individual assembly operators. By providing an efficient platform and 'virtual assembly line twin' the collaboration between Manufacturing Engineering and Production Operations can be significantly improved providing an efficient platform for assembly validation, ramp-up, operator guidance and virtual try-outs of improvements and changes to the assembly line. The main target is to provide a further strengthened platform for Human Centric Experiential Discovery and Validation, providing a rich virtual twin of the assembly environment, thus enabling efficient and reliable decision making by the key stakeholders involved in the manufacturing engineering, ramp-up and production operation processes, while providing digital continuity with upstream and downstream workflows for efficient integration within the customer processes. This session highlights most valuable IC.IDO (I See I Do) themes supporting the virtual validation of human centric processes in the production line, supporting our customers to increase productivity while ensuring worker health and safety, minimizing waste (Muda) and human error throughout the product lifecycle fulfilled with some proven customer examples. The session will also highlight customer requirements from innovation perspective to improve future workflows to generate a higher level of working efficiency.

Keywords. Human Centric, Virtual Assembly, Operator 4.0, Process Validation, Virtual Reality

1. Introduction

While significant focus in context of Industry 4.0 is on extensive automation and digitalization of the production environment, this is not necessarily true for all assembly processes which remain human-centric in practice. As new technology transforms many aspects of the assembly process including future employment rates and job profiles; there is common agreement that most tasks in general assembly will stay human-centric for any foreseeable future. Production flexibility required by novel and transformative new products can result in processes for which humans are still superior to machines [1]. At the same time there will be new challenges in introducing new processes, tools and human-machine interactions that needs to be efficiently validated from a human-centric perspective, requiring efficient ramp-up and knowledge transfer to the final production environment and human operators.

[1] Corresponding Author, Email: andre.rueckert@esi-group.com.
[2] Corresponding Author, Email: marc.niemann@esi-group.com.
[3] Corresponding Author, Email: eric.kam@esi-group.com.

2. Customer challenges for human centric assembly process validations

What does a Program Manager do when faced with a start of production pulled ahead by four months for the product to launch ahead of competition and a design and validation budget slashed at the 11th hour to match the competitor's offer or if your customer reduces their aerospace program lead-time by 18 months from 5 years to 42 months [2]?

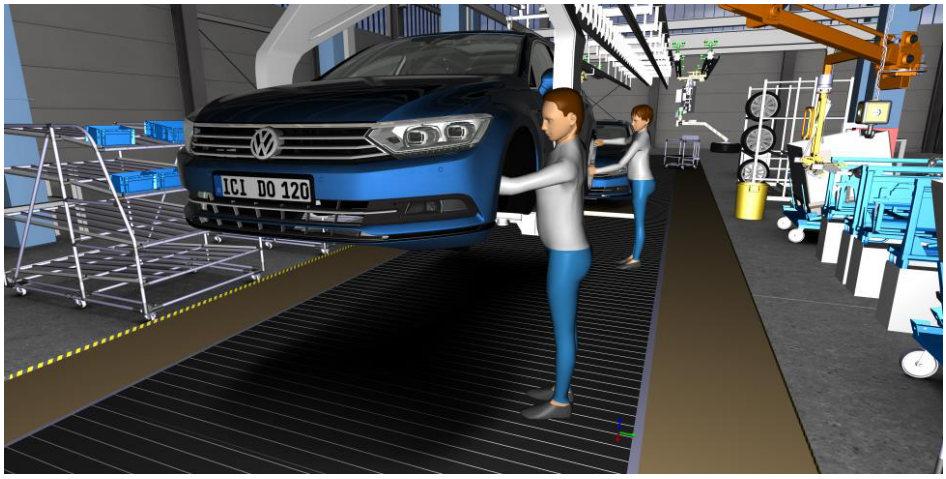

Figure 1. Experience assembly process with Digital Human Models. Model data is Courtesy of Volkswagen.

There is neither time nor resources available to work according to standard processes anymore: activities must be rushed, reduced and/or bypassed and key design decisions considered "good enough", making risk mitigation pivotal.

2.1. Keeping up with market disruptions

Every day, new disruptive companies emerge and challenge the established organizations with compelling products, lower structural costs, more nimble processes, and a simpler approach. Smart, dynamic entrepreneurs devise clever strategies leveraging new technologies and new mentalities to overrun the slower, historical processes of larger corporations. Existing companies must align to the new market conditions or dwindle. To cut costs and hope to reduce lead times, Program Managers can no longer afford to design iteratively based on physical prototype trial and error. Design, validation, and manufacturing teams must be involved from the start, to reach a common understanding of the design without constructing a prototype. They must understand and experience the product before it exists. This is as true for manufacture and assembly on the factory floor as it is for the engineering design of the product.

2.2. Recognizing the interactions of people with proposed products and processes

Conducting an experiential process validation, an immersed engineer might conclude that a virtual build or service task as performed in fully physical context is "feasible" to complete, but that the process is sub-optimal for comfort or ease, in the space provided with the proposed tools.

In contrast to a deterministic simulation that might compute that a motion path is plausible for the installation of a component, a human operator will observe that, without super-human powers, they might not be able to see the workspace clearly enough to complete the task. Computer animations to illustrate a proposed process can take hours to prepare, requiring specialized skills to manipulate a digital human model like puppeteering and could still fall short of proving the validity of the procedure. Working in a Virtual Reality (VR)-enabled Virtual Build (Figure 1), an engineer can, within seconds, evaluate, perform, and optimize an assembly sequence and tooling manipulation intuitively, just like they would in a pilot production facility.

First-person exploration only gets you so far because the circumstances are unique to the individual. Production will likely be distributed to different locales and performed by the local population, for localized product variants, in a unique production environment. Adding the ability to record and playback object animations, extends that singular experience over the potential a range of localizations in real-time. Capturing the assembly experience of other individuals in VR not only reaches the value of physical pilot assembly lines, it can reflect plausible production conditions that would take years of production to observe, mitigate, improve, and resolve.

3. Enhancing productivity and processes for the factory of the future

Sequences coupled with advance anthropometric digital human models, allows virtual build users to apply their first-person actions to “manikins” reflecting any number of regionalities, gender, and proportions. It becomes easy to explore, in the virtual environment, building a new product, and directly arrive at objective analytics for a diverse range of potential workers. Thereby it is possible, for example, to learn that, a 95% European male who performed an assembly action with ease could assign that same action to a 5% Asian female manikin and discover that she would find the same task uncomfortable or even unfeasible.

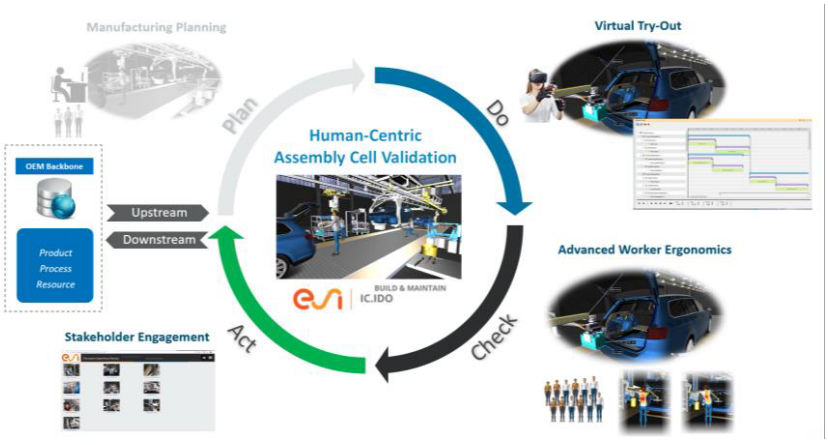

Figure 2. Digitally guided assembly process with Digital Human Models. Model data is Courtesy of Volkswagen.

3.1. Augmented Reality and Virtual Reality

Assembly sequences are also required for creation of documentation and deployment of work instructions. Recent technology advances in the factory of the future point to a range of digitally guided assembly processes (Figure 2). Augmented Reality (AR) is one hot topic in this area, wherein digital model data can be overlaid with the real product to indicate the required sequence of operations. AR technology is lauded for its ability to enhance spatial understanding of complex tasks and communicate in 3D object visual overlays, like "holograms", what would take mountains of words and static illustrations to convey.

It does not, however, invalidate the need to prove and validate assembly processes and sequences; it instead increases the stakes that an expensive deployment of digital work instructions exposes production risks if the AR process is not feasible. In a Virtual Reality environment, one can validate assembly sequences using purely digital data. The findings from Virtual Builds can then be captured and exported as the basis for Augmented Reality digital guided assembly operations. It is not a question of VR versus AR, but instead that Virtual Reality can be used to validate what will eventually be deployed on Augmented Reality, before the physical products are ready.

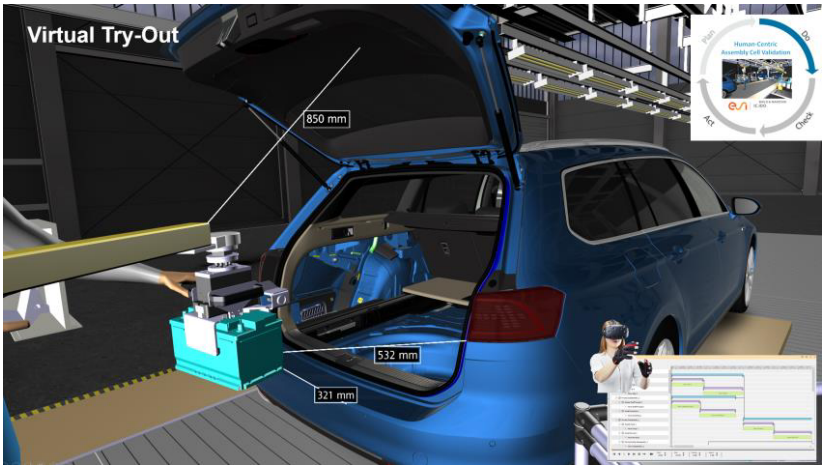

Figure 3. Human centric assembly cell validation. Model data is Courtesy of Volkswagen.

3.2. Validating the production process across multi-disciplinary teams

Bringing in more competencies for a product evaluation is always beneficial. That is why modern design methodologies usually call for a "multi-disciplinary approach" or simultaneous engineering in design reviews and risk assessments. Additional sets of eyes spot more risks, alternative perspectives identify more trade-offs, different minds find more solutions. Where a test engineer might confirm that a button is too hard to press, an ergo-nomics engineer might point out that it is too small and not easily accessible, a safety engineer might note that it reduces accidental actuation, and a sales manager might wonder why there is even a button to begin with. The more interaction, the richer the analysis and the more potential to confirm solutions or to identify problems, then as a group explore design opportunities. The design team can then rework the product, or the affected procedure, with confidence that all parties are aware and on board with the improved solution.

The ability to experience and interact with products, before they are ever physically manufactured—on screen, with a head-mounted display, on a power wall or in a Cave, as an individual engineer, as a group, with a supplier or with a customer team, across a global enterprise—is invaluable. The discussions engaging team members and other stakeholders in an interactive quest for issues and improvements so early in the program, before tools are even kicked-off, inevitably lead to a stronger confidence in the design and manufacturability of the product from all involved, and ultimately from the whole company.

4. IC.IDO for human-centric assembly cell and line validation

With IC.IDO [3], ESI [4] offers a solution for Human-Centric Assembly Process Validation. This immersive virtual workspace (Figure 3) enables multi-disciplinary evaluations, discussions, and resolutions to the challenges that new products and processes bring to the factory of the future. It allows individuals or teams, together or from remote sites, to experience and interact with digital designs, so that engineering teams can identify necessary improvements and engineer corrections before construction starts on tooling for the manufacturing plants.

ESI IC.IDO solution helps product and manufacturing engineering managers address challenges brought by shorter product lifecycles, globalization and new technology trends, to better manage the risk of missed production targets (delivery, cost, quality, safety); through real-time, rich-context, virtual (VR enabled) validation of human-centric production processes, facilitating early identification of issues and improvements while reducing reliance on traditional off-line simulation, costly physical trials, or limited expert opinions.

The goal is to provide a further strengthened platform for Human Centric Experiential Discovery and Validation, providing a rich virtual twin of the assembly environment, thus enabling efficient and reliable decision making by the key stakeholders. No matter if they are involved in the manufacturing engineering, assembly ramp-up, or production operation processes, a Collaborative Virtual Workspace expands digital continuity with upstream and downstream workflows for efficient integration within the customer processes.

Core focus also includes the progression toward ‘Operator 4.0’ [5] providing a human centric perspective on Industry 4.0. Focus is two-fold, on one hand side enabling virtual validation of new production technology in context of the worker of the future ‘Operator 4.0’, e.g. including increased automation of the assembly line, while also enabling VR and AR enabled workflows into new buying centers within Production and Service Operations to support efficient operator ramp-up through virtual try-outs, training and operator guidance.

5. Existing customer reference examples [6]

Fiat Chrysler Automobiles (FCA) [7] has production units in 40 countries and commercial presence in 150 countries. The group is home to brands like Alfa Romeo, Chrysler, Dodge, Fiat, Jeep, Lancia, Ram, SRT, Maserati, and Mopar (parts and services). As part of FCA’s ambitious MFG2020 initiative, an Industry 4.0 project, FCA Latin America (LATAM) considered how to further improve the engineering and

validation of assembly operations for the new Fiat Argo car model, seeking to further reduce costs and delays.

Figure 4. Human centric assembly cell validation at FCA. Model data is Courtesy of FCA.

For this action, they turned to ESI's Virtual Reality solution, ESI IC.IDO. The 'Fiat Argo' was the current program for FCA LATAM and had a strong focus on interior assembly and trim. It was the first time that FCA LATAM applied IC.IDO throughout an entire project, including in the validation of vehicle assembly. The Virtual Reality solution was used to identify risks in the product design before construction of a physical prototype.

All of FCA engineering groups – manufacturing, production, and ergonomic health & safety (EHS) – were involved in the action (Figure 4), which enabled them to reach an optimized solution for all areas reviewed. 18 months had been considered an acceptable ROI for this kind of Industry 4.0 technology investment. But in fact, the project reached full ROI after only eight months and FCA was able to successfully assemble the new vehicle as planned. ESI IC.IDO brought agility, reduced time and enhanced workplaces.

IC.IDO enabled FCA LATAM to experience the real process conditions of assembly and assure the conformity of the product by considering all the interferences in the virtual phase of development. IC.IDO enabled FCA LATAM to evaluate different process scenarios and design variants for the program, including the validation of the manipulator arms for passenger compartment assembly.

By evaluating the planned processes in advance, FCA LATAM was able to implement a corrective action plans to develop a new work cell device and validate assembly procedures to optimize and validate the proposed assembly process. It was crucial, prior to the following phases of the program, to assure the products were safe and feasible to assemble.

Today, FCA LATAM has IC.IDO installations at the Automotive Industrial Center of FIAT Betim and at Jeep Goiana, which allows them to use the tool across the entire range of FIAT's brands.

6. Scientific outlook and next generation HC assembly process validation

ESI is part of an ITEA 3 [8] driven project consortium called MOSIM [9] (**Mo**dular **Si**mulation of Human **M**otions) (Figure 5). In the project ESI has a role as system

integrator and industrial partner (Figure 6). MOSIM is an open modular framework for efficient and interactive simulation and analysis of realistic human motions for professional applications. The IC.IDO solution from ESI is one of the proposed target engines who wants to use the project outcome for later industrial use mainly to enhance the current capabilities within the human centric assembly validation area.

The impact of present engineering practices on the people who produce, use, and maintain products is often left unquantified until late in the product lifecycle; in some cases, too late to address in the immediate product design or even the next generation. The idea of MOSIM need to increase comprehension of current engineering and manufacturing paradigm the integration of products and processes on the people who build, use, and maintain products throughout their lifecycle. There is no holistic solution on the market which takes care of human factors during assembly including realistic human simulation capabilities on board. ESI's intention is to use these projects results for improving human centric manufacturing/manual assembly evaluations.

Figure 5. MOSIM consortium partners.

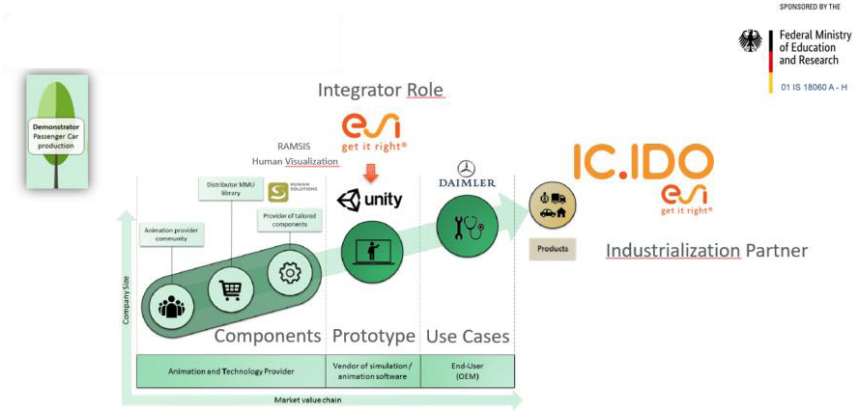

Figure 6. ESI main project role in the MOSIM consortium.

ESI expects a huge paradigm shift and implications for automotive production (Figure 7):

- From the viewpoint of an assembly station, nearly each **product** can be considered **unique**
- Associated **assembly tasks** may vary within each cycle
- Rising **complexity** and **efforts** for production planning departments
- Simultaneously, **changed paradigms**, are leading to a **decreasing prediction** quality of planning methods

Figure 7. Paradigm shift for simulating human motions in future.

ESI expects also a huge reduction of needed time effort compared to curren industrial practise (based on DMU related human task simulation).

The generation of a rich repertoire of realistic human motions in complex and possibly highly collision afflicted environments is not sufficiently addressed by commercial tools. Complex process workflows with an exhaustive number of possible manual task sequences can only be partly addressed today, since process variants must be modelled by hand. As manual modelling is inevitably linked with high additional effort, the potential cost reduction is significant. In order to introduce approaches and software solutions, which are capable to automatically simulating a rich repertoire of realistic human motions, MOSIM aims to develop and implement a generic concept which is inspired by the Functional Mock-up Interface (FMI) standard [10].

MOSIM transfers the idea of co-simulating models from different simulation environments to the field of human simulation by means of introducing the Motion Model Units (MMU). To achieve the mentioned goals, three main approaches, each incorporating various technical contributions which clearly go beyond the state of technology, will be explored within MOSIM.

The main ideas behind MOSIM are:

- Concept and Implementation of an extensive **library** consisting of **MMUs** encapsulating various human motions regardless of the respective use-case.
- Development of tailored approaches, enabling **autonomous generation** of plausible **MMU sequences** and context-dependent decision-making using recent AI methods.
- Unifying both approaches, a **co-simulator** will be implemented, generating natural and continuous human motions by **sequencing** and **executing** the obtained set of **MMUs** using generic transition models.

The main expected outcomes for the MOSIM outcomes are for ESI:

- Extension of IC.IDO assembly process validation module
- Validation of assembly sequence plan's out of workers perspective (people, tools, resources)
- Integration of MOSIM platform into IC.IDO "target engine" to simulate human centric assembly processes (automized)
- Integration of ergonomic analysis (e.g. RULA [12] and others [13]) using RAMSIS kernel (by Human Solutions GmbH [11]) and MOSIM MMUs in IC.IDO.

ESI wants to push the MOSIM concept [14] forward from an industrial perspective to relevant industry pillars like automotive, aerospace or heavy industry for example even though to define an industry standard within the consortium.

References

[1] Elon Musk drafts in humans after robots slow down Tesla Model 3 production. The Guardian. Link: https://www.theguardian.com/technology/2018/apr/16/elon-musk-humans-robots-slow-down-tesla-model-3-production

[2] SAFRAN Success Story using Virtual Reality. Safran Group. Link: http://usinedufutur.safran-group.com/en/virtual-reality/

[3] IC.IDO (I See I Do) Industrial Grade Virtual Reality Solution. ESI Group. Link: https://www.esi-group.com/software-solutions/virtual-reality/icido-industrial-grade-immersive-vr-solution

[4] ESI (Engineering Systems International). ESI Group. Link: https://www.esi-group.com/

[5] Wuest T, Romero D, Stahre J. Introducing 'Operator 4.0,' a tech-augmented human worker (April 2017). The Conversation. Link: https://theconversation.com/introducing-operator-4-0-a-tech-augmented-human-worker-74117

[6] FCA IC.IDO Success Story. FCA Article. Link: https://www.fcagroup.com/stories/latam/en-us/Pages/realidade-virtual.aspx

[7] FCA Group. FCA Group. Link: https://www.fcagroup.com/en-US/Pages/home.aspx

[8] ITEA 3 (ITEA is a transnational and industry-driven Research, Development and Innovation (R&D&I) program in the domain of software innovation. Link: https://itea3.org/about-itea.html

[9] MOSIM. An open modular framework for efficient and interactive simulation and analysis of realistic human motions for professional applications. Consortium. Link: https://mosim.eu/

[10] FMI Functional Mockup Interface. Modelica Association Project. Link: https://fmi-standard.org/

[11] Human Solutions GmbH, RAMSIS (3D manikin, ergonomic simulations). Link: https://www.human-solutions.com/en/products/ramsis-general/index.html

[12] McAtamney L, Nigel Corlett E. RULA: a survey method for the investigation of work-related upper limb disorders. Appl Ergon. 1993, 24(2), 91–99.

[13] Niemand P, Saladdin A. Management of ergonomic aspects in early design phases using virtual reality. 2018. Bachelor Thesis, University of Halmstad, Sweden. (2018-06-13). Link: http://www.diva-portal.org/smash/get/diva2:1218096/FULLTEXT02

[14] MOSIM Concepts & Architecture. Link: https://www.mosim.eu/results.html

DHM2020
L. Hanson et al. (Eds.)
© 2020 The authors and IOS Press.
This article is published online with Open Access by IOS Press and distributed under the terms of the Creative Commons Attribution Non-Commercial License 4.0 (CC BY-NC 4.0).
doi:10.3233/ATDE200036

Employing UX Processes for More Focused Development in Research Projects

Ari KOLBEINSSON[a,1], Jessica LINDBLOM[b] and Peter THORVALD[a]
[a] *University of Skövde, School of Engineering Science, 541 28 Skövde, Sweden*
[b] *University of Skövde, School of Informatics, 541 28 Skövde, Sweden*

Abstract. The aim of this paper is to highlight some benefits of incorporating usability/user experience (UX) approaches in the software development process of research projects advancing digital human modeling (DHM), and how these processes, approaches, and methods can help keeping the development process more focused and efficient. Research projects that contain large software development components may receive funding only to complete the core tasks, and including additional persons in a project may seem like a waste of resources. This paper introduces user research that relied on a UX approach called *contextual inquiry* to ascertain user goals and how those might be translated into features for DHM named IMMA that has been developed as a part of numerous research projects in the last decade. The goal of the study is to support DHM development in general through highlighting methods and approaches that can be used, with specific results aimed to support the continued development of IMMA. Results clearly show that existing functions do not support the goals of the user group examined, and highlights the need of understanding user goals and creating functions to support achieving those goals, rather than assuming what functionalities might be needed. By understanding user goals, interpreting those into activities and functionalities time and resources can be used more effectively, which is important for small to medium research projects, where both time and budget may be limited.

Keywords. Contextual Inquiry, DHM Development, UX, Activity Theory

1. Introduction

Clear development processes exist for products as well as software [1]. These processes include lessons learned to avoid common pitfalls, as well as allowing for iterative approaches [1, 2], and including sub-processes for mechanical safety, software quality assurance, as well as for ensuring good usability/user experience within the product. From the users' point of view, a technical system that is suitable for its purpose, easy to use, and fits into its intended context are just basic. Users have also started to demand a positive experience when interacting with technological artifacts, beyond utility, usability, and acceptance [1, 2]. Broadly speaking, UX, in addition to ensuring usability, addresses the feelings created and shaped by the use of technology and how technology can be designed to create a positive user experience [1]. For this to be possible, UX processes posit that first the intended users have to be identified and described, and then focused upon during the whole UX design (UXD) lifecycle process (described as

[1] Corresponding Author, Email: ari.kolbeinsson@his.se.

the UX wheel). The process is iterative and consists of the four key elements of UX activities; analyze, design, implement, and evaluate [1, 2].

Research projects differ from commercial development projects in many ways, one of which is that standard development processes often do not align with other requirements of projects, such as educational requirements of graduate students or the scientific contribution requirements of most members. This can lead to common development processes not being followed, and specialists who are not critical to the academic and scientific contribution of the system being developed may not be involved in the process to the required degree from the beginning. One such specialization is the UX specialist or the usability designer, a role often left out of smaller development projects.

It is widely recognized that there is a substantial gap between UX research and practice, where UXD approaches are rarely applied. Although there is a large interest in UXD, organizational priority and competence is often lacking. Instead one relies heavily on questionable approaches such as designing systems for "trained professionals" to excuse the low effort towards UXD processes [3]. Not following development or design processes, and not including relevant (but peripheral to the academic side) specialists and project managers is a known hazard that can lead to problems down the line [4], and can have negative consequences for the quality of whatever is being developed, as well as the scientific validity of the research conducted along the way [4].

The focus in this paper is to highlight why and how the inclusion of UX specialists and UX processes throughout a project may be beneficial, not only to the finished product and the bottom line when selling a system developed in research projects but also to optimize the rest of the development process through a having a stronger focus on the intended end-users and a clearer idea of what is actually needed from the project, as opposed to researchers' assumptions based on their own needs.

This was explored through the study of one identified user group that would benefit from the use of DHM software to support their own analyses, namely ergonomists who use existing manual tools to evaluate work in multiple companies. These ergonomists evaluate various tasks, including office tasks and industrial tasks in both large and small factories, relying heavily on their own expertise in applying standards (by law) and tighter constraints (guidelines within companies) and evaluating work activities based on observation, interviews, and other manual and digital tools.

The first steps of a user study will be examined where a projected primary user group of digital human modeling (DHM) software for ergonomics simulation is interviewed, and user goals (i.e. what users want to achieve) are mapped. These user goals are then translated into possible features, and these were compared to available features in the IMMA DHM software [5] through interviews with specialists in the software. The final section discusses the impact of any identified discrepancies between features that exist and features that would support achieving the goals required by this user group.

2. Method

This study relies on an approach used in the analyze activity of the UXD process, called *contextual inquiry*, which uses a master-apprentice approach to exploring the domain [1, 2]. Contextual inquiry is based on a 'quick and dirty' ethnographic

approach, and is useful in many parts of a development process, but can give particularly good insights into the domain being explored early in the analyze activity. Contextual inquiry allows UX specialists to learn what the relevant questions actually are through interviews, discussions, and observation of domain experts to [1, 2, 6, 7]. Applying the contextual inquiry approach requires first identifying some user groups, although these may be redefined during the process.

User groups were identified through discussions with stakeholders within the research project. One groups was identified as being important and interesting to study in more detail, and had in fact been discussed by stakeholders working on the IMMA DHM system during previous projects: practical ergonomists working in the field. This group was identified as being important as they constitute an envisioned target user group of the IMMA system, and interesting because this group has a very different background and skillset when compared to ergonomists working in research who may work more with DHM simulation software and CAD systems.

Identifying potential users in this way through discussions with stakeholders is commonly used method in the discovery and analyze activity of a development process [1, 2, 6], with more details emerging through interviews with these users that allow further defining primary, secondary, and tertiary (or supplemental) user groups.

This can be used later in the UXD process to identify candidates for creating personas for other approaches such as *scenario-based design* where identified user goals are first consolidated, and data is used to create personas (pretend users that are essentially aggregated from the data that has been gathered) and can be used for various methods of usability and UX evaluations [1, 2].

2.1. IMMA at a glance

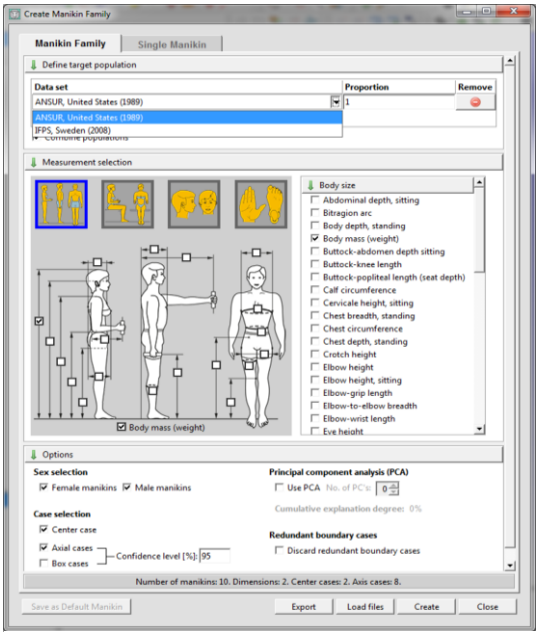

Figure 1. IMMA manikin family creation dialog. Here the user can create multiple manikins for testing based on anthropometric databases. Measurements can be selected as appropriate.

IMMA is a DHM tool created to allow the evaluation of ergonomic factors in assembly stations in manufacturing, even before the assembly station is created. As such, IMMA simulates a manikin or group of manikins (referred to as a manikin family, see Figures 1 and 2) in an environment, performing tasks such as assembly or climbing into the cab of a truck, and forces for each joint are calculated. This works with complex geometries, using path simulation software to generate paths which object will need to take to avoid collisions. IMMA can perform these calculations with families of manikins that are created from ergonomics databases, thus highlighting the ergonomic attributes of a task for different people.

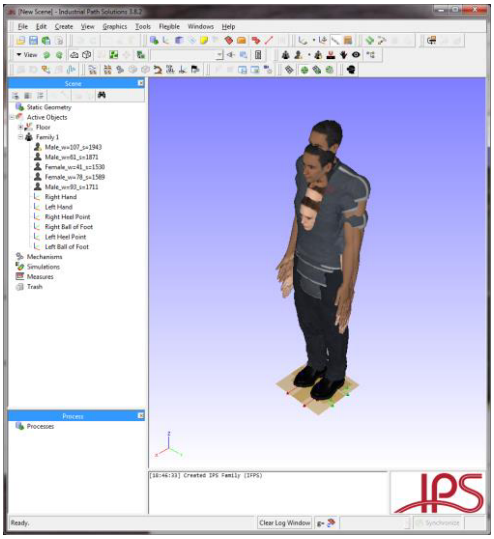

Figure 2. A family of manikins has be created and can now be used for ergonomic analysis of an activity for a range of "people".

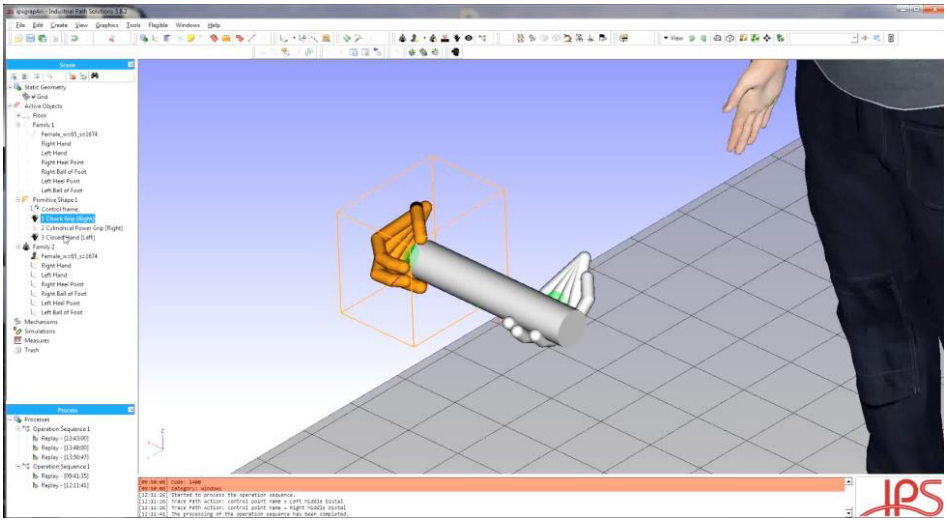

Figure 3. IMMA grip control interface. Here the user can select how the manikin(s) will hold onto the object that will be moved in the activity being analysed.

2.2. Identifying users

User groups require further verification as the project progresses, as current limitations on visits have led to a pragmatic approach being used. This is particularly important when it comes to UX work, as discussions with stakeholders are important for identifying user groups within the industrial use cases.

The IMMA program has been used by project partners for a number of years, with these partners including large industrial production companies as well as research institutions. This means that some user groups may be well established, but this can

complicate identifying prospective users [2]. That said, one partner in the SVE project is new to the system, and has specialist knowledge long been discussed as an important potential user group, in the form of practicing ergonomics evaluators who contract to companies. This user group was seen as both an important potential user group, but the actual project partners were also new to IMMA, as well as not having used any DHM software for ergonomic evaluations. Users without heavy exposure to the system are less likely to get stuck on existing functionality, making it easier to evaluate what functionalities might support their goals. Other user groups, such as engineers working with workstation development and ergonomics researchers, have been identified, and will be explored later in the project.

2.3. Interviews

The interviews were conducted using the *contextual inquiry* approach, which is an ethnographically inspired approach commonly used within UX research [1, 2]. Contextual inquiry is an approach widely used (and recommended) for exploratory user research [2, 6] and can be used to combine multiple field-study approaches and activities [7]. Contextual inquiry employs a master-apprentice model of learning, assuming that the interviewee is a master of their craft and the researchers are novices trying to learn [2]. Contextual inquiry further relies on four basic principles: *context*, *partnership*, *interpretation,* and *focus* [2].

- Context involves meeting users in their own work environments, rather than in a lab of some sorts
- Partnership means that the domain expert and the UX specialist are working together to create improvements.
- Interpretation is important because users, even experts, tend to focus on the tasks as they are performed today, not what the actual goal of the task is. This means that the UX specialist needs to "read between the lines" to identify goals in a holistic manner.
- Focus refers to how interviews and discussions are conducted. Although the interviews may feel open or free form they should be carefully guided by the UX specialists to capture information relevant to the design questions being explored.

The approach used was enhanced by employing recommendations for effectivising contextual inquiry. Examples of these effectivisation approaches are e.g.:

- Shortening the interviews, avoiding full day interviews and instead using interviews as short as an hour, so long as the approach is used in a targeted manner.
- Using smaller design teams. Older and more formal approaches assume a large team for interviews, observations, and analyses, but UX specialists have found that smaller teams can lead to all the UX specialists gaining direct interaction with all the domain experts, and have found that this can make analyses more effective [2].
- Using interviews and other contextual inquiry methods for identifying goals. This allows other parts of the development process to be more task focused.

Furthermore, contextual inquiry rewards "storytelling", i.e. allowing the experts being interviewed to explain through anecdotes (even going into seemingly unrelated details

to shine a light on goals that might otherwise be missed [2]. Analyses should then be performed by the interviewers discussing and comparing notes, highlighting patterns and *coding* the interviews [1, 2]. The participants were two ergonomists, one highly experienced with additional training and experience as a physical therapist, and the other with a few years of experience and a background in health care. Two interviews were conducted. The first interview was conducted online by two researchers and one ergonomist. The second interview was conducted some weeks later after a preliminary analysis of findings from the first interview, and involved the same two researchers, the ergonomist interviewed in the first interview, and a second ergonomist. This interview was conducted face-to-face, and was relatively short (under two hours).

2.3.1. Interview 1

The first interview was conducted in an exploratory manner with few assumptions being made, relaxed and questions were directed to explore mostly the current work practices of the ergonomist. This interview led to some points that needed further exploration. Differences in work practices, experience, and techniques also suggested that interviewing both main ergonomists would be beneficial.

2.3.2. Interview 2

The second interview was more focused on user goals when conducting ergonomics evaluations. The partnership model of contextual inquiry was employed, and the interview was less than 2 hours long. This interview was conducted in the ergonomists' workplace. Questions and discussions were guided by the understanding that had been gained from the first interview.

2.4. User Goals

One central principle of the UXD lifecycle process (see Figure 4) is the need to identify and characterize the user goals, with these goals being connected to the business goals, and subsequently the business goals connected to the user behaviors [9]. An important activity for the whole UX wheel is to extract, identify, and characterize user goals [1]. User goals are high-level objectives, which should be driven by the representative use of an envisioned interactive artifact or system. The user goals should identify what is important to the users, stated in terms of anticipated UX of an interaction design. User goals are important because they help and support the designers and developers to continuously focus on the intended experience when interacting with the envisioned interactive artifact. For that reason, they are referred to as "goals", instead of "requirements", since user goal fulfillment cannot be guaranteed for all intended end-users [1].

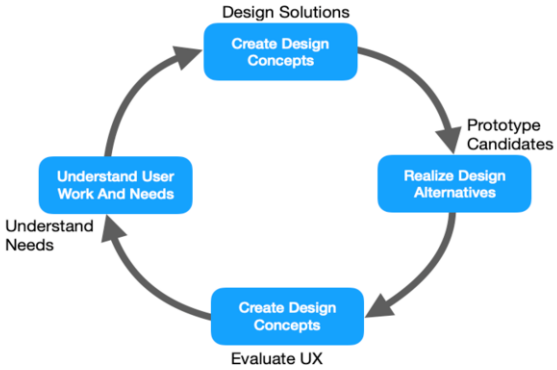

Figure 4. The UX design lifecycle (adapted from [1]).

User goals differ from features, actions or activities. In general, users do not want to use a feature or function, and do not want to perform an action. What the user wants to do is to fulfill a goal [1, 2, 8]. This distinction is important, as it allows us (the system designers) to focus on what the user wants to achieve rather than what actions are performed to achieve this goal [1, 2]. User goals can be simply defined as desired real-world end states, and can be split into many or few sub-goals [2].

Moreover (and in many ways even more importantly) users generally cannot put this into words. Users often explain the actions involved in currently fulfilling the goal, never explicitly explaining the goal, or what effect they want to achieve. This means that goals must be interpreted from interaction with users [1, 2].

Unfortunately, the extraction of user goals is an activity that is often overlooked, either because of lack of time or lack of knowledge [1], which may result in negative consequences for the final design of the system. Proper and relevant user goals that are extracted and characterized early on can simplify and strengthen the UX evaluation performed later on through pointing out exactly what should be investigated in order to enhance the positive UX of IMMA.

Identifying user goals from user interviews is a well documented approach [e.g. 1, 2]. Cooper et al. [2] also recommend observing users and their activities in their normal context, as that will result in the most accurate understanding of the work practice.

3. Results

The interviews led to a new understanding of user goals in ergonomic evaluations, as well as other general information that can be of importance to the development of the IMMA DHM software. These will be listed here, starting with general points that may be of interest, and then details that are clearly linked to initial user goals. Each point will be introduced and analyzed, identifying user goals.

3.1. Interview findings and interpreted user goals

The ergonomists explained that multiple people are involved in risk assessments of workstation design or work tasks, especially in manufacturing, and these risk

assessments require collaboration between various specialists. Visualizations support this communication early in the project.

> Identified User Goal: An ergonomic evaluation using knowledge and skills from all who can contribute to the ergonomics evaluation and risk assessment. Requires communication between stakeholders from beginning to end.

The ergonomists work with "persona-like" approaches. Personas are an accepted tool in UXD processes [10]. The ergonomists call their version MIP ("montör i projekt" or "assembly worker in project") and are similar to personas in many respects. Personas are seen as central to understanding the user, empathizing with the user, and communicating to stakeholders, including decision-makers.

> Identified User Goal: Ergonomic evaluation that supports empathizing with users and communicating user attributes in empathetic ways.

The ergonomists note that they are being taken onboard in projects earlier now than they used to, which is positive, especially by companies who have experience with involving specialists.

> Identified User Goal: Applying ergonomic evaluations throughout the process, as opposed to "painting on some ergonomics" at the end of the process.

The ergonomists focus a lot on *frequency*, i.e. how often a task is performed. This comes up repeatedly. Repetitive strain is clearly a central factor to take into account, and should be represented in any tool used (including DHM software). This is explained as being central to a holistic approach to ergonomic evaluations. In a case where physical load is within the (legal) standard, but outside of tighter company constraints then the frequency of the task becomes central. A once-per-day task that exceeds company constraints but is well within legal standards might be deemed as being acceptable if other factors are acceptable.

> Identified User Goal: Holistic evaluation of ergonomics, taking into account all major factors (e.g. frequency).

Tools and functions that visualize analyses and visualize ergonomic stresses in general and limits were described as being extremely helpful. A manikin that just performs the action is seen as possibly useful up to a point, but seeing forces in action while performing actions is considered central. This was further discussed as being beneficial to comparing standards and also for comparing observed work to simulated work.

> Identified User Need: Ergonomic evaluation where forces, standards, and observations have been taken into account.

Rules/standards and company guidelines (which must be tighter than the laws) were discussed. The possibility of visualizing constraints (laws or company-set guidelines) is seen as potentially extremely helpful in holistically evaluating the ergonomics of a workplace.

> Identified User Goal: Holistic evaluation of workplace, taking into account standards and company imposed constraints (Standards)

An important part of regular (non-DHM) analysis of tasks when performing risk assessments in practice involves observing natural body positions, including grip (which may be shifted during a task) which is seen as supporting the holistic approach to ergonomics evaluations mentioned previously.

> Identified User Goal: Naturalistic, holistic evaluation of workplace, taking into account body positions, stance, and grip (Body position and grip)

Rules/standards that need to be considered when performing a risk assessment:

- Formal standards (Arbetsmiljöverkets) rules should be included, possibly selectable for different regions.
- A major manufacturing company's own standards should be includable.
- Tasks may go beyond a company's guidelines, but an expert holistic evaluation takes into account frequency and additional aspects (including cost of changes) when assessing whether it is acceptable to go over guideline limits.

This resulted in the need to include different "limits", and visualize these in the tool in the form of constraints (Spärrgränsar), which is the term used by the ergonomists.

> Identified User Goal(s): An ergonomic evaluation where standards, rules, and constraints are linked to the rest of the evaluation; understanding forces holistically even while focusing on one aspect of the evaluation (i.e. keeping an overview while focusing on a detail).

The core goals that have been identified are primarily that the evaluation should be holistic, and that collaboration between specialists will be required throughout the whole process.

The overarching UX goal *to holistically evaluate ergonomic factors in a work context* is hard to interpret into features; this is where the detail level offered in the interviews is helpful. Note that the overarching goal is not always to reduce ergonomic strain, but rather ensure that strains are sustainable and balance that with the needs of the company. Multiple factors should be taken into account during these ergonomic evaluations, which involves high levels of expertise and expert judgment.

3.2. Further results

Although the interviews focused on how the ergonomists approach their analyses and how their current tools are used, the discussion also highlights the ergonomists' experience with IMMA and other technical tools they have either worked with or observed specialists working with.

When discussing the IMMA DHM software as it is today the ergonomists discuss how complex the software seems, and how importing geometry seems to require trained specialists in CAD/IMMA. This highlights their view that interacting with the IMMA software as being for experts in the software (see Figures 1, 2 and 3), not necessarily for specialists in ergonomics such as themselves. Further interviews and observations were planned, but have been delayed due to constraints imposed by the COVID-19 pandemic. Observations, in particular, proved impossible to organise at this time. Further interviews, as well as observations, will be conducted later this year.

3.3. Interview: IMMA experts

An interview with specialists familiar with the IMMA software was conducted by one of the researchers to compare the identified goals to existing functionality. This interview revealed that only some of the identified goals are currently supported by the IMMA software. In particular, the current visualization has certain limitations in visualizing real-time ergonomic information, and getting out information in the form of

reports was explained as being limited or missing. While it is possible to select a measure (e.g. a joint) for monitoring, it is not easy to view the action being performed and get data about forces and constraints (e.g. standards or guidelines) at the same time.

More importantly, comparing multiple versions of the same task (e.g. after iteration of the workstation) or observing differences between different manikins is not directly supported. The concept of seeing multiple levels of standards, such as legal, standards (e.g. RULA), and company specific guidelines/standards visualized was novel to the specialists, but immediately seen as being potentially useful, as were many of the visualization needs lifted by the user goals.

A functionality that was pointed out as being potentially useful, especially if comparison functions are implemented, is IMMA's support for motion capture (mocap) which allows the IMMA tool to record and evaluate a real user performing the task. This would fit in directly with the user goals if comparisons can easily be made between the mocap manikin and the data-generated manikin.

The specialists also pointed to the anthropometric module for IMMA as potentially being of interest to implement some features that would support user goals, especially surrounding persona concepts (communicating an empathetic version of the manikin) and for further analyses and evaluations.

4. Discussion

A comparison of the findings from the ergonomists and the findings from the IMMA DHM specialists makes it clear that opportunities have been missed by not engaging with one of the user groups expected to have much to gain from the use of the IMMA software. This does not suggest that the software lacks power or other qualities; rather that resources might have been more effectively used to support multiple user groups during the product development process. Indeed, the potential power and flexibility of the software is apparent, and the modularity of the software may prove to be a great asset.

All interviews turned out to be extremely rewarding, with the IMMA experts stating that the found the identified needs and goals interesting and expressed an interest in further incorporating this kind of UXD approach into the development process. An acceptance of unfamiliar development processes and an openness to including user perspectives have been shown to have a positive effects on product usability [1, 2] which means that this introduction of UX approaches into DHM software development should be seen as an opportunity, which is how the specialists considered the discussion.

Acknowledgement

This work has been made possible by the Knowledge Foundation and the INFINIT research environment (KKS Dnr. 20180167) who have supported the Synergy Virtual Ergonomics project (SVE), as well as partner organizations.

References

[1] Hartson R, Pyla PS. The UX Book: Process and guidelines for ensuring a quality user experience. Elsevier, 2012.
[2] Cooper A, Reimann R, Cronin D, Noessel C. About face: the essentials of interaction design. John Wiley & Sons, 2014.
[3] Andreasson R, Lindblom J, Thorvald P. Towards an increased degree of usability work in organizations. Procedia Manufacturing, 2015, 3, 5739-5746.
[4] Kolbeinsson A, Falkman G, Lindblom J. Showing uncertainty in aircraft cockpits using icons. Procedia Manufacturing, 2015, 3, 2905-2912.
[5] Hanson L, Högberg D, Carlson JS, Delfs N, Brolin E, Mårdberg P, … Ore F. IPS IMMA – Intelligently Moving Manikins. In: Scataglini S, Paul G, editors. DHM and Posturography. Elsevier Academic Press, London, 2019, 115–124.
[6] Rosala M. The Discovery Phase in UX Projects, 2020. Available from: https://www.nngroup.com/articles/discovery-phase/.
[7] Herzon C, DeBoard D, Wilson C, Bevan N. Contextual Inquiry, 2010. Available from: http://www.usabilitybok.org/contextual-inquiry.
[8] Farrell S. Field Studies, 2016. Available from: https://www.nngroup.com/articles/field-studies/.
[9] Kaasinen E, Roto V, Hakulinen J, Heimonen T, Jokinen JP, Karvonen H, Keskinen T, Koskinen H, Lu Y, Saariluoma P, Tokkonen H. Defining user experience goals to guide the design of industrial systems. Behaviour & Information Technology, 2015, 34(10), 976-991.
[10] Harley A. Personas Make Users Memorable for Product Team Members, 2015. Available from: https://www.nngroup.com/articles/persona/.

DHM2020
L. Hanson et al. (Eds.)

© 2020 The authors and IOS Press.
This article is published online with Open Access by IOS Press and distributed under the terms of the Creative Commons Attribution Non-Commercial License 4.0 (CC BY-NC 4.0).
doi:10.3233/ATDE200037

The Need for Faster and More Consistent Digital Human Modeling Software Tools

Dan LÄMKULL [1] and Maciej ZDRODOWSKI
Volvo Car Corporation, Dept. 81412, Manufacturing Technology, SE-405 31, Göteborg, Sweden

Abstract. The vehicle industry is a common user of Digital Human Modeling Software (DHMS) tools, both for product development and production process development. One of three major risk factors interacting and contributing to the level of risk for an assembly worker is working posture (the two others are time and force). To achieve a working posture that is likely to happen in reality when using a DHMS tool is therefore crucial. Realistic posturing is required to obtain accurate quantitative assessments of human performance, as it has been shown that the performance models are sensitive to the postural condition. The need for faster and more consistent human simulation tools has motivated most commercial digital human modeling tool suppliers to implement various posture / motion wizards. However, these wizards are designed for certain types of tasks (e.g. ingress, egress or driving postures), and can not be utilized as a general solution for obtaining correct assembly/working postures. This paper shows examples of where working postures, achieved through manual use of DHMS tools, and discrete motions, achieved through use of a motion wizard, often considerably differ from working postures compiled during VR/AR sessions. This way of working (using VR/AR) is used to achieve more realistic working postures and a further development of the DHMS tools and working procedures should lead to faster and more consistent human simulation tools. The paper also justifies several research projects, which purposes are to decrease the gaps between wanted and existing functionalities.

Keywords. Digital Human Modeling Software (DHMS), VR/AR, Human Posturing, Ergonomics Simulation, Ergonomics Assessment

1. Introduction

Digital Human Modeling Software (DHMS), both for product development and production process development, are frequently used within automotive industry [1]. The software is typically installed on desktops and operated with mouse and keyboard (manually using a DHMS), and the software is normally used early in development processes to consider ergonomics in design, development, and pre-planning, and the results are visualized by numbers, pictures and, less regularly, movies. To continue to provide essential support in development processes, DHMS technology needs to be adapted to new digitalization techniques and trends. Therefore, DHMS technology needs to be able to work together with head mounted display VR (virtual reality) and AR (augmented reality) technologies, as new immersive ways to control inputs, present simulation results and enhance understanding. Such technologies are available and

[1] Corresponding Author, Email: dan.lamkull@volvocars.com.

established within the gaming/entertainment industries. Furthermore, DHMS technology needs to be developed to function in digital twin solutions. This means that DHMS technology needs functionality for simulations in the virtual world in order to feed the reality with information (i.e. as used today), but also have functionality to work the other way around, i.e. to be fed with information from the real world in order to continuously learn and improve, and thereby gain future designs and simulations made in the virtual world. Information from the real world could be fed from smart textiles/sensorized garments. Smart textiles have the potential to radically change the way industry performs evaluations of ergonomics. Clothes with integrated sensors exist on the market and prototypes have shown that piezoelectric fibers can be used to detect finger flexion and piezoresistive fibers for registration of foot pressure [2,3]. Additionally, other wearable sensors, such as smart watches and wristbands, are changing the traditional interaction with operators in assembly industries. Wearable solutions may be a natural way to improve the usability of measurement systems by avoiding the use of cables and sticky electrodes and ensuring correct electrode placement by novice users [4,5].

One of three major risk factors interacting and contributing to the level of risk for an assembly worker is working posture (the two others are time and force) [6]. To achieve a working posture that is likely to happen in reality when manually using a DHMS tool is therefore crucial. Realistic posturing is required to obtain accurate quantitative assessments of human performance, as it has been shown that the performance models are sensitive to the postural condition [7]. The need for faster and more consistent human simulation tools has motivated some commercial human modeling tool suppliers to implement various posture/motion wizards. These task animation wizards allow a more rapid definition of task sequences [8,9]. However, these wizards are designed for certain types of tasks (e.g. ingress, egress or driving postures), and can not be utilized as a general solution for obtaining correct assembly postures or motions. These wizards seem not yet to be a successful way of eliminating, or at least minimizing, the inconsistency in results within or among simulation engineers. Fully functional self-posturing (and motion) calculation is needed by DHMS tool users [10]. There are numerous examples of posture and motion prediction research and implementations, e.g. [11-15]. Most of the research results are not yet available in commercial DHMS tools but implemented in research applications.

This paper shows examples of where work postures, achieved through manual use of DHMS tools (posturing the manikin with manual joint manipulation or by instructing the manikin to perform a certain grasp task), or by using task animation wizard, considerably differ from “real” postures compiled during VR/AR sessions. VR/AR is used to achieve more realistic (likely to happen) working postures and a further development of the DHMS tools and work procedures should lead to faster and more consistent digital human simulation tools. The paper also justifies several mentioned research projects that is supported by the authors’ employer both by financial means but also by collaboration.

2. Examples of achieved working postures

This section presents three working postures achieved with manual joint manipulation (manual use) of DHMS tools and one motion sequence achieved by the use of a task animation wizard. The DHMS tools used are IMMA [16] (Figure 2 and 3) and

JACK/JILL [17] (Figure 4). The motion sequence is generated in the IMMA manikin software.

2.1. *Manual use of DHMS tools*

Volvo Cars uses a generic work process for performing DHM task analysis suggested by, among others, Green [18] and Hanson et al. [19]. The work process includes the following seven steps: 1) understanding the task, 2) understanding the work environment, 3) understanding the worker population, 4) understanding the limits of the software used, 5) performing the analysis, 6) analysing and applying judgements to the results, and 7) reporting the results of the analysis. This work process is used to support both the customers of the simulation tasks and the simulation engineers performing the tasks. By this approach the simulation engineers are given vital information about the task; what is the working height, what is the weight of the assembled part, is the task allowed to be carried out as a blind operation, is the operator allowed to lean on the car, is the operator leaning on the car, etcetera.

It could be argued that the unrealistic postures achieved with manual joint manipulation (manual use) of DHMS tools are due to inexperienced simulation engineers or poor manual execution of DHMS tasks. However, the simulation engineers at Volvo Cars have been working, in average, 21.6 years (n=5, s.d.=0.8) as simulation engineers within the Final Assembly Manufacturing Engineering organization; and during the last 23 years Volvo Cars has used several different DHMS tools. Figure 1 shows the different DHMS tools and the period of usage. Thus, it should be possible to reject that inexperience and poorly executed simulations are the cause of the unrealistic postures.

Figure 2-4 (the figures have been partly blurred due to confidentiality reasons) show three working postures that are unnatural (unlikely to happen). Unfortunately the "real" postures derived from VR/AR sessions are not possible to show due to confidentiality reasons. However, the figures are rather self-explanatory – the working postures are really unnatural; but it is a subjectively based statement of the both authors. Comparisons between experienced operators' (used in VR/AR sessions) preferred working postures and the working postures achieved through manual joint would probably objectively reject them as natural working postures.

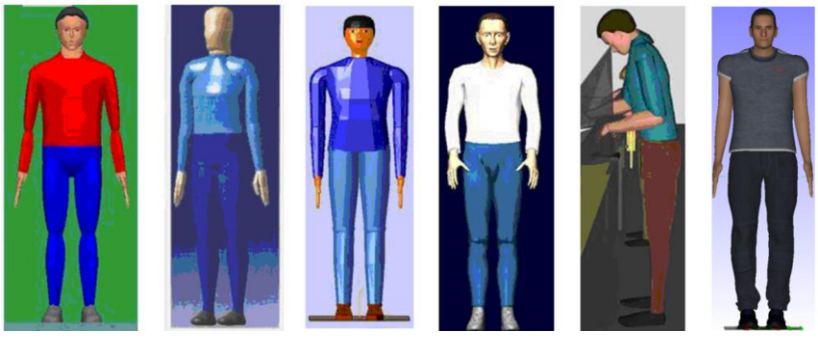

Figure 1. The different DHMS tools used at Volvo Cars during the last 23 years. From left to right and the period the DHMS tool was/is used: IGRIP/VMAP 1998-2000, Catia V5 Human 2000-2002, Robcad/Man 2000-20004, eM-RAMSIS 2004-2010, JACK/JILL 2010-today, IMMA 2015-today.

Furthermore, the simulation engineers' greatest concern is that the simulation tasks appear to be correct as well as being correct [20,21]. If the simulation task does not appear realistic, the analysis might also be questioned. Consequently, simulation engineers manipulate the manikins to achieve as realistic postures as possible and be in congruent with the information given by the customers in the generic work process.

Figure 2. Assembly of tailgate sealing. (IMMA manikin)

Figure 3. Assembly of a part in the tunnel console. (IMMA manikin)

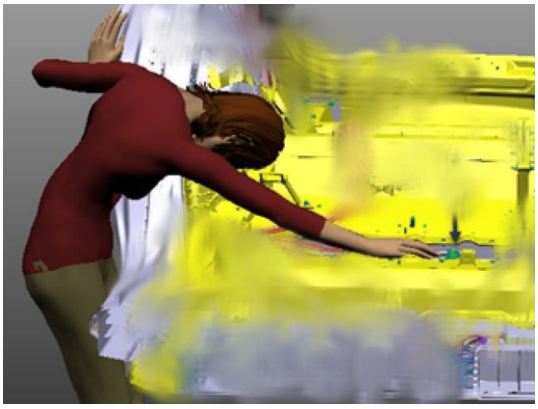

Figure 4. Electrical connection in the proximity of the tunnel console area. (JACK/JILL manikin)

2.2. *Using task animation wizard*

Figure 5 shows the interface of the task animation wizard in the DHMS tool IMMA. To instruct the manikin (manikin family) to get into the rear part of the car the simulation engineer has created 34 sub-tasks (such as attach, detach, look at, follow, pause, grasp etcetera). The 34 sub-tasks' basic motion is shown in Figure 6.

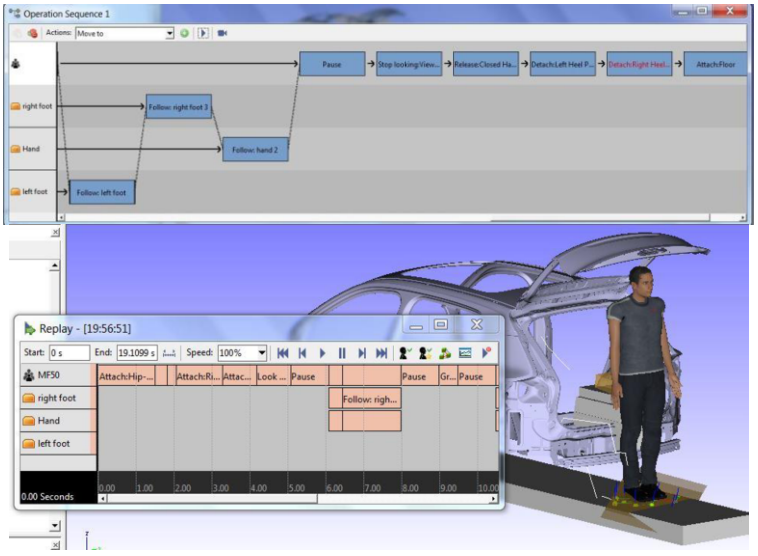

Figure 5. The interface of the task animation wizard in the DHMS tool IMMA. The operation sequence consists of 34 sub-tasks.

Figure 6. The 34 sub-tasks' basic motion pattern. (All 34 pictures are not possible to show due to restricted space in the form of a conference paper).

The task animation wizard is used when the manikin task consists of a longer and rather complex motion. It is the only way to, inside the DHMS tool, manually instruct the manikin to perform a movement over a longer period of time. Thus, it can be seen as a complement, or substitute, for motion capture.

3. Discussion and concerns about achieved working postures

3.1. *The working postures achieved by manual use of the DHMS tool*

The working postures in Figure 2-4 achieved by manual use of the DHMS tools are not likely to happen in reality. However, the simulation engineers within the Final Assembly Manufacturing Engineering organization, at Volvo Cars, state that it is often when the human (manikin) has to reach a certain part or location in its boundary of reach of motion that the unrealistic working postures occur. Sometimes the unrealistic working postures occur when the manikin has to support the body with one hand. Figure 4 shows a typical working posture that is the result of a change of a hand position – in this case the left hand has been moved to the door pillar to support the body; and that change makes the manikin to occupy an awkward body posture. The simulation engineers try to avoid these awkward body postures but have no, or little, knowledge about what is causing the manikin to suddenly occupy an unwanted and unrealistic body posture. The simulation engineers often restrict the manikin to move as much as possible by entering certain constraints such as attach some body parts to different car components or demand a particular line of sight to avoid a rapid change of the neck angle. However, that trick is not very useful since it will, if used too much, completely freeze the manikin and it will not be possible to move the manikin at all. Another concern is that the manikin is taught (programmed) to avoid collisions and

therefore behaves as if the car body is lethal to touch; Figure 2 and Figure 3 are typical examples of such behaviour. This is the case for all DHMS tools that have collision avoidance, e.g. IMMA and eM-RAMSIS [22]. If the manikins in these two cases lean with the hip, or the thighs, on the car body they will occupy a much better ergonomics posture. In the software IMMA it is possible to synthesize collision-free and ergonomic motions for a system consisting of a manikin and the part being assembled using the manikin motion generator inside IMMA [23]. However, many assembly tasks are related to engage clips and connectors. Thus, there is no part that shall be taken from the material facade to a nominal part in the car. Therefore the motion generator can not be used – there is simply no part to connect to the motion generator.

The manual use of the DHMS tools to achieve working postures are full of flaws and it is well known that this method is not very suitable for ergonomics analyses [24]. However, it is still the most common method to manipulate a manikin since it is a basic functionality in all DHMS tools and manual adjustments of body angles continue to be a common method to manipulate a manikin [25].

3.2. *The working postures achieved by using a task animation wizard*

A motion over a long period of time is not possible to create with manual use of a DHMS tool. If the DSHMS tool is not equipped with an animation wizard an imported stream of motion must be used, e.g. motion capture. The working postures (or discrete motion cycle/time frame capture) achieved by using a task animation wizard is therefore the most realistic motion that can be generated manually. However, it is an extremely time consuming procedure and the discrete motion jumps are not collision free and the motion pattern is rather "robot like" in its motion behaviour. The simulation engineer can try to avoid this "robot like" behaviour by adding more (sub) tasks, but that would take even more time, and the benefit between creating more (sub) tasks and a better motion behaviour is not worthwhile. Due to the vast time needed to carry out a motion sequence by using a task animation wizard, and the rather jerky motion pattern (and not 100% collision free) achieved, are two of the reasons why animation wizard based motions are not commonly performed at Volvo Cars.

3.3. *An intermediate period when complementary technologies are used together with DHMS tools for ergonomics simulations*

Many of the shortcomings and difficulties described in this paper could be avoided, or at least reduced, by the use of complementary technologies such as:

- Motion Capture (recording the movements of objects and/or people)
- VR[2] and/or Mixed Reality where physical and digital objects co-exist and interact in real time (also called AR – Augmented Reality)
- Virtual Gloves (capturing full hand and finger actions in virtual reality)

Considering the many recent advancements in capability from the movie animation and gaming industries. The quantity and quality of computer generated movies and computer games have increased greatly over the past 15 years. The realism of humans

[2] In this descriptive paper we do not explicitly distinguish between VR and AR, although there are distinct differences; but in this context we consider it being more of a semantic issue and consider them being synonyms.

represented in these models and their associated movements are attracting customers and driving new business opportunities. DHMS tool developers and providers should investigate the technologies used in these industries for application in commercial DHMS software. Today, there are many available motion capture programs that are both affordable in price, easy to use and that reproduce sufficiently accurate motion recordings, e.g. [26-28]. In the VIVA project [29] an add-on application for motion capture has been developed for IMMA and it is Volvo Cars' intention to implement this motion capture add on. This complementary technology will be used to achieve more realistic working postures for assemblies in the outmost reachability area of the operators. When (not if) the DHMS tools have been improved, and motion capture no longer is needed for these kind of assembly simulations, Volvo Cars will abolish the motion capture technology.

To further improve the use of motion capture Volvo Cars will also combine it with mixed reality so physical and digital objects co-exist and interact in real time. Already today Volvo Cars uses mixed reality without combining it with motion capture. Once the COVID 19 pandemic is over, testing of motion capture will be performed and successful tests will lead to a launch of motion capture. Figure 6 shows an example of mixed reality.

The hands are an operator's most valuable tools. Many simulation tasks are ordered in the purpose to get an answer if a part is possible to handle with the hands; are there sufficient space, are the handles good etcetera. The simulation engineers might spend up to 50% of the simulation time to tune the hands and fingers to a realistic configuration [21]. Thus, virtual glove technology is something that interests Volvo Cars. Furthermore, hand, wrist and finger injuries are the most common MSDs in Volvo Cars' final assembly plants (48% of all reported MSDs).

Figure 6. An example of mixed reality. The "operator" is wearing a head mounted display (HMD) and is working in a room where props like aluminum frames and wooden parts have been installed to mimic a car body. The HMD is displaying a virtual car made of CAD parts – positioned in relation to the props.

4. Research projects supporting the need for faster and more consistent human simulation tools

The following three mentioned research projects have all been initiated to deal with the shortcomings and difficulties described in this paper. Beyond dealing with these issues the research projects are dealing with numerous other research questions; all in attempt to close, or decrease, gaps in functionalities and efficiency of DHMS tools. These research projects' aims and purposes are justifying the authors' employer to participate in the research projects and partly financing them. The following three paragraphs, 4.1-4.3, are coarsely describing the three research projects' objectives and research topics.

4.1. *VIVA – VIrtual vehicle assembler*

VIVA – VIrtual Vehicle Assembler [29] is a research project that started in 2019. It will continue for three years and will end in April 2022. The total funding from VINNOVA is 4.6 MSEK. The overall aim is to develop a supportive DHMS tool that:

- automatically can predict human behaviour considering dynamic effects and analyze human work in manual work stations from a musculoskeletal viewpoint
- automatically can optimize workstations where humans are supported with exoskeletons or collaborative robots.
- considers human diversity in terms of appearance, shape, clothes, and safety equipment used during work.
- easily can be understood, used and manipulated as well as adapted to recent developments within immersive VR and digital twin solutions.

4.2. *SVE – Synergy Virtual Ergonomics*

SVE – Synergy Virtual Ergonomics [30] is a research project that started in 2019 and will end in September 2023. The total funding from the Knowledge Foundation (KK) is 12 MSEK. The project has three themes: 1) Modeling behaviour and appearance, 2) Assessment and 3) Interaction.

The research contributions will include techniques and methods for making well-informed design decisions related to ergonomics, mainly at the virtual stages of the product realization process, including representing human diversity, digital twin solutions, modeling and assessing cognitive ergonomics, instructing manikins from demonstrations, applying persona descriptions to manikins, and interacting with manikins in immersive virtual reality (VR).

4.3. *DIPPA – Digitalization of Product- and Production design to increase Automation*

DIPPA – Digitalization of Product- and Production design to increase Automation [31] is a research project that started in April 2019 and will end in April 2021. The total funding from VINNOVA is 3 MSEK. The purpose and goal of the DIPPA project is to increase the interaction between product and production design to increase automation in the final assembly. In the context of DHMS tools DIPPA will carry out research in the topic of Human Robot Collaboration (HRC).

5. Conclusion

In the meantime, before a ”perfect” task animation wizard is realized, motion capture will probably be the predominant technology to use when it comes to generate complex motions for digital human models in a manufacturing context. DHMS technology needs functionality to be fed with information/data from the real world in order to continuously learn and improve, and thereby gain future designs and simulations made in the virtual world. Information from the real world could be fed from smart textiles/sensorized garments. Wearable sensors, such as smart watches and wristbands, are changing the traditional interaction with operators in assembly industries. Wearable solutions may be a natural way to improve the usability of measurement systems by avoiding the use of cables and sticky electrodes and ensuring correct electrode placement by novice users. DHMS tools could also be connected with motion databases with MTM-based annotations in order to synthesize natural looking motions, as suggested by Keyvani et al. [32].

Acknowledgement

It is not the authors' intention to completely disqualify the use of DHMS tools. These tools are indispensable in the development of new vehicles and play a crucial role in virtual product simulation and production simulation. The development that these tools have undergone over the past thirty years is outstanding and it is important to recognize the focused work of DHMS developers and researchers that is supporting and enabling the automotive industry's virtual way of working. The authors also would like to thank both *VINNOVA* and *The Knowledge Foundation* for financially supporting the research projects mentioned in this paper.

References

[1] Lämkull D. Computer Manikins in Evaluation of Manual Assembly Tasks. Doctoral Thesis, ISBN 978-91-7385-236-4, Chalmers University of Technology, Göteborg, Sweden, 2009.
[2] Lund A. Melt spun piezoelectric textile fibres - an experimental study. Doctoral Thesis, ISBN 978-91-7385-889-2, Chalmers University of Technology, Sweden, 2013.
[3] Rundqvist K, Sandsjö L, Lund A, Persson N-K, Nilsson E. Registrering av fotnedsättning baserat på piezoelektriska fibrer, Medicinteknikdagarna, October, Göteborg, Sweden, 2014.
[4] Abtahi F. Towards Heart Rate Variability Tools in P-Health: Pervasive, Preventive, Predictive and Personalized. Doctoral Thesis. KTH-Royal Institute of Technology, Stockholm, Sweden, 2016.
[5] Vega-Barbas M, Diaz-Olivares JA, Lu K, Forsman M, Seoane F, Abtahi F. P-Ergonomics Platform: Toward Precise, Pervasive, and Personalized Ergonomics using Wearable Sensors and Edge Computing. Sensors (Basel). 2019, 19(5), 1225. doi:10.3390/s19051225.
[6] Sperling L, Dahlman S, Wikström L, Kilbom A, Kadefors R. A cube model for the classification of work with hand tools and the formulation of functional requirements. Applied Ergonomics, 1993, 24(3), 212–220.
[7] Chaffin DB, Erig M. Three-Dimensional Biomechanical Static Strength Prediction Model Sensitivity to Postural and Anthropometric Inaccuracies. In: IIE Transactions, 1991, 22(3), 215–227.
[8] Mårdberg P, Yan Y, Bohlin R, Delfs N, Gustafsson S, Carlson JS. Controller Hierarchies for Efficient Virtual Ergonomic Assessments of Manual Assembly Sequences. In: Proceedings of the 6th CIRP Conference on Assembly Technologies and Systems (CATS), 2016, May, Volume 44, 435–440.
[9] Raschke U, Kuhlmann H, Hollick M. On the Design of a Task Based Human Simulation System. In: Proceedings of the 2005 SAE Digital Human Modeling for Design and Engineering Symposium (DHM2005), 2005, June, Iowa City, Iowa, USA.

[10] Wegner D, Chiang J, Kemmer B, Lämkull D, Roll R. Digital Human Modeling Requirements and Standardization. In: Proceedings of the 2007 SAE Digital Human Modeling for Design and Engineering Symposium Conference (DHM2007), 2007, June, Seattle, Washington, USA.
[11] Yang J, Marler RT, Kim HJ, Farrell K, Mathai A, Beck S, Abdel-Malek K, Arora J, Nebel K. Santos: A New Generation of Virtual Humans. In: Proceedings of the 2005 SAE World Congress, 2005, April, Detroit, MI, USA.
[12] Yang J, Marler T, Beck S, Kim J, Wand Q, Zhou X, Pena Pitarch E, Farrell K, Patrick A, Potratz J, Abdel-Malek K. Arora JS, Nebel K. New Capabilities for the Virtual-Human Santos. In: Proceedings of the 2006 SAE World Congress, 2006, April, Detroit, MI, USA.
[13] Han Kim K, Martin BJ, Brent Gillespie R. Posture and Motion Prediction: Perspectives for Unconstrained Head Movements. In: Proceedings of the 2006 SAE Digital Human Modeling Design and Engineering Conference and Exhibition (DHM2006), 2006, July, Lyon, France.
[14] Rasmussen J, Tørholm S, Christensen S, Rausch J. Posture and Movement Prediction by Means of Musculoskeletal Optimization. In: Proceedings of the 2006 SAE Digital Human Modeling Design and Engineering Conference and Exhibition (DHM2006), 2006, July, Lyon, France.
[15] Obentheuer M, Roller M, Björkenstam S, Berns K, Linn, J. Human like Motion Generation for Ergonomic Assessment – A Muscle driven Digital Human Model using Muscle Synergies. In: Proceedings of the ECCOMAS Thematic Conference on Multibody Dynamics, June, 2017. Prague, Czech Republic.
[16] Högberg D, Hanson L, Bohlin R, Carlson, JS. Creating and shaping the DHM tool IMMA for ergonomic product and production design. International Journal of the Digital Human, 1(2), 132–152, January 2016.
[17] Badler N. Computer Graphics Animation and Control. Simulating Humans, Oxford University Press, New York, USA, 1993.
[18] Green RA. Generic Process for Human Model Analysis. In: Proceedings of the Digital Human Modeling Conference, Munich, Germany. SAE 2000-01-2167, 2000.
[19] Hanson L, Blomé M, Dukic T, Högberg D. Guide and documentation system to support digital human modeling applications. International Journal of Industrial Ergonomics, 2006, 36(1), 17–24.
[20] McDaniel JW. The Need for Better Human Performance Models. In: Proceedings of the 1999 SAE Digital Human Modeling for Design and Engineering. International Conference and Exposition, The Hague, The Netherlands. SAE 1999-01-1895.
[21] Lämkull D, Hanson L, Örtengren R. Uniformity in manikin posturing: A comparison between posture prediction and manual joint manipulation. International Journal of Human Factors Modelling and Simulation, 2008, 1(2), 225–243.
[22] Seidl A. Das Menschmodell RAMSIS. Analyse, Synthese und Simulation dreidimensional Körperhaltung des Menschen. (The Man Model RAMSIS: Analysis, Synthesis and Simulation of Three-dimensional Human Posture). Ergonomics and Human Factors, Technical University of Munich, Germany, Doctoral thesis (In German), 1994.
[23] Lia Y, Delfs N, Mårdberg P, Bohlin R, Carlson JS. On motion planning for narrow-clearance assemblies using virtual manikins. In: Proceedings of the 51st CIRP Conference on Manufacturing Systems, 2018, May, Stockholm, Sweden.
[24] Artl F, Bubb H. Development of movement functions for the CAD human model RAMSIS. In: Landau, K. editor. Ergonomics Software Tools in Product and Workplace Design, A review of recent developments in human modelling and other design aids: Verlag ERGON GmbH; 2000. Stuttgart, Germany.
[25] Lämkull D, Hanson L, Örtengren R. Uniformity in manikin posturing: a comparison between posture prediction and manual joint manipulation. International Journal of Human Factors Modeling and Simulation, 2008, 1(2), 225–243.
[26] Qualisys Automotive Application. Available from: https://www.qualisys.com/applications/engineering/qualisys-automotive-driving-innovation/ [Accessed 16 May 2020].
[27] Becoming One: Assessing Ford's Exoskeletons With Inertial Motion Capture. Available from: https://www.xsens.com/cases/becoming-one-assessing-fords-exoskeletons-with-inertial-motion-capture. [Accessed 16 May 2020].
[28] The biomechanical measuring system industrial athlete. Available from: https:// neuronmocap.com/portfolio/scalefit-industrial-athlete. [Accessed 16 May 2020].
[29] VIVA - the Virtual Vehicle Assembler. Available from: https://www.vinnova.se/en/p/viva---the-virtual-vehicle-assembler/ [Accessed 16 May 2020].
[30] SVE – Synergy Virtual Ergonomics. Available from: https://www.his.se/en/research/virtual-engineering/user-centred-product-design/virtual-ergonomics/ [Accessed 16 May 2020].

[31] DIPPA (Digitalization of Product- and Production design to increase Automation). Available from: https://www.vinnova.se/en/p/dippa-digitalisation-of-product--and-production-design-to-increase-automation/ [Accessed 16 May 2020].
[32] Keyvani A, Lämkull D, Bolmsjö G, Örtengren R. Using Methods-Time Measurement to Connect Digital Humans and Motion Databases. In: Duffy V, editor. Digital Human Modeling and Applications in Health, Safety, Ergonomics, and Risk Management. Human Body Modeling and Ergonomics, Vol. 8026, 343–352, Springer Berlin Heidelberg. 2013.

DHM2020
L. Hanson et al. (Eds.)

© 2020 The authors and IOS Press.
This article is published online with Open Access by IOS Press and distributed under the terms of the Creative Commons Attribution Non-Commercial License 4.0 (CC BY-NC 4.0).
doi:10.3233/ATDE200038

Narrowing the Gap of Cognitive and Physical Ergonomics in DHM Through Embodied Tool Use

Jessica LINDBLOM[a,1], Ari KOLBEINSSON[b] and Peter THORVALD[b]
[a] *University of Skövde, School of Informatics, 541 28 Skövde, Sweden*
[b] *University of Skövde, School of Engineering Science, 541 28 Skövde, Sweden*

Abstract. The fields of human factors and ergonomics are systemic by nature, focusing on studying complex interaction between human and technology. However, the levels of explanation have resulted in physical or cognitive ergonomics. Modern understandings of human cognition and technology-mediated interaction, such as embodied cognition, activity theory and user experience (UX) is used as a frame of reference to analyze and illustrate the usage of a digital human modeling (DHM) tool in practice. We try to narrow the gap between physical and cognitive ergonomics through embodied tool use. An identified core problem is to understand how 2D devices should properly interact within 3D objects and manikins in DHM. Some future work is presented, which could be beneficial for DHM, and, in the long run, promote a positive UX at work for various end-users of DHM tools in general.

Keywords. Ergonomics, Embodied Tool Use, DHM, User Experience

1. Introduction

The fields of human factors and ergonomics (HF/E) are systemic by nature, focusing on studying complex interaction between human and technology [1-3]. In spite of this, the common practice in HF/E is to split the human into 'neck up' and 'neck down', which has resulted in cognitive ergonomics and physical ergonomics [2]. Although this division makes it easier to study certain aspects of ergonomics, it runs the risk of not portraying the whole picture of the embodied human being situated in the world of technology [4]. Indeed, it should be acknowledged that both cognitive and physical ergonomics are dominant and well justified fields that have been successfully for a long time, but where the common practice is to mainly focus on performance-related aspects [4, 5]. However, it has been argued that one current challenge of HF/E is that that they are not aligned with the more modern approaches for studying human cognition and technology-mediated interaction, including embodied interaction and cognition, activity theory (AT), and user experience (UX) [4, 5]. Briefly stated, embodied cognition emphasizes that traditional cognitive science as well as HF/E has largely ignored the role and relevance of the lived body in human cognition, viewing the body more as a passive input and output device. Embodied cognition, on the other hand, argues that human cognition emerges via close couplings of brain, body and environment, stressing the active process

[1] Corresponding Author, Email: jessica.lindblom@his.se.

of bringing fourth the experience of being situated within the material and social world [6-14].

Recently, several initiatives have been performed to include embodied interaction and cognition into the equation of HF/E [1-5, 15]. One initiative is to include some aspects of embodied cognitive actions into digital human modeling (DHM) that merely models physical aspects of human bodies, focusing on anthropometry and physical strain on the body, which is also the case with most current DHM tools [2, 16, 17]. Another initiative is to study the use of DHM tools in practice from an embodied interaction and UX perspective. To the best of our knowledge, in the DHM domain, the combination of embodied cognition and interaction, tool use, and UX have received limited attention in practice and in theory/research. In addition, UX lacks proper theoretical frameworks, and we also want to contribute to this challenge, suggesting that embodied tool use would fit as hand in glove for addressing UX aspects within DHM.

In this paper, the focus is on the latter initiative, and the component of discussion is the digital DHM software called IPS IMMA [18]. This work is motivated from two overlapping perspectives. On the one hand, Dourish [14, 19] quests to investigate and analyze how human-technology interaction is embodied, studying how the visibility and availability of the interface is designed so it affords for a wider range of relevant engagements and embodied interactions. On the other hand, Grundgeiger et al. [20] argue that considering and improving users' experience (UX) is one of the fundamental aims of the ISO standards on human factors and human–computer interaction [21]. They point out that embodied interaction and cognition as well as tool use is a feasible approach for considering complementary views on *interaction* that cultivates a positive UX [20].

The next section briefly presents and discusses the underlying theoretical and methodological foundation for embodied tool use, and its relationship to UX. The discussion is illustrated with an illustrative example of the DHM tool IMMA from an end-user's perspective, focusing on activities and relevant embodied engagements that have an impact on UX. The paper ends with a short discussion.

2. Embodied Cognition and UX as Embodied Experience

The mainstream study of human cognition has since the inception of cognitive science in the mid-1950s mainly focused on studying individual's internal mental representations in form of symbol manipulation inside the head [6-14]. Cognition is viewed as information-processing of these more or less explicit internal symbolic representations, being the "internal content" of the external world, following the so-called computer metaphor of mind, and almost nothing outside "the skull" is taken into account. It presents a centralized view of cognition with the body only serving as some kind of input and output device, i.e. a physical interface between an internal program (cognitive processes) and an external world [6-14]. It should be pointed out that the information-processing view still dominates the fields of HF/E as well as traditional cognitive science.

Starting in the late 1970s, several lines of criticism arose about the fundamental assumptions of the computer metaphor of mind. It was argued, for example, that bodily and neurological aspects should be taken into account more seriously in explaining cognition. Another much discussed issue were if cognition should rely that much on mental representations and how the connection between the external world and the internal representations was realized. Some researcher started to study cognition as it unfolded in everyday life together with other people and various artefacts. The so-called

'turn to the wild' approach in cognitive science and human-computer interaction (HCI) questioned the nature of human cognition and how it should be studied [6-14, 22-23].

2.1. Various stances of embodied cognition

Since the 1980s, the cognitive sciences have (re-)introduced more elaborate views on cognition that are commonly referred to as dynamical, embodied, extended, distributed, and situated theories of cognition. A body of research now provides compelling empirical evidence and theoretical explanations that the human mind is the result of human's bodily interactions with a social and material environment within a broader unit of analysis "beyond the brain/skull" [6-14, 22-23]. Several characterizations of embodied cognition exist (see [10] for a review). Here we describe embodied cognition from three complementary stances, as a way to simplify, ranging from *sensori-motorness* and *situatedness* to *embeddedness*.

First, the *sensori-motorness* of embodied cognition commonly refers to structural couplings that usually are considered the core of embodied cognition [6], meaning the action-perceptions loops that span the agent-environment interaction unit [7, 9]. The claim is that knowledge and cognition is the result of an active and ongoing interpretation that emerges from biologically embodied structures of understanding, which makes it possible for us to "make sense" of our human being in the world [6, 9-13]. Most attention is placed on how the individual agent's physical body is mutually sensori-motor coupled to the material and social world, and how the agent continuously perceives feedback on its actions, which affects what is being perceived, and then the perceptions affect the actions, etc. A key aspect in embodied cognition is that the same dynamical processes which emerge through action-perception loops are also used in more advanced forms of cognition [6, 9-13]. The underlying assumption is that the acting and perceiving body as a whole organism is able to move and act in the world, manipulate objects, communicate, where these sensorimotor couplings are the pillar for human cognition. During the course of development and learning, an increasing ability to accomplish more advanced action-perception loops emerge via the growing ability to coordinate the lived body in relation to environmental constraints. As a result, stable patterns of behavior through which the body 'gets a grip' on the surroundings emerge [9, 11-12]. This implies that different kinds of bodies (morphology and structure) result in different kinds of cognition.

Second, the above stance of sensori-motorness enables us to be *situated in* the world, emphasizing the 'here and now' of a certain situation. This stance expands the unit of analysis to also consider what kind of social and material environment the embodied agent is situated within, i.e. to get a grasp of what is going on [7, 10-13]. This aspect of embodied cognition puts the sensorimotor coordination into a meaningful context, very often a social and material one [8-9]. Here the human needs to coordinate and collaborate her actions with other people and artefacts. A central focus is to describe and investigate what happens when cognition unfolds 'in the wild', studying how real humans enact their actions, and lot of ethnographic work has been performed that consider how complex patterns of collaboration emerge via distribution of cognitive processes between various kind of artefacts like calendars, cameras, pens, hammers, and other kinds of technology, and other humans, emphasizing the importance of studying practice as it occurs in real situations [11, 13, 15, 22-23]. It is highlighted that the social dimension of situatedness, i.e. other peers and caregivers, bootstrap the embodied agent into its particular niche and provide scaffolds for actions [22]. Moreover, this aspect also stresses that the cognitive system as a whole is able to perform cognitive phenomena at a systems level that cannot

be explained by an individual person alone. Example of this is the distributed cognition approach by Hutchins [23] where ship navigation is considered as a distributed phenomenon spanning several people, the tools and artefacts used, which considers the possibilities and constraints that affect the work practice of navigation as a cognitively distributed phenomenon.

The last stance stresses the *socio-cultural embeddedness* of embodied cognition, which refers to the social and cultural norms and values that shape the individual agent's development into being a full-blown member of society. Much focus here is on learning and developmental processes of children and adults, including acquiring various competences and skills as well as language and other external symbol systems. The research is dominated by a focus on social and communicative aspects of being socially embodied and socially situated in the socio-cultural world. Another strand of research is focusing on the use of tools as well as the historical development of various kind of tools in order to enhance cognitive abilities, studying the material engagement of tools both for the individual, but also in society [22-23]. During the years, it has been stressed that embodied cognition is relational, i.e., although an act or gesture is carried out individually, the act itself is social in nature, and the human brain is considered as a mediating social organ [10-13]. When it comes to human language, it is argued that language has roots in sensori-motorness and many abstract concepts are metaphors of concrete actions; i.e., the expressions "grasping an idea" or "life is a journey" [10-13, 24].

Although we have disentangled various stances of embodied cognition, they should not be considered as distinct levels that could be investigated in isolation. These stances of embodied cognition are inseparably intertwined, as Johnson [24, p.155] phrases it "*in order to have human meaning, you need a human brain, operating in a living human body, continually interacting with a human environment that is at once physical, social, and cultural. Take away one of these three dimensions, and you lose the possibility of meaning*". This way of considering human cognition also have methodological implications. Propose that the unit of analysis for HF/E and DHM research should include all aspects of embodied cognition, future research needs to consider some critical reflections on how to conduct and to what extent to cover this broader scope on the embodied human mind. This argument holds both when implementing the digital twin manikins used for simulations in the DHM tools as well as when end-users use the DHM tools to make risk assessments digitally.

2.2. Embodied interaction and UX

When it comes to applying embodied cognition to human-technology interaction and HCI, the *embodied interaction* approach received increased attention when the phenomenological dimension of HCI was stressed in the late 1980s. The previous mentioned 'turn to the wild' in studying cognition, particularly the seminal work by Suchman [22] on situated actions when interacting with a photocopier machine and Hutchins's [23] work on distributed cognition in ship navigation, focuses primarily on the body as being situated and embedded in a particular context, not considering the sensori-motorness of embodiment, but include interaction with various kinds of technology. Building on these pillars, Dourish [14] claims that embodied interaction offers a new model or framework of interaction, which is suggested fundamental for the future development of human-technology interaction in the early 2000s. He stresses the need to develop more plausible interactive modes than the traditional graphical user

interfaces, interactive modes which are physically and socially more similar to how tasks are performed in the real world. Dourish [14] emphasizes three elements in his work, in which embodiment is the key element in the analysis and design of interactive technology. He characterizes embodiment as meaning "grounded in everyday, mundane experience" [14, p. 125]. Another element is the focus on practice, which he describes as "everyday engagement with the world directed towards the accomplishment of practical tasks" [p. 125]. The third element is embodied practice that is the source of meaning: "we find the world meaningful primarily with respect to the ways in which we act within it" [p. 125].

Dourish's work [14-19] has been very influential in HCI, but he has been criticized for the lack of the actual body in his work. He does not merely consider physical embodiment, i.e. the physical instantiation of our living body. Instead, he focuses on the *participative status* of embodiment when describing interaction as an embodied phenomenon, which takes place in the real material and social world that affords form, substance and meaning to the interaction. Dourish argues that interaction should still be considered embodied, although there is no concrete contact between the human fingers and the computer mouse, because the interaction unfolds within a setting of specific knowledge, circumstances, and 'know how' that provides meaning and value. This 'background' should not be considered as a problem space to cope with. Instead, the background provides an essential and constitute component of the activity, we do not interact with an environment, were are *situated within* an environment.

Dourish's work [14-19] resulted in a focus on the aspects of social and tangible computing that contrasted the traditional desktop computing, as new modes of interacting with technology. This way of working resulted in a major misreading, namely that embodied interaction is only related to tangible computing, distinguishing between modes of interaction that are either 'embodied' or 'dis-embodied', explaining that embodiment cannot be 'turned off'. On the contrary, his intention was to compare and contrast between tangible computing and other forms of interactivity, suggesting that they should be analyze from the same point of view. This means that traditional desktop computing using mouse and keyboard is also embodied interaction [14, 19].

A lot of empirical studies of situated and embodied cognition has been conducted 'in the wild', which indicates that embodiment and situatedness requires a naturalistic environment to emerge. However, Rooksby [25] emphasizes that the 'in-the-wild' metaphor is not synonymous with applied research conducted outside the laboratory. He explains that Suchman's [22] work on situated action has been used as the ultimate ticket for leaving the contrived laboratory settings when studying cognition, is a total misconception of her work. Instead, Suchman introduced a new analytic model to study cognition where the relevant actions are driven by its context, reframing the issue of *interaction* per se in terms of sense-making practices [25]. Humans' sense-making practices may afford fewer degrees of freedom in a contrived laboratory setting, but still it is irrevocably a *situated activity* whether or not it is studied in 'the wild' or 'the laboratory'. It is quite ironic that Suchman's own work [23] was conducted in a laboratory setting. Consequently, there are no such claims that there are circumstances where human cognition is considered "dis-embodied" or "non-situated". Humans do not "think" differently in the laboratory, but the access to social and material scaffolds may be reduced. This aspect has been misinterpreted as "any human action that occurs in a laboratory is itself artificial" [25, p. 12]. Rooksby [25] argues that it is not a choice between 'artificial' or 'natural', rather it is possible to perform studies of embodied and situated activity that spans both the lab and the field [9]. To summarize, Grundgeiger et al. [20] claim that considering interaction as embodied, the intentionality of the user is

emphasized, which is mediated via the structural couplings with the technical devices and the context of use (i.e., the social and material environment that the user and the tolls/devices are embedded within).

2.3. UX as embodied tool use

Turning to the UX perspective, some criticism has been raised towards the embodied interaction approach for being too vague in informing design and development of technology. More recently, Van Dijk et al. [26] present several approaches and principles for how to design for embodied engagements for a person's being-situated-in-the-hybrid world of digital and real world interaction. It is pointed out that describing cognition as embodied interaction implies that user's embodied actions constitute underlying intentions and motives, which means that these actions are fundamentally emotive and intentional [26]. Grundgeiger et al. [20] suggest several reasons why users' experience should be considered when interacting with technology in the workplace, and DHM tolls are no exception. Grundgeiger et al. [20] emphasize that *interaction* per se is as an ongoing experience, implying that interaction with technology always has an associated UX, which is ubiquitously present whether or not it is explicitly addressed by researchers or designers [20]. The UX does not only occur during interaction, but also the time before and after usage [21]. Moreover, it is not enough to ensure pragmatic qualities, e.g., error reduction, effective performance, and reduced cognitive load when humans are interacting with technology such as DHM tools in the workplace. Much more emphasis needs to be focused on hedonic qualities, e.g., satisfying humans' motives and psychological needs, including expectations, emotions, and wellbeing [5, 26-28].

Grundgeiger et al. [20] also consider interaction as tool use, and this claim is grounded in Activity theory (AT). AT [27-29] focuses on human tool use to manipulate, perceive and interact with the world in order to fulfill activities. What an activity is could be understood on an intuitive level, but in AT, the notion of "activity" is central, being characterized as a purposeful, transformative, and developing interaction between users and the world [27]. Hence, its focus is on understanding and describing human activity in context, i.e., stressing that the human mind can only be understood in the context of human interaction with the world, and that this interaction, i.e., *activity*, is socially and culturally determined [27-29]. This socio-cultural embeddedness is stressed by the co-operative nature of human activity. Hence, every *activity* consists of a set of intentionally performed goal-directed actions that could be described as an interaction between a user and an environment, e.g., professional ergonomists' workplace, with the aim of transforming the workplace through the use of mediating artefacts like DHM tools and additional artefacts. In so doing, individual users have to be perceived active actors who intentionally engage in tool-mediated interaction process [20, 27-29]. The tool mediates the relationship between the users and the environment to fulfill the activity, where both the users and the environment are affected by the mediating tool. The DHM tool could be considered as a mediating tool that foster new ways of working practice as well as the users is affected by learning additional functionality of the DHM tool. It should be stressed that a DHM tool is typically not an object of activity but rather a *mediating* tool, because the object of activity is the workplace and settings in which the DHM tool is used.

The three-level *hierarchical structure of activity* is the backbone of AT. The structure frames the activity into the levels of activity, action, and operation, which are related to motive, goal and condition, respectively [27-29]. The top layer is the *activity*

itself, which is undertaken in order to fulfil some motive that corresponds to certain needs [27-29]. *Actions* refer to what must be done, and are conscious processes subordinated to activities, and they are directed at specific goals. These goals could be decomposed to sub-goals, sub-sub-goals, etc. Actions are similar to what usually is denoted as tasks within the HF/E literature. Actions are implemented through lower-level units called *operations* that describe how it can be done, defined by the prevailing conditions or circumstances under which they are carried out. Operations are routine processes that do not have their own goals, instead they provide an adjustment of actions to the ongoing situations. Operations are oriented toward the conditions under which the subject is trying to reach a goal, and humans are commonly not fully aware of their operations. Operations could be the result of an automatization of prior conscious actions, which over time may be transformed into a routine operation that may not require conscious control.

By combining the view of interaction as tool use from AT with the idea of interaction as fluent and intentional embodied ways of acting and being in the material and social world, implies that a transparent and useful tool amplifies the users' capabilities of bodily engagement in the material and social environment. This means that a positive UX is not only tied to a single entity in the interaction with a DHM tool in specific situations, or a moment of pleasure or joy when interacting with technology in general, but to the fulfillment of a successful embodied tool use of the activity.

Taking a UX perspective can be beneficial in the design and development of better DHM tools. Norros [4], Savioja et al. [5] as well as Hartson and Pyla [30] emphasize the need to include the intended end-users, i.e., the domains experts and professionals that will use the envisioned technology in accomplishing tasks in their daily work practice. In the case of DHM tool; ergonomists, several kinds of healthcare practitioners, and workstation designers in manufacturing are tentative primary user groups. In so doing, these domain experts are able to assess the potential and efficiency of the envisioned future technology. Considering UX early on can result in DHM tools that are usable, accepted, and support a positive UX [5, 30-31]. In addition, this way of involving und-users in the process can also support current work practices. It is widely acknowledged that professionals have to make workarounds to fill the gaps when technology rather hinders than supports the users' competence in their work practices, forcing them to pay attention to reducing the gaps in information flow, handling task interruptions, keeping various processes running smoothly, and enabling or recreating safety [20]. It should be emphasized that much work practice is based on tacit knowledge, originating in embodied and situated knowledge that sometimes is hard to articulate [32]. Neglecting various aspects of UX may cause poor interaction design and decreased interaction quality, which in turn may have a negative impact on acceptance of technology such as DHM tools to a wider group of end-users. This can be manifested in anxiety about digital and technical competence, reduced trust in data credibility, altered or even undermined professional autonomy and competence [20].

3. Illustrative example of the IMMA tool from an embodied tool use perspective

To illustrate these concepts and present how an embodied tool use approach could be used to study DHM tools in practice, we take a closer look at a tentative usage situation of the digital DHM software called IPS IMMA [18] where two professional ergonomists are going to evaluate and assess physical strain in the hand's grip for an assembly task

for an operator virtually, even before the assembly task is implemented at the shop floor (Figure 1). IMMA digitally simulates a manikin of the operator's performance and the objects used in the assembly situation, and the forces for each joint are calculated. IMMA can perform these calculations with families of manikins that are created from ergonomics databases, thus highlighting the ergonomic attributes of a task for several kinds of operators [18].

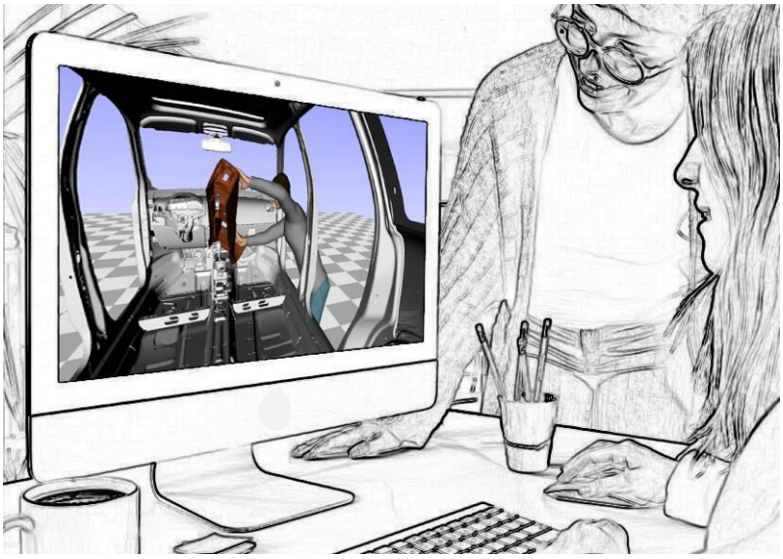

Figure 1. Illustration of the sensori-motorness, situatedness, and embeddedness of embodied interactions in relation to UX using the mediating IMMA tool in practice.

Referring to *embeddedness*, the ergonomists perform this task in a background of acquired embodied skills and situated knowledge of doing risk assessments in general, and for the particular manufacturing company. Beside the IMMA tool, multiple persons are involved in risk assessments of workstation design and work tasks that require collaboration between various specialists and company representatives. Moreover, additional tools and techniques should be included, e.g., legislation, company standards, additional risk assessment techniques based on field observation, interviews, and other manuals. The templates provided by the Swedish Work Environment Authority (SWEA) offer detailed instructions for the application of the assessment models denoted Key Indicator Methods Manual Handling Operations (KIM MHO) [33], which are commonly used, among others, in their current work practice. KIM I is about manual lifting and carrying [34], KIM II is about manual pushing and pulling of heavy objects [35], and KIM III deals with assessment of the probability of physical overload of repetitive work [36]. The available KIM assessment templates can be filled in directly on the screen at the SWEA's website and then a risk assessment score is calculated automatically (or be printed to be filled in and calculated manually). In the *activity* of doing risk assessments of manual operations in assembly for the particular company, all available digital and physical tools, and acquired skills and knowledge should be properly aligned with credible trade-offs in order to balance cost justification between competing financial and ergonomic goals as well as wellbeing at work.

From the stance of *situatedness*, the ergonomists perceive themselves from a first person point of view, in the unfolding social interaction when doing the risk assessment 'here and now' through the material and social constraints present at the current situation, which can be considered as a whole cognitive system. When the emergent participation in social and structural couplings evoke the experience of running smoothly and fluently, it can evoke the experience of a fluent interaction. This experience is bodily based, enable them to pay attention on the actual task (or actions), and the mediating IMMA tool could enable the structural coupling via acquired bodily skills to cope with the software and its input and output devices, which are not that easy to accomplish. Such a fluent interaction may promote a sense of competence that is likely to satisfy some of the emotional and psychological needs of the end-users.

The difference between *activities*, *actions* and *operations* in AT can be explained how to master the simulated movements of a manikin's various grips of a virtual object in manual assembly when learning to use the IMMA tool, being able to perform virtual risk assessments of manual assembly tasks, portraying the dynamic nature between these concepts. The overall motive here is to perform digital risk assessment by learning to use the IMMA tool, where manipulating the mouse, cursor and key board, the IMMA functions and 3D controls while using the IMMA tool is the fundamental activity in the very beginning. The focus on the hand-eye coordination of the structural couplings when creating the simulated manikin's basic grip points, grasp points, release points and viewpoints requires the full attention of the learner initially, perhaps on a non-complicated grasp for a 3D object. The new activity is then to conduct rather simple grips with the manikin's hand on typically object shapes, and these simple hand grips is now an *action* that is performed consciously since the learner is still a novice user of the IMMA tool, and soon, as a result of prolonged practice, moving the mouse, controlling the cursor, and using the controls become *operations* that are done without too much effort. Eventually, for the skilled super-user of IMMA, manipulating the manikin's various grips on several objects is no longer an *activity* in itself, but just an *action* as part of another activity, for example, virtually evaluating a new work station layout or designing a new assembly sequence for a new product component in order to increase operators wellbeing or the company's profit. Hence, the action of creating the simulated manikin's basic grip points, grasp points, release points and viewpoints has transform into routine operations, which does not require conscious control. An *activity* both mediates, and is mediated by, the physical and psychological *tools* used, as well as the social context of the activity. Viewing human activity as a three-layer systems provides the possibility for doing a combined analysis of motivational, goal-directed, and operational aspects of human activity in the socio-cultural and material environment, by interrelating the issues of "why", "what", and "how" within the AT framework [27-29].

However, it should be emphasized that working in a 3D environment using screen, mouse, cursor, and keyboard, as done in the IMMA tool, spans several *layers* of complex embodied interaction [37] (see Figure 2).

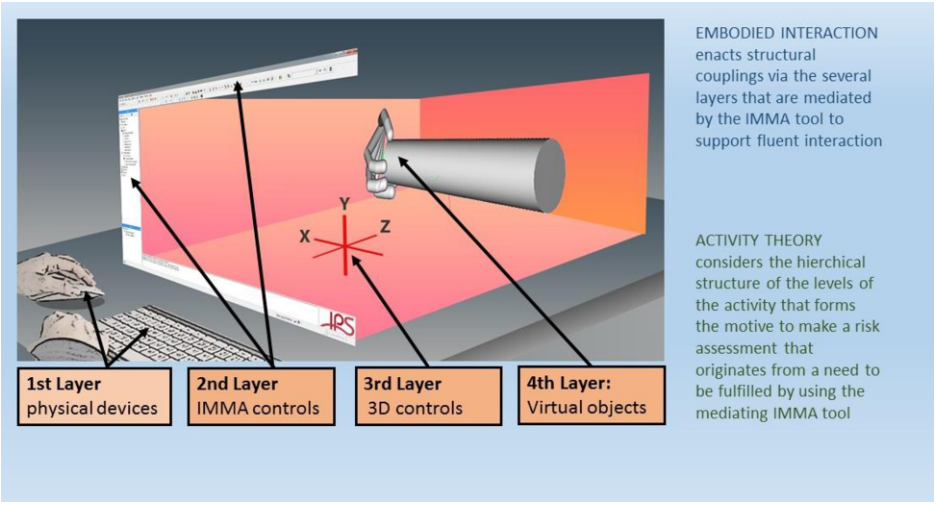

Figure 2. Illustration of the several layers of sensori-motorness in IMMA.

As Kolbeinsson [30] describes, the first layer is the real physical and social world, in which basic input/output devices like the screen, the keyboard and the mouse are physically situated. The second layer consists of the application controls, e.g., buttons and menus in the software interface as well as the mouse cursor, being two-dimensional in nature. The third layer represents the controls for manipulating the simulated three dimensional objects in IMMA software. These controls are three dimensional in nature, displaying a direct link to the manipulated object. The fourth layer is the three dimensional manikin's hand and the virtual objects themselves [37]. Hence, all the prevailing layers are made for the purpose for interacting with the fourth layer, the manikin hand's grip and the object it touches. Consequently, these various layers cover several forms of *sensori-motorness*. Every action performed via the hands that controls the keyboard and mouse, is intentional in itself, resulting in a bodily felt phenomenological experience. The IMMA tool will only achieve the anticipated outcome and functionality in the hands of a very skillful user. In order to accomplish this level of skill, the user needs to develop complex action-perception couplings that encompass complex hand manipulations of the input devices available – requiring well-acquired *handedness* skills as well as advanced sensorimotor coordination between what the hands do and what the user sees on the screen, which span several of the layers of interaction with the IMMA tool.

Upon closer analysis, it is revealed that manipulating the 3D world via 2D controls has a negative impact on the UX experience. The critical identified aspect is how to design the interface for the translation from the 3D entities of the interface to the 2D devices. In other words, the core problem is in understanding how a mouse cursor should interact within 3D objects and manikins in a 3D environment. As pointed out by Kolbeinsson [37], the lack of specific guidelines to handle this translation is surprisingly absent in theory and practice of interaction design, although the symptoms are addressed. Cooper et al. [38], for example, highlight three symptoms of the core problem: *drag thresholds* (translating a 2D dragging motion into 3D), *the picking problem* (picking objects at various depths in the simulated scene), and the *object rotation/viewpoint movement* problem [37]. However, Cooper et al. [38] mainly discuss these issues, but do

not provide any concrete guidelines, tentative solutions how to overcome these issues or any underlying principles that may provide some support for tentative solutions. A tentative explanation to reduce the gap is found in the concept of body schema [10, 12] that clarifies *why* the translation between the 2D layer and the 3D layer causes negative UX. Body schema results in the accomplishment of movement, referring to the phenomenological aspect of having a *capacity to move* or to exist in the action of one's own body. The body schema supports intentional activity, accomplished by almost automatic sensori-motor processes, given that the attention mostly is focused on external objects, and not on the particular accomplishment of movement [10, 12]. The body schema concept explains the problem's underlying cognitive foundation that results in a confusion that occurs when the mismatch in the visual perception provided that appears to be three dimensional, and the interaction mode provided by the IMMA tool that is two dimensional. Hence, the experienced dimensionality of movement gap between on the one hand the 2nd layer, and on the other hand, the 3rd and 4th layers, is the tentative underlying cause to the core translation problem (for more details about body image and body schema and their interrelatedness, see [10,12]).

4. Discussion

This work is initial steps in viewing the IMMA tool from an embodied tool use perspective, being aligned with UX that is one fundamental part of the ISO standards [21]. The identified core problem in understanding how 2D devices should properly interact within 3D objects and manikins in a DMH tool that results in negative UX. More detailed analysis and actions taken how to reduce this gap in DHM tools to improve a positive UX will be conducted. We will focus on more detailed and systematic analysis of DHM tools like IMMA in theory and practice, and include additional aspects and concepts from embodied cognition. The development of an evaluation framework of embodied tool use from a UX perspective is planned. To conclude, we want to enhance the embodied experience of interacting with DHM tools and improving their UX, contributing to the well-being of ergonomists and other user groups of IMMA, and, in the long run, the operators of the factories of the future, to promote a positive UX at work.

Acknowledgements

The authors wish to thanks the two ergonomists at Feelgood for their valuable input. This work has been realized by the Knowledge Foundation and the INFINIT research environment (KKS Dnr. 20180167) who have financially supported the Synergy Virtual Ergonomics project (SVE), as well as partner organizations.

References

[1] Bagnara S, Pozzi S. Embodied cognition and ergonomics. Journal of Ergonomics, 2015, 5(1), e129.
[2] Thorvald P, Högberg D, Case K. Applying cognitive science to digital human modelling for user centred design. International Journal of Human Factors Modelling and Simulation, 2012, 3(1), 90-106.
[3] Lindblom J, Thorvald P. Manufacturing in the wild–viewing human-based assembly through the lens of distributed cognition. Production & Manufacturing Research, 2017, 5(1), 57-80.

[4] Norros, L. Developing human factors/ergonomics as a design discipline. Applied Ergonomics, 2014, 45(1), 61-71.
[5] Savioja P, Liinasuo M, Koskinen H. User experience: does it matter in complex systems? Cognition Technology & Work, 2014, 16, 429-449.
[6] Varela FJ, Thompson E, Rosch E. The embodied Mind. MIT Press, Cambridge, 1991.
[7] Clark A. Being there – putting brain, body and world together again. MIT Press Cambridge, MA, 1997.
[8] Chemero A. Radical Embodied Cognitive Science. MIT Press, Cambridge, 2009.
[9] Wilson S, Golonka AD. Embodied cognition is not what you think it is. Frontiers in Psychology, 2013, 4(58), 1-13.
[10] Lindblom J. Embodied Social Cognition. Springer, Cham, 2015.
[11] Fuchs T. Ecology of the brain. Oxford University Press, Oxford, 2018.
[12] Gallagher S. Action and Interaction. Oxford University Press, Oxford, 2020.
[13] Lindblom J. A Radical reassessment of the body in social cognition. Frontiers in Psychology, 2020, 11, 987.
[14] Dourish P. Where the Action is. MIT Press, Cambridge, MA, 2001.
[15] Kolbeinsson A, Lindblom, J. Mind the body: how embodied interaction matters for multimodal human-technology interactions. Procedia Manufacturing, 2015, 3, 5184-5191.
[16] Scataglini S, Paul G, editors. DHM and Posturography. London, Elsevier, Academic Press, London. 2019.
[17] Billing E, Hanson L, Lamb M, Högberg D. Digital Human Modelling in Action. In: Holm L, Billing E, editors. Proceedings of the 15th SweCog Conference, 2019, Skövde, University of Skövde, 25-28.
[18] Hanson L, Högberg D, Carlson JS, Delfs N, Brolin E, Mårdberg, P, … Ore F. IPS IMMA – Intelligently Moving Manikins. In: Scataglini S, Paul G, editors. DHM and Posturography. Elsevier, Academic Press, London, 2019, 115–124.
[19] Dourish P. Epilogue: Where the action was, wasn't, should have been, and might yet be. ACM Transactions on Computer-Human Interaction, 2013, 20, 1, Article 2, 1-13.
[20] Grundgeiger T, Hurtienne J, Happel O. Why and how to approach user experience in safety-critical domains: the example of health care. Human factors, 2020.
[21] ISO DIS 9241-210. Ergonomics of human system interaction - part 210: Human-centred design for interactive systems. International Organization for Standardization, Switzerland, 2019.
[22] Suchman LA. Plans and situated actions. Cambridge University Press, New York, 1987.
[23] Hutchins E. Cognition in the wild. MIT Press Cambridge, MA, 1995.
[24] Johnson M. The meaning of the body. University of Chicago Press, Chicago, 2007.
[25] Rooksby J. Wild in the laboratory: A discussion of Plans and Situated Actions. ACM Transactions of Computer-Human Interaction, 2013, 20(3), Article 19, 17 pages.
[26] Hummels C, Van Dijk J. Seven principles to design for embodied sensemaking. In Proceedings of the Ninth International Conference on Tangible, Embedded, and Embodied Interaction, 2015, ACM, 21-28.
[27] Kaptelinin V. Activity Theory. In The Encyclopedia of Human-Computer Interaction, 2nd ed.; Soegaard, M., Dam, R.F., Eds. The Interaction Design Foundation: Aarhus, Denmark, 2013. https://www.interaction-design.org/literature/book/the-encyclopedia-of-human-computer-interaction-2nd-ed/user-experience-and-experience-design
[28] Engeström Y. Learning by expanding: An activity-theoretical approach to developmental research, 2nd ed. Cambridge University Press, New York, USA, 2015.
[29] Leontiev AN. Activity, consciousness, and personality. Prentice-Hall, New Jersey, USA, 1978.
[30] Hartson HR, Pyla PS. The UX Book. Morgan Kaufmann, Amsterdam, Netherlands, 2018.
[31] Hassenzahl M. The thing and I. In: Blythe M, Monk A, editors. Funology 2: From Usability to Enjoyment. 2018. Springer, Cham, 17-31.
[32] Andreasson R, Lindblom J, Thorvald P. Interruptions in the wild: portraying the handling of interruptions in manufacturing from a distributed cognition lens. Cognition, Technology & Work, 2017, 19(1), 85-108.
[33] Steinberg U. New tools in Germany: development and appliance of the first two KIM ("lifting, holding and carrying" and "pulling and pushing") and practical use of these methods. Work, 2012, 41 Suppl 1, 3990-3996.
[34] https://www.av.se/globalassets/filer/publikationer/broschyrer/bedom-risker-vid-manuell-hantering-lyfta-bara-broschyr-adi627.pdf
[35] https://www.av.se/globalassets/filer/publikationer/broschyrer/bedom-risker-vid-manuell-hantering-skjuta-dra-broschyr-adi668.pdf
[36] https://www.av.se/globalassets/filer/checklistor/riskbedomning-repetitivt-arbete-kim-3-checklista.pdf?hl=kim%203
[37] Kolbeinsson A. Mind the gap: Extending the body into 3D environments using 2D tools for interaction. Bachelor thesis, University of Skövde, Skövde, 2011.
[38] Cooper A, Reimann R, Cronin D. About Face: the essentials of interaction design. Wiley Indianapolis, 2007.

DHM2020
L. Hanson et al. (Eds.)

© 2020 The authors and IOS Press.
This article is published online with Open Access by IOS Press and distributed under the terms of the Creative Commons Attribution Non-Commercial License 4.0 (CC BY-NC 4.0).
doi:10.3233/ATDE200039

Gamification of DHM Software

Juan Luis JIMÉNEZ SÁNCHEZ [a,1] and Adam PALMQUIST [b,2]
[a] *Scania CV AB, Global Industrial Development, 151 32 Södertälje, Sweden*
[b] *University of Skövde, School of Informatics, 541 28 Skövde, Sweden*

Abstract. This study concerns the implementation of a gamified API in a digital human modelling simulation software, Industrial Path Solutions – Intelligently Moving Manikin (IPS-IMMA). The software has been identified as complex to learn and use, requiring a high level of expertise and involvement in order to interpret the interface and finding the correct tool for each task, causing disengagement from the users. To solve this issue, the study has looked into the concept of gamification to increase user activity by using elements and techniques from game design and applying them in a non-game context. Research on gamification in learning and training indicate increased engagement from the user, quicker on-boarding to a system as well as potential increases in learning outcome.

The gamified API implementation in this project has the purpose of increasing user engagement when utilizing the tool, increase the retention rate of users, as well as smoothing the learning curve for the user, producing an optimal learning trajectory that will make the novice user become a skilled user within a shorter period of time. To achieve this, an API widget package has been connected to IPS-IMMA to create one of the first gamified interfaces for a digital human modelling software.

Keywords. Gamification, Ergonomics, Simulation, Digital Human Modelling, On-the-job-training

1. Introduction

1.1. Digital Human Modelling tools

Digital Human Modelling (DHM) tools use digital representations of humans (also called manikins) to simulate and visualize their behavior, and then optimize their workspace and interactions with products in terms of ergonomics. Nowadays there is a number of DHM software commercially available in the market, such as RAMSIS [1], Jack [2], and SAFEWORK [3]. However, the present study has focused on the tool IPS-IMMA [4] [5], developed by the Fraunhofer-Chalmers Research Centre (FCC) [6].

Although the focus for the use case of this paper is placed on one particular tool, all of the existing software products for DHM share the same characteristic of being complex to use and requiring expert knowledge and substantial amount of time invested in order to produce a representative simulation output [7] [8] [9].

[1] Corresponding Author, Email: juan-luis.jimenez.sanchez@scania.com.
[2] Corresponding Author, Email: adam.palmquist@his.se.

1.2. Gamification

The concept of gamification is the application of game-design elements and game principles in non-game contexts [10] [11]. Through applying these elements, gamification aims to improve the user engagement, productivity, learning, and more.

Research on the topic of gamification shows that a majority of studies have found it has a positive impact on individuals [12], such as increased engagement from users, quicker on-boarding to a system as well as increases in learning outcome.

Gamification strategies commonly use a reward system for players that accomplish their tasks; this type of reward may include points, achievement badges, levels, or virtual currency. The accomplishment of these tasks can also be made visible to other players, in order to promote engagement and competition.

Aside of the reward system, another approach to gamification would be to make existing tasks feel more like games by using techniques such as onboarding tutorials, scaling difficulty, or adding narrative [13].

1.3. Purpose of this study

The aim of this paper is to study the feasibility of using gamification in order to address two of the main shortcomings of DHM software, namely the complexity to learn and substantial time requirement to become an expert in the tools, and the lack of user engagement when utilizing them. To achieve this, a demonstrator of the gamification service Gamify the World Engine (GWEN) [14] in connection with IPS-IMMA has been developed as a starting point for future testing of the gamified DHM concept.

The study has focused on the gamification approach to tackle these issues, but other alternatives like conventional user interface design could already solve some of the challenges of DHM software today. These alternatives, as well as other issues of DHM systems such as the required understanding of ergonomics or interpreting the information the program gives the user, are out of the scope of this project.

2. Method

In order to implement the gamification concept within IPS-IMMA, the GWEN platform provided by the company InsertCoin AB [15] has been utilized. GWEN provides a series of configurable gamification modules that can be bundled together in order to serve as a relevant solution for the specific context.

2.1. Technical implementation

On a technical level, the connection of the GWEN platform and the IPS-IMMA tool has been made through an external widget, due to the time limitations to make a fully integrated interface inside the software. The frontend widget is implemented through Javascript in an HTML web environment. Then, by sending an authentication token to GWEN with the same user credentials as the IPS-IMMA login, the widget will establish connection between the software and the GWEN backend. After that connection is made, every time the user interacts with an item inside the IPS environment (e.g. pressing a button, selecting an object in the scene), a call will be sent to the gamification platform

indicating what action the user has performed. Based on the type of action, a response will be sent to the widget to update as necessary, e.g. complete a mission, advance a level, complete an achievement, etc. A simple diagram displaying the connection between the different elements can be seen in Figure 1.

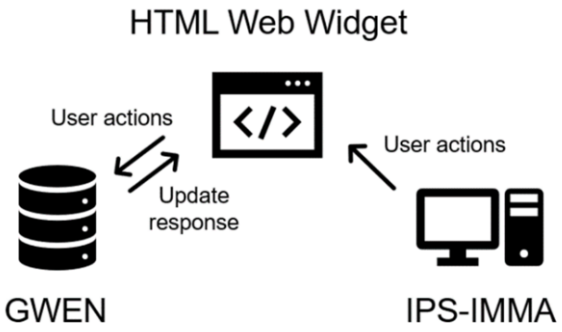

Figure 1. IT architecture diagram of the technical implementation.

2.2. Game design elements

Game design elements are the basic building blocks of gamification applications [16]. For this case, the following elements have been utilized:

- Avatars: a simple 2D avatar can be chosen by the player from a predetermined set in order to represent themselves, and set each player apart from each other.
- Levels & experience points: levels are used to numerically represent the player's progress, and they are basic elements of a multitude of games and gamified applications. In order to advance through levels, the user will have to earn experience points through completion of achievements and missions.
- Badges: achievement badges can be used by the player to confirm their merits and visibly show their accomplishments. They function as goals and can influence the player's behavior, leading them through selected routes and challenges in order to earn the associated badges [17].
- Currency: another type of points, virtual currency can serve as a continuous and immediate feedback as well as a reward that can be spent to purchase other classes of rewards.

3. Results

An initial demonstrator of a gamified IPS-IMMA application has been developed. This first implementation has been made through an external html-based widget, which can be seen in Figure 2 and Figure 3 (right). The widget displays the gamified interface, granting access for the user to the following GWEN modules:

- Level module (Figure 3, left): in this module, the user will see displayed their avatar and level, as well as the experience points required to progress to the next level, and the reward they will receive once they reach it. Here the user is also able to change their avatar, as well as see their Event Log to keep track of their activity within IPS and the communication to GWEN. Moreover, a "Cooldowns" tab is present and can be potentially used to show the user the amount of time they need to wait before repeating a certain task or event.

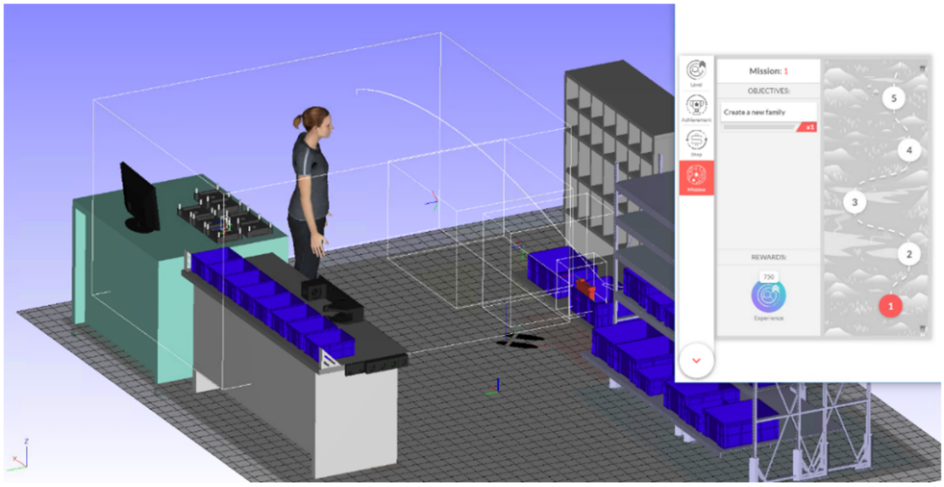

Figure 2. The IPS software in combination with the external GWEN widget.

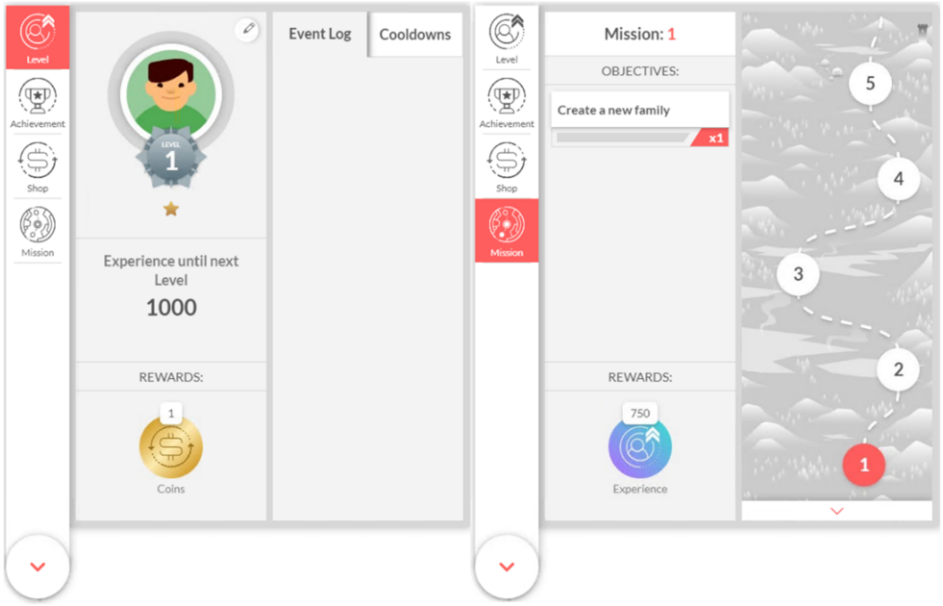

Figure 3. Widget modules for Level (left) and Mission Path (right).

- Mission module (Figure 3, right): this module will display the currently active mission path for the user. It is the primary tool used for onboarding and smoothing the learning curve for the user. It consists on a series of missions, or tasks, that will have to be gradually completed by the user in a serial manner in order to earn different rewards and proceed through the path. It is meant to guide the user through a series of introductory tasks, and gradually increase the difficulty to show most of the functionalities that are available in the IPS-IMMA tool and that the user will need when running their simulations.
- Achievement module (Figure 4, left): this module is aimed towards increasing the user engagement and their skill retention. Achievements are a series of background objectives that are always possible to attain, and can require the user to complete a task repeatedly (for example, run a progressively higher number of simulations, with increasingly better rewards for each achievement in the chain), or to complete a particularly difficult task (e.g. run a simulation with a certain number of elements or for a minimum time duration).

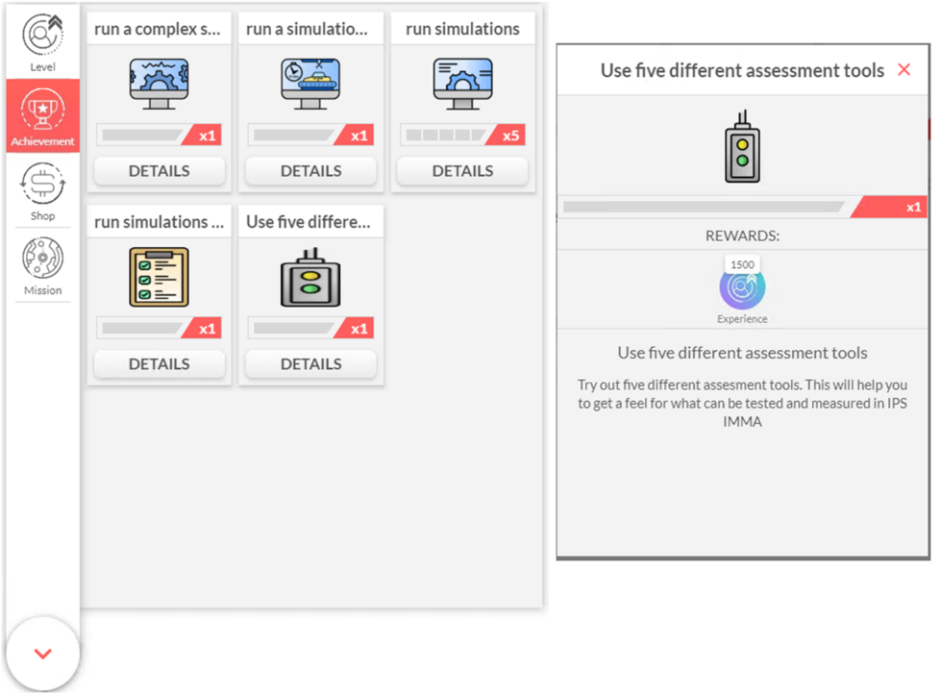

Figure 4. Widget module for Achievements (left) and example achievement (right).

- Shop module (Figure 5, left): finally, the shop module offers the user the possibility of purchasing different badges of recognition as a confirmation of their skill with the IPS tool, by employing the currency earned as they gain levels.

The gamified interface is connected to the IPS environment, so whenever the user performs a certain action, IPS sends an event call to GWEN, triggering a response in the widget. For example, when the user completes the first mission of the path, which is

creating a Manikin family inside the scene, the mission module will move on to the next mission (e.g. placing a geometry in the scene), and it will grant the user the rewards for having completed the mission (i.e. experience points). This, by itself, may trigger a level-up event, which will prompt the Level module to advance to the next level and give the appropriate rewards.

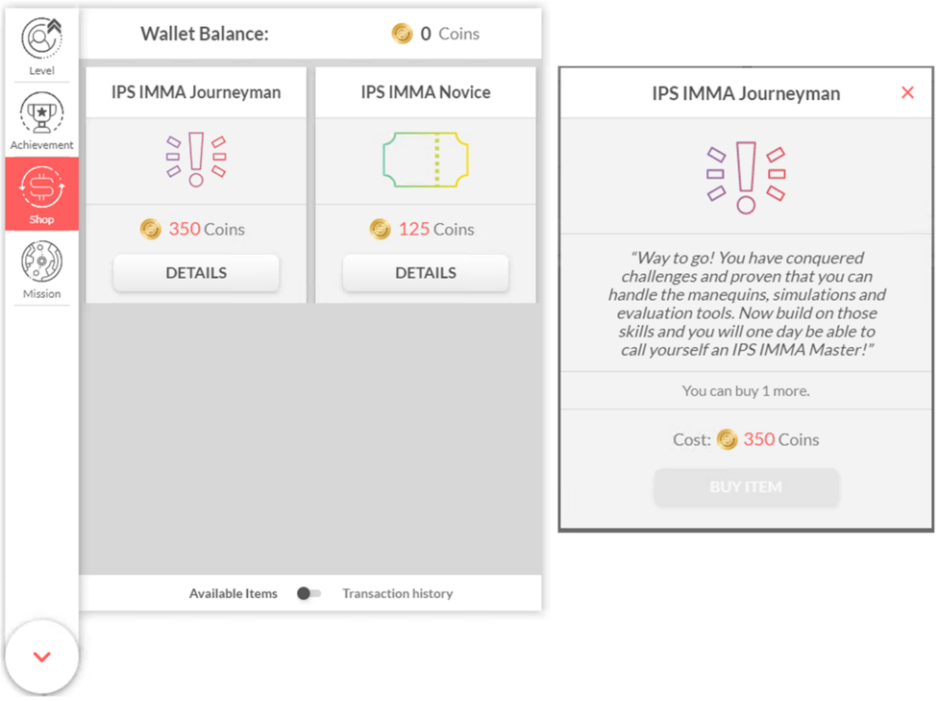

Figure 5. Widget module for the Shop (left) and example shop item (right).

4. Discussion

The initial demonstrator of a gamified DHM tool has been carried out successfully and has the potential of tackling the issues of user engagement and training. It provides the users of IPS-IMMA the possibility of following a mission system to familiarize with all of the different features of the program and their different degrees of complexity, making their onboarding easier and providing an optimal path to become expert users in a short time. Furthermore, it also provides a reward system for continuous use of the tool, giving an incentive to users to keep using the tool and completing all of the different achievements and earn rewards, increasing their engagement and skill retention.

Future work of this study includes carrying out an evaluation by users of the IPS-IMMA tool from different backgrounds, to evaluate the effectiveness of the gamified application. Moreover, the integration of the widget within the IPS environment will be necessary in order to provide the users with a smoother experience. Other future improvement will be offering users the possibility of finding other users that have completed certain achievements or earned certain badges, so that they know who has a certain skill with the tool and can seek assistance more easily. In the end, involvement

from the end-users in the development of this solution will prove crucial to the gamification of DHM applications.

Acknowledgement

This work has been made possible with support the Knowledge Foundation and the associated INFINIT research environment at the University of Skövde, in the Synergy Virtual Ergonomics (SVE) project, and by the participating organizations. This support is gratefully acknowledged.

References

[1] Seidl A. RAMSIS, a new cad tool for ergonomic analysis of vehicles developed for the German automotive industry. Automotive Concurrent/Simultaneous Engineering, 1997, 1233.
[2] Badler NI, Phillips CB, Webber BL. Simulating Humans: Computer Graphics Animation and Control. Oxford University Press, New York, 1993.
[3] Fortin C, Gilbert R, Beuter A, Laurent F, Schiettekatte J, Carrier R, et al. Safework: a microcomputer-aided workstation design and analysis. New advances and future developments. In: Karwowski W, Genaidy AM, Asfour S. Computer Aided Ergonomics. Taylor & Francis, London, 1990, 157-180.
[4] Hanson L, Högberg D, Carlson JS, Delfs N, Brolin E, Mårdberg P, et al. Industrial Path Solutions - Intelligently Moving Manikins. In: Scataglini S, Gunther P, editors. DHM and Posturography. Elsevier, London, 2019, 115-124.
[5] IPS AB. Industrial Path Solutions - IPS IMMA. [Online]. [cited 2020 May 15. Available from: http://industrialpathsolutions.se/ips-imma.
[6] FCC. Fraunhofer-Chalmers Centre - Industrial Path Solutions. [Online]. [cited 2020 May 15. Available from: http://www.fcc.chalmers.se/software/ips/.
[7] Busch F, Wischniewski S, Deuse J. Application of a character animation SDK to design ergonomic human-robot-collaboration. In: Proceedings of the 2nd International Digital Human Modeling Symposium (DHM2013), 2013, Ann Arbor, 1-7.
[8] Fritzsche L. Ergonomics risk assessment with digital human models in car assembly: simulation versus real life. In: Human Factors and Ergonomics in Manufacturing & Service Industries. 2010, 287-299.
[9] Scataglini S, Paul G, editors. DHM and Posturography. 1st ed. Elsevier, London, 2019.
[10] Huotari K, Hamari J. Defining Gamification - A Service Marketing Perspective. In: Proceedings of the 16th International Academic MindTrek Conference, 2012, Tampere.
[11] Robson K, Plangger K, Kietzmann JH, McCarthy I, Pitt L. Is it all a game? Understanding the principles of gamification. Business Horizons. 2015 July-August; 58(4).
[12] Hamari J, Koivisto J, Sarsa H. Does Gamification Work? - A Literature Review of Empirical Studies on Gamification. In: Proceedings of the 47th Hawaii International Conference on System Sciences, 2014, Hawaii.
[13] Reeves B, Read LJ. Total Engagement: Using Games and Virtual Worlds to Change the Way People Work and Businesses Compete: Harvard Business Press, 2009.
[14] AB I. GWEN - Gamify the World Engine. [Online]. [cited 2020 May 16. Available from: https://insertcoin.se/our-solutions/gwen/.
[15] AB I. InsertCoin. [Online]. [cited 2020 May 16. Available from: https://insertcoin.se/.
[16] Deterding S, Dixon D, Khaled R, Nacke L. From Game Design Elements to Gamefulness: Defining "Gamification". In: Proceedings of the 15th International Academic MindTrek Conference, 2011, Tampere.
[17] Wang HSCT. Game Reward Systems: Gaming experiences and social meanings. In: Proceedings of the 2011 DiGRA International Conference: Think Design Play, 2011, Utrecht.

DHM2020
L. Hanson et al. (Eds.)
© 2020 The authors and IOS Press.
This article is published online with Open Access by IOS Press and distributed under the terms of the Creative Commons Attribution Non-Commercial License 4.0 (CC BY-NC 4.0).
doi:10.3233/ATDE200040

Digital Human Modeling Technology in Virtual Reality - Studying Aspects of Users' Experiences

Julia ROSÉN [a,1], Jessica LINDBLOM [a], Maurice LAMB [a] and Erik BILLING [a]
[a] *Interaction Lab, University of Skövde, Sweden*

Abstract. Virtual Reality (VR) could be used to develop more representative Digital Human Modeling (DHM) simulations of work tasks for future Operators 4.0. Although VR allows users to experience the manikin as rather realistic in itself, there are still several aspects that need to be considered when shifting from tasks performed in the real world into a virtual one, adding cognitive and user experience (UX) aspects. Currently, there is limited research of UX in VR. The overall aim was to gain deeper insights into how users' experiences can ultimately help us to improve how VR can aid in DHM. A pilot study examined how users perceived and experienced actions performed by a humanoid hand (manikin) in VR. Users' perceived presence indicates how well they are immersed in the virtual environment, and Proactive eye gaze (PEG) was used to measure the realism of the virtual hand. The obtained findings indicate some potentially surprising outcomes and some tentative explanations for these are discussed. The lessons learned from this pilot will be used as input to a future larger study that continues to highlight how UX aspects can be useful in a DHM context.

Keywords. digital human modeling, virtual reality, UX, proactive eye gaze

1. Introduction

In this paper we address how digital human modeling (DHM) could benefit working environments for future industrial operators interacting with various kinds of enabling technologies in manufacturing. In order to achieve the goals for the industrial operators at the shop floor, DHM provides tools for analyzing physical ergonomics during the whole design and development cycle [1]. DHM tools enable interaction with manikins in the form of digital twins of human operators that provide support to DHM practitioners and users to view, foresee, investigate, plan, and evaluate work tasks and perform risk assessments while still being in the digital world [1].

The usage of Virtual Reality (VR) and digital twins allows both the DHM practitioners and the future human operators to consider and experience the envisioned work tasks and interaction before being physically manifested and situated. There are several benefits aligned with this way of working, e.g., reducing costs, enabling rapid design of work stations and tasks, and more usable DHM tools. However, this approach requires that the

[1] julia.rosen@his.se

digital twin is reliable and credible in itself. Although VR allows users to experience the digital twin in a way that is in many ways realistic, there are still several user aspects that ought to be considered when we move from tasks performed in the real physical world into a simulated one. Presence, for instance, aims to address how well a user is immersed in the virtual environment; higher presence means the user feels that the environment is responding authentically (i.e. similar to the non-virtual world) to the users senses and actions [2, 3]. Subsequently, higher presence is linked to higher realism and thus gaining higher validity and credibility in evaluations [3]. A study by Faas et al. [2] found that designers who scored higher on presence and immersion oftentimes scored higher on design performances as well. The authors conclude that presence can be used as an indicator of performance and learning in design-and-build activities. Thus, presence is a method to evaluate how well users adapt to a virtual world. Presence has also been shown to increase when the user's move their body in the virtual world (e.g.[4, 5, 6, 7]).

Eye-tracking systems in VR have become more precise which has made it possible to study various aspects of eye gaze behavior in a virtual environment [8]. In this work, we are investigating proactive eye gaze (PEG) as a way to quantify presence and immersion, thus studying how realistic a VR environment could be. The phenomenon of PEG illustrates a certain kind of eye-hand coordination pattern during object manipulation and action observation, where the eye-gaze behaviors precede hand behaviors [9]. We also argue that DHM tools could be further developed by adding such cognitive aspects, because traditionally the field of ergonomics predominantly addresses the assessment of anthropometry and physical strains on the body in DHM [10, 11, 1]. We use Virtual Reality (VR) to support the development of more representative DHM simulations of work tasks and actions. Our proposed use of PEG in DHM is thus two-fold – measuring the level of realism a specific VR experience provides and offer a potential tool for measuring and/or predicting behaviors of future industrial operators. Our focus in this paper will be the former.

Our primary aim is to perform an initial investigation into how users perceive and experience actions being performed by a humanoid hand (manikin) in VR. Regarding users' perceptions, we want to investigate whether and to what extent users exhibit PEG when observing a simulated agent's hand movements. Regarding users' experiences, we want to understand how the overall user experience (UX) [12] is affected when observing the agent's hand movements in the simulated environment, because limited research of UX in VR exists [13, 14]. Deeper insights into user perception an experience in VR can ultimately help us to gain a deeper understanding of how VR can aid in DHM.

We report findings from a small pilot study that was performed in preparation for an upcoming larger experiment. These findings are tentative and used as input to frame the broader discussion in this paper. While the findings from present pilot should not be interpreted as conclusive results, they represent important steps toward a larger study of the use of VR in DHM tools. We employ an UX approach to enhance the ability of DHM tools to generate realistic and credible simulations and evaluations of bio-mechanical and cognitive ergonomics, including the use of digital twins; thus, supporting the envisioned digital work space for Operator 4.0 [15].

2. Background

Industrie 4.0 is characterized by the recent and rapid advances in digitalization and intelligent autonomous technologies, e.g. internet of things, augmented reality, VR, and collaborative robots that are entering the manufacturing domain [16, 17]. For the manufacturing industry, the intended benefits of this revolution is expected to result in shorter development periods, individualization on demand for the customers, flexibility, decentralization and resource efficiency [16]. One consequence of this revolution is a shift in working environments throughout all aspects of the manufacturing industry towards increasingly advanced digital work spaces.

A central issue of Industrie 4.0's digital work space is the development with respect to Operator 4.0 [15]. Operator 4.0 refers to smart and skilled operators of the future, who are assisted by various kinds of intelligent automated systems that provide sustainable physical and cognitive support, allowing operators to achieve and develop a high degree of cognitive, collaborative, and innovative knowledge and skills - without compromising safety, competitiveness and productivity [15]. Two examples of proposed of Operator 4.0 types that involve augmentations of human capabilities are the Virtual Operator and the Healthy Operator. The Virtual Operator will use various kinds of VR technologies to digitally replicate a production line, work station design, assembly tasks or a manufacturing environment, enabling the operator to interact with various tools, artifacts and robots found in a factory with real-time feedback and reduced risk. Via advanced software, various tools and manual assembly tasks could be transformed into a digital twin world, in which interactive virtual simulations of assembly sequences could be used for designing and evaluating work tasks as well as for training these smart operators in complex assembly tasks. In other words, VR enacts the envisioned 'virtual factory' as an integrated simulation model [15]. The Healthy Operator will be equipped with several wearable devices and trackers that will measure aspects like exercise activity, stress, heart rate and other biometrics as well as location. The Healthy Operator will be able monitor both the physical workload and cognitive workload on specific tasks or during the work-shift, receiving alerts and warnings regarding proper workloads.

However, the future digital work space of Operator 4.0 poses several interrelated challenges, of which two are addressed below [18]. First, the need to enhance the quality of the interaction between humans and autonomous systems in general, and enabling technologies in particular. Second, changes of work roles and work practices due to more advanced forms of human-technology interaction at the shop floor will make work more demanding and flexible, and an interest in human-centered aspects has the potential to promote well-being and professional development in order to be a desired workplace.

However, the envisioned digital work space of Operator 4.0 will not materialize automatically [19, 18]. Of particular note for this paper, it requires careful design and evaluation of future enabling technologies like human-robot collaboration (HRC) systems where the interaction quality between operators and collaborative robots should be experienced positively and well suited to their purposes, being smooth, safe, trustworthy and satisfying to interact with [20, 18]. Taking a human-centered design approach [21] for the envisioned digital workplaces has an important influence to the job satisfaction, safety, and operator well being, which previous research on these topics rarely considered [19]. The fields of human factors/ergonomics, human-computer interaction (HCI), and UX have a great deal in common, although some differences exist. These approaches origi-

nate from the human-centered design perspective, having its foundation in the Standard Ergonomics of human-system interaction [21], which has become invaluable to evaluate the quality of human-system interaction in general.

UX in particular is more general than ergonomics because it considers and characterizes *"how users encompass all aspects of the interaction with a service/system or products"* [21, 12, 22]. Usability is a component of UX, but UX also encompasses additional components that go beyond the more instrumental usage of usability in ergonomics and HCI. Usability is defined as: *"the **effectiveness, efficiency** and **satisfaction** with which specified users achieve specified goals in particular environments*, in which **'effectiveness'** is defined as: *"the accuracy and completeness with which specified users can achieve specified goals in particular environments"*, **'efficiency'** is defined as *"the resources expended in relation to the accuracy and completeness of goals achieved*", and **'satisfaction'** as: *"the comfort and acceptability of the work system to its users and other people affected by its use"* [21].

In the above ISO standard [21], there are two additional notes to the above characterization of UX that go as follows: Entry 1: *"Users' perceptions and responses include the users' emotions, beliefs, preferences, perceptions, comfort, behaviours, and accomplishments that occur before, during and after use"*. Entry 2: *"User experience is a consequence of brand image, presentation, functionality, system performance, interactive behavior, and assistive capabilities of a system, product or service. It also results from the user's internal and physical states resulting from prior experiences, attitudes, skills, abilities and personality; and from the context of use"*. This means that it is not possible to guarantee a certain user experience, because it is the outcome of the subjective inner state of a human user. Although, by designing a high quality interaction with the intended users and the usage context in mind it is possible to positively impact the users' experiences.

Hence, UX aspects can be aligned with a broader meaning of topics, changing from pragmatic and hedonic qualities [12], to emotional aspects of the experience when interacting with robots or other enabling technologies [23]. Pragmatic quality refers to fulfilling the so-called "do-goals" of the user, which means that the interactive system makes it possible for the user to reach the task-related goals in an effective, efficient, and satisfying way. Hence, pragmatic aspects relate to the usability component of UX [21]. Hedonic quality refers to the so-called "be-goals" of the user, which relates to psychological, subjective and emotional needs that can have a great impact on how enabling technologies are experienced [22]. A central activity in UX is to extract, identify, and characterize UX goals [19, 12]. UX goals are high-level objectives, which should be driven by the representative use of an envisioned interactive system. The UX goals should identify what is important to the users, stated in terms of anticipated user experience of an interaction design. The UX goals are expressed as desired effects, for example the interactive artifact's ease-of-use, perceived safety, quality-of-use, acceptance, immersion, trust, or emotional arousal [12]. It should be emphasized that the major focus of study in UX is not the user's behavior as a response of a certain condition, as commonly done in experimental psychology. Instead, the focus is on several aspects of the users' experiences of interacting with the robot or any kind of enabling technologies in a particular context to achieve a certain task/goal or fulfill a need, which is a significant difference.

The kinds of enabling technologies required for Industrie 4.0 and Operator 4.0 are not yet fully realized, and there is a need to include an understanding of Operator 4.0

early in the analysis and design phases. One way to achieve this is through visualization software early in a design process in order to optimize the design of a product. With regards to DHM software, it can be argued that along with a focus on realistic digital simulations of the physical human bodies, user context and cognition should also be considered to be important aspects of DHM [10, 11]. In the specific case of HRC development, DHM could be used to support and assess both physical and cognitive aspects of the future digital workplaces which include HRC systems. The proposed UX perspective may improve insights provided by DHM software regarding work performance, ergonomics, cognitive and physical fatigue, trust and expectations, and potential errors [24], which are aligned with several UX perspectives. This could substantially improve the effectiveness of DHM tools which focus almost exclusively on bio-mechanical constraints. Currently, most DHM tools simulate tasks and actions for a specified work situation given a set of physical and bio-mechanical constraints, without consideration of the emergence of cognitive constraints such as cognitive goals and intentions [10]. For example, insights from embodied cognitive science have revealed that cognition is the emergent result of complex systems of agent-environment interaction where perception, bio-mechanics, environment, and action mutually constrain one another [25].

However, prior work has shown that using VR technology itself may result in negative user experience, and ultimately may produce results that do not match real-world behaviors. As pointed out by Papadimitriou [13], UX in VR both "includes the aspects of the experience and is influenced by them simultaneously." The author argues that the increased popularity of VR has resulted in efforts to design and evaluate which aspects and characteristics influence a positive user experience in VR environments, although limited research has been conducted so far.

While rapid development of VR systems as a part of Industrie 4.0 has occurred in recent years, it is important to be aware of the ways in which VR experiences do not completely match reality, just as it is important to understand how digital or physical models of tasks, workstations or products may not match actual implementations. Hence, the user's performance and experience must be interpreted and understood in relation to the specific VR conditions and digital context. Commonly identified potential problems, now and then, with VR include head-mounted display weight or fit, limited motion tracking and/or control, system latency, lack of visual realism, limited haptic and/or non-visual feedback, nausea, and lack of presence [24, 26, 13, 27]. The latter concept – presence is commonly defined as the feeling of "being there" in a virtual environment [3]. Presence is closely linked to the concept of immersion and as there is no consensus on the definitions between these concepts, we will take the stance that presence is achieved by way of immersion [3]. The level of presence in a VR environment has been shown to correlate with how much interaction and movement is being expressed by the user[4, 5].

Presence by immersive VR systems has been studied since the conception of VR (for a fuller review on presence in VR see [3, 28, 3]). As early as 1998, Slater et al. [4] saw how participants initially viewed the VR environment as a screen with low presence, but once the users realized that they could move around in VR, they experienced a higher presence as if they were "stepping through" the screen. In that study participants were asked to bend down and to rotate their heads in order to make them aware of their body in relation to the environment. The study concluded that increased body movements increase the presence in VR. Presence has continued to be of interest in the field of VR. More recently, Lee et al. [5] showed that presence was assessed higher when partici-

pants could interact more within the VR environment by being more embodied, i.e. using their own legs to walk around in the environment in contrast to using a gamepad control method or hand-based walking control interface for walking.

While the specifics of embodied theories of cognition can at first seem overwhelming in a DHM context, there are specific hypotheses which should be relatively easy to apply. In this paper we specifically focus on the idea that cognition is for action and anticipation of action. PEG is a way to quantify how realistic a VR environment may be. PEG is observed both in nonsocial settings, where eye-gaze precedes one's own actions and in social settings where eye-gaze precedes the actions of a co-actor. Moreover, PEG is considered to be an important mechanism for producing the kind of smooth and intuitive human-robot interaction [29] that is the basis for successful HRC in Industrie 4.0. While PEG phenomena are relatively well established in tightly constrained research contexts, the extent to which PEG occurs in naturalistic and repetitive conditions similar to manufacturing and assembly contexts is not yet well explored. In order to better understand PEG in these contexts and provide relevant insights for DHM of these phenomena, we investigated PEG in a VR environment.

3. Method: Pilot study

VR can be useful in a DHM context to test worker environments virtually before building the physical instantiation. With this in mind, we present a pilot study investigating PEG in virtual environments in order to understand how well PEG behaviors in VR environments match the PEG behaviors in physical environments. We want to stress that the study presented here is a pilot and is only a indicative of our future larger experiment. In this within-subject pilot study, participants observed a virtual humanoid hand that performed several kinds of reaching and grasping tasks (Fig. 1). This movement is inspired by a pick and place action, where an actor is, as the name suggests, picking up and placing an object. In this case, the participants observed an object being picked up and placed rather than performing the action themselves.

Procedure After the participants (N=5) signed a consent form, they were instructed to step into the VR room where they would sit in front of a table and observe an object moving in front of them. They were asked to simply observe the scene until the experiment ended. After the instructions, the participants put on the HTC Vive Pro Eye. The session started by calibrating the participant's eye gaze, followed by starting the experiment. Before the experiment began, the participant was re-centered in the virtual environment to ensure that all participants had the same initial view point of the stimulus objects. In the experiment, a cylindrical object moved either by itself (self-propelled condition), or was moved by a virtual hand (humanoid hand condition), 20 times each with a counterbalanced starting order. Both conditions were driven by the same prerecorded biological motion profiles. The experiment took about 10 minutes in total.

Material The virtual environment was developed in Unity3D 2018 LTS and is illustrated from the participant's point of view in figure 1. The virtual environment was displayed on an HTC Vive Pro Eye with a display frequency of 90 Hz. Position and rotation of the headset were tracked at 90 Hz and eye-tracking was recorded at 120 Hz. Eye tracking data was provided via the HTC SRanipal v1.1.0.1 SDK. SRanipal provides processed eye values relative to the headset with a delay from eye record to provided data due to

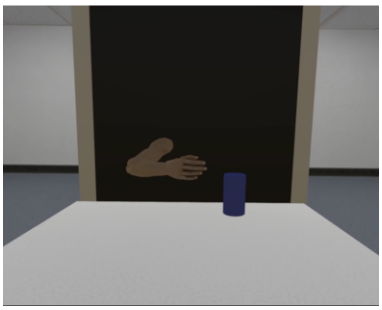

Figure 1. The field of view for the participants in VR with the humanoid hand condition. The humanoid hand reaches out from the black box and moves the object.

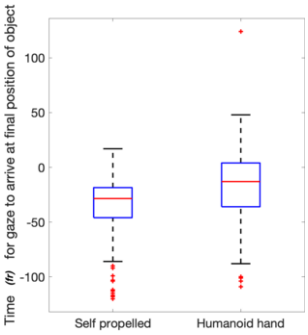

Figure 2. The box plot to the right illustrates the amount of time (fr) between the arrival of the gaze and the object at its final position.

processing of approximately 16.6 ms. As a result, given Unity's 90 Hz frame rate for the HTC Vive, eye tracking values have an expected latency of up to 33.2 ms. Focus objects were calculated in real-time based on the current position and orientation of the headset and an average gaze vector provided by the SRanipal SDK. The stimulus motions were driven by prerecorded data of a single individual engaged in an object pick and transport task, inspired by a pick and place action. The positions and orientations of both the individual's hand and the transport object were recorded at 90 Hz using two HTC Vive Trackers (2018). For playback, position and orientation were used for the transport object. However, due to technical challenges, only position was used to drive the stimulus hand. The stimulus arm was a part of the First Person Generic Arms Pack (BlocBros Studio) Unity asset package and arm kinematics were driven by the FinalIK (RootMotion) Unity asset package. The collected data included gaze location on a plane relative to the stimulus objects as well as comments gathered from the participants afterwards.

4. Findings

A within-subject analysis of repeated measure (ANOVA) was conducted to compare the two conditions for the time (in frames) between the arrival of the gaze and the object at its final position. The analysis indicated that the onset activation of PEG was significantly earlier in the self-propelled condition ($F(1,4) = 25.12$, $P < 0.01$) than in the humanoid hand condition. This is illustrated in figure 2: a strong negative value implies strong PEG and a positive value means that the first gaze onto the object came after the object was placed in its final position. Interestingly, these findings suggest the opposite of previous results on PEG from e.g., Flanagan and Johansson [9] and Falck-Ytter et al. [30]. However, we are aware that any interpretation of the findings is tentative, given the sample size and novelty of the particular VR implementation in this context.

5. Discussion

The analysis of the collected data from the pilot study suggests some potentially surprising findings; PEG was elicited later when a humanoid hand was present rather than when

no hand was present. We provide some tentative explanations for the initial findings. Although VR can enact a strong sense of presence, it involves numerous modifications, simplifications, and omissions of real world features and thus, should not be uncritically considered to be relevantly similar to real world stimuli. It is therefore possible that there is a difference between PEG in the real world and in VR. This relates to both the VR environment as a whole and the specific profile of the hand condition. For example, previous studies have suggested that a more natural hand interaction in VR, with complex hand grasp- and rotation options, resulted in a higher sense of presence. In contrast, a less natural hand interaction, with one default grasp option and one rotation option, resulted in participants scoring lower on presence in VR [7]. A similar phenomenon may be occurring here such that the virtual hand in VR was experienced differently than a movement is done by a real human hand. Perhaps the issue lies in how this hand is interpreted: not a real hand but one closely similar to it. This could result in a visual disturbance or discomfort (e.g. uncanny valley) when viewing this virtual hand.

Turning to the UX perspective, one participant reported that the head-mounted display was experienced as narrowing the field of vision, causing some degree of vertigo, and the feeling of wearing cyclops. There was also some difficulty to get the head-mounted display to fit comfortably as indicated by some of the participants. Experiences of vertigo and possible limited presence are related to being situated in a virtual environment by the users and head mounted display discomfort are related to experienced comfort and satisfaction of the VR equipment.

Although we cannot say with confidence that the VR setting is the reason for the current direction of these findings, we believe it is important to not discount the possibility that some aspects of the virtual presentation and the task of the participant had an impact on the current findings. However, it is not totally clear whether this impact is the outcome of how the users perceived and experienced the virtual humanoid's hand movements, not manipulated the object themselves, or the fact of being situated in a virtual world, or a combination of all. It is obvious that the virtual hand and its movements and the VR environment are not isomorphic to reality, i.e, they are not a one-to-one match, and therefore some relevant dimensions may be missing or inadequately represented and realized in our study (see Kolbeinsson et al. [31] for a discussion on fidelity, representativeness, and immersion in simulations). A UX evaluation of these aspects may provide more systematic insights into their impact on user behavior and experience.

VR has been increasingly popular in recent years, and has contributed to making development cycles shorter, safer, and more flexible. It has also been a popular tool for many industries to train their workers in a variety of workplace domains, e.g. safety, onboarding, and running scenarios [3]. It is important to understand the users' experience of VR and specifically how the VR equipment and being situated in the VR environment potentially can influence how users understand, enact and act in the artificial world. By employing a more systematic UX approach, a deeper understanding could be gained how new technology and new modes of interacting with technology, not only results of some after aspects of the users' visual and cognitive behaviors [32], but also how VR supports users to achieve their aims and goals.

In parallel to the present work, we have conducted a study of eye gaze behavior in a pick and place task performed in VR [33]. Participants were asked to move around in a VR environment and pick up objects from a table and place them in a bin. In contrast to the findings of the present work, Billing et al. [33] conclude that the eye gaze

behavior of participants executing the pick and place task in VR has many similarities to that of a pick and place action performed in real life. One important difference between these studies was that Billing et al. [33] investigated a task that participants executed themselves, while in the present work we investigated a setting where participants were observers. As discussed in the introduction, presence increases with greater interaction with a virtual environment [4, 5, 6]. As such, it is likely that the level of presence experienced by participants is higher when executing a task [33], compared to the observer condition used in the present work. This could be interpreted as an indication that the level of presence may directly influence the results of evaluations performed in VR, and to what extent these results are transferable to tasks performed in real life. We believe presence should therefore be addressed through UX evaluation in our future study and could aid other VR studies in order to understand both the user experience and how the user experience affects results.

For our future study, we intend to build on our pilot with a larger sample size and to systematically evaluate the UX perspective. The design will change in three ways. First, to avoid participants getting more information in the hand condition, the reaching for the object will be removed and only the transport of the object will be included. As a hand is not visible in the self-propelled condition, there is no reach and grasp action here compared to the hand condition. This inconsistency might also give enough time for the participants to observe incongruences, such as the lack of preshape of the hand and hand rotation. Second, the end position of the object will be marked on the table as this visual information could elicit faster PEG. This is commonly used in PEG studies and is therefore reasonable to add in order to compare our results to similar studies. Lastly, the conditions will be expanded with both one more hand profiles and one more movement profile. For the hand profiles, we will explore a third condition: a robot hand which has been previously shown to elicit PEG in a real world human-robot interaction [29]. Furthermore, besides the biological motion that was included in our pilot, we intend to add a mechanical motion stimuli. Research on point light displays has indicated that biological motion, as opposed to visual cues, elicit PEG [34].

Regarding UX evaluation in VR, it has been argued that traditionally established evaluation approaches may not fit or are irrelevant, because of the unique ways that users can interact with the content and do tasks via VR technologies. Papadimitriou [13] points out that the increased popularity of VR has resulted in efforts to design and evaluate which aspects and characteristics influence a positive user experience in VR environments, although limited research has been conducted so far. Indeed, Stanney et al. [35] have developed a taxonomy of criteria and heuristics called the Multi-criteria Assessment of Usability for Virtual Environments (MAUVE), with the aim to systematically focus on usability and UX aspects when designing and evaluating VR environments. The MAUVE taxonomy includes the following criteria: 1) wayfinding, 2) navigation, 3) object selection and manipulation, 4) visual output, 5) auditory output, 6) haptic output, 7) simulator-sickness, 8) engagement, 9) presence, and 10) immersion. A tentative way of systematically evaluating users' perceptions, expectations and experiences of the hand simulations in VR may be to use a modified version of the MAUVE taxonomy, focusing on the comfort, presence, and representativeness aspects of the experience, where both quantitative and qualitative data will be collected. Furthermore, we also want to evaluate the dimensions of the users' perceptions and experiences of being situated in the VR environment as well as their experiences of virtual hands with different profiles and grasp-

ing movements. Another significant modification to the above work of UX evaluation in VR is that we will include pragmatic and hedonic UX goals for these aspects and dimensions, because this fundamental aspect of conducting proper UX evaluation is lacking in the works by Papadimitriou [13] and Stanney et al. [35].

Furthermore, Stephanidis et al. [14] have recently identified seven grand challenges for HCI, where some main research issues are addressed that consider living and interacting in technology augmented environments. In particular, they highlight the need to develop proper UX evaluation in VR environments towards the assessment of VR attributes beyond subjective assessments only, the need to design VR environments that achieve realistic user experience, and finally to support social interaction in the VR environment. We hope to contribute to some of these identified issues in our upcoming work of using the digital twin approach when continuing our work on studying UX aspects of digital human modeling technology.

6. Conclusion

The initial intent with the work presented in this paper was to present the obtained results from the larger study, including the experiment and the proposed UX evaluation, but due to the unforeseen covid-19 situation across the globe, it became impossible to perform. Our pilot study can therefore be seen as lessons learned.

To conclude, as we move towards Industrie 4.0, research in DHM is advancing rapidly in order to accommodate future workers in the digital work space. Not only is it necessary to consider changes in physical environments and actions, but it is also important to consider how these changes are interconnected with some aspects of human cognition. In this context, the use of VR in DHM tools enables ergonomics and other specialists involved in the design of future workstations for Operator 4.0, to simulate and evaluate the worker environment of the digital work space of the factories of the future virtually before building the physical instantiations. This way of working may be more cost efficient and faster than the traditional way of working as well as increasing the well-being of the operators. We therefore suggest that a more diverse use of methods and taking a UX approach in DHM will benefit the field as a whole, and the future Operators 4.0 in the envisioned digital work space will benefit even more.

Acknowledgment

Special thanks to Erik Lagerstedt for his valuable input. This work has been made possible with support the Knowledge Foundation dnr 20180167 and the associated INFINIT research environment at the University of Skövde, in the Synergy Virtual Ergonomics (SVE) project, and by the participating organizations.

References

[1] Raschke U, Cort C. Siemens Jack. In Scataglini, Paul (Eds.). DHM and Posturography. Academic Press; 2019.

[2] Faas D, Bao Q, Frey D, Yang M. The influence of immersion and presence in early stage engineering designing and building. Artificial Intelligence for Engineering Design, Analysis and Manufacturing. 2014;28(2):139–151.
[3] Skarbez R, Brooks F Jr, Whitton M. A survey of presence and related concepts. ACM Computing Surveys (CSUR). 2017;50(6):1–39.
[4] Slater M, McCarthy J, Maringelli F. The influence of body movement on subjective presence in virtual environments. Human Factors. 1998;40(3):469–477.
[5] Lee J, Kim M, Kim J. A study on immersion and VR sickness in walking interaction for immersive virtual reality applications. Symmetry. 2017;9(5):78.
[6] Hameed A, Perkis A. Affects of Perceived-Actions within Virtual Environments on User Behavior on the Outside. In: 2020 Twelfth International Conference on Quality of Multimedia Experience (QoMEX); 2020. p. 1–6.
[7] Rosén J. The importance of natural hand interaction in virtual reality [master thesis]. Lund University; 2017.
[8] Clay V, König P, König S. Eye tracking in virtual reality. Journal of Eye Movement Research. 2019 4;12(1).
[9] Flanagan J, Johansson R. Action plans used in action observation. Nature. 2003;424(6950):769–771.
[10] Billing E, Hanson L, Lamb M, Högberg D. Digital Human Modelling in Action. In: SweCog 2019, the 15th SweCog conference, Umeå, Sweden, November 7-8, 2019. University of Skövde; 2019. p. 25–28.
[11] Thorvald P, Högberg D, Case K. Applying cognitive science to digital human modelling for user centred design. International Journal of Human Factors Modelling and Simulation. 2012;3(1):90–106.
[12] Hartson H, Pyla P. The UX Book: Process and guidelines for ensuring a quality user experience. Elsevier; 2012.
[13] Papadimitriou D. User experience evaluation in virtual reality [master thesis]. Tampere University; 2019.
[14] Stephanidis C, Salvendy G, Antona M, Chen JY, Dong J, Duffy VG, et al. Seven HCI grand challenges. International Journal of Human–Computer Interaction. 2019;35(14):1229–1269.
[15] Romero D, Bernus P, Noran O, Stahre J, Fast-Berglund Å. The operator 4.0: human cyber-physical systems & adaptive automation towards human-automation symbiosis work systems. In: IFIP international conference on advances in production management systems. Springer; 2016. p. 677–686.
[16] Lasi H, Fettke P, Kemper H, Feld T, Hoffmann M. Industry 4.0. Business & information systems engineering. 2014;6(4):239–242.
[17] Kagermann H, Helbig J, Hellinger A, Wahlster W. Recommendations for implementing the strategic initiative INDUSTRIE 4.0: Securing the future of German manufacturing industry; final report of the Industrie 4.0 Working Group. Forschungsunion; 2013.
[18] Kaasinen E, Schmalfuß F, Özturk C, Aromaa S, Boubekeur M, Heilala J, et al. Empowering and engaging industrial workers with Operator 4.0 solutions. Computers & Industrial Engineering. 2020;139:105678.
[19] Kaasinen E, Roto V, Hakulinen J, Heimonen T, Jokinen J, Karvonen H, et al. Defining user experience goals to guide the design of industrial systems. Behaviour & Information Technology. 2015;34(10):976–991.

[20] Alenljung B, Lindblom J, Andreasson R, Ziemke T. User experience in social human-robot interaction. In: Rapid Automation: Concepts, Methodologies, Tools, and Applications. IGI Global; 2019. p. 1468–1490.

[21] ISO 9241-210: 2019. Ergonomics of human system interaction-Part 210: Human-centred design for interactive systems (formerly known as 13407). Geneva, CH: International Standardization Organization (ISO). Switzerland; 2019.

[22] Hassenzahl M. The Thing and I (Summer of'17 Remix). In: Funology 2. Springer; 2018. p. 17–31.

[23] Lindblom J, Alenljung B, Billing E. Evaluating the User Experience of Human–Robot Interaction. In: Jost C. et al. (eds) Human-Robot Interaction. Springer Series on Bio- and Neurosystems. vol. 12. Springer, Cham; 2020.

[24] Leskovskỳ R, Kučera E, Haffner O, Matišák J, Rosinová D, Stark E. A Contribution to Workplace Ergonomics Evaluation Using Multimedia Tools and Virtual Reality. In: 2019 Federated Conference on Computer Science and Information Systems (FedCSIS). IEEE; 2019. p. 317–326.

[25] Gazzaniga M, Ivry R, Mangun G. Cognitive Neuroscience: The Biology of the Mind. 4th ed. W. W. Norton & Company; 2014.

[26] Nichols S. Physical ergonomics of virtual environment use. Applied Ergonomics. 1999;30(1):79–90.

[27] Wilson J. Virtual environments and ergonomics: needs and opportunities. Ergonomics. 1997;40(10):1057–1077.

[28] Mütterlein J. The three pillars of virtual reality? Investigating the roles of immersion, presence, and interactivity. In: Proceedings of the 51st Hawaii International Conference on System Sciences; 2018. p. 1407–1415.

[29] Sciutti A, Bisio A, Nori F, Metta G, Fadiga L, Sandini G. Anticipatory gaze in human-robot interactions;. Gaze in HRI from modeling to communication" workshop at the 7th ACM/IEEE international conference on human-robot interaction, Boston, Massachusetts, USA. 2012.

[30] Falck-Ytter T, Gredebäck G, von Hofsten C. Infants predict other people's action goals. Nature Neuroscience. 2006 jul;9(7):878–879.

[31] Kolbeinsson A, Thorvald P, Lindblom J. Coordinating the interruption of assembly workers in manufacturing. Applied ergonomics. 2017;58:361–371.

[32] Szpak A, Michalski SC, Saredakis D, Chen CS, Loetscher T. Beyond Feeling Sick: The Visual and Cognitive Aftereffects of Virtual Reality. IEEE Access. 2019;7:130883–130892.

[33] Billing E, Bampouni E, Lamb M. Automatic Selection of Viewpoint for Digital Human Modelling;. To appear in Advances in Transdisciplinary Engineering (ATDE). ISSN 2352-7528, IOS Press. 2020.

[34] Elsner C, Falck-Ytter T, Gredebäck G. Humans Anticipate the Goal of other People's Point-Light Actions. Frontiers in psychology. 2012;3:120.

[35] Stanney M K, Mollaghasemi M, Reeves L, Breaux R, Graeber A D. Usability engineering of virtual environments (VEs): identifying multiple criteria that drive effective VE system design. International Journal of Human-Computer Studies. 2003;58(4):447–481.

DHM2020
L. Hanson et al. (Eds.)
© 2020 The authors and IOS Press.
This article is published online with Open Access by IOS Press and distributed under the terms of the Creative Commons Attribution Non-Commercial License 4.0 (CC BY-NC 4.0).
doi:10.3233/ATDE200041

Integration of Simulation and Manufacturing Engineering Software - Allowing Work Place Optimization Based on Time and Ergonomic Parameters

Oskar LJUNG[a,1], Aitor IRIONDO PASCUAL[b], Dan HÖGBERG[b], Niclas DELFS[c], Tobias FORSBERG[c], Pierre JOHANSSON[d], Johanna DAHLVIK[e], Juan Luis JIMÉNEZ SÁNCHEZ[f] and Lars HANSON[b,f]
[a] *SOLME AB, 412 50 Gothenburg, Sweden*
[b] *University of Skövde, School of Engineering Science, 541 28 Skövde, Sweden*
[c] *Fraunhofer-Chalmers Centre, Geometry and Motion Planning, 412 58 Gothenburg, Sweden*
[d] *Volvo Group Trucks Operation, Dept. BE18210, 405 08 Gothenburg, Sweden*
[e] *Virtual Manufacturing Sweden AB, 412 50 Gothenburg, Sweden*
[f] *Scania CV AB, Global Industrial Development, 151 32 Södertälje, Sweden*

Abstract. There is a constant strive in industry to be competitive on the market, to manufacture with quality and productivity. At the same time, it is important to offer workers a sustainable work life. Research has shown a clear relationship between poor ergonomics and productivity losses and quality deficiencies, e.g. due to assembly errors, which also causes large costs for companies. In spite of the above-mentioned relationship, productivity, ergonomics and quality are commonly treated separately in factory, line and workstation planning. To improve the factory, line and workstation planning, make it more efficient, ergonomic and to improve quality this paper proposes a concept that enables line balancing that considers two parameters in parallel, assembly time and ergonomic load as well as add possibility for mathematical optimization. The concept has been developed in a participative and iterative process. Two software tools and a simulation platform, the digital human modelling tool IPS IMMA, the balancing tool AVIX and the optimization platform EPP, have been used to demonstrate the concept. An integrated solution is formed. The integrated demonstration tool shows promising results. The demonstrator provides the possibility to manually optimize ergonomics and time in parallel, a relatively unique functionality.

Keywords. Line Balancing, Digital Human Modelling, Process Planning, Multi Variable Optimization

1 Introduction

There is a constant strive in industry to be competitive on the market, to manufacture with quality and productivity. At the same time, it is important to offer workers a sustainable work life. Research has shown a clear relationship between poor ergonomics

[1] Corresponding Author, Email: oskar.ljung@solme.com.

and productivity losses and quality deficiencies, e.g. due to assembly errors, which also causes large costs for companies [1]. In spite of the above-mentioned relationship, productivity, ergonomics and quality are commonly treated separately in factory, line and workstation planning. In manufacturing, traditional line balancing is conducted with focus on achieving a certain volume capacity with low amount of waste, e.g. walking. With this approach, one parameter is primarily being optimized, time. As time is considered and visual in the optimization, productivity is in focus and prioritized. Ergonomics is considered, but not prioritized and not visual in the balancing activity. Ergonomics is commonly in focus at later stages, when constraints from the initial optimization round focusing on productivity limits the degrees of freedom for improvements and optimization of other parameters than time. Time and ergonomics being considered and optimized in sequence is not optimal.

Industry uses different kinds of software in the production development process to represent, analyze and simulate production, in order to predict productivity, behaviors, calculate times and plan production in advance [2]. Production/process engineers use software tools for factory and line balancing. There is a number of software available supporting manual assembly balancing in manufacturing suites such as Technomatix from Siemens and DELMIA 3DEXPERIENCE from Dassault Systèmes, and also specialized ones as AVIX from Solme and Casat from MVV Information Technology. In order to simulate workers and ergonomics digital human modeling (DHM) software is used [3]. There are numerous DHM software to perform human simulations and evaluate ergonomics, for example Siemens Jack [4], Santos [5], Ramsis [6] and IPS IMMA [7]. These human simulations are usually carried out by human factors engineers to validate workstations or specific tasks. As a result, also in the simulation software, time and ergonomic are separated and treated in sequence. This can easily lead to a slow process and result in suboptimal design solutions based mainly on manual optimization from a combined productivity and ergonomics perspective. To improve the factory, line and workstation planning, make it more efficient, ergonomic and to improve quality this paper proposes a concept that enables line balancing that considers two parameters in parallel, assembly time and ergonomic load as well as add possibility for mathematical optimization. The concept is illustrated with a pedal car assembly balancing task.

2 Method

2.1 Software and methods

Two software tools and a simulation platform: the digital human modelling tool IPS IMMA, the balancing tool AVIX and the optimization platform EPP, have been used to demonstrate the concept. AVIX is a software that supports analysis of manual assembly processes by combining video analysis with time and motion studies based on standard times such as MTM [8] and MTM-UAS [9]. The applications are within the fields of productivity, production development, production optimization and production efficiency which are all closely related to work measurement and time study.

IPS IMMA is a digital human modelling tool including a biomechanical model of a human, motion generator based on inverse and forward kinematics and comfort algorithms as well as CAD functionality to create active parts that the manikin are interacting with and also an environment that the manikin need to consider e.g. avoid

collision. The digital human modelling tool simulates manikins performing tasks and generating data used for measuring workload, e.g. joint angles. In this study REBA [10] is used for analyzing joint angles.

EPP is developed within the research presented here, and is essentially a platform for multi-variable optimization. In this concept, i.e. workplace optimization based on time and ergonomic parameters, EPP is used to optimize parameters such as assembly table height from time and ergonomic perspectives with IPS IMMA as a data provider. EPP can also be used as a service to be integrated with other data providers than IPS IMMA.

2.2 Use case and procedure

A pedal car assembly use case represents a typical assembly line of an automotive industry. This pedal car assembly line includes about 70 assembly value adding tasks, e.g. assemble part, and about 100 necessary but not value adding tasks, e.g. walk and pick part at logistic rack, and an undefined number of waste tasks. Pedal car assembly or other similar simplified productions are commonly used to teach new employees the philosophy of a company specific production system. The pedal car assembly exists both in a physical lab/teaching area and in a virtual model, both to test and evaluate different production concepts and educate employees in production.

The concept has been developed in a participative and iterative process. The end users and developers have worked side by side. The end users specified the needs and requirements. The developers created a demonstrator that users can evaluate and give feedback on. This demonstrator is one of the first iterations.

3 Results

An integrated solution is formed by AVIX, IPS IMMA and EPP and their interactions. IPS IMMA is used as the digital human simulation tool, AVIX as the manual balancing tool and process planning tool, and EPP as an optimization tool on workstation level, as opposed to AVIX that is more biased towards the optimization of the assembly line. The interaction between these software tools covers both the manual optimization by balancing the tasks and the automatic workplace design optimization (Figure 1). In the first iteration of the demonstrator a json-format and Lua scripting are used for communication between the different software tools.

The user starts by planning the processes in AVIX (Figure 2 - left). The task sequence is set and the time the operator needs to perform each task is estimated. Time estimation is done manually using any of the, in the AVIX application, available techniques for time estimation. MTM-UAS, MTM-SAM or the AVIX proprietary time estimation technique are examples of such techniques.

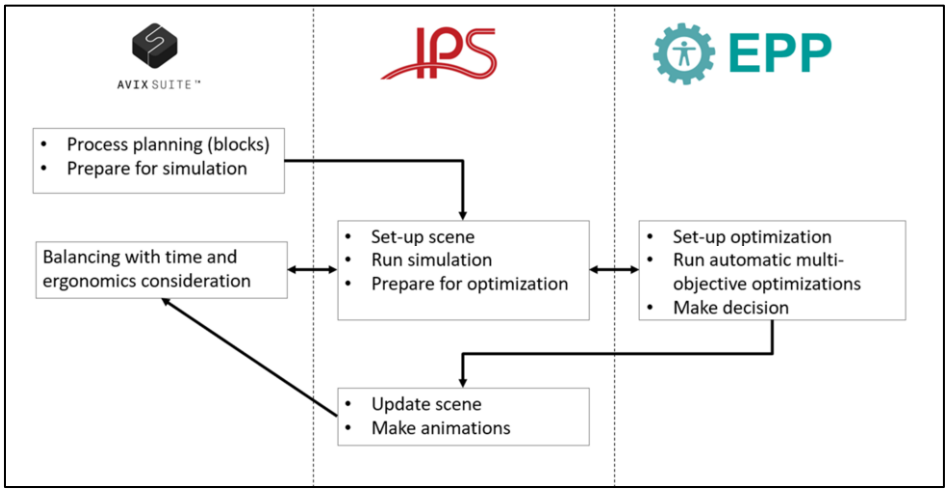

Figure 1. The workflow of the integrated solution.

As a second step a simulation model, with manikins representing the operator and objects representing the layout and parts are created in IPS IMMA (Figure 2 - right). Once the scene and manikins have been defined and set-up in the CAD environment of IPS IMMA the process from AVIX is imported into the task sequence editor. The sequence editor controls what tasks the manikins should be performing. Once these steps have been defined, the digital human modelling tool simulates the tasks and records the joint angles for each task.

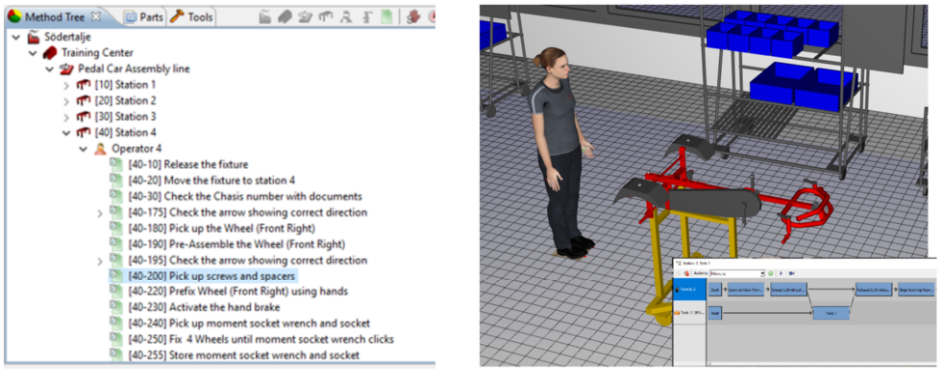

Figure 2. AVIX interface with task sequence (left). The same sequence, lower right, in the sequence editor of IPS IMMA.

As a third step, the information, process with task sequence and joint angles are exported back to AVIX. In the current version of the demonstrator is delimited to consider ergonomic risks due to static postures using the REBA method. AVIX has a graphical and interactive interface and offers the user the possibility to drag and drop, to manually place the tasks on the workstations on the assembly line to receive both balance in time (visualized with size of the task block) and ergonomics (visualized with colour to the right of the task block) (Figure 3).

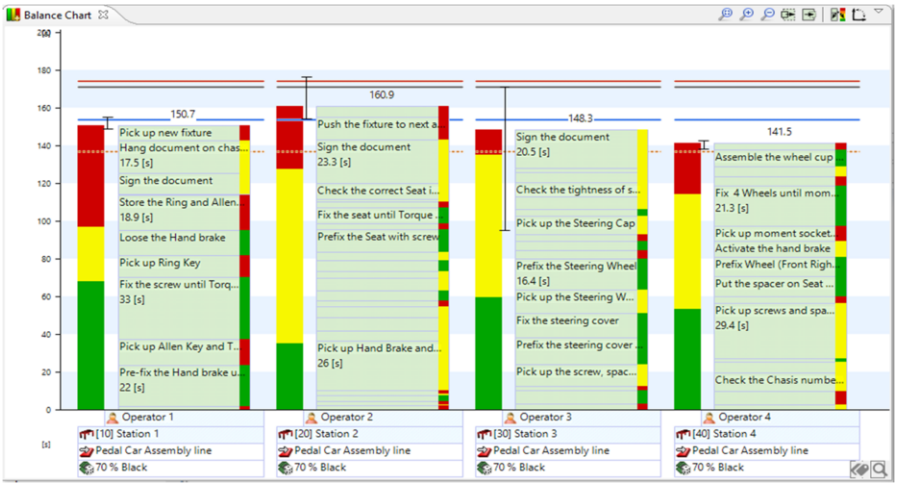

Figure 3. Balance chart showing ergonomics and total time of workstations.

The EPP platform is used to optimize the design of the workplace, first the variables to optimize are defined, in this case the assembly height of the pedal car. Afterwards, EPP can be launched to start the optimization process. The optimization will start by EPP automatically running the simulation in IPS IMMA. Next, EPP obtains the motion data from the manikin in IPS IMMA, and EPP performs ergonomic evaluations. As an alternative, EPP can use ergonomics evaluation data exported from IPS IMMA. The ergonomics evaluations data is sent to the chosen optimization algorithm, which will provide new values for the variables to optimize. Once the new values for the variables are set in the scene, the simulation is run and the new motion data from the manikin is sent to EPP.

4 Discussion

There are producing companies developing solutions considering time and ergonomics in parallel, in some cases even integrated. There are software companies and organizations developing solutions, e.g. EMA - Editor for Manual Work Activities [11] ErgoSAM [12] and MTM-HWD from the MTM Association, to integrate time and ergonomics domains. However, in general, there is a large potential in the industry to explore this approach further and to prioritize ergonomics more than done today. The integrated demonstration tool shows promising results. The demonstrator provides the possibility to manually optimize ergonomics, time and line balancing in parallel, a relatively unique functionality. Several challenges still exist, to improve both functionality and user friendliness. These challenges may be solved in the participative and iterative development process. The final demonstrator will most likely improve both the effectiveness and efficiency of the factory, line and/or workstation planning and follow the current trend towards multi objective optimization. The first final demonstrator includes manual multi objective optimization, which in future next step can be automatized.

There are many different digital human modelling tools, e.g. Siemens Jack, Santos, Ramsis and IPS IMMA and many different process planning simulations tools used for balancing, e.g. Tecnomatix from Siemens, DELMIA 3DEXPERIENCE from Dassault

Systèmes and AVIX from Solme. Furthermore, there are several methods for estimating time, e.g. MTM-1, MOST [13] and MTM-2, MTM-3 and MTM-UAS and several different methodologies for estimating ergonomic scores, e.g. OWAS [14], OCRA [15], REBA [10], RULA [16] and EAWS [17]. The demonstrator uses a selection of software and selection of time and ergonomic methods. Still, the concept will most likely work with any software and methods combination. The current demonstrator is based on standard methods and software that project partners develop and maintain. To have direct access to the core of the software is most likely a success factor. Equally important is the deep involvement of the end-user in research and development process.

Acknowledgment

This work has been made possible with support from ITEA3 and Vinnova in the project MOSIM and by the participating organizations. This support is gratefully acknowledged.

References

[1] Falck A-C, Örtengren R, Högberg D. The impact of poor assembly ergonomics on product quality: A cost–benefit analysis in car manufacturing. Hum Factors Ergon Manuf Serv Ind, 2010, 20(1), 24–41.
[2] Negahban, A, Smith, JS. Simulation for manufacturing system design and operation: Literature review and analysis. Journal of Manufacturing Systems, 2014, 33(2), 241–261.
[3] Scataglini S, Paul G. DHM and Posturography, Academic Press, 2019, ISBN 9780128167137.
[4] Badler NI, Phillips CB, Webber BL. Simulating humans: Computer graphics animation and control. Oxford University Press, New York, USA, 1993.
[5] Yang J, Marler T, Kim H, Farrell K, Mathai A, Beck S, Abdel-Malek K, Arora J, Nebel K. Santos™: A new generation of virtual humans, SAE Technical Paper No 2005-01-1407, Warrendale, USA, 2005.
[6] Seidl A. RAMSIS, a new CAD tool for ergonomic analysis of vehicles developed for the German automotive industry. Automotive concurrent/simultaneous engineering, SAE Special Publications, Vol. 1233, 51–57, 1997.
[7] Högberg D, Hanson L, Bohlin R, Carlson JS. Creating and shaping the DHM tool IMMA for ergonomic product and production design. Int J Digit Hum, 2016, 1(2), 132–152.
[8] Meynard HB, Stegemerten GJ, Schwab JL. Method-time-measurement. McGraw-Hill, New York, 1948.
[9] Matias AC. Work measurement: Principles and techniques. In: Salvendy G, editor. Handbook of Industrial Engineering: Technology and Operations Management. John Wiley & Sons, New York, 2001, 1409–1462.
[10] Hignett S, McAtamney L. Rapid entire body assessment (REBA). Appl Ergon, 2000, 31(2), 201–205.
[11] Fritzsche L, Jendrusch R, Leidholdt W, Bauer S, Jäckel T, Pirger A. Introducing ema (Editor for Manual Work Activities) – A New Tool for Enhancing Accuracy and Efficiency of Human Simulations in Digital Production Planning. In: Duffy VG, editor. Digital Human Modeling. ICDHM 2011. Lecture Notes in Computer Science, 2011, vol 6777. Springer, Berlin, Heidelberg.
[12] Laring J, Christmansson M, Kadefors R, Örtengren R. ErgoSAM: A preproduction risk identification tool. Human Factors and Ergonomics in Manufacturing, 2005, 15(3), 309–325.
[13] Zandin K. MOST Work Measurement Systems. Marcel Dekker, New York, 1990, ISBN 0824776046.
[14] Karhu O, Kansi P, Kuorinka I. Correcting working postures in industry: A practical method for analysis. Appl Ergon, 1977, 8(4), 199–201.
[15] Occhipinti E. OCRA: a concise index for the assessment of exposure to repetitive movements of the upper limbs. Ergonomics, 1998, 41(9), 1290–1311.
[16] McAtamney L, Nigel Corlett E. RULA: a survey method for the investigation of work-related upper limb disorders. Appl Ergon, 1993, 24(2), 91–99.
[17] Schaub K, Karlheinz G, Mühlstedt J, Illmann B, Bauer S, Fritzsche L, Wagner T, Bullinger-Hoffmann A. Ergonomic assessment of automotive assembly tasks with digital human modelling and the 'ergonomics assessment worksheet' (EAWS). Int. J. Human Factors Modelling and Simulation, 2012, 3(3/4).

DHM2020
L. Hanson et al. (Eds.)
© 2020 The authors and IOS Press.
This article is published online with Open Access by IOS Press and distributed under the terms of the Creative Commons Attribution Non-Commercial License 4.0 (CC BY-NC 4.0).
doi:10.3233/ATDE200042

Digital Human Models of Lower Limb Amputees for Socket Modelling and Simulations: An Overview of Current Technologies, Limitations and Future Possibilities

Vasja PLESEC [1] and Gregor HARIH
Laboratory for Intelligent CAD systems, Faculty of Mechanical Engineering, University of Maribor, Slovenia

Abstract. Discomfort when using lower limb prostheses is still a major problem, leading to limited use of the prostheses and reduced mobility of the patient. The production of the socket is still more or less handcrafted, and modern Computer Aided Engineering (CAE) technologies are rarely used due to the time-consuming and complex process. However, several researchers have already shown that the transfer of Computer-Aided Design and Finite Element Modelling to the practical work of socket and liner design, a better fit socket can be obtained for improved comfort and safety. In Finite Element Modelling, static analysis has been predominant until now, although many previous researchers have suggested that dynamic computer simulations should be used to simulate the socket-limb interaction. This paper aims to present past efforts in Computer Aided Design and simulations of prosthesis socket fit, and to present state-of-the-art technologies. Also presented are the capacity and limits of transient computer simulations. Furthermore, based on the paper review, we want to investigate to what extent this technology is used in everyday prosthetic work. As we can see, the technology for the data-driven design of lower limb prostheses is already available, and provides improved results in comparison to traditional methods. However, CAE and numerical simulations still present too high an effort to benefit ratio.

Keywords. Finite Element Method, Lower Limb Amputees, Prosthetics, Socket Fit

1. Introduction

The loss of limbs is a traumatic event for a person, putting them in a challenging psycho-physical situation. Among all amputations, lower limb amputations due to trauma or disease are the most common. We can divide leg amputation into transfemoral (above the knee) and transtibial (below the knee), the latter being the most common [1]. Prostheses are a replacement for the musculoskeletal system of the leg, which enables the amputee to stand upright and walk. The forces transmitted from the socket to the limb often cause discomfort, skin problems and soft tissue soreness, which can lead to chronic pain. On a monthly average, patients experience three different skin problems such as

[1] Corresponding Author, Email: vasja.plesec@um.si.

dermatitis, skin oedema, hyperaemia, redness, hygiene problems, etc., which force them to limit the use of the prosthesis [2]. This leads to a poorer quality of life and the inability to integrate normally into social life.

Adequate socket fit and a suitable liner can improve the user experience significantly, and, thus, influence the amputee's mobility and quality of life directly. The evaluation of the prosthesis is still determined by the subjective assessment of the user and Prosthetist, and is not based on an objective scientific method. It is, therefore, difficult for Prosthetists to understand the relationship between the properties of the socket and the comfort of use. In recent years, great effort has been made to describe and understand the mechanical behaviour of the socket and the residual limb – the desire is to describe the behaviour in a quantitative manner [3-6]. The progress is more than obvious, but, due to its subjective nature, the problem is still solved largely in an artisan way, and, therefore, the successful fit depends mainly on Prosthetists` skills and experiences.

Currently, in lower limb prosthetics, in order to distribute pressure more evenly over the amputated limb, mostly, (up to 85%) soft and flexible elastomeric liners are used mainly in combination with a TSB (Total Socket Bearing) socket [7]. In contrast to older foam liners (Pelite) which are attached directly to the socket, usually PTB (Patellar Tendon Bearing) elastomeric liners are donned on the residual limb similar to a sock, creating an intimate interaction due to the sticky properties of the elastomeric material, which is beneficial in terms of limiting relative movement and transferring shear forces between the liner and the limb. According to amputees, the most common problem is a change in volume of the residual limb, which can lead to premature replacement of the liner, or even the socket [8].

In the current socket manufacturing process, the Prosthetist first examines and assesses the condition of the limb. Then a mould (negative) is produced, which is made by the technician by shaping the plaster directly onto the limb. The negative is used to produce a positive mould, which is then reshaped artificially. This step emphasises the practical skills of the Prosthetist, who removes or adds material manually in areas where he or she wants to relieve or burden the limb further. The shape is also adjusted according to the patient's age and lifestyle – younger and more active users generally want a tighter fit than older people and people with sensitive skin [9]. The next step is to shape the thermoplastic material thermally onto a positive mould, in order to obtain a test socket which is later validated by the user. At this stage, certain modifications can still be made to the socket before the final phase begins. Typically, the final socket is made of lightweight composite materials (usually carbon fibre) with a total thickness of approximately 4 mm.

In the first year following the amputation, an average of nine corrections of the socket are required [10]. The development of computer technology and numerical methods has the potential to reduce the number of iterations required to fabricate the final socket and determine the appropriate liner drastically. For several decades, attempts have been made to simulate the interactions between the residual limb, the liner and the socket. The beginnings of the use of the Finite Element Method (FEM) in Prosthetics for the productions of leg prostheses date back to the late eighties of the last century [11]. During this period, a number of numerical models of the residual limb, the liner and the socket were developed, to describe the interaction between them as accurately as possible. The method is suitable, because it provides us with results that are very difficult, in some cases even impossible, to obtain with experimental tests. A good feature of the computer procedure is also the provision of repeatability. Despite all these advantages, the mass use of numerical methods in Prosthetics is still not noticeable.

2. Data-driven process

The proposed data-driven procedures to produce sockets for lower amputees are based on similar basic steps. Instead of using a plaster mould to capture the geometry of the limb, it is proposed to capture the external shape with a 3D scanner and the internal structure with Magnetic Resonance Imaging (MRI) or Computed Tomography (CT) [9, 12, 13]. The acquired data are imported into a computer program that prepares the geometry of the limb automatically, including the corresponding internal structure. At this point, the Prosthetist can use various commands on the virtual model to change the size by adding or removing material in certain areas and, thus, adjusting the shape. Once we have a desired virtual limb with the corresponding socket, an FEM analysis is carried out automatically [9]. The purpose of the analysis is to inform about inner stresses and contact pressure. With the results we can modify the socket further. When we are satisfied with the design, the final socket is produced using additive technologies (3D printer). Newer printers with multiple nozzles enable multi-material printing, which allows us to change the material properties in different areas of the socket gradually [9, 13].

The idea of the described procedure is to reduce the number of iterations by omitting the test socket and producing the final version directly. New additive technologies allow us to print complex shapes from variable materials, creating a flexible socket with perfect fit to the limb. There is currently no standardised procedure which is necessary to introduce a computer-controlled process for manufacturing a socket, although the idea is more than a decade old [12]. The described data-driven process with basic steps is shown in Figure 1.

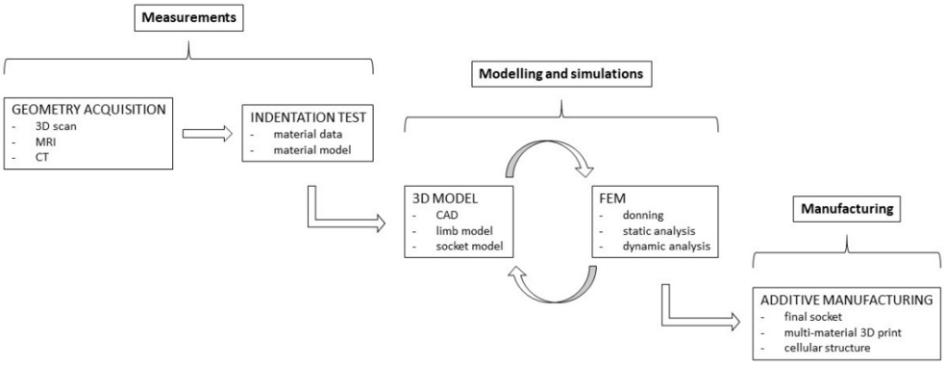

Figure 1. Data-driven process.

2.1. Data acquisition

The first step in a standardised, data-driven prosthesis manufacturing process for a given amputee is to capture the geometry of the limb using either a 3D scanner, MRI or CT. The data obtained from the measurements are converted by software into a single representative 3D model of the limb. For an accurate numerical description we also need material data, which can vary greatly from person to person. One of the proposed methods is to perform an indentation test in vivo on the amputee's limb [6]. An inverse FEM simulation was performed using force, displacement and time from the test, to

acquire a material model that describes the mechanical properties of the limb (Ogden 2nd order). Two material models have been developed, one for the description of skin-adipose and one for the description of muscle-soft tissue, including their hyperelastic and viscoelastic properties. Previous research on the material properties of biological tissues has concerned mainly animal tissue [14-16]. Due to the specific nature of biological material, the results of these studies have been difficult to use directly to describe the properties of human tissue.

MRI is used not only to obtain the geometry of the limb and the internal structure, but also to assess the quality of the fit between the plaster and the limb at the time of mould making. Different materials used in the mould can influence the accuracy. An initial study was conducted on this subject [17]. Safari and colleagues in the study tested 7 different materials commonly used to make a mould, and their influence on the accuracy of the results obtained by MRI [18]. The obtained analysis of the 3D geometry showed small deviations, which confirmed the accuracy. The development of an indentation device for non-invasive measurement of soft tissue material properties compatible with an MRI device was described by Moerman et al. [19, 20]. An automatic 3D reconstruction of the limb using MRI images was proposed by Colombo et al. [21]. The procedure consisted of three steps: Image preprocessing, voxel segmentation, 3D model generation. In addition to the MRI, the author also proposed the use of a 3D scanner for the precise acquisition of an external topology [9]. CT would be the best measurement method solely for the automatic generation of a 3D model. However, since CT is an invasive method that is harmful to the patient, MRI is the better choice, which can be used several times without major consequences for the patient. MRI data may also be useful for designing a variable-impedance prosthetic socket for transtibial amputees [22].

In addition to capturing the geometry, experimental measurements of the contact pressure at the stump-socket or liner-stump interface are common, which are carried out with a pressure sensor inserted into the prosthesis [23, 24]. The results of a dynamic or static experiment can be used to validate computer simulations. Dynamic measurements are particularly important because only in this way can a dynamic process such as walking be fully described. Until now, not many researchers have used a motion capture system to simulate the amputees' gait kinematics. However, it is a crucial step to completely record and simulate the entire gait cycle. The motion analysis system was used to compare the piston movement of the transtibial prosthesis socket using two different types of suspension liners [25]. Besides gait simulation, dynamic analysis can also be used to simulate other amputee activities such as cycling [26].

2.2. Modelling and simulations

So far, much has been done in the field of virtual representation and simulation. Computer technology can reduce drastically the time required to produce a prosthesis and ensure a better fit. With the help of FEM, we can predict the stress concentrations and high-pressure areas in the limb that have a negative impact on comfort. This is also the reason for the great interest in computer technology in the prosthetic field since the early days of 3D modelling and computer simulation. Figure 2 shows the results obtained on a generic 3D model of a transtibial limb and the prosthesis by FEM (a) Displacement in the sagittal plane (b) Contact pressure at the socket-liner interface.

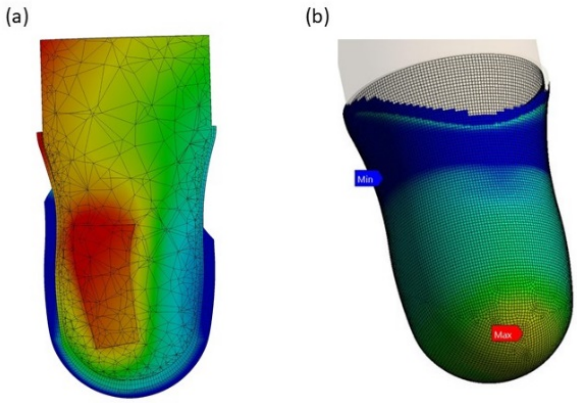

Figure 2. FEM results (a) Displacement (b) Contact pressure.

At first, 2D geometry and simple linear elastic material models were used, which tried to describe the behaviour of the limb. Over time, it became apparent that we need nonlinear material models for an accurate description. In 1999, Fisher and his colleagues took an important step towards reducing stresses and redistributing loads in a prosthesis with polyurethane liner using the nonlinear Finite Element Method [27]. The well-known Mooney-Rivlin material model and the 2D limb geometry were used to simulate the liner. A similar analysis was carried out by Zhang and co-workers, who simulated the donning of a socket [28]. The 3D model predicted pressure, shear stress and slippage between the residual limb and the socket under various loading conditions. In the same year, Zhang compared the numerical model with clinical measurements of interface pressure in a transtibial socket [29]. He proposed the use of nonlinear mechanical properties for soft tissue and dynamic gait simulation. A research team with Fisher updated their 2D model and extended it with a 3D design [30]. Their main purpose, like many others, was to minimise discomfort and pain when using prostheses. In his dissertation, Faustini described the modelling and fabrication of prostheses using the selective laser sintering process [31]. He proposed the use of the above-mentioned process to make the fabrication of complex prosthesis shapes more precise and easier. The same author conducted a study of the quasi-static reaction of a transtibial socket [32]. The problem of hyperthermia in the residual limb when wearing a prosthesis was raised by Peery, who created a 3D numerical model to simulate the temperature in the socket [33]. The analysis was validated by measurements on five amputees. A comparison of different liners for TSB prostheses using FEM was conducted by Wu et al. [34]. As expected, the simulation shows that the contact pressure increases with increasing stiffness of the liner. One of the few who have used explicit dynamic analysis is Lacrox, with which they have simulated the donning of a prosthesis [35]. Rotariu and colleagues developed a numerical model to understand better the interaction between limb, socket and liner [36] – the results show the pressure distribution in the socket. In his dissertation, Cagle provided a detailed analysis of the various liners and a tool to help facilitate the choice between different suppliers [37]. He also proposed a method for measuring the mechanical properties for an objective comparison of the different liners, and made a 3D numerical simulation of three amputees to compare them with limb injuries caused by wearing prostheses. The model had proven to be good, because it predicted the areas where the damage occurred fairly accurately. For future work, he proposed a more robust numerical

model that would allow the simulation of the entire gait. Fatone carried out extensive research on transfemoral amputees, with the aim of producing a flexible prosthesis for active users [38]. Moerman and his colleagues took an important step towards automation and standardisation of the prosthesis manufacturing process when they attempted to implement a non-invasive method of geometry acquisition, indentation tests to obtain material data, automatic generation of a given 3D design, the Finite Element Method of a 3D model, and final production with additive technologies [13]. In 2018, an article was published on the use of additive technologies for ankle-foot orthoses using the Finite Element Method [39]. Constitutive material models of biological tissue can also be taken from modelling studies of other body parts, such as a healthy leg [40], where much has already been developed.

To date, not much has been done in the field of transient simulations for leg amputees. The reason for this is the high computing intensity (non-linear behaviour, contacts, complex geometry ...), which requires computing time and advanced computer equipment. A major problem in the calculation of complex nonlinear dynamic load cases is also the achievement of convergence. In order to prepare the dynamic load case accurately, the motion capture experiment should be performed to preserve the amputee's gait kinematics. Jia et. al. used quasi-dynamic and dynamic nonlinear FEM analysis to investigate the mechanics of load transfer between the lower leg prosthesis socket and residual limb [41-43]. They suggested that it is preferable to consider the material inertia effect in a dynamic FE model.

2.3. Additive manufacturing

In contrast to the traditional manufacturing process, where the Prosthetist forms a thermoplastic test socket on the mould, and only later forms the final composite socket, the proposed computer-controlled method uses additive manufacturing to produce the final socket directly. This reduces the number of iterations, and ensures repeatability. With the development of 3D printing, the possibilities for the production of complex shapes have expanded greatly. The range of materials that can be printed has also increased. Additive technologies, combined with a data-driven process, provide an advanced tool that reduces socket manufacturing time.

The advanced idea of multi-material printing enables the production of a socket with graded stiffness. Where the thickness of the soft tissue is the smallest, the material with the lowest stiffness should be used, and vice versa. Doubrovski and colleagues proposed an innovative process for simultaneous 3D printing of multiple materials, based on a voxel-based fabrication rather than the traditional volume-based workflow of 3D printing [44]. They achieved a graded stiffness of the material along the desired areas of the transtibial socket, which is determined by inverse FEM analysis. MRI data of the stump, a 3D scan of the inner surface of the existing well fitted socket and the contact pressure at the limb-socket interface are used, measured with custom made sensors in the unloaded state. In addition to the fabrication of the graded socket, they also propose the production of built-in sensors using multi-material printing. 3D-printed capacitive elastomer sensors for measuring pressure and shear loads at the limb-socket interface have been proposed by Laszczak et al. [45]. The results showed that the sensors were capable of measuring both compressive and shear stresses up to 380 kPa and 80 kPa respectively. The separation of loads into compressive and shear stresses is particularly promising for understanding the behaviour within the stump. A similar use of additive technology is also used for amputees of the upper extremity [46]. As part of this research,

they used a 3D printer to produce a socket for an amputated arm and a silicone cast for the rest of the arm. The geometry of the arm was obtained with a CT device. The study is a successful presentation of advanced computer-controlled procedures (CT imaging, CAD, 3D printing and silicone casting). The additive technologies are also used in Orthotics for the production of leg splints. The paper describes the performance of a 3D printed splint using FEM [39].

3. Discussion and conclusions

3.1. Discussion

The presented computer-controlled processes show great potential for a faster, more cost-effective, more accurate and repeatable socket manufacturing process. The results provide the predicted stresses within the stump and the contact pressure at the limb-socket interface. Hereby, we can determine objectively the sensitive areas that will help us design the socket. Mainly static analyses are used, which are simpler, but only describe one loading situation. Since walking is a highly dynamic process, more attention must be paid to transient numerical simulations that describe the entire gait. To validate the transient simulation, it is necessary to capture and describe the movement with motion capture systems. The transition from time-independent to dynamic analysis is crucial for a more accurate description of the entire gait and the conditions within the residual limb. In addition to the gait cycle, dynamic analysis can also be used to analyse the donning of a socket where a pre-stress condition occurs in the stump.

The final step of the computer-controlled process is the production of the socket. Due to the above listed advantages, 3D printing is currently the most efficient technology for the final production of the socket. Additive manufacturing opens up new possibilities for designing complex shapes, such as cellular structures. Such structures enable us to control the properties by changing the porosity, gradation and shape, so that, with the right design, we can improve the comfort of the prosthesis significantly. One of these structures is the well-known gyroid structure. Figure 3 shows (a) The schematic σ-ε diagram of this structure, and (b) A visual representation of the gyroid model with Gaussian curvature. The advantage of such a structure is a plateau that follows the linear elasticity. This plateau provides deformation at the point where the critical load is exceeded. With the correct design of the cell structure we can adjust the plateau according to the position in the socket. This helps to distribute the pressure over a larger area while maintaining stability.

Research on porous structures fabricated with additive technologies yields promising results, which are also of interest for use in Biomechanics and Prosthetics [47-49]. The main advantages are the lightweight structure, good vibration damping and the possibility of a continuously graded design. The aim of the graded structure is to adjust the stiffness over the socket as required. In practice, we find the use of such structures for the liners of bicycle helmets [50]. In the paper they test the applicability of a 3D printed structure made of TPU material.

The idea of the data-driven process is more than 10 years old and the required technologies are already at a high level, but we still have to overcome difficult obstacles. The question is, why do we not see such a process in practice yet? There are several reasons for that. The first is the expensive equipment we need, which represents a major initial investment. We need an MRI or a CT machine to capture the geometry, suitable

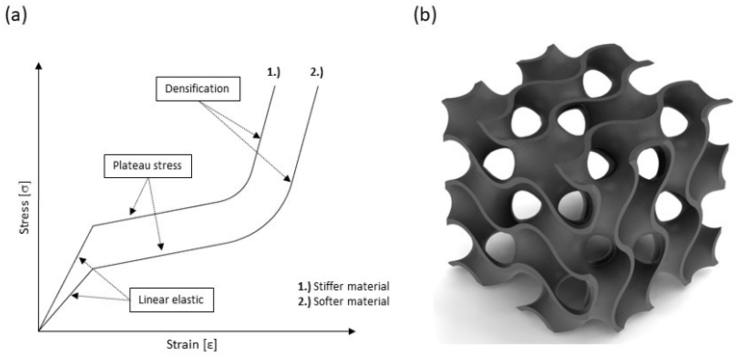

Figure 3. Gyroid structure (a) Schematic σ-ε diagram (b) Virtual model.

software and hardware to perform FEM, and a high-quality 3D printer for production. In addition to the expensive hardware, the limitation is also the current software, which does not yet provide a sufficiently fast and automated procedure that would be easy enough for the Prosthetist to use.

Despite the large initial investment, the cost of fabricating a prosthesis using the data-driven process is reduced significantly over a longer period of time, due to the reduction of iterations. Although the computer procedure requires more time in the initial phase, this time is compensated for by the reduction, or even elimination, of corrections. However, the data-driven process should be more cost and time efficient, and it is only a matter of time before the traditional process will become obsolete. Before this happens, it is necessary to introduce a standard procedure that guarantees the quality of the work. In addition to the procedure, the development of new materials and structures, such as cell structures, will also contribute to the comfort of using a leg prosthesis.

3.2. Conclusions

Currently, the use of advanced procedures in prosthesis design is mainly useful for research purposes to design new materials and structures. FEM is very useful for simulating internal stresses, which is difficult, if not impossible, with experimental testing. The development of additive technologies allows multi-material printing and, thus, graded stiffness. This step can improve the comfort of the prosthesis significantly during the time of use, as, so far, only the shape of the socket has been adjusted to fit the stump. The flexible socket is also more favourable in terms of changing the stump volume, which varies both daily and over a longer period. Furthermore, various mechanical properties of the socket can also be ensured by the cellular structure. For a data-driven socket manufacturing process, it is also necessary to develop and adapt software that enables easy use for Prosthetists. Before the advantage of these ideas can be confirmed, several experiments have to be performed, including the users who can best evaluate the effectiveness of the new socket.

References

[1] Dillingham TR, Pezzin LE, MacKenzie EJ. Limb amputation and limb deficiency: Epidemiology and recent trends in the United States. Southern Medical Journal, 2002,95(8), 875-883.

[2] Meulenbelt HEJ, Geertzen JHB, Jonkman MF, Dijkstraa PU. Skin Problems of the Stump in Lower Limb Amputees: 2. Influence on Functioning in Daily Life. Acta Dermato-Venereologica, 2011, 91(2), 178-182.

[3] Steer JW, Worsley PR, Browne M, Dickinson AS. Predictive prosthetic socket design: part 1—population-based evaluation of transtibial prosthetic sockets by FEA-driven surrogate modelling. Biomechanics and Modeling in Mechanobiology, 2019.

[4] Cagle JC, Reinhall PG, Allyn KJ, McLean J, Hinrichs P, Hafner BJ, et al. A finite element model to assess transtibial prosthetic sockets with elastomeric liners. Medical & Biological Engineering & Computing, 2018, 56(7), 1227-1240.

[5] Sankaran S, Murugan PR, Johnson JC, Abdullah HJS, Raj CMN, Ashokan D, editors. Prevention of skin problems in patients using prosthetic limb: A review of current technologies and limitations. Proceedings of the 2019 IEEE International Conference on Communication and Signal Processing, ICCSP 2019, 2019.

[6] Sengeh DM, Moerman KM, Petron A, Herr H. Multi-material 3-D viscoelastic model of a transtibial residuum from in-vivo indentation and MRI data. Journal of the Mechanical Behavior of Biomedical Materials, 2016, 59, 379-392.

[7] Whiteside SR. Practice Analysis of Certified Practitioners. edited by SR Whiteside: American Board for Certification in Orthotics, Prosthetics, & Pedorthotics, Inc, 2015.

[8] Ahmad A. Prosthetic problems of transtibial amputee. Journal of Postgraduate Medical Institute, 2009, 23, 153-158.

[9] Colombo G, Rizzi C, Regazzoni D, Vitali A. 3D interactive environment for the design of medical devices. International Journal on Interactive Design & Manufacturing, 2018, 12(2), 699.

[10] Pezzin LE, Dillingham TR, MacKenzie EJ, Ephraim P, Rossbach P. Use and satisfaction with prosthetic limb devices and related services. Archives of Physical Medicine and Rehabilitation, 2004, 85(5),723-729.

[11] Zachariah SG, Sanders JE. Interface mechanics in lower-limb external prosthetics: a review of finite element models. IEEE Transactions on Rehabilitation Engineering, 1996, 4(4), 288-302.

[12] Colombo G, Filippi S, Rizzi C, Rotini F. A new design paradigm for the development of custom-fit soft sockets for lower limb prostheses. Computers in Industry, 2010, 61(6), 513-523.

[13] Moerman K, Sengeh D, Herr H. Automated and Data-driven Computational Design of Patient-Specific Biomechanical Interfaces. Germany, Europe: engrXiv, 2016.

[14] Safari MR, Rowe P, Buis A. Accuracy Verification of Magnetic Resonance Imaging (MRI) Technology for Lower-Limb Prosthetic Research: Utilising Animal Soft Tissue Specimen and Common Socket Casting Materials. Scientific World Journal, 2012, 156186.

[15] Bosboom E, Hesselink M, Oomens C, Bouten C, Drost M, Baaijens F. Passive transverse mechanical properties of skeletal muscle under in vivo compression. Journal of biomechanics, 2001, 34(10), 1365-1368.

[16] Palevski A, Glaich I, Portnoy S, Linder-Ganz E, Gefen A. Stress relaxation of porcine gluteus muscle subjected to sudden transverse deformation as related to pressure sore modeling, 2006.

[17] Buis AWP, Condon B, Brennan D, McHugh B, Hadley D. Magnetic resonance imaging technology in transtibial socket research: a pilot study. Journal Of Rehabilitation Research And Development, 2006, 43(7), 883-890.

[18] Safari MR, Rowe P, Buis A. Examination of anticipated chemical shift and shape distortion effect on materials commonly used in prosthetic socket fabrication when measured using MRI: A validation study. Journal of Rehabilitation Research & Development, 2013, 50(1), 31-41.

[19] Moerman KM, Sprengers AMJ, Simms CK, Lamerichs RM, Stoker J, Nederveen AJ. Validation of continuously tagged MRI for the measurement of dynamic 3D skeletal muscle tissue deformation. Medical Physics, 2012, 39(4), 1793-1810.

[20] Moerman KM, Sprengers AMJ, Nederveen AJ, Simms CK. A novel MRI compatible soft tissue indentor and fibre Bragg grating force sensor. Medical Engineering and Physics, 2013, 35(4), 486-499.

[21] Colombo G, Facoetti G, Rizzi C, Vitali A, Zanello A. Automatic 3D reconstruction of transfemoral residual limb from MRI images. Lecture Notes in Computer Science (including subseries Lecture Notes in Artificial Intelligence and Lecture Notes in Bioinformatics), 2013, 324-332.

[22] Sengeh DM, Herr H. A variable-impedance prosthetic socket for a transtibial amputee designed from magnetic resonance imaging data. Journal of Prosthetics and Orthotics, 2013,25(3), 129-137.

[23] Eshraghi A, Abu Osman NA, Gholizadeh H, Ali S, Abas WABW. Interface stress in socket/residual limb with transtibial prosthetic suspension systems during locomotion on slopes and stairs. American Journal of Physical Medicine and Rehabilitation, 2015, 94(1), 1-10.

[24] Sewell P, Noroozi S, Vinney J, Amali R, Andrews S. Static and dynamic pressure prediction for prosthetic socket fitting assessment utilising an inverse problem approach. Artificial Intelligence In Medicine, 2012, 54(1), 29-41.
[25] Gholizadeh H, Abu Osman NA, Kamyab M, Eshraghi A, Wan Abas WAB, Azam MN. Transtibial prosthetic socket pistoning: Static evaluation of Seal-In(®) X5 and Dermo(®) Liner using motion analysis system, 2011.
[26] Childers WL, Perell-Gerson KL, Gregor RJ. Measurement of motion between the residual limb and the prosthetic socket during cycling. Journal of Prosthetics and Orthotics, 2012, 24(1), 19-24.
[27] Fisher C, Simpson G, Reynolds D. Development of a finite element model of a transtibial socket liner--an initial study. Biomedical Sciences Instrumentation, 1999, 35, 39-44.
[28] Zhang M, Mak AF, Fan Y. Three-dimensional finite element analyses on the transtibial residual limb and its prosthetic socket. Journal Of Biomedical Engineering, 2000, 17(4), 403-406.
[29] Zhang M, Roberts C. Comparison of computational analysis with clinical measurement of stresses on below-knee residual limb in a prosthetic socket. Medical Engineering and Physics, 2000, 22(9), 607-612.
[30] Fisher C, Simpson G, Reynolds D. Development of a three-dimensional, non-linear finite element model of a transtibial socket liner. Middleton J, Jones ML, Shrive NG, Pande GN, editors. 1062 Ev Amsterdam: Gordon and Breach Science Publ, 2001, 319-324.
[31] Faustimi MC. Modeling and fabrication of prosthetic sockets using selective laser sintering. United States, North America, 2004.
[32] Faustini MC, Neptune RR, Crawford RH. The quasi-static response of compliant prosthetic sockets for transtibial amputees using finite element methods. Medical Engineering and Physics, 2006, 28(2),114-121.
[33] Peery JT, Klute GK, Blevins JJ, Ledoux WR. A Three-Dimensional Finite Element Model of the Transibial Residual Limb and Prosthetic Socket to Predict Skin Temperatures. IEEE Transactions on Neural Systems & Rehabilitation Engineering, 2006, 14(3), 336.
[34] Wu CL, Lin CC, Wang KJ, Chang CH. Effect of prosthesis liner material properties on interface stresses between stump and trans-tibial socket. Herzog W, editor. Anaheim: Acta Press Anaheim, 2007, 135-140.
[35] Lacroix D, Patiño JFR. Finite element analysis of donning procedure of a prosthetic transfemoral socket. Ann Biomed Eng, 2011, 39(12), 2972-2983.
[36] Rotariu M, Filep R, Turnea M, Ilea M, Arotăriţei D, Popescu M. Analyse of socket-prosthesis-blunt complex for lower limb amputee using objective measure of patient's gait cycle. Revista Medico-Chirurgicala A Societatii De Medici Si Naturalisti Din Iasi, 2015, 119(1), 281-286.
[37] Cagle J. A Computational Tool to Enhance Clinical Selection of Prosthetic Liners for People with Lower Limb Amputation. United States, North America, 2016.
[38] Fatone S, Caldwell R, Gard S, Major M, Wilken J, Komolafe O, et al. Development of Subischial Prosthetic Sockets with Vacuum-Assisted Suspension for Highly Active Persons with Transfemoral Amputations, 2016.
[39] Volpini M, Alves D, Horta A, Borges M, Reis P. Orthosis And Finite Elements: A Study For Development Of New Designs Through Additive Manufacturing, 2018.
[40] Perrier A, Luboz V, Bucki M, Cannard F, Vuillerme N, Payan Y. Chapter 25 - Biomechanical Modeling of the Foot. In: Payan Y, Ohayon J, editors. Biomechanics of Living Organs. 1. Oxford: Academic Press, 2017, 545-563.
[41] Jia X, Zhang M, Lee WCC. Load transfer mechanics between trans-tibial prosthetic socket and residual limb—dynamic effects. Journal of Biomechanics, 2004, 37(9), 1371-1377.
[42] Jia X, Zhang M, Li X, Lee WCC. A quasi-dynamic nonlinear finite element model to investigate prosthetic interface stresses during walking for trans-tibial amputees. Clinical Biomechanics, 2005, 20(6), 630-635.
[43] Jia X, Zhang M, Wang R, Jin D. Dynamic investigation of interface stress on below-knee residual limb in a prosthetic socket. Tsinghua Science and Technology, 2004, 9(6), 680-683.
[44] Doubrovski EL, Tsai EY, Dikovsky D, Geraedts JMP, Herr H, Oxman N. Voxel-based fabrication through material property mapping: A design method for bitmap printing. Computer-Aided Design, 2015, 60, 3-13.
[45] Laszczak P, Jiang L, Bader DL, Moser D, Zahedi S. Development and validation of a 3D-printed interfacial stress sensor for prosthetic applications. Medical Engineering and Physics, 2015, 37(1), 132-137.
[46] Cabibihan JJ, Abubasha MK, Thakor N. A Method for 3-D Printing Patient-Specific Prosthetic Arms with High Accuracy Shape and Size. IEEE Access, 2018, 6, 25029-25039.
[47] Bates SRG, Farrow IR, Trask RS. Compressive behaviour of 3D printed thermoplastic polyurethane honeycombs with graded densities. Materials and Design, 2019, 162, 130-142.

[48] Habib F, Iovenitti P, Masood S, Nikzad M, Ruan D. Design and evaluation of 3D printed polymeric cellular materials for dynamic energy absorption. International Journal of Advanced Manufacturing Technology, 2019, 103(5-8), 2347-2361.
[49] Mansouri MR, Montazerian H, Schmauder S, Kadkhodapour J. 3D-printed multimaterial composites tailored for compliancy and strain recovery. Composite Structures, 2018, 184, 11-17.
[50] Soe S, Martin P, Jones M, Robinson M, Theobald P. Feasibility of optimising bicycle helmet design safety through the use of additive manufactured TPE cellular structures. International Journal of Advanced Manufacturing Technology, 2015, 79(9-12), 1975-1982.

Part 6

Production Planning and Ergonomics Evaluation

This page intentionally left blank

DHM2020
L. Hanson et al. (Eds.)

© 2020 The authors and IOS Press.
This article is published online with Open Access by IOS Press and distributed under the terms of the Creative Commons Attribution Non-Commercial License 4.0 (CC BY-NC 4.0).
doi:10.3233/ATDE200044

Implementation of Ergonomics Evaluation Methods in a Multi-Objective Optimization Framework

Aitor IRIONDO PASCUAL [a,1], Dan HÖGBERG [a], Anna SYBERFELDT [a], Erik BROLIN [a], Francisco GARCÍA RIVERA [a], Estela PÉREZ LUQUE [a] and Lars HANSON [a,b]
[a] *University of Skövde, School of Engineering Science, 541 28 Skövde, Sweden*
[b] *Scania CV, Södertälje, Sweden*

Abstract. Simulations of future production systems enable engineers to find effective and efficient design solutions with fewer physical prototypes and fewer reconstructions. This can save development time and money and be more sustainable. Better design solutions can be found by linking simulations to multi-objective optimization methods to optimize multiple design objectives. When production systems involve manual work, humans and human activity should be included in the simulation. This can be done using digital human modeling (DHM) software which simulates humans and human activities and can be used to evaluate ergonomic conditions. This paper addresses challenges related to including existing ergonomics evaluation methods in the optimization framework. This challenge arises because ergonomics evaluation methods are typically developed to enable people to investigate ergonomic conditions by observing real work situations. The methods are rarely developed to be used by computer algorithms to draw conclusions about ergonomic conditions. This paper investigates how to adapt ergonomics evaluation methods to implement the results as objectives in the optimization framework. This paper presents a use case of optimizing a workstation using two different approaches: 1) an observational ergonomics evaluation method, and 2) a direct measurement method. Both approaches optimized two objectives: the average ergonomics results, and the 90th percentile ergonomics results.

Keywords. Ergonomics, Optimization, DHM, Simulation

1. Introduction

Research has shown a clear relationship between poor ergonomics and productivity losses and quality deficiencies such as assembly errors, which incur significant costs for companies [1]. Hence, when designing factories and workstations or making other decisions that affect ergonomic conditions, it is important to proactively ensure proper ergonomic conditions for workers. Doing this reduces the risk of work-related musculoskeletal disorders (WMSDs), supports high product quality and productivity, and reduces the associated costs to the industry and society [2,3]. There are several digital human modeling (DHM) tools available that consider ergonomics at the design stage of workstations in the virtual world. These include Santos™ [4], Siemens Jack™ [5], and

[1] Corresponding Author, Email: aitor.iriondo.pascual@his.se.

IPS IMMA™ [6]. These tools typically facilitate studies related to anthropometric variability among workers [7], simulation of work tasks [8], and assessments of ergonomics according to established ergonomics evaluation methods. These evaluation methods enable the DHM tool user to assess alternative workstation design proposals from an ergonomics perspective by simulating workers performing work tasks. The types of ergonomics evaluation methods commonly implemented in DHM tools are digitalized versions of observation-based methods. Examples of such methods include RULA (rapid upper limb assessment) [9], OWAS (Ovako working posture assessment system) [10], NIOSH (National Institute for Occupational Safety and Health) Lifting Equation [11], OCRA (occupational repetitive actions) [12] and REBA (rapid entire body assessment) [13]. Observation-based methods are sometimes based on subjective measurements. For example, "trunk twisted" in RULA [9] is not defined as a specific angle and is therefore hard for computers to interpret. There are also ergonomics evaluation methods based on direct measurements of ergonomic exposures [14]. Rather than being based on a person making manual observations of work, these direct measurement methods use technical devices such as digital goniometers [15], IMUs (inertial measurement units) [16,17], or EMG (electromyography) sensors [15] to measure exposure factors. The direct measurement methods can also be based on using different kinds of image recognition technologies to capture postures and motions [18,19].

Both observational and direct measurement methods are used to measure the ergonomics and to change the design of workstations to improve the ergonomics for the workers. The redesign of the workstations is typically done manually by ergonomists and design engineers since current DHM tools do not include optimization tools to automatically optimize the ergonomics. There are some ergonomic optimization studies that suggest automatic optimizations for ergonomics, for example [20]. However, it is more difficult to define metrics for improved ergonomics than metrics for improved production, where increasing production and reducing times or costs are always positive.

Some studies have tried to solve the lack of ergonomic evaluation methods for optimization by analyzing different ergonomic evaluation methods [21]. However, in most of these studies the common approach when optimizing ergonomics parameters is to use results from different observational ergonomics evaluation methods and optimize the ergonomics risk score of those methods [22]. The goal of this study was to compare the effectivity of observation-based methods, for example RULA [9], with direct measurement methods in an automatic optimization process performed with evolutionary algorithms. For this purpose, a use case was defined to perform two optimizations and compare both approaches.

2. Method

The study used a case study-based method. First, a use case was defined and a simulation model corresponding to the use case was created in the DHM tool. Next, two approaches to evaluate the ergonomics in each iteration were used to study the influence of each method on the optimization process: (A) an observational method approach, and (B) a direct measurement method approach. Finally, the optimization process was defined and the comparison method was described.

2.1. Use case and simulation model

A use case was defined to perform an optimization of ergonomics by changing the design parameters of a workstation. The digital human modeling tool IPS IMMA [6] was used because it is possible to perform optimizations by communicating with IPS IMMA through a LUA script [23]. The use case represents one of the workstations in a pedal car assembly factory at Scania. Scania use this testing environment to train assembly line workers; they assemble pedal cars before entering the real production line. The pedal car factory is modelled on the production processes of the real production line at Scania. The pedal car factory has four workstations, and each workstation has several assembly tasks that the workers need to perform. In this use case, one task from the first workstation was chosen for optimization. This task is part of attaching the front frame to the chassis of the pedal car. The model and simulation were created in IPS IMMA (Figure 1).

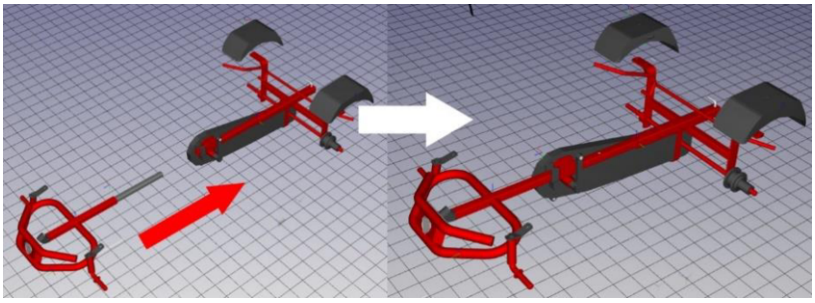

Figure 1. Simulation model of the assembly of the front frame on the chassis of the pedal car in IPS IMMA.

The pedal car has a stand that regulates the height of the pedal car. The height is measured from the ground to the lowest point of the pedal car, being zero when the pedal car touches the floor (**Figure 2**). This height was chosen as the variable to optimize.

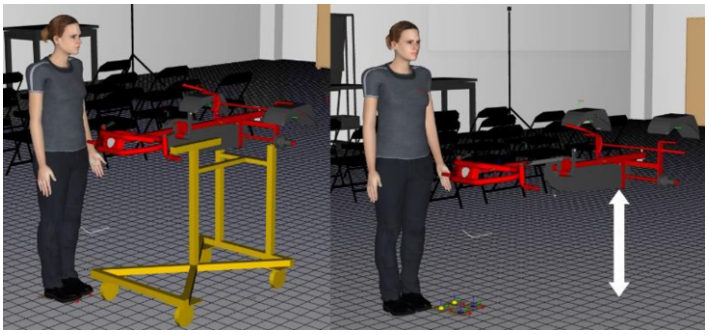

Figure 2. Stand and height of the pedal car.

The manikin randomly created for this use case was a female manikin with a body mass of 62 kg and anthropometrics as shown in Table 1. The manikin's biomechanical definition and the generated motions correspond to the IPS IMMA software [6,24].

Table 1. Anthropometrics of the manikin.

Measure name	Value [mm]
Stature	1629
Shoulder height	1334
Elbow height	985
Shoulder-elbow length	336
Elbow-wrist length	258
Elbow-grip length	326
Shoulder biacromial breadth	363
Shoulder bideltoid breadth	433

To analyze the effect of the height of the pedal car, only the assembly of the front frame was simulated, without simulating picking up the front frame from the shelf and other actions such as walking. The entire simulation consisted of grasping the front frame with both hands at a height of 650 mm and assembling the front frame on the pedal car. The height of 650 mm is a fixed height representing the shelf on which the front frame is located. The operation sequence defined in IPS IMMA was grasping the front frame, moving the front frame, and releasing the front frame **(Figure 3)**.

Figure 3. Operation sequence in IPS IMMA.

2.2. Evaluation of ergonomics

For this use case, the objective was to reduce the ergonomic exposure of the upper arms by adjusting the height of the pedal car until the position that leads to the lowest exposure was found. Two different approaches were used to assess the exposure: an observational method based on the upper arm criteria in RULA [9], and a direct measurement method based on measuring upper arm angles.

For both approaches, the upper arm (left/right) with the highest value was chosen, corresponding with the way it is done in RULA [9]. To evaluate the entire simulation and not a single posture, each frame of the simulation was evaluated using both evaluation methods. The simulations in IPS IMMA can be evaluated at a rate of 30 frames per second. However, since that would be very process-consuming, the simulations were evaluated at a frequency of 5 frames per second. Two values were calculated to represent ergonomic exposure over the entire simulation:

- Average value
- 90^{th} percentile value

2.2.1. Approach A - RULA-based upper arm criteria

Approach A uses the upper arm criteria defined in the ergonomics evaluation method RULA [9] **(Figure 4)**. The criteria evaluate the risk of WMSD with a number between 1 and 6, based on the upper arm sagittal angle, shoulder raised distance, upper arm abduction angle, and support of the arm.

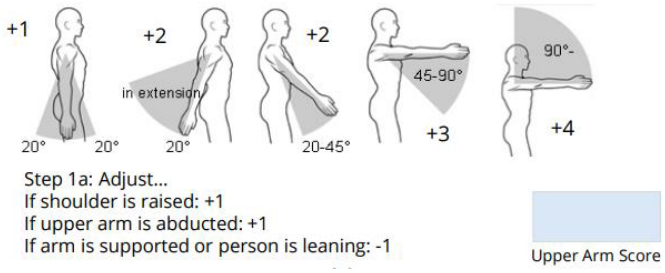

Figure 4. RULA-based upper arm criteria [9].

2.2.2. Approach B - Direct measurement of upper arm angle

Approach B uses the direct measurement of the angle of the upper arms, measured as the absolute value of the angle between two vectors: the back vector and the upper arm vector **(Figure 5)**. The back vector is the vector from the T1T2 joint to the L5S1 joint, and the upper arm vector is the vector from the glenohumeral joint to the elbow joint.

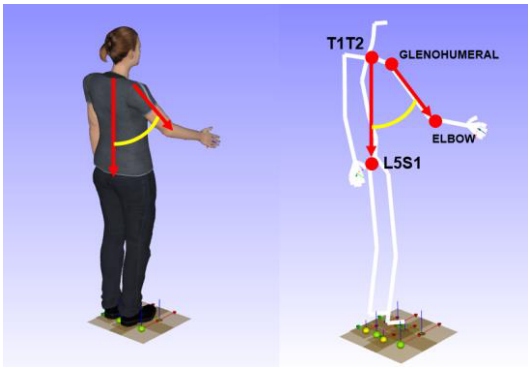

Figure 5. Back and upper arm vectors (red) and absolute angle (yellow).

2.3. Optimization of the pedal car height

In this case, the NSGA-II optimization algorithm [25] was used for the optimization. NSGA-II is an evolutionary algorithm known to be able to efficiently handle complex optimization problems. NSGA-II is commonly used for multi-objective optimizations, but also works well for single-objective problems. By choosing an algorithm that can deal with multiple objectives, it becomes possible to later optimize more complex workstations with numerous design criteria. The NSGA-II algorithm uses an iterative optimization process. In this use case, for each iteration the algorithm generates a new value for the height of the pedal car **(Figure 6)**. The new height is set in the simulation model, and the simulation is run again to obtain new motions of the manikin. The motion data of the manikin are evaluated to obtain ergonomic evaluations data, and these evaluations data are sent to the NSGA-II optimization algorithm. This process is repeated until the number of iterations defined for the optimization process is reached.

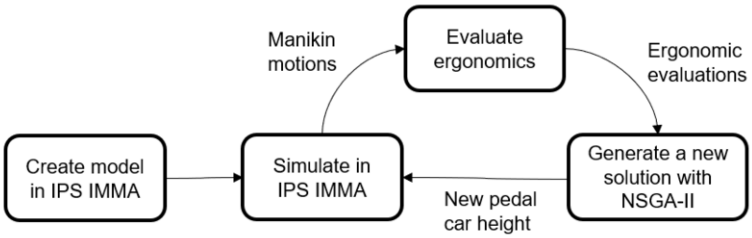

Figure 6. Optimization process workflow.

The NSGA-II optimization algorithm [25] was configured with a population size of 4, a crossover probability of 0.9, a mutation probability of 0.3, and a tournament size of 2. In order to maintain a feasible height of the pedal car, its height was constrained between 0 and 2000 mm. The initial solutions for the population were generated randomly.

2.4. Comparison between approach A and B

Two optimizations of 200 iterations were run to study the entire solution space, one for approach A and one for approach B. The objective of performing 200 iterations was to study the behavior of both approaches while optimizing using NSGA-II [25].

In addition, the convergence of each of the approaches was compared to find which approach could be applied more effectively in an optimization problem by performing fewer simulations while finding more optimal solutions. This step compared the convergence of the pedal car height in each approach. Afterwards, another study investigated whether optimizing for the RULA-based approach also optimized the direct measurement approach.

3. Results

The iterative optimization process varied the height of the pedal car and then simulated the manikin assembling the front frame. The height of the pedal car caused significant changes in the manikin's motions **(Figure 7)**.

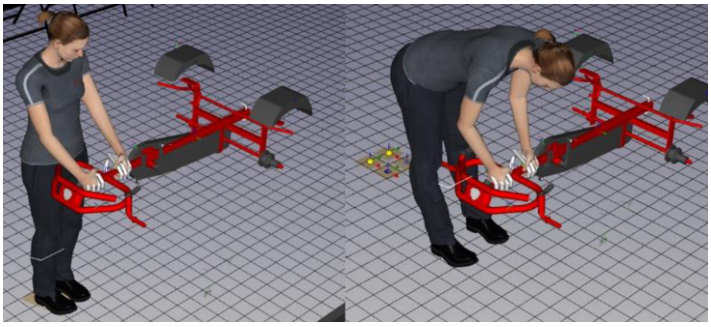

Figure 7. Manikin in IPS IMMA holding the pedal car at different heights.

The entire solution space was studied for both approaches, for both average results and 90th percentile results. The iterations performed for this optimization generated 200 solutions generated by the NSGA-II algorithm, simulated in IPS IMMA [6], and evaluated with the RULA-based criteria and direct measurement approaches.

3.1. Approach A - RULA-based criteria

As **Figure 8** shows, heights of the pedal car in the range of 380–820 mm provided the best results for the RULA-based criteria average values (orange dots). For the RULA-based criteria 90th percentile, the range is the same but the results are more separate due to the percentile calculation (**Figure 8**, blue circles).

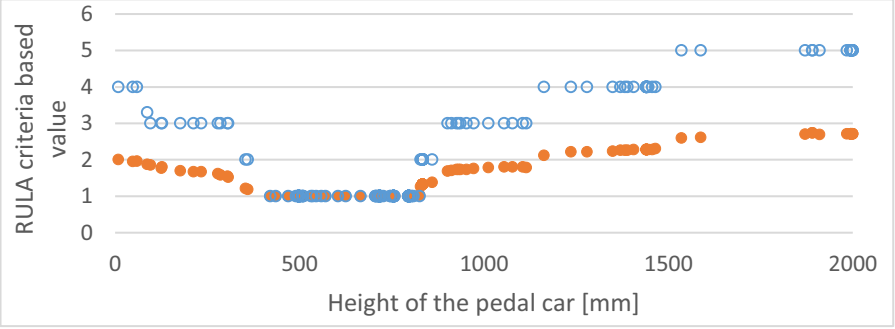

Figure 8. RULA-based criteria average (orange) and 90th percentile (blue) results depending on the height of the pedal car.

3.2. Approach B - Direct measurement

The results are more continuous and show fewer jumps in the evaluation values (**Figure 9**) in the direct measurement approach. Due to this continuity in values, it is easier to locate the minimum value at 565 mm using the measurement average. In addition, this continuity also exists in the direct measurement 90th percentile results (**Figure 9**), also showing a minimum at 565 mm.

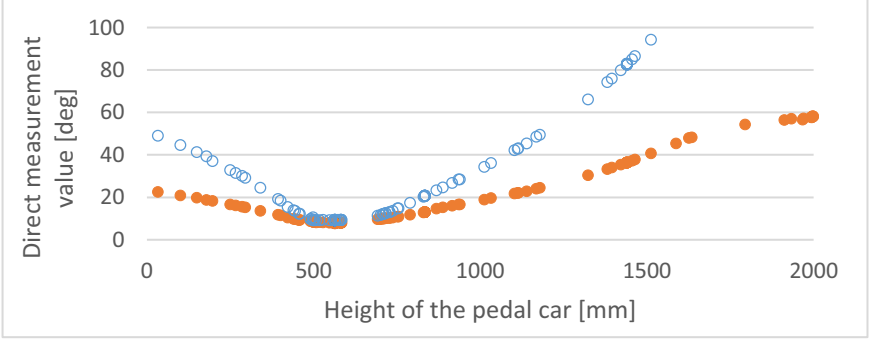

Figure 9. Direct measurement average (orange) and 90th percentile (blue) results depending on the height of the pedal car.

3.3. Comparison between approach A and B

The two optimizations made with the RULA-based criteria and direct measurement approaches were compared by comparing the convergence of the height of the pedal car among the iterations. The convergence of RULA-based criteria results was also compared for the optimization with both approaches.

3.3.1. Comparison of the convergence of the pedal car height

The direct measurement approach was observed to converge at iteration 50 **(Figure 10)**, meaning that NSGA-II found a minimum value for a given height of the pedal car and the following solutions stayed close to that minimum. Due to the nature of the NSGA-II optimization algorithm and the configured mutation rate, after converging the algorithm still tries solutions far from the minimum to find if there is a better minimum value to avoid getting stuck in a local minimum **(Figure 10)**.

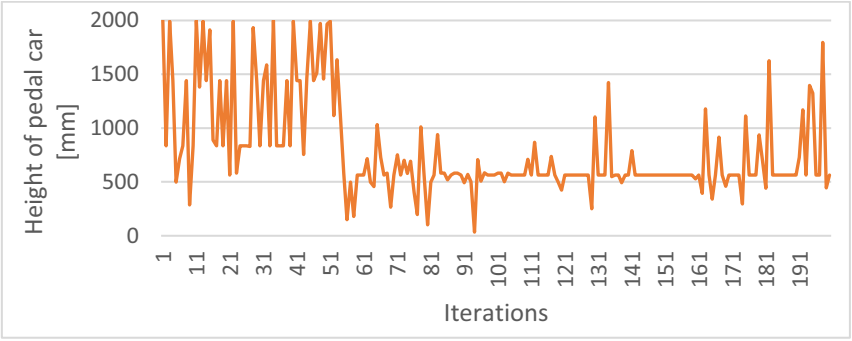

Figure 10. The convergence of pedal car height in the direct measurement optimization.

In the case of the RULA-based criteria approach, the results converged at around iteration 50, but instead of staying close to a single value, the optimization algorithm yielded solutions between a range of values **(Figure 11)**. This is due to the thresholds of the RULA-based criteria approach.

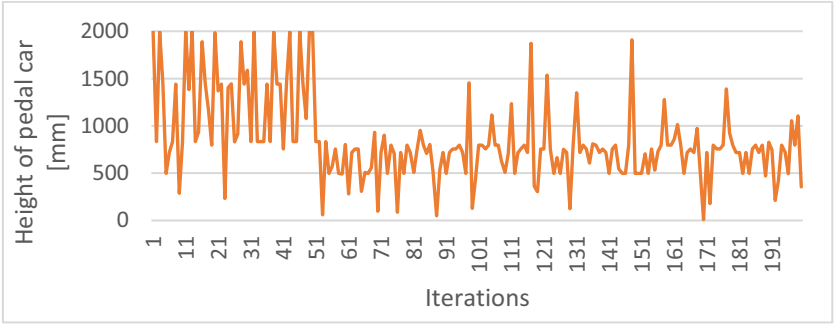

Figure 11. The convergence of pedal car height in the RULA-based criteria optimization.

3.3.2. Comparison of the convergence of RULA-based criteria results in both approaches

If the direct measurement approach is used for the optimization, and the results are reevaluated using the RULA-based criteria approach, the optimal results for direct measurements are also optimal for the RULA-based criteria approach **(Figure 12)**.

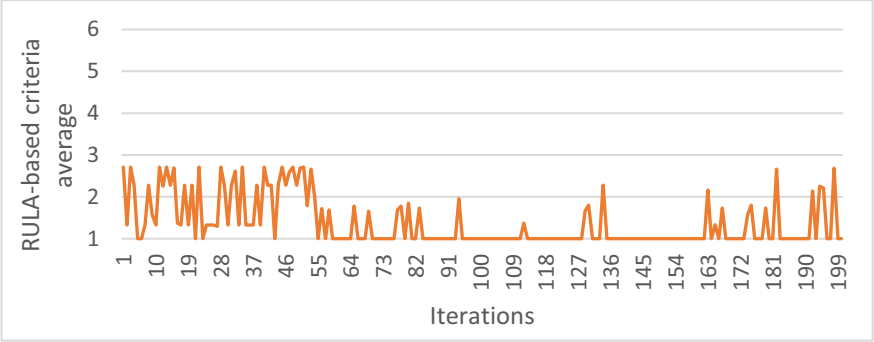

Figure 12. The convergence of RULA-based criteria average in the direct measurement optimization.

However, if the RULA-based criteria approach is used for optimization, **Figure 13** shows that the results do not converge as well as the direct measurement optimization **(Figure 12)**.

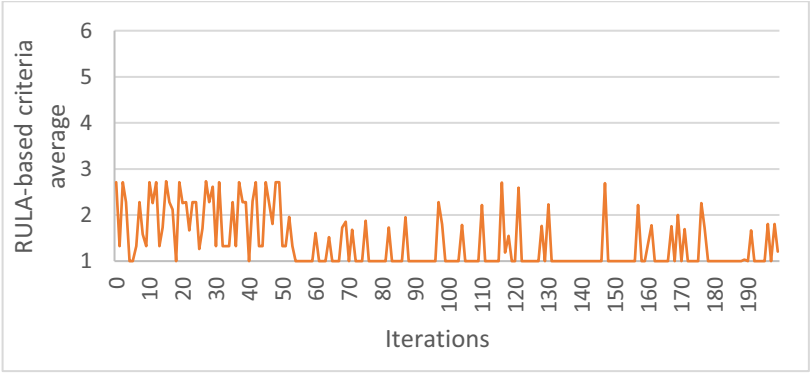

Figure 13. The convergence of RULA-based criteria average in the RULA-based criteria optimization.

4. Discussion

This study is considered an initial study. A single variable, the pedal car height, was optimized by using evolutionary algorithms with two objectives: 1) the minima of the average ergonomic evaluation of the upper arms, and 2) the extreme ergonomic evaluation (90^{th} percentile) of the upper arms. Thus, the study represents a single variable multi-objective optimization problem, where the optimization was performed for two different cases: 1) optimization with the RULA-based criteria approach, and 2) optimization with the direct measurement approach.

The optimization process found a single good ergonomic solution for the recommended height of the pedal car when using the direct measurement approach. However, for the RULA-based criteria approach, the recommended height was between 380 and 820 mm, which is less supportive for making a design decision. Hence, the results show that the pedal car height converged to a single solution when using the direct measurement approach, while the RULA-based criteria approach did not converge to a single solution. These results are however not surprising considering the step-wise nature of the scoring system in the RULA method. Still, the results also show that optimizing with the direct measurements approach also gave the best RULA-based criteria results, and converged faster than the RULA-based criteria approach. These results indicate that it is advantageous to optimize ergonomics by using the direct measurements approach, since the optimization process will be faster and it will converge into a single solution. The results can later be presented in both direct measurement format and RULA format regardless of the approach used for the optimization. The direct measurement approach, as applied in this study, assists finding ergonomic design solutions by favoring joint angles closer to neutral postures, hence improving ergonomics by reducing exposure to postural stress. However, the direct measurement approach does not provide risk levels for WMSDs, as observational ergonomics evaluation methods like RULA typically do. Obviously, being able to estimate the risk for WMSDs is essential for being able to assess if a solution is appropriate or if changes are needed. Hence, it becomes important to be able to present the results by using observational ergonomic evaluation methods after performing the optimizations, even if the optimization was performed using the direct measurement approach. This in order to provide the decision maker with information about estimated risk levels for WMSDs.

This study will be extended in future research, for example, by including more exposure variables and more design variables for the workstation. In addition, more manikins with different anthropometrics will be added to include diversity by optimizing the ergonomics of different manikins. Different configurations of NSGA-II and more optimization algorithms will be tested to find the most suitable configurations for optimization problems of this nature.

Acknowledgment

This work has been made possible with support from ITEA3 in the project MOSIM, and with the support from the Knowledge Foundation and the associated INFINIT research environment at the University of Skövde, within the Virtual Factories – Knowledge-Driven Optimization (VF-KDO) research profile and the Synergy Virtual Ergonomics (SVE) project, and by the participating organizations. This support is gratefully acknowledged.

References

[1] Falck A-C, Örtengren R, Högberg D. The impact of poor assembly ergonomics on product quality: A cost–benefit analysis in car manufacturing. Hum Factors Ergon Manuf Serv Ind, 2010, 20, 24–41. https://doi.org/10.1002/hfm.20172.

[2] Sultan-Taïeb H, Parent-Lamarche A, Gaillard A, Stock S, Nicolakakis N, Hong QN, et al. Economic evaluations of ergonomic interventions preventing work-related musculoskeletal disorders: a systematic

review of organizational-level interventions. BMC Public Health, 2017, 17, 935. https://doi.org/10.1186/s12889-017-4935-y.
[3] European Agency for Safety and Health at Work. An international comparison of the cost of work-related accidents and illnesses, 2017.
[4] Abdel-Malek K, Arora J, Bhatt R, Farrell K, Murphy C, Kregel K. Chapter 6 - Santos: An integrated human modeling and simulation platform. In: Scataglini S, Paul G, editors. DHM Posturography, Academic Press, 2019, 63–77. https://doi.org/10.1016/B978-0-12-816713-7.00006-4.
[5] Raschke U, Cort C. Chapter 3 - Siemens Jack. In: Scataglini S, Paul G, editors. DHM Posturography, Academic Press, 2019, 35–48. https://doi.org/10.1016/B978-0-12-816713-7.00003-9.
[6] Högberg D, Hanson L, Bohlin R, Carlson JS. Creating and shaping the DHM tool IMMA for ergonomic product and production design. Int J Digital Human, 2016, 1, 132–152. https://doi.org/10.1504/IJDH.2016.077413.
[7] Brolin E, Högberg D, Hanson L, Örtengren R. Development and evaluation of an anthropometric module for digital human modelling systems. Int J Hum Factors Model Simul, 2019, 7, 47–70.
[8] Mårdberg P, Carlson JS, Bohlin R, Delfs N, Gustafsson S, Högberg D, et al. Using a formal high-level language and an automated manikin to automatically generate assembly instructions. Int J Hum Factors Model Simul, 2014, 4, 233–249. https://doi.org/10.1504/IJHFMS.2014.067180.
[9] McAtamney L, Nigel Corlett E. RULA: A survey method for the investigation of work-related upper limb disorders. Appl Ergon, 1993, 24, 91–99. https://doi.org/10.1016/0003-6870(93)90080-S.
[10] Karhu O, Kansi P, Kuorinka I. Correcting working postures in industry: A practical method for analysis. Appl Ergon, 1977, 8, 199–201. https://doi.org/10.1016/0003-6870(77)90164-8.
[11] Waters TR, Putz-Anderson V, Garg A, Fine LJ. Revised NIOSH equation for the design and evaluation of manual lifting tasks. Ergonomics, 1993, 36, 749–776. https://doi.org/10.1080/00140139308967940.
[12] Occhipinti E. OCRA: a concise index for the assessment of exposure to repetitive movements of the upper limbs. Ergonomics, 1998, 41, 1290–1311. https://doi.org/10.1080/001401398186315.
[13] Hignett S, McAtamney L. Rapid entire body assessment (REBA). Appl Ergon, 2000, 31, 201–205.
[14] David GC. Ergonomic methods for assessing exposure to risk factors for work-related musculoskeletal disorders. Occup Med, 2005, 55(3), 190–199. https://doi.org/10.1093/occmed/kqi082.
[15] Hansson G-Å, Balogh I, Ohlsson K, Granqvist L, Nordander C, Arvidsson I, et al. Physical workload in various types of work: Part I. Wrist and forearm. Int J Ind Ergon, 2009, 39, 221–233. https://doi.org/10.1016/j.ergon.2008.04.003.
[16] Robert-Lachaine X, Mecheri H, Larue C, Plamondon A. Validation of inertial measurement units with an optoelectronic system for whole-body motion analysis. Med Biol Eng Comput, 2017, 55, 609–619. https://doi.org/10.1007/s11517-016-1537-2.
[17] Vega-Barbas M, Diaz-Olivares JA, Lu K, Forsman M, Seoane F, Abtahi F. P-Ergonomics platform: Toward precise, pervasive, and personalized ergonomics using wearable sensors and edge computing. Sensors, 2019, 19. https://doi.org/10.3390/s19051225.
[18] Plantard P, Shum HPH, Le Pierres A-S, Multon F. Validation of an ergonomic assessment method using Kinect data in real workplace conditions. Appl Ergon, 2017, 65, 562–569. https://doi.org/10.1016/j.apergo.2016.10.015.
[19] Sandoval J, Laribi MA, Zeghloul S. Validation of an Ergonomic Contactless Master Device for a Teleoperation Platform. In: Berns K, Görges D, editors. Adv. Serv. Ind. Robot., Cham: Springer International Publishing; 2020, 421–429. https://doi.org/10.1007/978-3-030-19648-6_48.
[20] Butlewski M, Czernecka W, Pajzert A, Radziejewska M, Suszynski M, Feniser C. Ergonomic Criteria in the Optimization of Assembly Processes. In: Abrudan I, editor. Perform. Manag. Manag. Perform., Cluj-Napoca: Todesco Publishing House; 2018, 424–431.
[21] Berlin C, Kajaks T. Time-related ergonomics evaluation for DHMs: a literature review. Int J Hum Factors Model Simul, 2010, 1, 356–379. https://doi.org/10.1504/IJHFMS.2010.040271.
[22] Bortolini M, Faccio M, Gamberi M, Pilati F. Multi-objective assembly line balancing considering component picking and ergonomic risk. Comput Ind Eng, 2017, 112, 348–367. https://doi.org/10.1016/j.cie.2017.08.029.
[23] Ierusalimschy R. Programming in Lua. Lua.org; 2006.
[24] Hanson L, Högberg D, Carlson JS, Delfs N, Brolin E, Mårdberg P, et al. Chapter 11 - Industrial Path Solutions – Intelligently Moving Manikins. In: Scataglini S, Paul G, editors. DHM Posturography, Academic Press; 2019, 115–124. https://doi.org/10.1016/B978-0-12-816713-7.00011-8.
[25] Deb K, Pratap A, Agarwal S, Meyarivan T. A fast and elitist multiobjective genetic algorithm: NSGA-II. IEEE Trans Evol Comput, 2002, 6, 182–197. https://doi.org/10.1109/4235.996017.

DHM2020
L. Hanson et al. (Eds.)
© 2020 The authors and IOS Press.
This article is published online with Open Access by IOS Press and distributed under the terms of the Creative Commons Attribution Non-Commercial License 4.0 (CC BY-NC 4.0).
doi:10.3233/ATDE200045

Data-Based Parametric Biomechanical Models for Cyclic Motions

John RASMUSSEN [a,1], Morten Enemark LUND [b]
and Rasmus Plenge WAAGEPETERSEN [c]
[a] *Aalborg University, Department of Materials and Production, Fibigerstræde 16, 9220 Aalborg Ø, Denmark*
[b] *AnyBody Technology, Niels Jernes Vej 10, 9220 Aalborg Ø, Denmark*
[c] *Aalborg University, Department of Mathematical Sciences, Skjernvej 4A, 9220 Aalborg Ø, Denmark*

Abstract. We present a method to convert motion capture data and anthropometric statistics into parametric biomechanical models of cyclic motions, such as walking, cycling and running. The motivation is ease of modelling and the desire to make models prospective. We have developed a data processing pipeline, which pre-compiles a large amount of motion capture trials into a parametric model relying on the correlations between the input variables. The compilation converts optical motion capture data into anatomical joint angle variations and anatomical body dimensions. Finally, a quadratic programming method with a closed-form solution is developed to predict motion patterns meeting subject-specific requirements. The method is demonstrated on running models, and we conclude that the method can facilitate new uses of biomechanical models.

Keywords. Running, Anthropometry, Statistics, Principal Component Analysis

1. Introduction

One of the trends in biomechanics from the past two decades is individualization of model to specific subjects or patients. The importance of this topic was illustrated by the "Grand Challenge Competition to Predict in Vivo Knee Loads": a blinded conference competition to predict measured forces in knee implants [1]. Such carefully implemented subject-specific models typically require advanced medical imaging input to obtain correct geometries of internal anatomical structures. Despite recent advances in automatic processing of medical image data [2], this process tends to be cumbersome and not tractable for clinical workflows.

In terms of movement, such models typically require subject-specific motion capture data. The prior collection of motion data means that subject-specific models can only be retrospective, in the sense that they represent movements that happened in the past in a laboratory. This contradicts the purpose of many models, which is to predict what will happen if a prospective intervention is performed.

There are many applications of human models which do not require accurate representations of single individuals but rather statistical representations of populations;

[1] Corresponding Author, Email: jr@mp.aau.dk.

in terms of anthropometry, digital human models for ergonomics and product design have successfully relied on population statistics for decades [3].

While skilled and repetitive movements, such as walking, running and cycling, differ between people, they do seem to show more similarity than difference, and there may be notable connections between movement patterns and anthropometry. For instance, a positive correlation between leg length and step length seems plausible. Such correlations are important to recover, because they can potentially reduce the need for subject-specific model input and thereby facilitate the development of truly predictive models. The idea of investigating skilled movements based on many motion capture trials was pursued successfully in the HUMOSIM framework from the University of Michigan [4]. In this paper, we report on the development of a unified statistical model for anthropometry and movement patterns for cyclic motions exemplified by running.

2. Methods

Kinematics of a total of 285 treadmill running trials were collected from 80 subjects using an optical motion capture system (Qualisys AB, Gothenburg, Sweden). 180 trials were from male subjects, and 105 trials were from female subjects. The subjects were recreational and skilled runners. Informed consent was obtained, and the data were handled in accordance with the GDPR regulations. Statistical summaries are presented in Table 1.

Table 1. Summary of data of running trials.

Property	Mean	Standard deviation	Range
Velocity [km/h]	12.48	2.79	6-20
Subject age [years]	35.8	12.0	19-65
Body Mass [kg]	73.0	10.7	51-105
Stature [m]	1.77	0.0807	1.58-1.95

The marker trajectories were imported into the AnyBody Modelling System ver. 7.2 (AnyBody Technology, Aalborg, Denmark) [5] for the initial compilation. Using an algorithm for identification of model kinematics and segment parameters [6], each trial was converted into an individualized, full-body musculoskeletal model. The model comprises 67 anatomical segments and 52 anatomical joints with a total of 104 joint degrees-of-freedom. The variation of each joint degree-of-freedom over a typical running cycle was recovered from the model, and these time functions are parameterized with Fourier series truncated to 11 terms.

Each running trial is now represented by parameters, which are the Fourier coefficients for each degree-of-freedom, subject-specific segment lengths identified from the motion capture data, and meta data, such as gender, age, body weight, stature and running speed. This comprises a total of 1224 parameters from which each trial can be recreated. Parameters from all trials are collected into a standard-scaled matrix, $\mathbf{X}$, where each row represents a trial, and each column is a parameter. The matrix is subjected to principal component analysis (PCA):

$$\mathbf{y} = \mathbf{A}(\mathbf{x} - \boldsymbol{\mu}) \tag{1}$$

where **A** is the PCA transformation matrix, **x** is a set of running parameters, **μ** is the vector of mean values of **X**.

The orthonormal properties of **A** enable the opposite transformation:

$$\mathbf{x} = \mathbf{A}^{\mathbf{T}}\mathbf{y} + \boldsymbol{\mu} \tag{2}$$

The principal components can be ordered in terms of variance, thus offering an opportunity to investigate which generic features of the running style and anthropometry primarily distinguish runners from each other.

Performing PCA leads to a convenient parametric running model, because the components of **y**, unlike the primal parameters in **x**, are orthogonal and therefore can be varied independently to create new running patterns. The procedure is to select a set of transformed parameters, **y**, within a reasonable statistical range, transform them back to primal space, **x**, through (2), feed **x** back into the biomechanical simulation model and recreate the running style.

However, the transformed parameters, **y**, are linear combinations of **x** and may or may not lend themselves to physical interpretation. From a user's perspective, it would be more practical to be able to specify primal parameters, **x**, with a physical or physiological interpretation, for instance running speed, step length, leg length, gender or BMI. However, changing a single parameter in **x** is not immediately possible because the parameters in **x** are statistically correlated, i.e. changing a single primal parameter will lead to unrealistic combinations. To combine the benefits of the primal and transformed space, we formulate parameter identification as an optimization problem. We first observe that the average runner corresponds to **y** = **0**. Minimizing a weighted norm of **y** given one or more constraints on the primal parameters will therefore lead to a running pattern that is as probable as possible, given the constraints on primal variables:

Minimize

$$\mathbf{y}^{\boldsymbol{T}}\mathbf{C}^{-\mathbf{1}}\mathbf{y} \tag{3}$$

Subject to

$$x_j = f_j \text{ for } j \in \boldsymbol{J} \tag{4}$$

where **C** is a diagonal matrix of eigenvalues of **X**, f_j is a prescribed value of primal parameter x_j and ***J*** is the set of primal variables that are constrained. We express x_j in terms of **y** using (2) and obtain a quadratic optimization problem with linear constraints in the transformed variables:

Minimize

$$\mathbf{y}^{\boldsymbol{T}}\mathbf{C}^{-\mathbf{1}}\mathbf{y} \tag{5}$$

Subject to

$$\sum_i a_{ij} y_i + \mu_j = f_j \text{ for } j \in \boldsymbol{J} \tag{6}$$

where a_{ij} is the ij^{th} entry in **A.** Defining **B** as the subset of **A** corresponding to the indices $\boldsymbol{J}$, this mathematical program has a closed form solution:

$$\begin{bmatrix} \mathbf{C}^{-1} & \mathbf{B}^T \\ \mathbf{B} & \mathbf{0} \end{bmatrix} \begin{Bmatrix} \mathbf{y} \\ \boldsymbol{\lambda} \end{Bmatrix} = \begin{Bmatrix} \mathbf{0} \\ \boldsymbol{f} - \boldsymbol{\mu} \end{Bmatrix} \tag{7}$$

where $\boldsymbol{\lambda}$ is a vector of Lagrange multipliers corresponding to the constraints on primal parameters. Equation (7) makes it possible to specify constraints on primal parameters in the transformed, orthogonal space.

2.1. Software implementation

For the purpose of demonstration, the technology has been encapsulated into a demonstrator app, Runover, working as a front end to the AnyBody Modeling System. Runover is programmed in Python using the cross-platform user interface framework kivy [7], so it is theoretically deployable on mobile devices running Android or iOS. Runover collects user input, executes the biomechanical analysis, displays the running animation, and reports key figures for the running pattern biomechanics, for instance ground reaction forces, Achilles tendon forces or patella ligament forces.

3. Results

3.1. Data processing

The processed running trials show differences as well as similarities. Figure 1 illustrates these differences with selected joint angle variations resulting from the compilation process.

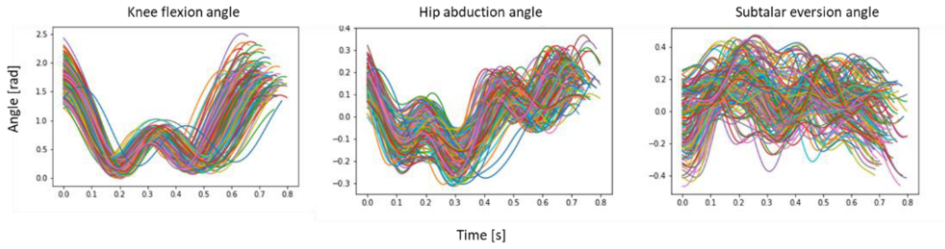

Figure 1. Populations of selected anatomical angles.

The explained variance from the principal components is illustrated in Figure 2, which shows that 40 principal components explain 90% of the total variance of the 1224 primal parameters. Although the figure is truncated after 40 parameters, PCA was not used to reduce the dimensionality of the system. There is no practical reason to do so since the PCA analysis is easily manageable on an ordinary desktop computer.

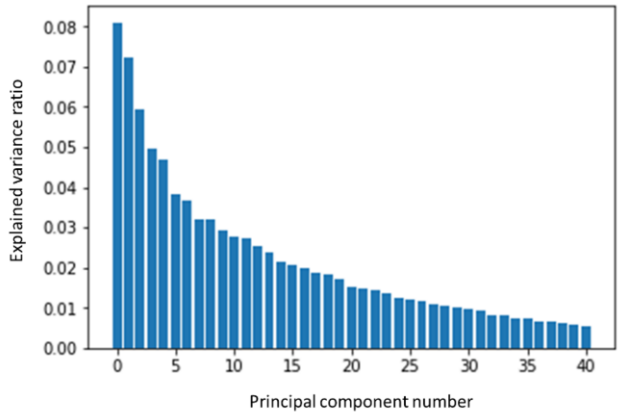

Figure 2. Explained variance ratio from the principal component analysis.

The average runner corresponding to the mean values listed in Table 1, and the runner's biomechanics output are depicted in Figure 3. Please notice that the computed parameters are slightly asymmetric because the runners compiled into the model were also asymmetric to some extent.

Figure 3. Average runner and computed biomechanical parameters.

3.2. Interpretation of principal components

Direct variation of each parameter in transformed space reveals, by visual inspection of the model animations, that the first principal component is primarily associated with running speed, while the second appears to be related mostly to the stature of the runner. Subsequent parameters are more difficult to interpret visually but seem to concentrate

their influence on movements of specific body regions: core movements for the third principal component, shoulder and arm movements for the fourth component and leg movements—specifically knee extension—for the fifth component.

3.3. Control of primal parameters

Any subset of the primal parameters, **x**, i.e. the 1224 parameters for each runner, can be specified as constraints in (6). Constraining the running speed to 6 and 30 km/h respectively for the otherwise average runner leads to the running styles depicted in Figure 4.

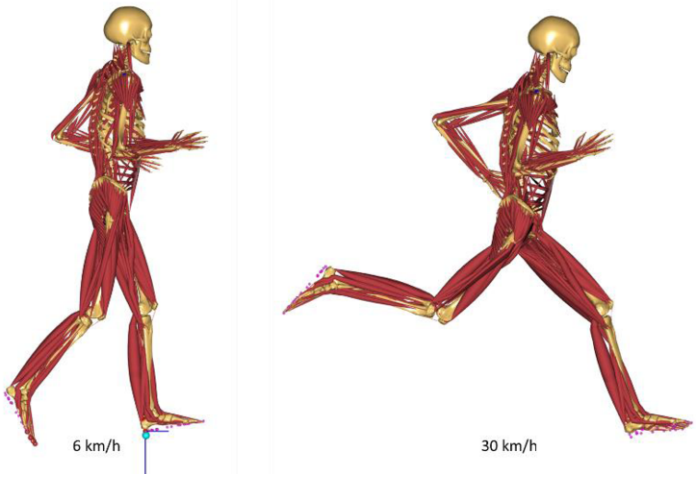

Figure 4. Synthesized running patterns for speeds of 6 km/h (left) and 30 km/h (right).

A debated issue in running biomechanics is whether forefoot running might entail biomechanical advantages with respect to running with heel strike [8]. During the processing of the statistical data, the angle of the foot with respect to the ground at foot strike is registered and stored as a primal parameter in **X**. It is therefore subsequently possible to constrain the foot strike angle along with the running speed as primal parameters and obtain models that are similar, except for the foot strike pattern. Such models running at 13 km/h are depicted in Figure 5, and their simulated biomechanical parameters are compared in Table 2. The peak ground reaction forces are, perhaps surprisingly, a bit higher for forefoot running, while the patella ligament force is reduced at the cost of increasing the Achilles tendon load. The running economy in terms of metabolism seems to be slightly better for the heel strike running pattern.

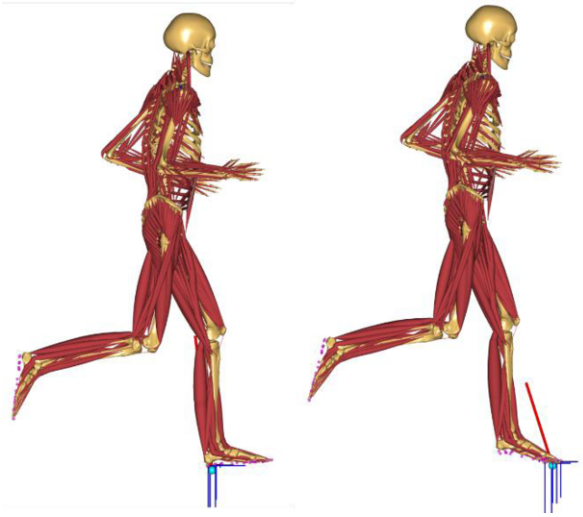

Figure 5. Synthesized running patterns for heel strike (left) and forefoot running (right) at 13 km/h.

Table 2. Simulated biomechanical parameters of heel strike and forefoot running at 13 km/h.

Property	Heel strike	Forefoot
Peak GRF [BW]	2.03	2.17
Peak patella lig. force [BW]	6.6	5.84
Peak Achilles tend. force [BW]	7.38	9.05
Metabolism [J/(kg km)]	3714.0	3858.0

4. Discussion

The proposed method can be regarded as a machine learning algorithm, which appears to be able to generate a statistical variation of plausible running models. The underlying PCA approach is not confined to normally distributed data, but the optimization problem formulation relies on an assumption of normality. It is certain that this condition is not fulfilled for all of the underlying data in the sense that male and female trials are mixed, and the gender variable is categorical. Other gender-dependent variables, such as anthropometrical dimensions, probably do not meet the criteria for normal distribution in their merged form.

Despite these reservations, the method seems to work well, even to the extent of producing surprisingly good results in some cases. The fastest speed in the empirical data is 20 km/h, but the model reproduces notable features of sprint running, such as high heel elevation in the forward swing, when the speed is extrapolated to sprint at 30 km/h as shown in Figure 4.

It is obvious that the validity of the synthetically generated running styles is inferior to recorded empirical data. However, for comparison of related but different conditions, the synthetic approach offers the advantage that selected parameters can be changed while keeping other parameters constant, which is rarely possible in empirical studies. While doing so, users should observe that the optimization problem in the interest of

orthogonality is formulated in the set of transformed parameters, **y**. The effect of this choice is that unconstrained primal variables will change during the solution of the optimization problem, so it is necessary to explicitly constrain the variables that must remain unchanged between conditions. This should also be done with caution, because constraining too many or unlikely combinations of primal variables can lead to improbable running patterns.

The method has the potential to facilitate the use of digital human models for prospective purposes because it allows for generation of anthropometry and motion with minimal subject-specific input. The method should be directly extensible to other cyclic motions, where walking will probably be the more important application.

Acknowledgement

The authors thank Kaiser Sport & Ortopædi A/S for cooperation on data collection. This work was supported by the Innovation Fund Denmark.

References

[1] Fregly BJ, Besier TF, Lloyd DG, Delp SL, Banks SA, Pandy MG, et al. Grand challenge competition to predict in vivo knee loads. J Orthop Res, 2012, 30(4), 503–513.
[2] Klein A, Warszawski J, Hillengaß J, Maier-Hein KH. Automatic bone segmentation in whole-body CT images. Int J Comput Assist Radiol Surg, 2019, 14(1), 21–29.
[3] Ulin SS, Armstrong TJ, Radwin RG. Use of computer aided drafting for analysis and control of posture in manual work. Appl Ergon, 1990, 21(2), 143–151.
[4] Reed MP, Faraway J, Chaffin DB, Martin BJ. The humosim ergonomics framework: A new approach to digital human simulation for ergonomic analysis. SAE Tech Pap, 2006.
[5] Damsgaard M, Rasmussen J, Christensen ST, Surma E, de Zee M. Analysis of musculoskeletal systems in the AnyBody Modeling System. Simul Model Pract Theory, 2006, 14(8).
[6] Andersen MS, Damsgaard M, MacWilliams B, Rasmussen J. A computationally efficient optimisation-based method for parameter identification of kinematically determinate and over-determinate biomechanical systems. Comput Methods Biomech Biomed Engin, 2010, 13(2).
[7] Ulloa R. Kivy: Interactive Applications in Python. cs_python_in. 2013. 138 p.
[8] Gruber AH, Boyer KA, Derrick TR, Hamill J. Impact shock frequency components and attenuation in rearfoot and forefoot running. J Sport Heal Sci, 2014, 3(2), 113–121.

DHM2020
L. Hanson et al. (Eds.)
© 2020 The authors and IOS Press.
This article is published online with Open Access by IOS Press and distributed under the terms of the Creative Commons Attribution Non-Commercial License 4.0 (CC BY-NC 4.0).
doi:10.3233/ATDE200046

Evaluation of Physical Workload Using Simulation Versus Motion Capturing Data for Biomechanical Models

Markus PETERS[1] and Sascha WISCHNIEWSKI
Federal Institute for Occupational Safety and Health (BAuA), 44149 Dortmund, Germany

Abstract. Throughout Europe, work-related musculoskeletal disorders (WRMSD) are still a major problem as they are most often associated with lower back pain or other physical complaints. In order to improve workplace safety and avoid WRMSD, it is therefore essential to analyse physical risk factors. Digital Human Models (DHM) can help to estimate ergonomic risks in working conditions. Traffic light schemes are commonly used to quantify the physical strain, while biomechanical loads are often neglected. The limitation of biomechanical models is, however, that they require motion data for their predictions. These data are time-consuming to capture and require camera-based or sensor-based methods. For this reason, a coupling between the "AnyBody Modeling System" and the "Editor for manual work activities" (ema) was developed to expand ergonomic evaluation with biomechanical parameters, without using motion capturing data. The findings indicate that the computer-generated motions of the interface rarely match real motions, therefore, the results of biomechanical loads have to be interpreted with caution. However, the coupling between AnyBody and ema allows to estimate the physical stress of specific activities. For a better understanding of physical workload another research approach is proposed taking kinematic and kinetic real-time data of workers into account to improve physical risk assessment in future.

Keywords. Ergonomics, Biomechanics, DHM, WRMSD, Inverse Dynamic, Risk Assessment

1. Introduction

Although the topic of work-related musculoskeletal disorders (WRMSD) has been frequently discussed in the last decades it is still up to date. Since the consequences of WRMSD are manifold as they result in substantially economic costs and impair the quality of life of the affected employees. About 60% of the workers in the EU-27 suffering from musculoskeletal complains, while shoulder, neck, upper limbs and lower back are often affected [1, 2]. Many of these diseases are linked to overexertion caused by manual material handling (MMH), which include unaided lifting, lowering, holding, carrying as well as pushing and pulling tasks. They result in high physical loads and can be indicators of an ergonomic risk. In this context, biomechanical loads can provide helpful information to estimate physical stress on the musculoskeletal system in working conditions. Compression forces of the lumbar spine, for example, are influencing factors

[1] Corresponding Author, Email: peters.markus@baua.bund.de.

considering lumbar diseases in occupational tasks [3-5]. In addition, high reaction forces in the shoulder girdle, caused by external loads, are also considered as risk factors [6-7] and may lead to permanent restrictions. Therefore, human-centered design of workplaces is essential to avoid WRMSD and maintain physical health of employees. In accordance with the Framework Directive [8], the employer is obliged by law to perform a risk assessment for reasonable working conditions.

Today a variety of tools, ranging from checklists to complex virtual simulations and real-time measurements, are available to estimate physical risk factors and improve work safety. The advantage of paper based risk assessment methods, e.g. Key Indicator Method (KIM) or Ergonomic Assessment Work-Sheet (EAWS), is that they do not require much preparation time. The disadvantage, however, is that biomechanical loads cannot be estimated with these approaches. The limitation of biomechanical models instead is that they require comprehensive data to run virtual simulations. The data acquisition e.g. with motion capturing is time consuming and less practical but the results provide more detailed information. With this in mind, an interface has been developed to exchange computer generated motion data of the Editor for manual work (ema) to run biomechanical analyses in the AnyBody modeling system without using motion capturing data. The main goal of the research project ema2AnyBody was to enrich ergonomic analysis with biomechanical parameters, on the one hand, and facilitating biomechanical analysis for physical risk assessment, on the other.

2. Method

A major challenge in exchanging data between Digital Human Models (DHM) are non-standardized protocols, concerning skeleton configurations and data file formats. This problem was frequently addressed in the literature [9-12]. Until today, for several reasons, no general recommendation is at hand. In the research project, the Biovision Hierarchical (BVH) file format was therefore used to exchange skeleton configurations, movements and forces between the ema and AnyBody model. These information are necessary to determine biomechanical joint load. To overcome the challenge of scaling a standardized DHM in ema and AnyBody was used, representing the 50th percentile male (body height) in Germany [13]. Another key issue is that computer generated movements, especially when forces are applied, do not change their movement strategies in an appropriate way. This can lead to problems during invers dynamic analysis as the movements become dynamically inconsistent. To prevent these problems the *over-determinate kinematics* algorithm [14] was used to optimize the movements before running invers dynamic calculations. More detailed information about the AnyBody model can be found here [15]. Furthermore, the optimization should additional contribute to a more realistic movement strategy. To ensure that the interface between ema and AnyBody provide reasonable data an investigation was performed taking kinematic data of subjects during MMH tasks into account. Kinematic data were used to run the same body model of the interface.

Nine healthy male subjects, stature 1.75 (0.04) m, 76 (9.1) kg, age 29 (5), participate in the study. Several MMH task had to be performed by each subject include lifting and lowering boxes as well as assembly activities with a drilling machine (Figure 1). Kinematic data were recorded using an inertial sensor based motion capturing suit (Perception Neuron). The weight of the boxes (5 kg, 10 kg, 15 kg) as well as the distance to the lifting object (0.4 m, 0.7 m) and lifting height (0.8 m, 1.1 m) was randomly

assigned. During the assembly activities the subjects had to apply a force of 50 and 100 Newton with the drilling machine in three different postures (below = b, neutral = n and above = a). To measure the forces the drilling machine was equipped with a one-component force sensor (ALMEMO®). For visualization of the force applied to the sensor, a tablet was installed at the working station. A Visual Analog Scale (VAS) was used to measure the perceived stress of the subjects on scale between 0 and 100. The study was conducted in 2019 under the supervision of the author and the approval of an ethics committee (No. 16.08.2018). A supervision was required to give the same movement instructions to all subjects. Furthermore, the IMU sensors of the motion capturing suit had to be attached on the same anatomical landmarks to reduce the measurement error.

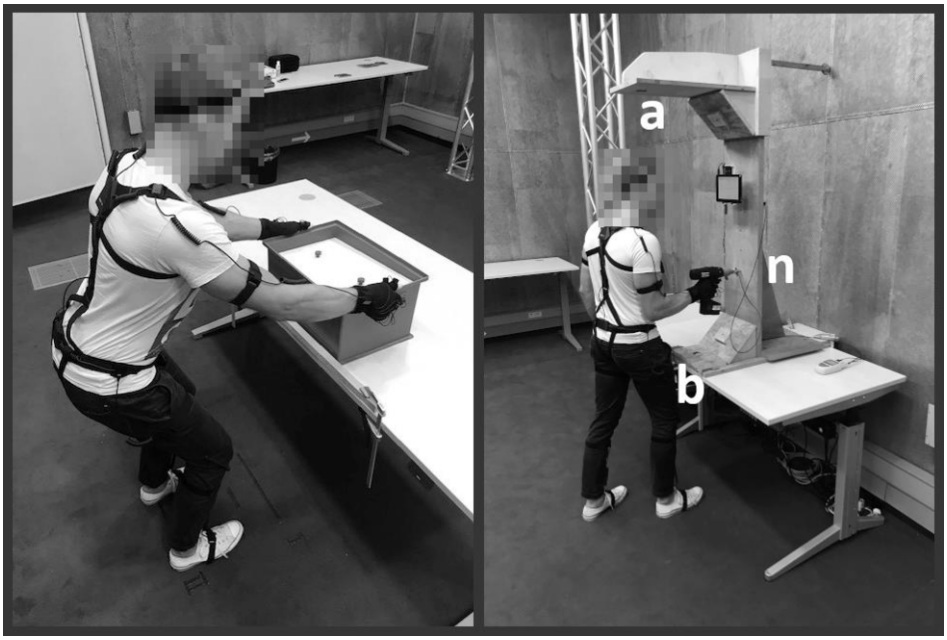

Figure 1. MMH task and assembly activity with a drilling machine in neutral posture.

The kinematic analysis during MMH tasks refer to the time when the boxes were lifted, and while assembly activities to that time period when force was applied to sensor. In the lifting process of MMH tasks subjects were not allow to change their standing position, while during the assembly actives, they could choose a preferred position. Data analyses and statistics were performed with Matlab (Mathworks, Natick, USA), SPSS (IBM Corp., Armonk, NY, USA), ema (imk automotive GmbH, Chemnitz, Germany) and AnyBody (AnyBody Technology, Aalborg, DK).

3. Results

Figure 2 shows angular trajectories of the elbow, shoulder and thorax in MMH task, where the subjects lifted a box of 5 kg with a distance of 0.4 m and lifting height of 0.8 m compared to the computer-generated results of the ema and the interface. Figure 3

reveals angular trajectories of subjects during assembly activity with a contact pressure of 50 N in body posture b. All kinematic results were time normalized. Figure 4 shows some results of the perceived stress of the subjects during lifting and assembly activities. Table 1 presents the maximum joint reaction forces calculated by the interface at the beginning of the lifting process. The shoulder moment (reported in Nm) and the compression force of the L4/L5 joint in N are listed. Table 2 is showing the mean joint reaction forces of the same joints during the assembly activities, calculated by the interface. Mean values were taken while reaction force of the drilling machine was applied. The stress of the shoulder joint and the compression forces of the lower back was of particular interest since they are often associated with WRMSD.

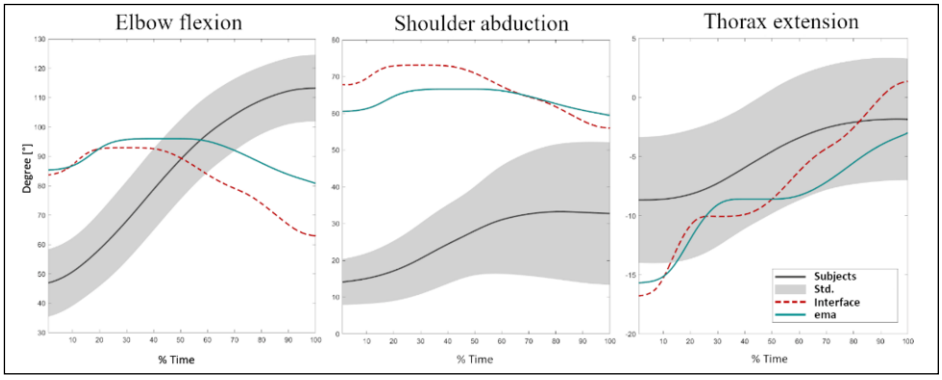

Figure 2. Angle trajectories of movement analyses in lifting condition 80_40_05.

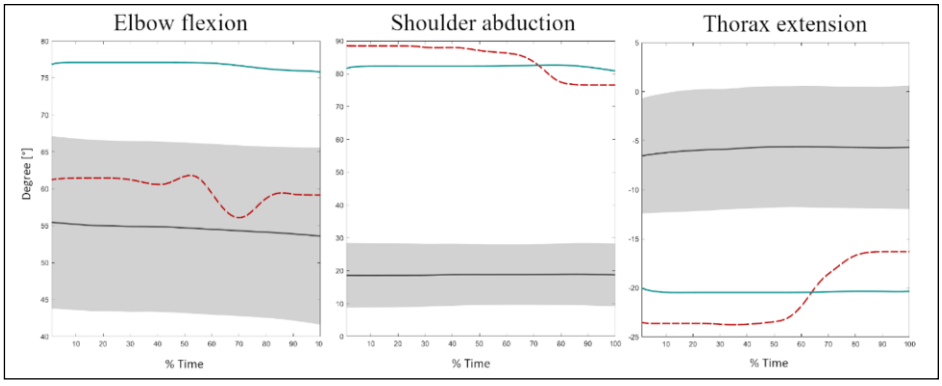

Figure 3. Angle trajectories of movement analyses during assembly activity b_50.

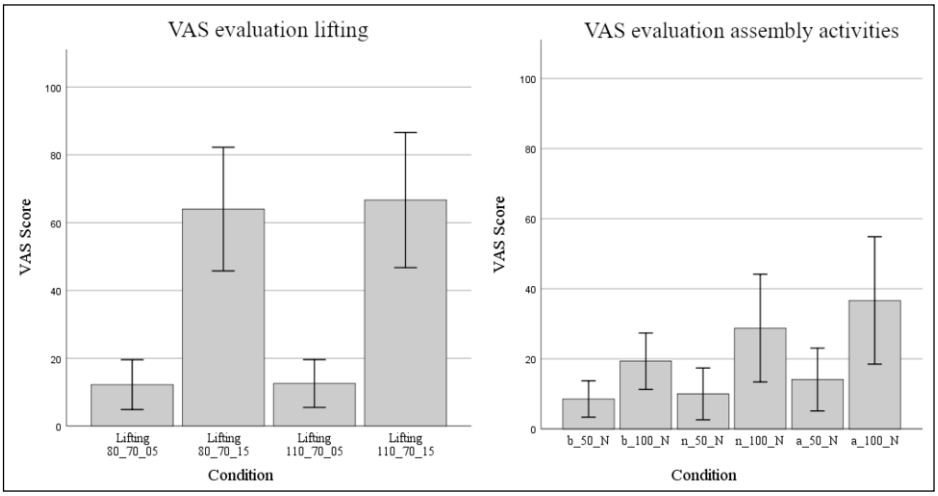

Figure 4. VAS evaluation of subjects.

Table 1. Maximum joint reaction forces of simulated lifting tasks with the interface.

Condition	Compression force L4/L5 [N]	Shoulder moment [Nm]
Lifting_80_70_05	2522	21.5
Lifting_80_70_15	4043	49.3
Lifting_110_70_05	1854	26.7
Lifting_110_70_15	3810	56.2

Table 2. Mean joint reaction forces of simulated assembly activities with the interface.

Condition	Compression force L4/L5 [N]	Shoulder moment [Nm]
b_50_N	525	11.8
n_50_N	911	19.8
a_50_N	1030	25.6
b_100_N	1311	36.5
n_100_N	1435	24.3
a_100_N	1644	41.9

4. Discussion and further steps

For the time being, the results show that an automated data exchange between an ergonomic and biomechanical DHM is possible. In this case, joint loads can be used to enrich ergonomic analysis with biomechanical parameters to provide a more detailed evaluation of workload. On the downside, however, the results indicate that computer-generated movements often differ significantly compared to the movements of the subjects. In some cases, the angle trajectories presented in figure 2 show even opposite directions (e.g. elbow flexion and shoulder abduction in lifting condition 80_40_05). These abnormalities could also be observed in other lifting conditions with short lifting distances. In contrast, the thorax extension show good agreement in all lifting conditions. As a first conclusion it can be summarized that the movement optimization of the interface do not necessarily provide more physiological movements, but is required to

run invers dynamic simulations with the computer-generated motion data of ema. Nevertheless, from a descriptive point of view the interface seems to provide in some cases angle trajectories that are closer to those of the subjects (e.g. elbow flexion during assembly activity b_50). However, these cases appear to be incidental, rather than a systematic improvement. It should be mentioned that the main goal of the research project was not the creation of computer-generated movement patterns that are close to human ones, but to establish a data exchange between the ema and the AnyBody modeling system. The perceived stress of the subjects show good agreement in almost all conditions compared to the joint reaction forces of the interface. However, it is noticeable that the joint compression force at L4/L5 during the assembly activity b_50_N is remarkably low, which may indicate limitations of the interface handling several restrictions at the same time. In this case, the reaction force of the drilling machine as well as dynamic inconsistencies that had to be solved may have led to the result. Particular care must be taken in the interpretation of shoulder moments. As already mentioned the shoulder and elbow joint showing substantial deviations between subjects and the interface, which hinders the interpretation of biomechanical loads. Also the intraindividual difference between subjects showing large deviations and complicate the evaluation. The standard deviation can be explained by individual movement strategies of the subjects and inaccuracies of the measurement system. For this reason, the significance of shoulder moment is limited. The huge variance between experimental and simulated joint angels is attributed to the fact that the artificial movement of ema is not affected by the load to be lifted. Thus, the shoulder abduction or elbow flexion undergoes only slight changes in almost all lifting conditions. Furthermore, there were greater differences in the anthropometry between both DHM concerning body segment lengths, as well as joint centers. The issues of posture prediction and coupling of DHM with biomechanical models have already been reported in literature [16, 17]. An approach to address this problem is a similar kinematic skeleton configuration to reduce the errors in the optimization process. This will help to better adapt the kinematics of both models and overcome scaling problems. For the dynamic interaction with the working environment, it is also possible to consider CAD models during the simulation with AnyBody [17].

Nevertheless, the results of compression forces of the lower spine in lifting conditions are more reliable, due to the minor deviation concerning the angular trajectories of the thorax. Accordingly, this biomechanical parameter can be considered as a reference in an ergonomic analysis. Several limitations have to be mentioned: Based on the small sample size, only potential benefits and no general statements can be highlighted. Furthermore, the IMU motion capturing suit, used in this study, does not necessarily provide accurate data, since the sensors can easily be affected by many environmental influences. Finally, the body model was not adjusted to the individual segment proportions of the subjects. Future research should take movement strategies in terms of ergonomics and plausibility into account when data are exchanged with biomechanical models. Since reliable biomechanical simulations can only be guaranteed if the movements correspond to physiological ones.

Due to several limitations mentioned above, biomechanical simulations with computer-generated movement data seems to be difficult at present. Therefore, a new research project was assigned to investigate the risk assessment of workers with a biomechanical model and real-time kinematic data. The aim of the project “Body Information on an Intelligent Chip” (BIONIC) is to develop smart working clothes with integrated IMU sensors to record kinematic data of workers during occupational tasks.

In addition, ground reaction forces are to be measured for a better estimation of physical workload. Based on the data collected, ergonomic risks factors should be identified to detect potentially hazardous body postures during work and to prevent WRMSD. The system is being developed for the ageing workforce but can also be used by others. Individual parameters are taken into account to achieve more accurate ergonomic risks. A challenge in the project will be to develop a system, which generates reliable data over a long period e.g. a working shift or at least several hours, to run biomechanical models. In contrast to the research approach presented in this paper, the focus is on precise movement data and a reduced biomechanical model complexity, which allows calculations in real-time. To evaluate the results of the Body Sensor Network (BSN), a further investigation is planned taking the accuracy of the body model into account, since IMU sensors a highly affected by environmental influences.

However, IMU systems with integrated ergonomic and biomechanical models seem to be of growing interest in occupational safety and health lately, as they offer potential new opportunities to facilitate risk assessment. One concern, though, is that the quality of automated ergonomic systems cannot replace the evaluation of an ergonomist and therefore potential risk factors may be overseen.

Acknowledgement

The Project BIONIC is receiving funding from the European Union's "Horizon 2020" research and innovation programme as part of grant agreement no. 826304. The research project "ema2AnyBody" was founded by the Federal Ministry for Economics Affairs and Energy on the basis of a decision by the German Parliament (Funding no. ZF4263601BZ6).

References

[1] Eurofound. Fifth European Working Conditions Survey. Luxemburg: Publications Office of the European Union, 2012.
[2] Eurostat, Labour Force Survey ad hoc module. Accidents at work and other work-related health problems. In: European Communities, 2013.
[3] Frymoyer JW, Pope MH, Clements JH, Wilder DG, Mac-Phearson B, Ashikaga T. Risk factors in low back pain. Journal of Bone and Joint Surgery, 1983, 65(2), 213-218.
[4] Kelsey JL, Githens PB, White AA, Holford TR, Walter SD, O'Connor T, Ostfeld AM, Weil U, Southwick WO, Calogero JA. An Epidemiologic Study of Lifting and Twisting on the Job and Risk for Acute Prolapsed Lumbar Intervertebral Disc. Journal of Orthopaedic Research, 1984, 2(1), 61-66.
[5] Swensson HO, Andersson GGJ. Low back pain in 40 to 47 year old man: work history and work environment factors. Spine, 1983, 8(3), 272-276.
[6] Wiker S, Chaffin DB, Langolf GD. Shoulder posture and localized muscle fatigue and discomfort. Ergonomics, 1989, 32(2), 211-237.
[7] Halsegrave C, Tracy M, Corlett E. Force exertion in awkward postures strength capability while twisting or work overhead. Ergonomics, 1997, 40(12), 1335-1362.
[8] 89/391/EEC, Council Directive of 12 June 1989 on the introduction of measures to encourage improvements in the safety and health of workers at work. The council of the European communities, 1989.
[9] Peters M, Wischniewski S, Paul G. DHM data exchange protocols. In: Scataglini S, Paul G, editors. DHM and Posturography. Academic Press, London, 2019, 663-670.
[10] Keyvani A, Lämkull D, Bolmsjö G, Örtengren R. Considerations for aggregation of motion-captured files in structured databases for DHM applications. Proceedings of the 2nd International Digital Human Modeling Symposium (DHM2013), 2013 June, Ann Arbor, USA.

[11] Bonin D, Wischniewski S, Wirsching H-J, Upmann A, Rausch J, Paul G. Exchanging data between Digital Human Modelling systems: a review of data formats. Proceedings of the 3rd International Digital Human Modeling Symposium (DHM2014), 2014 May, Tokyo, Japan.
[12] Paul G, Wischniewski S. Standardisation of digital human models. Ergonomics, 2012, 55(9), 1115-1118.
[13] DIN 33402-2:2005-12. Ergonomie - Körpermaße des Menschen - Teil 2: Werte. DIN Deutsches Institut für Normung e.v.
[14] Andersen MS, Damsgaard M, Rasmussen J. Kinematic analysis of over-determinate biomechanical systems. Computer methods in biomechanics biomedical engineering, 2009, 12(4), 371-384.
[15] Wolf A, Wartzack S. Parametric movement synthesis: towards virtual optimisation of man-machine interaction in engineering design. Proceedings of the DESIGN 2018 15th International Design Conference, 2018 May, Dubrovnik, Croatia, 941-952.
[16] Paul G, Lee WC. Interfacing Jack and AnyBody: Towards Anthropometric Musculoskeletal Digital Human Modeling. Proceedings of the 1st International Symposium on Digital Human Modeling (DHM2011), 2011 July, Lyon, France.
[17] Jung M, Damsgaard M, Andersen M, Rasmussen J. Integrating Biomechanical Manikins into a CAD Environment. Proceedings of the 2nd International Digital Human Modeling Symposium (DHM2013), 2013 June, Ann Arbor , USA.

DHM2020
L. Hanson et al. (Eds.)
© 2020 The authors and IOS Press.
This article is published online with Open Access by IOS Press and distributed under the terms of the Creative Commons Attribution Non-Commercial License 4.0 (CC BY-NC 4.0).
doi:10.3233/ATDE200047

The Use and Usage of Virtual Reality Technologies in Planning and Implementing New Workstations

René REINHARD [a,b,1], Peter MÅRDBERG [c], Francisco GARCÍA RIVERA [d], Tobias FORSBERG [e], Anton BERCE [f], Mingji FANG [f] and Dan HÖGBERG [d]
[a] *Fraunhofer-Institut für Techno- und Wirtschaftsmathematik ITWM, 67663 Kaiserslautern, Germany*
[b] *University of Kaiserslautern, Center for Cognitive Science, 67663 Kaiserslautern, Germany*
[c] *Fraunhofer-Chalmers Centre, 412 88 Gothenburg, Sweden*
[d] *University of Skövde, School of Engineering Science, 541 28 Skövde, Sweden*
[e] *Industrial Path Solutions AB, 412 58 Gothenburg, Sweden*
[f] *China-Europe Vehicle Technology CEVT, 417 55 Gothenburg, Sweden*

Abstract. Virtual reality (VR) technologies can support the planning and implementation of new workstations in various industry sectors, including in automotive assembly. Starting in the early planning stages, VR can help in identifying potential problems of new design ideas, e.g. through ergonomics analyses. Designers can then quickly change the virtual representations of new workstations to test solutions for the emerging difficulties. For this purpose, the actions and motions of prospective workers can be captured while they perform the work tasks in VR. The information can also be used as input for digital human modelling (DHM) tools, to instruct biomechanical human models. The DHM tools can then construct families of manikins that differ on anthropometric characteristics, like height, to simulate work processes. This paper addresses both existing technologies for gathering data on human actions and motions during VR usage and ways in which these data can be used to assist in designing new workstations. Here, a novel approach to translate a VR user's actions into instructions for DHM tools through an event-based instruction sampling method is presented. Further, the challenges for utilizing VR are discussed through an industrial use case of the manual assembly of flexible cables in an automotive context.

Keywords. Digital Human Modelling, Virtual Reality, Motion Tracking, Ergonomics, Assembly Path Generation, Automated Manikins, Flexible Cables, Automotive Assembly

1. Introduction

Virtual reality (VR) technologies find increasing application in many industrial settings, including automotive assembly, construction, or energy technologies [1]. This does not only include the assistance of product design through virtual prototypes [2] and VR-

[1] Corresponding Author, Email: rene.reinhard@itwm.fraunhofer.de.

based personnel training [3], but also the planning, evaluation, and optimization of assembly processes [4, 5]. For these purposes, VR technologies allow for the interaction with digital prototypes and with virtual representations of planned workstations even during the early planning stages [6]. Industrial case studies indicate the usefulness of VR assisted design of manufacturing workstations compared to design work with only a desktop computer set-up [7]. Thus, in the planning and design of workstations, VR can be used to generate feedback from relevant groups quickly and early in the process, leading to more rapid iterations without the need for costly physical prototypes.

On one hand, experts in subjects like ergonomics can experience and interact with the proposed workstations. Here, the virtual setups can further be used to visualize the results from path planning and digital human modelling (DHM) tools. Thus, the experts can assess the results of assembly simulations and the predicted human motions in an intuitive manner and help evaluate the feasibility, accessibility, and visibility during the installation of digital prototypes, and provide impressions for ergonomic analyses. The gained insights can then be used to adjust the digital work site, to further refine the assembly path and to add to or alter the constraints for the prediction of human motion in DHM tools.

On the other hand, members of the prospective workforce can perform the planned actions in VR while their motions are being tracked [8]. This allows for ergonomics evaluations that take individual characteristics of the workers, their specific restraints and abilities into account. But it also allows for the extraction of data from their tracked movements, which can in turn be used as input for DHM tools.

In this paper, we review currently available VR and tracking technology options and explore their usage in planning new and evaluating existing workstations. In this context, we present a novel event-based instruction sampling approach, in which the actions of VR users are tracked while they are interacting with the digital workstation. This is then used to create a simulation of the manufacturing task, where a digital manikin is instructed based on the actions the VR user performed. This makes it possible to evaluate ergonomics and to repeat the simulation using manikins with different anthropometrics than the original VR user. Moreover, this approach reduces the time needed to setup a DHM simulation and offers a more intuitive approach to construct simulations for non-expert users.

2. Capturing human motions and actions in VR

In order for a VR user to experience a virtual environment and interact with the virtual objects therein, both visualization and tracking technologies are required. In an industrial context, the most commonly utilized VR visualization approaches are projection-based systems and head-mounted displays (HMD) [1, 9]. Projection VR systems include single or multiple projector-based powerwalls, as well as surrounding, walk-in setups, based on multiple projection screens (e.g. Cave Automatic Virtual Environment (CAVE) or CAVE-like systems). However, the current paper focuses on HMD solutions, i.e. display devices which are affixed to the VR user's head and typically include one or two displays as the image source, as well as collimating optics between the eyes and the display.

These systems also typically include on-board inertial measurement units (IMUs) to track rotational movements of the head which are then translated into corresponding orientation changes in the virtual environment [10]. This can further be combined with methods that track the position of the HMD to allow for full 6-DoF movement. This

positional tracking usually uses accelerometer dead reckoning as its basis, which is combined with various additional tracking methods to correct the inertial measurement drift [11]. These methods may make use of external hardware, e.g. an external camera that detects infrared signals send from the HMD [12], or lighthouse tracking, where external base stations with stationary LED arrays and active spinning laser emitters send out LED flashes followed by laser sweeps, that are registered by photodiodes on the headset [11, 12]. The positional tracking can also be based on inside-out tracking methods, where cameras on the device estimate the motions of the camera itself relative to the environment they model based on the recorded input [13].

Besides head tracking, modern VR devices often integrate motion tracked handheld controllers, that are tracked and visualized in 3D space and also allow for abstract inputs via button presses [14]. Hereby, they also track the approximate spatial position of the hand holding the controller. Newer VR controller concepts also expand these capabilities with, as of yet, limited finger tracking based on sensors in the controller [15]. This already allows for the usage of some natural motions to interact with virtual objects, like grasping a virtual object by gripping the controller. Some motions, like a pinch grip, can, however, be hindered by the geometry of the controller in the user's hand. Finger tracking can be further extended by other hand and finger tracking technologies, like data gloves or optical tracking, which can translate more natural hand and finger motions into the virtual world. Some data gloves can also expand the feeling of touching virtual objects through tactile feedback, such as actuators on the glove that touch the hand across its surface, or through force feedback, i.e. mechanical forces applied to the finger tips to provide a resistance consistent with touching the object [16].

Lastly, body movements of workers at workstations can be captured. This can be relevant for a range of questions, focusing on topics from posture for ergonomics evaluations, upper body movements for capturing workers performing a task, to gait analyses for logistics analyses on a factory floor. The motion capture can be achieved by a wide variety of approaches: optoelectronic measurements, image processing systems, ultrasonic localization systems, and electromagnetic- or IMU-based systems [17]. Different motion capture systems may be more or less appropriate for certain use cases. As an example, optoelectronic measurements, i.e. active or passive marker-based tracking with usually fixed cameras, offer the most accurate tracking, but can be negatively impacted by obstructions to the line-of-sight or large distances from the cameras [17]. By contrast, IMU systems do not need additional external apparatus, are useful in a mobile context, and are capable of capturing highly dynamic motions, but also need additional information, e.g. from human rigid-body models, to actually offer positional data [17].

In industrial use cases, more elaborate tracking options have been established in the assessment of ergonomics. For example, Daria et al. [18] combined an IMU-based motion capture system connected to Siemens Jack with ErgoLog to perform ergonomics evaluations for workstation simulations. Similarly, Caputo et al. [19] also used an IMU-based motion capture system with Siemens Process Simulate to track posture, which, together with risk screening methods, was used as the basis for ergonomics evaluations.

But the tracked movements of VR users can also be useful for other use cases, e.g. VR-based training. Also, the usage of tracked motions as inputs for DHM tools should be mentioned. For example, Peruzzini et al. [20] used a Vicon optical motion capture system for posture tracking with a Delmia V5-6 for workstation digitalization. Here, they used Catia manikin digitalization and Haption RTI Delmia to connect the VR users' real movements to the virtual manikin's movements. Similarly, Garcia et al. [21] used IPS

VR with IPS IMMA manikins and Smart Textiles to track user movement. These applications in ergonomics evaluations and manikin instruction will be the focus of the following sections.

2.1. VR assisted ergonomics evaluations

The cost of work-related musculoskeletal disorders is considerable both for companies and for the afflicted workers [22]. This includes both direct costs, such as healthcare [23], and indirect losses, e.g. through reduced quality in the production [24]. Such disorders are also psychologically taxing for those who suffer them [25]. The combination of motion capture and VR can help in developing new methods to address these problems.

As the health risks are closely related to the posture of the workers while they perform their jobs, corrective approaches can target posture either via active or passive measures. In active corrections, the operators are informed that their posture is potentially harmful [26], while in passive correction, the workstation's design is improved to facilitate better posture [27]. In order to design workstations that minimize the workers' health risks, standardized ergonomics evaluation methods such as rapid upper limb assessment (RULA), rapid entire body assessment (REBA), or the Ovako working posture analysis system (OWAS) are being utilized [28]. To apply these standards, experts have to either simulate the workers' movements at the workstation using DHM tools, or to run tests by observing real life motions. Traditionally, this design process makes use of 2D screens and physical prototypes. Both approaches have advantages and disadvantages.

DHM tools can be used to economically test design ideas even during early phases of the process and thus spot and address potential problems early on, since they allow for rapid design changes to the workstation, to the performed task and to the anthropometric characteristics of the simulated workers. Yet, the DHMs need to be instructed, which requires expertise, time, and effort to come to representative results. Tests with physical prototypes make direct and easy observations of workers performing the tasks possible, but are also more costly and make changes to the workstation design more complicated. Physical tests will therefore often be used later in the design process.

By including VR in the design process, the designer can conduct studies of ergonomics earlier, without costly physical prototypes, and with the possibility of rapid changes. For this purpose, VR has often been combined with motion capturing technologies [18, 19]. The virtual environment also offers a high degree of control over the situation, including over factors like lighting and noise. However, the use of VR can also have drawbacks. The heavy emphasis on the sense of touch during assembly processes and the expectation of a physical resistance when interacting with virtual structures can often not be adequately simulated. Further, some people may feel less present in the virtual environment, or may even react adversely to VR usage, by developing motion sickness-like symptoms [29]. These individual reactions to VR can in turn impact task performance [29]. Consequently, the face validity of motions tracked in VR may not be as clearly established as it is for real life tests on prototypes. Still, VR can be especially useful for early tests of design ideas and to support the creation of simulations in DHM tools. In order for VR to assist in working with DHM tools, the information about the VR user's actions and motions have to be made usable within the tools. In the following, a new event-based instruction sampling approach is presented, to show how this can be achieved and what requirements it entails.

2.2. VR assisted ergonomics evaluations in DHM tools: An event-based instruction sampling approach

For VR to be of assistance in working with DHM tools, the relevant information from the VR session has to first be recorded and then translated into a form that can be utilized in later simulations. Here, we present a method that approaches this issue through the analysis of a VR user's actions at the virtual workstation, which results in instructions for a DHM tool that uses IPS IMMA [30]. This approach has several requirements, both for the used VR technology and for the DHM tool.

On the side of the adopted VR technology, information about the VR user's movements and interactions in the virtual space have to be captured. This can be realized even with the minimal tracking equipment provided by most current HMD-based VR options, namely the HMD itself and standard handheld VR controllers. While additional tracking information, e.g. from finger or full body tracking, could be gainfully employed, the following will not presuppose access to any additional VR or tracking technology beyond this typical setup, i.e. an HMD that is capable of both rotational and positional tracking and motion tracked VR controllers. On the side of the DHM tool, two functionalities are fundamental to this new method:

- An automated manikin that can interpret and automatically perform instructions with ergonomically sound postures and motions.
- An instruction language that can be mapped against the events in the VR session and that can be interpreted by digital manikins and other objects in the scene.

2.2.1. Automated manikins

A manikin in a DHM system can be said to be automated, if it is able to automatically perform an assembly operation. Thus, if instructed, it will perform a task automatically, without any additional help from the user of the DHM tool. Moreover, the task needs to be performed with ergonomically sound postures and motions which, for instance, need to consider the balance and weight of the manikin's body parts and of any carried objects [31, 32]. The simulation should also consider external forces and torques, while ensuring that the postures and motions are collision free with respect to both the manikin's body parts and the objects in the environment [31, 32].

2.2.2. Instruction language

The instruction language should not be limited to only manikins, since the manikin may interact with other objects in the simulation. All objects used in the simulation can be seen as actors that are performing a set of instructions. Such actors may include geometries, manikins, or mechanical structures, with each actor having its own set of instructions to execute. Thus, simulations with both manikins and other objects in the simulation can be created from the same instruction language [33, 34].

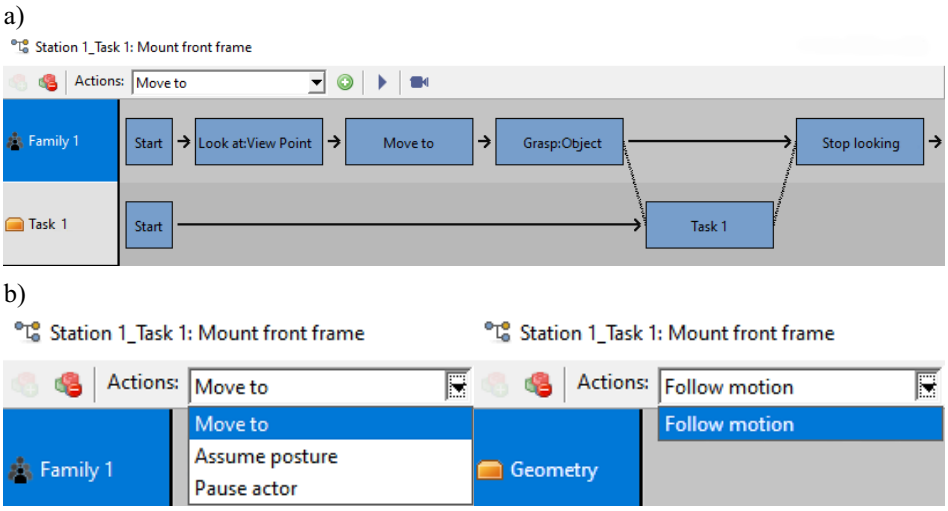

Figure 1. Example of events in the IPS instruction language. a) Interactions between the manikin and an object in the scene with which a task is performed. b) Examples of possible actions for a manikin and object.

The set of instructions that the actors may perform during a simulation should depend on the current state of the actor and on the objects in the simulation. For instance, if the manikin grasps an object with the right hand, then it is not possible for the manikin to grasp another object with the same hand unless the first object has been released [33, 34]. An example of such instructions in the IPS software is illustrated in Figure 1.

Moreover, each instruction must have a corresponding action event in the simulation. For instance, a *grasp* instruction may only be used if there is an object that is available for the manikin to take a hold of. Hence, properties of an object, such as grip, view, and attach points, also define the set of possible instructions for the actors.

Depending on the state of the manikin and on the objects in the environment, work tasks are translated to a sequence of low-level instructions in a controller structure [35]. By following the instruction sequence, a DHM tool like IPS automatically generates collision-free and ergonomically sound manikin motions that accomplish the assembly tasks [35].

2.2.3. Instruction of DHM manikins through event sampling actions in VR

To instruct the manikin, the presented approach uses a sampling procedure that considers all the events that occur while the VR user manipulates virtual objects with the controllers. Each manipulation corresponds to at least one sampled event. Such events may for example include the interaction when the user takes the virtual object, followed by the motion of the object while the VR user holds and moves it to another location. During the VR session, this interaction would correspond to the user pressing a button on the controller to hold the object, to moving it with the motion tracked controllers, and then to releasing the button to let go of the object.

In the presented method, the interaction events in the VR session are translated to the instruction language by mapping them to a fixed set of manikin actions. As an example, when the user is *taking* and *placing* an object, this is translated into corresponding actions of the instruction language, such as *grasp* and *release*. The IMMA manikin uses grip, view, and attach points to interact with objects in the environment. Predefined grip

points are automatically created when a VR controller is used to manipulate an object. Currently, a new predefined grip is created where the object is grasped as soon as the VR user takes hold of it.

Moreover, the movements of all objects that the VR user manipulates are also documented in IPS. As an example, during the VR session, the motions of a tracked controller are translated onto a gripped object. The resulting motions are logged and then movement trajectories are created accordingly. These trajectories can then be included in the simulation and correspond to a *follow* instruction in the instructional language. Since all events and trajectories are time stamped, it is possible to construct an instruction sequence for the manikin and all other objects used in the VR session. By following the resulting instruction sequence, a digital simulation of the VR session is created, where the user is represented by the manikin.

2.2.4. Discussion of an event-based instruction sampling approach

In the presented event-based instruction sampling approach, it is possible to capture the actions of VR users to quickly create simulations in a DHM tool, thereby lowering the expertise requirements of using these software options while allowing for their effective usage. In the resulting simulations, it is possible to change the anthropometric characteristics of the manikin and then repeat the simulation for different workers. IPS IMMA contains a built-in functionality to simulate an entire manikin family [36, 37]. Thus, this approach offers a straight forward and cost effective path to ergonomics evaluations of new workstation designs that consider workforce diversity through limited motion capture efforts in VR.

Still, there remain challenges to this approach. When a user picks up an object, a grip point is created. The currently automatically chosen grip type is similar to the way that one grasps the handheld controller, but this might not reflect the VR user's intentions. While grip types can be adjusted later in the DHM tool, this is an additional time demand. One approach to overcome this issue could be to let the user select a grip from a list of predefined grip types which is then automatically aligned, adjusted, and attached to the object. This would reduce the time that is later spend on adjusting the grips in the DHM software, but it also constitutes an action besides naturally interacting with the objects in VR and necessitates a certain degree of expertise to select the correct grip type. Another approach would be to use information from finger tracking technologies to automatically select a fitting grip type. With classical VR controllers, even with the newer models that try to estimate finger positions based on sensors on the controller, this can be a problem. Currently, these controllers can e.g. let VR users naturally grasp a spherical object in the palm of their hand, which corresponds to gripping the controller, but other grip types are not as intuitively translated into VR. In these cases, other finger tracking methods, like data gloves [16], could be useful. However, these options are more costly and come with higher initial time demands for equipping and calibrating the devices. New optical tracking options based on cameras in the HMD could also be useful, but they require a clear line-of-sight to the hand while performing the task, which may not always be possible.

The presented implementation could also be extended by motion tracking for body movements to include complex postural data and actions like squatting or kneeling in the instruction sequence. Future implementations will also focus on capturing interactions with complex objects, including collaborative robots and flexible cables.

Figure 2. An IPS VR user fastening a flexible cable with clips during an assembly task. Courtesy of CEVT.

2.3. Challenges for using VR in planning and implementing workstations exemplified by a use case from the automotive industry

The manual assembly of flexible cables is a common task in the automotive industry today. A corresponding industrial use case from the China Euro Vehicle Technology AB (CEVT) is illustrated in Figure 2. In this use case, the worker should assemble a cable from the floor to the roof of a car along its b-pillar. Here, the cables were fastened into particular places with clips, which are specifically designed for these circumstances. To assemble the cable, it needed to be unfolded, routed, and fastened in a certain order. All of this had to occur while the internal torques and forces of the cable, as well as the forces of the clips needed to be considered. An assembly of this type may also be performed in narrow regions and it may lead to uncomfortable postures for the assembly worker.

As shown in Figure 2, the assembly can be performed by a VR user who guides a manikin to assemble each of the clips along the pillar. The cable can be realistically fastened to the car by stepwise changing the boundary conditions of the cable during the simulation, i.e. by adding constrains to the clips on the cable. This example showcases many of the challenges that VR can encounter when it is applied to complex industrial use cases. To work with the clips, the manikin was instructed to utilize a pinch grip, which did not correspond to the VR users grip on the controller. Further, the assembly occurred at the b-pillar of a car and the VR users would have both expected its resistance when affixing the clips and may have wished to lean on the structure during the assembly. While VR users can be shown a visual impression of their avatar leaning on a virtual object, they themselves are not provided with its physical support. Even current haptic feedback options cannot accurately let the VR users touch and interact with such virtual structures, especially for demanding actions like bodily leaning against them. In addition, the work task required physically correct behavior from the flexible cable in real time at a high frame rate, which, while possible in IPS's VR implementation, can become performance intensive. While some of these challenges can be conquered with new advances in DHM and VR software, as well as with tracking-related hardware, complex bodily interactions with virtual structures can likely only be approached by the introduction of real life elements, like a b-pillar replica in a mixed-reality setup.

3. Conclusion

VR offers many potential benefits for the planning, design, and implementation of new workstations. It can allow for ergonomic assessments even early in the planning phases and, through new methods like the presented event-based instruction sampling approach, VR can also support the work in DHM-related software. The usage of VR does, however, also come with challenges that should be considered. VR can especially be of help in rooting out potential problems early in the design process, while during later stages real life prototype tests and ergonomics assessments may still have clear advantages in some complex use cases.

Acknowledgements

This work has been made possible with support from the Swedish Governmental Agency for Innovation Systems (VINNOVA) within the VIVA and SUMMIT projects, and the Knowledge Foundation within the Synergy Virtual Ergonomics (SVE) project, and the Eurostar project ED-VIMA (E!113330) supported by VINNOVA under the grant number (2019-03534), as well as by the participating organizations. It is also part of the Sustainable Production Initiative and the Production Area of Advance at Chalmers University of Technology. This support is gratefully acknowledged.

References

[1] Berg LP, Vance JM. Industry use of virtual reality in product design and manufacturing: a survey. Virtual Reality, 2017, 21, 1–17.
[2] Wolfartsberger J. Analyzing the potential of Virtual Reality for engineering design review. Automation in Construction, 2019, 104, 27–37.
[3] Gorecky D, Khamis M, Mura K. Introduction and establishment of virtual training in the factory of the future. International Journal of Computer Integrated Manufacturing, 2017, 30, 182–190.
[4] Maropoulos PG, Ceglarek D. Design verification and validation in product lifecycle. CIRP Annals, 2010, 59, 740–759.
[5] Abidi MH, Ahmad A, Darmoul S, Al-Ahmari AM. Haptics Assisted Virtual Assembly. IFAC-PapersOnLine, 2015, 48, 100–105.
[6] Pontonnier C, Dumont G, Samani A, Madeleine P, Badawi M. Designing and evaluating a workstation in real and virtual environment: toward virtual reality based ergonomic design sessions. Journal on Multimodal User Interfaces, 2014, 8, 199–208.
[7] Peruzzini M, Pellicciari M, Gadaleta M. A comparative study on computer-integrated set-ups to design manufacturing systems. Robotics and Computer-Integrated Manufacturing, 2019, 55, 265–278.
[8] Grajewski D, Górski F, Zawadzki P, Hamrol A. Application of Virtual Reality techniques in design of ergonomic manufacturing workplaces. Procedia Computer Science, 2013, 25, 289–301.
[9] Liagkou V, Salmas D, Stylios C. Realizing Virtual Reality learning environment for Industry 4.0. Procedia CIRP, 2019, 79, 712–717.
[10] Desai PR, Desai PN, Ajmera KD, Mehta K. A review paper on Oculus Rift: A Virtual Reality headset. International Journal of Engineering Trends and Technology, 2014, 13, 175–179.
[11] Niehorster DC, Li L, Lappe M. The Accuracy and precision of position and orientation tracking in the HTC Vive Virtual Reality system for scientific research. Iperception, 2017, 8, 2041669517708205.
[12] Borrego A, Latorre J, Alcañiz M, Llorens R. Comparison of Oculus Rift and HTC Vive: Feasibility for Virtual Reality-based exploration, navigation, exergaming, and rehabilitation. Games for Health Journal, 2018, 7, 151–156.
[13] Gourlay MJ, Held RT. Head-Mounted-Display tracking for Augmented and Virtual Reality. Information Display, 2017, 33, 6–10.
[14] Reski N, Alissandrakis A. Open data exploration in Virtual Reality: A comparative study of input technology. Virtual Reality, 2020, 24, 1–22.

[15] Arimatsu K, Mori H. Evaluation of machine learning techniques for hand pose estimation on handheld device with proximity sensor. In: CHI Conference on Human Factors in Computing Systems, 2020, New York, USA, 1–13.
[16] Perret J, Poorten EV. Touching Virtual Reality: A review of haptic gloves. In: Borgmann H, editor. ACTUATOR 2018: 16th International Conference on New Actuators, 2018, Bremen, Germany, 1–5.
[17] van der Kruk E, Reijne MM. Accuracy of human motion capture systems for sport applications: State-of-the-art review. European Journal of Sport Science, 2018, 18, 806–819.
[18] Daria B, Martina C, Alessandro P, Fabio S, Valentina V, Zennaro I. Integrating mocap system and immersive reality for efficient human-centred workstation design. IFAC-PapersOnLine, 2018, 51,188-193.
[19] Caputo F, Greco A, d'Amato E, Notaro I, Spada S. A preventive ergonomic approach based on virtual and immersive reality. In: Rebelo F, Soares M, editors. Advances in Ergonomics in Design, Springer International Publishing, Cham, Switzerland, 2018, 3–15.
[20] Peruzzini M, Carassai S, Pellicciari M. The benefits of human-centred design in industrial practices: Re-design of workstations in pipe industry. Procedia Manufacturing, 2017, 11, 1247–1254.
[21] García Rivera F, Brolin E, Syberfeldt A, Högberg D, Iriondo Pascual A, Perez Luque E. Using Virtual Reality and smart textiles to assess the design of workstations. In: Proceedings of the 9th Swedish Production Symposium (SPS2020), 2020, Oct 6-9, Jönköping, Sweden.
[22] Bhattacharya A. Costs of occupational musculoskeletal disorders (MSDs) in the United States. International Journal of Industrial Ergonomics, 2014, 44, 448–454.
[23] Ramos DG, Arezes PM, Afonso P. Analysis of the return on preventive measures in musculoskeletal disorders through the benefit-cost ratio: A case study in a hospital. International Journal of Industrial Ergonomics, 2017, 60, 14–25.
[24] Falck A-C, Rosenqvist M. A model for calculation of the costs of poor assembly ergonomics (part 1). International Journal of Industrial Ergonomics, 2014, 44, 140–147.
[25] Jose JA. Outcome measures and prognosis of WRMSD. Work, 2012, 41 Suppl 1, 4848–4849.
[26] Mahdavian N, Lind CM, Diaz-Olivares J, Pascual A, Högberg D, Brolin E, et al. Effect of giving feedback on postural working techniques. In: Advances in transdisciplinary engineering, 2018, 247-252.
[27] Shikdar AA, Al-Hadhrami MA. Smart workstation design: An ergonomics and methods engineering approach. International Journal of Industrial and Systems Engineering, 2005, 2, 363–374.
[28] David GC. Ergonomic methods for assessing exposure to risk factors for work-related musculoskeletal disorders. Occupational Medicine, 2005, 55, 190–199.
[29] Weech S, Kenny S, Barnett-Cowan M. Presence and cybersickness in Virtual Reality are negatively related: A review. Frontiers in Psychology, 2019, 10, 158.
[30] Högberg D, Hanson L, Bohlin R, Carlson JS. Creating and shaping the DHM tool IMMA for ergonomic product and production design. International Journal of the Digital Human, 2016, 1, 132–152.
[31] Bohlin R, Delfs N, Hanson L, Högberg D, Carlson JS. Automatic creation of virtual manikin motions maximizing comfort in manual assembly processes. In: Hu SJ, editor. 4th CIRP Conference on Assembly Technologies and Systems, 2012, Ann Arbor, USA, 209–212.
[32] Delfs N, Bohlin R, Hanson L, Högberg D, Carlson J. Introducing stability of forces to the automatic creation of digital human postures. In: 2nd International Digital Human Modeling Symposium (DHM2013), 2013.
[33] Mårdberg P, Carlson JS, Bohlin R, Delfs N, Gustavsson S, Keyvani A, Hanson L. Introducing a formal high-level language for instructing automated manikins. In: 2nd International Digital Human Modeling Symposium (DHM2013), 2013.
[34] Mårdberg P, Carlson JS, Bohlin R, Delfs N, Gustafsson S, Hanson L. Using a formal high-level language to instruct manikins to assemble cables. Procedia CIRP, 2014, 23, 29–34.
[35] Mårdberg P, Yan Y, Bohlin R, Delfs N, Gustafsson S, Carlson JS. Controller hierarchies for efficient virtual ergonomic assessments of manual assembly sequences. Procedia CIRP, 2016, 44, 435–440.
[36] Hanson L, Högberg D, Carlson JS, Delfs N, Brolin E, Mårdberg P, et al. Chapter 11 - Industrial Path Solutions – Intelligently Moving Manikins. In: Scataglini S, Paul G, editors. DHM and posturography: Academic Press, Cambridge, 2019, 115–124.
[37] Brolin E. Anthropometric diversity and consideration of human capabilities: Methods for virtual product and production development [PhD Thesis]. Göteborg: Chalmers University of Technology, 2016.

DHM2020
L. Hanson et al. (Eds.)
© 2020 The authors and IOS Press.
This article is published online with Open Access by IOS Press and distributed under the terms of the Creative Commons Attribution Non-Commercial License 4.0 (CC BY-NC 4.0).
doi:10.3233/ATDE200048

Digital Human Modeling as a Risk Assessment Tool for Maritime Workers

Sander ZELCK [a,1], Stijn VERWULGEN [a], Lenie DENTENEER [b] and Sofia SCATAGLINI [a,c]

[a] *Department of Product Development, Faculty of Design Sciences, University of Antwerp, Antwerp, Belgium*
[b] *Department of Rehabilitation Sciences and Physiotherapy, Faculty of Medicine and Health Sciences, University of Antwerp, Antwerp, Belgium*
[c] *Military Hospital Queen Astrid, 1120 Brussels, Belgium*

Abstract. Safeguarding the health of dockworkers in maritime transportation represents a high priority with employer's organizations within the port facilities and maritime organizations. Riggers responsible for container lashing secure a high amount of containers on the ship while working with heavy equipment on a tight schedule and therefore risking musculoskeletal disorders. In addition there is a gap discovered between the learned practices at the training facility and the behavior applied on the work floor. As a result it is necessary to provide a risk assessment tool for maritime workers. Firstly, non-intrusive motion capture method can be used to map their posture and movements with the possibility to emphasize on causing factors of repetitive strain injuries. Secondly, a DHM representing the rigger in maritime environment is created in Blender. Finally, an inertial mocap system is used to monitor kinematic lashing movements and to create a musculoskeletal model. The output can be used to create a framework for future observations with focus on developing a product-service-system (PSS) and smart personal protective equipment (PPE) tools.

Keywords. Wearable Motion Capture Inertial System, Product-Service-System (PSS), Digital Human Modeling, Marine (transportation), Occupational Repetitive Actions (OCRA), Health Monitoring, Marine Workers

1. Introduction

1.1 Background

Dockworkers or stevedores are indispensable in lashing and de-lashing of containers that enter the ports facilities and use a lashing technique conform with the learned craftsmanship respecting the safety measurements and prevailing legislation [1]. Container lashing is one of the high-risk professions in marine cargo [2]. Hence dockworkers responsible for container lashing (riggers) in the harbor of Antwerp can suffer from upper body chronic pains (neck, low back…). Due to continuous involvement of these body parts in lashing and de-lashing operations, the combination

[1] Corresponding Author, Email: sander.zelck@uantwerpen.be.

of a bad posture and incorrect applying force onto the turnbuckle, the risk of musculoskeletal disorders can be increased [2].

Prevention and training play a role in the risk assessment of musculoskeletal disorders in maritime workers. In fact, in Antwerp (Belgium), Cepa (employer's organization) and Ocha (port labor training center) are investing resources for training and prevention, are donating a dedicated training course of lifting techniques and ergonomic behavior to correctly lash containers[3–6].

1.2 Lashing and de-lashing technique

Container lashing is divided into two activities: lashing and de-lashing of containers. A container lashing consists of a turnbuckle and a lashing bar. Within these two domains, riggers work with small and big lashing bars. Small bars are used to constrain containers to the deck of the ship and have a length of 2,5 meters and weight of 11,9 kilograms [7]. The big lashing bars are used for securing containers with the already lashed containers underneath them with a length of 5 meters and weight of 21,1 kilograms [7]. A turnbuckle connects the lashing bar with the deck of the ship while adjusting also the tension on the lashing turnbuckles that have an approximate weight of 12,2 kilograms [8]. Container lashing crews are advised to work in pairs. One rigger (rigger1) raises the lashing bar and locks the top hook in place on the container. While the second rigger (rigger2) is in charge of securing the turnbuckle at the deck of the ship. Both riggers walk towards each other to connect the lashing bar with the turnbuckle (Figure1).

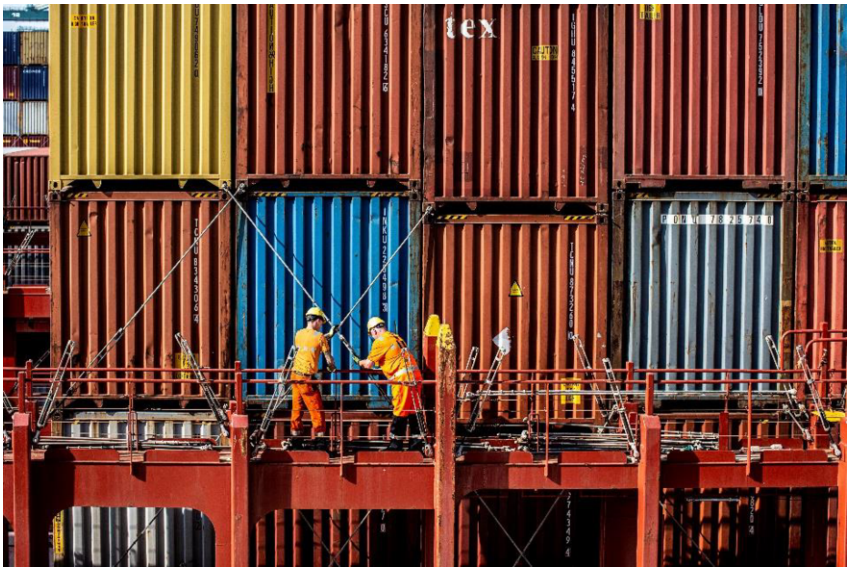

Figure 1. Lashing and de-lashing in Antwerp port (photo courtesy of Cepa).

Rigger 1 is in charge of locking the screw pin shackle from the turnbuckle in the lashing eye connected to the deck of the ship. While rigger 2 holds both items in place, rigger 1 fastens the turnbuckle, using first his hands to tighten and afterwards a fastening tool, which can be a metal bar or a dedicated tool [3–6].

1.3 Aim of the preliminary study

This study seeks to build an identification tool for incorrect behavior shown in previous interviews using motion capture analysis in combination with risk assessment tools. In order to fully understand this abnormal behavior, observations of the current work ethics and methods are required. To that end, a structured observation protocol to monitor container lashing crew and their behavior using at non-intrusive method is presented in this paper.

2. Methods

The validated observational method for motion capturing consists of video-cameras mounted in the environment port. But this method is intrusive because the participants feel observed and as a consequence react to correct their gestures and thus distorting the resulting data [9]. Inertial measurement units (IMU) allow to increase the detail in observational results in comparison with the markerless system available and therefore provide profound observational data [10]. As the usable surface to operate while observing riggers on a ship is very small [1], implementing an IMU in this environment would increase the efficiency of the observation.

2.1. *The Lashing and de-lashing gestures classification*

Using video footage of container lashing, the portrayed movements are classified in 4 different activities divided in gestures made to fulfil the task:

1) lashing with a small lashing bar;
2) de-lashing with a small lashing bar;
3) lashing with a big lashing bar;
4) de-lashing with a big lashing bar.

1) The first activity, lashing with a small lashing bar, consists of the following gestures:
   A. bending forward to reach the lashing bar or the turnbuckle;
   B. leaning forward to tighten the turnbuckle;
   C. leaning forward while having arms stretched out horizontal by before torso to fasten the turnbuckle with a fastening tool;
   D. straighten the posture to rest or reposition the movement;
   E. while in a straight posture raising the arms vertically above the body to lock lashing bar into place.
2) The second activity is lashing containers with big lashing bars. This operation was divided into the following gestures: All the above (A,B,C,D and E) including F.
   F. squatting, holding a straight posture to lift the lashing bar, locking it into place.
3) De-lashing with a small lashing bar is the third activity. The consecutive gestures are:
   A. bending forward to lay the lashing bar or the turnbuckle on the ground or to release the turnbuckle from the lashing eye;
   B. leaning forward to loosen the turnbuckle and to disconnect the turnbuckle from the lashing bar;
   C. leaning forward while having arms stretched out horizontal by before torso to loosen the turnbuckle with tool if necessary;

D. straighten the posture to rest or reposition the movement;
E. while in a straight posture raising the arms vertically above the body to unlock the lashing bar from container.

4) The last activity is described as de-lashing with a big lashing bar. This activity was also divided into smaller gestures: All the above (A,B,C,D and E)

2.2. *Motion capturing*

A test subject performed five repetitions of the four activities that represented lashing and de-lashing in a simulated environment. The test was segmented into two focusses: in the first one the test subject performed the gestures as accurately as possible while the second focus relies on mimicking the gestures from the lashing video footage as accurately as possible. Every activity was performed five times followed by a rest in the N-pose for five seconds between each activity. These gestures were recorded using a wearable motion capturing system called Xsens (MVN Awinda, The Netherlands) [11], and reconstructed in Blender [12].

The emphasis of this test laid on translating the range of motion of the riggers into a Digital Human Model (DHM) representation of the dockworkers gestures while lashing containers. In addition, the kinematics of the dockworkers gestures were also analyzed.

2.3. *DHM for container lashing crews*

A dedicate DHM was created in MakeHuman [13] and imported as COLLADA (.dae) in Blender [12]. Successively the subject was captured during lashing and de-lashing simulation gestures using the mocap system [11] and exported as BVH file [14]. Using the parenting and retargeting tool in Blender it was possible to transfer the motion of the test subject into the human base mesh model [15].

2.4. *Dedicated PSS to visualize potential injuries and its potential origin*

For better understanding of the presented injuries within a maritime environment, a broader observational system should be designed. As validated ergonomic assessment tools rely on empiric manual input [16], an utilization of kinematic data from IMU [11] has the possibility to decrease the margin of error and increase efficiency. Explorative research indicates that PPS implementation in health care is quite novel and therefore provides great potential [17]. In advance of conducting observations a dedicated protocol should be designed. This protocol will prelude as fundament for further iterations of the PSS [18]. Where Bortolini M, et.al. [19] concentrates on implementing kinematic data for higher accuracy and efficiency, our protocol should also focus on transparent communication to the participant and therefore enrich their perspective on injury prevention.

Results from Blender and a mocap system [11] will be combined to visualize problems in a simplified manner and have the ability to train the correct movements without constant supervision of a rehabilitation specialist. The kinematic data retrieved from the IMU [11] was utilized as input data for validated ergonomic risk-assessment tools [19,20]. A 3D model of the dockworker can be integrated with the information of the Anybody software [21] for musculoskeletal modelling simulation giving a predictive vision of the executed gestures from riggers preventing injury and preserving their performances.

3. Results

3.1. *DHM proposal for riggers*

The subject was wearing a full mocap system while performing in a simulated environment as shown in Figure 2 (on the left). Successively, the BVH was imported into Blender and used for rigging the mesh representing the movements performed by a rigger (Figure 2, on the right). A texture was made to embody the rigger's equipment (Figure 3). Containers were created in Blender as OBJ file into Blender to reproduce the digital human system interaction and integration in a virtual environment as in Figure 4. Finally, a virtual or a real scene was added as background (Figure 5).

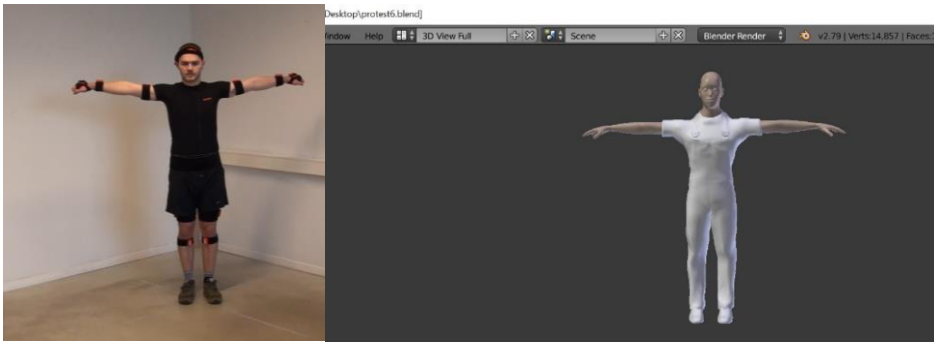

Figure 2. Acquisition of the subject using a mocap system in a real environment (left) and DHM created in Blender (right).

Figure 3. Rigging in Blender.

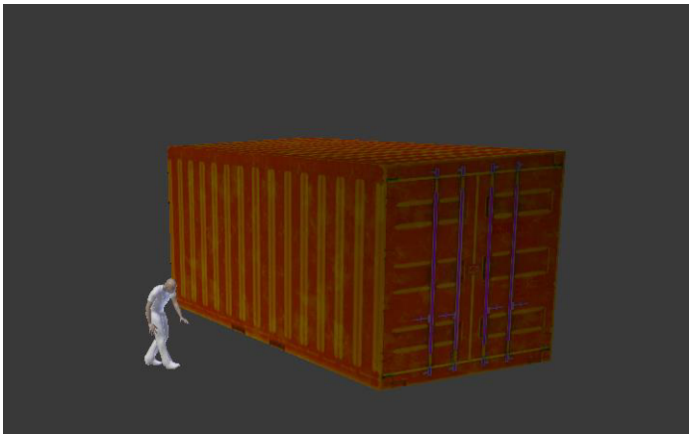

Figure 4. DHM of the stevedores and recreation of a container in Blender.

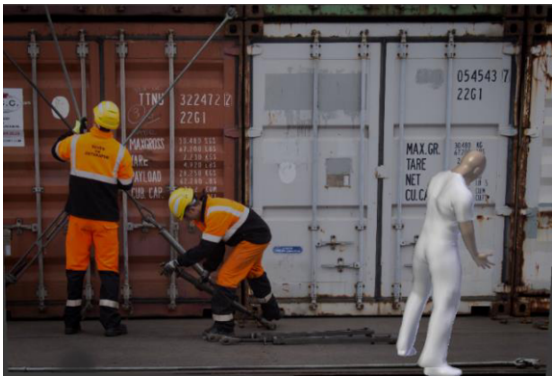

Figure 5. DHM into a real scene.

3.2. *PSS as tool in maritime workplace*

Within the current business environment the ability to reinforce existing business models with the integration of PSS, the focus shifts towards smart PSS [22]. With the presented product-service-system, the emphasis lays on creating a learning system. Focusing on digital resource driven value the PSS has the ability to create a monitorial structure [23]. Clarifying incoming kinematic data and outputting ergonomic suggestions, employer's organization have a risk assessment and training tool for study and improving worker 'safety and well-being, workplace design reducing injuries without affecting their performances. Indeed, the combination of Kinematics, Kinetics and Dynamic data could also constitute a computationally efficient posture and motion prediction of the worker (Figure 6). As a result, the PSS will constitute a valid follow-up for ergonomist, rehabilitation specialist and designer of dockworker system integration and interaction for designing new products, environments, systems and services for improving the quality of work-life of the dockworkers.

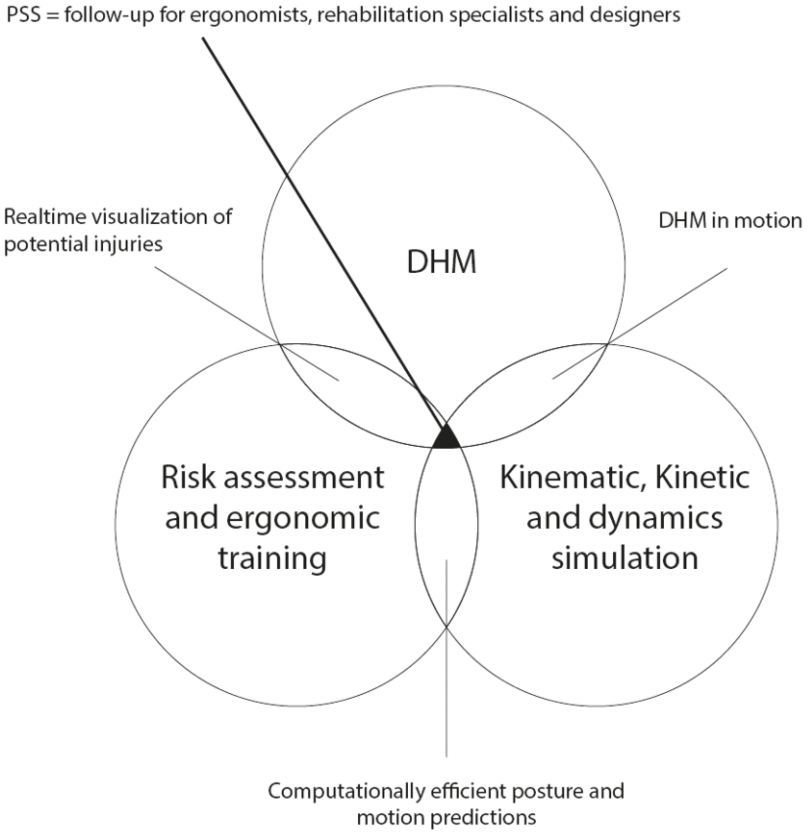

Figure 6. Proposition of a smart PSS as tool in maritime workplace.

4. Discussion

4.1. *Combining IMU and DHM: a trial and error process*

The two IMU systems used to form the baseline for the observations were Wearnotch [24] and Xsens Awinda [11]. Metal interference of the containers and the lashing bars used in container lashings, create disturbance on a IMU that can affect the results. Wearnotch [24] suffered greatly from the interference, not giving a consistent output while working next to the metal containers and shutting down while the test subject held a metal lashing bar. Xsens has experience with countering this metal interference, seen in the cases shown on their website [11]. To secure the more expensive Xsens mocap system [11], the lashing and de-lashing actions were mimicked by a test subject in different environments. Both systems mounting mechanisms provide no additional support in securing the sensors. To minimize potential damage, they are placed

underneath the safety equipment made of fabric. Sudden movements or even an acute vibration can cause the sensor to move its position or get damaged. While Wearnotch [24] uses a system where sensors are snapped into clips on straps, these straps are difficult to adjust, resulting in discomfort. Xsens Awinda [11] uses Velcro patches on the back of the sensors and comfortable specified bands with an adhesive surface to ensure a more comfortable experience, but makes securing the sensors more difficult. A preliminary test with two subjects evidenced that the provided gloves and soles for the shoes to mount the Xsens Awinda [11] on, are not comfortable. And consequently it is necessary to redesign them and test them in a broader population.

Kinematic data can be extracted from mocap systems into excel datasheet for evaluating joint angle data of the upper extremity (L5S1, C1, T4 left and T4 right shoulder). These can be included in the model comparing the different gestures made during each activity representing the joint angle of the maritime worker's upper body. Due to the small operational surface to work on while lashing, the high mass of operable equipment and the time sensitive work scheduled, the likelihood of losing one's equilibrium could be a potential threat. Therefore, our protocol will include next to range of motion (ROM) evaluation also posturographic analysis of the workers using the center of mass (COM) of the subject [25].

4.2. *Implementation of a behavioral monitoring system within maritime transportation*

Executing a behavioral monitoring system would be beneficial for long term supervision of riggers and dockworkers. The system can decrease work for instructors, supervisors and physiotherapist while improving the performance of new recruits. The combination of 3D visualization and kinematic information allows expressing a fast and specific solution for sustained injuries. This would grant better interpretation and understanding in performing correct gestures and therefore result in less injuries. Simultaneously a broader comprehension of the work culture should be established. The contribution of service design tools will grant the ability to better understand the work culture and origin of the incorrect behavior.

4.3. *Future perspective on DHM in maritime transportation*

Future perspective will be to address the creation of a dedicated application for linking kinematic data with 3D models to automatically categorize certain movements and give an early diagnose of potential injuries [26][27]. Using Matlab [28] a plugin can be built as prototype for this application and therefore almost directly be included within future observations. Early observations with riggers in the port of Antwerp will monitor not more than 12 participants, due to the voluntarily nature of the enrolment of the participants. Forthcoming tests with the plugin will examine if a machine learning character improves the results shown by the plugin. If the amount of participants would rise in later observation, data will become more detailed and more specific problems can be presented by the application. To further automize the presented system, Statistical Body Shape Modeling (SBSM) can be implemented [29].

Furthermore, thorough research is needed to create a smart protective garment for maritime workers. The combination of intellectual safety equipment and a motion analysis system provides the opportunity to build a product-service-system (PSS) within a maritime environment. A seamless calibration between product and service provides possibilities for increasing workflow efficiency within maritime transportation.

Upcoming research of the implementation of a PSS in the dockworker training program can be extrapolated to engineering PPE for dockworkers resulting in specialized garments regarding the practiced profession [30].

Acknowledgement

This research was supported by Cepa, OCHA, the Military Hospital Queen Astrid of Brussels and the University of Antwerp. This paper was written as preliminary investigation in Digital Human Modeling within a broader PhD study concerning the implementation of PSS in maritime transportation inducing injury prevention with its dockworkers.

References

[1] Cepa cvba [homepage on the Internet]. Antwerp: Cepa, employer's organisation for freight handlers; c2019 [cited 2019 Dec 17]. Available from: https://www.cepa.be/
[2] Sedilla K, Matias A. Prevalence, severity, and risk factors of work-related musculoskeletal disorders among stevedores in a Philippine break-bulk port terminal. Advances in Intelligent Systems and Computing, 2018, 90–100.
[3] Cepa. Beroepskwalificatie Kuiper, 2016.
[4] Cepa. werkpostfiche, 2009.
[5] Cepa cvba [homepage on the Internet]. Antwerp: OCHA, trainungscentrum for dockworkers; c2019 [cited 2019 Dec 17]. Available from: http://www.ocha.be/nl
[6] Cepa. BEROEPSKWALIFICATIEDOSSIER Kuiper, 2016.
[7] Container Technics N.V. [homepage on the Internet]. LR-63 Lashing Rod; c2020 [cited 2020 Apr 22]. Available from: https://www.containertechnics.com/en/online-catalogue/loose-lashing/lr-63
[8] Container Technics N.V. [homepage on the Internet]. S-32B Turnbuckle jaw step pickup; c2020 [cited 2020 Apr 22]. Available from: https://www.containertechnics.com/en/online-catalogue/loose-lashing/s-32b
[9] Preece J, Rogers Y, Sharp H. Interaction design : beyond human-computer interaction. Wiley, USA 2015.
[10] Kim S, Nozaki T, Murakami T. An approach to categorization analysis for human motion by Kinect and IMU. In: Proceedings 42nd Annual Conference of the IEEE Industrial Electronics Society (IECON2016), 2014, Oct, Florence, Italy, 6158–6162.
[11] Xsens [homepage on the Internet]. MTw Awinda; c2020 [cited 2020 Apr 22]. Available from: https://www.xsens.com/products/mtw-awinda
[12] Blender Foundation. [homepage on the Internet]. blender.org - Home of the Blender project - Free and Open 3D Creation Software; c2020 [cited 2020 Apr 22]. Available from: https://www.blender.org/
[13] MakeHuman. [homepage on the Internet]. c2020 [cited 2020 Apr 22]. Available from: http://www.makehumancommunity.org/
[14] Scataglini S, Paul G, editors. DHM and posturography, Elsevier, London, 2019.
[15] Scataglini S, Danckaers F, Huysmans T, Sijbers J, Andreoni G. Design smart clothing using digital human models. In: Scataglini S, Paul G, editors. DHM and Posturography, Elsevier, London, 2019, 683–698.
[16] ErgoPlus. Step-by-step Guides to Recommended Ergonomic Assessment Tools.
[17] Xing K, Rapaccini M, Visintin F. PSS in Healthcare: An Under-Explored Field. In: McAloone T, Pigosso D, Mortensen N, Shimomura Y, 9th CIRP IPSS Conference: Circular Perspectives on PSS (CIRP2017), 2017 June, Copenhagen, Denmark, 241–246.
[18] Rexfelt O, Hiort Af Ornäs V. Consumer acceptance of product-service systems: Designing for relative advantages and uncertainty reductions. Journal of Manufacturing Technology Management, 2009, 20, 674–699.
[19] Bortolini M, Gamberi M, Pilati F, Regattieri A. Automatic assessment of the ergonomic risk for manual manufacturing and assembly activities through optical motion capture technology. Computers & Industrial Engineering, 2018, 139, 81–86.
[20] Colombini D, Occhipinti E, Álvarez-Casado E. The revised OCRA Checklist method, Editorial Factors Humans, Barcelona, 2013.
[21] Rasmussen J. The AnyBody modeling system. In: Scataglini S, Paul G, editors. DHM and Posturography,

Elsevier, London, 2019, 85–96.
[22] Zheng P, Lin TJ, Chen CH, Xu X. A systematic design approach for service innovation of smart product-service systems. Journal of Cleaner Production, 2018, 201, 657–667.
[23] Chowdhury S, Haftor D, Pashkevich N. Smart Product-Service Systems (Smart PSS) in Industrial Firms: A Literature Review. Procedia CIRP, 2018, 73, 26–31.
[24] Wearnotch [homepage on the Internet]. Wearnotch | Wearable 3D motion capture; c2020 [cited 2020 May 1]. Available from: https://wearnotch.com/
[25] Najafi B, Lee-Eng J, Wrobel J, et al. Estimation of center of mass trajectory using wearable sensors during golf swing. Journal of Sports Science and Medicine, 2015, 14(2), 354-363.
[26] Olivas Padilla BE, Glushkova A, Menychtas D, Manitsaris S. Designing a web-based Automatic Ergonomic Assessment using Motion Data. In: Proceedings of the 12th ACM International Conference on PErvasive Technologies Related to Assistive Environments (PETRA2019), 2019 July, Rhodes, Greece, 528–534.
[27] Gläser D, Fritzsche L, Bauer S, Sylaja VJ. Ergonomic Assessment for DHM Simulations Facilitated by Sensor Data. In: 48th CIRP Conference on MANUFACTURING SYSTEMS (CIRP CMS 2015), 2015 June, Naples, Italy, 702-705.
[28] MathWorks. MATLAB - MathWorks - MATLAB & Simulink [Internet]. 2020 [cited 2020 May 6]. Available from: https://nl.mathworks.com/products/matlab.html
[29] Danckaers F, Scataglini S, Haelterman R, Van Tiggelen D, Huysmans T, Sijbers J. Automatic generation of statistical shape models in motion. In: Advances in Intelligent Systems and Computing. In: International Conference on Applied Human Factors and Ergonomics (AHFE2019), 2019 July, Washington D.C., USA, 170–178.
[30] Scataglini S, Moorhead AP, Feletti F. A Systematic Review of Smart Clothing in Sports: possible Applications to Extreme Sports. Muscle, Ligaments and Tendons Journal, 2020, 10, 333-342.

DHM2020
L. Hanson et al. (Eds.)
© 2020 The authors and IOS Press.
This article is published online with Open Access by IOS Press and distributed under the terms of the Creative Commons Attribution Non-Commercial License 4.0 (CC BY-NC 4.0).
doi:10.3233/ATDE200049

Closing the Gender Gap in DHM

Sofia SCATAGLINI [a,1] and Estela PEREZ LUQUE [b]
[a] *University of Antwerp, Faculty of Design Sciences, Department of Product Development, Antwerp, Belgium*
[b] *University of Skövde, School of Engineering Science, Skövde, Sweden*

Abstract. Digital Human Modelling by Women (DHMW) is an international group of women and supporters with the main purpose of eliminating the gender gap, empowering women to exchange ideas, results, visions, and promote the women's participation in the STEM (science, technology, engineering, and math) and DHM fields. This study presents a demographic investigation of human factors and behaviors affecting women in the DHM field. A questionnaire composed of several items was set up to analyze the situation: demographic map of women in DHM (age, country, and level of education), the field of application, factors related to career progression, and correct instruments to change the current situation of underrepresentation. Our results show a gap of women working in the DHM field in the industry or research institutes (21% and 8% respectively). While, the 56% are involved in the Academic world, with a 30% PhD and 26% PostDoc level. Work-life-balance (WLB), career progress (CP), family-balance vs career (FB VS C), and work schedule flexibility (WSF) resulted lower in women of 30-34 and 35-39 years old. As a result, it is necessary to adopt strategies focus on support mentoring programs, career progress, childcare support, and flexible work schedule aiming to eliminate women inequality and stigmatization. This will open up borders in Academics, Industry, and Research education closing the gap in the DHM field.

Keywords. Women, STEM, DHM, DHMW, Modelling, Gender Balance

1. Introduction

Over the years, women in Europe and all over the world are increasingly pursuing jobs that have been traditionally considered for males. However, women continue to be underrepresented in the STEM field (science, technology, engineering, and math fields) [1], where men's employment is still very high covering over 80% [2].

Several studies have shown that although girls and boys perform similar in math and science, there continue to be factors and biases relating to a poor and lower achievements perception of girls [3-4]. The root of the lack of girls and women involved in STEM comes with biological factors, education policy, social and cultural context as well as early experience more than cognitive aptitudes or sex brain differences [3-5].

To overcome this situation, numerous studies propose strategies that highlight the need of reducing and breaking down the stereotyping [3], [5-7], and the challenges it supposes to the administrative, financial and cultural current environment [3], [8].

The European Commission's strategic plan for gender equality 2016-2019 points out to that. This report proposes four strategic areas for independence between gender: equal pay, equality in decision making, ending gender violence, and equality between

[1] Corresponding Author, Email: sofia.scataglini@uantwerpen.be; sofia.scataglini@gmail.com.

the European Union's [8]. When moving to leadership positions this number is even lower [9]. In particular, the European University Association (EUA) analyzed the representation of female leaders in Europe's universities and found that only 15% of all rectors are female in 48 countries. Notably, 20 countries do not have any female rectors currently. Although the situation of female leaders is increasing yearly, there is still the gap.

Programs such as Hypatia chair were introduced in the University of Twente in the Netherlands for increasing the number of women in STEM to obtain academic top positions [10]. Dublin also approved a program to close the gender gap called "20 women only professor position" in 2020 [11]. Besides, the creation of tenure track policy resulted in increasing representation of women in senior academic positions but still this solution did not solve the problem in the transition from associate to full professor position. L'Oréal UNESCO for women in Science International programs recognize every year also women researchers around the world but apparently, highlighting again the existing gaps [12].

To confirm that, the study of Stefanie Jonson et al. [13] found that eliminating the gender information in funding application make more success for women passing from 18 to 30%. Understanding the current cause of underrepresentation and gender gap is important to open the borders and closing the gap [14]. For that, it is necessary to avoid discrimination for grant funding, journal reviewing, hiring female manager, researcher, and professor, and all this start from us. More dedicated and mentoring programs should grow up since primary school [15-16]. Together with that, stereotypes also need to be eliminated providing more role models. STEMinism campaigns are growing up but if these campaigns are promoted by only women the engagement will be more difficult [17-18]. To promote both gender engagement is necessary to build up an initiative where women are supported by also men looking into the role of "model" but also modelling.

In particular, Digital Human Modelling (DHM) is the "science of representing humans with their physical properties, characteristics, and behaviors in computerized virtual models" [19]. DHM is becoming an essential tool for the evolution of the society, going from a society 4.0 to a human-centred society 5.0 that aims to be much more smart, digital and address the well-being of the population [19]. In this evolution, it is important to ensure women are represented to the same degree as men.

DHM group started to promote the increment of women involved in the field by constituting an international group that aims to eliminate the gender gap, addressing the empowerment of women to exchange ideas, results, and visions in the multidisciplinary DHM and STEM field. This group entitled "Digital Human Modelling by Women" (DHMW) was born during the DHM Symposium 2017 [20], with the main purpose of increasing the women participation, reaching the gender balance by exploring the current barriers and issues that are affecting them, and constituting an essential "model" for women scientists that also inspires girls around the world. It constitutes a promising community of women and men that promotes sharing the feeling of struggling and engagement in improving the environment for women not only in the DHM area but STEM. Starting from the previous assumptions, this study presents a demographic investigation looking to human factors and behaviors that affects women in the DHM field.

2. Method

Twenty-three women, in the range of 18 and 67 years old, were investigated to study women's situation in the DHM field by using a questionnaire design form in GoogleDocs (Figure 1) [21]. The questionnaire (Table 1) admitted one or multiple responses, and is composed of several items that are addressed to:

1) create a demographics map of DHMW looking at their age, country(e.g. born, live/work today) and level of education;
2) explore the sectors and the field of application;
3) identify the factors and behaviors that affect their career progression, work and personal/family balance;
4) claim and find the instruments and the way for closing the gap.

The questionnaire was submitted to the DHMW group by email and shared in the LinkedIn social network group ("DHMW"). The responses were statistically elaborated by the authors in using the Statistical Package for Social Science, SPSS (IBM Corp., Armonk, NY, USA). The women involved were informed by a description of the research and all of them provided informed consent to be part of the study.

Figure 1. DHMW Survey.

Table 1. DHMW Questionnaire.

1	Gender
2	Age
3	Country of birth
4	Level of Education
5	Degree
6	Current work placement
7	Do you work in a country where you were born?
8	Did you move to another country for a non-professional reason?
9	If yes, why did you move?
10	Are you willing to move to another country in case you find an opportunity?
11	If you don't want to move, why?
12	Domain. If it is in academics (I am...)
	Domain. If it is in the industry (I am...)
13	Areas of practice/expertise
14	Topic
15	Areas of practice/expertise (software experience)
16	Which membership do you have?
17	Which DHM conferences did you attend?
18	Which networks do you use for work?
19	Projects Request Participation
20	Work-life balance (punctuation 0 to 10)
21	Do/did you find it difficult to find a job?
22	If you find/found it difficult, why?
23	Where do/did you search for jobs?
24	Career progress (punctuation 0 to 10)
25	Family balance VS Career (punctuation 0 to 10)
26	Work schedule flexibility (punctuation 0 to 10)
27	How many children do you have?
28	Parenthood flexibility (punctuation 0 to 10)
29	Do you get additional household support? (e.g. childcare, cleaning service,...)
30	What is the gender of your mentor?
31	Who is your mentor?
32	In which groups do you participate to promote specific populations?
33	Why is the participation useful?
34	Additional remarks?
35	Do you like to have a website (DHMW)?
36	Do you like the idea to have an association to share ideas, workshop, job, fellowship?

3. Results

The four different research objectives previously presented in the method were investigated, elaborated, and classified using the SPSS software.

3.1. Demographics

Data showed a geographical distribution that is limited in specific country areas where the DHMW number fluctuates from one to three (Figure 2).

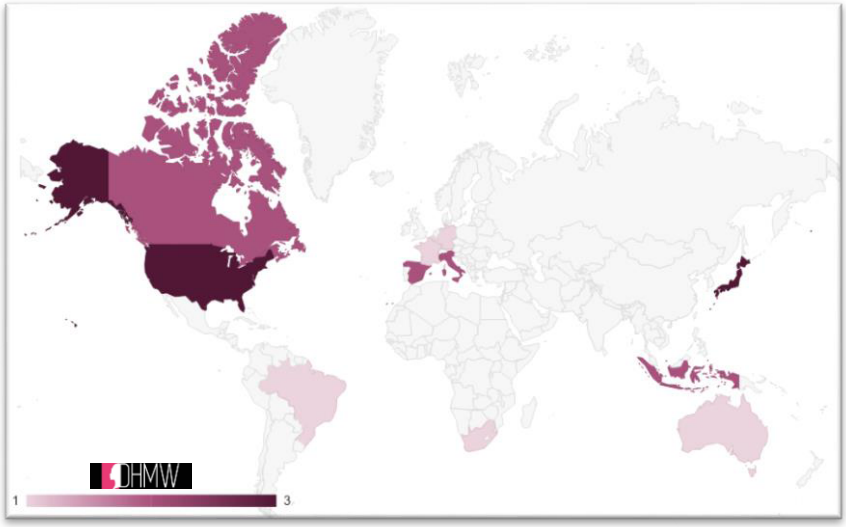

Figure 2. Map of DHMW population (light color represent lower density, dark color represent higher density) that participated in this study.

43% of DHMW participants are located in the European countries while 57% are not in the European zone. Within the EU zone, we can see that 17% of women are from France, 9% from Italy, 4% from Belgium, 9% from Spain and 4% from Germany. While from areas outside the EU, we have 4% of women participation in Australia, 4% in Brazil, 4% in South Africa, 14% in the United States, 13% in Japan, 9% in Indonesia, and 9% in Canada. Figure 3 shows the variation of the population considering the age distribution. The population of women has been classified by age groups of 18-24y, 25-29y, 30-34y, 35-39y, 40-54y, 55-67y. Age range values were established according to the academic's career structure. 48% of the women involved have ages between the 40-67 years. 22% age between 18-34 years while 30% between 35-39 years (Figure 3).

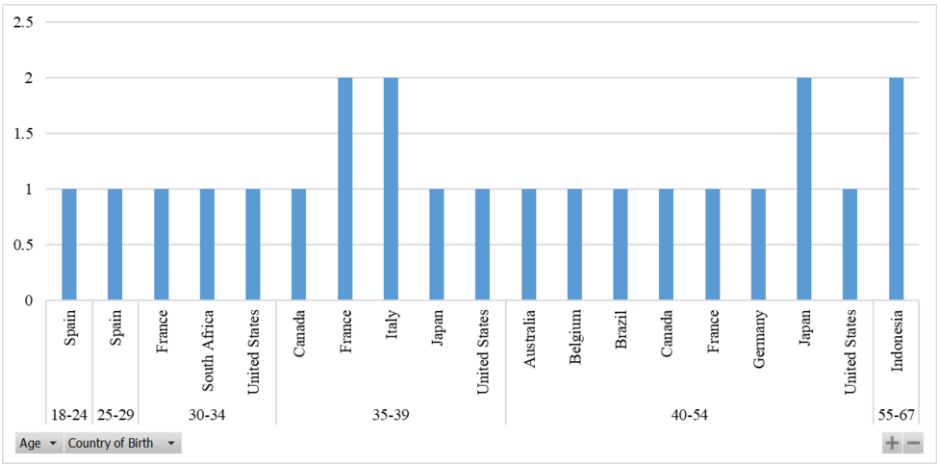

Figure 3. Age group distribution by country of birth of the DHMW population considered in this study.

3.2 Education, Career, Work-life balance

In terms of the level of education, 22% work in Industry, 9% in research institutes, and 56% in Academics (Figure 4).

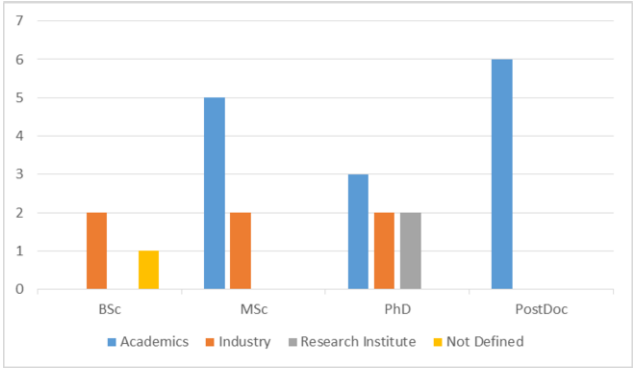

Figure 4. Number of DHMW per education level and workplace field considered in this study.

Seventy percent of them work in the country where they were born. From the overall population, 57% moved for their career (internship, job position, fellowship, change career), while 70% of them moved abroad for a non-professional reason (sabbatical year, family). Also, 52% of the women involved are willing to move to another country in case they find another opportunity. While 31% responded not because they do not like to do (16%) or they have family reasons (16%). Finally, 17% of women responded they cannot for reasons that are beyond their will (they mentioned family restriction). The women that responded they cannot for family reason are women that obtained rank as senior researchers, assistant or full professor.

61% did not find difficulties to get a job, while 39% found difficulties because there was no job in their countries (Italy, France, Spain, Belgium, and South Africa), the competitiveness of academics positions, and difficulties in their field.

Table 2. Age, Work-life balance (WLB), career progress (CP), family-balance vs career (FB VS C), work schedule flexibility (WSF) and number of child (NC) average score (0=low to 10=high) of the DHMW population that participated in this study.

Age	WLB	CP	FB VS C	WSF	NC
18-24	7	7	8	0	0
25-29	8	8	8	8	0
30-34	4.33	5.00	4.00	8.00	0
35-39	4.57	4.93	5.21	5.29	3.29
40-54	6.44	6.67	6.44	8.00	2.22
55-67	7.5	7.5	7.5	7.5	0
Mean	**6.31**	**6.52**	**6.53**	**6.13**	**0.92**
SD	**1.40**	**1.17**	**1.49**	**2.91**	**1.33**
Min	**4.33**	**4.93**	**4.00**	**0.00**	**0**
Max	**8.00**	**8.00**	**8.00**	**8.00**	**3.29**

Table 2 shows the average scores (from 0 meaning low to 10 meaning high) of every range of age regarding their work-life balance (WLB), career progress (CP), family balance vs career (FB vs C), and work schedule flexibility (WSF). It also shows the minimum, maximum, standard deviation and means scores of each aspect. Table 1 also describes the average number of children by age group, 57% of the women have at least one child. To this group, we asked also parenthood flexibility score (0=low to 10=high) obtaining an average of 6.36 for our population. 38% of them obtained also household support.

3.3 Area of expertise and the simulation tools in the different field of applications

DHM serves computer-based tools that simulate human-system interaction in a virtual environment applied in several fields such as rehabilitation, aerospace, medicine, space, forensic, automotive, elderly care, sports, orthopedics and robotics (Figure 5) [19]. These fields contain also areas of expertise such as virtual reality (VR), clothing, motion capturing, anthropometry, posture, mental/cognitive, musculoskeletal, standardization, and impact analysis (Figure 6).

From our analysis emerged that automotive and transportation are the main fields that are covered by our population, followed by robotics, elderly care, and then orthopedics. These results are followed by sport and military and successively clothing. Motion capturing and posture are the main areas of expertise with 43% each. These are followed by musculoskeletal and anthropometry and successively virtual reality, mental and cognitive modelling. Impact analysis covers only 8% of our population. This number becomes lower in the case of clothing and standardization.

Figure 7 shows the simulation tools used by our population in DHM as AnyBody [22], Biomechanics (e.g. kinematics data in Matlab,…), Blender [23], Delmia [24], Dhaiba [25], ESI [26], Gazebo simulator [27], HumanCad [28], IMMA [29], Jack [30], NetLogo [31], Opensim [32] and Posture (e.g. posturography).

Biomechanics is the most simulation tool used, followed by Jack, OpenSim, and Anybody. The field of application confirmed also the tools used by our population (Figure 7).

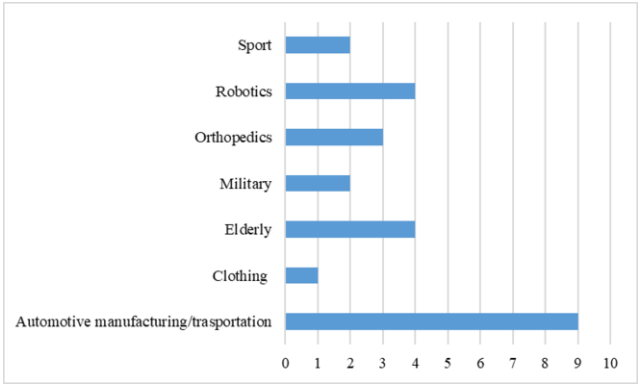

Figure 5. Number of DHMW for field application that participated in this study.

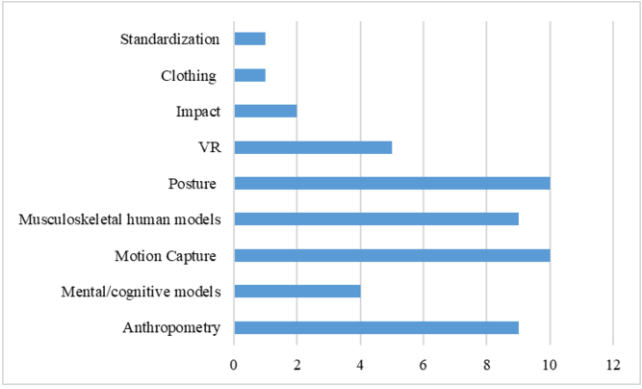

Figure 6. Number of DHMW in each area of expertise that participated in this study.

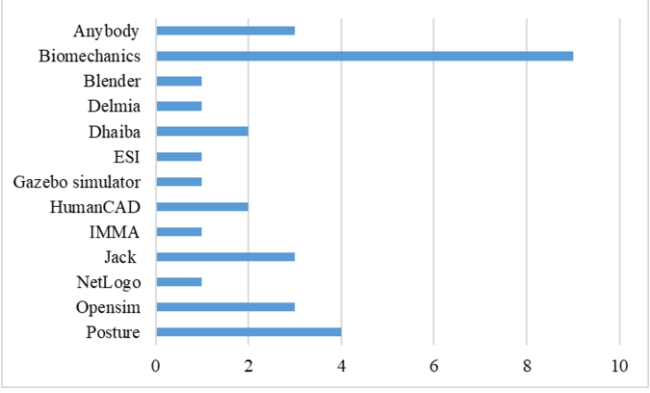

Figure 7. Number of DHMW that used the simulation tools considered in this study.

3.4 Network and conference participation

Networking and conference participation are also important for closing the gap. Figure 8 shows that DHM Symposium is the most specific congress in DHM with the majority of the participants with 52%. This is followed by the triennial International Conference

of Ergonomics (IEA) were also DHM group participates. 26% participates also at Applied Human Factors and Ergonomics (AHFE) that normally is held in the USA.

Finally, 4% follow the VPH Institute (Virtual Physiological Human) and the related conference in biomedicine.

The majority of the population use LinkedIn as a social network for sharing information, research, and job position (Figure 9). In terms of sharing research and papers, they prefer ResearchGate to Academia or Mendeley (Figure 9).

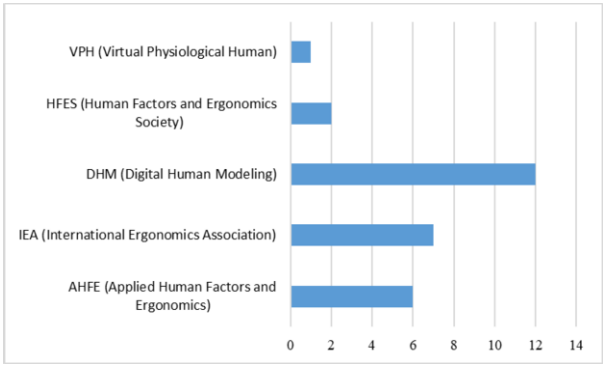

Figure 8. Number of DHMW that participate in each conference.

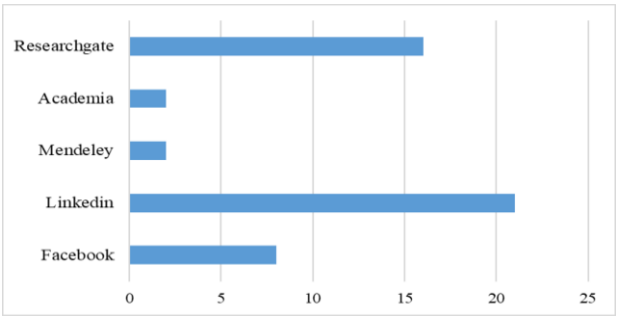

Figure 9. Number of DHMW that participate in each network.

4. Discussion

This paper aims to study the current situation of women involved in the DHM field. Different factors regarding age, nationality, experience, mobility, maternity, and career progression were taken into account to analyze in which order or how these aspects affect them and consequently try to find tools/solutions to improve it and close the gap.

A questionnaire form created using GoogleDocs was the used method in this study due to the easiness to spread by email or social network.

Results show a multicultural and a mixed-age environment of women working in the DHM area. Looking at their level of education and their workplace situation (Figure 4) is evident the gap of women working at the DHM field in the industry or research institutes (22% and 9% respectively). 56% are involved in the Academic world, with a 30% PhD and 26% PostDoc level. These numbers could mean the gender gap in Academia is smaller than in the industry, as some studies have also explained [11].

Another result to highlight is how work-life-balance (WLB), career progress (CP), family-balance vs career (FB VS C), and work schedule flexibility (WSF) decrease in the range of 30-34 and 35-39 years old when the number of child increase (Table 1).

Although 61% did not find difficulties getting a job, the remaining 39%, which is still a high number, found difficulties because there was no job in their countries. Also, from the entire population, 52% reported willing to move abroad in case of a career opportunity while 16% said they have family restrictions and 17% responded they cannot for reasons that are beyond their will. The women that responded they cannot for family reason are women that obtained rank as a senior researcher, assistant, or full professor, which correspond to the range of ages where the number of child increase. With these data, we could reflect again on how the maternity limit somehow the career progression of women in DHM. That points out the high importance of establishing strategies for the women's career progression and the equality between genders during parenthood.

Nowadays, social media as LinkedIn, ResearchGate, Mendeley (Figure 9) as well as conferences (Figure 8) are good tools or scenarios to expose and visualize the situation and promote the women's participation in both the DHM and the STEM fields.

5. Conclusion

This paper aims to study the current situation of women involved in the DHM field. Different factors regarding age, nationality, experience, mobility, maternity, and career progression were taken into account to analyze in which order or how these aspects affect them and consequently try to find tools/solutions to improve it and close the gap. Our results demonstrated that DHMW between 30 and 39 years old have a lower score of work-life-balance (WLB), career progress (CP), family-balance vs career (FB VS C), and work schedule flexibility (WSF) respect to the other age groups.

As a consequence, it is necessary to create and promoting strategies addressed to closing the gap for recreating gender balance. Mentoring programs, career progress aim to promoting female positions, childcare support, and flexible work schedule are necessary for closing the gap. The closing gap starts also from men putting more efforts to close it by promoting more women in STEM, opening borders in Academic, Industry and Research, and in this case in DHM.

Acknowledgement

This work was supported by University of Skövde (Synergy Virtual Ergonomics project) and the University of Antwerp. We would like to thank all the DHMW who participated in making the first draft of the survey during the last DHM Symposium 2017, where the DHMW group was born. This support is gratefully acknowledged.

References

[1] Meyer M, Cimpian A, Leslie S-J. Women are underrepresented in fields where success is believed to require brilliance, Front. Psychol, 2015, (6), 235.
[2] Lekfuangfu WN, Lordan G. Cross Cohort Evidence on Gendered Sorting Patterns in the UK: The Importance of Societal Movements versus Childhood Variables, 2018, 47.
[3] Halpern DF, Benbow CP, Geary DC, Gur RC, Hyde JS, Gernsbacher MA. The Science of Sex Differences in Science and Mathematics. Psychol. Sci. Public Interest J. Am. Psychol. Soc, 2007, 8(1), 1–51.

[4] Modi K, Schoenberg J, Salmond K. Generation STEM: what girls say about science, technology, engineering, and math, Girl Scout Research Institute, 2012, New York. Available from:http://www.girlscouts.org/content/dam/girlscouts-gsusa/forms-and-documents/about-girl-scouts/research/generation_stem_full_report.pdf>, (accessed 12 Jun 2020).
[5] Gunter C. Science: it's a role model thing. Genome Biol, 2013, 14(2), 105.
[6] Ehrlinger J, Plant EA, Hartwig MK, Vossen JJ, Columb CJ, and Brewer LE. Do Gender Differences in Perceived Prototypical Computer Scientists and Engineers Contribute to Gender Gaps in Computer Science and Engineering?. Sex Roles, 2018, 78(1), 40–51.
[7] Moè A, Hausmann M, Hirnstein M. Gender stereotypes and incremental beliefs in STEM and non-STEM students in three countries: relationships with performance in cognitive tasks. Psychol. Res., Jan. 2020.
[8] 2019 Report on equality between women and men in the EU. European Commision, ISSN 2443-5228. Availablefrom:https://ec.europa.eu/info/sites/info/files/aid_development_cooperation_fundamental_rights/annual_report_ge_2019_en.pdf, (accessed 14 May 2020).
[9] European University Association EAU, Male vs female university leaders: the hard facts on International Women'sDay. Available from:https://eua.eu/news/467:male-vs-female-university-leaders-the-hard-facts-on-international-women%E2%80%99s-day.html, (accessed 14 May 2020).
[10] University of Twente introduces Hypatia chairs for female professors | Home (EN). Universiteit Twente. Availablefrom:https://www.utwente.nl/en/news/2018/7/260065/university-of-twente-introduces-hypatia-chairs-for-female-professors (accessed 27 April 2020).
[11] Gorey C. 20 women-only professor positions approved to close academic gender gap. Silicon Republic, Jan. 03, 2020. Available from:https://www.siliconrepublic.com/innovation/women-only-professor-positions-sali-ireland (accessed 27 April 2020).
[12] L'Oréal-UNESCO For Women in Science Programme. UNESCO, Feb. 12, 2019. Available from:https://en.unesco.org/science-sustainable-future/women-in-science (accessed 6 May 2020).
[13] Johnson SK, Kirk JF. Dual-anonymization Yields Promising Results for Reducing Gender Bias: A Naturalistic Field Experiment of Applications for Hubble Space Telescope Time. Publ. Astron. Soc. Pac, 2020, 132:034503.
[14] Ceci SJ, Williams WM. Understanding current causes of women's underrepresentation in science. Proc. Natl. Acad. Sci, 2011, 108(8), 3157–3162.
[15] Improving the pathway from school to STEM careers for girls and women. Available from:https://blogs.worldbank.org/opendata/improving-pathway-school-stem-careers-girls-and-women (accessed 28 April 2020).
[16] Berwick C. Keeping Girls in STEM: 3 Barriers, 3 Solutions. Edutopia. Available from:https://www.edutopia.org/article/keeping-girls-stem-3-barriers-3-solutions (accessed 28 April 2020).
[17] STEMinism | Teach First. Available from:https://www.teachfirst.org.uk/steminism (28 April 2020).
[18] Sundorph E. Missing Elements, Teach First. Available from:https://www.teachfirst.org.uk/sites/default/files/202002/teach_first_steminism_report.pdf, (28 April 2020).
[19] Scataglini S, Paul G. DHM and posturography. London (UK): Elsevier Inc. : Academic press, 2019.
[20] Standing straight | IEC e-tech | Issue' 05/2019. IEC e-tech. Available from:https://www.iecetech.org/issue/2019-05/Standing-straight (28 April 2020).
[21] Rayhan RU, Zheng Y, Uddin E, Timbol C, Adewuyi O, Baraniuk JN. Administer and collect medical questionnaires with Google documents: a simple, safe, and free system. Appl. Med. Inform, 2013, 33(3), 12–21.
[22] Anybodytech.com: Frontpage. Available from:https://www.anybodytech.com/ (accessed 13 May 2020).
[23] Blender.org - Home of the Blender project - Free and Open 3D Creation Software, blender.org. Available from:https://www.blender.org/ (accessed 13 May 2020).
[24] DELMIA Global Operations – Dassault Systèmes. Available from:https://www.3ds.com/products-services/delmia/?woc=%7B%22brand%22%3A%5B%22brand%2Fdelmia%22%5D%7D (accessed 13 May 2020).
[25] Endo Y, Tada M, Mochimaru M. Dhaiba: Development of Virtual Ergonomic Assessment System with Human Models, Proceedings of the 3rd International Digital Human Modeling Symposium (DHM2014), 2014, Tokyo, Japan.
[26] E. S. I. Group. ESI Group. Available from:https://www.esi-group.com/ (accessed 13 May 2020).
[27] Gazebo. http://gazebosim.org/ (accessed 13 May 2020).
[28] NexGen Ergonomics - HumanCAD - Welcome. http://www.humancad.com/ (accessed 13 May 2020).
[29] IPS IMMA. Available from:https://industrialpathsolutions.se/ips-imma (accessed 13 May 2020).
[30] Human Modeling and Simulation. Siemens Digital Industries Software. Available from:https://www.plm.automation.siemens.com/global/en/products/tecnomatix/human-modeling-simulation.html (accessed 13 May 2020).

[31] NetLogo: Resources and Links. Available from:https://ccl.northwestern.edu/netlogo/resources.shtml (accessed 13 May 2020).
[32] OpenSim - Home. Available from:https://opensim.stanford.edu/ (accessed 13 May 2020).

DHM2020
L. Hanson et al. (Eds.)

© 2020 The authors and IOS Press.
This article is published online with Open Access by IOS Press and distributed under the terms of the Creative Commons Attribution Non-Commercial License 4.0 (CC BY-NC 4.0).
doi:10.3233/ATDE200050

Aiding Observational Ergonomic Evaluation Methods Using MOCAP Systems Supported by AI-Based Posture Recognition

Víctor IGELMO [1], Anna SYBERFELDT, Dan HÖGBERG, Francisco GARCÍA RIVERA and Estela PÉREZ LUQUE
University of Skövde, School of Engineering Science, Sweden

Abstract. Observational ergonomic evaluation methods have inherent subjectivity. Observers' assessment results might differ even with the same dataset. While motion capture (MOCAP) systems have improved the speed and the accuracy of motion-data gathering, the algorithms used to compute assessments seem to rely on predefined conditions to perform them. Moreover, the authoring of these conditions is not always clear. Making use of artificial intelligence (AI), along with MOCAP systems, computerized ergonomic assessments can become more alike to human observation and improve over time, given proper training datasets. AI can assist ergonomic experts with posture detection, useful when using methods that require posture definition, such as Ovako Working Posture Assessment System (OWAS). This study aims to prove the usefulness of an AI model when performing ergonomic assessments and to prove the benefits of having a specialized database for current and future AI training. Several algorithms are trained, using Xsens MVN MOCAP datasets, and their performance within a use case is compared. AI algorithms can provide accurate posture predictions. The developed approach aspires to provide with guidelines to perform AI-assisted ergonomic assessment based on observation of multiple workers.

Keywords. Artificial Intelligence, Machine Learning, Motion Capture, Wearable Inertial Sensors, Ergonomic Assessment, Ergonomic Evaluation

1. Introduction

The novel Industry 4.0 (also called the 4th industrial revolution), based on digitalization and future-oriented technologies in the field of "smart" objects, is changing the way companies understand and approach their processes [1]. Industry 4.0 comprises a large variety of concepts, where the most relevant for this paper are cyber-physical systems (CPS), adaptation to human needs, and corporate social responsibility [1].

CPS can be defined as "integration of computation and physical processes, where embedded computers and networks monitor and control the physical processes, usually with feedback loops where physical processes affect computations and vice versa" [2]. Physical measures are digitalized using sensors to reach this integration. However, this digitalization focusses more on produced goods, services, and the components to create

[1] Corresponding Author, Email: victor.igelmo.garcia@his.se.

them, rather than focusing on the role of human beings in the design of smart factories. Monitoring technologies allow the integration of human-related data into the design process, along with machines and their connectivity and interoperability features [3], making it more socially sustainable, intelligent, and flexible [4].

Monitoring technologies which focus on movement-related data are called motion capture (MOCAP). They have applications in several fields such as filmmaking, videogames, robotics, healthcare, ergonomics, and mechanics. There are three main technologies currently used within MOCAP: wearable inertial sensors, smart textiles, and image/video recognition. Wearable inertial sensors include gyroscopes and accelerometers to record motion. Inertial/magnetic measurements units are often added to compensate for possible drawback of the other sensors [5]. On the other hand, smart textiles provide standard fabrics with some kind of extra functionality, mostly within monitoring health-related variables [6]. Lastly, the current advances in artificial intelligence (AI), especially in the field of image recognition, have helped include this technology into the MOCAP field [7]. While some authors' research is done within pose estimation, where 2D images or videos are the primary sources of information [8–11], others have their focus on applying MOCAP directly to different processes/fields [12]. 2D image recognition can accurately predict specific anthropometric measurements [13], but it does not seem powerful enough to perform when the subject is moving or within the whole range of postures. On the other hand, 3D cameras (or depth cameras) can reach the highest accuracy among MOCAP systems, but they have disadvantages such as the need to have a clear sight on the target.

One application of MOCAP systems is aiding within physical ergonomic evaluations, seeking the prevention of work-related musculoskeletal disorders (WMSDs) [12]. Risk factors for WMSD include rapid work pace, repetitive motion patterns, forceful extensions, non-neutral body postures, heavy lifting, and vibration [14]. WMSDs have a high health and economical cost [15], due to factors such as work absence [16], healthcare expenditure [17], or loss of quality and productivity [18,19] among others, as well as the personal cost such as the physiological and stress problems suffered by the workers [20].

Posture-related ergonomic evaluations (referred just as ergonomic evaluations in this paper) can help to decrease the effect of these problems either by letting workers know when their postures are not good enough [21] or by designing workstations that lead the workers to have a better one [22], among others. Ergonomic evaluation methods can serve these purposes since they are applied to identify and assess risk factors in the workplace. These evaluation methods can be divided into several categories: self-report, simple observational techniques, advanced observational techniques, and direct measurement [23]. Direct measurement methods are the most objective since the results are based on analytic data, in contrast with observational methods, which rely on the subjective ergonomist´s judgment to assess the work task [24]. Observational methods are performed by looking at the work task (or on a videotape for example) and taking a few staple measures, such as the weight of the objects that the workers manipulate. Ergonomists can make use of either an existing evaluation method (Rapid Upper Limb Assessment (RULA) [25], Rapid Entire Body Assessment (REBA) [26], and Ovako Working Posture Assessment System (OWAS) [27], among others), or a custom one.

Traditionally, the attempts to automatize observational methods with MOCAP data have been based upon the premise that it is better to strictly apply the guidelines of certain method rather than apply these methods with the implicit human subjectivity. However, the judgment of an expert is not necessarily the wrong criteria for evaluation. Instead,

given the power of human reasoning, they can consider several variables omitted in the ergonomic assessment method used.

Experts might have different opinions about the same posture or task when applying an ergonomic evaluation method, e.g. about whether someone is bending instead of standing straight when the posture is unclear. If a particular set of variables are analysed to differentiate between postures, and these variables are measured using MOCAP equipment, the subjectivity of the evaluation can be taken away. While MOCAP systems can accurately measure anthropometric variables, posture classification (or labelling) is done by a human. AI can both directly learn from human classification, and it can adjust its predictions to the fine refinement that the human might apply to the assessment.

This study aims to investigate the advantages of approaching observational methods with combined use of AI and MOCAP systems. In the next section, an AI-based approach to observational ergonomic evaluation methods is presented. Section 3 presents, an example of the proposed approach, applying AI-based working posture detection within OWAS evaluation method, is described, followed by a discussion of the results and a summarize of the outcome in Section 4.

2. Proposed AI-based approach to observational ergonomic evaluation methods

Humans are valuable limited resources, and many might find observation to be a tedious, time-consuming process. Moreover, observation is based on the observers' perception [24]. When it comes to perception, AI algorithms (sometimes referred to as AI models) can provide with predictions, which are probabilistic outputs of the model trained using datasets built based perception. These models are capable of achieving even lower error rate results than humans in some fields, e.g., visual recognition algorithms, which have surpassed humans in several visual tests [28]. Preventing misuse of human resources would enable performing tasks in which humans are much better than machines, such as understanding complex problems and identifying underlying patterns.

To perform the search for previous work, the following string was defined:

$$(wearable\ OR\ inertial\ OR\ mocap\ OR\ motion\ capture)\ AND\ (ergonomics\ OR\ ergonomic\ assessment\ AND\ (learning\ OR\ machine\ learning\ OR\ artificial\ intelligence)$$

From the 34 results in the Scopus database, 21 abstracts were screened, and only 7 of them were relevant for this paper [29–37]. None of the reviewed papers was using or aiding existing ergonomic assessments through learning from multiple experts' knowledge or perception. Selection schema is presented in Figure 1.

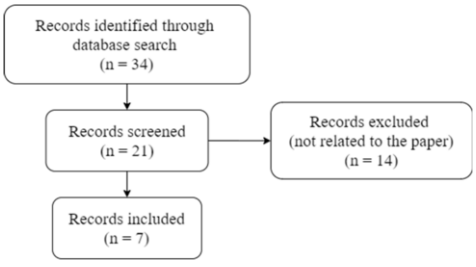

Figure 1. Flow chart of literature search and selection schema.

For the sake of generalization, fifteen different observational ergonomic evaluation methods were considered. The inputs required to perform each method can be classified into two groups [23]:

- **Objective inputs** are feasible to apply direct measurement and computing, since they rely on accurate data, such as mean power frequency (MPF).
- **Subjective inputs** are inherent to perception [38], and therefore problematic when deciding how to measure and compute them: working posture, recovery, and complex factors (environmental conditions, psychological, and individual factors, among others).

2.1. Workflow and components

In the following section, the suggested workflow is presented: from defining the problem to applying an operational AI-based solution to observational ergonomic evaluation methods using MOCAP systems. The starting point should always be particular ergonomic needs. Different problems, and ergonomic assessments available to handle them, shape the solution.

Depending on what kind of postures need to be measured, a specific MOCAP system will be more or less suitable than others. While the market is moving towards a new generation of low-cost MOCAP systems [39], certain MOCAP technologies might involve a trade-off between budget, desired accuracy, reliability, and extension of the ergonomic assessment to cover.

Existing solutions could also be a determinant factor, where used MOCAP would be a suitable, directly applicable solution. When selecting a MOCAP system, one of the criteria should be whether it is aimed to cover the entire ergonomic assessment (all the input variables are measured using MOCAP) or part of it (only certain variables).

Once data is collected, it might be possible to use an existing compatible solution (one which has the same MOCAP data). If there is no solution available, a custom one will be required, where MOCAP data will also be used to train an AI model. It will be necessary to carefully study the variables, and not include in training those not used to define a specific posture. For instance, a variable such as a neck angle most likely should not be included when aiming to predict lower limbs posture.

The AI model to use could differ from case to case. Evaluation is needed for the trained model, where MOCAP system feeds the AI model to check its feasibility. If the model is not good enough (most likely according to subjective criteria), the AI model would need to be retrained. This approach can be illustrated, as shown in Figure 2.

3. Evaluation of the suggested approach

Regardless of theoretical advantages, empirical results are desired when trying to demonstrate the feasibility of AI models. With this objective, the following use case is presented: building an AI model for posture prediction using the OWAS ergonomic evaluation method. OWAS inputs (postures) are defined descriptively in the assessment, instead of numerically, as it is done in other ergonomic assessments, such as RULA or REBA, where specific angle values are provided. Therefore, OWAS postures are subjective by nature, and different evaluations have been performed with different

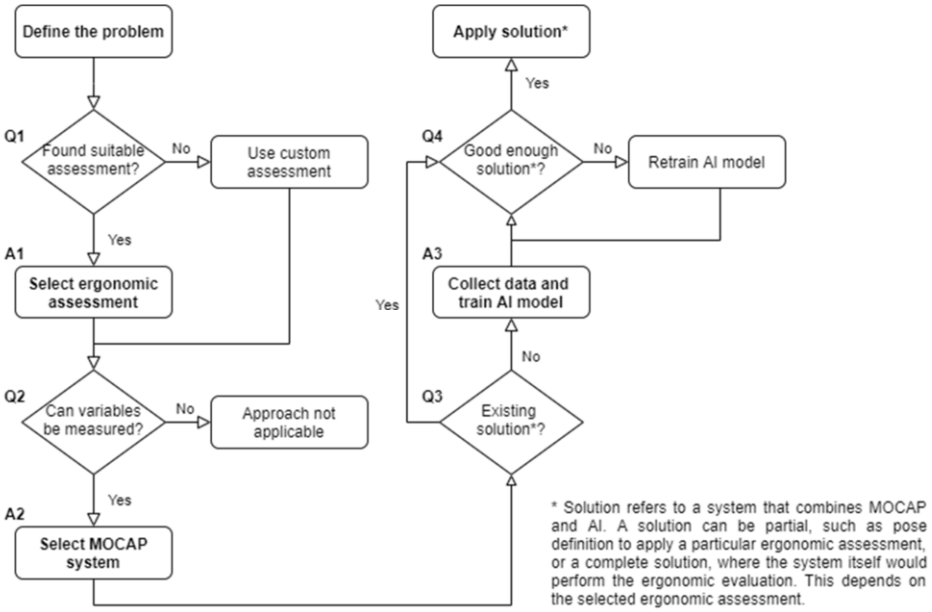

Figure 2. Suggested workflow for the presented AI-based approach.

criteria. Within OWAS, there are four different categories for back postures, three for upper limbs postures, and seven for lower limbs postures. AI can help by learning from the humans' classification, based on perception, and providing with predictions based on that training.

Other ergonomic evaluation methods would be also suitable for the case. The method itself would be a starting point for training, and the main task for AI would be to modify the original parameters of the method according to the humans' final refinement.

The task performed by the subject under study is hypothetical, where the subject moves within the range of postures which would fit in the different OWAS categories. This use case is focused on the OWAS postures detection, rather than applying the assessment strictly.

Following the presented approach, questions are answered as follows:

Q1: Found a suitable assessment?

A1: Rather than looking at suitability, OWAS is selected given its subjective nature [40], so an AI-based solution is built to potentially aid observers to have a more consistent judgement of posture classification when using OWAS.

Q2: Can variables be measured?

A2: As mentioned, OWAS does not provide with information about how to classify postures through anthropometric measurements. However, posture-related variables can be measured, since MOCAP systems provide enough information to accurately relate these variables to the labels in OWAS. The set of variables, picked to relate perception into OWAS labels, are back (in terms of inclination and rotation), upper limbs (shoulders angle), and legs (lower limbs angles). Several solutions are available to measure these variables. It is decided to use Xsens MVN [41], due to its current availability at the University of Skövde.

Q3: Existing solution?
A3: No, there are no AI models already trained for OWAS ergonomic assessment. A custom solution is required (See section 3.1).

Q4: Good enough solution?
A4: Solution is evaluated in Section 3.3.

3.1. Building an AI-based solution for the use case

A database is needed to build a custom solution, where MOCAP systems input is related to the different inputs required to perform the selected ergonomic assessment. In this case, Xsens' input is related to one of the OWAS categories [27], required to determine the posture: back posture, upper limbs posture, and legs. The database is generated using the answers from an online distributed questionnaire created by the authors of this paper. On it, participants were asked to classify 60 postures by selecting between two options, each shown in a figure including a real picture and the associated virtual representation (manikin), in one of the OWAS categories (Figure 3). At the beginning of the questionnaire, participants were asked to read the original OWAS study. The questionnaire was answered by 7 participants, being their area of expertise ergonomics (within either industry or research) and healthcare.

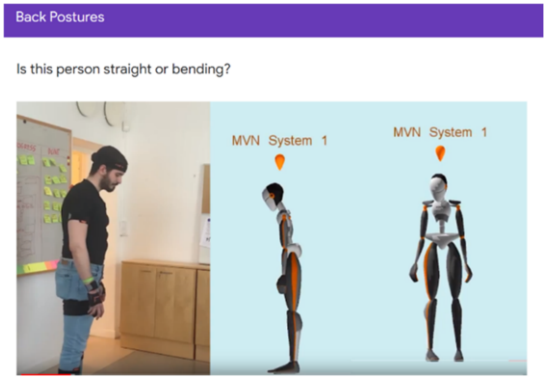

Figure 3. Example a question within the questionnaire.

Results are tabulated for AI training in Matlab. During the training stage, using Statistics and Machine Learning Toolbox and Deep Learning Toolbox in Matlab, the AI algorithms will map inputs (MOCAP data) to outputs (OWAS posture category). Ten different supervised learning algorithms (both input and corresponding output are provided during the training stage) are trained: Fine decision tree, medium decision tree, coarse decision tree, fine k-nearest neighbours (KNN), medium KNN, coarse KNN, cubic KNN, weighted KNN, and convolutional neural network (CNN). CNNs, are less sensitive to the training datasets, and therefore less affected by outliers. However, when using CNNs, it is challenging, if not impossible, to interpret the model and analyse useful information, such as the correlation between variables.

From 60 questions and 7 answers per question, the total size of the built dataset is 420. To prevent overfitting, decision trees and KNN models were trained with 70% of the dataset, with cross-validation set to 5 folds. The CNN was trained with 70% of the

dataset, leaving 15% for validation and 15% for verification, using the Levenberg-Marquardt training algorithm.

The inputs used for training were joint angles values coming from Xsens. Domain knowledge is applied to reduce the number of variables, reducing the risk of misclassification, and only variables related to the posture aimed to classify are used for prediction, as is shown in Table 1. For instance, limbs information is deleted from the dataset used to predict back postures.

Table 1. Example of dimensionality reduction for AI training, divided by category. The variables (joint values) presented are named as they are defined by the Xsens system.

OWAS category	Variables used for training (joint values)
Back	Pelvis, Lower back (L5 + L3), Chest (T8 + T12)
Upper limbs	Shoulder (left and right), Upper arm (left and right)
Legs	Pelvis Lower back (L5 + L3), Upper leg (left and right)
	Lower leg (left and right)

3.2. Questionnaire results

Results from the questionnaire show how experts might differ when classifying certain poses. For instance, in the question shown in Figure 3, 57% of the participants classified the posture as "bent", in contrast to 43% who classified it as "straight". Significant differences can be found when comparing straight and bending postures. Legs and upper body rotation appear to be less problematic among the participants, with a lower degree of disagreement.

Questionnaire sections are related to the type of posture to classify: questionnaire section 1 compares straight and bent back postures back, questionnaire section 2 compares bent and a combination of bent and twisted back postures back, questionnaire section 3 classifies upper limbs posture, and questionnaire section 4 classifies lower limbs postures. Questionnaire section 5 compares two postures not included in OWAS, in which a comparison between bent and straight back, having bent legs, is made. This last section is included to compare the different experts' judgment when classifying a posture not included in the ergonomic assessment. Figure 4 shows the disagreement ratio, comparing dominant options (the ones selected by most of the participants) with the other ones. Figure 5 illustrates an example of a uniform answer and an example of a non-uniform answer.

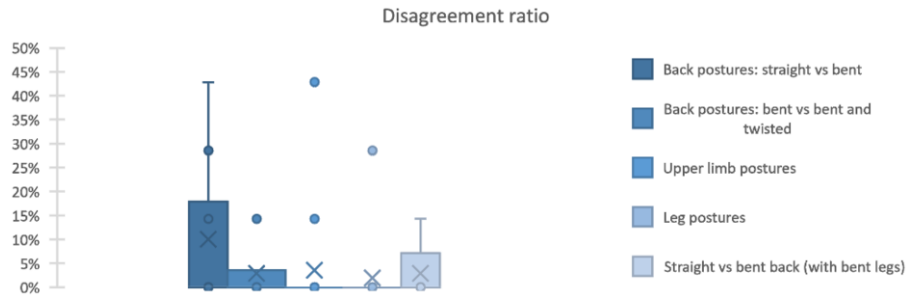

Figure 4. Disagreement ratio from the online questionnaire, comparing dominant options (the ones selected by most of the participants) with the other ones.

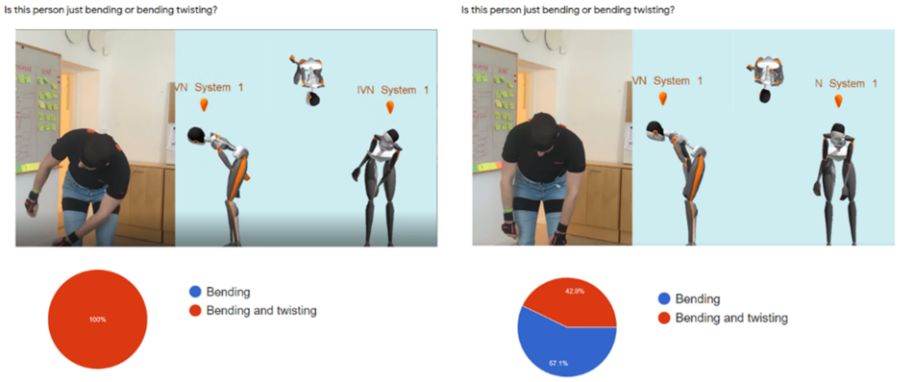

Figure 5. Example a uniformly answered question vs non-uniformly answered question.

3.3. Implementation results

Training results for each trained model are provided in Table 2. Training time for each model was shorter than a few seconds, except for the CNN, where training time was 25 seconds. When using larger datasets, training time is expected to stay relatively short in all the models, except for CNN.

Table 2. Training results for each trained model and its accuracy with the different OWAS categories. Most of the models result in high performance, indicating potential suitability of their use.

Model	Back OWAS accuracy (%)	Upper limbs OWAS accuracy (%)	Legs OWAS accuracy (%)	Avg. (%)
Fine tree	91.8	98.1	97.1	**95.7**
Medium tree	91.8	98.1	97.1	**95.7**
Coarse tree	85.7	98.1	97.1	**95.6**
Fine KNN	85.4	95.2	97.1	92.6
Medium KNN	90.7	98.1	97.1	**95.3**
Coarse KNN	79.3	55.2	97.1	77.2
Cosine KNN	92.1	98.1	97.1	**95.8**
Cubic KNN	90.7	98.1	97.1	**95.3**
Weighted KNN	92.9	98.1	97.1	**96.0**
Convolutional Neural Network	99.9	99.9	99.9	99.9

Resultant accuracy values in the OWAS back category suggest that these kinds of models are suitable for posture classification when the dataset is large enough. Upper limbs and legs predictions accuracy for the different models are the same, which would be a rare situation when using more data. More significant results would be expected if the upper limbs and legs datasets used was as large, and as varied, as the back dataset. The results obtained with CNN suggests that it is overfitting the dataset, most likely making the solution not suitable for other datasets.

4. Discussion and future work

Simple tasks, such as posture estimation within ergonomic evaluations, should not consume human time, and it could be done in an automatic, large-scale manner. Using a

systematic AI-based approach to ergonomic evaluation methods, where AI is considered from the beginning, has potential future applications, including but not limited to: the study of workers behaviour to optimize workstation design and prototyping, the study of patterns which might affect the long-term worker health, or workstation reconfiguration and optimization based on worker's movements. Furthermore, the existence of MOCAP would enable the implementation of human-related data into CPS and other platforms.

Results suggest that applying AI algorithms to observational ergonomic evaluation methods could be suitable for aiding in the computation of ergonomic assessments. AI-based solutions can be built by training models based on the experts' judgment applied to data extracted from body movement. While the results are promising, some models, like CNN, seem to be overfitting, providing exceedingly high accuracy for the current dataset. Overfitting makes difficult to predict how these models would behave when using new datasets. Further testing is required to validate the different models. AI-based ergonomic evaluations are most likely to improve over time, with ergonomic experts' feedback and with the use of new datasets for training. Moreover, further study about how AI-related parameters affect predictions when using MOCAP systems is needed.

AI can work with a dataset of a particular moment in time, e.g., recognizing working postures, but also with cumulative data, using models like recurrent neural networks (RNN). These kinds of AI-models would enable the recognition of an entire range of motion-related variables, such as current working tasks or precedent postures [7]. One of the topics for future research is using task recognition for suggesting the most suitable ergonomic assessment for each case.

One of the main challenges of the presented approach is to generalize it to multiple MOCAP systems, given their differences when it comes to digitalization of motion-related data. Each system might provide data in different formats, lacking some parts of the body, or use postprocessing for various reasons, such as global position calibration. In future studies, and if a comprehensive database is aimed to be created, further discussion about a common ground for multiple MOCAP systems would be required.

Acknowledgement

This work has been made possible with the support of the Knowledge Foundation and the associated INFINIT research environment at the University of Skövde, in the Synergy Virtual Ergonomics (SVE) project, and by the participating organizations. This support is gratefully acknowledged.

References

[1] Lasi H, Fettke P, Kemper HG, Feld T, Hoffmann M. Industry 4.0. Bus Inf Syst Eng, 2014, 6, 239–242. https://doi.org/10.1007/s12599-014-0334-4.

[2] Lee EA. Cyber physical systems: Design challenges. Proc - 11th IEEE Symp Object/Component/Service-Oriented Real-Time Distrib Comput ISORC, 2008, 363–369. https://doi.org/10.1109/ISORC.2008.25.

[3] Uhlemann THJ, Lehmann C, Steinhilper R. The Digital Twin: Realizing the Cyber-Physical Production System for Industry 4.0. Procedia CIRP, 2017, 61, 335–340. https://doi.org/10.1016/j.procir.2016.11.152.

[4] Peruzzini M, Grandi F, Pellicciari M. Exploring the potential of Operator 4.0 interface and monitoring. Comput Ind Eng, 2020, 139, 105600. https://doi.org/10.1016/j.cie.2018.12.047.

[5] Lopez-Nava IH, Angelica MM. Wearable Inertial Sensors for Human Motion Analysis: A review. IEEE Sens J, 2016, PP. https://doi.org/10.1109/JSEN.2016.2609392.

[6] Stoppa M, Chiolerio A. Wearable electronics and smart textiles: A critical review. Sensors (Switzerland),

2014, 14, 11957–92. https://doi.org/10.3390/s140711957.
[7] Fragkiadaki K, Levine S, Felsen P, Malik J. Recurrent network models for human dynamics. Proc IEEE Int Conf Comput Vis, 2015, Inter:4346–54. https://doi.org/10.1109/ICCV.2015.494.
[8] Alikarami H, Yaghmaee F, Fadaeieslam MJ. Sparse representation and convolutional neural networks for 3D human pose estimation. Proc. - 3rd Iran. Conf. Signal Process. Intell. Syst. ICSPIS 2017, vol. 2017- Decem, Institute of Electrical and Electronics Engineers Inc, 2018, 188–192. https://doi.org/10.1109/ICSPIS.2017.8311614.
[9] Eichner M, Ferrari V. Human pose co-estimation and applications. IEEE Trans Pattern Anal Mach Intell, 2012, 34, 2282–2288. https://doi.org/10.1109/TPAMI.2012.85.
[10] Yao A, Gall J, Van Gool L. Coupled action recognition and pose estimation from multiple views. Int J Comput Vis, 2012, 100, 16–37. https://doi.org/10.1007/s11263-012-0532-9.
[11] Yeh C, Matsuda N, Huang X, Li F. Computer Vision – ECCV 2016 Workshops, 2016, 9915, 738–752. https://doi.org/10.1007/978-3-319-49409-8.
[12] Yan X, Li H, Li AR, Zhang H. Wearable IMU-based real-time motion warning system for construction workers' musculoskeletal disorders prevention. Autom Constr, 2017, 74, 2–11. https://doi.org/10.1016/j.autcon.2016.11.007.
[13] Akbarnejad F, Osqueizadeh R, Mokhtarinia HR, Jafarpisheh AS. A novel technique for rapid-accurate 2D hand anthropometry. Iran J Public Health, 2017, 46, 865–866.
[14] Punnett L, Wegman DH. Work-related musculoskeletal disorders: The epidemiologic evidence and the debate. J Electromyogr Kinesiol, 2004, 14, 13–23. https://doi.org/10.1016/j.jelekin.2003.09.015.
[15] Ramos DG, Arezes PM, Afonso P. Analysis of the return on preventive measures in musculoskeletal disorders through the benefit–cost ratio: A case study in a hospital. Int J Ind Ergon, 2017, 60, 14–25. https://doi.org/10.1016/j.ergon.2015.11.003.
[16] Antwi-Afari MF, Li H, Edwards DJ, Pärn EA, Seo J, Wong AYL. Biomechanical analysis of risk factors for work-related musculoskeletal disorders during repetitive lifting task in construction workers. Autom Constr, 2017, 83, 41–47. https://doi.org/10.1016/j.autcon.2017.07.007.
[17] Piedrahita H. Costs of work-related musculoskeletal disorders (msds) in developing countries: Colombia case. Int J Occup Saf Ergon, 2006, 12, 379–386. https://doi.org/10.1080/10803548.2006.11076696.
[18] Falck AC, Örtengren R, Rosenqvist M. Assembly failures and action cost in relation to complexity level and assembly ergonomics in manual assembly (part 2). Int J Ind Ergon, 2014, 44, 455–459. https://doi.org/10.1016/j.ergon.2014.02.001.
[19] Falck AC, Rosenqvist M. A model for calculation of the costs of poor assembly ergonomics (part 1). Int J Ind Ergon, 2014, 44, 140–147. https://doi.org/10.1016/j.ergon.2013.11.013.
[20] Jose JA. Outcome measures and prognosis of WRMSD. Work, 2012, 41, 4848–9. https://doi.org/10.3233/WOR-2012-0775-4848.
[21] Mahdavian N, Lind CM, Olivares JAD, Iriondo A, Högberg D, Brolin E, et al. Effect of giving feedback on postural working techniques. Adv. Transdiscipl. Eng., vol. 8, IOS Press BV, 2018, 247–252. https://doi.org/10.3233/978-1-61499-902-7-247.
[22] Garcia Rivera F, Brolin E, Syberfeldt A, Högberg D, Iriondo Pascual A, Perez Luque E. Using Virtual Reality and Smart Textiles to Assess the Design of Workstations (Accepted). SPS2020, 2020.
[23] David GC. Ergonomic methods for assessing exposure to risk factors for work-related musculoskeletal disorders. Occup Med (Chic Ill), 2005, 55, 190–199. https://doi.org/10.1093/occmed/kqi082.
[24] Eliasson K, Palm P, Nyman T, Forsman M. Inter - and intra - observer reliability of risk assessment of repetitive work without an explicit method. Appl Ergon, 2017, 62, 1–8. https://doi.org/10.1016/j.apergo.2017.02.004.
[25] McAtamney L, Nigel Corlett E. RULA: a survey method for the investigation of work-related upper limb disorders. Appl Ergon, 1993, 24, 91–99. https://doi.org/10.1016/0003-6870(93)90080-S.
[26] Hignett S, McAtamney L. Rapid Entire Body Assessment (REBA). Appl Ergon, 2000, 31, 201–205. https://doi.org/10.1016/S0003-6870(99)00039-3.
[27] Karhu O, Kansi P, Kuorinka I. Correcting working postures in industry: A practical method for analysis. Appl Ergon, 1977, 8(4), 199-201. https://doi.org/10.1016/0003-6870(77)90164-8.
[28] Gams M, Gu IYH, Härmä A, Muñoz A, Tam V. Artificial intelligence and ambient intelligence. J Ambient Intell Smart Environ, 2019, 11, 71–86. https://doi.org/10.3233/AIS-180508.
[29] Nath ND, Chaspari T, Behzadan AH. Automated ergonomic risk monitoring using body-mounted sensors and machine learning. Adv Eng Informatics, 2018, 38, 514–526. https://doi.org/10.1016/j.aei.2018.08.020.
[30] Antwi-Afari MF, Li H, Yu Y, Kong L. Wearable insole pressure system for automated detection and classification of awkward working postures in construction workers. Autom Constr, 2018, 96, 433–441. https://doi.org/10.1016/j.autcon.2018.10.004.
[31] Walsh P, Dunne LE, Caulfield B, Smyth B. Marker-based monitoring of seated spinal posture using a calibrated single-variable threshold model. Annu. Int. Conf. IEEE Eng. Med. Biol. - Proc., 2006, 5370–

5373. https://doi.org/10.1109/IEMBS.2006.259806.
[32] Yu Y, Li H, Yang X, Kong L, Luo X, Wong AYL. An automatic and non-invasive physical fatigue assessment method for construction workers. Autom Constr, 2019, 103, 1–12. https://doi.org/10.1016/j.autcon.2019.02.020.
[33] Maurice P, Malaisé A, Amiot C, Paris N, Richard GJ, Rochel O, et al. Human movement and ergonomics: An industry-oriented dataset for collaborative robotics. Int J Rob Res, 2019, 38, 1529–1537. https://doi.org/10.1177/0278364919882089.
[34] Conforti I, Mileti I, Del Prete Z, Palermo E. Measuring biomechanical risk in lifting load tasks through wearable system and machine-learning approach. Sensors (Switzerland), 2020, 20. https://doi.org/10.3390/s20061557.
[35] Yang K, Ahn CR, Kim H. Deep learning-based classification of work-related physical load levels in construction. Adv Eng Informatics, 2020, 45. https://doi.org/10.1016/j.aei.2020.101104.
[36] Cerqueira SM, Moreira L, Alpoim L, Siva A, Santos CP. An inertial data-based upper body posture recognition tool: A machine learning study approach. 2020 IEEE Int. Conf. Auton. Robot Syst. Compet. ICARSC 2020, Institute of Electrical and Electronics Engineers Inc, 2020, 4–9. https://doi.org/10.1109/ICARSC49921.2020.9096167.
[37] Márquez BY, Vargas AR, Palencia JSM, Castillo JD, Arévalo DÁ. Development and biomechanical analysis through inertial sensors for human motion. ACM Int. Conf. Proceeding Ser., Association for Computing Machinery, 2018. https://doi.org/10.1145/3302425.3302453.
[38] Kadir BA, Broberg O, Conceição CS da. Current research and future perspectives on human factors and ergonomics in Industry 4.0. Comput Ind Eng, 2019, 137, 106004. https://doi.org/10.1016/j.cie.2019.106004.
[39] Thewlis D, Bishop C, Daniell N, Paul G. Next-generation low-cost motion capture systems can provide comparable spatial accuracy to high-end systems. J Appl Biomech, 2013, 29, 112–117. https://doi.org/10.1123/jab.29.1.112.
[40] Gómez-Galán M, Pérez-Alonso J, Callejón-Ferre ÁJ, López-Martínez J. Musculoskeletal disorders: OWAS review. Ind Health, 2017, 55, 314–337. https://doi.org/10.2486/indhealth.2016-0191.
[41] Roetenberg D, Luinge H, Slycke P. Xsens MVN: Full 6DOF human motion tracking using miniature inertial sensors, 2009.

This page intentionally left blank

L. Hanson et al. (Eds.)
© 2020 The authors and IOS Press.
This article is published online with Open Access by IOS Press and distributed under the terms of the Creative Commons Attribution Non-Commercial License 4.0 (CC BY-NC 4.0).

Subject Index

3D body scanning 11
3D statistical shape model 40
accidents 121
active human body models 227
activity theory 288
aircraft pilot seat 259
anthropometry 3, 18, 28, 40, 372
artificial intelligence 419
assembly path generation 388
automated driving 178
automated manikins 388
automatic differentiation 82
automotive assembly 388
autonomous driving 131
Bayesian Theory of Mind (BToM) 51
biomechanical modelling 197
biomechanics 380
blind spot 121
boundary cases 18
clothing modeling 166
cognitive modelling 61
confidence ellipses 18
contextual inquiry 288
curved surface 217
data comparison 11
DHM 28, 61, 99, 178, 197, 259, 269, 311, 323, 330, 342, 361, 380, 388, 398, 408
DHM development 288
DHMS 299
DHMW 408
digital hands 91
direct vision 99, 121
discrete mechanics 82, 115
driver mental model 51
driver monitoring 187
driver posture 187
dynamic driving 269
dynamic precision 145
embodied tool use 311
ergonomic(s) assessment 299, 419
ergonomic evaluation 419
ergonomics 28, 311, 323, 361, 380, 388
ergonomics simulation 299
ESI's virtual seat solution for aero 259
eye-hand coordination 61
finite element method 166, 348
flexible cables 388
gait analysis 197
gamification 323
gender balance 408
grasp synthesis 91
grasping 206
grasping movement 178
hand kinematics 206
hand trajectories 178
health monitoring 398
hill muscle 269
human body models 166
human body shape 40
human centric 279
human kinematics 197
human modelling 99
human motion planning 115
human-exoskeleton interaction 217
human-seat interaction 249
human posturing 299
interface forces 217
interpersonal communication 131
inverse dynamic 380
inversed dynamics 108
jaw motion 108
joint attention 131
law enforcement officer 3
line balancing 342
linear mixed effects models 178
lower limb amputees 348
machine learning 419
manikins family 28
manual anthropometry 11
marine (transportation) 398
marine workers 398
model order reduction 206

modelling 408
monitoring 197
motion capture 419
motion database 187
motion reconstruction and animation 187
motion tracking 388
multi variable optimization 342
multimodal interaction 131
multivariate 28
muscle activation 227
musculoskeletal model 217
musculoskeletal modeling 108
musculoskeletal optimal control simulations 82
naturalistic perception 131
neural networks 71
Occupational Repetitive Actions (OCRA) 398
on-the-job-training 323
Operator 4.0 279
optimal control 115, 269
optimization 361
Partially Observable Markov Decision Processes (POMDPs) 51
passive exoskeleton 217
PCA 40
personal protective equipment 166
postural comfort 259
postural synergies 206
posture 156
posture simulation 249
pre-crash 227, 269
precision of human movement 145
pressure ulcer 237
principal component analysis 372
proactive eye gaze 330
procedural animation 71
process planning 342
process validation 279
Product-Service-System (PSS) 398
prosthetics 348
rehabilitation 237
reinforcement learning 51
risk assessment 380
running 372
safety 121
seat cushion 237
simulation 323, 361
simulation of human movements 145
skewness 18
smart clothing 197
socket fit 348
spatio-temporal parameters 197
stability 156
standardization 99
standards 121
static comfort 259
static precision 145
statistics 28, 372
STEM 408
stepping 156
subject-specific calibration 227
take-over 178
temporomandibular disorder 108
thermal comfort 259
trucks 99, 121
universal design 91
upholstery database 249
upholstery stiffness measurement 249
user experience (UX) 288, 311, 330
variational motion synthesis 71
vehicle accommodation 3
vibratory comfort 259
virtual assembly 279
virtual evaluation 91
virtual prototyping 259
virtual reality 131, 279, 330, 388
VR interaction using collider 145
VR/AR 299
vulnerable road users 99
wearable inertial sensors 419
wearable motion capture inertial system 398
wheelchair 237
women 408
WRMSD 380
zero moment point 156

L. Hanson et al. (Eds.)
© 2020 The authors and IOS Press.
This article is published online with Open Access by IOS Press and distributed under the terms of the Creative Commons Attribution Non-Commercial License 4.0 (CC BY-NC 4.0).

Author Index

Abran, G. 197
Aissaoui, R. 156
Bampouni, E. 61
Bechler, F. 227
Bengler, K. 178
Berce, A. 388
Beurier, G. 40, 187
Bhatt, M. 131
Billing, E. 61, 330
Björkenstam, S. 115, 269
Boebel, A. 206
Boljen, M. 166
Bonin, D. 11
Borot, C. 259
Bradtmiller, B. 3
Brolin, E. v, 18, 361
Bullinger, A.C. 145
Cabane, C. 259
Carlson, J.S. 115
Cavatorta, M.P. 217
Chander, D.S. 217
Charland, J. 156
Cheema, N. 71
Dahlvik, J. 342
Darwish, A. 51
Delfs, N. 342
Denteneer, L. 398
Domi, A. v
Dörlich, V. 269
Du, H. 71
Eland, A. 99, 121
Fang, M. 388
Fehr, J. 227
Fischer, K. 71
Fleischer, M. 178
Forsberg, T. 342, 388
Fragoso, P.E. 28
García Rivera, F. 361, 388, 419
Haelterman, R. 197
Hagemeister, N. 156
Hanson, L. v, 18, 342, 361
Harih, G. 348
Hause, M. 3
Hetzenecker, A. 178
Högberg, D. v, 18, 342, 361, 388, 419
Hsiao, H. 3
Igelmo, V. 419
Iriondo Pascual, A. 342, 361
Jenerowicz, M. 166
Jiménez Sánchez, J.L. 323, 342
Johansson, P. 342
Kaiser, A. 145
Kam, E. 279
Kempter, F. 227
Klein, H. 166
Klingspor, P. v
Kolbeinsson, A. 288, 311
Kondyli, V. 131
Lafon, Y. 40
Lamb, M. 61, 330
Lämkull, D. 299
Latour, F. 156
Lee, Y.J. 237
Leyendecker, S. 82, 206
Lindblom, J. 288, 311, 330
Linn, J. 269
Ljung, O. 342
Lund, M.E. 372
Maeda, Y. 91
Mårdberg, P. 115, 269, 388
Marshall, R. 99, 121
Miyata, N. 91
Niemann, M. 279
Palmquist, A. 323
Paterson, A. 99, 121
Paul, G. 237
Peng, J. 40
Penner, J. 82
Pérez Luque, E. 361, 408, 419
Peters, M. 11, 380
Phutane, U. 206
Plesec, V. 348
Radke, D. 11
Rasmussen, J. 108, 372
Regnault, J. 259
Reinhard, R. 388

Rockwell, B. 3
Roller, M. 115, 206, 269
Roosens, E. 197
Rosén, J. 330
Rueckert, A. 279
Sasaki, K. 108
Scataglini, S. 197, 398, 408
Shigemitsu, R. 108
Slattery, P. 237
Slusallek, P. 71
Sprenger, J. 71
Steinhauer, H.J. 51
Summerskill, S. 99, 121
Syberfeldt, A. 361, 419
Takahashi, R. 91
Thorvald, P. 288, 311
Trube, N. 166
Van Tiggelen, D. 197
Verwulgen, S. 197, 398
Waagepetersen, R.P. 372
Wagner, F. 249
Wang, H. 187
Wang, X. 40, 187
Wirsching, H.-J. 249
Wischniewski, S. 11, 380
Zdrodowski, M. 299
Zeighami, A. 156
Zelck, S. 398
Zhao, M. 187